Thesis Topic:

BUCKLING MODES IN CONTINUOUS COMPOSITE BEAMS

Vol. 1

By:

ZORA VRCELJ

A thesis Submitted as Partial Fulfilment of The Requirements For The Degree of

DOCTOR OF PHILOSOPHY

October 2004

SCHOOL OF CIVIL AND ENVIRONMENTAL ENGINEERING
THE UNIVERSITY OF NEW SOUTH WALES

*In memory of **Braco**, my beloved brother*

SYNOPSIS

This thesis addresses primarily the issue of restrained-distortional buckling (RDB) in both half-through girder bridges and composite tee-beams in hogging bending regions. RDB is fundamentally different to the more commonly studied distortional buckling of laterally unrestrained beams and can have a profound influence on the buckling of beams with a continuous restraint.

Buckling of continuous composite beams and half-through girder bridges is usually modelled in design codes using the so-called U-frame method. The U-frame approach is simplistic, and finite element calibrations have shown it to be inaccurate. Furthermore, significant differences exist between the buckling behaviour of composite tee-beams and reasonably well-researched steel I-beams in the negative-moment regions. Local, lateral and distortional instabilities of the steel section occur in the hogging-moment regions of continuous composite tee-beams and these forms of buckling have been recognised to be highly interactive.

Following a concise review of the available literature, the elastic buckling modes in continuous composite beams are investigated. In this study, an in-plane analysis of a two-span continuous composite beam and a rational model for the out-of-plane buckling are combined, so as to study the elastic restrained distortional buckling of composite beams cast unpropped and propped over one internal support. The main focus of this investigation are restraint conditions at the internal support, the effects of bracing in the hogging bending region, the ratio of the axial and bending actions in the bottom flange along the length of the beam, the destabilising nature of the compressive actions in the hogging moment region and the dependence of the elastic buckling load factor of a continuous composite beam caused by shrinkage and creep for a multiplicity of geometric and loading configurations.

A rational model is then developed to investigate the elastic RDB of I-section members, under moment gradient and varying axial force, restrained fully against translation and lateral rotation and elastically against twist rotation at one flange. This method of analysis has its application in the buckling analysis of through girders under moment gradient and continuous composite beams in which both varying axial force and moment gradient are present. The generic model selected has identified a unique distortional buckling parameter that quantifies the effect of cross-sectional distortion, and which allows the high multiplicity of buckling curves in the design space associated with distortional instability to be reduced to only a few.

The above method is then modified to account for the inelastic range of structural response, as the strength of steel members of low to intermediate slenderness is generally reduced below the elastic buckling value due to premature yielding as a result of the combined effects of the stresses caused by the applied loads and of the residual stresses which are developed during the cooling of a welded/hot-rolled steel member. This analysis is concerned primarily with welded sections as these are normally used in half-through bridge girders. The usual idealised stress-strain relationship is used for the analysis, while the 'tendon force concept' of residual strains is assumed for the flanges and web.

The conventional semi-analytical finite strip method for elastic local buckling has then been modified and augmented with so-called bubble functions in the form of Legendre polynomials for the transverse buckling displacements. The results show that the use of bubble functions significantly improves the efficiency of the finite strip method in terms of strip subdivision. It is found that only one bubble strip for each flat was needed to model the topology, compared with conventional finite strips, in order to achieve comparable accuracy. It is also shown that augmentation of bubble terms, in modelling plate assemblies where membrane actions are significant, such as I and T-beam sections, does not improve the efficiency of the finite strip method in terms of discretisation. Similarly, there was no significant improvement in convergence for members where lateral buckling precedes local buckling.

A bubble based spline finite strip method of analysis is then formulated. A simple technique for replacing the specification of amended splines, used conventionally to model the variety of end conditions and internal restraints that may occur (clamped, simply supported, sliding or free), is developed so that freedoms may be assigned in the same manner as is usually employed in the finite element method. The method is then employed to study the interactive nature of local and distortional buckling of different plate assemblies, and it is applied specifically to the RDB of beams that is addressed in this thesis. The difference in the buckling behaviour of plates and plate assemblies in elastic and inelastic range of structural response is assessed.

PREFACE

This thesis is submitted for the degree of Doctor of Philosophy at the University of New South Wales, Australia. Some of the work described in this thesis has already been published in journals or presented at conferences. These supporting papers are:

1. Vrcelj, Z., Bradford, M.A. and Uy, B. (1999). Elastic buckling modes in unpropped continuous composite tee-beams, *ACMSM16*, Dec. 8-10, Sydney, 325-331.

2. Vrcelj, Z. and Bradford, M.A. (2001). A rational model for the elastic restrained distortional buckling of half-through girder bridges, *Third International Conference on Thin-Walled Structures*, Jun. 5-7, Cracow, 153-160.

3. Vrcelj, Z., Bradford, M.A. and Ronagh, H. (2001). Elastic stability of half-through girder bridges, *ISEC*-01, Jan. 24-27, Hawaii, 687-692.

4. Bradford, M.A. and Vrcelj, Z. (2001). Instabilities in continuous composite beams induced by quasi-viscoelastic slab behaviour, *ISEC*-01, Jan. 24-27, Hawaii, 937-941.

5. Vrcelj, Z., Bradford, M.A., Uy, B. and Wright, H.D. (2002). Buckling of the steel component of a composite member caused by shrinkage and creep of the concrete component, *Progress in Structural Engineering and Materials*, **4**(2), 186-192.

6. Vrcelj, Z. and Bradford, M.A. (2002). Inelastic restrained distortional buckling of half-through girder bridges under transverse loading, *Sixth Int. Conf. on Short & Medium Span Bridges*, Vancouver, Canada, 161-168.

7. Vrcelj, Z. and Bradford, M.A. (2002). Elastic restrained distortional buckling modes in continuous composite T-beams, *Sixth Int. Conf. on Short & Medium Span Bridges,* Vancouver, Canada, 169-176.

8. Vrcelj, Z. and Bradford, M.A. (2004). An efficient bubble-based spline finite strip method of buckling analysis, *Communications in Numerical Methods in Engineering* (accepted for publication).

9. Vrcelj, Z. and Bradford, M.A. (2004). Elastic buckling modes of two-span continuous composite beams (submitted for publication).

10. Vrcelj, Z. and Bradford, M.A. (2004). Inelastic buckling modes of two-span continuous composite beams (submitted for publication).

11. Vrcelj, Z. and Bradford, M.A. (2004). Restrained distortional buckling of half-through girder bridges (submitted for publication).

12. Vrcelj, Z. and Bradford, M.A. (2004). Inelastic restrained distortional buckling of monosymmetric I-sections subjected to moment gradient (submitted for publication).

13. Vrcelj, Z. and Bradford, M.A. (2004). Restrained distortional buckling strength of I-section beam-columns subjected to moment gradient (submitted for publication).

ACKNOWLEDGEMENTS

I am indebted to a number of people for their help in the preparation of this thesis. Without them this thesis would never have come into realisation.

First at all, I would like to express my profound gratitude to my supervisor, Professor Mark Bradford, for his outstanding guidance and support during my PhD studies. Mark is a brilliant researcher and a fascinating teacher, and I benefited greatly from working under his guidance. He is also an attentive mentor and his encouragement and friendship have been invaluable throughout my studies at UNSW. Mark's academic excellence continues to be a source of inspiration, but beyond that I am especially grateful for his limitless patience and fatherly support during trying times.

Special thanks are due to Professor Brian Uy who co-supervised the work in this thesis and who also supervised my undergraduate thesis. I owe much of my insight and interest in structural engineering research and teaching to his inspiring lectures and exceptional guidance during my undergraduate studies. Brian's unfailing support, friendship and encouragement throughout the years are greatly appreciated.

My sincere thanks are due to Professor Ian Gilbert, the Head of School, who has been most accommodating and caring over last few years. I would also like to thank all the rest of the academic and general staff in the School for their help with the preparation of this thesis. Further thanks must also be warmly extended to my students here at UNSW for making this whole experience such an enjoyable one.

I am very grateful to the Faculty of Engineering for providing a scholarship that enabled me to join the School.

For all the good time during the PhD years, I am thankful to my family, colleagues and friends from UNSW and around the world. But above all, I would like to express my loving appreciation to my parents, who are never-ending source of love, support and inspiration.

TABLE OF CONTENTS

VOLUME II

Chapter 6 Bubble Augmented Harmonic Semi-Analytical Finite Strip Method

Chapter 7 Elastic Bubble Based Spline Finite Strip Method

Chapter 9 Concluding Remarks

REFERENCES

APPENDIX

NOTATION

A	Cross-sectional area;
A, B, C, D	Bubble polynomial coefficients;
A_c	Concrete cross-sectional area;
A_r	Reinforcement cross-sectional area;
A_S	Cross-sectional area of the joist;
A_w	Area of the added weld metal;
$\overline{A}$	$\overline{K}(\lambda)-\overline{G}(\lambda)$;
B	Welding process constant (8,000 N/mm^2);
$\overline{B}$	Strain matrix;
$\overline{B}_F$	Flange strain matrix;
$\overline{B}_W$	Web strain matrix;
$\overline{C}$	Coefficients matrix;
D_{11}, D_{12}, D_{33}	Plate properties;
D_x, D_y, D_{xy}	Plate properties;
$\overline{D}$	Elasticity matrix;
$\overline{D}_F$	Flange elastic property matrix;
$\overline{D}_W$	Web elastic property matrix;
E	Young's modulus of elasticity;
E_s, E_c	Young's modulus of elasticity for steel and concrete respectively;
E_{st}	Tangent modulus;
E_x, E_y	Young's modulus in x and y direction respectively;
EI_F	Flexural rigidity of the flange about an axis through the web;
EI_W	Warping rigidity;
E_1, E_{12}, E_2	Plate properties;
F	Tendon force;
$F(t)$	Compliance function;
G	Shear modulus;
G_{st}	Inelastic shear modulus;
GJ_T, GJ_B	Top and bottom flange Saint-Venant's torsional rigidity;
$\overline{G}, \overline{K}$	Stability and stiffness matrix of folded plate system;

I_F	Second moment of inertia of flange = (1/12) $t_f b_f^3$;
I_w	Warping constant;
I_x, I_y	Second moment of inertia of cross section about x and y-axis respectively;
J	Torsional constant;
J_T, J_B	Top and bottom flange Saint-Venant's torsional constant;
K	Dimensionless beam parameter;
$\overline{K}$	Monosymmetric I-beam parameter;
L	Beam length; Length of a strip;
M	Bending moment;
M_a	Applied bending moment;
M_E	Elastic critical buckling moment, distortional buckling;
M_o	Reference value of $M(\xi)$, numerically greatest bending value; First order bending moment; Primary structure bending moment;
M_{ob}	Elastic critical buckling moment, classical solution;
M_{od}	Elastic critical buckling moment, distortional buckling;
M_{cr}	Elastic critical buckling moment;
M_{Icr}	Inelastic critical buckling moment;
M_P	Plastic moment;
M_S	Bending moment in the joist;
M_{sd}	Bending strength of the steel in the absence of compression;
M_x, M_y, M_{xy}	Bending moments about x and y axis and twisting moment;
M_Y	First yield moment;
$\overline{M}$	Flexural and membrane displacements equations matrix;
N	Axial load;
N_a	Applied axial load;
N_{cr}	Elastic critical buckling load;
N_o	Reference value of $N(\xi)$, numerically greatest axial value;
N_{od}	Elastic critical buckling load, distortional buckling;
N_{ol}	Euler buckling load;
N_S	Axial force in the joist;
N_{sd}	Compressive strength of the steel in the absence of bending;
N_Y	Section capacity in compression;

N_1, N_2	Membrane (linear) interpolation polynomials;
N_3, N_4	Flexural (cubic) interpolation polynomials;
N_5	Bubble function polynomial;
P	Applied point load;
P_u	Ultimate point load;
R	Support reaction;
$\overline{R}$	Transformation to global coordinates matrix;
$\vec{R}$	Vector of incremental actions;
S_1, S_2, S_4	Plate properties;
$\overline{T}$	Tangent stiffness matrix;
$\overline{T}^*$	Transformation matrix for boundary and interior supports;
U	Total strain energy stored during buckling;
U_F, U_W	Flange and web contributions to U;
U_F	Flexural strain energy;
U_M	Membrane strain energy;
U_R	Restraint contribution to U;
V	Total work done during buckling; Shear force;
V_a	Applied shear Force;
V_F, V_W	Flange and web contributions to V;
V_F	Flexural contribution to total work done during buckling;
V_M	Membrane contribution to total work done during buckling;
X_B	Bubble polynomial;
X_i	Redundant unknown reaction;
Z	Elastic section modulus = I_x/y;
Z_S	Elastic section modulus of the joist;
$a_1,\ldots,a_4$	Coefficients in the expression $M(\xi) = M_o\,(a_1 + a_2\xi + a_3\xi^2 + a_4\xi^3)$;
b	Strip width;
b_f	Flange width;
b_s	Stiffener width;
c	Constant;
c_f	The half-width of the residual tensile stress block;
c_m	Moment gradient caused by unequal end moments;
d_s	Longitudinal stiffener position;

e	Eccentricity;
e_0, e_L	End eccentricities;
f'_c	Concrete compressive strength (28 days);
f_{ij}	Flexibility coefficient;
f_t	Flexural tensile strength of concrete;
f_y	Yield stress;
$\bar{g},\bar{k}$	Strip stability and stiffness matrix respectively;
$\bar{g}_e,\bar{k}_e$	Kernel strip stability and stiffness matrix respectively;
$\bar{g}_F,\bar{g}_M$	Strip stability flexural and membrane matrix, respectively;
h	Section width; Web depth;
h_w	Web depth;
k	Local buckling coefficient;
k_e	Column effective length factor;
k_t	Continuous translational restraint;
k_z	Continuous twist rotation stiffness;
$\bar{k}$	Member stiffness matrix;
$\bar{k}_F,\bar{k}_W$	Flange and web stiffness matrix, respectively;
$\bar{k}_F,\bar{k}_M$	Strip stiffness flexural and membrane matrix, respectively;
$\bar{k}_R$	Restraint stiffness matrix;
m	Number of sections; Bending moment due to unit value of the redundant action;
n	Number of nodal lines; Number of terms in the Fourier expansion; Number of buckling half wavelengths over the length L of the strip
ns	Number of strips;
r_x	Radius of gyration about x-axis;
$\vec{r}$	Vector of generalised incremental displacements;
$\bar{s}$	Member stability matrix;
$\bar{s}_F,\bar{s}_W$	Flange and web stability matrices, respectively;
sgn	Sign (+ve or –ve);
$\vec{q}$	Maximum values of buckling deformations; Vector of buckling displacements, eigenvector;
q_1, q_2, q_3	Buckling degrees of freedom;

t	Strip thickness; Time in days;
t_f	Flange thickness;
t_s	Stiffener thickness;
t_w	Web thickness;
u, v, w	Strip deflections in x, y, z direction respectively;
u'_b	In-plane lateral rotation of the bottom flange;
u_T, u_B	Top and bottom flange lateral deformations;
u_t, u_b	Top and bottom flange lateral deformations;
u_t	Flange strut buckling deformation;
u_1, u_2	Support displacements;
$\vec{u}$	Buckling deformations vector;
w	Uniformly distributed load in z-direction;
w_B	Bubble degree of freedom;
w_u	Ultimate uniformly distributed load;
x, y, z	Cartesian axes aligned with strip;
Δ	Web flexibility per unit length in U-frame model;
$\vec{\Delta}$	Vector of buckling displacements, eigenvector;
$\vec{\Delta}_e$	Vector of buckling displacements in global direction;
Π	Total potential energy;
α	Dimensionless twist restraint parameter; Stress gradient;
$\alpha, \beta, \gamma, \delta, \omega$	Displacement coefficients;
α_s	Critical buckling moment coefficient;
α_t	Stiffness in Winkler type tensionless foundation;
α_w	Brace location parameter;
$\vec{\alpha}$	Vector of coefficients;
β	Orientation of a strip; Ratio of the smaller to the larger end moment; $Et^3/12(1-\nu^2)$;
β_T, β_B	Ratios of the inelastic to total areas of the full top and bottom flanges respectively;
β_x	Monosymmetry section constant;
δ	First variation; Beam-column deflection;
δ_b	Approximate factor for amplifying the first order moments;

δ_{mi}	Fourier series coefficients;
δ'	Beam-column slope;
δ''	Beam-column curvature;
$\vec{\delta}$	Vector of buckling displacements in local coordinate system;
ε_a	Applied strain;
ε_h	Strain-hardening strain;
$\varepsilon_L, \varepsilon_N$	Linear and non-linear component of strain in strip, respectively;
ε_{oi}	Strain at the top of cross-section;
ε_r	Residual strain;
ε_{rc}	Residual compressive strain;
ε_{sh}	Shrinkage strain;
ε^*_{sh}	Shrinkage strain final value;
ε_y	Yield strain;
$\vec{\varepsilon}_F$	Generalised flange strain vector;
$\vec{\varepsilon}_L$	Linear strain vector;
$\vec{\varepsilon}_N$	Non-linear strain vector;
$\vec{\varepsilon}_W$	Generalised web strain vector;
ϕ	Creep coefficient;
ϕ^*	Creep coefficient final value;
ϕ_T, ϕ_B	Top and bottom flange twist;
ϕ_t, ϕ_b	Top and bottom flange twist;
γ	Proposed restrained-distortional buckling parameter;
γ_r	Web distortion parameter;
$\vec{\gamma}$	Vector of local degrees of freedom;
η	y/b;
κ	Curvature;
λ	Load factor;
λ_{cr}	Critical buckling load factor;
λ_L	Long term buckling load factor;
λ_r	Modified slenderness $\lambda_r = \sqrt{M_P/M_{ob}}$;

λ_{ref}	Reference buckling load factor;
λ_S	Short term buckling load factor;
ν	Poisson's ratio;
ν_x, ν_y	Poisson's ratio in x and y direction respectively;
π	3.1415927;
ρ	Monosymmetry parameter;
ρ_x, ρ_y, ρ_{xy}	Curvature in the x and y directions and shear strain, respectively;
θ	Rotation about z-axis of edge of strip;
σ	Buckling stress = $M(\xi)/Z$;
σ_A	Axial stress;
σ_B	Bending stress;
σ_{cr}	Critical buckling stress;
σ_{el}	Lateral-torsional critical buckling stress;
σ_r	Residual stress;
σ_{rc}	Residual compressive stress;
σ_T	Total buckling stresses;
σ_x, σ_y	Longitudinal and transverse stresses, respectively;
σ_y	Yield stress;
σ_1, σ_2	Longitudinal compressive stress at nodal lines 1,2 respectively of a strip;
τ, τ_{xy}	Shear stresses;
ξ	z/L;
ψ	Local B_3-spline function;
ψ_B	Bubble degree of freedom;

[ ]	Matrix;
$\mid \; \mid$	Determinant of matrix;
$\lfloor \; \rfloor$	Diagonal matrix;
$\langle \; \rangle$	Row vector;
$\{ \; \}$	Column vector.

VOLUME I

Chapter 1

INTRODUCTION

TABLE OF CONTENTS

1.1 STATEMENT OF THE PROBLEM

Instability is probably the most common cause of failure of a steel member, and may be instigated by various buckling phenomena. From a fundamental point of view, these buckling phenomena can be divided into three main categories, namely local, global and distortional. Local buckling is a characteristic form of instability in members composed of slender plate elements in which the member element is considered to buckle by locally distorting over a short length of the member with a half-wavelength of the order of the member width, as shown in Fig. 1.1a. Global or lateral instability (Fig. 1.1b) occurs when a laterally unbraced member, which is bent about its stiffer plane, buckles out of the plane of loading by deflecting laterally and twisting with a half-wavelength of the order of the member length without any distortion of the cross-section. On the other hand, lateral- distortional buckling is basically an interaction mode between lateral-torsional and local buckling. This buckling mode takes place at longer half-wavelengths than local buckling and is characterised by simultaneous lateral deflections and cross-sectional distortion (Fig. 1.1c). The usual buckling assumption in overall buckling that no distortion of the cross-section occurs during buckling (Vlasov 1961) does not apply to this buckling mode. These instability modes are all bifurcative, which has proven to be a convenient way to study the phenomenon, in that they occur at a point of bifurcation from a stable primary straight unbuckled configuration to a stable or neutral secondary buckled configuration.

Distortional buckling of unrestrained beams of practical configuration usually takes place at a load that is not significantly less than that for lateral buckling. Restrained-distortional buckling (RDB), however, is fundamentally different to the more commonly studied distortional buckling of laterally unrestrained beams and can have a profound influence on the buckling behaviour of beams with continuous restraint at the level of the tension flange (Bradford 1998a; Ronagh & Bradford 1998; Lee 2001). The overall mode of buckling in composite steel-concrete tee-beams in regions of negative bending (Fig 1.2) and in half-through girder bridges (Fig. 1.3) is what is herein termed restrained-distortional buckling. Many other structural elements, such as roof and wall cladding, which are intended primarily for other purposes, also provide restraints against buckling, as illustrated in Fig. 1.4, and advantage is taken of this in design. For example, rafters in industrial buildings are usually restrained against buckling by purlins attached to one flange, and which when spaced reasonably close enough can be considered as continuous since the purlin/cladding system provides diaphragm and flexural restraint.

The buckling aspects involved in continuously restrained members are far more complex, and much less understood, than those involved in lateral or local buckling of bare steel beams. Distortional buckling analyses are invariably more complex than either local or lateral buckling analyses alone, since each cross-section of a member is free to both distort and displace. The distortional nature of this buckling mode, with its inherent additional complexities, means that no tangible closed form solution has yet been developed for this type of buckling. While research findings that deal with restrained beams are fairly plentiful, most have incorrectly ignored the effects of cross-sectional distortion.

One of the most difficult beam buckling problems to analyse accurately is the buckling of a steel joist in a continuous composite beam, and despite many investigations, the mechanics of this problem has not yet been correctly or comprehensively quantified. These difficulties arise because the buckling mode is lateral-distortional rather than lateral-torsional, because the joist is subjected to combined bending moments and axial forces that vary along the length of the span, as shown in Fig. 1.5, and because there is no evidence that the conversion of the elastic buckling load factor to a strength load factor that incorporates yielding is the same for lateral-distortional buckling as it is for lateral buckling. In negative bending the slab restrains the tension region of the steel and the neutral axis is not located at the mid-height of the web. The neutral axis is shifted towards the top flange, and in negative bending the steel region is subjected to predominantly compressive loading. The steel joist in such a composite beam is not only subjected to varying bending moments, but also to varying axial actions that can be compressive at the internal support and tensile near the simply supported end. Unbalanced axial force in the joist arises from maintaining equilibrium of the monosymmetric steel/concrete cross-section at the level of the shear connection, and varies along the length of the joist in accordance with the gradient of the bending moment. Few studies, if any, have addressed the problem of the buckling of a steel beam-column with both continuously varying axial force and bending moment. In addition, the web usually carries proportionally higher shear loads than in ordinary steel beams (Climenhaga & Johnson 1972). The lateral-distortional buckling resistance of the steel portion in continuous composite beams is therefore dependent on the extent to which the web can provide a restraining action to the unstable compression flange. This form of buckling is usually prevented in bridge girders by the cross bracing as illustrated in Fig. 1.6, and the common view amongst engineers is that such bracing is excessive and uneconomical.

The utilisation of half-through girders in bridge construction is most usually a result of constraints on headroom. They find very frequent use in railway bridges over roadways, where the flat grade of the railway is predetermined and it is difficult to provide a substructure to support the bridge deck. Half-though girder bridges provide a load path from the bridge deck to the bearing supports by means of bottom flange loading of parallel steel I-section beams. Because of this, the I-section beams of simply supported half-through girders experience compression in their top flanges and tension in their bottom flanges. At the level of the bottom (tension) flange, the deck restrains the flange against lateral and minor axis rotational deformations during buckling, and depending on the stiffness of the deck in flexure transverse to the longitudinal axis of the bridge, it provides some theoretically quantifiable degree of twist rotational restraint. At the level of the top (compression) flange of the I-section, restraint of this critical flange against buckling is provided only by the flexural stiffness of the web in the plane of its cross-section, or by the flexural stiffness of the web/stiffener contribution. The major consideration in the design of half-through girders is that of instability of the steel beams, and this mode of instability must necessarily be that of RDB (Bradford 1997a; Ronagh & Bradford 1998), as shown in Fig. 1.3.

The most common model for considering RDB in design is the so-called U-frame method (Oehlers & Bradford 1995, 1999), in which the top compression flange of the I-section is considered as a strut compressed uniformly along its length by the maximum bending stress that is induced in it, and which is restrained by a continuous Winkler spring whose stiffness is that of the web in the plane of its cross-section acting as a cantilever, as illustrated in Fig. 1.7. This simplistic model appears in some national bridge codes. In reality, half-through girder bridges and continuous composite beams are generally used in situations in which there is considerable moment gradient, and so the U-frame approach tends to be conservative, excessively so in most cases.

Local and distortional instabilities of the steel beam occur in the hogging-moment region in a continuous composite beam and these forms of buckling have been recognised to be highly interactive (Dekker *et al.* 1995). Existing studies (Bradford & Kemp 2000) have indicated that significant differences exist between the behaviour of composite and steel beams, and their study identifies that further research is required to understand the implications of these differences, specifically:

(i) the influence of distortional restraint provided by the slab and the shear connection to combined global and local buckling of the compression flange and adjacent web, and the interactive nature of this buckling;
(ii) the area of longitudinal slab reinforcement at internal supports relative to the area of the steel section;
(iii) the difference in the buckling behaviour of elastic, inelastic and plastic members.

Although buckling of plain steel beams in both the elastic and inelastic ranges of structural response has been studied extensively and a great deal of research work has been devoted to the understanding of their buckling modes, and codes of practice for the design of structural steelwork contain relevant clauses that presently are considered to be quite accurate, buckling of the steel component in composite beams still represents a grey area in structural engineering research and is much less well documented. Whilst buckling of the steel component in a continuous composite beam and a half-through girder bridge is of major practical significance, and significant research has been devoted into its prediction, the development of even moderately accurate design rules suitable for practising structural engineers has not been achieved to date. Designers need simpler and less conservative methods of checking the resistance to buckling of such commonplace structural configurations.

This thesis thus addresses comprehensively the issue of restrained-distortional buckling in both half-through girder bridges and composite tee-beams in hogging bending regions.

1.2 AIM AND SCOPE OF THE THESIS

The aim of this thesis is to study theoretically the behaviour of continuously restrained structural systems, such as continuous composite beams and half-through girder bridges, and to provide some practical guidance pertaining to their design. This aim is achieved by developing theoretical models for studying the RDB of half-through girder bridges and continuous composite beams under transverse loading and moment gradient. These numerical models have been programmed for a digital computer, and the results have been compared with independent theoretical solutions and published test results where possible. Furthermore, a bubble based spline finite strip method of analysis has been formulated in order to investigate the interactive nature of local and distortional buckling, as well as the difference in the buckling behaviour of plates and plate assemblies in the elastic and inelastic range of structural response.

In Chapter 2, the existing work reported in the published literature on the buckling modes of I-section beams, columns and beam-columns is reviewed. A review of the classical local, lateral and lateral-distortional modes of buckling, and their interaction is presented and this is followed by a chronological development of the spline finite strip method of analysis for buckling problems.

Chapter 3 presents the results of a numerical buckling analysis of a two-span composite tee-beam that is cast unpropped, as would normally be the case for highway overpass bridges. The elastic solutions presented indicate the effect of restraint conditions over the interior support and of bracing of the bottom flange of the composite beam, the ratios between axial and bending stresses in the steel joist for both propped and unpropped construction and the influence of the time effects of shrinkage and creep of the slab on the erosion of the buckling load factor.

The elastic buckling of simply supported I-section members is considered in Chapter 4. By invoking a Ritz-based procedure, a simple generic model is developed that may be used for studying the elastic RDB of I-members restrained completely and continuously against lateral translation and lateral rotation at one flange level, but elastically against twist rotation at this flange level, when subjected to moment gradient. This situation is encountered in half-through girder bridges. A unique dimensionless parameter that quantifies the influence of a number of material and geometric factors on the restrained-distortional buckling solutions is identified in the model, and is used to provide useful design graphs. Some guidance pertaining to the design of half-through girders is provided, and this is illustrated with an example.

The analysis developed in Chapter 4 is extended in Chapter 5 to include inelasticity as well as residual stresses, so that predictions of buckling strengths may be made. Inelasticity is of particular significance in fabricated I-section members, such as welded plate girders, because the welding process results in levels of residual stresses that are typically higher than those in hot-rolled beams. The variations of the residual stresses across the flanges are nearly uniform in welded beams, and once flange yielding is initiated, it spreads quickly through the flange with little increase in moment. This causes large reductions in the inelastic buckling moments of members. The energy method is employed to study the relationship between elastic RDB and yielding for an I-section member restrained by concrete medium at the tension flange level and some results are reported that address the influence of geometry, residual stresses, member length and restraint stiffness for the inelastic RDB.

In Chapter 6, the traditional harmonic based finite strip method is augmented by so-called bubble functions in the form of orthogonal Legendre polynomials in order to evaluate their efficiency in calculating the elastic buckling capacities of isolated plates and their assemblies, which may buckle locally, laterally or in a distortional mode.

In Chapter 7 a bubble-augmented elastic spline finite strip method of analysis is developed. The finite strips admits both flexural and membrane buckling deformations. The method allows for consideration of structures with intermediate supports and a variety of conditions that may be prescribed at the ends of a plate or plate assembly. The method is deployed to study parametrically elastic behaviour of plates and plate assemblies.

Chapter 8 then modifies the bubble augmented spline finite strip method to account for inelastic behaviour, so that buckling strengths may be predicted. The numerical studies of this chapter focus on buckling characteristics of single span and two-span composite T-section beams in the inelastic range of structural response.

Finally, Chapter 9 summarises some of the most important conclusions, which have resulted from the work presented in this thesis. Also included in this chapter is an outline of future research, which would extend and augment the numerical studies presented in this thesis by suggesting possible avenues for further research.

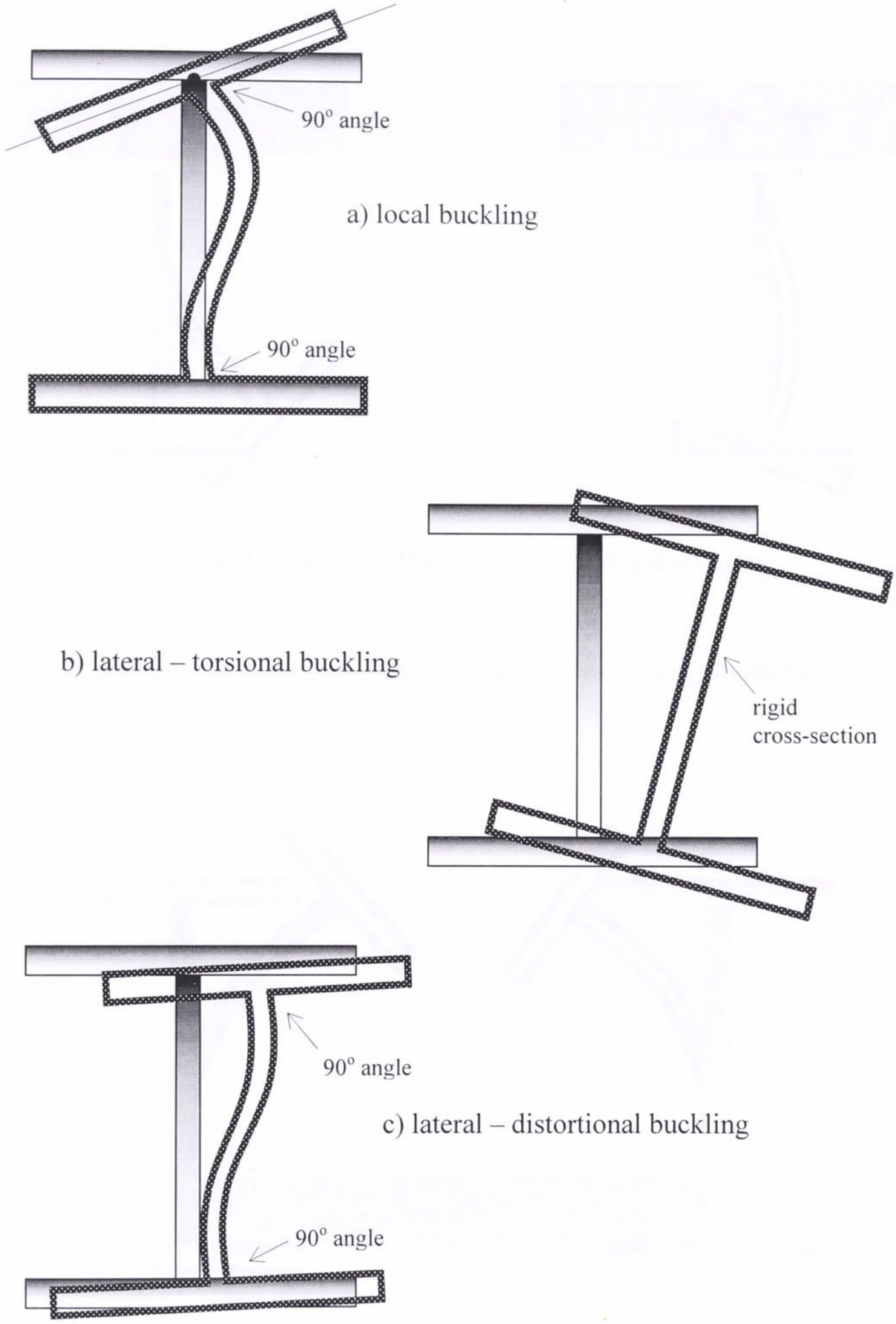

Figure 1.1 Buckling deformations of unrestrained I-section

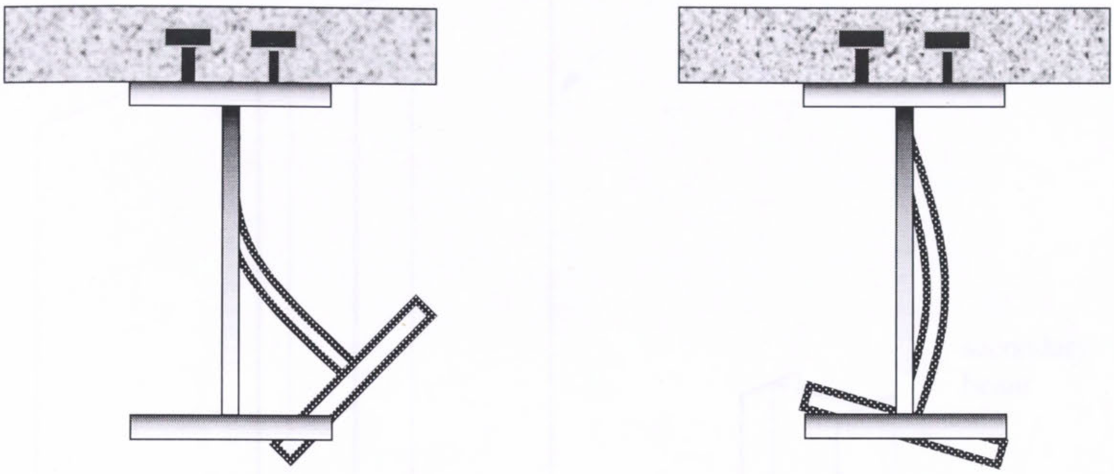

a) restrained distortional buckling (RDB) b) local buckling

Figure 1.2 Buckling deformations of restrained I-section in hogging-moment region

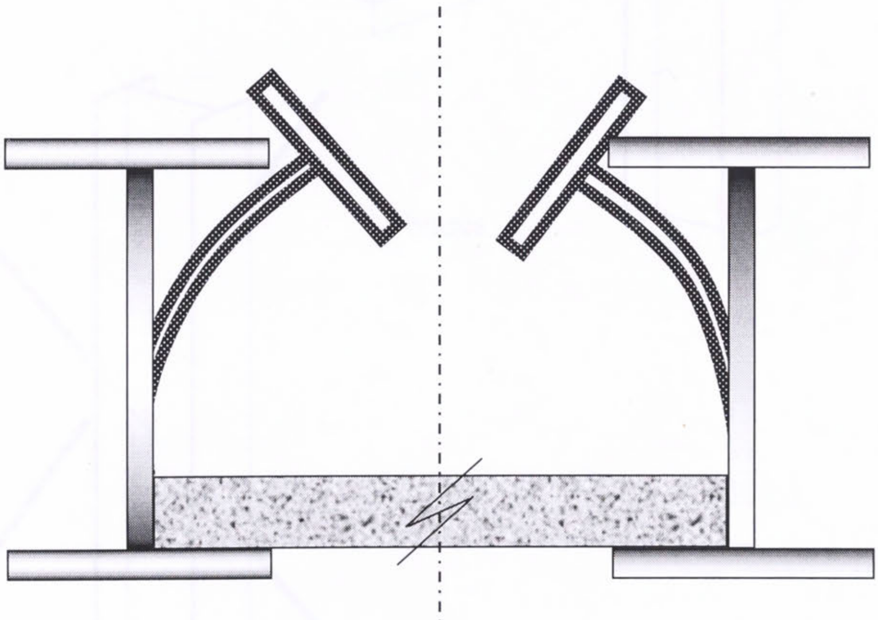

Figure 1.3 Buckling deformations of half-through girder bridge

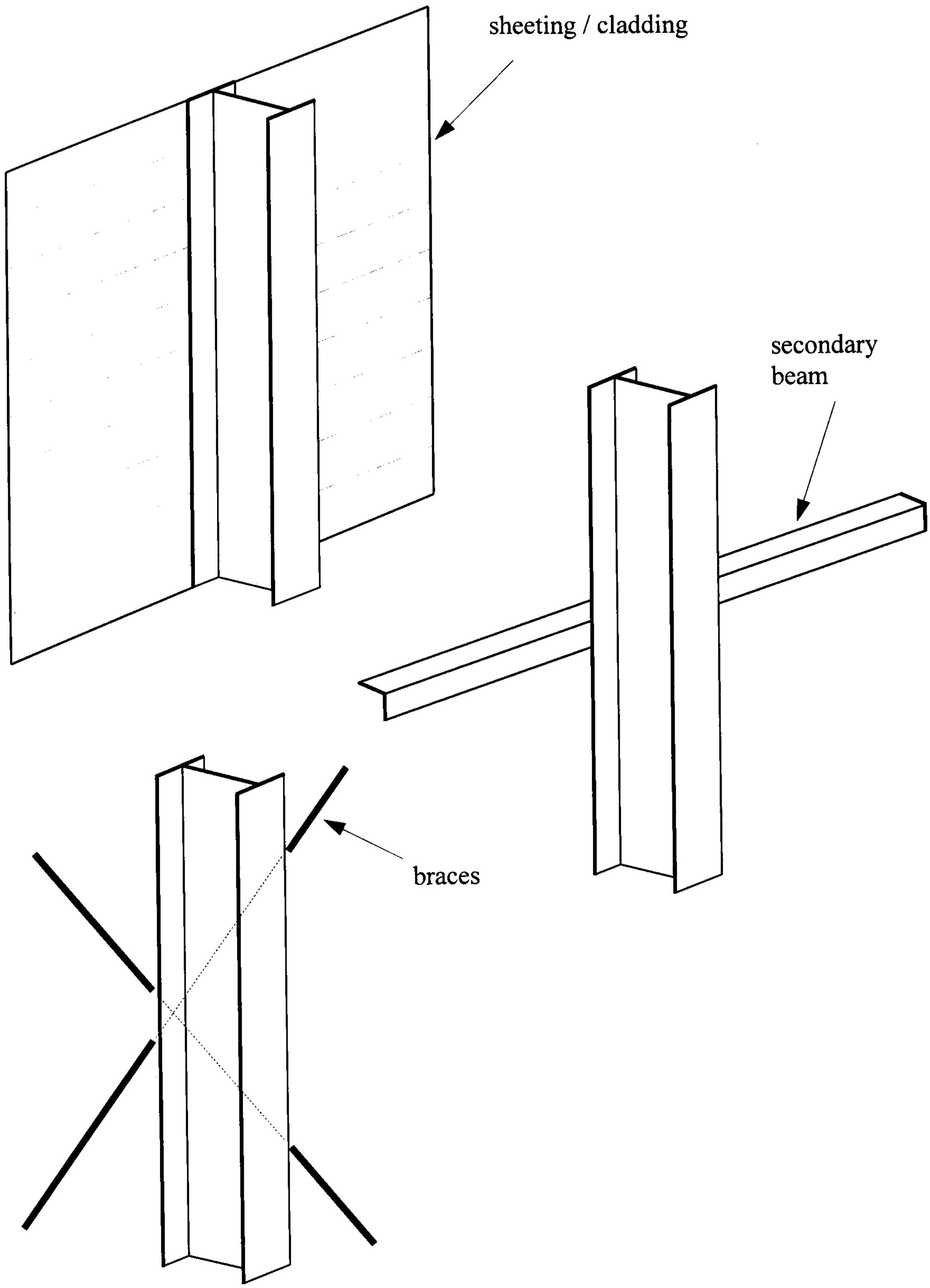

Figure 1.4 Restrained members

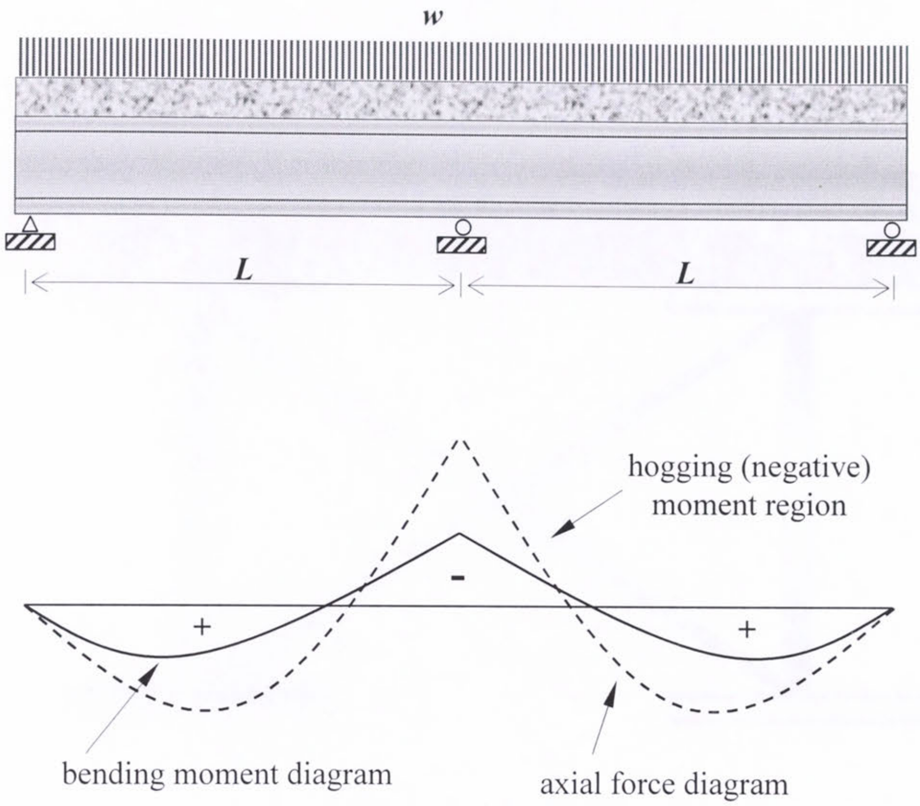

Figure 1.5 Two span continuous composite beam; bending moment and axial force distribution in the steel joist

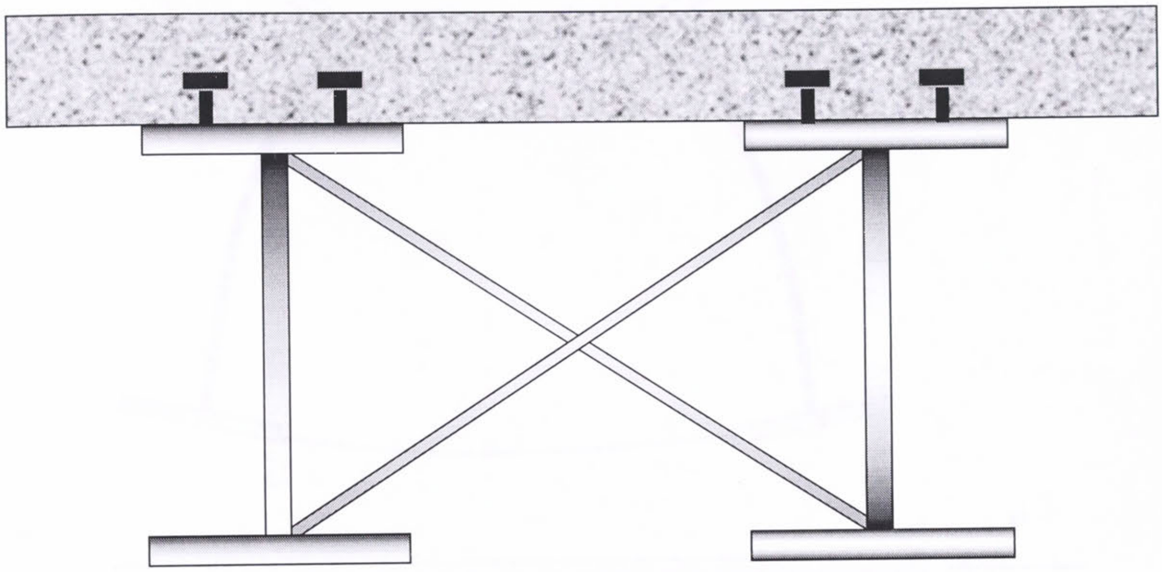

Figure 1.6 Cross-bracing

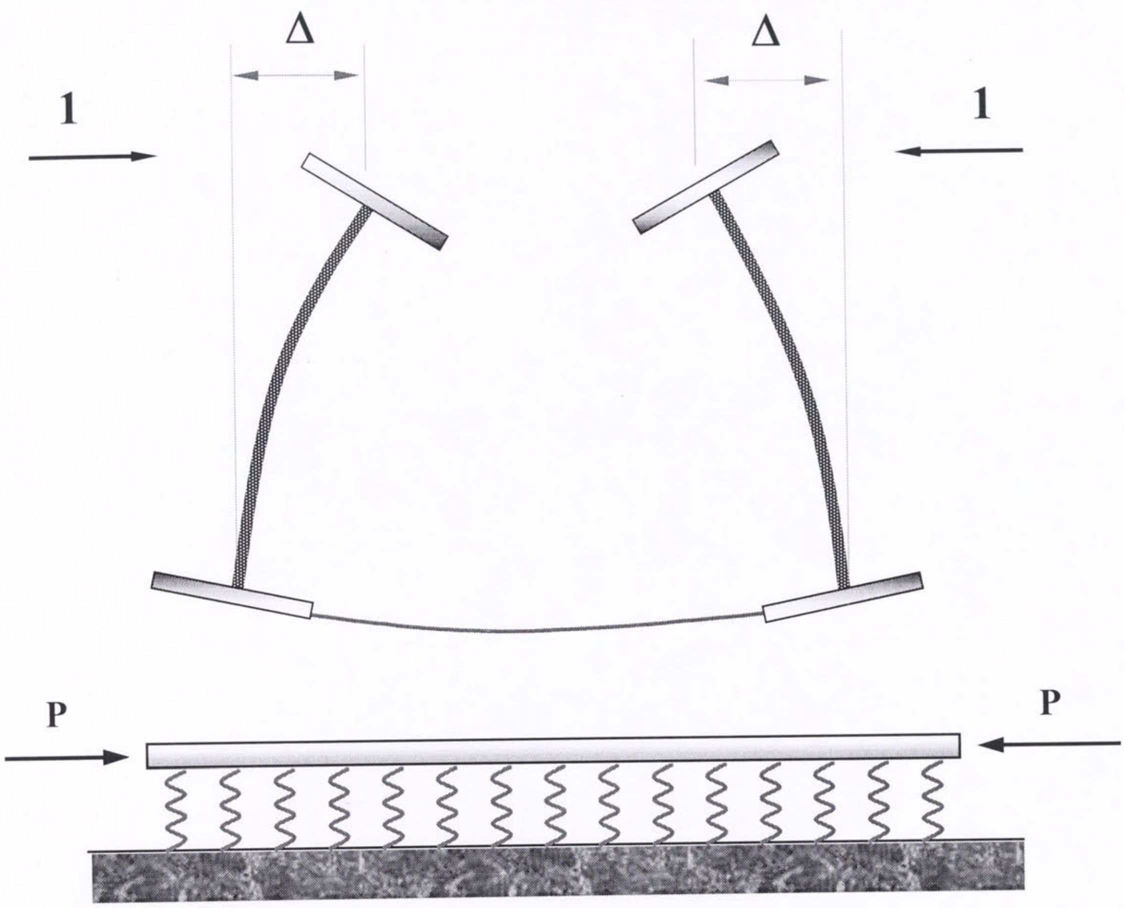

Figure 1.7 U-frame model

Chapter 2

LITERATURE REVIEW

TABLE OF CONTENTS

2.1 INTRODUCTION

In a composite steel-concrete tee-beam subjected to negative or hogging bending and in a simply supported I-section half-through girder bridge, instability of the steel web and compression flange becomes a design problem. The most important modes of failure occurring in continuous composite beams and simply supported half-through girder bridges are local flange, local web and lateral-distortional buckling, and these forms of buckling have been identified as being highly interactive in the hogging moment region of continuous composite beams. If these buckling modes are prevented, large rotational capacities can be achieved beyond the plastic moment of resistance and advantageous plastic design is possible. Consequently, significant economies can be achieved in continuously restrained I-beams that are designed using rigid-plastic principles (Oehlers & Bradford 1999), and the moment redistribution that is possible due to the ductility of such beams is desirable prior to failure.

Whilst cross-sectional proportioning to achieve the necessary moment redistribution in the hogging region has been quantified fairly accurately (Bradford & Kemp 2000), the problem of overall or global member buckling has received much less attention. Although the lateral-distortional buckling of isolated beams has been studied quite extensively (Bradford 1992a; Lee 2001), there appears to have been very little research undertaken on the distortional buckling of continuous beams (Svensson 1985; Johnson & Fan 1991; Bradford & Ge 1997; Lee 2001).

The distortion of the web during buckling could be significant in a variety of problems, and if not considered may lead to erroneous results. Essa and Kennedy (1994, 1995), who investigated a collapsed roof structure in Vancouver, have shown that the reductions of the lateral-torsional buckling load due to web distortion for restrained I-section members are substantial. Because lateral-distortional buckling is basically an interaction mode between lateral-torsional buckling and local buckling (Hancock *et al.* 1980), there are many factors influencing the phenomenon, and the derivation of general solutions is not straightforward even for an unrestrained section. The amount of distortion depends on various parameters such as the degree of flange restraint, torsional stiffness of flanges, web/flange thickness ratio, member slenderness, boundary conditions at the supports and the moment distribution along the beam. Although an approximate closed-formed solution for the case of uniform bending has been derived (Hancock *et al.* 1980), its use is cumbersome and the general lateral-distortional buckling solution for the case of moment gradient and with the incorporation of restraints requires a computer program, which is generally only a research tool, and was unavailable until the last few decades which have seen the development of high-speed digital computers and 'advanced' commercial software packages. Design codes of practice attempt to approximate this behaviour, but when applied particularly to distortional buckling their accuracy is at best questionable.

Thin-walled structures, especially columns and beams, are able to sustain load after local buckling; the determination of their load carrying capacity requires consideration of the interaction of buckling modes and imperfections in the non-linear analysis of stability. Due to inevitable imperfections, the actual buckling behaviour of a beam is different from that of the idealised one. It is well known that under certain conditions of geometry and loading, linear analysis of structures leads to unacceptable and inaccurate results. Thus numerous methods have been developed for nonlinear analysis, which usually permit simultaneous analysis for bifurcative buckling in the form of a linear eigenproblem. However, to ensure safe, reliable structures, accurate deterministic numerical methods for nonlinear analysis (along with probabilistic methods) are needed.

This thesis therefore addresses the issue of restrained-distortional buckling (RDB) in both half-through girder bridges and composite tee-beams with hogging bending regions, and considers the most important buckling modes and their interactions that are typical in such structural systems. This chapter reviews the phenomenon of lateral-torsional and lateral-distortional (unrestrained and restrained) buckling, considering elastic and inelastic behaviour separately. Experimental and theoretical results and design implications are considered. Subsequently, the local buckling phenomenon and recent research into elastic postbuckling behaviour and nonlinear interaction of buckling modes are presented. Azhari (1993) reviewed the literature on the elastic, inelastic and post-local buckling behaviour of plates and plate assemblies extensively prior to 1993, as well as the literature on their methods of analysis. Since an extensive review of local buckling in plates and plate assemblies has already been given by a number of authors (Timoshenko & Gere 1970; Allen & Bulson 1980), the review of work on local buckling behaviour is limited in this chapter primarily to local buckling in restrained I-sections. Finally, the finite strip method of analysis, with main emphasis on spline finite strip method for buckling analysis, is reviewed at the end of this chapter.

2.2 LATERAL-TORSIONAL BUCKLING

This form of buckling is also called flexural-torsional buckling and is significant for slender I-section members whose resistances to lateral bending and torsion are low. The elastic flexural critical load of a centrally loaded prismatic column was first derived by Euler in 1744 (Euler 1759). At this load, buckling occurs in a principal plane without rotation of the cross-section. However, for some thin-walled open sections, such as an I-section, torsional buckling may occur, and indeed does occur for many cross-sections such as cruciform shapes.

The early investigations on lateral-torsional buckling of I-section members date back to the beginning of the last century (Prandtl 1899; Michell 1899; Timoshenko 1910, 1913) when the closed form solutions for beams under equal and opposite end moments were first launched. The work by the Australian engineer Michell (1899) is usually acknowledged to be the foundation study. Timoshenko and Gere (1970) studied the buckling behaviour of transversely loaded I-beams and cantilevers, and reported many previous studies. Lateral-torsional buckling of beams, columns, beam-columns and frames has been a subject of widespread research since the early twentieth century and general design methods have been proposed by Timoshenko (1924), De Vries (1947), Salvadori (1955), Kerensky *et al.* (1956), Clark and Hill (1960), Trahair (1966), Nethercot and Rockey (1971), Nethercot and Trahair (1975, 1976), Cuk (1984), SSRC (1988), Trahair (1993) and Trahair and Bradford (1998). The effects of monosymmetry were addressed by Kitipornchai and Trahair (1980), Kitipornchai *et al.* (1986), Kitipornchai and Wang (1988a, 1988b) and Bradford and Cuk (1988). The first comprehensive studies on tapered I-steel beams appear to be those of Kitipornchai and Trahair (1972, 1975) followed by investigations carried out by Lee *et al.* (1972), Nethercot (1973b), Bradford and Cuk (1988), Bradford (1988c), Bradford (1989a) and Bradford and Ronagh (1997b).

The elastic lateral-torsional buckling of I-sections is well understood and full treatments are given in standard texts (Bleich 1952; Vlasov 1961; Timoshenko & Gere 1970; Allen & Bulson 1980; Trahair & Bradford 1998; Trahair *et al.* 2001), with a highly comprehensive treatment being given by Trahair (1993). Although the studies of elastic lateral-torsional buckling of I-sections appear plentiful, a somewhat more limited amount of research is available on inelastic lateral-torsional buckling of steel I-sections. The main reason for this deficiency is the need for a complex buckling theory that incorporates the effects of monosymmetry in the cross-section and non-uniformity effects along the beam that follow the commencement of yielding.

2.3 UNRESTRAINED LATERAL-DISTORTIONAL BUCKLING

2.3.1 General

The first reported study of distortional buckling appears to be that of Nylander (1943), although it appears the topic had been researched a little earlier. Nylander investigated the effect of web distortion on the lateral buckling of I-beams. Later Okumura (1950) and Naka and Kato (1961) extended these studies into the buckling of I-shaped girders. Scheer (1959) considered the web plate as an assembly of longitudinal strips subjected to pure compression. Suzuki and Okumura (1961) investigated the influence of cross-sectional distortion on the flexural-torsional buckling using a closely related folded plate method of analysis. A more refined folded plate analysis, which accounted for the plate torsion actions in the web, was developed later by Kollbrunner and Hajdin (1968).

Goldberg *et al.* (1964) presented a set of eight coupled first order differential equations for the distortional buckling analysis of members of arbitrary cross-section. The differential equations were formed by coupling the membrane and plate bending equations. Baar (1968) also derived a set of four differential equations connecting the displacements and twists of the flanges of an I-section member. His model could account for the presence of elastic translational restraint of one of the flanges.

Kristek and Studnicka (1975) presented a matrix method for analysing stability problems in thin-walled structures based on their so-called elasticity theory of folded plates. The method covered the distortional buckling of thin-walled members of deformable cross-section. The analytical technique was based on the static solution of folded plates using a harmonic technique. Studies into lateral-distortional buckling based on energy methods were pioneered by Protte (1961), Schmied (1967) and Fischer (1967). Early attempts at applying an accurate analysis appear to be that of Goldberg *et al.* (1964), followed by studies of Rajasekaran and Murray (1973), Bartels and Bos (1973) and Johnson and Will (1974).

Although ground-breaking studies into distortional buckling date back to the 1930's, and this concept was presented in Bleich (1952), studies into this buckling mode have been limited to the last thirty years or so, while many lateral-torsional and local buckling problems were solved earlier this century. The numerical methods used to determine accurately the buckling loads of structures have changed significantly, particularly with the advent of high speed computers.

2.3.2 Elastic Distortional Buckling

Elastic unrestrained distortional buckling is characteristic for intermediate length members with thin webs (Bradford 1992a). Distortional buckling analyses are invariably more complex than either local or lateral buckling analyses alone, since each cross-section of a member is free to both distort and displace. Extensive studies of elastic distortional buckling (Hancock *et al.* 1980; Bradford 1983; Lee 2001) have indicated that distortional buckling will occur at a lower load than elastic lateral buckling for short beams with slender webs, but often the disparity in these buckling loads for unrestrained beams is not great. The majority of the systematic studies available in the published literature on elastic lateral-distortional buckling have only been attempted in the last two decades or so, originating mainly from the work of Australian researchers (Bradford 1992a).

Rajasekaran and Murray (1973) developed a finite element analysis approach of coupled local and lateral buckling for the wide flange beam-columns. Their analysis used one dimensional beam elements for North American flanges and flexural plate elements for the web. A total of eleven degrees of freedom were required at each longitudinal node. Johnson and Will (1974) later developed a three dimensional assemblage of thin plate elements having both membrane and bending stiffnesses, which was a more powerful method than the method of Rajasekaran and Murray. Plate elements were used for the web and flanges, and therefore the cross-section was allowed to distort freely. The procedure was advantageous in that it could simulate complex structures, although its merits were outweighed by computational effort due to considerable number of degrees of freedom and the restricted capabilities of the computers at the time. Akay *et al.* (1977) then refined this rather complex procedure into a two-dimensional analysis taking advantage of symmetry about the mid-surface of the web for the I-sections. Hancock *et al.* (1980) presented an energy method of analysis for distortional buckling, which was amenable to simply-supported doubly symmetric I-beams. Their method made use of a sinusoidal shape function and arrived at a fourth-order eigenproblem. With some simplification, this eigenproblem was reduced to a closed form equation.

Some notable studies of the distortional buckling of beams using the finite strip method belong to Plank (1973), Plank and Wittrick (1974), Hancock (1978, 1980), Sangakkara (1978), Lau and Hancock (1986) and Bradford (1989b). Conventional rectangular finite elements with a plane stress-bending formulation result in an extremely inefficient modelling of the distortional buckling problem. This inefficiency was successfully overcome by Bradford and Trahair (1981), who developed a beam or line-type element that incorporated six nodal degrees of buckling freedom. Cubic polynomials are adopted to model the lateral displacements of the flanges and the web distortion. Using this method, Bradford and Trahair (1983) investigated the stability of beams on seats. Bradford (1985b, 1990a, 1990b) investigated the distortional buckling of monosymmetric I-beams and T-section beams and Bradford (1990c) provided design formulae for beams with partial end restraints. This element was extended subsequently to handle flanges of arbitrary shape by Bradford and Trahair (1982), and this extension was applied to analyse continuous composite bridge girders by Johnson and Bradford (1983). Subsequent analyses using the method were reported, in which presence of elastic restraints (Bradford 1988a) and the inclusion of axial force (Bradford 1990c) were considered. The method, too, provided considerable insight into the distortional buckling phenomenon for composite tee-beams. Bradford and Gao (1992) employed the same beam element in an elastic study, which motivated Williams *et al.* (1993) to investigate the composite beam buckling problem using their transcendental buckling formulation.

Bradford (1990b) investigated the stability of monosymmetric beam-columns with thin webs. Wang *et al.* (1991) presented a parametric study of the elastic distortional buckling of simply supported monosymmetric I-section members under a uniform moment and an axial force. Based on their investigations, a simple empirical buckling formula was proposed for predicting the moment distortion factor for monosymmetric beam-columns having equal flange thicknesses. Van Erp and Menken (1991) studied the buckling behaviour of simply supported T-beams subjected to a central concentrated load. The spline finite strip method was adopted with Koiter's initial post-buckling analysis.

Ronagh and Bradford (1994a) considered the lateral-distortional buckling of tapered doubly symmetric I-section beam-columns. The finite element method used in their study is similar to that used by Bradford and Trahair (1981), but they argued their approach was approximate as the flanges contain in-plane moments (that are akin to a bimoment) but which are not orthogonal to the shear centre. Ronagh and Bradford (1994b) considered the parameters affecting distortional buckling of tapered I-section members and the finite element method developed by the same authors (1994a) was modified to include the effects of off-shear centre loading and was augmented to include elastic restraints. Ronagh and Bradford (1994c) made some observations that are relevant to the finite element method of analysis of lateral buckling from the two previous studies of elastic lateral-distortional buckling tapered beams. They discovered that a boundary term was absent in a very commonly cited formulation, which can produce erroneous results in some cases. Ronagh and Bradford (1996) presented a two-dimensional consistent structural idealisation of the finite element method for linear elastic distortional buckling of tapered I-section members. The flanges were modelled as beam type elements and the web by serendipity plate elements. The effectiveness of the method was demonstrated by considering the distortional buckling of a gable frame. This formulation is not approximate, but may be somewhat inefficient.

Ma and Hughes (1996) developed the energy method to investigate the distortional buckling of monosymmetric I-beams under distributed vertical load. They employed a fifth order polynomial for the web displacement and non-linear elastic theory to attain the external work due to buckling.

Pi and Trahair (1999) investigated the elastic lateral-distortional buckling behaviour of simply supported beams subjected to uniform bending. Their study showed that cross-sectional distortion and unequal twist of the flange decreased the torsional rigidities of the cross-section. A simple approximation for the elastic lateral-distortional buckling of the beam was proposed by replacing the effective torsional and warping rigidities in the flexural-torsional buckling equations.

2.3.3 Inelastic Distortional Buckling

While studies of elastic lateral-distortional buckling of I-sections have received quite a deal of attention in the literature, a very limited amount of research has been reported on inelastic lateral-distortional buckling of steel I-sections. The main reason for this dearth of literature is the complexity added to the buckling theory due to the monosymmetry and non-uniformity in the cross-section and along the member caused by yielding, in addition to the complexities associated with cross-sectional distortion and that of the relevant plasticity theory.

The first rational analysis of inelastic lateral-distortional buckling appears to be that of Bradford (1986a). Bradford (1986a) developed a plate-type element to study the inelastic buckling of hot-rolled beams. A parametric study was undertaken to explore the effect of web distortion on beams subjected to uniform bending and moment gradient. The study demonstrated that the effect of the web distortion on inelastic lateral-torsional buckling was minimal for longer span beams, which are governed by the lateral-torsional buckling.

Bradford (1988b) investigated the inelastic lateral-distortional buckling of welded monosymmetric I-beams under uniform bending. The energy-based method developed for elastic distortional buckling by Bradford and Waters (1988) was modified to incorporate inelasticity and to take account of the effects of monosymmetry caused by the yielding of the cross-section. The 'tendon force model' of the residual stresses, developed by the Cambridge group, was utilised. The flanges were modelled as beam elements, and the minor axis flexural rigidity and torsional rigidity of the flanges as determined as by Trahair and Kitipornchai (1972). A plate theory was used for the web, and isotropic and orthotropic plate theory based on the flow theory of plasticity was deployed for elastic and inelastic regions respectively. The results of Bradford's study demonstrated a similarity between the inelastic lateral-torsional and lateral-distortional buckling loads excluding the case of extremely short beams.

Dekker and Kemp (1998) have shown using a spring model how the elastic warping coefficient, second moment of area in lateral buckling and the Saint Venant torsion constant should be adapted to allow for distortional buckling and inelastic behaviour. The loss in moment resistance caused by cross-sectional distortion was confirmed as being small.

It is worth pointing out that these studies of inelastic buckling are really 'quasi-elastic' since they reduce the cross-section to an effective section whose properties are determined by the extent of yielding using an appropriate constitutive relationship for these regions. The buckling solution then reduces to an eigenproblem, albeit that is generally nonlinear, to define a bifurcation of the equilibrium path. Correct modelling of inelastic buckling would assume a yield surface (such as von Mises' yield criterion) with an associated plasticity rule (such as the flow rule) and hardening. This requires the finite post-buckling deformations to be monitored whereas the studies cited above assume implicitly that these deformations are infinitesimal. It is worth noting too that a number of 'advanced' software packages (ABAQUS 1998) have become available over the past few years. These differ from the specialist numerical treatments of many researchers in structural instability, in that they do not, a priory, address the issue of a generic modelling that identifies the significant parameters in the design space.

2.4 RESTRAINED LATERAL-DISTORTIONAL BUCKLING

2.4.1 General

RDB is fundamentally different to the more commonly studied and familiar lateral-distortional buckling of unrestrained beams, and it can have a profound influence on the buckling behaviour of beams with continuous restraint at the level of the non-critical flange (Bradford 1998a, 1998b; Ronagh & Bradford 1998). Despite RDB being the governing buckling mode for many engineering structures that are commonly designed, such as continuous composite beams and half-through girder bridges, its accurate prediction is still a grey area in structural mechanics. Even for elastic buckling, the problem is complex, and recourse needs to be made to a suitable numerical procedure to handle each individual case.

2.4.2 Elastic Distortional Buckling

The first study of distortional buckling in composite beams appears to be that carried out by Hamada and Longworth (1974) using the finite element method. Hancock (1978) extended his finite strip method to beams subjected to lateral displacements and continuous torsional elastic restraint applied at the level of the tension flange. Hancock (1978), Hancock *et al.* (1980) and Robers and Jhita (1983) showed that during buckling, laterally unsupported hot-rolled I-beams that are restrained laterally and torsionally at the supports only remain almost rigid in cross-section. The situation may be different, however, when a member is fabricated with a slender web, and indeed is substantially different when one of the flanges (the non-critical flange) is restrained against rigid cross-sectional movement. In these cases the member may buckle with the web distorting, where the deflection and twisting are accompanied by a change in the shape of the cross-section due to this distortion.

Bradford (1988a) augmented the energy-based method developed by Bradford and Waters (1988) to include continuous elastic restraints, and investigated the elastic lateral-distortional buckling of monosymmetric I-beams under uniform bending. Bradford and Trahair (1981) considered the effects of different end conditions on the elastic distortional buckling of I-beams under uniform bending using their finite element method with 6 degrees of freedom at each node. The end conditions considered in their study ranged from complete restraint to the bottom flange being restrained against displacement and twist as would occur on a seat support. The effects of web distortion are increased for short and intermediate length beams where end displacement or rotations are allowed. Recently, Pi and Trahair (1999) considered the elastic warping stiffness caused by beam end support conditions and based on their findings, proposed an approximation for the elastic lateral-distortional buckling of beams under uniform bending with end warping restraints. Bradford and Trahair (1983) and Bradford (1989c) studied the lateral-distortional buckling of beams on seat supports using the beam-element method of analysis developed by Bradford and Trahair (1981). Bradford and Trahair (1983) proposed a simple design method for beams under uniform bending with an unrestrained top flange that buckles symmetrically.

Several studies of the distortional buckling of composite beams also appear in the literature. Johnson and Bradford (1983) and Bradford and Johnson (1987) used the model of Bradford and Trahair (1982) to conduct a finite element parametric study of distortional buckling in laterally unstiffened fixed-ended composite bridge girders. Each beam was modelled as an inverted T-section, which consisted of only the web and the bottom flange, with the top flange being fully prevented from lateral and rotational movements. Based on their study, they proposed a design formula against the attainment of distortional buckling, which was based on a modified slenderness parameter related to the web depth to thickness ratio.

The most common model for considering RDB in design, although overconservative, is the so-called U-frame method (Oehlers & Bradford 1995, 1999), in which the top compression flange of the I-section is considered as a strut compressed uniformly along its length by the maximum bending stress that is induced in it, and which is restrained by a continuous Winkler spring whose stiffness is that of the web in the plane of its cross-section acting as a cantilever (Fig. 1.7). This produces a simple closed form solution for the buckling load. A very useful modification of the U-frame model was developed by Svensson (1985), in which account was taken of the variation of the bending stress in the strut model, but which retained the tensionless Winkler concept of restraint by the web. Williams and Jemah (1987) argued that the Winkler model did not account for torsional restraint, and based on numerical studies suggested that the flange-strut should be considered as a tee-section with the flange section as its table, and 15% of the web depth as its stem. This suggestion is empirical, and does not produce exact results for the elastic critical stress in the flange. Svensson (1985) also presented a useful modification of the U-frame model to estimate the elastic distortional buckling stress of composite beams. The method takes into account the variation of the bending stress in the strut model, by treating the unsupported flange as a column on an elastic foundation (tensionless Winkler concept) representing the web. Svensson's method neglected the contribution of the Saint Venant torsion. Later Goltermann and Svensson (1987) modified Svensson's model by allowing for arbitrary continuous rotational restraint of the upper flange, representing its attachment to the concrete slab. They also included the contribution of Saint Venant torsion. Williams *et al.* (1993) further refined this method by making an allowance for different end conditions and cracking of the concrete in the tension region. Design curves were presented for the distortional buckling of a wide range of composite steel-concrete beam sections with the bottom flange having clamped, simply supported, or free boundary conditions for buckling in its own plane.

Bradford (1991) presented charts for the prestressing force required to cause elastic distortional buckling of externally prestressed slender plate girders by using the analytical method developed by him (Bradford 1990c). Bradford and Gao (1992) presented a simple method for analysing fixed-ended composite steel-concrete beams taking into account the difference between its sagging and hogging bending rigidities, due to the concrete cracking in tension. Their composite beam was subjected to a uniformly distributed load and was continuous over an internal support. Using the virtual work theorem, they were able to determine the moments, shears and axial forces that are present in the steel joist. These forces were then used in a distortional buckling analysis to determine the moment at the support, which causes instability of the joist. A comprehensive range of section properties was analysed, and based on the results a design proposal to convert the elastic buckling moments into strengths was given. Williams *et al.* (1993) followed the simple idea of Bradford and Gao (1992) and provided design curves for any combination of clamped, simply-supported and free in-plane end conditions. Their model varied from the method of Bradford and Gao (1992) in that it compared areas under the curvature diagram of the beam, rather than using the virtual work approach.

Ronagh and Bradford (1994a) considered the effects of different end conditions on the distortional buckling of tapered I-beams under uniform bending. The reduction in buckling stress due to the web distortion was emphasized as the degree of the end restraint increased. Ronagh and Bradford (1994b) considered restrained tapered I-section members by augmenting elastic continuous and discrete restraints to the finite element method developed by the same authors (1994a). The amount of distortion increases as the restraint is increased, and the presence of these restraints may increase the unrestrained buckling load. Later Ronagh and Bradford (1996) modified a finite element method of analysis, previously used by the authors to investigate the elastic distortional buckling of doubly symmetric tapered I-section beam-columns, to consider the effects of off-shear centre loading and discrete elastic restraints applied anywhere in the cross-section or along the length of the beam-column.

Bradford (1997a) developed a rational model for predicting the elastic buckling load of thin-walled I-section columns, restrained fully against translation and elastically against twist at one flange and subjected to a uniformly distributed axial force. This study showed that when the assumption of a rigid cross-section is relaxed, the restrained column will buckle in a lateral-distortional buckling mode, in which the web of the column distorts in the plane of its cross-section. In addition, an energy method was employed to develop an equation for the critical load of an elastically restrained flange in the so-called U-frame model (Fig. 1.7). The study has confirmed that the buckling mode with twist restraint is lateral-distortional, with the free flange, restrained only by the stiffness of the web, displacing and twisting and the web distorting in the plane of its cross-section.

Bradford and Ronagh (1997a) concluded that the 12 degree of freedom line element developed by Bradford and Trahair (1981) is not able to predict the distortional buckling of restrained I-section members accurately, and as a result extended the number of degrees of freedom to 16 to investigate the elastic distortional buckling behaviour of restrained I-section beam-columns by considering a half-through girder.

Bradford and Ronagh (1997b) considered the elastic lateral-distortional buckling of composite cantilevers, whose steel portion is tapered, under moment gradient. The finite element method developed by Ronagh and Bradford (1996) was employed in this study. This study illustrated the effects of the web distortion that occurs in the hogging region and the differences between the cantilever representation and the continuous beam were highlighted. This study has shown that the buckling moment of resistance may be improved significantly by using a vertical stiffener in the region where the lateral movement of the bottom flange is greatest.

Bradford (1998b) included continuous elastic restraint and discrete flange and web restraint in the finite element method developed by Bradford and Ronagh (1997a) to study the elastic distortional buckling behaviour of a cantilever subjected to a tip load. The buckling loads obtained for translational restraint applied at the top and bottom flange are not equal to the equivalent minor axis rotational restraint applied at the top and bottom flange, which is in contrast to Trahair's (1979) solution based on Vlasov theoy. There is a discrepancy between his study and AS4100 (1998) for cantilevers subjected to full continuous restraint at the top flange, but with nodal twist restraint applied at the nodes, in that the elastic buckling load of a restrained cantilever was much lower than AS4100 and the prediction of Woolcock *et al.* (1999). The distortional buckling load was increased when translational nodal web restraint was applied at the top flange but little increase was evident when the bottom flange was restrained, and the elastic buckling load was not increased when restraint was applied at the cantilever tip.

Kina and Hanswille (1996) described the basic mechanical models of the design method in Eurocode 4 for lateral tosional buckling and compared the design rules of Eurocode 4 with test data (Johnson & Molenstra 1990; Johnson & Fan 1991). The comparisons of design rules with available test data demonstrated good agreement between both.

Lindner (1998) studied a steel-concrete composite section consisting of a steel I-section beam and a concrete slab seated on the top of the beam. Two different solutions (simplified and more general solution), based on the buckling curves of the Eurocode, were presented to investigate the minimum coefficient of torsional restraint that causes web distortion. Hanswille (2000) described a method to determine the elastic critical moment based on the analogy between the differential equilibrium equations of the compression member on an elastic foundation and the lateral-torsional buckling problem. The method was then compared with Eurocode 4 design guidance and it was found that the method given in Eurocode 4 can lead to unsafe results in the case of members with unequal end moments and for the end spans of continuous beams.

Bradford's (1999) study of T-beams was extended to include a rigid brace on the flange that was assumed to inhibit lateral displacement and twist on the top of the stem. The presence of a brace increased the buckling load substantially for the more stocky webbed tees, but had little effect when the web or stem was slender.

2.4.3 Inelastic Distortional Buckling

For plastic design, it is important to ensure that attainment of a plastic mechanism with its associated redistribution of bending moment will precede inelastic distortional buckling. The transition from elastic to plastic behaviour in a continuous composite beam under increasing load involves redistribution of longitudinal bending moments, to an extent that is greater in a composite beam than in a steel beam. The method reported by Nethercot and Trahair (1976) established a relationship between the plastic moment at which inelastic buckling will occur and the elastic buckling moment, so that this study forms the basis of the lateral buckling strength curves in a number of national steel standards. However, it appears that the relationship between the full plastic moment and the elastic buckling moment at which lateral buckling occurs is different from that at which distortional buckling occurs (Bradford 1989b), especially if the beam has a continuous restraint. The beam or line type element method of analysis, originally developed by Bradford and Trahair (1981), was modified by Bradford (1986a) to account for inelastic buckling by using the flow theory of plasticity with Lay's (1965) shear modulus. It was shown that there was a significant reduction of the elastic distortional buckling load due to the effects of inelasticity when the tension flange was completely restrained. Bradford and Johnson (1987) applied the same method to composite bridge girders and suggested a design rule which was somewhat different to, and an improvement on that published in 1983 by the same authors. Bradford's study in 1989 has reported that the existing design provisions, particularly the Australian AS4100 Steel Standard and British Bridge Code, are conservative for composite beams.

Bradford (1989b, 1990d) further extended the finite element method developed in 1986 to consider the inelastic distortional buckling behaviour of restrained I-section members. Bradford (1989b) considered the inelastic distortional buckling behaviour of I-beams with completely restrained top flanges of a composite girder under moment gradient. Design curves were proposed based on a parametric study carried out by the author. Bradford (1989c) studied the inelastic distortional buckling of hot-rolled beams with seat supports under moment gradient and this was verified experimentally by Bradford and Wee (1994).

An energy-based method developed earlier by Bradford (1988a) was augmented to include continuous elastic restraint to investigate the inelastic distortional buckling of a restrained beam by Bradford (1990a). The inelastic lateral-distortional buckling moments were almost identical for translational and minor axis rotational restraint applied at the level of the tension flange. The buckling of monosymmetric beams subjected to torsional restraint exhibits similar behaviour to that of beams subjected to translational and minor axis rotational restraint, except for long beams which exhibited almost constant distortional buckling moment when highly restrained in a similar fashion to local buckling with a large number of half-wavelengths.

Bradford (1990d) studied the elastic and inelastic buckling of hot-rolled I-beams restrained laterally at the tension flange level by purlins and subjected to unequal end moments. The cross-sectional distortion in the elastic buckling range was very small. The inelastic distortional buckling curves of a restrained beam were different from those of the inelastic lateral-torsional buckling curves of unrestrained beams. A design method was proposed to calculate the buckling strength of portal frames, and which was conservative to allow for the effects of geometric imperfection that were not included in the buckling study.

Johnson and Fan (1991) compared the distortional buckling capacities in two Class 2 U-frame tests in negative bending with the theoretical approaches of Bradford and Johnson (1987), Weston *et al.* (1991) and the Eurocode (1981). This comparison showed that the Eurocode method is the most versatile of the four methods. In all these tests a complex interaction between local and distortional buckling that takes place at or near the maximum load was observed.

Weston *et al.* (1991) presented an inelastic distortional buckling method for composite beams in which they used a nonlinear non-bifurcative finite element method for plastic analysis developed elsewhere. These results were considered to be accurate, although computationally very inefficient. In 1997, Gioncu and Peteu deployed a major extension of Climenhaga and Johnson's (1972) yield line approach, which includes both local and distortional buckling and the assessment of available rotation capacity.

Essa and Kennedy (1994, 1995) investigated the cause of the collapse of part of the roof structure of a newly constructed supermarket in Vancouver, Canada using the finite element method. This work presented a simple design procedure for a cantilever-suspended span subjected to a multiplicity of loading and restraint conditions based on the distortional buckling model. The design method accounts for the effects of lateral and torsional restraints provided to the beam open-web steel joist it supports. The beam stability was enhanced by the torsional restraint.

Dekker *et al.* (1995) investigated the factors influencing the strength of composite beams in negative bending and developed a theoretical model by introducing an equivalent spring system to account for the effect of the web distortion. They concluded that for the case of inelastic buckling, the flexural resistance of the steel beam is determined by lateral-distortional buckling, while for the case of plastic buckling the flexural resistance is controlled by a combination of local flange/web and lateral-distortional buckling. Kemp *et al.* (1995) studied two-span continuous beams subjected to uniformly distributed loads. The required inelastic rotation capacity of the composite beam prior to strain weakening is larger than that of equivalent steel I-sections. This results from the negative moment region being short and the elastic rotation of the composite beam being small.

Bradford and Ronagh's (1997b) study into tapered composite beams has demonstrated that the buckling moment may be enhanced significantly by using a vertical stiffener in the region where the lateral movement of the bottom flange is greatest, and the stiffener is most effective when placed at the point corresponding to the largest lateral movement in the eigenmode.

Bradford (1998a) extended the energy method (Bradford 1988b) to study the inelastic distortional buckling of welded columns fully restrained against translation and with elastic twist restraint at the level of one flange. The numerical results were compared with the U-frame model often used in bridge design and it was again demonstrated that the U-frame model is conservative.

Recently, Bradford (2000) investigated the inelastic distortional buckling behaviour of compact beams subjected to moment gradient and which were partially restrained. This study demonstrated that the prediction of lateral buckling strength using conventional or Vlasov theory might overestimate the buckling strength, overly so in many cases.

2.4.4 Experimental Investigations

Experimental studies of distortional buckling of composite beams are very rare and elastic distortional buckling experiments on I-section beams have received very little treatment (Woods & Watson 1977) in comparison to other section profiles (Zhao *et al.* 1995).

Bartels and Bos (1973) performed some tests to investigate the effect of boundary conditions on the buckling of both simply-supported and continuous beams. Their tests were performed in two series. The first comprised three tests on 1:5 scale model beams of an IPE 270 (Dutch) section, and the second comprised eight tests on 1:10 scale models of an IPE 600 section. The loading consisted of several equally spaced loads applied to the top flange. The support conditions were: (i) 'forked bearings', in which lateral deflections and twists of both flanges were prevented: (ii) 'semi-forked bearings', in which lateral deflections of both flanges as well as twisting of bottom flange were prevented: and (ii) 'bottom flange restraint', in which only the bottom flange was laterally and torsionally restrained. The experimental studies were compared with theoretical results and it was found that they were in good agreement.

Hamada and Longworth (1974) tested a series of composite beams of 8-ft span under a concentrated load at midspan. The beams were tested "upside down" to create the conditions of negative bending. Hamada and Longworth (1974) reported that the buckling configuration for a composite beam in negative bending indicated that only the inverted T-section needs to be considered in a lateral buckling analysis. They concluded that the ratio of the lateral buckling moment to the simple plastic moment decreases significantly with increase in the span length and is slightly affected by the amount of longitudinal slab reinforcement and the size of the cover plate on the compression flange.

Johnson and Fan (1991) conducted an experimental study on lateral-distortional buckling of continuous composite beams. They tested at realistic scale composite T-sections and inverted U sections of double-cantilever with unstiffened webs. The results showed that interaction between local and lateral-distortional buckling governs the ultimate strength of the test specimens and is strongly influenced by initial imperfections. It was concluded that local buckling initiated lateral buckling and buckling did not begin until the bottom flange was fully yielded adjacent to the central support. Johnson and Chen (1993) conducted an experiment on continuous composite beams by considering a centrally supported pair of double-cantilever plate girders. The configuration of the experiment can be interpreted as inverted U sections. The slender cross-section of the composite beams had either stiffened or unstiffened web. The results were similar to those of Johnson and Fan (1991).

Albert *et al.* (1992) conducted an experimental study consisting of 33 full-scale tests to investigate the stability of steel beams in cantilever-span structures. The number of beam specimens comprised of seven W360x39 and four W310x39 sections. The experiments were conducted with the three different top flange restraint conditions of no restraint, lateral restraint only and lateral and torsional restraint, while the restraint conditions at the column were lateral and torsional restraint at the bottom flange. The results of this experimental study demonstrated that a beam subjected to torsional restraint buckles in lateral-distortional mode.

Bradford and Wee (1994) reported experimental tests on eight light full-scale hot-rolled universal beams (180UB18.1) supported on seats. The length of three beam specimens was 2770 mm and they were placed under a central concentrated load. Another three beam specimens were subjected to a third point loading with the same length as the previous specimens. Finally, two beam specimens were 1500 mm long and were placed under a central concentrated load. The experimental results were compared with the finite element method of analysis that incorporates distortional buckling developed by Bradford (1986a) and overall, the computer solutions agreed well with the test results.

Kemp *et al.* (1995) studied the difference in behaviour between steel and composite beams experimentally by testing steel I-sections of the same size.

2.5 LOCAL BUCKLING

2.5.1 General

Local buckling is a major cause of failure in thin steel plates and in plate assemblies. Local buckling of thin plate assemblies is characterized by localized distortions of the cross-section of the member, with the line junctions between intersecting plates remaining straight. This differs from lateral buckling where buckling is of an overall mode and the cross-section does not distort, and from distortional buckling where local and overall buckles interact.

The thin plate analysis is based on the use of classical plate theory. It is recognised widely (Allen & Bulson 1980; Timoshenko & Gere 1970; Azahri 1993) that exact analytical solutions for buckling loads are possible only for rectangular plates under certain boundary and loading conditions. For the instability analysis of plates of arbitrary shape, numerical methods such as the finite difference method, finite element method or finite strip method are usually applied to the problem, while some non-discretisation techniques such as the Galerkin method are being revisited (Saddatpour *et al.* 1998; Azhari *et al.* 2004). Elastic local buckling experiments on plates with various boundary and loading conditions have been reported extensively in the literature (Donald 1990), and have formed a means of validating a number of theoretical studies. In some cases, it is also necessary to understand the ensuing behaviour after buckling. Thus, the determination of the critical load and the clarification of the postbuckling behaviour under various loads are some of the most important problems for the development of lightweight structures, particularly with aerospace applications.

2.5.2 Local Buckling in Continuous Composite Beams

Continuous composite beams can only be designed by simple plastic theory if the hinges at the supports have adequate rotation capacity. This is often controlled by local buckling of the webs and flanges. The adverse effect that local buckling has on the rotation capacity of steel I-beams is well known. In design by plastic theory, limits are placed on the slenderness ratios of the flanges and webs of members required to participate in a collapse mechanism.

One of the first studies into local buckling in composite beams appears to be that of Climenhaga and Johnson (1972) who studied both elastic and inelastic local buckling when the slab restrained the top flange of the steel I-section. The underlying assumption in this yield line analysis of local buckling is that longitudinal line junctions between intersecting plates remain straight, and this occurs at short wavelengths. These line junctions move sideways with longer length distortional buckling, which was only considered subsequently to this study. The same study has shown that apart from the restraint of the top flange, the main parameters that affect local buckling are the width to thickness ratio of the web and free flange outstand.

Research on local flange buckling of steel beams has resulted in the establishment of flange proportions that guarantee that local flange buckling does not occur prior to the onset of strain hardening (Hamada & Longworth 1974). While the local buckling characteristics of composite steel-concrete and plain steel beams are similar, it is still not apparent that the design rules that exist for plain steel beams are appropriate for continuous composite beams.

Dawe and Kulak (1984a) considered a pseudo-strip method for handling inelastic local buckling, and compared the solutions with tests on North American WF sections in the inelastic range of structural response. Bradford (1986b) independently developed an inelastic finite strip method of analysis based on the flow theory of plasticity. Bradford and Johnson (1987) employed the same method to study inelastic local buckling of composite beams. Because of the limiting assumptions of the harmonic-based semi-analytical method, the solution was approximate. The inelastic finite strip method, originally developed by Bradford (1986b), was also employed to calibrate the width to thickness limits in the British BS5950 Steel Standard (1990).

Bradford (1986b) developed a finite strip method of analysis to study the local buckling behaviour of composite beams in negative bending. Inelastic material behaviour and residual stresses were included in the analysis. The method was in a good agreement with independent test results on hot-rolled composite beams, reported by Ansourian (1981, 1982).

It was shown that the development of longitudinal stiffeners improves significantly the buckling capacity of the web in bending. Based on the position of the neutral axis, the optimum position of the longitudinal stiffener varies between 0.255 and 0.375 times the depth of the web above the bottom flange (Azhari & Bradford 1993).

Aribert (1994) showed that for continuous composite beams subjected to increasing loads up to collapse, a very large extent of bending moment redistribution may appear in spite of the occurrence of local buckling with a possible interaction of global buckling of a web panel in shear.

From the experimental studies carried out by Dekker *et al.* (1995), Johnson and Fan (1991), Hamada and Longworth (1974), Climenhaga and Johnson (1972) and Johnson *et al.* (1967) it is evident that interactive lateral-distortional and local buckling results in lower rotation capacity than local flange and/or local web buckling. These studies further indicate that large areas of longitudinal reinforcement relative to the area of the steel section produce lower rotation capacities due to the larger web depth in compression and the reduced curvature at which the critical strain occurs in the flange. In addition, the studies have reported that web stiffeners can improve local buckling behaviour.

The technique of stiffening a plate by stiffeners is rather common as it gives higher values of strength to weight ratio of the structure. This makes the structure economically more attractive in practice, in spite of fabrication costs. Srinivasan and Ramachandran (1977) considered linear and nonlinear analysis of stiffened plates. Carlsen (1980) presented a parametric study of collapse of stiffened plates in compression. Bedair and Sherburne (1995) investigated the influence of the geometric interaction on the local stability of stiffened plates and the influence of the plate/stiffener geometric proportion on the overall stability of stiffened plates under uniform compression. Bedair (1997a, 1997b) studied the influence of stiffener location on the stability of stiffened plates under compression and in-plane bending and presented an approach for optimum location of the stiffener. Gronding *et al.* (1999) considered the stability of plates stiffened with tee-shape stiffeners using a finite element method. The model developed by the authors was verified using the results of tests on full-size stiffened plate specimens and was subsequently used to perform the study of various parameters. Koko and Olson (1991) performed a nonlinear analyis of stiffened plates using superelements. Investigations on the behaviour of stiffened plates have been carried out for a long time (Satsangi & Mukhopadhyay 1989), but most of these works are confined to linear analysis only.

2.5.3 Nonlinear Buckling

The nonlinear interaction mode takes place when the lateral buckle at a long wavelength interacts with local buckling at a short wavelength. The phenomenon of nonlinear buckling has over last few decades inspired a large amount of attention in the literature. This is largely due to the fact that the post-critical behaviour of structural members is strongly influenced by the occurrence of simultaneous or nearly simultaneous buckling modes. In fact, in such situations, structures are highly susceptible to initial imperfections and exhibit limit loads that are often well below the bifurcation load.

Nonlinear analysis of thin-walled structures is an important tool to investigate their post-buckling behaviour and ultimate strength. Thin-walled sections may buckle in a local, a distortional or an overall mode before yielding (Hancock 1978; Desmond *et al.* 1981; Sridharan 1982). However, these modes usually have a post-buckling strength reserve depending on the buckling mode. For example, in the post-locally buckled domain, the buckled form of the plates is stable owing to the membrane actions. Because of this, plate assemblies usually have a significant reserve of strength prior to collapse, which is instigated by plasticity. For such thin-walled structures, the evaluation of the post-local buckling response is of great interest and significant weight savings can be achieved by considering the postbuckling behaviour of plate structures. This fact influences the design of advanced technology structures for which it is permitted to use allowable design loads greater than their critical buckling loads.

A rapid growth of theoretical studies began in the 1970s. This problem was first studied by Koiter (1976) and subsequently investigated by numerous authors for thin-walled members by using numerical analysis based on the finite strip method.

The interaction behaviour of thin-walled structural elements loaded in compression has received a great deal of attention. The first detailed investigations of the interaction between global and local buckling of a column are due to Graves-Smith (1968) and Van der Neut (1969). Van der Neut created a simple mechanical model of a column, whose two plate flanges were capable of independent local buckling. This model exhibited a rather strong interaction with overall buckling, resulting in a marked sensitivity to imperfections. Graves-Smith (1968) studied a square tube and the interaction appeared to be of minor importance. Several other authors, notably Koiter and Kuiken (1971), Tvergaard (1973), Pignataro *et al.* (1985), Sridharan (1983) and Hancock (1984) contributed to the further study of compressed members.

Research into interaction buckling of members loaded in bending and/or shear has so far received little attention. Cherry (1960) presented a simple analytical model and test results for beams in uniform bending, whose compression flanges had prematurely buckled locally. Similar studies were made by Reis and Roorda (1977), Wang *et al.* (1977) and Bradford and Hancock (1984).

There are basically two strategies for studying interaction buckling:

(i) The stiffness of the locally buckled member is calculated first, and then this stiffness is used to evaluate the overall buckling;

(ii) The analysis of the interaction is performed on the basis of the general Koiter theory (Koiter 1945).

The studies of interaction buckling under bending by Cherry, Reis and Roorda, Wang *et al.* and Bradford and Hancock, belong to the first category. In all these cases the concept of the effective width was used to account for the postbuckling stiffness of the locally buckled plate component. Koiter (1969), Tvergaard (1973), Sridharan (1983) Benito (1983) and Pignataro *et al.* (1985) used the second approach.

Usami (1982) considered the postbuckling behaviour of plates in compression and bending. Bradford and Hancock (1984) employed finite strip method to investigate the elastic interaction of local and lateral buckling in beams, while Bradford (1985a) studied the postubuckling of box-section beams. Using the finite strip method, the postbuckling behaviour of I-beams in uniform bending was studied by Hancock (1985). Bradford (1989d) employed the finite strip method to study the postbuckling of longitudinally stiffened plates in bending and compression. Galkiewicz (1990) studied post-buckling behaviour and load carrying capacity of thin-walled plate girders. Van Erp and Menken (1991) studied the initial postbuckling behaviour of thin-walled beams loaded by a concentrated force using spline finite strip method.

The tests by Kwon and Hancock (1993) have shown that a significant postbuckling reserve of strength exists beyond the elastic distortional buckling stress in a similar manner to that which normally occurs for local buckling. The post-buckling reserve can be considered in the design of thin-walled sections to improve the design strength. Kwon and Hancock (1993) presented a nonlinear elastic spline finite strip method for predicting the post-local buckling behaviour of thin-walled sections to study the influence of the interaction between local and distortional buckling modes for channel columns. Their results are particularly important for very thin-walled cold formed members. Guo and Lindner (1993) developed a material and geometric nonlinear spline finite strip method to carry out a theoretical study on the elastic-plastic interaction buckling of imperfect longitudinally stiffened panels under axial loads. Ronagh *et al.* (1997) described a formulation for linear, nonlinear, buckling and postbuckling analysis of tapered symmetric beam-columns. Recently, Pi and Bradford (2001) considered elastic lateral-torsional buckling and postbuckling of arches subjected to a central concentrated load.

2.6 SPLINE FINITE STRIP APPROACH

2.6.1 General

The well-known finite element method is regarded as the most powerful and versatile numerical tool for complex structural and other problems. Theoretically, the finite element method can be applied to the analysis of most structures. However, in practice its application is even today very often limited because of high expense in terms of computer time, particularly where fine discretization of the problem is required or where the problem is nonlinear. In addition, it is not always clear what parameters affect the solution in a more generic fashion.

The earliest general stiffness method for stability problems to be programmed employed finite elements. This method of analysis was used by Kapur and Hartz (1966), Gallagher *et al.* (1967), Navaranta *et al.* (1968), Gallagher and Yang (1969) and many others to analyse local buckling of structural sections under uniform compression. The finite element method is computationally inefficient, and has not been applied notably to the analysis of buckling modes and their interactions for plates and plate assemblies. In view of this, and also of the fact that the topology of many types of commonly used structures is quite regular, a simple and economical approach, known as the finite strip method, was successfully developed some thirty years ago (Wittrick & Williams 1974; Cheung 1976). In many cases this now well-known method provides a significant reduction of the degrees of freedom of a strip as only one set of cross-sectional degrees of freedom are required. The method essentially transforms a three-dimensional problem to a two dimensional one.

2.6.2 Finite Strip Method of Analysis

There are a number of different types of the finite strip method and these are distinguishable principally by the type of displacement functions used to describe longitudinal variation of displacements. The 'exact' finite strip method has its origin in work presented by Wittrick and his colleagues (1968, 1971 & 1973). The main advantage of this method is that it is not necessary to subdivide the component plates into finite strips and the buckling stresses can be calculated at any wavelength. However, this method does have some disadvantages in solving the ordinary differential equations, especially when the longitudinal stress varies across the width of the plate and this method has been deployed only on rare occasions since 1970 (Bradford 1992a).

The conventional finite strip method (hereafter called the semi-analytical finite strip method), in which plates and plate assemblies are discretized into longitudinal strips, is an alternative and attractive method of numerical analysis. This method differs from the finite element method in that the displacements are represented by Fourier terms in the longitudinal direction, which satisfy the end conditions of a strip a priori, and by simple polynomial functions in the transverse direction (Cheung 1976). By using polynomial interpolating functions, the differential equations that are produced by the 'exact' finite strip method do not need to be solved, so that in this sense the semi-analytical method is a classical stiffness type finite element method as presented by Zienkiewicz and Taylor (2000).

The advantage of this method is that the coefficients in the overall stiffness matrix are linear functions of the load factors and that the matrix is often highly banded, and standard eigenvalue routines can be used to extract the critical or buckling load factors λ. Nevertheless, the semi-analytical finite strip experiences difficulties in dealing with concentrated forces, multiple spans, discrete supports at strip ends etc. In the semi-analytical form presented by Przemieniecki (1973), Cheung (1976), Hancock (1978) and others, the method is unable to model supports other than simple, nor loading which varies in the longitudinal direction, since the longitudinal variation of buckling displacements is represented by single sine curves. The latter restriction was overcome by Plank and Wittrick (1974), who utilised complex arithmetic to impose phase change between the sinusoidal varying displacements to handle shear in long plates, in a similar way to the handling of capacitance and inductance in electrical engineering (Bradford & Kemp 2000). Azhari and Bradford (1993) modified Plank and Wittrick's analysis, and undertook an elastic buckling study of a composite beam that included a longitudinal stiffener, which Climenhaga and Johnson (1972) found delayed significantly the onset of local buckling. This implies that the method, when shear is present, is only applicable if the overall length of the structure is significantly greater than the half-wavelength of the mode. Their plates, though, were assumed to have infinite length.

2.6.3 Spline Finite Strip Method

To overcome these difficulties and to retain the advantages of the finite strip method, a mathematical tool called a 'spline' function has been used as displacement functions to form spline finite strips. A spline was originally the name of a small flexible wooden strip used by draughtsmen as a tool for drawing a continuous smooth curve segment by segment and became a mathematical tool only after the work of Schoenberg (1946). It was further developed by Ahlberg *et al.* (1967), Greville (1969), Schultz (1973), Birkhoff (1965) and de Boor (1978) and others, but unfortunately has attracted little attention from engineering analysts as highlighted by Prenter (1975).

The last two decades have seen a re-emergence of the use of spline functions as tools for research in numerical structural analysis for a wide range of engineering problems. Polynomials are historically the most popular tools of approximation, since they are easy to implement in numerical schemes. Spline functions, which are piecewise polynomials, are very convenient for interpolation and approximation. This is especially true of the practically important and often used family of *B*-splines, which have variation-diminishing properties.

The most notable stiffness approach using spline functions is the spline finite strip method developed by Cheung *et al.* (1982). In this method, the longitudinal trigonometric series functions, used previously in the semi-analytical finite strip method, were replaced by cubic B_3-spline functions.

The use of spline functions has enjoyed continuous development chronologically, and they have been applied to the solution of a broad range of linear and nonlinear engineering problems. For example, Fan and Cheung (1983a, 1983b) studied right box girder bridges and shallow shell structures by applying the spline finite strip method of analysis. Lau and Hancock (1986) utilised spline functions to depict the longitudinal variation of buckling displacements. This method was an extension of the stiffness analysis of Fan and Cheung (1983a). Rong (1983) reported an application of uniform *B*-splines to approximate the variables in plate bending analysis. Liu and Zheng (1987) and Wang *et al.* (1994) employed the same concept for foundation plates and rotating discs of variable thickness respectively. Shen and Wang (1987a, 1987b) studied the static and vibration responses of flat shells using B_3 and B_5 spline functions and beam functions, while Zhu and Cheung (1996) utilised the spline finite strip method to conduct a postbuckling analysis of shells. Van Erp and Menken (1990) also employed this method of analysis to study the buckling of prismatic thin-walled structural members under arbitrary loading, and Tham and Szeto (1990) applied the B_3-spline finite strip method to the buckling analysis of arbitrarily shaped plates. A numerical method, that combines Koiter's (1976) initial postbuckling theory with the spline finite strip method to carry out the initial postbuckling analysis of folded plate structures, was presented by Van Erp and Menken (1991). The postbuckling behaviour of circular cylindrical shells of finite length, under the combined action of external pressure and axial compression, was studied by Zhu and Cheung (1996) using the spline finite strip method of analysis. By utilising the same method, Guo and Lindner (1993) presented a theoretical study of the elastic-plastic interaction buckling of imperfect longitudinally stiffened panels under axial loads. A material and geometric nonlinear spline finite strip method was developed in this study to analyse such interaction problems, with initial geometric imperfections and residual stresses due to welding being included in the analysis. Kwon and Hancock (1993) also presented a method for predicting the postbuckling behaviour of thin-walled sections based on spline finite strip method of analysis. Wang and Dawe (1999) employed the spline finite strip method for the prediction of the geometrically non-linear response of rectangular, composite shear-deformable rectangular laminated plates to progressive in-plane loading.

Nevertheless, the spline finite strip method requires many more degrees of freedom than the conventionally harmonic-based finite strip method, and this has detracted from its popularity. However, Azhari *et al.* (2000) have included so-called bubble functions, which represent nodeless but additional strip degrees of freedom in the form of higher order orthogonal polynomials, into the expressions for the transverse buckling displacements, and have demonstrated great computational savings in this configuration of spline finite strip method.

Lawther (1990) and Stefani and Lawther (1990) also showed that using bubble functions in the buckling analysis of framed structures produced very good accuracy for a coarse mesh subdivision. In their study, they employed two types of symmetric and antisymmetric bubble functions in order to investigate frame stability. Studies by Szabo and Babuska (1991) and by Kasagi and Sridharan (1992) have also demonstrated the power of bubble functions in dealing with stability problems.

Bradford and Azhari (1993) included bubble functions into the expressions for the transverse buckling displacements and have demonstrated great computational saving in this augmentation of the finite strip method based on complex arithmetic. Hitherto, these serendipity type bubble strips have only been used for buckling modes that involve plate flexure such as local buckling.

Bradford and Azhari (1995) used a finite strip method of analysis using complex arithmetic that incorporated inelasticity, augmented by bubble functions. The analytical procedure was then used to study the inelastic local buckling of plates in compression and shear, stiffened plates in compression and I-section beams in shear. It was shown that by implementing bubble functions in the inelastic complex finite strip analysis, it is possible to obtain results that are very close to the exact solution by subdividing the plates into only one or two strips, which is a significant saving of computational time and storage. The method was also used by Azhari and Bradford (1995) for the nonlinear (postbuckling) analysis of plate structures, and they again demonstrated computational savings by a coarser discretization and more rapid convergence of the nonlinear tangent stiffness equations.

Della Croce and Scapolla (2000) included the bubble function concept into a hierarchic finite element method for thin and thick plates analysis, and showed that the cost of the increase of the number of degrees of freedom is negligible compared with the improvement of the result with coarser discretization. All these studies have illustrated the power of the bubble function based method for studying the elastic and inelastic bifurcative stability of plates and plate assemblies.

All these studies have illustrated the power of the bubble function based method for studying the elastic and inelastic stability of plates and plate assemblies. As mentioned earlier, the work by Azhari *et al.* (2000) appear to be the first such study to augment the bubble functions to the spline finite strip method. It is worthwhile noting that this study deals with plain and stiffened plates only, and does not consider plate assemblies such as I-sections and the like.

2.7 SUMMARY

This chapter has presented a literature review on theoretical and experimental studies related to lateral-torsional, lateral-distortional (unrestrained and restrained), local and interactive local and distortional buckling in the negative bending moment region in continuous composite beams and simply supported half-through bridge girders. The development of theoretical modelling and numerical studies of lateral-distortional buckling of I-sections has also been reviewed with major emphasis on the spline finite strip method of analysis.

Although buckling of plain steel beams in both the elastic and inelastic ranges of response has been studied extensively, and is now considered to be fairly well understood and quantified, buckling in continuously restrained beams is much less researched and understood. Further directions in research and its interpretation have been noted to illustrate the necessity for additional research to obtain a global method for modelling the behaviour that will lead to accurate and uniform design rules. This thesis addresses this deficiency by presenting a detailed study of lateral-distortional and local buckling, and their interactive nature for restrained I-section beams in elastic and inelastic range of structural response.

TABLE OF CONTENTS

3.1 INTRODUCTION

This chapter investigates the elastic restrained-distortional buckling (RDB) of two-span continuous composite steel-concrete tee-beams. In a composite tee-beam subjected to negative or hogging bending, instability of the steel web and compression flange becomes a design problem. Because of the rigidity provided by the concrete slab, although cracked, and because of the significant flexibility of the thin web, the overall buckling mode is not of a lateral-torsional type, but rather it is lateral-distortional (Johnson & Bradford 1983; Bradford & Johnson 1987), as illustrated in Fig. 3.1. Significant economies can be achieved in composite beams with compact joists that are designed using rigid-plastic principles (Oehlers & Bradford 1995, 1999), and while cross-sectional proportioning to achieve the necessary moment redistribution in the hogging region has been quantified fairly accurately (Bradford & Kemp 2000), the problem of overall member buckling has still to be addressed properly. Plastic design of continuous composite beams is advantageous, but this can only be achieved if buckling is prevented.

Whilst the distortional buckling of isolated beams has been studied quite extensively, there appears to have been somewhat less research undertaken and reported on the distortional buckling of continuous composite beams. Only a few experimental results are available for composite beams in hogging bending where all the parameters are documented in the test reports. Johnson and Fan (1990) reported four tests on rolled steel sections. Additional tests were carried out by ARBED Recherches (Schaumann 1991). In general, the buckling resistance of a continuous beam is affected by the interaction between adjacent segments of the beam. The interaction, and hence the buckling load, depend on such aspects as the loading pattern, restraint conditions, span ratios, section geometry and beam slenderness (Trahair 1993). The interaction between the parameters that influence the distortional buckling of isolated composite beams is difficult enough in itself to quantify, and incorporating the restraining or destabilizing effects of an adjacent span only adds another dimension of difficulty to the problem. Even for elastic buckling, the problem is complex, and recourse needs to be made to a suitable numerical procedure to handle each individual case.

In this chapter, an in-plane analysis of a two-span continuous composite beam and a rational model for out-of-plane distortional buckling are combined to study the elastic restrained distortional buckling of composite beams. The results of the in-plane analysis are used in the finite-element based out-of-plane analysis to determine the load factor against out-of-plane (restrained-distortional) buckling. The ratio between axial and bending actions in the bottom flange along the beam length and the destabilizing nature of the compressive actions in the hogging moment region are investigated for a variety of geometrical, loading and bracing configurations, as well as incorporating propped and unpropped construction. The method is then used to give some indication of the accuracy of existing design procedures and earlier studies based on less accurate assumptions. The study is of significance, as contemporary design techniques tend to be on the conservative side, and with the motivation for more economic and efficient design it is most important to identify the factors that may lead to premature buckling.

This chapter then describes the rational in-plane analysis of continuous composite beams subjected to creep and shrinkage of the slab, coupled with the out-of-plane analysis of the buckling of the steel joist. This problem is a generalisation of a more generic situation where quasi-viscoelastic rheology in one component is coupled with instability in the other component of a bi-material composite. Although the quasi-elastic shrinkage and creep behaviour in concrete are conventionally associated with serviceability limit states, it is shown that this rheology can in theory reduce the load factor against buckling in the steel, which is a strength limit state. This situation has hitherto not been a design consideration, nor thought to be important in conventional practice, as contemporary design techniques are quite conservative. The ramifications of this erosion of the buckling load factor are illustrated quantitatively and discussed, in the light of seeking more accurate solutions for the buckling of continuous composite beams.

3.2 CONTINUOUS COMPOSITE BEAMS

Steel and concrete provide an ideal combination of strength, with concrete efficient in compression and steel in tension. Steel provides fast erection, lightweight construction and increased span capability, whilst concrete is the most economical material when used in compression, as it provides compressive capacity, mass, stiffness and damping. Concrete provides corrosion and fire resistance and prevents slender steel sections from buckling. Continuous composite beams are a common form of composite construction in multi-storey buildings and bridges. Continuity in construction is a desirable feature, and substantial benefits can be attained by providing continuity in composite beams, particularly if the member possesses the necessary ductility to develop the plastic moment resistances at both the internal supports and mid-span regions. However, continuous composite beams consist of positive moment regions, in which the slab is subjected to compression and the steel component mainly to tension, and negative moment regions at the internal support, in which the concrete has cracked but still able to provide restraint to the steel and the reinforcement carries the tensile force, with the steel component subjected to a combination of negative bending and compression (Bradford & Kemp 2000). Thus, the ideal combination of these two construction materials is unavoidably violated in the negative moment region where the steel component is subjected to potential buckling, and the capacity of the concrete to resist tensile stresses is usually ignored as it is generally assumed that in the hogging region the concrete cannot transfer tensile stress, but the longitudinal slab reinforcement is effective in tension (Oehlers & Bradford 1995).

Continuous composite beams are widely used in multi-storey buildings, where they are continuous at the column connection, and in bridges. For the purpose of flexural strength calculations, such beams may be divided lengthwise into two distinct regions, namely regions of negative and regions of positive bending. The flexural strength of composite beams in positive bending is governed by the strength of the concrete and the steel beam and simple calculations based upon fully plastic stress blocks provide acceptable accuracy in predicting ultimate bending moment capacities, provided that the cracking of the concrete produces a ductile positive hinge (Ansourian 1982). In regions of negative bending moments, however, local and lateral instabilities of the steel section and cracking of the concrete influence not only the ultimate bending strength of the composite section, but also the ability of the section to redistribute bending moment by absorbing inelastic rotations. The ductility of composite beams in negative bending is affected by considerations of the stability of the steel component (Bradford 1986b). Local, lateral and distortional instabilities of the steel beam occur in the hogging-moment region and these forms of buckling have been recognised to be highly interactive. Furthermore, basic beam buckling theory (Vlasov 1961) that assumes no distortion of the section during buckling, does not apply to the hogging moment region of continuous beams.

The buckling in composite beams is even more special, as in negative bending the slab restrains the tension region of the steel and the neutral axis is not located at the mid-height of the web. In these regions the neutral axis is shifted towards the top flange, and in negative bending the steel part is subjected mainly to compressive strains. It is important to recognise that the compression zone of the beam in the negative moment region is not directly restrained by the concrete slab, as in the case of the sagging-moment region of a continuous composite beam. In addition, the web usually carries proportionally higher shear loads than in ordinary steel beams (Climenhaga & Johnson 1972). The hogging moment resistance of composite beams is determined by the magnitude of the tensile force in the reinforcing steel in the concrete slab, the compressive force in a portion of the steel beam (namely the bottom flange and the portion of the web) and the distance between these stress resultants (Oehlers & Bradford 1995).

The most important buckling modes of failure occurring in composite beams are local flange, local web and lateral-distortional buckling (Fig 1.2). If these are prevented, large rotational capacities can be achieved beyond the plastic moment of resistance, with the negative hinge being classified as "strain hardening" (Barnard & Johnson 1965). Because lateral-distortional buckling is basically an interaction mode between lateral-torsional buckling and local buckling (Hancock *et al.* 1980), there are many factors influencing the phenomenon, and the derivation of general solutions is not straightforward. Although a closed-formed solution for the case of uniform bending has been derived (Hancock *et al.* 1980), the general lateral-distortional buckling solution for the case of moment gradient and with the incorporation of restraints requires a specialist computer program, which is generally only a research tool.

The factors influencing the strength of continuous composite beams in negative bending may be summarised as follows:

(a) *Amount of steel reinforcement in the slab.* The depth of the web in compression is controlled by the amount of reinforcement in the slab. Local buckling of the web and compression flange limits the amount of active reinforcement in the slab. The rebar content in turn determines the magnitude of the negative moment.

(b) *Lateral-distortional buckling of the steel section.* Significant restraint, both lateral and torsional, is provided by the concrete slab to the tension flange of the steel section. The lateral-torsional buckling resistance of the steel beam is therefore dependent on the web's ability to convey this restraining action to the unrestrained compression flange.

In the following study of this distortional mode of lateral buckling, it is assumed that the shear connection between the steel flange and the restraining slab has sufficient strength, and that its flexibility in the transverse plane is negligible. These assumptions can be shown to be valid when the steel web is unstiffened, except at supports, because the transverse flexibility of webs is high. They may not be valid where there are vertical web stiffeners, because the transverse stiffness of the resulting cruciform or tee section far exceeds that of the web alone, so that the transverse restraining moments applied by the slab are concentrated at the stiffened cross-sections of the beams.

3.3 DESIGN METHODS FOR DISTORTIONAL BUCKLING

Design for lateral-distortional buckling is generally based on procedures for steel structures in which an elastic analysis is carried out to determine the actions in the steel portion or steel component of a cross-section subjected to negative bending. One of the impediments of this analysis is that the steel component is subjected to combined compression and negative moments, where the compression force equilibrates the tensile force in the reinforcement, and that the axial compression varies along the beam. The buckling strength of the steel component is then calculated, and this is used in determining the strength of the composite cross-section. The combination of both bending and axial actions in the steel component appears to have been overlooked by many.

In the method of 'design by buckling analysis' (Trahair & Bradford 1998), the elastic buckling moment M_{od} and the elastic buckling load N_{od} for the steel component are converted into *strengths* using relevant prescriptive strength curves in national standards which account for the complex interaction between buckling and non-linear material behaviour in steel columns in a simplified way. Therefore in the failure envelope for the steel beam-columns, these curves relate the pure flexural strength and pure axial strength with both elastic buckling and the rigid plastic strengths.

The rationale of 'design by buckling analysis' requires the slendernesses to have been determined using the elastic distortional buckling moment M_{od} and load N_{od}, so that the bending strength of the steel in the absence of compression M_{sd} and the compressive strength of the steel in the absence of bending N_{sd} may be determined from design equations in codes. It must be noted that these prescriptive equations were developed for lateral-torsional beam buckling and flexural column buckling. Their use for lateral-distortional buckling is questionable (Lee 2001), but they are considered to be conservative. Finally, the bending strength must be reduced for the effects of axial compression if an 'accurate' analysis is being performed by treating the steel component as a beam-column. It is obvious that the calculation of the lateral-distortional buckling moment and load are based on very approximate design methods in lieu of complex finite element modelling, and that the member strengths that are based on combined elastic buckling and yielding are derived from lateral buckling results, and so their applicability to lateral-distortional member strengths is questionable. This issue has been addressed recently by Lee (2001).

The 'inverted U-frame approach' is based on the design philosophy for half-through girder bridges. For this, compression flange is modelled as a uniformly compressed strut restrained elastically against flexural buckling by the stiffness of the web, which represents a continuous Winkler foundation. The web is treated as a cantilever, and its stiffness may be determined by applying a fictitious unit horizontal force.

Fig. 1.7 shows the strut buckling model, in which the flange strut is subjected to an elastic Winkler restraint of stiffness α_t per unit length that produces a distributed restoring force of $\alpha_t\ u_t$ per unit length, where u_t is the buckling deformation which is assumed to be a sine curve. The elastic critical value of the force in the strut to cause buckling N_{cr} is

$$N_{cr} = \frac{\pi^2 E_s I_F}{L^2} + \frac{\alpha_t L^2}{\pi^2} \tag{3. 1}$$

where I_F is the second moment of area of the flange about the weak axis of the I-section. The relationship between N_{cr} and L is of a garland shape, and the minimum value of N_{cr} may be determined by setting $\mathrm{d}N_{cr}/\mathrm{d}L$ to zero. Therefore,

$$(N_{cr})_{\min} = 2\sqrt{E_s I_F \alpha_t} \tag{3. 2}$$

This design approach has been explained and criticised in detail (Johnson & Buckby 1986), and has been shown by numerical analyses (Bradford & Johnson 1987; Weston *et al.* 1991) to be very conservative. The main reasons for this conservatism are:

(a) the effective length of the bottom flange is based on the model of a restrained strut with constant axial compression, thus neglecting the benefit of the moment gradient;

(b) the torsional and warping stiffnesses of the strut are neglected.

Svensson (1985) suggested that the lateral-torsional critical buckling stress σ_{el} for a beam with one flange elastically restrained along its entire length could be obtained by solving the approximately equivalent buckling load problem obtained by treating the free flange as an elastically supported column and dividing the buckling load by the flange area. Williams and Jemah (1987) suggested that it would be safer to add 15% of the web area to the flange area when finding σ_{el}, on the basis of a comparison with accurate lateral-torsional critical buckling stresses which the exact thin plate theory computer program VIPASA produced for pure bending of four representatively chosen beam cross-sections. Goltermann and Svensson (1987) presented a method that allows for the rotational restraint at the tension flange to be quantified. Bradford and Gao (1992) presented a very interesting method of analysing fixed-ended composite steel-concrete beams, by using the principle of virtual work and taking into account the difference between the beam sagging and hogging bending rigidities. Williams *et al.* (1993) extended their previous investigations by developing a model with an additional spring having arbitrary stiffness to restrain in-plane rotation at each end, which can become infinite, and allows for difference between sagging and hogging bending rigidities along the member, using an approach of comparing areas under the curvature diagram of the beam. These authors presented a parametric study, covering a wide range of beam sections. Hanswille (2000) showed in his study that the method in Eurocode 4 (1996) leads to unsafe results in the case of members with unequal end moments and for the end spans of continuous beams. Although some design guidance and research into buckling behaviour of continuous composite beams are in existence, it is evident that designers need simpler and less conservative methods of checking resistance to buckling. More detailed critiques of the issue have been published by Ronagh (2001) and Ronagh and Bradford (2002).

3.4 THEORY

3.4.1 General

Conventionally, design against the limit state of lateral-torsional buckling is usually based on the results of an in-plane elastic (second order) analysis, or a plastic analysis. The rationale of an elastic analysis is conservative, and applicable to bare steel members for which elastic analysis is appropriate. The extension of an 'elastic' analysis to composite tee-beams could be open to debate, since in the negative region of a composite beam the slab is invariably cracked and so an elastic analysis (using transformed area principles) is invalid.

Nevertheless, in this study an 'elastic-cracked' analysis of a two-span continuous composite beam is undertaken first in order to determine the stress resultants that act in the steel joist. A rational beam-type finite element analysis is then invoked using these stress resultants as input to perform an elastic distortional buckling analysis, so as to determine the load factor against distortional buckling. Since the in-plane and out-of-plane analyses are well documented, they are described very briefly in the following two sub-sections.

3.4.2 In-Plane Analysis

A flexibility method of analysis developed by Bradford *et al.* (2002) has been used in this study to determine the short-term moments and axial actions in a two-span continuous composite beam, whose spans may have different lengths and with concentrated loads placed at specified positions within each span. This method allows for propped and unpropped construction. The method is in essence 'linear elastic', but accounts for cracking of the slab (of flexural tensile strength, f_t) in the negative moment regions, so that it resembles a close to non-uniform stepped beam, as shown in Fig. 3.2. The position of the step where the rigidities change is at the point of contraflexure (if for simplicity in the argument the tensile strength of the concrete is ignored), but this position is not known a priori and so an iterative scheme must be invoked to converge on its position and hence on the final bending moment distribution in the composite beam. While the entire composite cross-section is not subjected to axial actions under pure bending, these are present in the slab and in the joist, with equilibrium being maintained between these two components by means of the shear connection. Thus under a given geometry and loading, the in-plane analysis is able to generate the bending moment diagram and shear force diagram for the steel joist. It is assumed here that the shear connection is infinitely stiff.

3.4.3 Out-of-Plane Analysis

The beam or line-type finite element method for elastic distortional buckling analysis of I-sections developed by Bradford and Ronagh (1997a) is used for the out-of-plane analysis, that is mathematically uncoupled from the in-plane analysis. In their program FEDBA16 each end of the line element has eight buckling degrees of freedom, corresponding to the lateral displacements and twists of the top and bottom flanges, and their respective rates of change with respect to the beam longitudinal axis, as illustrated in Fig. 3.3. The web is allowed to distort as a cubic curve during buckling, with its flexural displacements being related to the flange buckling freedoms by imposing displacement and slope compatibility at the top and bottom of the web. All freedoms relating to buckling deformations of the top flange of the joist were suppressed in the present analysis, owing to the rigid restraint assumed to be provided by the slab and the shear connection.

Because of the linearity of the in-plane analysis, the geometric stiffness matrix $\overline{S}$ is assembled from the moments and axial forces in the joist due to a set of initially applied loads. These loads are then scaled by a buckling load factor λ, which is the eigenvalue of the well-known buckling problem

$$\{\overline{K} - \lambda\overline{S}\}\vec{\Delta} = \vec{0} \tag{3.3}$$

in which $\overline{K}$ and $\vec{\Delta}$ are the elastic stiffness matrix and vector of buckling displacements respectively.

3.5 NUMERICAL INVESTIGATIONS

3.5.1 General

Distortional buckling loads are dependent on a multiplicity of geometric and material properties, which when coupled with the in-plane analysis prohibit general solutions. Hence four different illustrative steel I-beam sections (J1,…,J4) have been chosen for this study, these being two universal and two welded doubly symmetric steel I-sections supporting a slab (S1, S2 and S3) cast propped and unpropped with 0.6, 1.8 and 3.6% (R1, R2 and R3) reinforcement throughout positioned 50 mm from the top of the slab. The concrete compressive strengths were taken as 25, 32, 40 and 50 MPa with tensile strengths of 3.0, 3.4, 3.8 and 4.2 MPa respectively. The span lengths considered in this study range from 10 to 40 metres. A wide range of loading configurations has been considered and these are illustrated in Fig. 3.4 (Cases 1-11). The steel section dimensions, slab geometry, reinforcement ratios, concrete strengths and beam span lengths, with the notation adopted in this chapter, are summarised in Table 3.1.

3.5.2 In-Plane Behaviour

In regions of negative bending, the joist of a composite beam is not only subjected to longitudinally varying bending moments, but also to varying axial actions that can be compressive at the internal support and tensile near the simply supported end support. Unbalanced compression in the joist of a composite beam arises from the geometric and material asymmetry of the total cross-section, so that in composite beam joists the axial forces vary in accordance with the moment gradient. Resulting errors in predicting buckling loads are on the safe side, however, if conditions at the point of maximum moment are considered.

While elastic distortional buckling of members subjected to pure bending has received a good deal of attention (Bradford 1992a), the effects of combined actions on the distortional buckling of isolated members has received very little attention (Bradford 1990b), and even studies of lateral-torsional buckling under combined actions when the axial force varies along the member appear to be very rare (Trahair 1993).

In order to illustrate the effects of the axial (N) and bending (M) actions, the ratio of the axial to bending stresses σ_A/σ_B in the bottom flange along the beam length has been determined, where

$$\sigma_A = \frac{N_S}{A_S} \tag{3. 4}$$

and

$$\sigma_B = \frac{M_S}{Z_S} \tag{3. 5}$$

with N_S and M_S being the axial force and moment respectively in the joist at a particular section obtained from the in-plane analysis, and with A_S and Z_S being its respective area and elastic section modulus, and in which

$$\mathrm{sgn}(\sigma_A / \sigma_B) = \mathrm{sgn}(\sigma_A + \sigma_B) \tag{3. 6}$$

so that the portions of the beam in sagging and hogging may be identified. For the graphical illustration compressive stresses are taken as positive.

3.5.2.1 Effects of the Steel Cross-Sectional Area Parameter

Figure 3.5 shows the lengthwise variation of the stress ratio for four different steel sections (J1,..., J4) when self-weight is ignored, while Fig. 3.6 plots this ratio when self-weight is included. The influence of self-weight is important in unpropped construction, as it generates bending stress only in the joist and no axial stress. In the absence of self-weight, the beam acts as if propped, and in Fig. 3.5 it can be seen that the axial stress is twice the bending stress for the 180UB (J4) section over most of the beam. However, as the cross-section dimensions increase the ratio between the stresses reduces and for the 1200WB (J1) section this ratio is as low as 0.39. On the other hand, the ratio in Fig. 3.6 is below 0.1 for the entire range of sections considered in this study, as the inclusion of self-weight increases the bending stress but not the axial stress as composite action is not achieved under self-weight. Furthermore, this ratio remains unaffected by different beam lengths (ie. L1,..., L7) and different loading configurations (ie. loading cases 1-5, 8-11) as illustrated in Figs. 3.7-3.10. The effects of the steel cross-sectional area parameter on the stress ratio for the entire range of sections and loading configurations considered in this study are presented in Figs. A1.1-A1.28 (Appendix).

3.5.2.2 Effects of the Concrete Slab Cross-Sectional Area Parameter

Three different concrete slab areas were considered in this study (ie. S1, S2 and S3) and it can be seen from Figs. 3.11 and 3.12, which represent propped and unpropped construction respectively, that the magnitude of the stress ratio increases with the increase of the cross-sectional area of the slab. However, this ratio is not excessively significant and becomes negligible as the size of the steel section decreases. Broader illustrations of this effect are presented in Appendix, Figs. A1.29-A1.34.

3.5.2.3 Effects of the Steel Reinforcement Area Parameter

A similar investigation has been carried out to quantify the influence of three different steel reinforcement areas (ie. R1, R2 and R3) on the longitudinal variation of the axial/bending stress ratio for propped and unpropped construction as illustrated in Figs. 3.13 and 3.14 respectively. It is evident that the effects of the reinforcement are of no consequence. Further evidence of this effect is included in Appendix, Figs. A1.35-A1.42.

3.5.2.4 Effects of the Concrete Compressive Strength Parameter

Four different concrete compressive strengths were investigated in this study (ie. F25, F32, F40 and F50). The results shown in Figs. 3.15 and 3.16 for propped and unpropped construction respectively indicate that the axial/bending stress ratio increases with an increase in the concrete compressive capacity. Nevertheless, this increase is inconsequential. The effects of this parameter have been considered in association with some other parameters such as steel sectional area, concrete slab cross-sectional area, loading configuration, different reinforcement ratio and the results are documented in Appendix, Figs. A1.43-A.1.50.

3.5.3 Out-of-Plane Behaviour

The steel section of an unpropped composite steel-concrete beam may experience overall member buckling under two loading conditions. First, the construction loading of the wet concrete may induce lateral-torsional buckling in regions of positive bending before the beam becomes composite. The second buckling condition occurs during live loading in regions of negative bending over an internal support after composite action is achieved, where the compressive stress in the bottom flange and lower portion of the web of the joist may induce lateral-distortional buckling. The first type of instability may be prevented by routine application of the lateral-torsional buckling provisions in the modern limit-state codes of practice. The use of these rules by designers is straightforward, and are usually quite accurate. This type of instability is not considered any further in this thesis.

The stress resultants obtained from the in-plane analysis have been used to assemble the stability matrix $\overline{S}$ in Eqn. 3.3 so that the eigenvalue or buckling load factor λ may be found. The eigenvector $\vec{\Delta}$ in Eqn. 3.3 represents the buckled shape, and this has also been calculated. Although many buckling models do not include the effects of self-weight, this clearly is important for composite beams if the buckling load factor is low. The out-of-plane analysis undertaken for an unpropped continuous beam includes self-weight in the finite element modelling of FEDBA16. For the purpose of this study, the self-weight is included in Eqn. 3.3 by the addition of a constant stability matrix $-\overline{S}_{sw}$ that is built-up using the self-weight stress resultants. Hence,

$$\left\{\overline{K} - \overline{S}_{sw} - \lambda\overline{S}\right\}\vec{\Delta} = \vec{0} \tag{3. 6}$$

The solution of both Eqn. 3.3 and Eqn. 3.7 using FEDBA16 is extremely rapid on a contemporary personal computer.

3.5.3.1 Model Verification

Table 3.2 compares the critical buckling stresses derived by the method adopted in this study, the 'inverted U-frame' design method and design suggestions given by Williams and Jemah (1987) and Williams *et al.* (1993). The cross-sections used, X1-X4 with three values of the span length for each, are the same as those employed by Williams *et al.* (1987, 1993). Table 3.2 shows a relatively large difference between results derived by the analysis presented here, those derived by the 'inverted U-frame approach' and the methods suggested by Williams *et al.* (1987, 1993). The latter two techniques did not account for the cracking of the concrete adequately (as the solutions are based on a buckling model for a steel section and do not consider the in-plane analysis appropriately), and interestingly the earlier (1987) recommendations of Williams and Jemah compare best until those of the current study. The results in Table 3.2 reinforce the disparity between the solutions to the problem given by various researchers and the need for further investigations of the phenomenon.

3.5.3.2 Buckling Behaviour

Figures 3.17 to 3.24 show some buckling characteristics for a number of continuous composite beams, built either propped or unpropped, both symmetric and asymmetric and with different geometries of the steel joist. The ratio of the buckling load factor for the loading cases 1-11 is normalised with the buckling load factor of loading case 2 and plotted as a function of the beam span length considered. It can be seen from the figures that the buckling load factors for the equal span beams with various loading configurations (ie. Cases 1-3 and Cases 8-11) are almost identical to that of L2, whilst the figures indicate that this difference in buckling behaviour is more pronounced for the asymmetric beams (ie. Cases 4-7). It is worthwhile noting that in the case of unequal span beams this ratio is quite substantial for the sections J3 and J4, and ranges between 10-30 for propped, and between 30-120 for unpropped construction.

The elastic distortional buckling resistance of two-span continuous beams decreases when the concentrated loads within each span are located toward the centre of each span, since the bending moment distribution is more uniform. When the ratio of span lengths is high, the buckling behaviour of the longer span dominates, and so cross-sectional distortion becomes less significant because of the increased length of the longer span.

3.5.3.3 Buckling Modes

In modelling the buckling restraints for a continuous beam, it is assumed that the top flange is completely restrained by the slab, and at the simple end supports that bottom flange displacement and twist (but not their rates of change) are also fixed. At the interior support, the bearing support would restrain the lateral displacement and twist of the bottom flange, but there may be some elastic restraint provided against the in-plane lateral rotation (u'_b) of the bottom flange. Figures 3.25-3.26 show the normalised buckling mode shapes for two identical spans with central concentrated loads when u'_b is completely fixed or restrained, whilst Figs. 3.27-3.28 plot the normalised buckling modes for the same beam when u'_b is unrestrained. It can be seen that the bottom flange buckling deformations are almost identical for the two cases.

Bracing of the bottom flange can have ramifications on the buckling loads and modes and is quite common in practice. Figures 3.25-3.32 show the bottom flange translation buckling mode (u_B) and bottom flange twist buckling mode (ϕ_B) for loading arrangements shown in Fig. 3.4 (case 1 and case 4) for unpropped and propped construction. In the figures the internal supports provide complete restraint against buckling deformations. Figures A1.51-A1.62, included in Appendix, show the buckling modes for loading configurations different to cases 1 and 4, as shown in Fig. 3.4. The plots of normalised buckling modes clearly indicate the critical points (the points equal to unity) along the span length subjected to the destabilising lateral-distortional buckling that need to be designed against and accordingly provided with bracing.

It is worth noting that in both cases the 'stabilising' influence of the sagging region of the span against buckling (where the bending stresses in the bottom flange are tensile) is enhanced somewhat by tensile stresses that equilibrate with compression in the slab. On the other hand, the compressive axial actions in the hogging region act with the hogging moment to destabilise that region against buckling.

3.5.3.4 Bracing Effects

The influence of the brace position and the load position has been investigated in this chapter for both symmetric and asymmetric two-span beams. For this, the brace is positioned $\alpha_w L$ from the internal support and the concentrated load is positioned, as shown in Fig. 3.4, some distance from the internal support, with the brace providing complete restraint against lateral deflection and twist. Such bracing may be typical of conventional cross bracing. The reference buckling load factor, λ_{ref}, has been taken to be that when the brace is not provided for the loading configuration considered.

Figures 3.33 to 3.35 show the effects of a single brace positioned within the span $0 \leq \alpha_w \leq 0.5$ for both symmetric and asymmetric unpropped two span beams. When the loads are placed in the positive region up to mid-span, the destabilising hogging moments and the associated hogging region result in an elastic buckling load factor ratio that increases only up to about 20% for equal and about 50% for unequal span beams. On the other hand, as the point load is placed closer to the internal support the hogging moment increases at the internal support (which of course is restrained from buckling), the extent of the hogging region decreases, and the larger sagging moment region (whose bottom flange tensile bending stress is enhanced by the axial tension in equilibrium with the slab compression) is very significant in restraining the beam against elastic buckling. Consequently, the buckling load factor for the braced continuous beam has increased two to three fold over that when the point load is placed closer to the mid-span for which providing a brace in this region will increase the buckling load factor, as can be seen in Figs. 3.33-3.35 for the brace positioned at a_w = 0.4. Braces further away from the internal support than this are in the sagging region, and have negligible effect on increasing the buckling load factor.

Similar behaviour has been observed for propped construction, as shown in Figs. 3.36-3.38, with the exception that the elastic buckling load factor ratio for the braced continuous beam increases three to four fold when the point load is placed closer to the internal support over that when the point load is placed closer to the mid-span. It is also worth noting that if the internal bearing is unable to provide lateral rotational restraint, the counterparts to Figs. 3.33-3.38 are almost identical to the latter figures.

3.6 QUASI-VISCOELASTIC SLAB BEHAVIOUR

3.6.1 General

Because the structural performance of a composite beam makes use of its extensive concrete component, it is subjected to the time-varying effects of creep and shrinkage. Conventionally, the quasi-viscoelastic rheology of reinforced concrete that induces shrinkage and creep deformations is associated with the serviceability limit state in engineering structures. The associated service load responses are usually those of time-dependent deflections and cracking and sometimes thermal straining, and provisions to control these are included in most national design codes of practice. The ramifications of these effects on the deformations of simply supported beams are quite well researched, with recent bibliographies being given by Dezi *et al.* (1998) and Ranzi (2004). Controlling deformations under service loading is a serviceability limit state problem, and although serviceability analyses are usually based on linear-elastic assumptions, the analysis of composite beams is non-linear owing to the cracking, creep and shrinkage of the slab (Bradford & Gilbert 1989). However, it has been shown that quasi-viscoelastic deformations in concrete and composite steel-concrete structures can lead to geometric instability or buckling, which is usually considered to be a strength limit state.

The so-called creep buckling behaviour of slender, eccentrically loaded concrete columns is fairly well known and documented (Gilbert 1988; Gilbert & Bradford 1990; Bradford 1997b, 1997c & 1998c). Less well-known is the instability which may occur in thin steel sheeting that is juxtaposed with concrete that undergoes quasi-viscoelastic deformation, and which acts compositely with the concrete. This behaviour has been observed in tests and quantified in composite profiled beams (Uy & Bradford 1995) and quantified theoretically in thin-walled concrete-filled tubes (Bradford 1998c; Uy & Das 1998) and composite profiled walls (Bradford *et al.* 1998). The purpose of the study in this chapter is to quantify the instability that may arise in the steel joist of a continuous composite beam due to quasi-viscoelastic creep and shrinkage deformations, which occur in the concrete slab.

Gilbert and Bradford (1995) presented a flexibility based approach for determining the response of a shored composite propped-cantilever beam which undergoes deformations due to creep and shrinkage, and showed that the bending moment redistribution that takes place predominantly due to shrinkage is substantial. Of particular significance is the increase in both the magnitude and extent of negative or hogging bending that occurs near the fixed support, and this was examined in the light of the serviceability limit states of deflection and concrete cracking. Bradford *et al.* (2002) extended the flexibility-based approach to consider two-span beams with point loads placed arbitrarily in within the spans, and which could model both propped and unpropped construction, and this modelling was used in section 3.4 of this chapter, albeit without the inclusion of time-dependence. While the time-dependent increase in the negative bending region was again quantified, the ramifications that this may have on instability of the joist were not alluded to in the work of Bradford *et al.* (2002).

Because the in-plane analysis including quasi-viscoelastic deformations developed by Bradford *et al.* (2002) is able to determine the varying stress resultants in the steel joist in the time domain, these stress resultants may be used as input for the out-of-plane method that uses the line-type finite element FEDBA16 developed by Bradford and Ronagh (1997a), and which was used in section 3.4. This study therefore makes recourse to the numerical uncoupled in-plane (quasi-viscoelastic) and out-of-plane (FEDBA16) methods of analysis to investigate erosion of the elastic buckling load factor, due mainly to shrinkage in unpropped continuous composite beams that would be typical of bridge girders. It is shown in this section that the elastic buckling load factor is indeed eroded quite significantly in the time domain in this theoretical treatment. With the fairly well-accepted knowledge that contemporary design of composite T-beams against buckling is very conservative, such an erosion of the elastic buckling load factor would not be considered to be of concern in existing beams. However, since more rational and accurate methods of predicting distortional buckling and which remove the conservatism of existing techniques are evolving and indeed extensively developed in this thesis, the consideration of quasi-viscoelastically induced buckling must be borne in mind in these more accurate buckling models.

3.6.2 Numerical Results

The in-plane quasi-viscoelastic analysis has been applied to an unpropped two-span composite beam subjected to a sustained uniformly distributed load of 1 kN/m. The slab has widths of 1500, 2500 and 3500 mm and a depth of 130 mm, and full interaction between the concrete slab and steel joist at the interface was assumed. Figures 3.39 to 3.43 show some results for different geometries of the steel joist, different span lengths, different concrete compressive strengths, different steel reinforcement ratios, symmetric and asymmetric spans constructed either unpropped or propped, in which the ratio of the long-term buckling load factor to its short-term counterpart, λ_L/λ_S is plotted as a function of time. In modelling the creep and shrinkage, the aging coefficient was taken as 0.8, and the creep coefficient ϕ and shrinkage strain ε_{sh} were assumed to be given by the same compliance function $F(t)$ as

$$\begin{pmatrix} \phi \\ \varepsilon_{sh} \end{pmatrix} = F(t) \begin{pmatrix} \phi^* \\ \varepsilon^*_{sh} \end{pmatrix} \tag{3.7}$$

where Terrey *et al.* (1994) defined the compliance function, $F(t)$ as

$$F(t) = \frac{t^{0.7}}{t^{0.7} + 32} \tag{3.8}$$

in which t is in days, and the values at $t \rightarrow \infty$ are $\phi^* = 3.5$ and $\varepsilon^*_{sh} = 1000 \times 10^{-6}$.

It can be seen from Figs. 3.39 to 3.43 that the elastic buckling load factor can be eroded due to the effects of creep and, particularly, shrinkage. With the combination of the final values ϕ^* and ε^*_{sh} and the compliance function $F(t)$, the short-term elastic buckling load factor is eroded in the long-term, up to about 80% in some cases.

The magnitude of the erosion of the load factor up to times of around 100 days is exaggerated, since significant shrinkage takes place during curing when the composite action has not mobilised. Nevertheless, the effects are seen to be quite severe, particularly for the span lengths ranging between 10 to 20 metres. This effect appears to amplify with the increased size of the steel cross-section and increased concrete compressive capacity. An increase in the slab cross-sectional area and reinforcement ratio does not contribute significantly to the reduction of the buckling load capacity due to the time effects. Further illustrations of the creep and shrinkage effects on the erosion of the buckling load factor are included in Figs. A1.63-A1.69.

It is also worth noting that the final buckling factor that determines the buckling strength of the beam is derived from both the elastic buckling load and the plastic moment of the cross-section, as noted in Oehlers and Bradford (1995). This effect reduces the severity of the time-dependent erosion of the load factor.

3.7 SUMMARY

This study has made recourse to two methods of analysis, a rational in-plane analysis of a two-span continuous beam, which may have different span lengths with arbitrary positions of the loads, married with a rational out-of-plane beam-type finite element procedure to determine the elastic buckling load factors under short-term loading and to address the interesting issue of the dependence of the elastic buckling load factor of a continuous composite beam on the effects of shrinkage and creep. Extensive numerical investigations have been carried out and various parameters such as the area of the steel section, beam slenderness, area of the concrete slab section, area of the secondary steel reinforcement, concrete compressive strength, propped and unpropped construction, symmetrical and asymmetrical beam configurations and different loading configurations were the subject of this analysis. The effects of these parameters on the in-plane behaviour, together with the effects of bracing and some buckling characteristics, are documented in Figs. 3.5 to 3.43, whilst more comprehensive investigations are included in Appendix.

The in-plane analysis accounts for the variation of both bending and axial actions in the steel joist, the latter of which seems to have been ignored by many investigators, and not previously quantified. The analysis also shows that there is a disparity between the results of this rational buckling analysis, which includes the effect of concrete cracking, and other techniques which do not include this effect or which are overly simplistic. However, converting the elastic buckling loads into design strengths is another problem, which requires recourse to inelastic distortional buckling solutions that are calibrated against test results, and this has been considered in Chapters 5 and 8 of this thesis.

Finally, a quasi-viscoelastic model has been used to determine the redistribution of bending moment and axial force within the steel joist in the time domain. The results of this in-plane analysis were then used as input data for a finite element method for analysing elastic distortional buckling. It was shown that the buckling load factor in the long term decreased somewhat from its short-term value owing to the quasi-viscoelastic rheology of the concrete slab.

This issue has hitherto been ignored in design, but the perceived conservatism of past and contemporary design methods, combined with the dependence of the strength load factor on both the elastic buckling load factor and on the plastic moment in the method of 'design by buckling analysis', would suggest that the propensity of existing bridge girders to buckle is remote. However, with the impetus of evolving advanced and rational design procedures, the possibility of quasi-viscoelastic induced instabilities, as have been observed in other steel/concrete composite applications, is at least a potential and interesting issue in structural mechanics that requires further investigation. The design of continuous composite beams is significantly influenced by lateral distortional buckling, yet research into its prediction is far from complete.

Table 3.1 Notation: a) steel section; b) slab cross-sectional area; c) reinforcement ratio; d) concrete compressive strength; e) span length

a)

Steel Section	Notation	b_f (mm)	t_f (mm)	h_w (mm)	t_w (mm)
1200WB	**J1**	500.0	40.0	1160.0	16.0
900WB	**J2**	400.0	32.0	892.0	12.0
250UB	**J3**	146.0	10.9	245.1	6.4
180UB	**J4**	90.0	10.0	169.0	6.0

b)

Slab dimensions	Notation
1500×130	**S1**
2500×130	**S2**
3500×130	**S3**

c)

Reinforcement ratio A_r/A_c (%)	Notation
0.6	**R1**
1.8	**R2**
3.6	**R3**

d)

Concrete Strength f'_c (MPa)	Notation
25	**F25**
32	**F32**
40	**F40**
50	**F50**

e)

Length (m)	Notation
10	**L1**
15	**L3**
20	**L3**
25	**L4**
30	**L5**
35	**L6**
40	**L7**

Table 3.2 Model verification

Section	t_w	h	t_f	b_f	L	This study (1) [MPa]	U-frame (2) [MPa]	Ref. 279 (3) [MPa]	Ref. 280 (4) [MPa]	(1)/(2)	(1)/(3)	(1)/(4)
X1	18.5	935	35	300	7396	2063	442	1904	1527	4.67	1.08	1.35
X1	18.5	935	35	300	12333	1751	475	1533	1229	3.69	1.14	1.42
X1	18.5	935	35	300	30827	701	545	769	617	1.29	0.91	1.14
X2	15.6	744.2	25.4	268	6013	2110	483	2299	1830	4.36	0.92	1.15
X2	15.6	744.2	25.4	268	10017	1916	511	1855	1477	3.75	1.03	1.30
X2	15.6	744.2	25.4	268	25042	916	570	930	740	1.61	0.99	1.24
X3	10.7	446.2	18.9	133.4	3324	2277	615	2468	1979	3.70	0.92	1.15
X3	10.7	446.2	18.9	133.4	5537	2157	643	1991	1597	3.35	1.08	1.35
X3	10.7	446.2	18.9	133.4	13841	1611	700	998	801	2.30	1.61	2.01
X4	5.8	195.4	7.8	133.4	2042	2808	1249	4939	4245	2.25	0.57	0.66
X4	5.8	195.4	7.8	133.4	3404	2293	1266	3979	3420	1.81	0.58	0.67
X4	5.8	195.4	7.8	133.4	8510	2025	1302	1995	1715	1.56	1.01	1.18

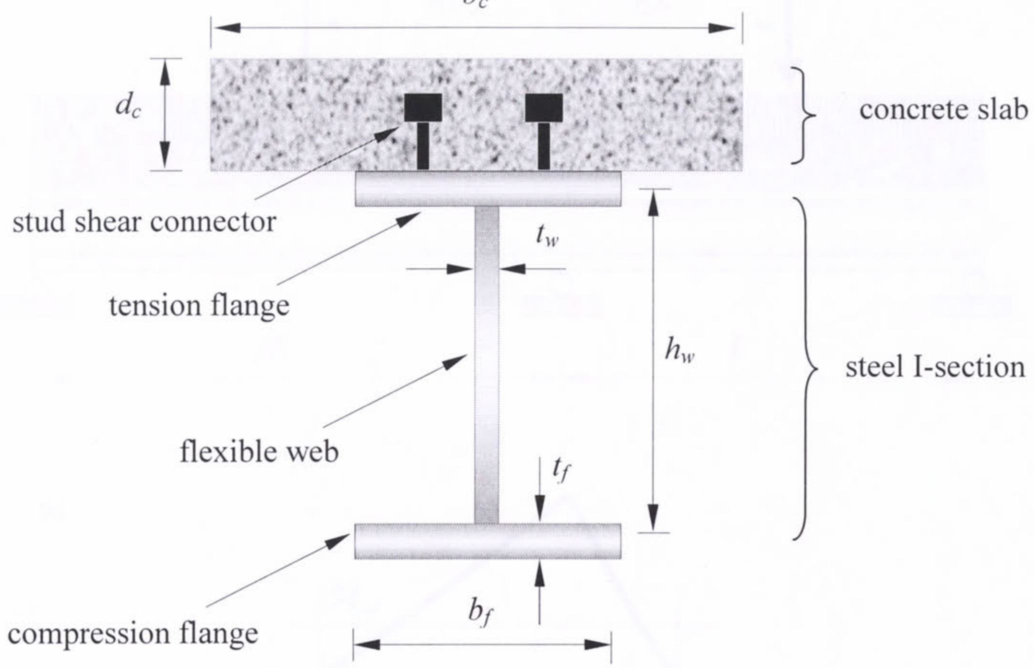

a)

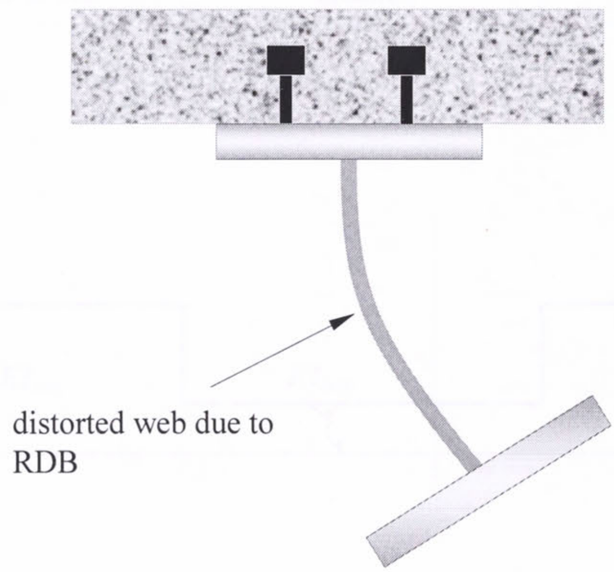

b)

Figure 3.1 Composite beam cross section: a) notation; b) RDB

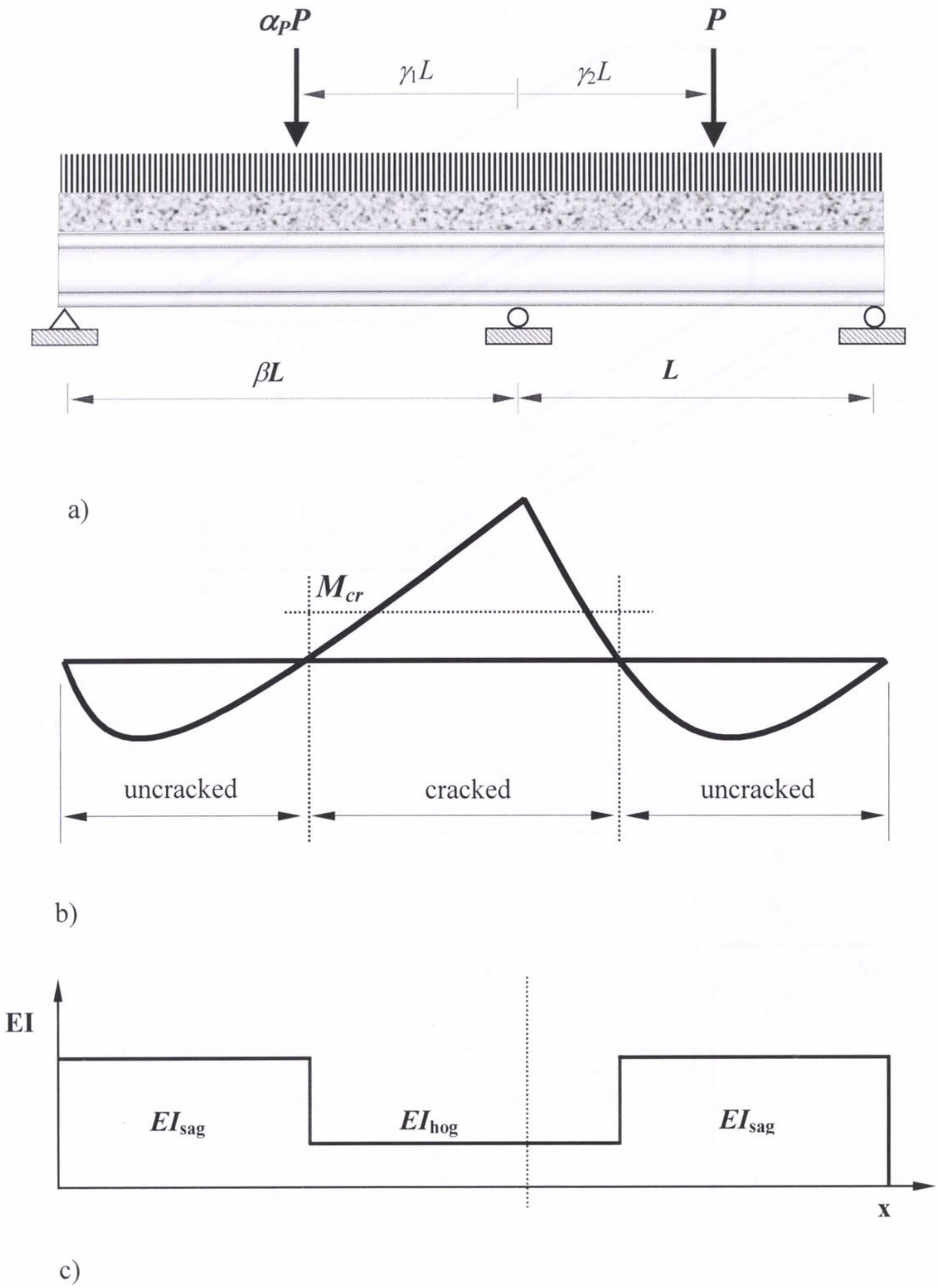

Figure 3.2 a) Two span continuous composite beam; b) bending moment diagram; c) flexural rigidity variation

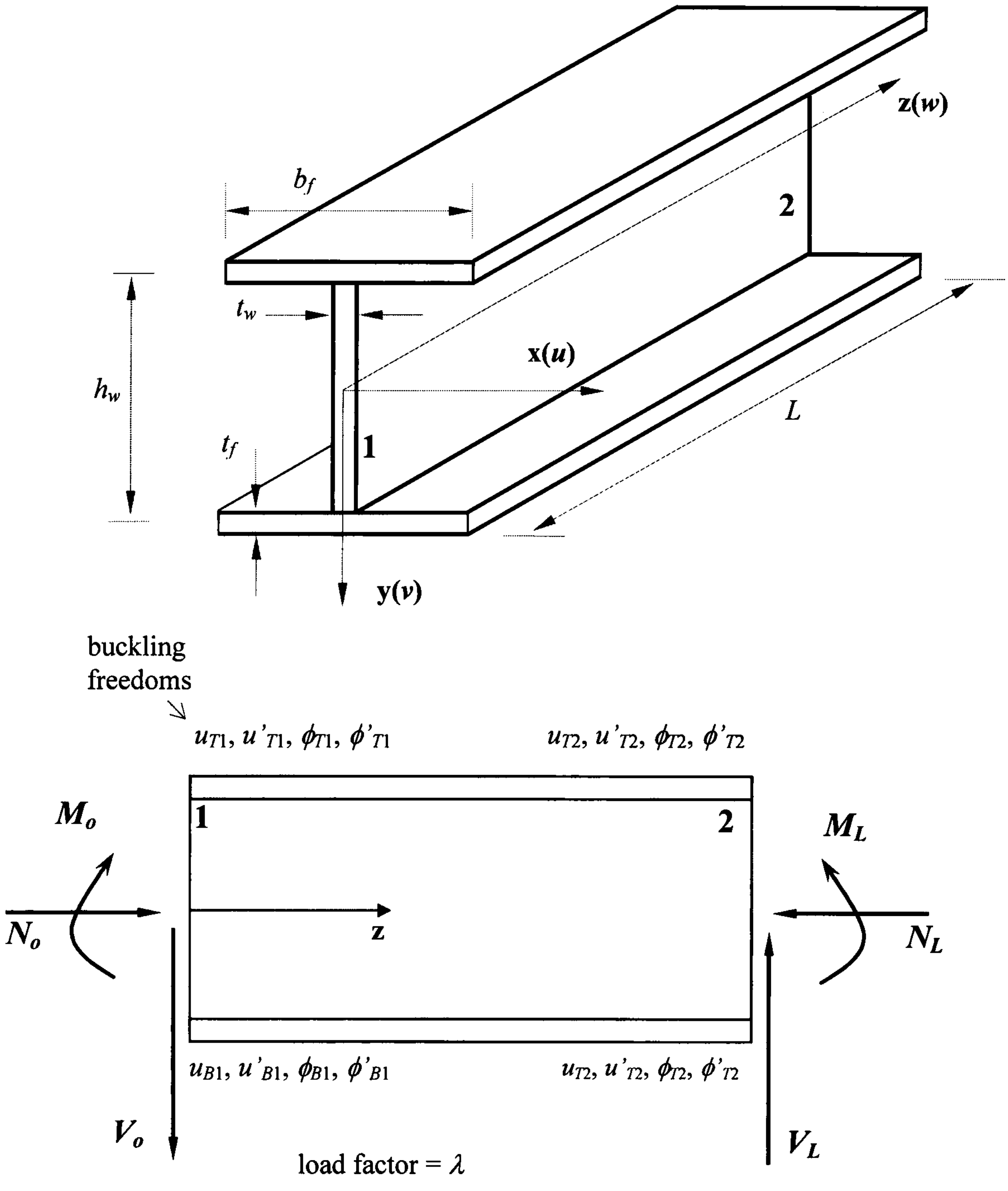

Figure 3.3 Beam or line finite element

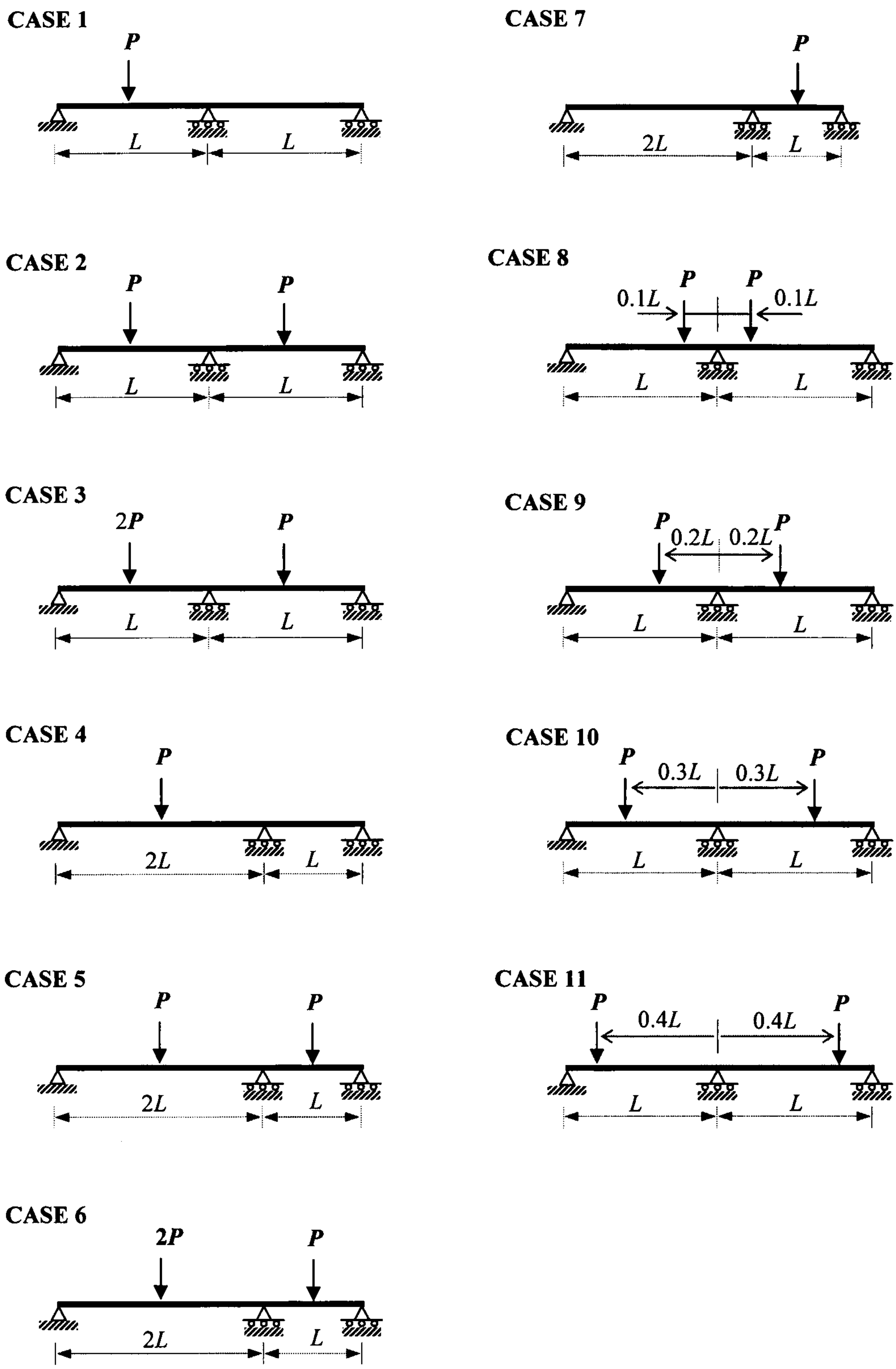

Figure 3.4 Loading cases

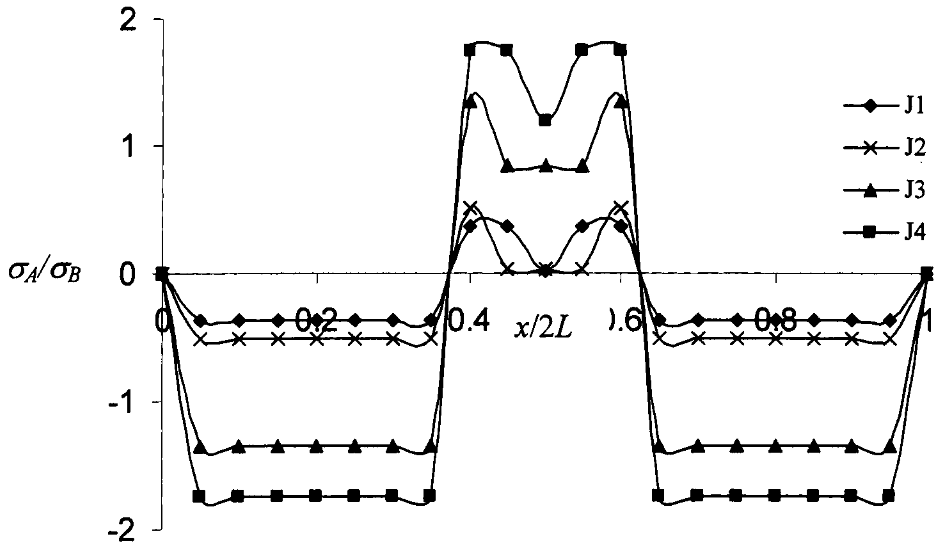

Figure 3.5 Stress ratio excluding self-weight (CASE 1, R1, S1)

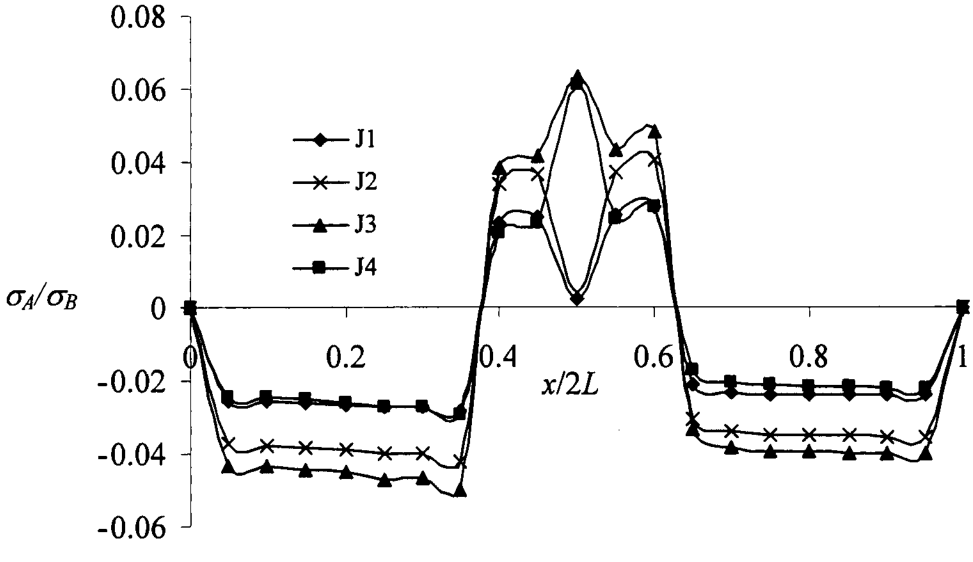

Figure 3.6 Stress ratio including self-weight (CASE 1, R1, S1)

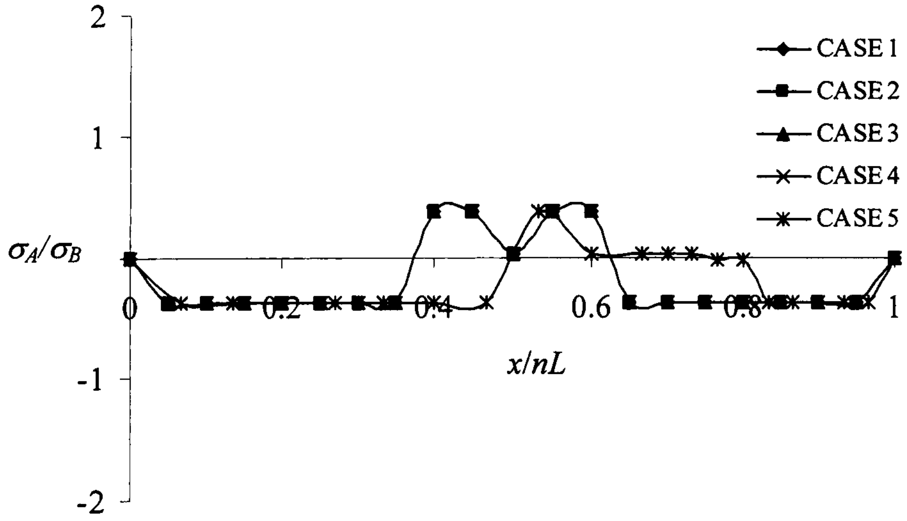

Figure 3.7 Stress ratio excluding self-weight (J1, R1, S1)

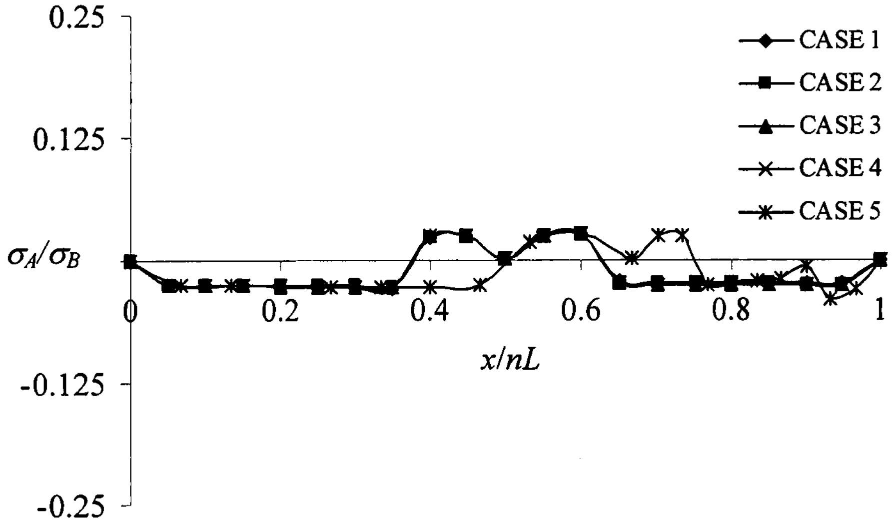

Figure 3.8 Stress ratio including self-weight (J1, R1, S1)

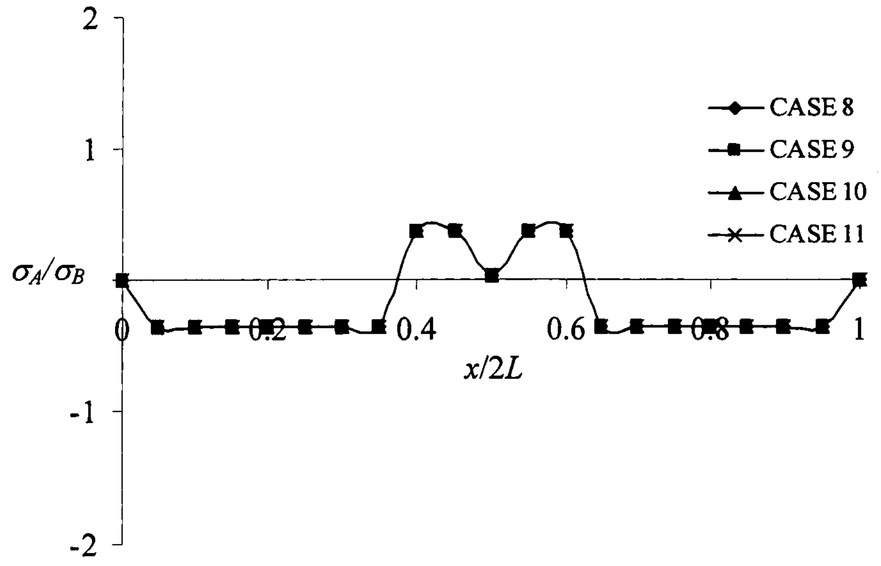

Figure 3.9 Stress ratio excluding self-weight (J1, R1, S1)

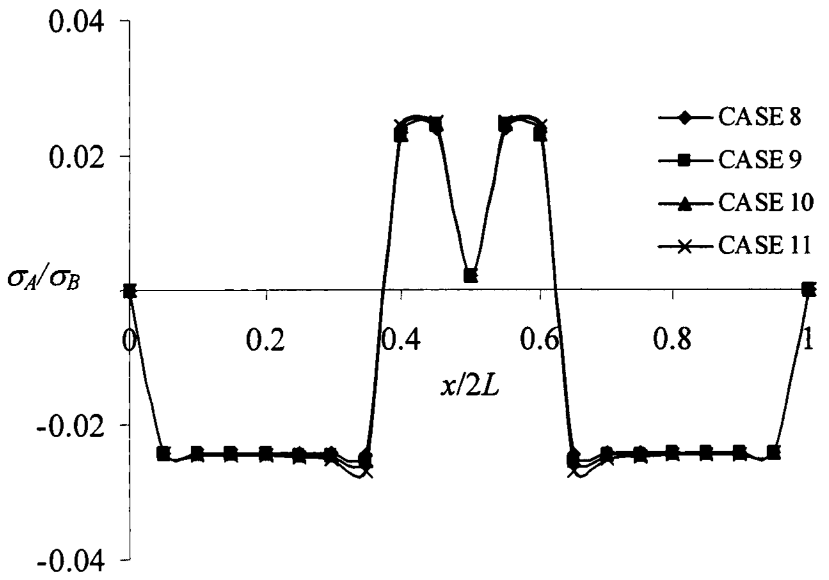

Figure 3.10 Stress ratio including self-weight (J1, R1, S1)

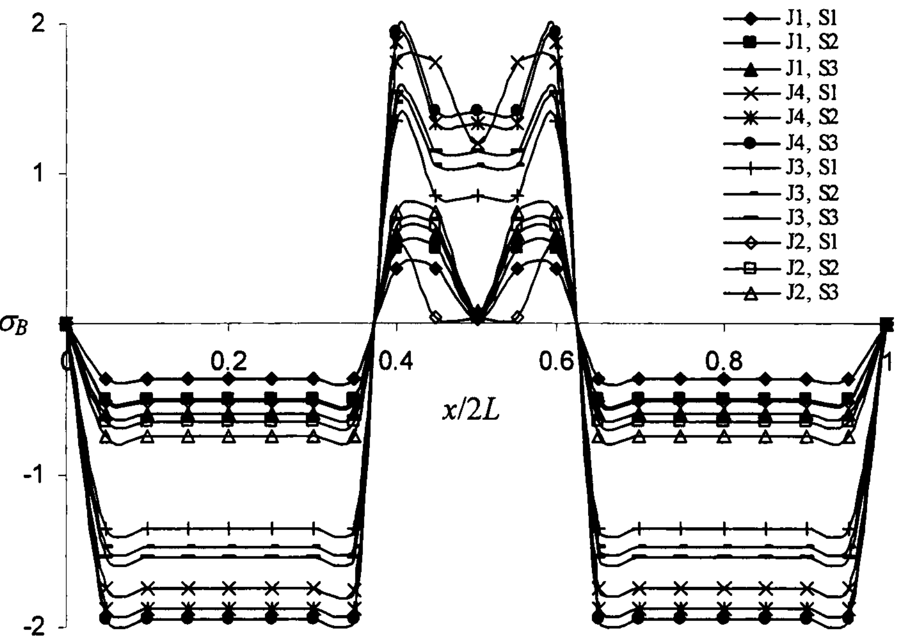

Figure 3.11 Stress ratio excluding self-weight (CASE 1, R1)

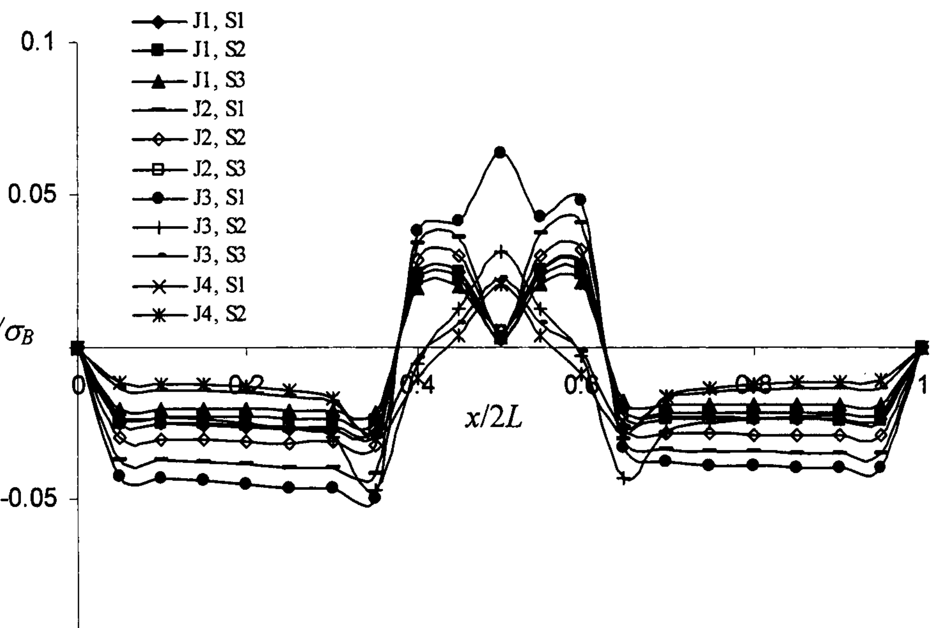

Figure 3.12 Stress ratio including self-weight (CASE 1, R1)

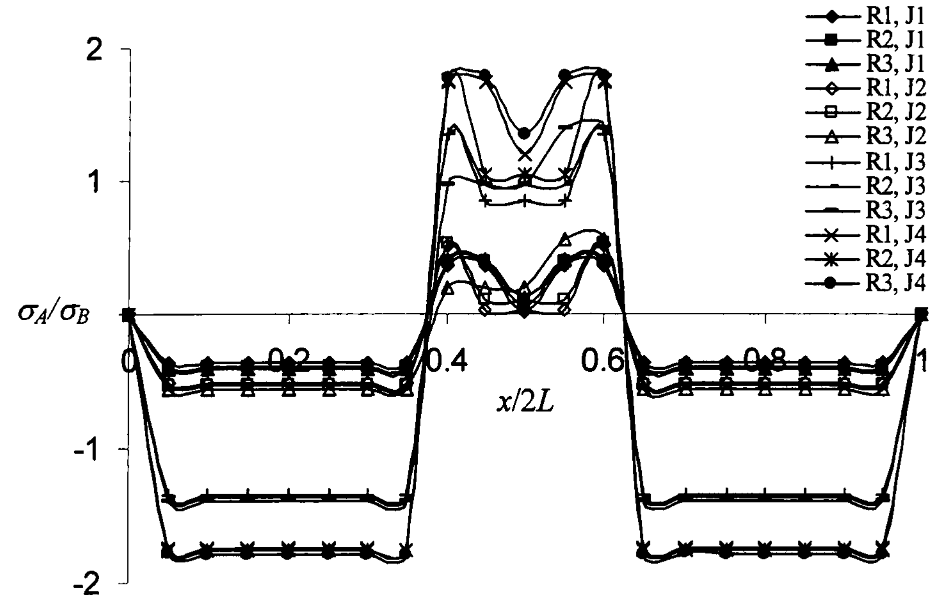

Figure 3.13 Stress ratio excluding self-weight (CASE 1, S1)

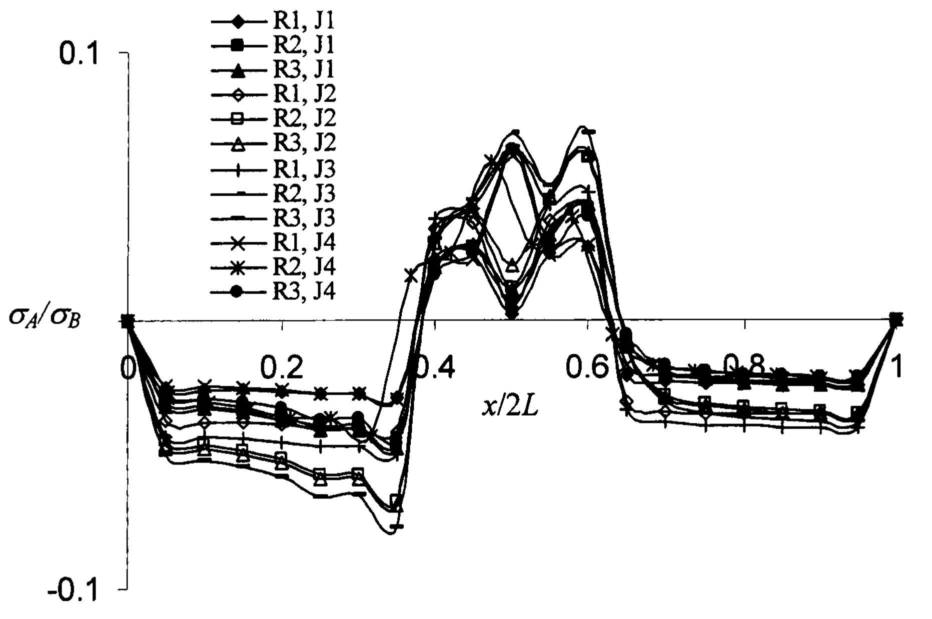

Figure 3.14 Stress ratio including self-weight (CASE 1, S1)

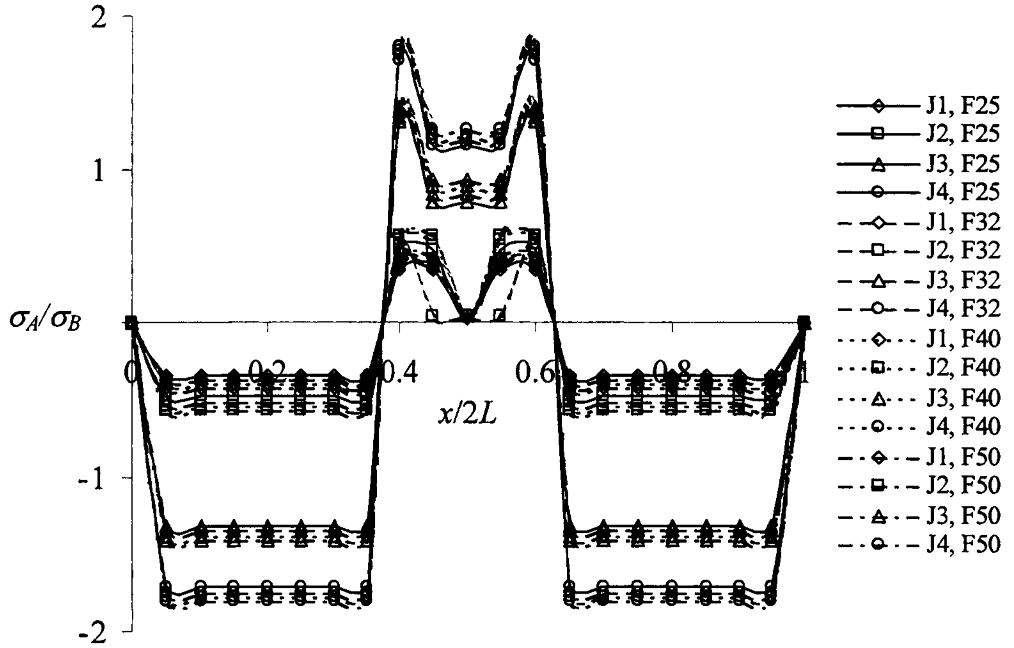

Figure 3.15 Stress ratio excluding self-weight (CASE 1, R1, S1)

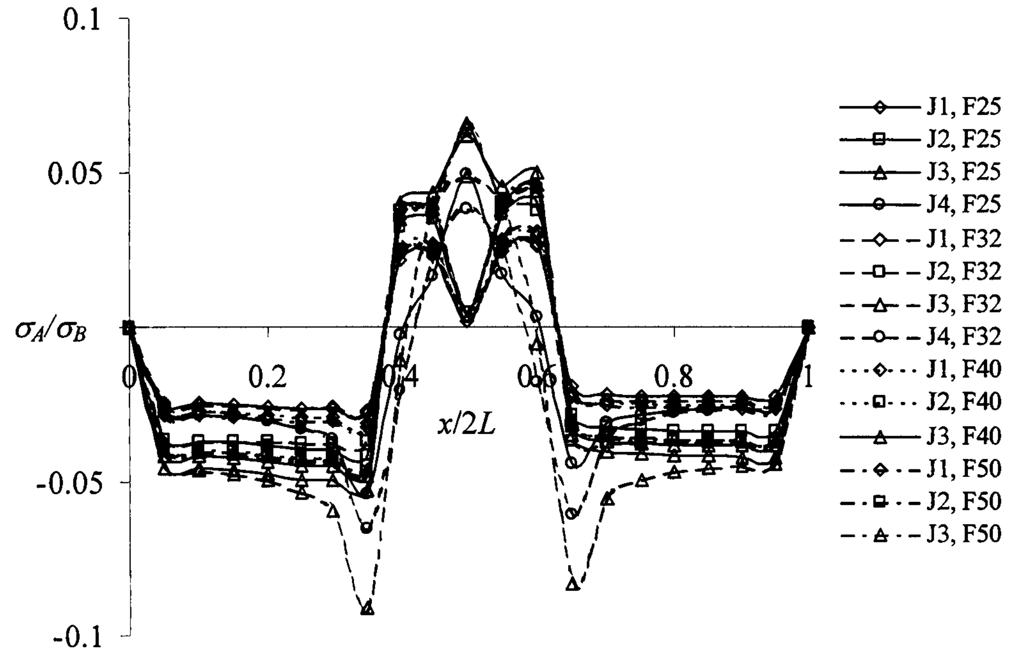

Figure 3.16 Stress ratio including self-weight (CASE 1, R1, S1)

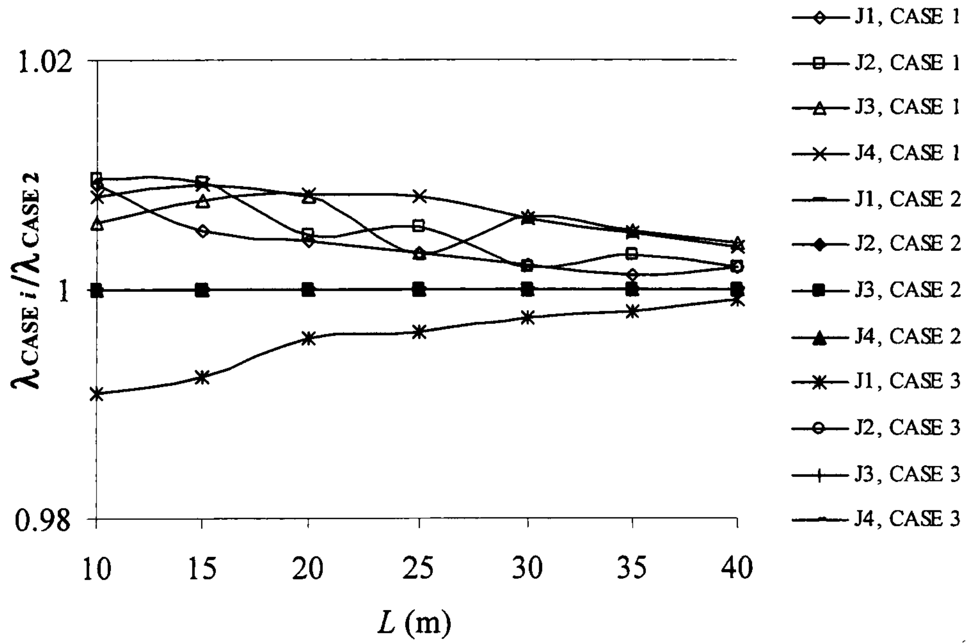

Figure 3.17 Buckling behaviour (R1, S1, propped construction)

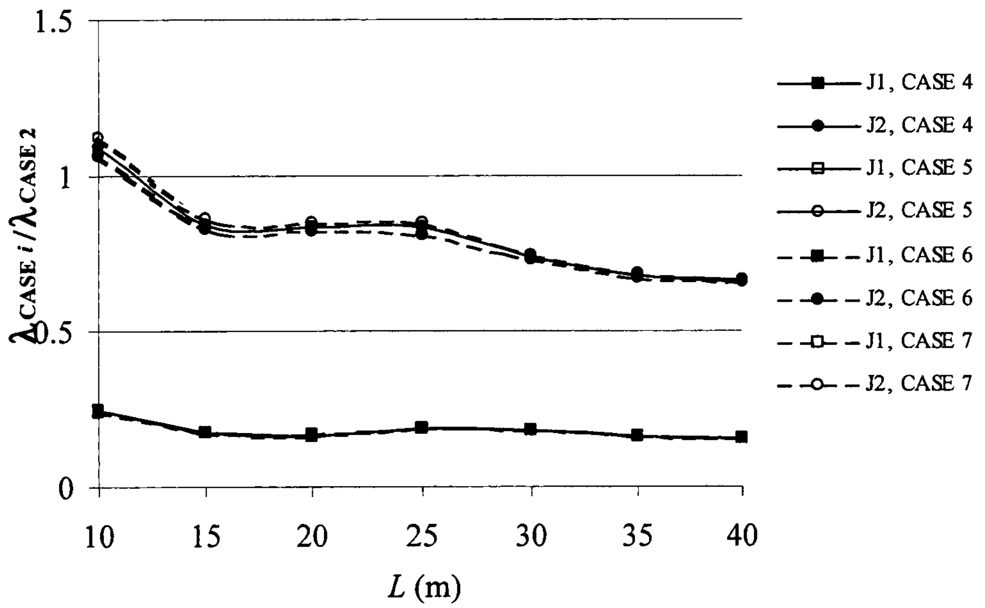

Figure 3.18 Buckling behaviour (R1, S1, propped construction)

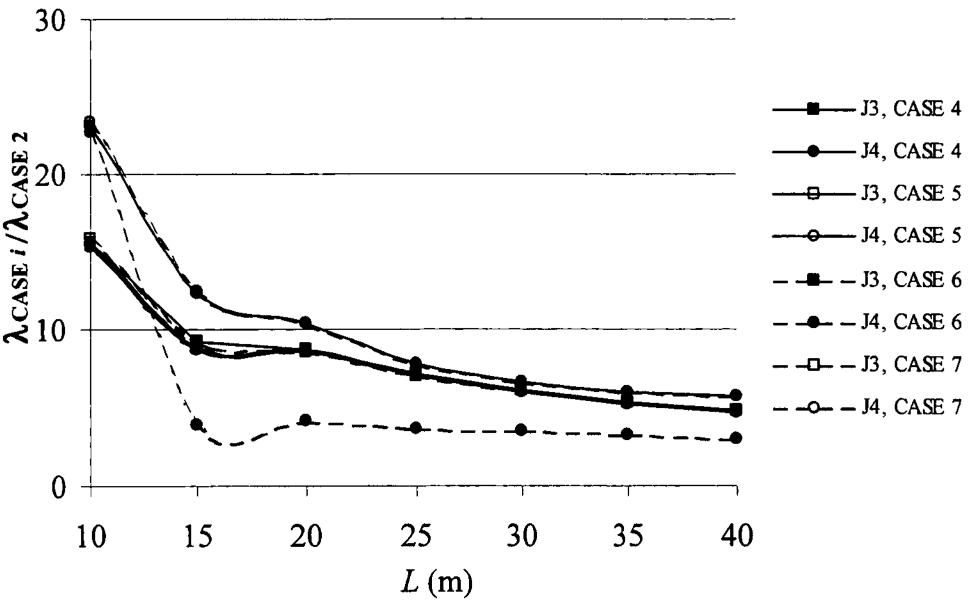

Figure 3.19 Buckling behaviour (R1, S1, propped construction)

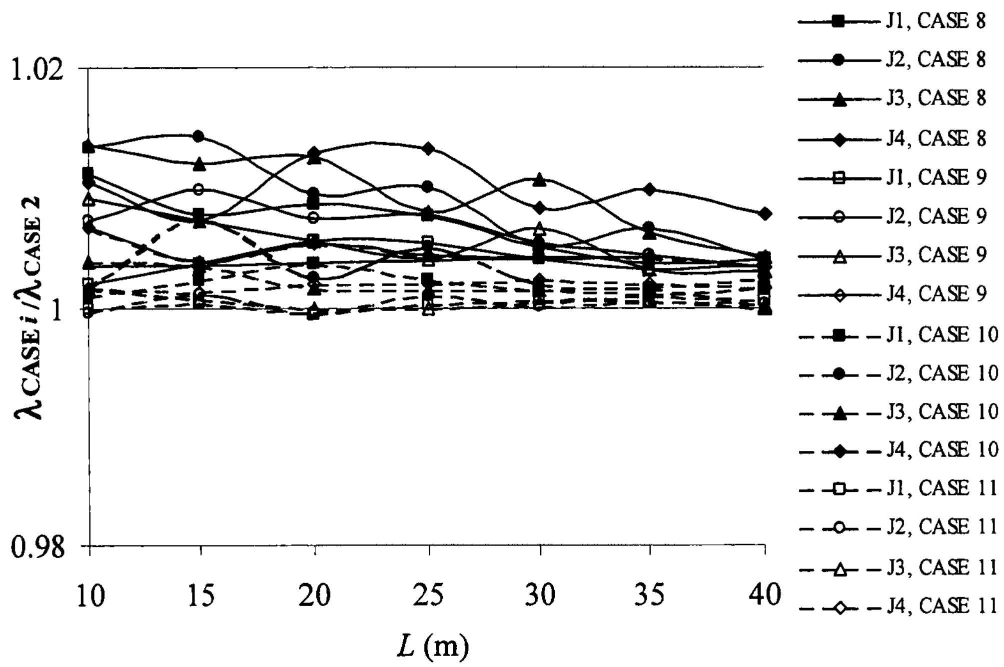

Figure 3.20 Buckling behaviour (R1, S1, propped construction)

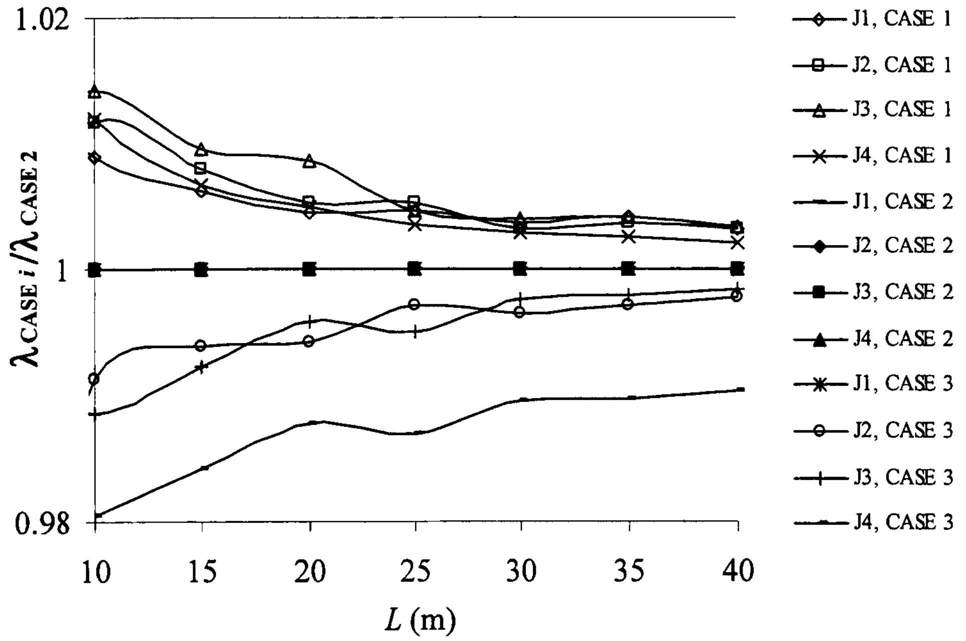

Figure 3.21 Buckling behaviour (R1, S1, unpropped construction)

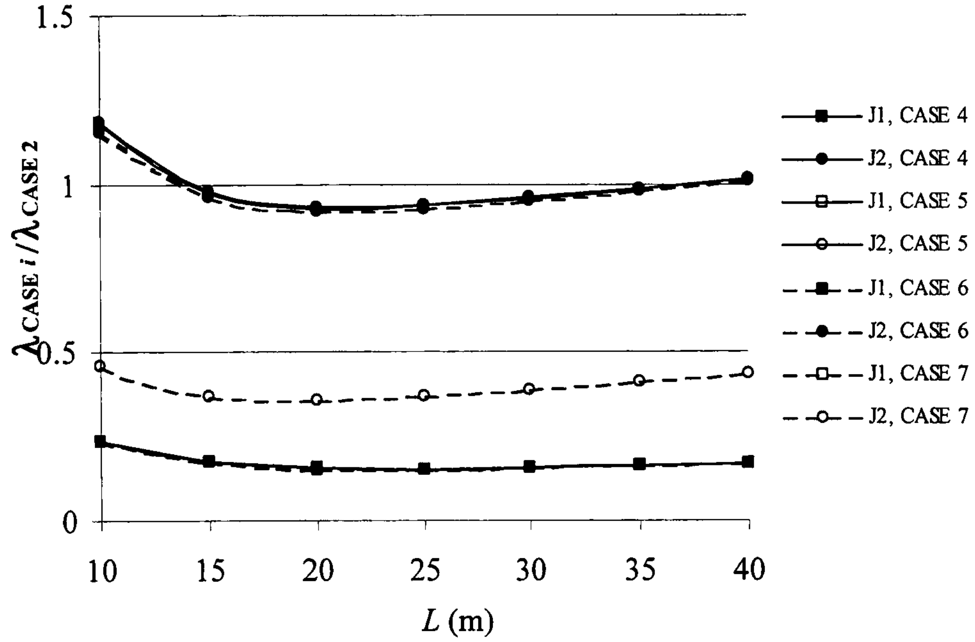

Figure 3.22 Buckling behaviour (R1, S1, unpropped construction)

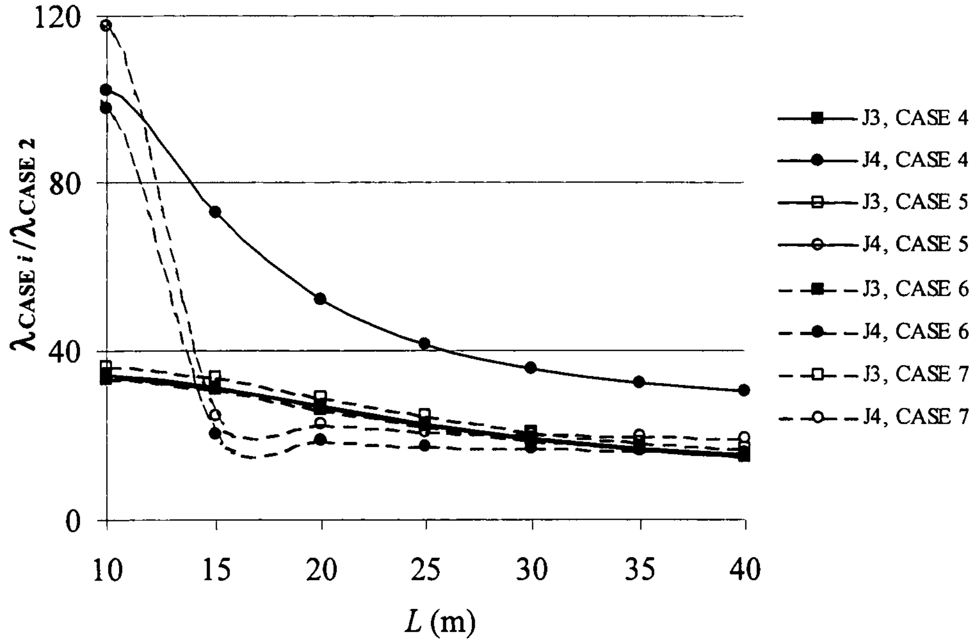

Figure 3.23 Buckling behaviour (R1, S1, unpropped construction)

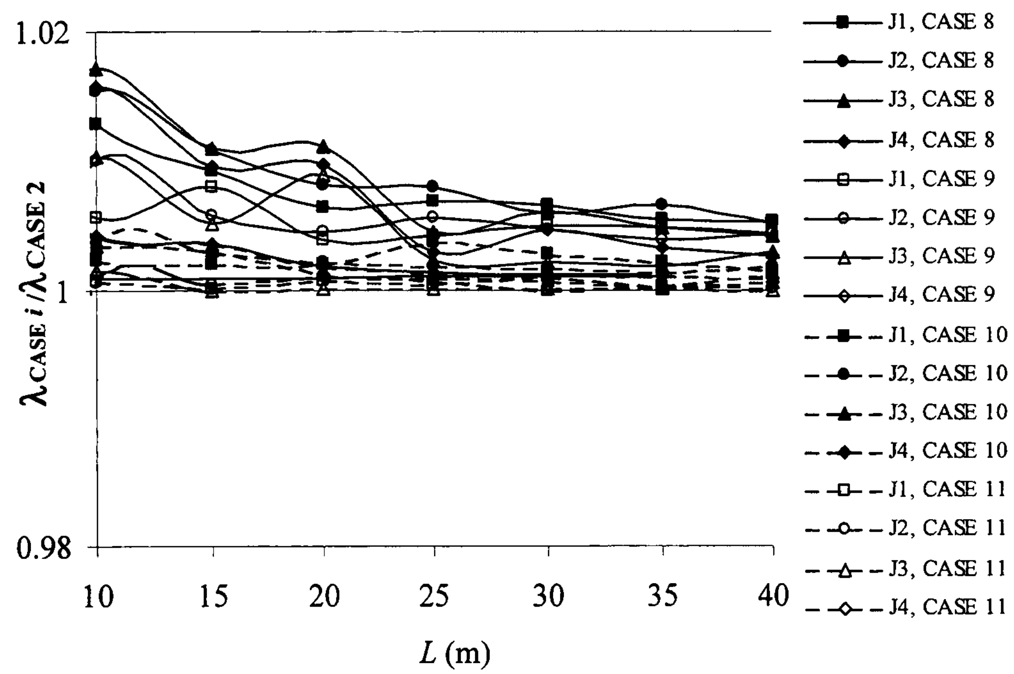

Figure 3.24 Buckling behaviour (R1, S1, unpropped construction)

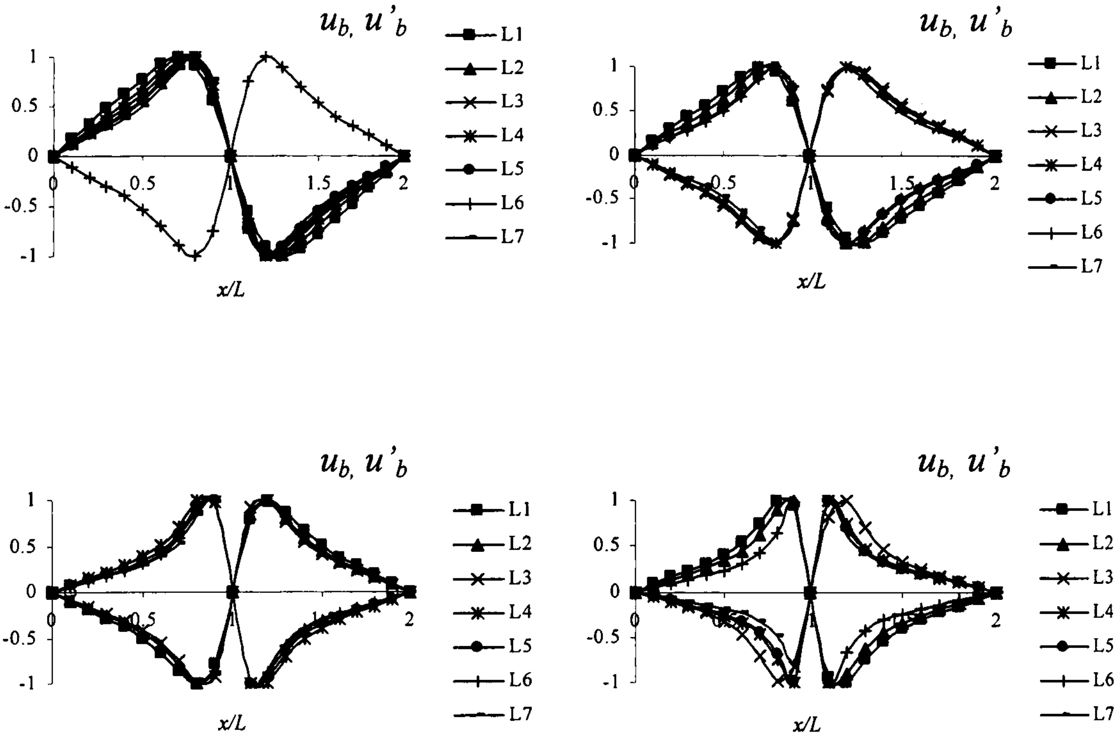

Figure 3.25 Buckling modes (CASE 1, R1, S1, unpropped construction):
(i) J1, (ii) J2, (iii) J3 and (iv) J4

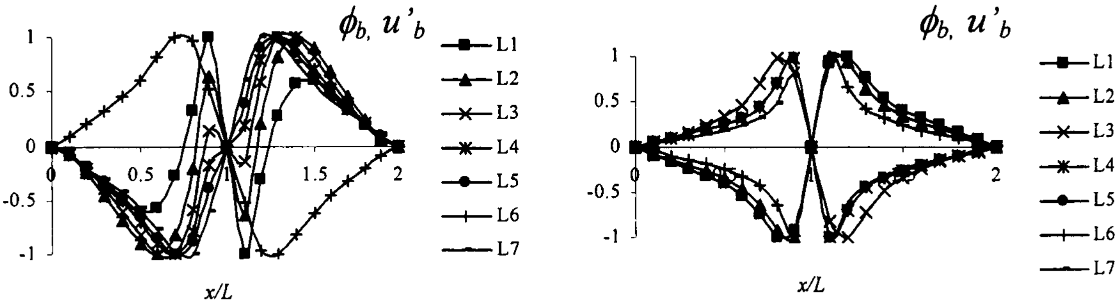

Figure 3.26 Buckling modes (CASE 1, R1, S1, unpropped construction):
(i) J1 and (ii) J4

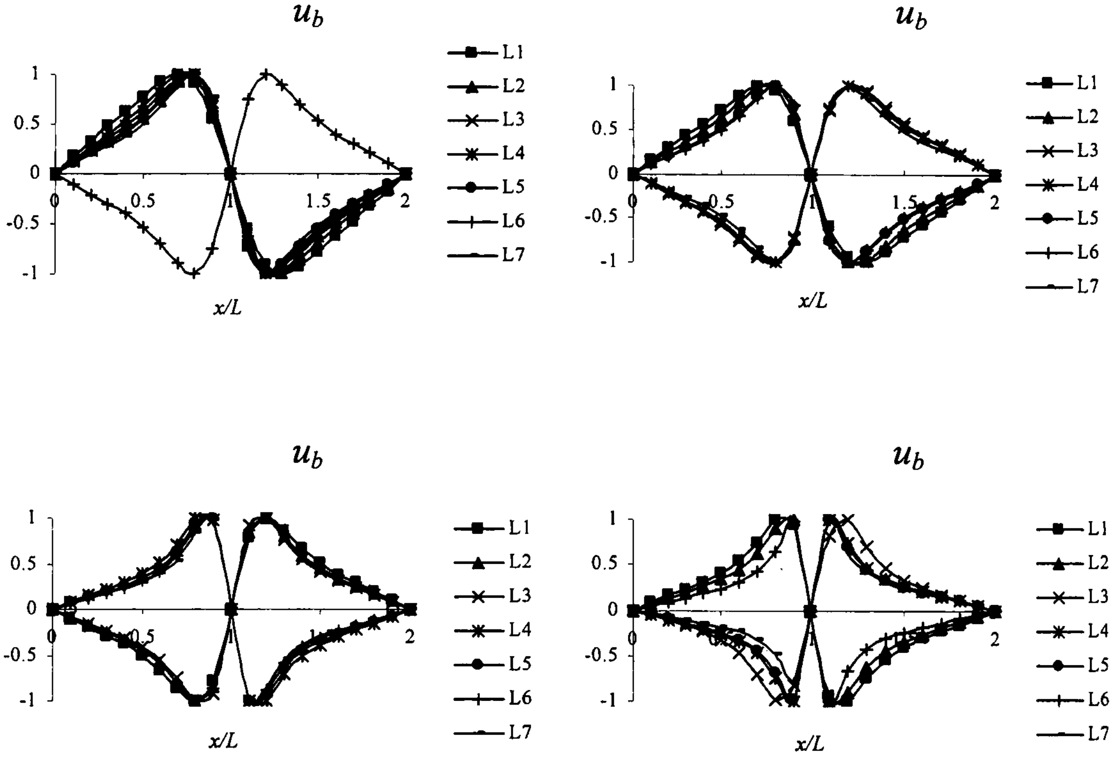

Figure 3.27 Buckling modes (CASE 1, R1, S1, unpropped construction):
(i) J1, (ii) J2, (iii) J3 and (iv) J4

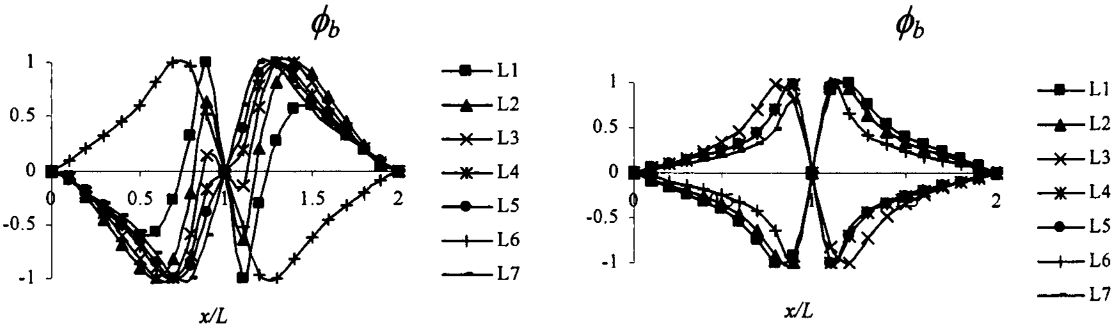

Figure 3.28 Buckling modes (CASE 1, R1, S1, unpropped construction):
(i) J1 and (ii) J4

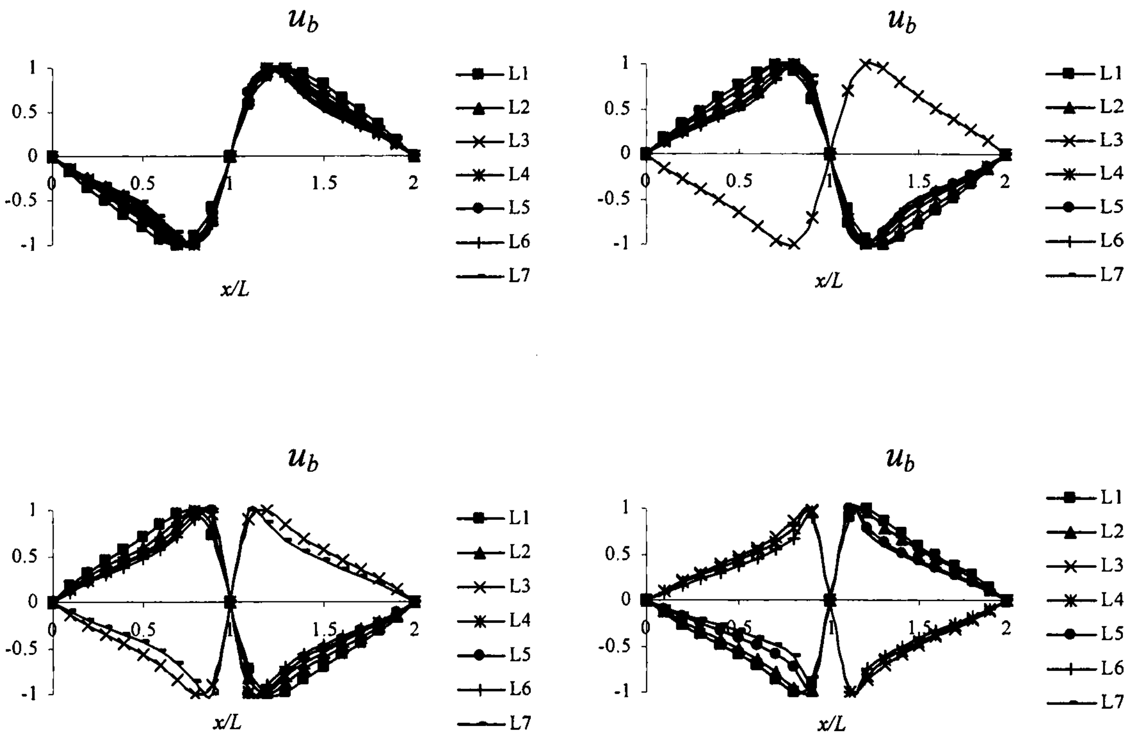

Figure 3.29 Buckling modes (CASE 1, R1, S1, propped construction):
(i) J1, (ii) J2, (iii) J3 and (iv) J4

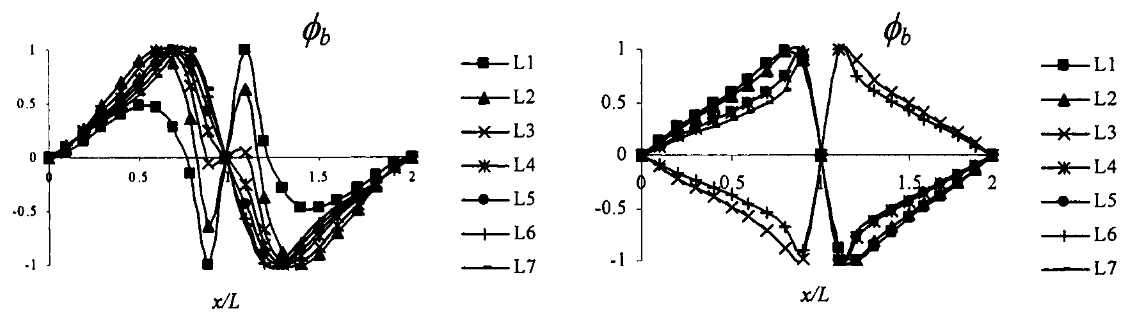

Figure 3.30 Buckling modes (CASE 1, R1, S1, propped construction):
(i) J1 and (ii) J4

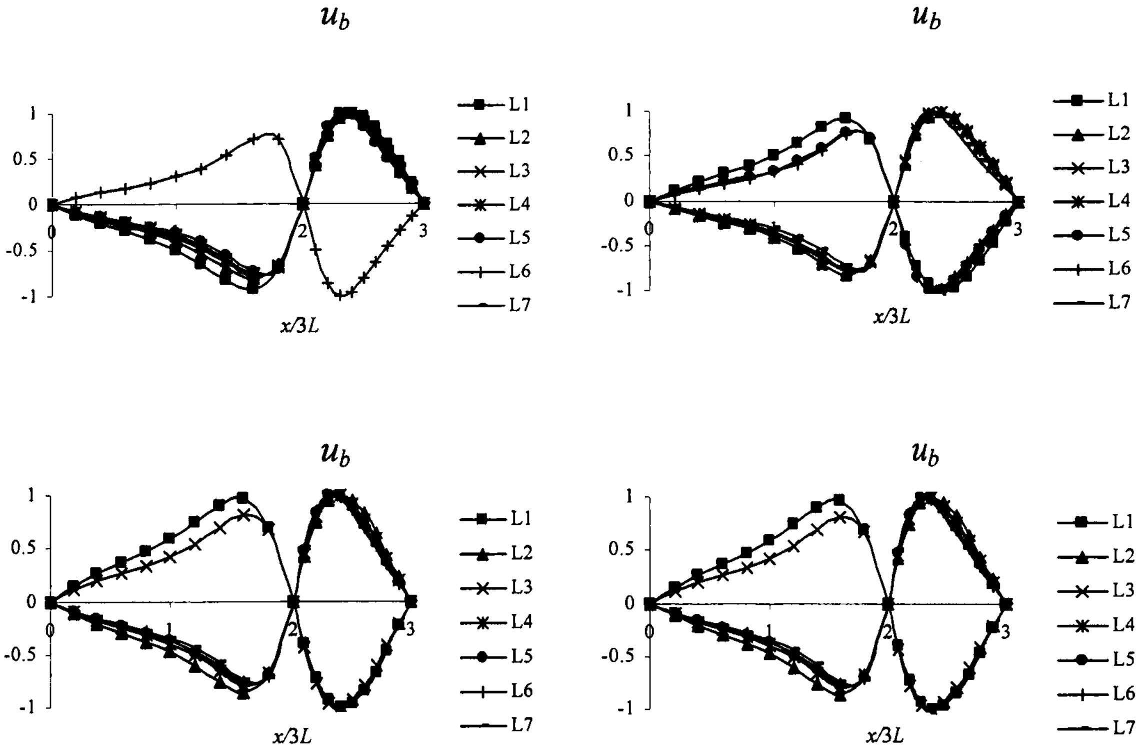

Figure 3.31 Buckling modes (CASE 4, R1, S1, unpropped construction):
(i) J1, (ii) J2, (iii) J3 and (iv) J4

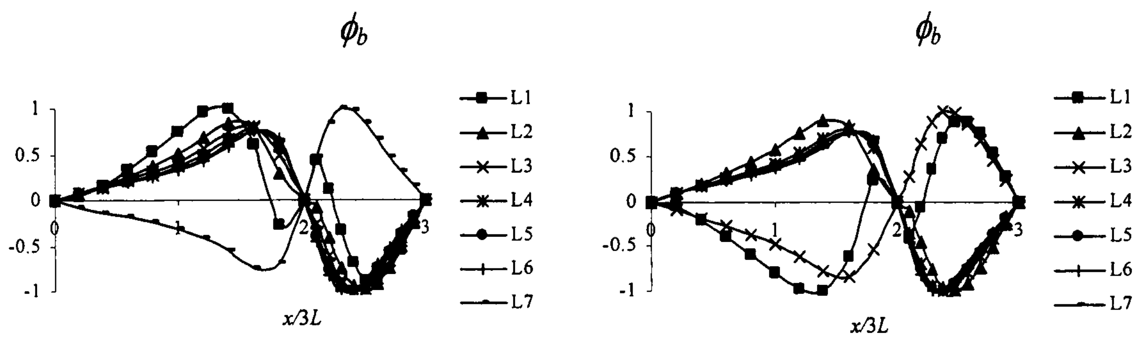

Figure 3.32 Buckling modes (CASE 4, R1, S1, unpropped construction):
(i) J1 and (ii) J4

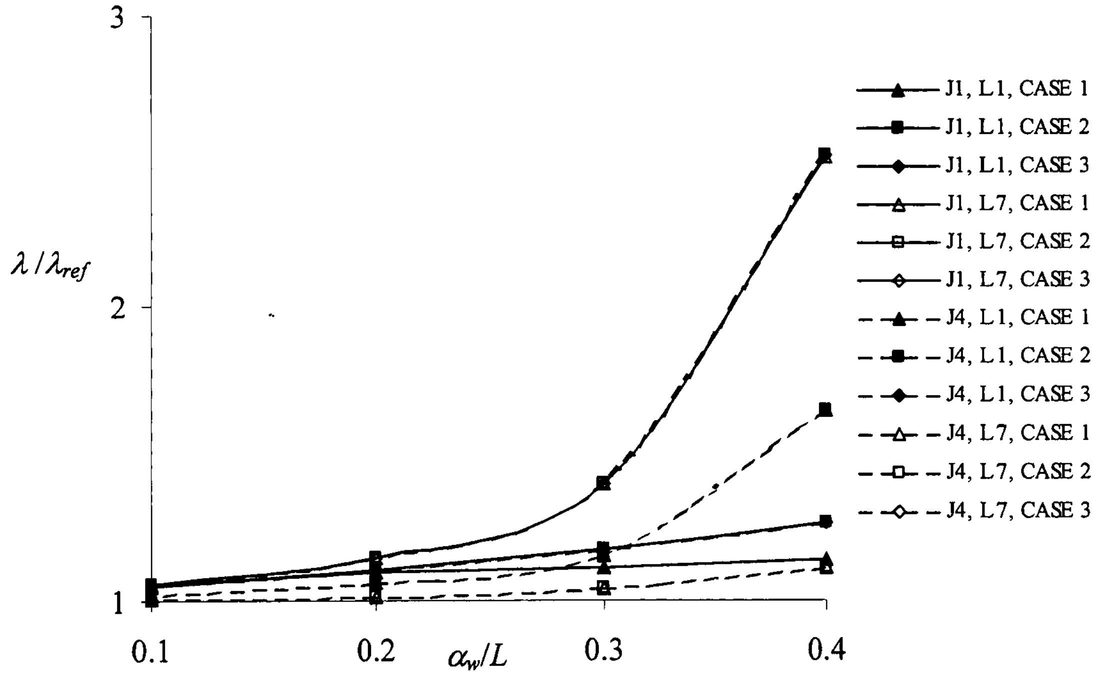

Figure 3.33 Bottom flange bracing (R1, S1, unpropped construction)

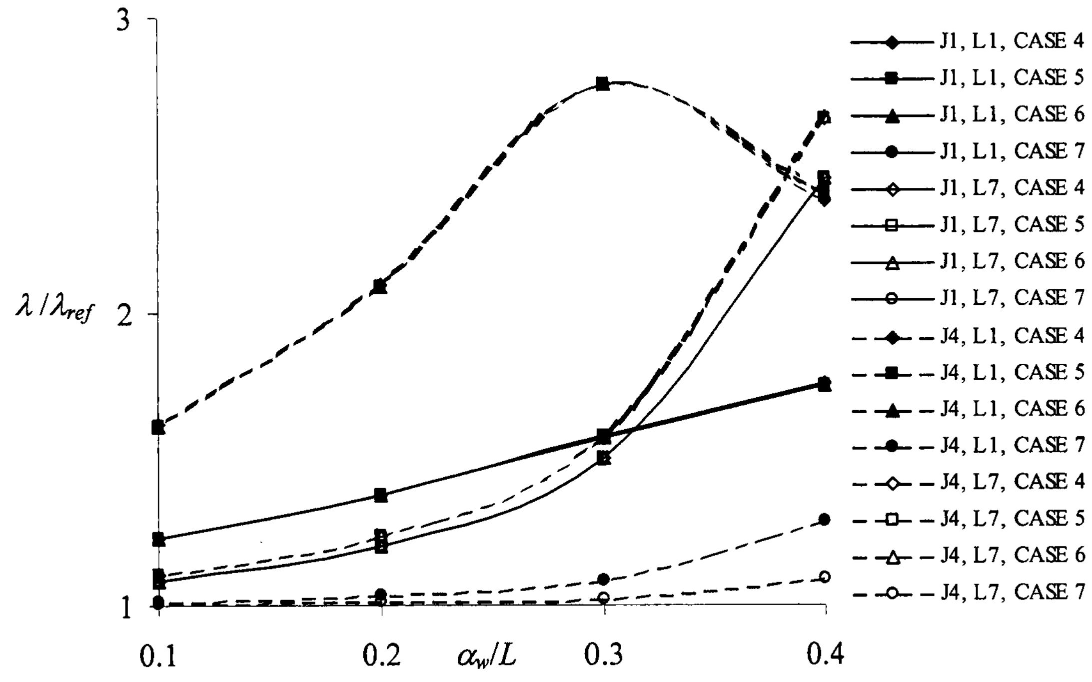

Figure 3.34 Bottom flange bracing (R1, S1, unpropped construction)

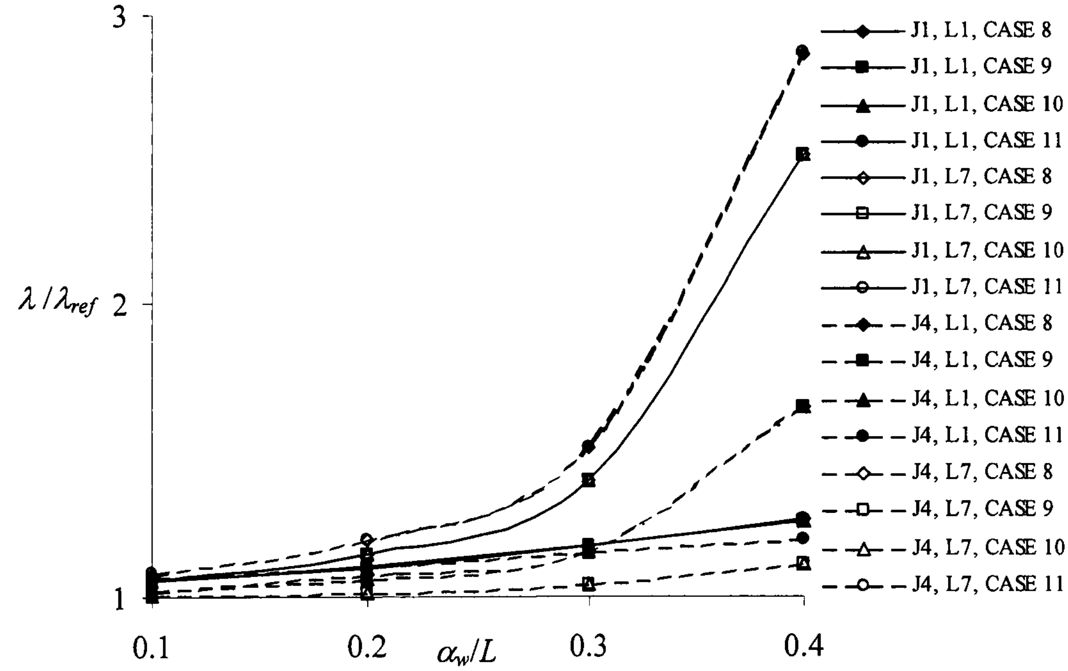

Figure 3.35 Bottom flange bracing (R1, S1, unpropped construction)

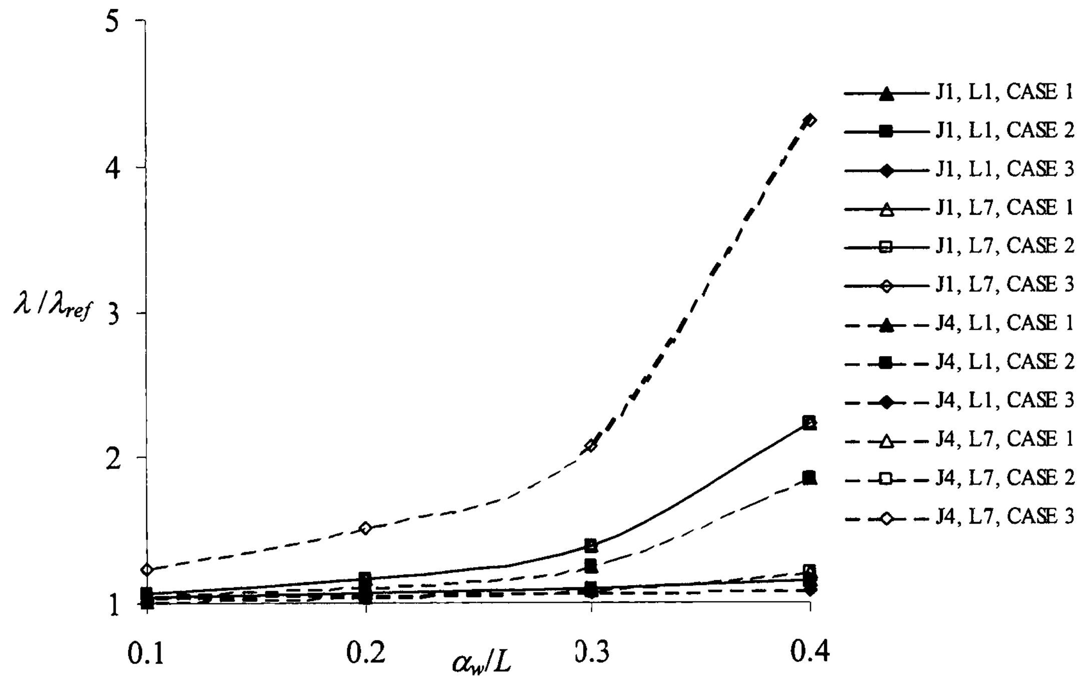

Figure 3.36 Bottom flange bracing (R1, S1, propped construction)

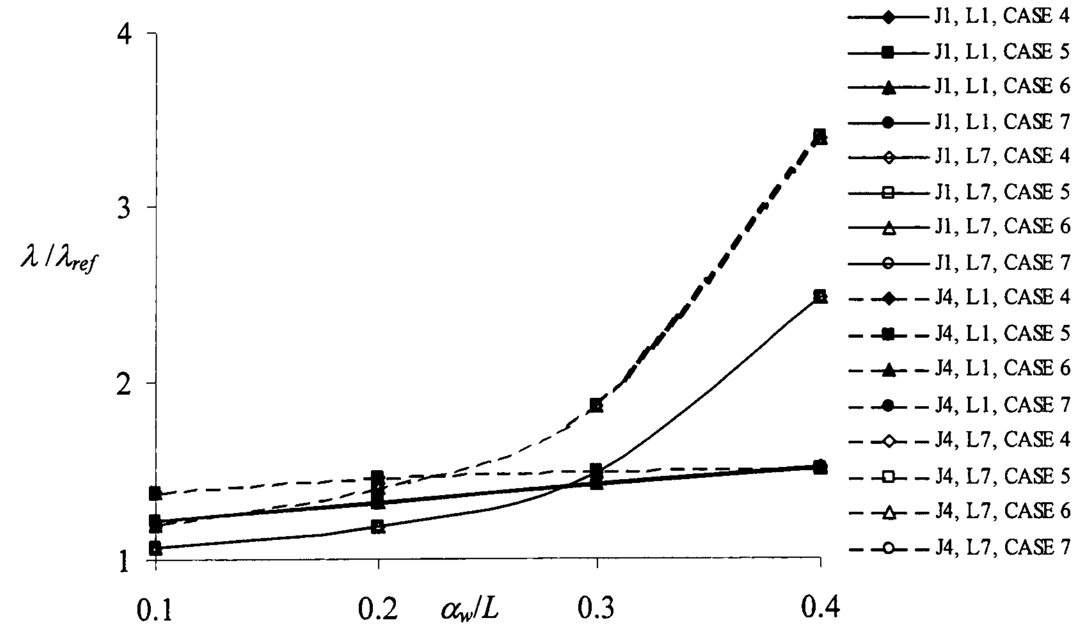

Figure 3.37 Bottom flange bracing (R1, S1, propped construction)

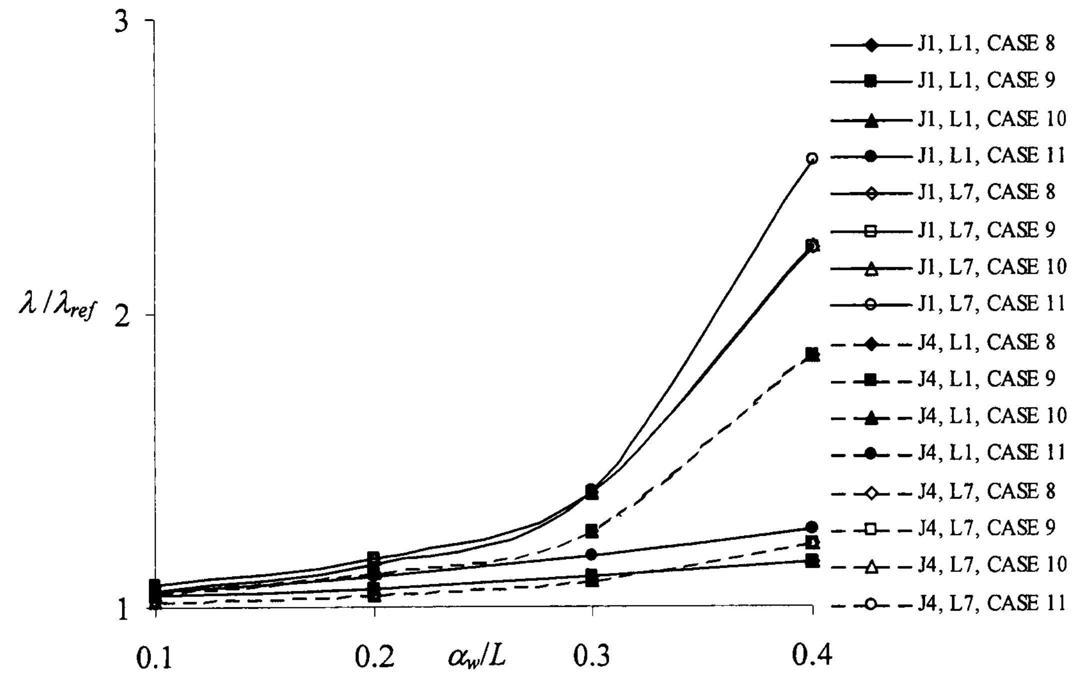

Figure 3.38 Bottom flange bracing (R1, S1, propped construction)

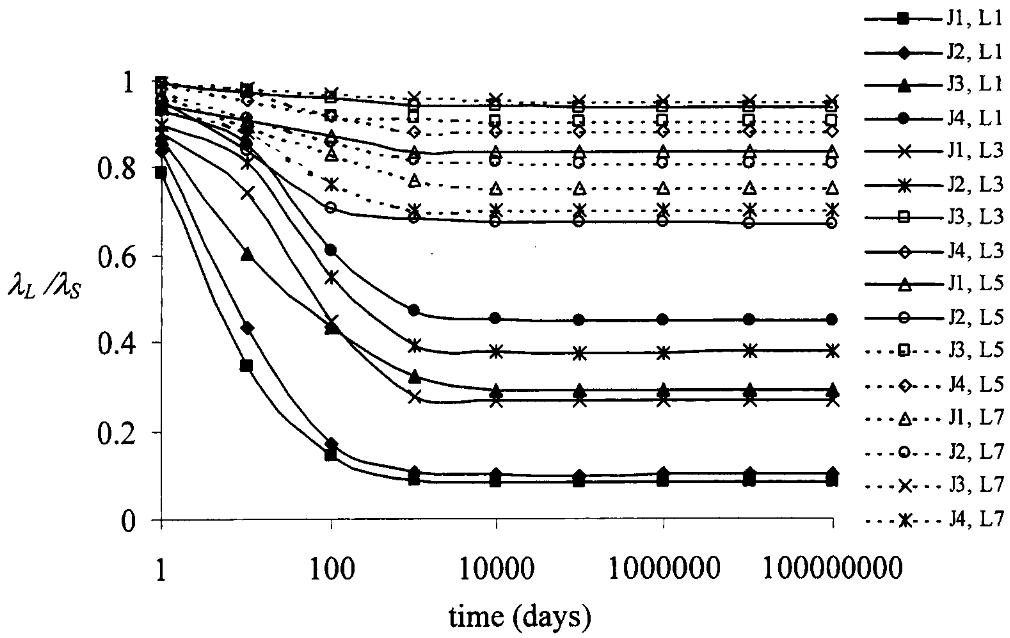

Figure 3.39 Creep and shrinkage effects (R1, S1, equal spans, unpropped construction)

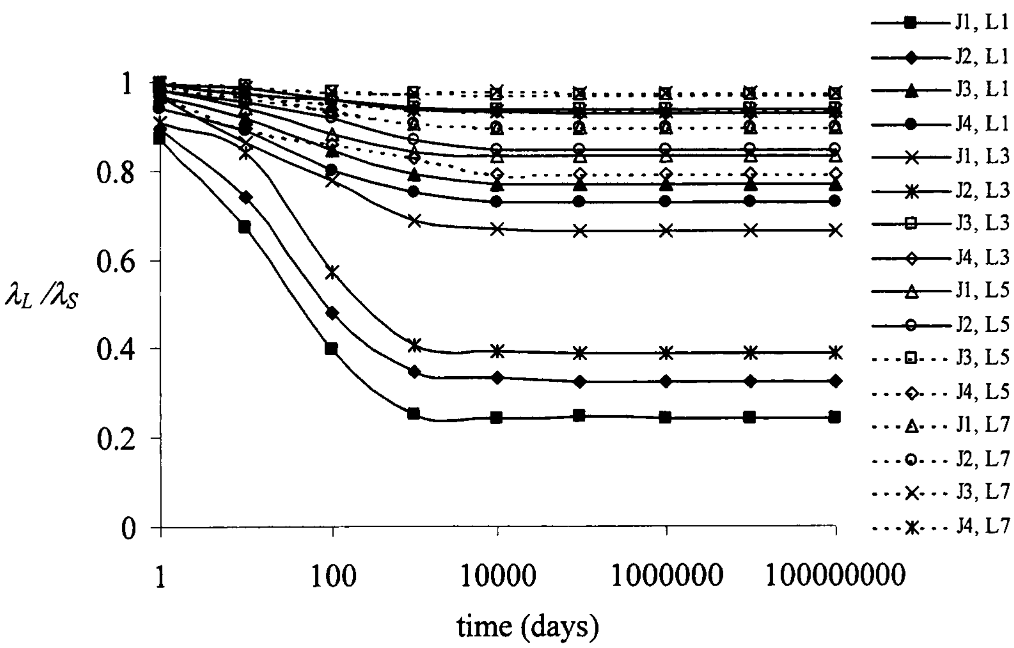

Figure 3.40 Creep and shrinkage effects (R1, S1, unequal spans, unpropped construction)

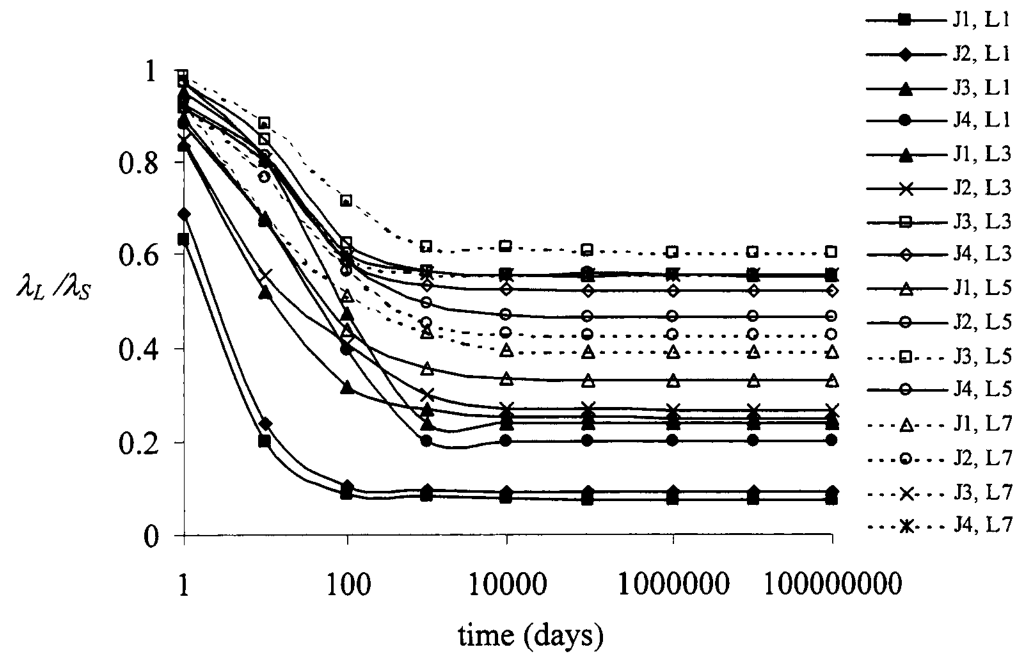

Figure 3.41 Creep and shrinkage effects (R1, S1, equal spans, propped construction)

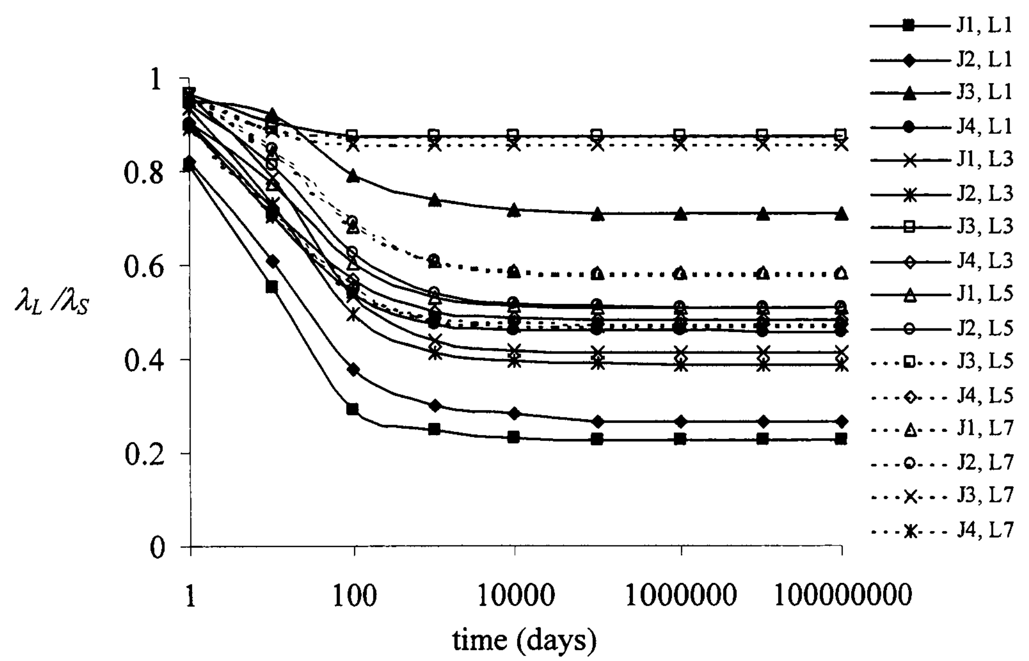

Figure 3.42 Creep and shrinkage effects (R1, S1, unequal spans, propped construction)

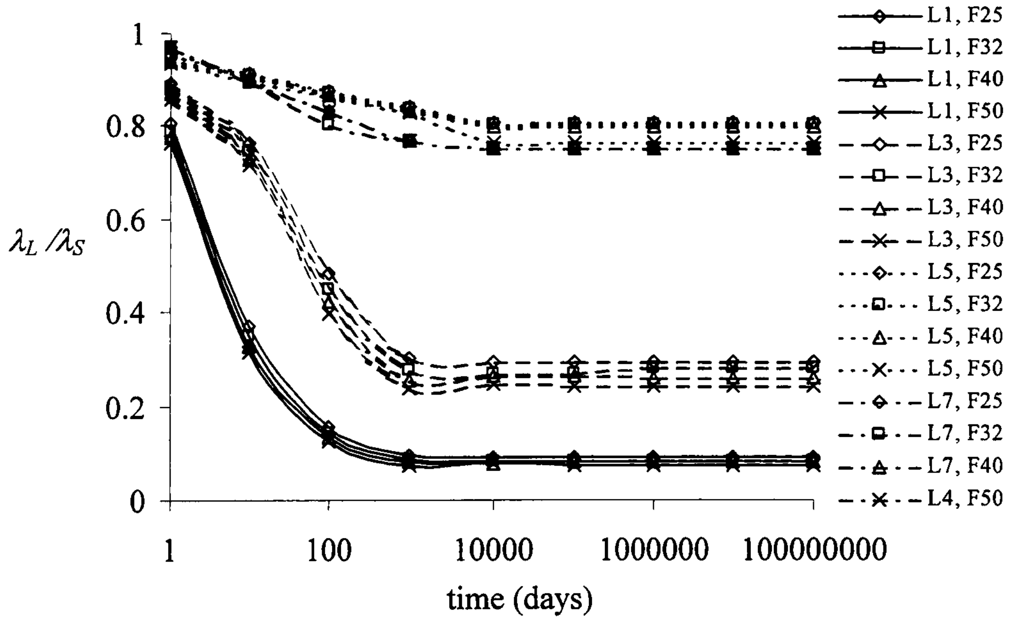

Figure 3.43 Creep and shrinkage effects (J1, R1, S1, equal spans, unpropped construction)

Chapter 4

ELASTIC RESTRAINED DISTORTIONAL BUCKLING OF I-SECTION MEMBERS

TABLE OF CONTENTS

4.1 INTRODUCTION

The purpose of this chapter is to present a simple generic model that may be used for studying the elastic restrained-distortional buckling (RDB) of I-section members restrained completely and continuously against lateral translation and lateral rotation at one flange level, but elastically against twist rotation at this flange level, when subjected to moment and axial force gradient. This situation is typically encountered in half-through girder bridges and in a composite steel-concrete tee-beam subjected to negative or hogging bending.

In a half-through girder bridge and in a composite steel-concrete tee-beam subjected to negative or hogging bending, instability of the steel section becomes a design problem. The overall mode of buckling in those two structural configurations must necessarily be restrained-distortional (Bradford 1997a), since continuous restraint exists at the tension flange level of the I-section girder and which inhibits buckling deformations at this position. The RDB takes place at longer half-wavelengths than local buckling, and is characterised by simultaneous lateral deflections and cross-sectional distortion at the bifurcation of equilibrium, as shown in Fig. 1.2a. Distortion during the buckling arises since the cross-section is physically unable to remain undeformed as would be predicted in the commonly adopted Vlasov (1961) thin-walled theory.

RDB is fundamentally different to the more commonly studied distortional buckling of laterally unrestrained beams (Ronagh & Bradford 1998), and can have a profound influence on the buckling of beams with a continuous restraint. The RDB resistance of the steel I-section component of a half-through girder and a composite steel-concrete tee-beam subjected to negative or hogging bending is dependent on the extent to which the usually slender web is able to transmit the restraining action, provided by the deck at the level of the tension flange, to the unstable compression flange. Conventionally I-sections have stockier flanges than webs.

Half-through girder bridges are in general comprised of two parallel I-section beams joined by a concrete deck at the bottom/tension flange level as illustrated in Fig. 4.1. The compression flange of the I-section is restrained only by the stiffness of the usually flexible web and the tension flange is provided with continuous torsional restraint through its connection to the concrete deck. An arrangement analogous to this one is that of a heavily loaded beam supported on seats and shown in Fig. 4.2. The utilisation of half-through girders in bridge construction is most usually a result of constraints on headroom. They find frequent use in railway bridges over roadways, where the grade of the railway is predetermined and it is difficult to provide a substructure to support the bridge deck. When the superstructure is in the form of I-section girders, the top flange of the girder is subjected to compression and cannot be easily braced laterally, except by the provision of transverse web stiffeners which may be used to design against buckling in shear. Conservatively, the girder may be designed against lateral buckling without bracing of the compression flange. However, this conservatism can be highly excessive, and advantage must be taken of the restraint provided at the tension flange level by the bridge deck.

A similar buckling mode to a half-through girder bridge occurs in the overall buckling of continuous composite tee-beams in regions of negative bending (Hamada & Longworth 1974; Johnson & Bradford 1983; Weston *et al.* 1991; Bradford & Gao 1992; Williams *et al.* 1993; Lindner 1998). Many other structural elements, such as roof and wall cladding, which are intended primarily for other purposes, also provide restraints against buckling. For example, rafters in industrial buildings are usually restrained against buckling by purlins attached to one flange, and which when spaced reasonably close enough can be considered as continuous since the purlin/cladding system provides diaphragm and flexural restraint.

As discussed in Chapter 3 (section 3.3) buckling of half-through girder bridges is usually and simplistically modelled in design codes using the so-called U-frame method, in which the top compression flange of the I-section girder is considered as a strut compressed uniformly along its length by the bending stresses induced in it, and which is restrained elastically and continuously in the transverse direction along its length by the web. This model is attractive, since a closed form solution exists for the elastic critical load of such a strut, and it is easy to determine the flexural stiffness of a web plate. However, half-through girder bridges are generally used in situations where there is considerable moment gradient and for that reason the U-frame approach is overly conservative since it ignores the effect of moment gradient, and does not include any instability effects that may also occur in the web.

Despite RDB being the governing buckling mode for many engineering structures that are commonly designed, such as a half-through girder bridge and composite steel-concrete tee-beam subjected to negative or hogging bending, its accurate prediction is still a grey area in structural mechanics. Even for elastic buckling, the problem is complex, and recourse needs to be made to a suitable numerical procedure to handle each individual case. Existing research into lateral-distortional buckling of restrained beams has been generally limited to a uniform bending, which cannot represent the realistic loading condition experienced in most composite steel-concrete structures.

This chapter, therefore, addresses the issue of the buckling of half-through girders by developing a generic approach to the problem using a Ritz-based procedure. The bridge girder is assumed to be of doubly-symmetric I-section, simply supported at its ends, and without web stiffeners that would be deployed for stiffening for shearing actions. The bottom flange of the girder is restrained at the deck level fully against translational and lateral rotational buckling deformations, but is restrained elastically against twist rotation by the flexibility of the deck between adjacent girders. The method is then modified to address the distortional buckling of continuously restrained monosymmetric beams and beam-columns under transverse load. In plain steel beams, most transverse loads are not applied directly at mid-height but instead are applied above or below this location. However, the height of transverse loading is only important if the point of load application can twist and this is clearly not the case for a half-through bridge girder or for a continuous composite beam.

While the results in this chapter provide useful additions to research findings, the main motivation is to develop an energy method that can be modified to handle the monosymmetry caused by residual stresses in the inelastic buckling analysis developed in subsequent chapters of this thesis.

4.2 BUCKLING MODEL

The method used in this study is a simple Ritz-based energy procedure. This energy approach requires assumptions for the deformations of the beam-column as it departs its (trivial) primary equilibrium path at bifurcation, and that the prebuckling deformations are not coupled with the buckling deformations. The deformations of the cross-section shown in Fig. 4.3 are defined as the lateral deformation u_T and twist ϕ_T of the top flange, and twist ϕ_B of the bottom flange as shown. If the assumption verified elsewhere (Bradford 1992a) that the stocky flanges do not deform during buckling, but that the web deforms in its cross-section as a cubic curve, then the buckling deformation

$$\vec{u} = \langle u_T, \phi_T, \phi_B \rangle^T \tag{4. 1}$$

defines the buckled configuration of the cross-section at any position z from the origin of the beam of length L.

It is assumed that the web is unstiffened, except for load bearing stiffeners at the ends, which provide simple support to the member against out-of-plane buckling. The buckling deformations consistent with the kinematic boundary conditions are taken as

$$\vec{u} = \vec{q}\sum_{i=1}^{n} \sin i\pi\xi \tag{4. 2}$$

in which $\vec{q} = \langle q_1, q_2, q_3 \rangle^T$ are the maximum values of the deformations $\langle u_T, \phi_T, \phi_B \rangle^T$ respectively, and $\xi = z/L$. The cubic deformation of the web during buckling is written as

$$u_W = h_w\left(\alpha_1 + \alpha_2\eta + \alpha_3\eta^2 + \alpha_4\eta^3\right)\sum_{i=1}^{n} \sin i\pi\xi \tag{4. 3}$$

and invoking the conditions of displacement and slope compatibility of the flanges and web at the two flange-web junctions (Bradford 1997a) allows the polynomial coefficients in Eqn. 4.3 to be expressed as

$$\vec{\alpha} = \overline{C}\vec{q} \tag{4.4}$$

$$\begin{Bmatrix} \alpha_1 \\ \alpha_2 \\ \alpha_3 \\ \alpha_4 \end{Bmatrix} = \begin{bmatrix} 1/2h_w & -1/8 & 1/8 \\ 3/2h_w & 1/4 & 1/4 \\ 0 & 1/2 & -1/2 \\ -2/h_w & -1 & -1 \end{bmatrix} \begin{Bmatrix} q_1 \\ q_2 \\ q_3 \end{Bmatrix}. \tag{4.5}$$

Equations 4.3, 4.4 and 4.5 thus define the web displacements in terms of the buckling degrees of freedom, q_1, q_2 and q_3.

The energy approach requires the calculation of the total change in potential

$$\Pi = U - V \tag{4.6}$$

where U = the strain energy stored during buckling and V = the work done by the applied actions. The strain energy U is composed of three components; viz. the strain energy stored in the top flange due to lateral deformation and twist rotation and the strain energy stored in the bottom flange due to twist rotation U_F, the strain energy stored in the web due to flexure U_W and the strain energy stored in the continuous bottom flange restraint during twist rotation U_R. The work done, V, during buckling is associated with fibre shortening during buckling under a stress $\sigma(y,z)$. In calculating the strain energy, the flange components are based on simple beam theory, while the web component is based on isotropic plate theory (Bradford 1997a). Hence,

$$U_F = \frac{1}{2}\int_0^L \left\{EI_{yF}u_T^2,_{zz} + GJ\left(\phi_T^2,_z + \phi_B^2,_z\right)\right\}dz \tag{4.7}$$

$$U_W = \frac{1}{2}\beta\int_0^L \int_{-h_w/2}^{\frac{h_w}{2}} \left\{u_W^2,_{yy} + u_W^2,_{zz} - 2(1-\nu)\left(u_W,_{yy}\, u_W,_{yy} - u_W^2,_{yz}\right)\right\}dydz \tag{4.8}$$

$$U_R = \frac{1}{2}\int_0^L k_z\phi_B^2 dz \tag{4.9}$$

where commas denote partial differentiation, ν = Poisson's ratio, k_z = the continuous twist rotation stiffness at the bottom flange, EI_F = flexural rigidity of the flange about an axis through the web, GJ = the Saint Venant torsional rigidity of the flange, and

$$\beta = \frac{Et_w^3}{12(1-\nu^2)}. \tag{4. 10}$$

The strain energy U_F stored in the flanges during buckling can be written as

$$U_F = \frac{1}{2}\int_0^L \bar{\varepsilon}_F \overline{D}_F \bar{\varepsilon}_F \mathrm{d}z \tag{4. 11}$$

where $\overline{D}_F$ is the appropriate flange property matrix given by

$$\overline{D}_F = \begin{bmatrix} EI_T & 0 & 0 \\ 0 & GJ_T & 0 \\ 0 & 0 & GJ_B \end{bmatrix}. \tag{4. 12}$$

The elastic shear modulus G is used to calculate the torsional strain energy stored during buckling of the flanges, where

$$G = \frac{E}{2(1+\nu)}. \tag{4. 13}$$

By making the assumption that the flanges deflect and twist as rigid bodies, the generalized strain vector is

$$\bar{\varepsilon}_F = \langle u_{T},_{zz},\ \phi_{T},_{z},\ \phi_{B},_{z} \rangle^T. \tag{4. 14}$$

The vector $\bar{\varepsilon}_F$ can be obtained by suitable differentiation of Eqn. 4.2 so that

$$\bar{\varepsilon}_F = \overline{B}_F \langle q_1, q_2, q_3 \rangle^T. \tag{4. 15}$$

Thus by substituting Eqns. 4.12 and 4.14 into Eqn. 4.11, the increase in strain energy due to lateral deflection and twist during buckling can be formulated as

$$U_F = \frac{1}{2}\bar{q}^T \bar{k}_F \bar{q} \tag{4. 16}$$

where $\bar{q} = \langle q_1, q_2, q_3 \rangle^T$ and the flange stiffness matrix $\bar{k}_F$ can be written in matrix form as

$$\bar{k}_F = \int_0^L \bar{B}_F^T \bar{D}_F \bar{B}_F \mathrm{d}z\,. \tag{4. 17}$$

The strain energy U_W stored during buckling of the flexible plate web may be obtained from

$$U_W = \frac{1}{2}\int_0^L \int_{-h_w/2}^{h_w/2} \bar{\varepsilon}_W^T \bar{D}_W \bar{\varepsilon}_W \mathrm{d}y\mathrm{d}z \tag{4. 18}$$

where the generalized web strain vector, $\bar{\varepsilon}_W$, since the web is modelled as a 'plate', is given by

$$\bar{\varepsilon}_W = \left\langle u_{W,zz},\ u_{W,yy},\ -2u_{W,yz} \right\rangle^T \tag{4. 19}$$

which may be obtained by suitable differentiation of Eqn. 4.3 as

$$\bar{\varepsilon}_W = \bar{B}_W \langle q_1, q_2, q_3 \rangle^T = \bar{B}_W \bar{C} \bar{q}\,. \tag{4. 20}$$

The web property matrix in Eqn. 4.18, applicable to isotropic plate buckling, may be written as

$$\bar{D}_W = \frac{t_w^3}{12}\begin{bmatrix} D_{11} & D_{12} & 0 \\ D_{21} & D_{22} & 0 \\ 0 & 0 & D_{33} \end{bmatrix}. \tag{4. 21}$$

For isotropic elastic buckling (ie. in regions of the web where the applied strain, ε_a is less than yield strain, ε_y), the well-known rigidities given by Timoshenko and Gere (1970) are used, so that

$$\begin{aligned} D_{11} &= D_{22} = E/(1-\nu^2) \\ D_{12} &= D_{21} = \nu D_{11} \\ D_{33} &= G \end{aligned} \quad . \tag{4. 22}$$

Thus by substituting Eqns. 4.19 and 4.21 into Eqn. 4.18, the strain energy stored in the web can be expressed as

$$U_W = \frac{1}{2}\vec{q}^T \bar{k}_W \vec{q} \tag{4. 23}$$

where the web stiffness matrix $\bar{k}_W$ is given by

$$\bar{k}_W = \bar{C}^T \left(\int_0^L \int_{-h_w/2}^{h_w/2} \bar{B}_W^T \bar{D}_W \bar{B}_W \mathrm{d}y\mathrm{d}z \right) \bar{C} \, . \tag{4. 24}$$

The integrals in the above equation are calculated by Gaussian quadrature and the pre- and post-multiplication by $\bar{C}^T$ and $\bar{C}$ is facilitated by computer.

If k_z is the continuous twist restraint of the restrained flange per unit length, then the strain energy is

$$U_R = \frac{1}{2}\vec{q}^T \bar{k}_R \vec{q} \tag{4. 25}$$

where $\bar{k}_R$ is the restraint stiffness matrix given by

$$\bar{k}_R = k_z \int_0^L \phi \cdot \phi \, \mathrm{d}z \, . \tag{4. 26}$$

The matrix $\bar{k}_R$ may be readily determined by hand manipulation.

Finally, the total strain energy stored during buckling can be expressed as

$$U = \frac{1}{2}\vec{q}^T \bar{k} \, \vec{q} \tag{4. 27}$$

where the stiffness matrix $\bar{k}$ is given by

$$\bar{k} = \bar{k}_F + \bar{k}_W + \bar{k}_R \tag{4.28}$$

and each of the matrices are given in Appendix 4.7. The order of these matrices depends on the number of Fourier terms n used in Eqn. 4.2 and is $3n \times 3n$.

During buckling the stresses $\sigma(y, z)$ caused by the axial force $N_{cr}(\xi)$ and the moment $M_{cr}(\xi)$ do work

$$V = V_F + V_W \,. \tag{4.29}$$

V_F is the work associated with the flange deformations and twists and V_W is the work associated with the web flexural deflections, and these are defined respectively as

$$V_F = \frac{1}{2}\int_A \sigma \int_0^L \left\{ u_T^2{}_{,z} + v_T^2{}_{,z} + v_B^2{}_{,z} \right\} \mathrm{d}z\mathrm{d}A \tag{4.30}$$

$$V_W = \frac{1}{2}\int_A \int_0^L \left\{ u_{W,z} \quad u_{W,y} \right\} \begin{bmatrix} \sigma & \tau \\ \tau & 0 \end{bmatrix} \left\{ u_{W,z} \quad u_{W,y} \right\}^T \mathrm{d}z\mathrm{d}A \tag{4.31}$$

where A = the area of the cross-section, and owing to the assumed rigidity of the flanges,

$$v_T = x\phi_T ; v_B = x\phi_B \,. \tag{4.32}$$

In the present application, the axial force $N_{cr}(\xi)$ is assumed without loss of generality to vary lengthwise as a cubic polynomial, and ξ is defined as z/L, so that

$$N_{cr}(\xi) = \lambda N_o \left(a_0 + a_1\xi + a_2\xi^2 + a_3\xi^3 \right) \tag{4.33}$$

where N_o = a predetermined reference value, λ = the buckling load factor, and $a_0,\ldots,a_3$ are predetermined constants specifying the given axial force distribution.

The bending moment $M_{cr}(\xi)$ is assumed to vary lengthwise as a cubic polynomial, so that

$$M_{cr}(\xi) = \lambda M_o \left(b_0 + b_1\xi + b_2\xi^2 + b_3\xi^3\right) \tag{4. 34}$$

where M_o = a predetermined reference value, λ = the buckling load factor, and $b_0,\ldots,b_4$ are predetermined constants specifying the given bending moment distribution. The stress σ in Eqn. 4.29 is then simply

$$\sigma = \frac{N_{cr}(\xi)}{A} + \frac{M_{cr}(\xi)y}{I_x} \tag{4. 35}$$

where I_x = major axis second moment of area of the I-section girder.

It is assumed that the average shear stress, τ is carried by the web only and is defined as

$$\tau = \frac{V(\xi)}{h_w t_w} \tag{4. 36}$$

in which

$$V(\xi) = \frac{\mathrm{d}M(\xi)}{\mathrm{d}\xi}. \tag{4. 37}$$

Again, substituting Eqns. 4.2 and 4.3 into Eqns. 4.29, 4.30 and 4.31 allows the work done during buckling to be expressed conveniently in matrix form as

$$V = \frac{1}{2}\lambda \bar{q}^T \bar{s} \bar{q} \tag{4. 38}$$

in which $\bar{s}$ is the stability matrix given by

$$\bar{s} = \bar{s}_F + \bar{s}_W \tag{4. 39}$$

and each of the matrices are given in Appendix 4.7.

If now the contributions in Eqns. 4.28 and 4.39 are substituted into Eqn. 4.6, the change in total potential Π takes the familiar form

$$\Pi = \frac{1}{2}\bar{q}^T\left(\bar{k} - \lambda\bar{s}\right)\bar{q}\,. \tag{4.40}$$

Neutral equilibrium is defined by $\delta\Pi = 0$ for any arbitrary variation $\delta\bar{q}$, so that

$$\delta\Pi = \delta\bar{q}^T\left(\bar{k} - \lambda\bar{s}\right)\bar{q} = \bar{0} \tag{4.41}$$

and if the neutral equilibrium is at the point of bifurcation from the primary path $\left(\bar{q} = \bar{0}\right)$ to the secondary path $\left(\bar{q} \neq \bar{0}\right)$, then the standard buckling eigenproblem in Eqn. 4.41 becomes

$$\left|\bar{k} - \lambda\bar{s}\right| = 0\,. \tag{4.42}$$

The eigenproblem in Eqns. 4.41 and 4.42 is of order $3n$, and amenable to standard eigensolvers (Garbow *et al.* 1977).

4.3 VERIFICATION OF MODEL

4.3.1 Convergence studies

Convergence studies have been conducted to determine the number of terms of the trigonometric series, n, required for accurate solutions. The number of terms required to achieve a sufficiently accurate solution will depend on the loading. Comparisons with the finite element program FEDBA16 (Bradford & Ronagh 1997a) for loading cases different from uniform bending have indicated that only nine to twelve terms in Fourier series are sufficient for critical buckling factor, λ, to converge. It was in general found that solutions for n = 9 and n = 12 where within 0.2%. Figure 4.4 shows the convergence characteristics for some considered bending distributions. For the sake of brevity, the results of the convergence study have been restricted to a selected few.

Since relatively few Fourier terms are required the solution of the eigenproblem is extremely rapid.

4.3.2 Model verification

Since experimental or closed form solutions are unavailable for elastic RDB of beams under moment gradient, the validity of the buckling analysis developed in this chapter was tested by comparing the critical moments with established finite element solutions. The accuracy of the theoretical model for the case of a column in uniform compression has been verified by comparisons with the results presented by Bradford (1997a) and good agreement has been demonstrated, as illustrated in Fig. 4.5. The model verification was then extended and the results were compared with the results which the finite element program FEDBA16 (Bradford & Ronagh 1997a) and ABAQUS gave for different loading configurations for four representatively chosen beam cross-sections with different α, γ and K values, as summarised in Table 4.1. The parameters α, γ and K are defined subsequently in Eqns. 4.44, 4.45 and 4.47.

In order to compare the current numerical model with the existing solutions for plain steel beams, either doubly-symmetric, monosymmetric or steel beam-columns, an additional degree of freedom was introduced and this amendment allowed for the tension/bottom flange to displace laterally as well. Distortion of the web in this amended analysis was suppressed by expressing the strain energy due to out-of-plane plate flexure of the web as

$$U_{Wf} = \frac{1}{2}\gamma_r \int_0^L \int_{-h_w/2}^{h_w/2} D_W u_{W,yy}^2 \, \mathrm{d}y\mathrm{d}z \tag{4. 43}$$

and allowing γ_r to approach infinity; where D_W is the relevant web rigidity applicable to elastic-plastic buckling. Thus, the elastic critical buckling moment values calculated for the plain steel sections (ie. translational restraint, $k_t = 0$, rotational restraint, $k_z = 0$ at the tension flange level) are elastic lateral-torsional buckling resistances and these values were compared to those calculated according to AS4100 (1998) as shown in Table 4.1b. Generally, these solutions agree with the present method within a tolerance of 2%.

4.4 PROPOSED DIMENSIONLESS PARAMETER, γ

The parameters that control the distortional buckling of isolated beams are numerous and their relationship is difficult to quantify, and consequently difficult to present in a systematic and concise manner. The buckling load depends on such aspects as the loading pattern, cross-section geometry, beam slenderness and restraint conditions. The relationship between the parameters that influence distortional buckling is difficult enough in itself to quantify, and incorporating the restraining effects adds another dimension of complexity to the problem.

To understand the relation between the most influential parameters that control the RDB phenomenon Eqns. 4.17, 4.24 and 4.39 were expanded and the significant relevance of such parameters with respect to each other was examined. The loading regime, L/h_w ratio and moment parameter β were recognised as the most dominant parameters. To take into account the torsional rigidity and to satisfy dimensional homogeneity the proposed dimensionless parameter, γ, takes the following form

$$\gamma = \frac{\beta L^2}{GJh_w}. \tag{4. 44}$$

4.5 NUMERICAL INVESTIGATIONS

4.5.1 General

The proposed parameter has been employed to carry out numerical analyses. Various dimensionless parameters such as L/h_w, h_w/t_w, b_f/t_f and torsional restraint parameter, α, given by

$$\alpha = \frac{k_z}{\pi^2 GJ / L^2} \tag{4. 45}$$

were covered in this parametric study. The results of this study are shown in Figs. 4.6-4.28. In the figures, M_{cr} is the elastic critical moment obtained from the RDB analysis and described in section 4.2, while M_{ob} is the elastic critical moment for the plain steel I-beam subjected to uniform bending moment, assuming rigidity of the cross section and defined by

$$M_{ob} = \sqrt{\left(\frac{\pi^2 EI_y}{L^2}\right)\left(GJ + \frac{\pi^2 EI_w}{L^2}\right)}. \tag{4. 46}$$

The ratio of M_{cr}/M_{ob} is plotted as a function of the dimensionless beam parameter, K, as generally deployed in plain steel sections (AS4100 1998), and given by

$$K = \sqrt{\frac{\pi^2 EI_y}{GJL^2}}, \tag{4. 47}$$

the proposed parameter, γ, and the torsional restraint parameter, α, for some typical loading configurations.

4.5.2 Continuously restrained I-beam

4.5.2.1 Doubly symmetric I-section

M_{cr}/M_{ob} ratios were computed for γ values of 5, 10, 20, 30, 40 and 50 for a wide range of loading configurations. The predicted RDB loads of simply supported beams are shown in Figs. 4.6-4.8. Analyses were made for varying amounts of rotational restraint k_z, herein expressed in terms of a dimensionless torsional restraint parameter, α. The rotational restraint parameter, α, was varied from 0 (no restraint) to 1000 (or ∞, rigid restraint). It can be seen that for $\alpha = 0$, where there is only translational restraint the beam buckles in a lateral-torsional mode. In general, the reductions in buckling resistance caused by distortion are moderate for medium spans, and increase as the span decreases. However, as the twist restraint, α, increases, the effect of web distortion increases and the buckling mode is lateral-distortional. The figures demonstrate that the elastic critical moment of beams with elastic torsional restraint of the tension flange asymptotes to a maximum value as the stiffness of the torsional restraint increases. It is further shown that the effects of the web distortion are the most severe for the case when α reaches 1000, and that the compression flange twists significantly. A plot of the normalised buckling mode, which is the eigenvector in Eqn. 4.41 is shown in Fig. 4.9.

The parametric studies undertaken have shown that the proposed parameter, γ, is useful in defining a unique value of critical buckling moment for any particular ratio of L/h_w, h/t_w and b_f/t_f and value of K. The results have demonstrated that the implementation of the proposed parameter, γ, together with the well-known beam parameter, K, results in curves that are much more comprehensive, principally because these curves fully cover member geometrical and elastic material properties for a particular loading pattern. It has been further observed that plotting the range of different γ values, as shown in Figs. 4.6-4.8, as a function of K, α, and a loading regime, intermediate values of the parameter γ may be easily interpolated. These curves may be used to estimate the elastic RDB moments of any general I-beam since the parameters K and γ proved to be very effective in defining a wide range of general I-beam dimensions.

4.5.2.2 Design Example

The application of the design graphs in Figs. 4.6-4.8 is best illustrated by an example. For the steel section of a half-through girder bridge simply supported over a span of 10 m and subjected to uniformly distributed load, determine the elastic critical buckling load.

It is assumed that the torsional restraint parameter, α, is 1000. It is further assumed that the relatively thin web has longitudinal stiffeners, which prevent local buckling without preventing the web distortion.

b_f = 300 mm

t_f = 30 mm

h_w = 1000 mm

t_w = 10 mm

E = 200 GPa

ν = 0.3

The procedure is as follows:

1. Determine I_y, I_w, J, G and β
2. Calculate γ

3. Calculate K
4. By using γ and K determine M_{cr}/M_{ob} by referring to Fig. 4.7
5. Calculate M_{cr}
6. Determine elastic buckling load

Solution:

1. Properties of the steel section:

$$I_y = 2\times\frac{300^3\times 30}{12}+\frac{1000\times 10^3}{12}=1.358\times 10^8 \text{ mm}^4$$

$$I_w = \frac{I_y h_w{}^2}{4}=\frac{1.358\times 10^8\times 1000^2}{4}=3.396\times 10^{13} \text{ mm}^6$$

$$J=\frac{1}{3}\sum bt^3 = \frac{1}{3}\left(2\times 300\times 30^3+1000\times 10^3\right)=5.733\times 10^6 \text{ mm}^4$$

$$G=\frac{E}{2(1+\nu)}=\frac{200{,}000}{2(1+0.3)}=76923.1 \text{ MPa}$$

$$\beta=\frac{Et^3}{12\left(1-\nu^2\right)}=\frac{200{,}000\times 10^3}{12\left(1-0.3^2\right)}=1.831\times 10^7 \text{Nmm}$$

2. The proposed dimensionless parameter:

$$\gamma=\frac{\beta L^2}{GJh_w}=\frac{1.831\times 10^7\times 10{,}000^2}{76{,}923.1\times 5.733\times 10^6\times 1000}=4.15$$

3. K-beam parameter:

$$K=\sqrt{\frac{\pi^2 EI_w}{GJL^2}}=\sqrt{\frac{\pi^2\times 200{,}000\times 3.396\times 10^{13}}{76{,}923.1\times 5.733\times 10^6\times 10{,}000^2}}=1.233$$

4. Therefore, with $K = 1.233$ and $\gamma = 4.15$ it is found from Fig. 4.7 that $M_{cr}/M_{ob} = 1.35$.

5. The elastic buckling moment

$M_{ob} = \sqrt{\left(\frac{\pi^2 EI_w}{L^2}\right)\left(GJ + \frac{\pi^2 EI_w}{L^2}\right)} = 1718.6$ kNm, and the critical buckling moment

M_{cr} = 1718.6 x 1.35 = 2320.1 kNm

6. Hence, the uniformly distributed load $w = \frac{8M_{cr}}{L^2} = 185.6$ kN/m.

4.5.2.3 Monosymmetric I-section

Monosymmetric I-sections are in general more efficient in resisting loads, provided the compressive bending stresses are taken by the larger flange, as shown in Figure 4.10. Contemporary and inexpensive fabrication techniques allow flanges of different widths and thicknesses to be welded to a slender web to maximise the buckling resistance of the resulting I-beam, while minimising the amount of material used. It has been shown in section 4.5.2.1 that the buckling modes of equal flange I-beams (called RDB in this thesis) may combine general lateral deflection and twist with general changes in the cross-sectional shape which arise from web distortion.

The analysis of the structural stability of continuously restrained or unrestrained monosymmetric beams has been generally lateral-torsional (Trahair 1993) which is based on the Vlasov assumption that the cross-sections do not distort. When this assumption is relaxed, the buckling of the I-section is lateral-distortional rather than lateral-torsional. Although research into the lateral-torsional buckling of unrestrained doubly and monosymmetric beams is bountiful, few studies have been conducted on the elastic lateral-torsional and lateral-distortional buckling of continuously restrained monosymmetric beams (Lee 2001). The closed form solution for monosymmetric beam-columns subjected to uniform bending with elastic torsional and translational restraints was presented by Vlasov (1961). Pincus and Fisher (1966) verified Vlasov's study by considering the effects of continuous diaphragms acting at the compression flange of a doubly-symmetric I-section. Trahair (1979) developed an accurate closed form solution for continuous elastically restrained monosymmetric beam-columns subjected to uniform bending. The continuous elastic restraints considered in that study were minor axis rotational and torsional restraint as produced by a continuous diaphragm restraint. Hancock and Trahair (1978) developed a line-type finite element with 8 degrees of freedom to study the elastic lateral-torsional buckling of restrained monosymmetric beams. The line element method developed by Hancock and Trahair was extended to study the elastic lateral-torsional buckling of simply supported doubly symmetric beams subjected to a uniformly distributed load with minor axis rotational restraints applied at the level of load application (Hancock & Trahair 1979). Bradford and Cuk (1988) developed a line-element based on an arbitrary axis system to eliminate the complications that arise when the shear centre and centroid of the cross-section are not parallel. The method was extended to the elastic lateral-torsional buckling of restrained doubly and monosymmetric beams subjected to uniform bending to verify the method (Cuk 1984), but parametric studies where not undertaken. As mentioned earlier, lateral-distortional buckling is profound for a beam subjected to torsional restraint, and this was demonstrated by Bradford (1988a, 1988b) who studied the elastic lateral-distortional buckling of restrained monosymmetric beams under uniform bending. In that study, he also found that the effect of web distortion is not significant for translational and minor axis rotational restraint. Nevertheless, research into lateral-distortional buckling of restrained beams has been generally limited to uniform bending, which cannot represent the realistic loading condition experienced in most structures.

The model described in section 4.2 is used here to study the effects of web distortion on the elastic distortional buckling of continuously restrained monosymmetric I-beams of practical geometry under transverse loading. The loading regimes considered in this study are concentrated and uniformly distributed loads with translational and minor axis rotational restraints at the bottom/tension flange. The method forms the kernel for inelastic buckling studies by the energy method in subsequent chapters.

The results derived in this study are shown in Figs. 4.11 to 4.14. The variation of the elastic critical buckling moment, M_{cr} normalised with respect to the elastic critical moment, M_{ob} for the plain monosymmetric steel I-beam, subjected to uniform bending moment and assuming rigidity of the cross-section, is plotted for a range of beam monosymmetry parameter, ρ (ρ = 0 to 1). The degree of beam monosymmetry is given as (Kitipornchai *et al.* 1986)

$$\rho = \frac{I_{y(compression)}}{I_{y(compression)} + I_{y(tension)}} = \frac{I_{y(compression)}}{I_y} \tag{4. 48}$$

in which $I_{y\,(compression)}$, $I_{y\,(tension)}$ and I_y are the second moments of area about the section y-axis of the top/compression flange, the bottom/tension flange, and the whole section, respectively. Although steel cross-sections with values of beam monosymmetry parameter of 0 and 1.0 were used in this study, the cross-sections are not authentic T-sections but have some minor top and bottom flanges respectively. Thus the values of 0 and 1.0 are to a certain extent approximate values (ie. 0.02% tolerance).

The elastic critical moment, M_{ob} for a plain monosymmetric steel I-beam subjected to uniform bending moment and assuming rigidity of the cross-section is defined by

$$M_{ob} = \sqrt{\frac{\pi^2 EI_y}{L^2}}\left\{\sqrt{GJ + \frac{\pi^2 EI_w}{L^2} + \frac{\beta_x^2}{4}\frac{\pi^2 EI_y}{L^2}} + \frac{\beta_x}{2}\sqrt{\frac{\pi^2 EI_y}{L^2}}\right\} \tag{4. 49}$$

in which the monosymmetry section constant, β_x is given by (Kitipornachi & Trahair 1975)

$$\beta_x = 0.8h_w\left[\frac{2I_{y(compression)}}{I_y} - 1\right]. \tag{4. 50}$$

The solutions are plotted for the beam parameter, $\overline{K}$ ranging from 0.5 to 2, and for the monosymmetric I-section defined as

$$\overline{K} = \sqrt{\frac{\pi^2 EI_y h_w{}^2}{4GJL^2}}. \tag{4. 51}$$

The values of $\overline{K}$ for practical beams are in the range of 0.5 and 2.5, with low values of the $\overline{K}$ beam parameter representing long beams and/or compact cross-sections, and high values corresponding to short beams and/or slender cross-sections. As shown in Figs. 4.11-4.14 the M_{cr}/M_{od} values, for a particular monosymmetry parameter, ρ curve, converge to a constant after $\overline{K} > 1.5$.

The results (Figs. 4.11 – 4.14) show the favourable effects of elastic translational and minor axis rotational restraints (α = 0, 10, 100 and 1000) applied at the bottom flange of a simply supported beam, as normally employed in half-through girder bridges. The increase in the buckling capacity is most pronounced for low values of the beam parameter, $\overline{K}$. A considerable increase in buckling capacity is demonstrated for beams with $\rho = 0.1$ to 1.0 and the slightest increase being for the case of a monosymmetric I-beam with $\rho = 0$ (ie. very narrow compression flange). It can be further observed from Figs. 4.11-4.14 that the increase in the degree of rotational restraint, α does not have an effect on the increase in the buckling capacity for the beams with $\rho = 0$.

The results also indicate that the effects of web distortion are significant when elastic translational and minor axis rotational restraints are applied at the tension flange level. Besides this, it is evident that the reduction of the elastic lateral buckling load due to web distortion increases as the stiffness of the restraint increases. In all cases, the effects of web distortion can be very pronounced, more so than for doubly symmetric beams.

For a beam whose tension flange is the smaller flange, the reductions in the elastic critical moment buckling capacity due to web distortion decrease as the degree of monosymmetry of the beam increases. On the other hand, when the smaller flange is the compression flange, the reductions in the buckling capacity increase as the degree of monosymmetry increases. This is because the buckling resistance is provided by smaller flange, and it has been shown that the distortion which reduces the buckling resistance of the member is most pronounced for beams with narrow stocky flanges (Bradford 1985b).

Figures 4.15 to 4.17 show the longitudinal distribution of normalised buckling mode shapes of the lateral displacements, u_T and the angle of twist, ϕ_T for the compression/top flange and the angle of twist, ϕ_B for the tension/bottom flange. These curves were derived from the energy method presented in section 4.2 (using $n = 18$) by solving for the eigenvectors in the determinantal equation 4.38 after λ had been found. It can be seen that as the value of ρ decreases from 1.0 to 0, and therefore the compression flange becomes stockier, the deflected shape changes from a half-sine wave to a full-sine wave and a two full-sine waves. Therefore, as the value of ρ approaches 0, the u and ϕ buckled shapes are more complicated functions and require at least two terms in the Fourier series to describe them closely.

4.5.3 Continuously restrained beam-column

4.5.3.1 General

The buckling behaviour of steel beam-columns has been the subject of considerable research (Trahair 1993; Trahair & Bradford 1998; Chen & Lui 1991). The interaction of bending moment and axial compressive loading has been investigated by a large number of researchers, and a wide variety of different interaction equations have been derived to take account of the complexities which arise when beam-columns of various cross-sections, with varying degrees of compactness, are subjected to combinations of axial load and moments which may vary to any specified degree along the length of the member. Numerical solutions and approximate buckling formulae for such members under a variety of loading and restraint conditions are available in standard texts.

Beam-columns may act as if isolated, or they may be continuous members that form part of a rigid frame. The analysis of a beam-column involves the features of both a deflection problem as a beam and a stability problem as a column. All members deflect under loading, but in the case of beams the effect of this upon the actions can usually be ignored for a buckling analysis. In the case of columns, however, the deflections may be such as to add a significant additional or secondary moment. This is the main reason that beam-column analysis is complicated compared with column analysis, which is a pure linear eigenvalue problem.

Most research work on the elastic buckling of I-section beam-columns has focused on unrestrained steel sections. Although for short span steel members the critical load is often less than the elastic value because the effective stifnesses are reduced by yielding within the member, the ultimate strength of a slender steel beam-column which is laterally unsupported is influenced by buckling by combined twist and lateral (sideways) bending of the cross-section. This well-known phenomenon is known as lateral-torsional buckling.

When a continuously restrained beam-column (Fig. 4.18) does not have a braced top (compressive) flange, its buckling mode must necessarily be distortional (Bradford 1992a), since the web must distort in the plane of its cross-section as it restrains the compressive flange during buckling. Further, because of the restraint provided at the tension flange level, cross-sectional distortion is more profound, and so this buckling mode is referred to as restrained distortional buckling (RDB).

The problem is compounded by the many effects, which have significant influence, including those of force and moment distribution, member and cross-section slenderness, continuity, restraints, and two- or three-dimensional behaviour of the beam-column.

4.5.3.2 Second-Order Non-Linear Elastic Analysis

An approximate solution for the maximum moment in a member with unequal end eccentricities is given in AS4100 (1998) as

$$M = \frac{Nec_m}{1 - N / N_{ol}} \tag{4. 52}$$

where e is the largest end eccentricity (e_0 or e_L) and c_m is a factor to account for the moment gradient caused by unequal end moments and is given by

$$c_m = 0.6 - 0.4\beta \leq 1.0 \tag{4. 53}$$

in which β is the ratio of the smaller to the larger end moment, as illustrated in Fig. 4.18, taken as negative if the member is bent into single curvature.

The geometric non-linearity is accounted for by amplifying the first order moments M_o (Ne) by the approximate factor δ_b given by

$$\delta_b = \frac{c_m}{1 - N_{cr} / N_{ol}} \tag{4. 54}$$

where N_{cr} is the applied axial load and N_{ol} is the Euler buckling load.

While having a closed form solution when elastic (Bradford 1997a), the investigations carried out in this study implement the following numerical procedure so that yielding may be introduced and for use in the out-of-plane analysis described subsequently.

Once loaded, the beam-column will deform $\delta(z)$ from its original undeformed position. The problem is non-linear, and δ depends on the end moments $M_{(0)}$ and $M_{(L)}$ respectively and magnitude of the load N. The appropriate boundary conditions at $z = 0$ and L are

$$\begin{array}{ll} \delta(0)=0 & \delta(L)=0 \\ EI\delta''(0)=-M_{(0)} & EI\delta''(L)=-M_{(L)} \end{array}. \tag{4.55}$$

An assumed function for the curvature that satisfies the boundary conditions is

$$\delta'' = c_0 + c_1 z + \sum_{i=1}^{n} \delta_{mi} \sin i\pi z / L. \tag{4.56}$$

Therefore, on integrating,

$$\delta = \frac{c_0 z^2}{2} + \frac{c_1 z^3}{6} + c_2 z + c_3 - \frac{L^2}{\pi^2} \sum_{i=1}^{n} \frac{\delta_{mi}}{i^2} \sin i\pi z / L. \tag{4.57}$$

Substituting the boundary conditions in Eqns. 4.56 and 4.57 produces

$$c_0 = \frac{-M_{(0)}}{EI}$$

$$c_1 = \frac{M_{(0)} - M_{(L)}}{EIL}$$

$$c_2 = \frac{L}{EI}\left(\frac{M_{(0)}}{3} + \frac{M_{(L)}}{6}\right) \tag{4.58}$$

$$c_3 = 0.$$

The analysis is elastic, and the geometric non-linearity is accounted for by the Fourier terms in Eqn. 4.56. The iterative technique proceeds as follows. The beam-column is divided into $n + 1$ segments containing n internal nodes. At each station, the moment is $M_j + N\delta_j$, and this is related to the curvature in Eqn. 4.56 by

$$\frac{M_j + N\delta_j}{EI} = -\left(c_0 + c_1 z + \sum_{i=1}^{n} \delta_{mi} \sin i\pi z / L\right). \tag{4.59}$$

Equation 4.59 may be solved for the n unknown Fourier coefficients δ_{mi} provided that the left hand side is known. Firstly, $\delta_j^{(0)}$ is set as zero, and Eqn. 4.59 is solved for $\delta_{mi}^{(0)}$. The values of $\delta_{mi}^{(0)}$ may then be substituted into Eqn. 4.57 to obtain $\delta_j^{(1)}$ at each of the j stations corresponding to $z = z_j$. The values of $\delta_j^{(1)}$ may then be substituted in Eqn. 4.59 to obtain n equations in $\delta_{mi}^{(1)}$. The procedure is thus continued, by solving the n equations for $\delta_{mi}^{(k)}$ at each *k-th* step, until convergence of the displacements δ_j occurs.

4.5.3.3 Verification of solution

The elastic second order behaviour of beam-columns is well-known in steel design. The deflected shape of an elastic beam-column $\delta(z)$ acted on by axial forces N and end moments M and βM, where β can have any value between −1 (single curvature bending) and +1 (double curvature bending) as shown in Fig. 4.18, is given by

$$\delta(z) = \frac{M_{(0)}}{N}[\cos\mu z - (\beta \operatorname{cosec}(\mu L) + \cot\mu L)\sin\mu z - 1 + (1+\beta)\frac{z}{L}] \tag{4.60}$$

in which β is the same ratio of end moments as $M_{(0)}/M_{(L)}$ in Eqn. 4.53 and where

$$\mu = \frac{\pi}{L}\sqrt{\frac{N}{N_{ol}}} \tag{4.61}$$

in which

$$N_{ol} = \frac{\pi^2 EI}{k_e^2 L^2} \tag{4.62}$$

and k_e is the effective length factor which for a simply supported beam-column is equal to unity.

Figure 4.19 shows a plot of $\delta(z)$ for β = -1, 0 and 1 for a beam-column with μ = 1.33×10^{-4} to 1.74×10^{-4} and $\mu = 1.70\times10^{-4}$ to 2.06×10^{-4}, with $\gamma = 5$ and $K = 0.7$ using the above numerical procedure with n = 9 segments. The solutions were obtained very rapidly on a personal computer, and are identical to those of the analytical solution, even for large non-linearities when N/N_{ol} approaches unity.

The maximum deflection of an elastic beam-column $\delta(z)$ with transverse loads (Fig. 4.20) can be obtained by using

$$\delta = \frac{\gamma_m (1-\gamma_s N/N_{ol})}{(1-\gamma_n N/N_{ol})} \tag{4. 63}$$

and values of γ_m, γ_s and γ_n are given for beam-columns with central concentrated load as 1.0, 1.0 and 0.18 and for beam-columns with uniformly distributed loads, w as 1.0, 1.0 and –0.03 (Trahair & Bradford 1998).

Figure 4.21 illustrates a plot of $\delta(z)$ for a beam-column with central concentrated load and uniformly distributed load, w and K = 0.65 and 1.23, using the above numerical procedures.

4.5.3.4 Buckling Analysis

The buckling analysis assumes that in cross-section the flanges remain straight, that the web flexes as a cubic curve, and that all deflections and twists vary as a cubic polynomial function along the member, as described in section 4.2. The bottom flange of the beam-column is restrained fully against translation and lateral rotational buckling deformations, but is restrained elastically against twist. The ends of the beam-column are assumed to be simply supported and free to warp but end twist rotations and lateral deformation are prevented. Furthermore, since the cross-section of the beam-column has two axes of symmetry the shear centre and centroid coincide.

For beam-columns, simple beam theory provides a good model for stress distribution and therefore is used in the study. The total buckling stresses σ_{jT} are

$$\lambda_a \sigma_{jT} = \lambda_a \sigma_{jA} \pm \lambda_a \sigma_{jB} \tag{4. 64}$$

where

$$\lambda_a \sigma_{Aj} = \frac{\lambda_a N_j}{A} ; \ \lambda_a \sigma_B = \frac{\lambda_a \left(N_j \delta_j^k + M_j\right) y}{I_x} \tag{4. 65}$$

in which M_j is the applied moment; N_j is the applied axial force; λ_a is the applied load factor; σ_{jB} is the bending stress and σ_{jA} is the axial stress; δ_j^k is the converged deformation as calculated in section 4.5.3.2 at each of the j stations due to applied N_j and M_j; A is the cross-sectional area; and I_x is the second moment of area about the major axis.

The total potential energy Π is the sum of the strain energy U (contributed to by the strain energies stored in flanges, web and elastic torsional restraint) and the potential energy of the applied load, V (containing flange and web potential energies)

$$\Pi = U_F + U_W + U_R - V_F - V_W \tag{4. 66}$$

which can be written as

$$\Pi = \frac{1}{2} \bar{q}^T \bar{k}(\lambda) \bar{q} \tag{4. 67}$$

where $\bar{k}$ is the stiffness matrix that depends non-linearly on λ owing to the term δ_j^k in Eqn. 4.65. Using the variational form of the neutral equilibrium at buckling, that $\delta\Pi = 0$ for any arbitrary variation of the buckling displacements $\delta \bar{q}$, leads to the familiar buckling condition

$$\bar{k}(\lambda) \bar{q} = \bar{0} . \tag{4. 68}$$

Equation 4.68 represents a routine linear eigenproblem that may be solved by standard numerical algorithms for the buckling load factor λ as well as the buckled shape that is defined by the normalized eigenvector $\bar{q}$ as illustrated in Fig. 4.9. Because the problem is actually nonlinear, Eqn. 4.68 must be solved sequentially until $\lambda = \lambda_a$. The iterative eigenproblem scheme thus linearises the nonlinear solution.

The numerical method has been used to study a simply supported continuously restrained I-section beam-column. For consistency with the numerical model, the continuous restraint provided at the bottom flange is assumed to restrain this tension flange fully against lateral deflection and minor axis rotation, but to provide partial restraint against twist rotations with the dimensionless stiffness α given in Eqn. 4.45.

In Figs. 4.22-4.27 the load factor is plotted in terms of the dimensionless ratios M_{cr}/M_{od}, and N_{cr}/N_{od}. M_{od} is the lateral-distortional buckling moment for a beam member restrained fully against lateral deformation and minor axis rotation at the tension flange level, but which is free to twist during buckling, as calculated in section 4.5.2.1 for doubly-symmetric I-beams. This buckling mode involves cross-sectional distortion. Similarly N_{od} is the lateral-distortional buckling load for a column with the same restraining arrangement and which also accounts for cross-sectional distortion.

The loading configurations considered in this study are uniform bending, uniformly distributed load and a concentrated load acting at the mid-span. The buckling load factor is plotted as a function of the restraint parameter, α, the proposed distortional parameter, γ and the beam parameter, K, as described in section 4.5.2.1. Different degrees of lateral-torsional restraint, α are considered, ranging from 0 to 1000. The proposed distortional parameter, γ varies from 5 to 50.

The numerical results shown in Figs. 4.22-4.24 demonstrate that for a particular loading configuration M_{cr}/M_{od} and N_{cr}/N_{od} are close to unique values for a range of γ, α and K values. Hence for particular stress distribution defined in Eqn. 4.64 the buckling load factor λ may be determined as a function of K, α and γ.

In Figs. 4.25-4.27 the interaction between axial and bending capacities is plotted for three different loading configurations considered in this study. In these figures the ratio between reference bending moment and axial load M_o/N_o is varied from 0 to 1 in order to plot the buckling envelope. The figures address the entire range of α and γ values considered in Figs. 4.22-4.24. The trends shown in Figs. 4.25-4.27 are very similar and can be simplified to the linear interaction equation given as

$$\frac{M_{cr}}{M_{od}} + \frac{N_{cr}}{N_{od}} = 1.0 . \qquad (4.69)$$

Figure 4.28 plots some typical longitudinal distribution of normalised buckling mode shapes of the lateral displacements, u_T and the angle of twist, ϕ_T for the compression/top flange and the angle of twist, ϕ_B for the tension/bottom flange for the beam-columns considered in this study.

4.6 SUMMARY

The Rayleigh-Ritz energy based method of analysis has been developed for the study of the restrained-distortional buckling (RDB) of half-through girder bridges. The developed model is used to predict the elastic buckling moments of I-beams where the compression flange is restrained by the stiffness of the web only, and the tension flange is provided with continuous torsional restraint. This analysis is applicable to members under various conditions of loading and degree of continuous restraint.

The results of the energy method have been used to develop a design procedure. The proposed design curves produce accurate estimates of the elastic RDB capacity over a practical range of cross-sectional geometry. The design curves for individual loading cases are applicable to the entire range (0 to 1000) of the torsional restraint parameter, α. The I-section properties required in the determination of the elastic RDB moment for a particular loading configuration may be grouped into three basic parameters: 1. γ – distortion parameter (proposed in this study); 2. K- beam parameter; and 3. α – torsional restraint parameter. Some guidance pertaining to the design of half-through girders was provided, and this was illustrated with an example.

A parametric study was then undertaken to investigate the factors influencing the lateral-distortional buckling behaviour of simply supported continuously restrained monosymmetric I-beams. The solutions, which are valid for any general monosymmetric I-beam with degree of twist restraint, α varying from 0 to 1000 (rigid restraint), were presented in design graphs in terms of the easily evaluated design parameters ρ and $\overline{K}$. The results have demonstrated the beneficial effect of twist restraint and that the effect of web distortion can be significant. This is caused by the combination of the degree of monosymmetry and distortion of the web imposed by the restraint at the tension flange level.

The developed method was then further modified to account for geometric nonlinearity and was used to investigate the effects of combined uniform axial force and moment gradient on the critical buckling load of simply supported isolated beam-columns. The results obtained in this study demonstrated that a linear interaction equation is suitable in determining the out-of-plane buckling capacity of beam-columns. It was confirmed that the stability criteria for beam-columns under moment gradient are greatly influenced by the beam parameter, K, torsional restraint parameter, α, distortional buckling parameter, γ and the loading configuration.

Thus, the presented model identifies a distortional buckling parameter that may be used to reduce the proliferation of design graphs normally associated with distortional buckling to comparatively few. The buckling parameter also identifies the relative importance of many geometric dimensions, as well as their interactions on this distortional mode of buckling. It is concluded that the design method developed in the present chapter, due to its generality and simplicity, provides an accurate and quick method for solving complex RDB problems of half-through girder bridges.

4.7 APPENDICES

4.7.1 Flange Stiffness Matrix

For $i,j = 1,2,\ldots n$, (n = number of Fourier terms) and $i = j$

$$k_F(i,j) = \frac{1}{2}\pi^4 \frac{EI_{yB}}{L^3}(ij)^2$$

$$k_F(n+i,n+j) = \frac{1}{2}\pi^2 \frac{GJ_T}{L} ij \tag{4.70}$$

$$k_F(2n+i,2n+j) = \frac{1}{2}\pi^2 \frac{GJ_B}{L} ij$$

while for $i \neq j$

$$k_F(i..n, j..n) = 0 \tag{4.71}$$

4.7.2 Flange Stability Matrix

For $i,j = 1,2,\ldots n$, (n = number of Fourier terms) and $i = j$

$$g_F(i,j) = \frac{ij\pi^2\left(\sigma_N + \frac{h_w\sigma_M}{2}\right)A_{BF}}{L^2}$$

$$g_F(n+i,n+j) = \frac{ij\pi^2\left(\sigma_N + \frac{h_w\sigma_M}{2}\right)\left(t_f b_f^3\right)_T}{12L^2} \tag{4.72}$$

$$g_F(2n+i,2n+j) = \frac{ij\pi^2\left(\sigma_N + \frac{h_w\sigma_M}{2}\right)\left(t_f b_f^3\right)_B}{12L^2}$$

where $\sigma_N = \dfrac{\lambda N_o}{A}$ and $\sigma_M = \dfrac{\lambda M_o}{Z_x}$, while for $i \neq j$

$$g_F(i..n, j..n) = 0 \tag{4. 73}$$

4.7.3 Restraint Stiffness Matrix

For $i,j = 1,2,\ldots n$, (n = number of Fourier terms) and $i = j$

$$k_R(n+i, n+j) = \frac{1}{2} L k_z \tag{4. 74}$$

while for $i \neq j$

$$k_R(i..n, j..n) = 0 \tag{4. 75}$$

4.7.4 Web Stiffness (Kernel) Matrix

For $i,j = 1,2,\ldots n$, (n = number of Fourier terms) and $i = j$

$$k_W(i,j) = \frac{1}{2} h_w^{\,3} (ij)^2 \eta^4 \beta L$$

$$k_W(i,2n+j) = \left(-h_w ij \eta^2 \nu + \frac{1}{24} h_w^{\,3} (ij)^2 \eta^4 \right) \beta L$$

$$k_W(n+i,n+j) = \left(\frac{1}{24} h_w^{\,2} (ij)^2 \eta^4 + ij\eta^2 (1-\nu) \right) \beta L h_w$$

$$k_W(n+i,3n+j) = \left(\frac{1}{160} h_w^{\,2} (ij)^2 \eta^4 - \frac{1}{2} ij \eta^2 \nu + \frac{1}{4} ij \eta^2 \right) \beta L h_w \tag{4. 76}$$

$$k_W(2n+i,2n+j) = \left(\frac{2}{h_w} - \frac{\eta^2 \nu}{2} + \frac{\eta^4 h_w^{\,2}}{160} + \frac{\eta^2}{3} \right) \beta L h_w$$

$$k_W(3n+i,3n+j)=\left(\frac{-3}{16}\eta^2 h_w \nu+\frac{3}{2h_w}+\frac{\eta^4 h_w^{\ 3}}{896}+\frac{9}{80}\eta^2 h_w\right)\beta L$$

while for $i \neq j$

$$k_W(i..n, j..n)=0 \tag{4. 77}$$

4.7.5 Web Stability (Kernel) Matrix

For $i,j = 1,2,\ldots n$, (n = number of Fourier terms)

$$g_W(i,j)=\begin{cases}\dfrac{ij}{2}\dfrac{h_w^{\ 3}\pi^2\sigma}{L}, & i=j\\ 0, & i\neq j\end{cases}$$

$$g_W(i,n+j)=\begin{cases}0, & i=j\\ (-1)^i\dfrac{4}{3}h_w^{\ 2}\tau, & i\neq j\end{cases}$$

$$g_W(i,2n+j)=\begin{cases}\dfrac{ij}{24}\dfrac{h_w^{\ 3}\pi^2\sigma}{L}, & i=j\\ 0, & i\neq j\end{cases} \tag{4. 78}$$

$$g_W(i,3n+j)=\begin{cases}0, & i=j\\ (-1)^i\dfrac{1}{3}h_w^{\ 2}\tau, & i\neq j\end{cases}$$

$$g_W(n+i,n+j)=\begin{cases}\dfrac{ij}{24}\dfrac{h_w^{\ 3}\pi^2\sigma}{L}, & i=j\\ 0, & i\neq j\end{cases}$$

$$g_W(n+i,2n+j)=\begin{cases}0, & i=j\\ \dfrac{(-1)^i}{9}h_w^{\ 2}\tau, & i\neq j\end{cases}$$

$$g_W(n+i,3n+j)=\begin{cases}\dfrac{ij}{160}\dfrac{h_w^{\ 3}\pi^2\sigma}{L}, & i=j\\ 0, & i\neq j\end{cases}$$

$$g_W(2n+i,2n+j)=\begin{cases}\dfrac{ij}{160}\dfrac{h_w^{\ 3}\pi^2\sigma}{L}, & i=j\\ 0, & i\neq j\end{cases}$$

$$g_W(2n+i,3n+j)=\begin{cases}0, & i=j\\ \dfrac{(-1)^i}{60}h_w^{\ 2}\tau, & i\neq j\end{cases}$$

$$g_W(3n+i,3n+j)=\begin{cases}\dfrac{ij}{896}\dfrac{h_w^{\ 3}\pi^2\sigma}{L}, & i=j\\ 0, & i\neq j\end{cases}$$

where σ and τ are defined in Eqns. 4.35 and 4.36 respectively.

Table 4.1 Comparisons: a) continuously restrained steel beam;
b) bare steel section (lateral torsional buckling)

a)

Loading Configuration	K	γ	α	**Model (1)**	**FEDBA16 (2)**	**ABAQUS (3)**	**(2)/(1)**	**(3)/(1)**
Uniformly distributed load	0.55	5	0	1098.1	1087. 1	1080.3	0.99	0.98
	0.73	20	10	1342.9	1302.6	1298.1	0.97	0.97
	0.83	40	100	950.2	915.0	913.4	0.96	0.96
	1.29	50	1000	851.9	817.8	815.2	0.96	0.96
Point load at 0.5L	0.55	5	0	1292.3	1266.5	1263.6	0.98	0.98
	0.73	20	10	1902.0	1844.9	1840.2	0.97	0.97
	0.83	40	100	1042.7	1001.0	999.6	0.96	0.96
	1.29	50	1000	893.4	857.7	856.2	0.96	0.96
Point load at 0.1L	0.55	5	0	1518.5	1503.3	1499.8	0.99	0.99
	0.73	20	10	2000.3	1940.3	1938.6	0.97	0.97
	0.83	40	100	909.9	882.6	879.2	0.97	0.97
	1.29	50	1000	852.3	818.2	817.3	0.96	0.96
2 point loads at 0.25L from support	0.55	5	0	662.8	636.3	634.1	0.96	0.96
	0.73	20	10	1504.7	1444.5	1442.2	0.96	0.96
	0.83	40	100	780.0	741.0	738.6	0.95	0.95
	1.29	50	1000	705.3	670.0	669.2	0.95	0.95
2 point loads at 0.4L from support	0.55	5	0	1132.2	1098.2	1095.5	0.97	0.97
	0.73	20	10	1693.0	1642.2	1638.7	0.97	0.97
	0.83	40	100	956.7	918.4	916.2	0.96	0.96
	1.29	50	1000	814.2	781.6	778.9	0.96	0.96

b)

Loading Configuration	K	γ	**Model (1)**	**AS4100 (1998) (2)**	**(2)/(1)**
Uniformly distributed load	0.41	5	902.9	898.2	0.99
	0.51	20	558.4	554.3	0.99
	0.60	40	568.9	279.1	0.99
	1.02	50	281.9	1073.0	0.99
Point load at 0.5L	0.41	5	1106.2	1073.0	0.97
	0.51	20	689.8	662.2	0.96
	0.60	40	701.9	673.8	0.96
	1.02	50	343.7	333.4	0.97
2 point loads at 0.25L from support	0.41	5	882.0	864.4	0.98
	0.51	20	549.9	533.4	0.97
	0.60	40	553.9	542.8	0.98
	1.02	50	276.9	268.6	0.97

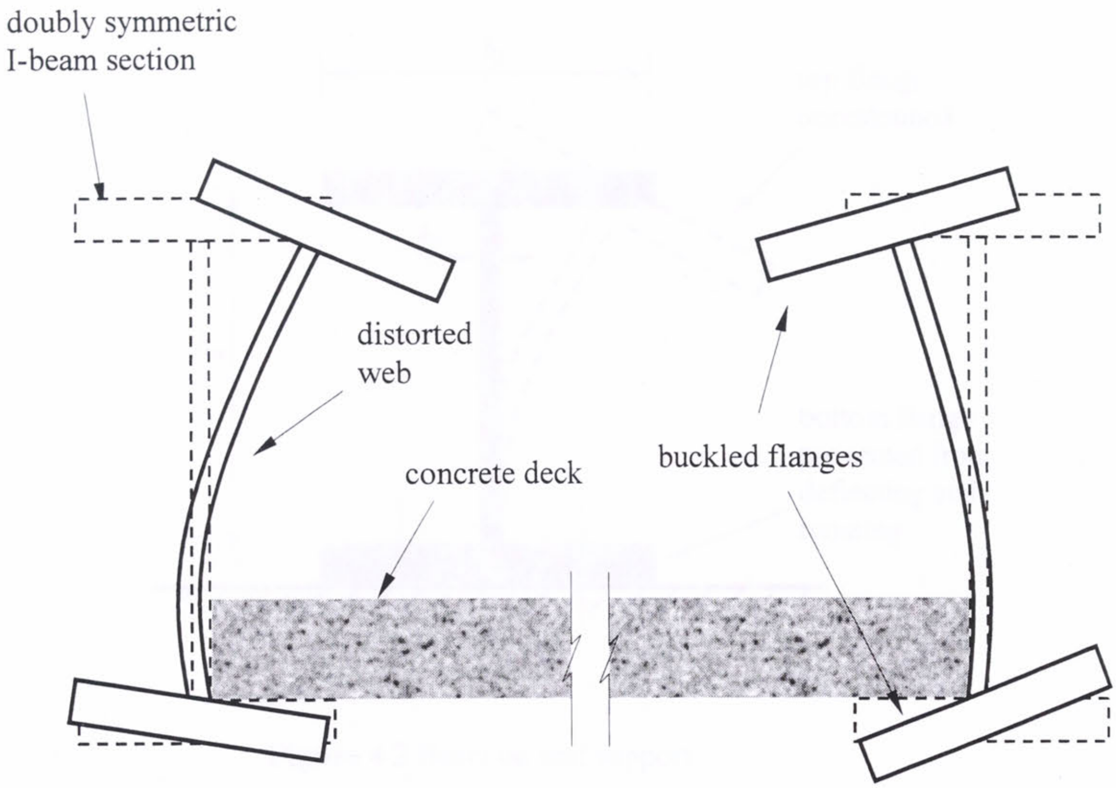

a) RDB of a half-trough girder bridge, cross-section elevation

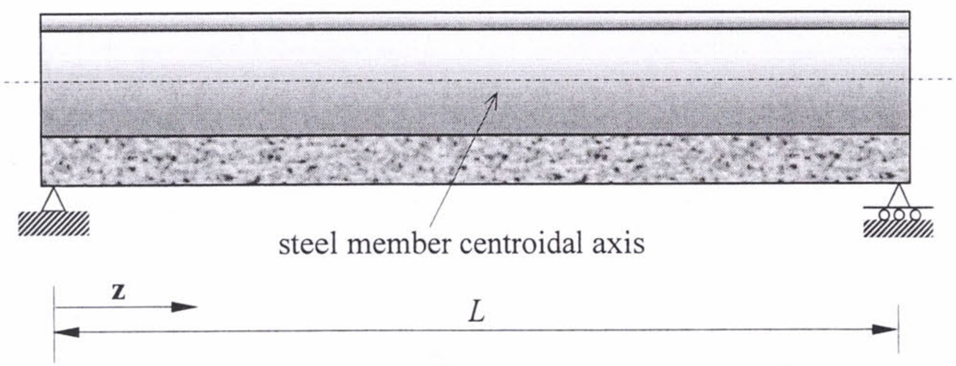

b) longitudinal elevation

Figure 4.1 Simply supported half-through girder bridge

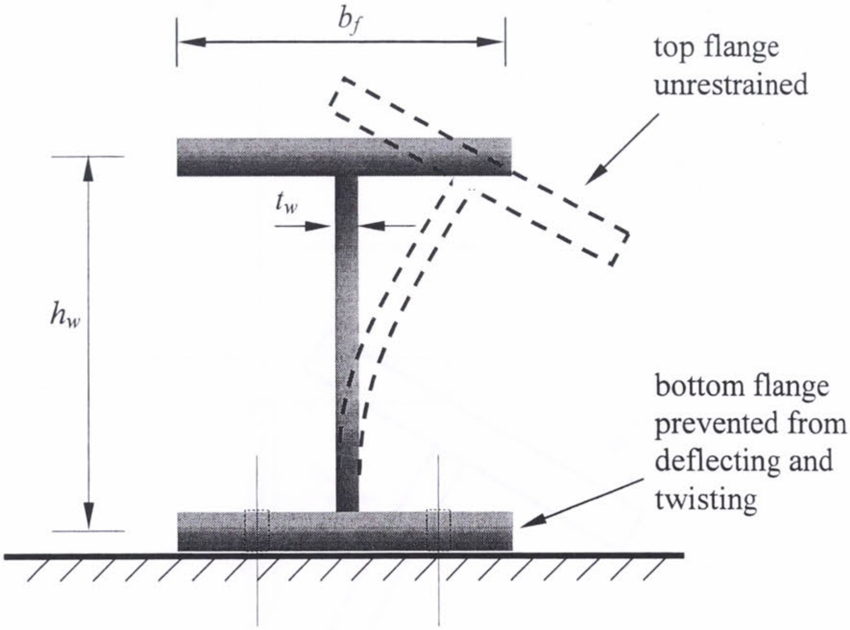

Figure 4.2 Beam on seat support

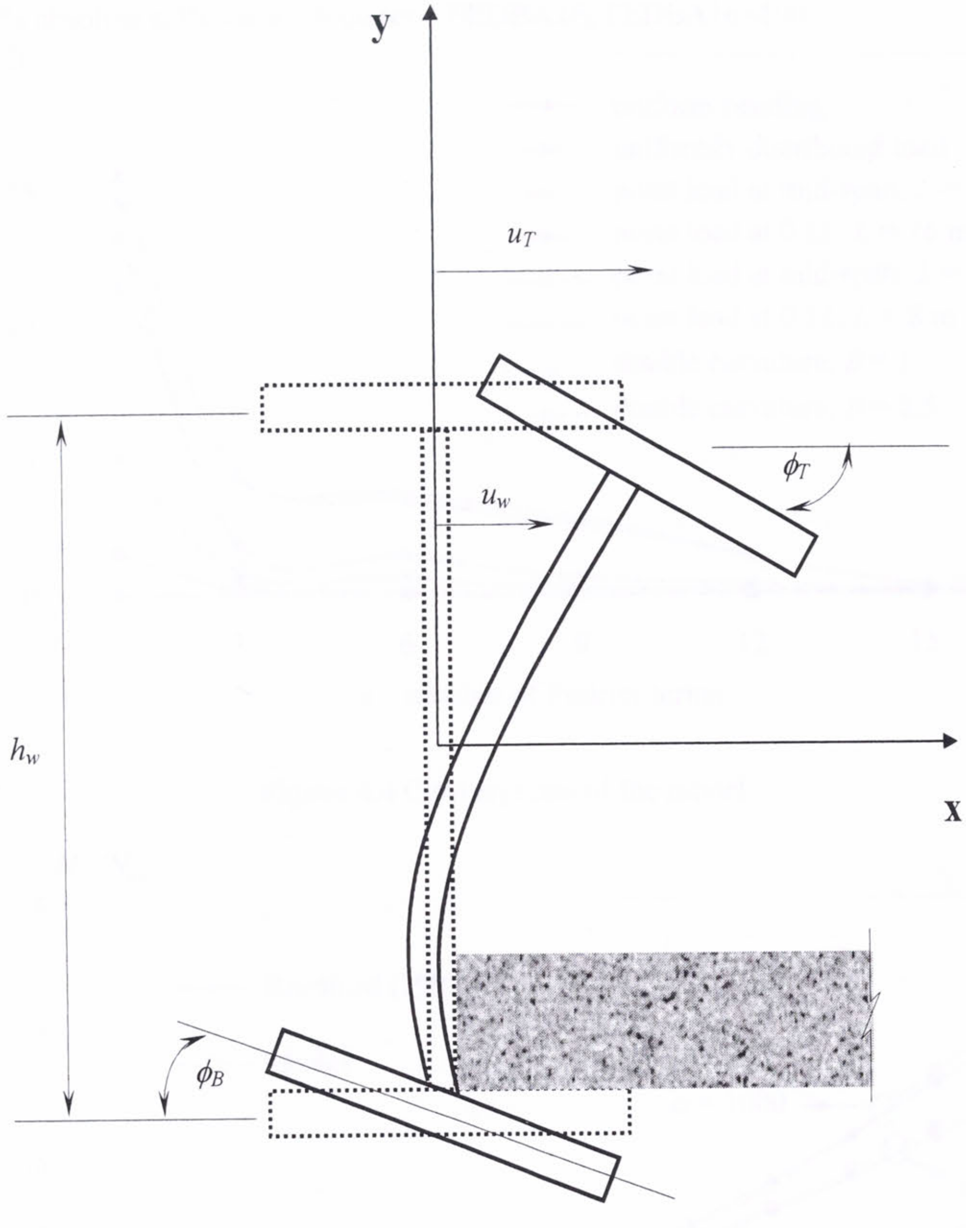

Figure 4.3 Buckling model

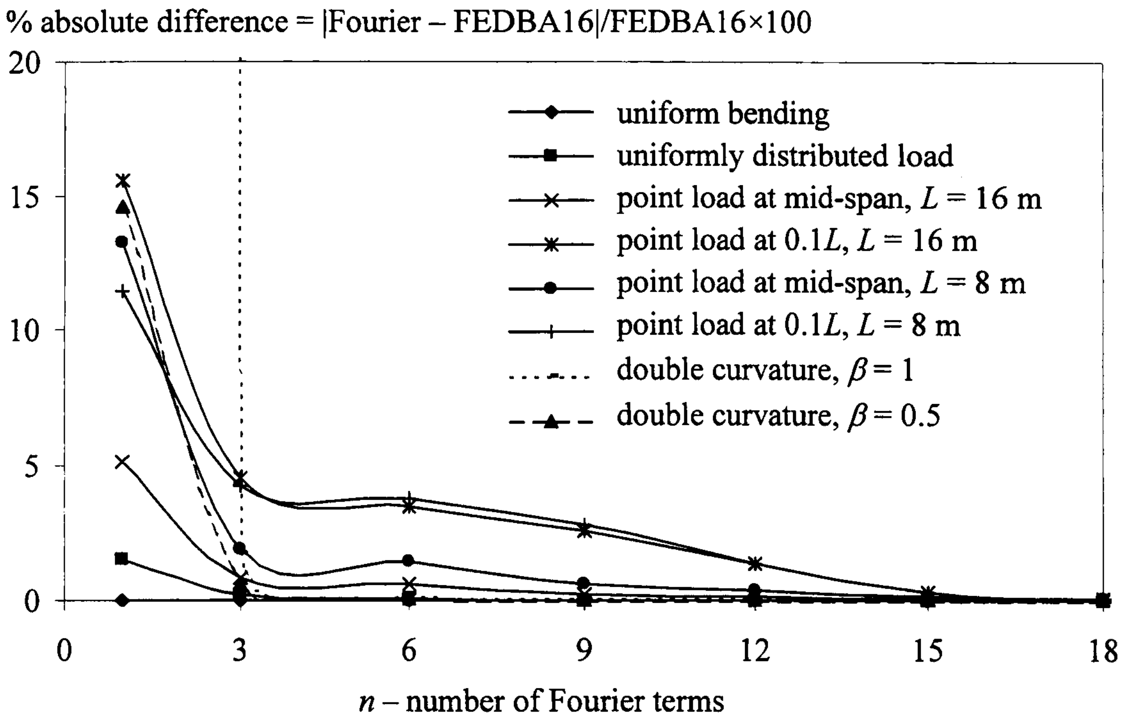

Figure 4.4 Convergence of the model

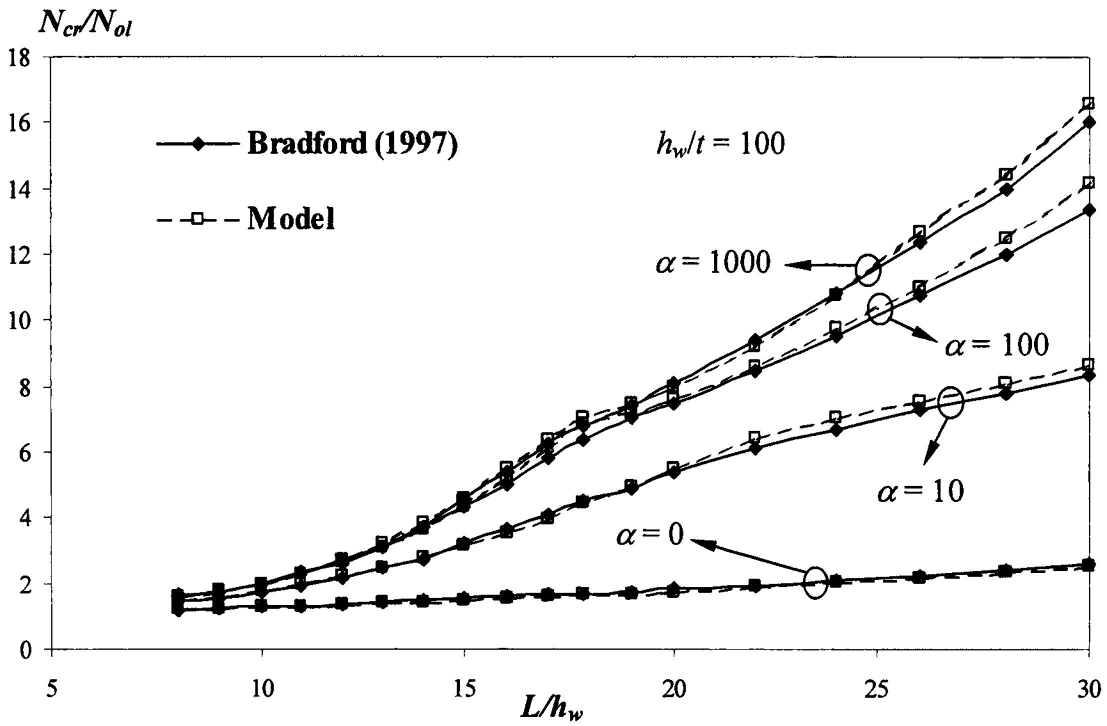

Figure 4.5 Buckling of doubly symmetric column with $h_w/t = 100$

a)

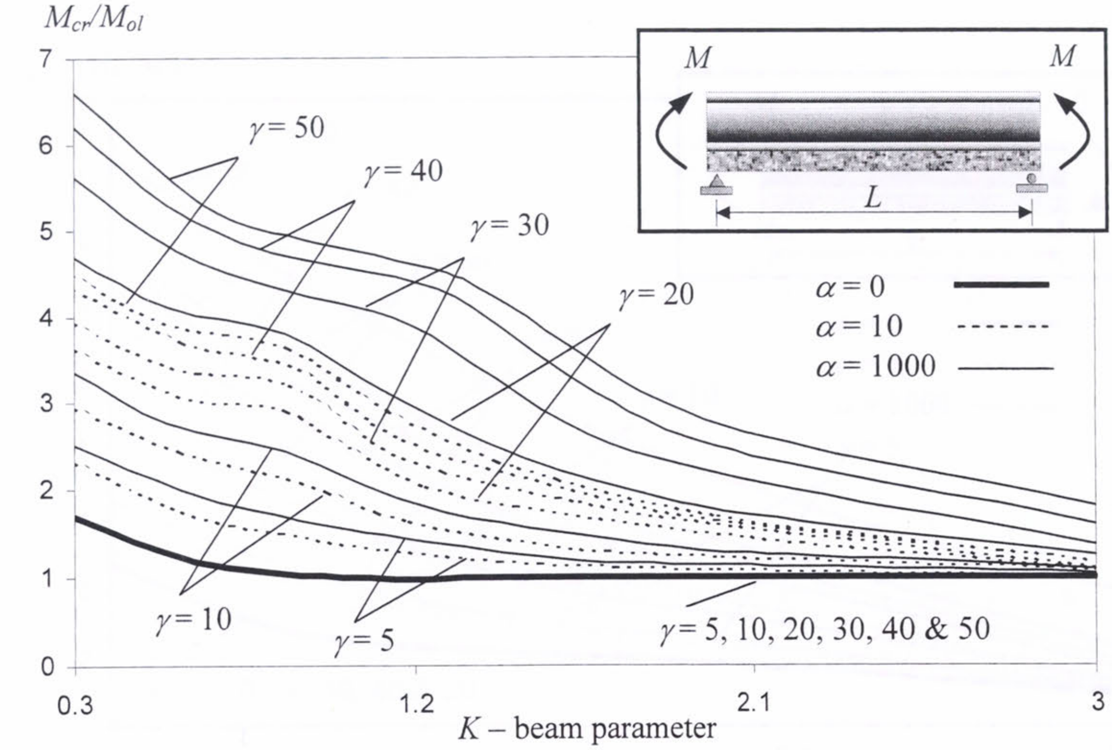
M_{cr}/M_{ol}
M
M
L
$\gamma = 50$
$\gamma = 40$
$\gamma = 30$
$\gamma = 20$
$\gamma = 10$
$\gamma = 5$
$\gamma = 5, 10, 20, 30, 40$ & 50
$\alpha = 0$
$\alpha = 10$
$\alpha = 1000$
K – beam parameter

b)

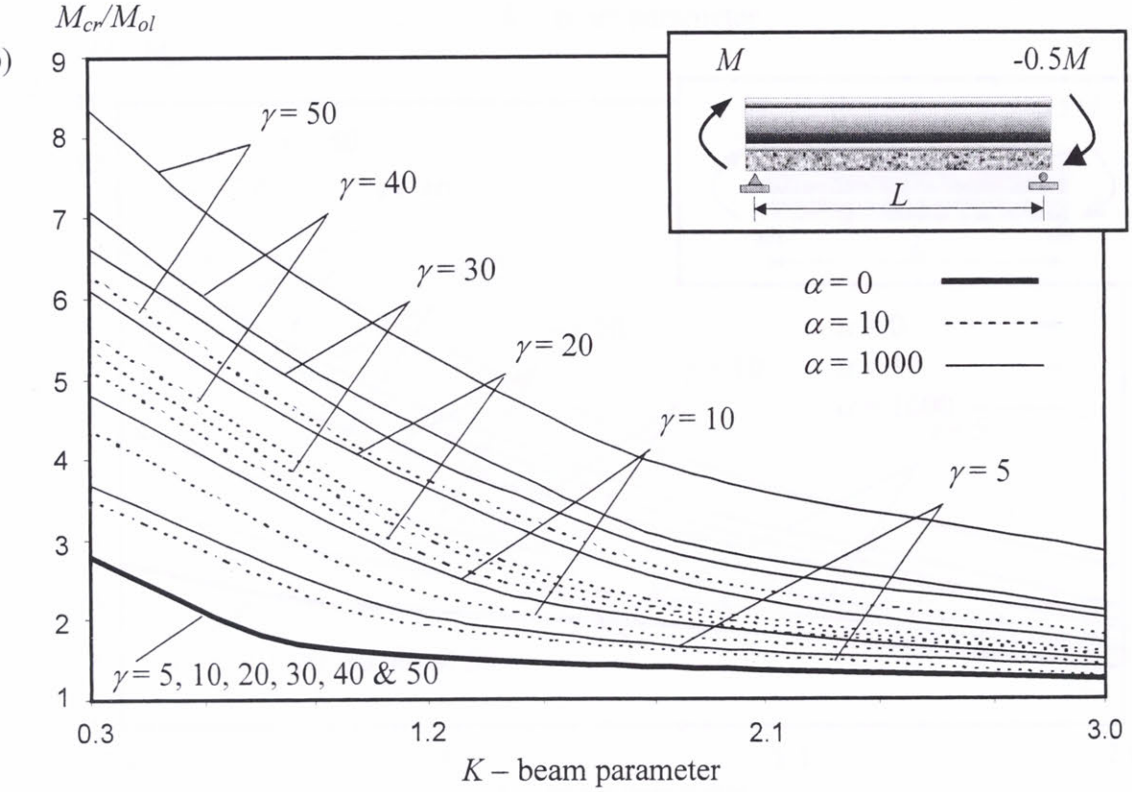
M_{cr}/M_{ol}
M
-0.5M
L
$\gamma = 50$
$\gamma = 40$
$\gamma = 30$
$\gamma = 20$
$\gamma = 10$
$\gamma = 5$
$\gamma = 5, 10, 20, 30, 40$ & 50
$\alpha = 0$
$\alpha = 10$
$\alpha = 1000$
K – beam parameter

c)

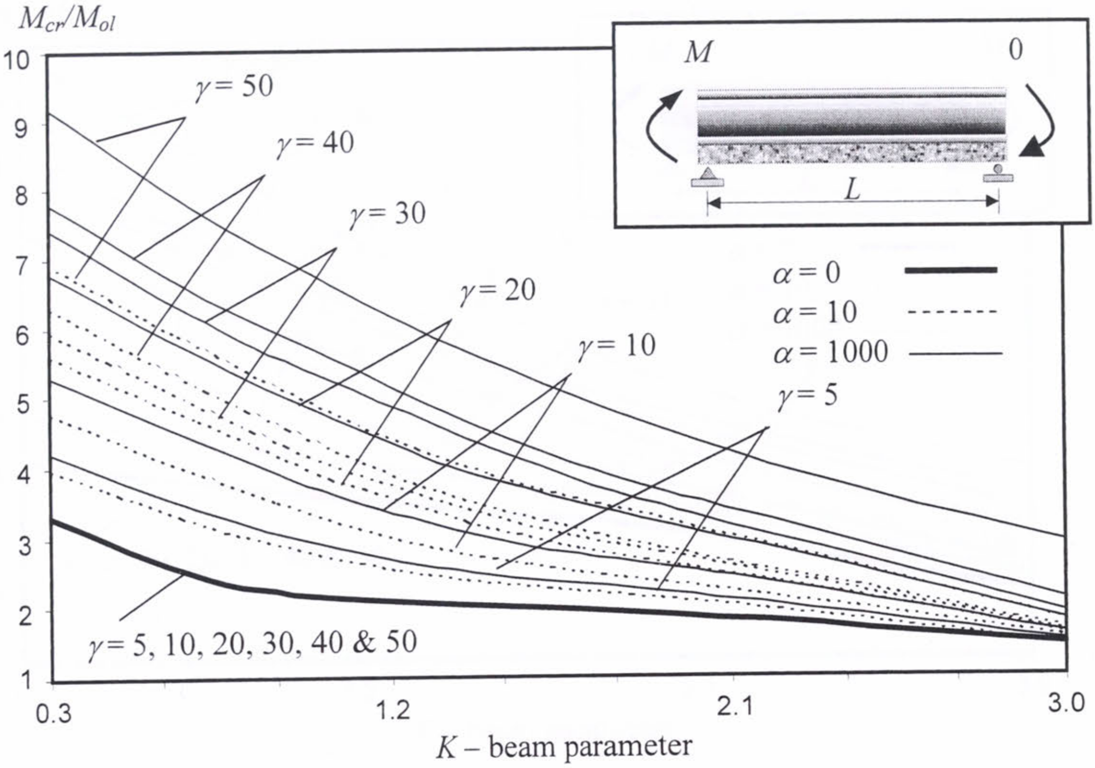

M_{cr}/M_{ol}
10
9
8
7
6
5
4
3
2
1
0.3
1.2
2.1
3.0
K – beam parameter
M
0
L
$\alpha = 0$
$\alpha = 10$
$\alpha = 1000$
$\gamma = 50$
$\gamma = 40$
$\gamma = 30$
$\gamma = 20$
$\gamma = 10$
$\gamma = 5$
$\gamma = 5, 10, 20, 30, 40$ & 50

d)

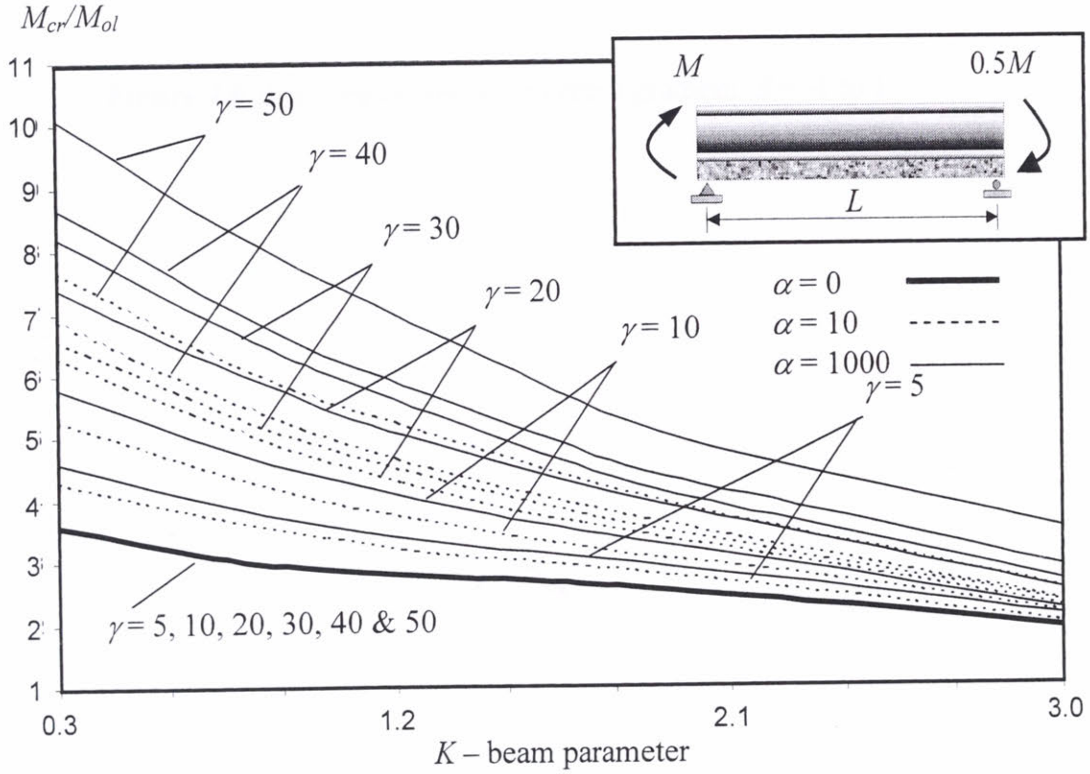

M_{cr}/M_{ol}
11
10
9
8
7
6
5
4
3
2
1
0.3
1.2
2.1
3.0
K – beam parameter
M
$0.5M$
L
$\alpha = 0$
$\alpha = 10$
$\alpha = 1000$
$\gamma = 50$
$\gamma = 40$
$\gamma = 30$
$\gamma = 20$
$\gamma = 10$
$\gamma = 5$
$\gamma = 5, 10, 20, 30, 40$ & 50

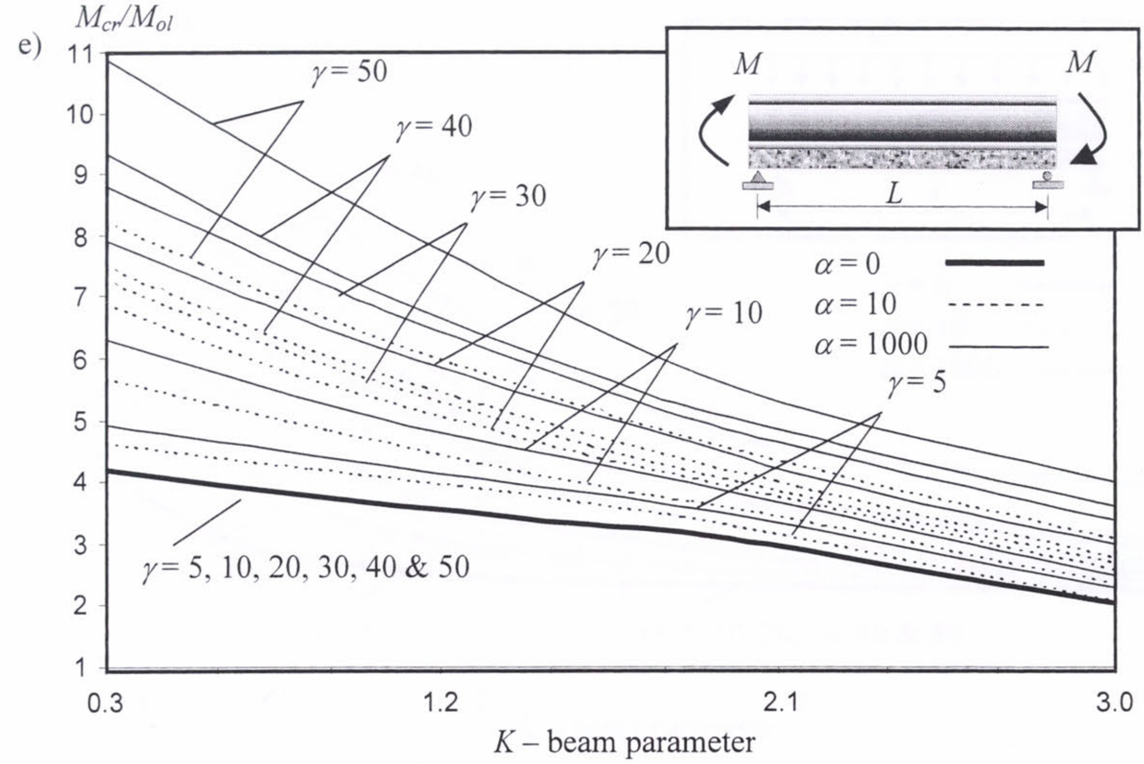

Figure 4.6 Buckling curves for moment gradient, $\beta = -1$ to 1

a)

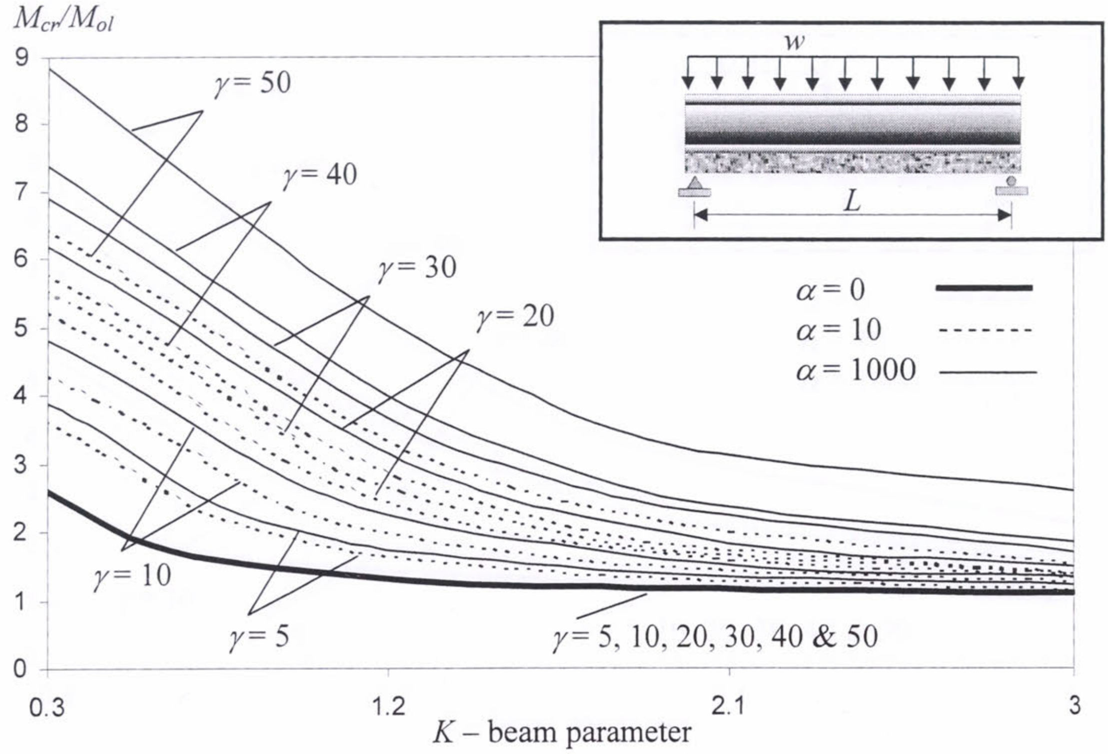

M_{cr}/M_{ol}
w
L
$\gamma = 50$
$\gamma = 40$
$\gamma = 30$
$\gamma = 20$
$\gamma = 10$
$\gamma = 5$
$\gamma = 5, 10, 20, 30, 40$ & 50
$\alpha = 0$
$\alpha = 10$
$\alpha = 1000$
0
1
2
3
4
5
6
7
8
9
0.3
1.2
2.1
3
K – beam parameter

b)

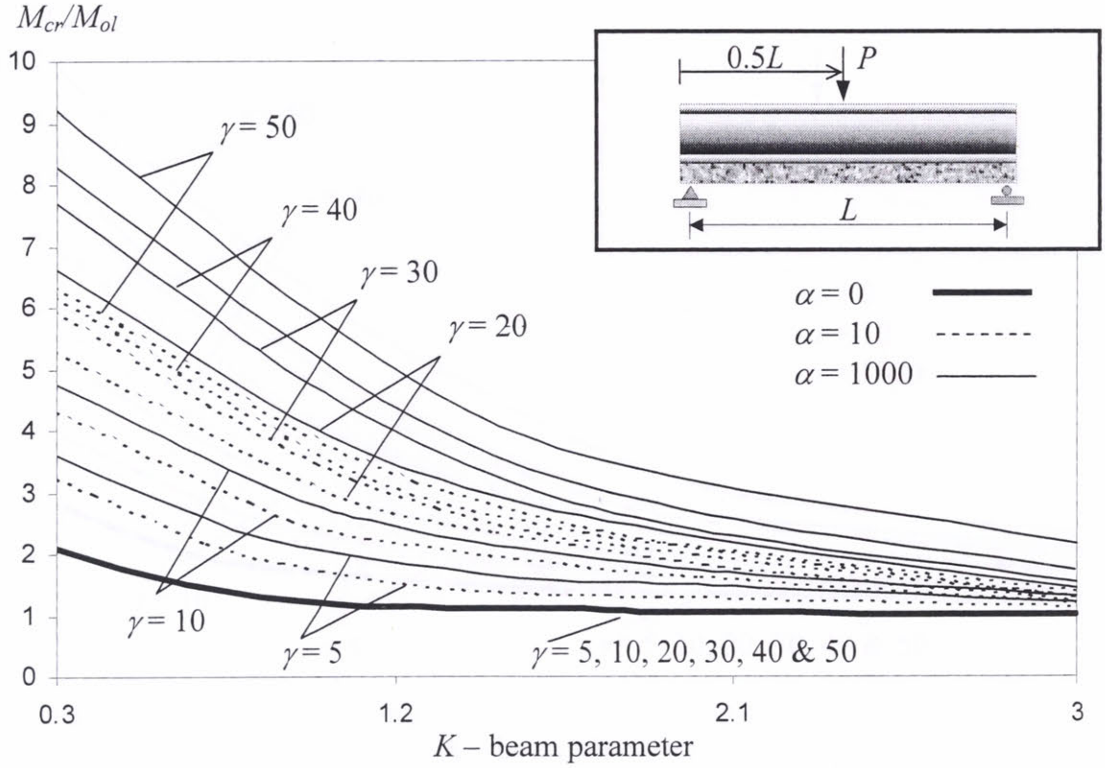

M_{cr}/M_{ol}
0.5L
P
L
$\gamma = 50$
$\gamma = 40$
$\gamma = 30$
$\gamma = 20$
$\gamma = 10$
$\gamma = 5$
$\gamma = 5, 10, 20, 30, 40$ & 50
$\alpha = 0$
$\alpha = 10$
$\alpha = 1000$
0
1
2
3
4
5
6
7
8
9
10
0.3
1.2
2.1
3
K – beam parameter

c)

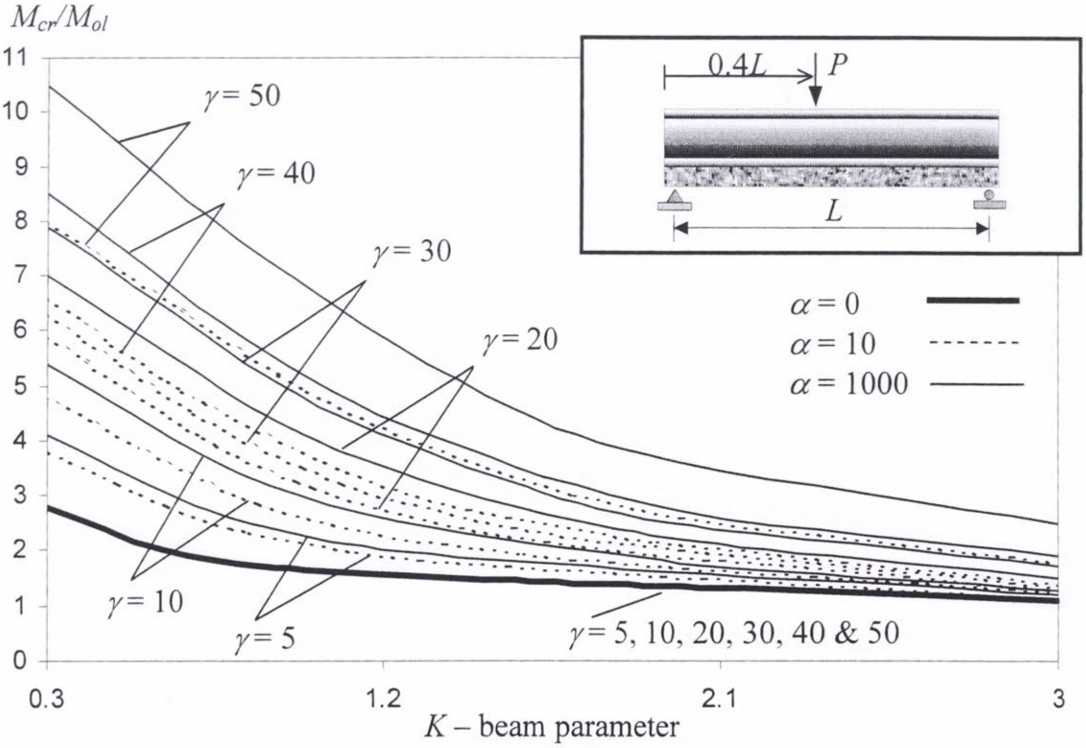
Mcr/Mol
0.4L
P
L
α = 0
α = 10
α = 1000
γ = 50
γ = 40
γ = 30
γ = 20
γ = 10
γ = 5
γ = 5, 10, 20, 30, 40 & 50
K – beam parameter
0
1
2
3
4
5
6
7
8
9
10
11
0.3
1.2
2.1
3

d)

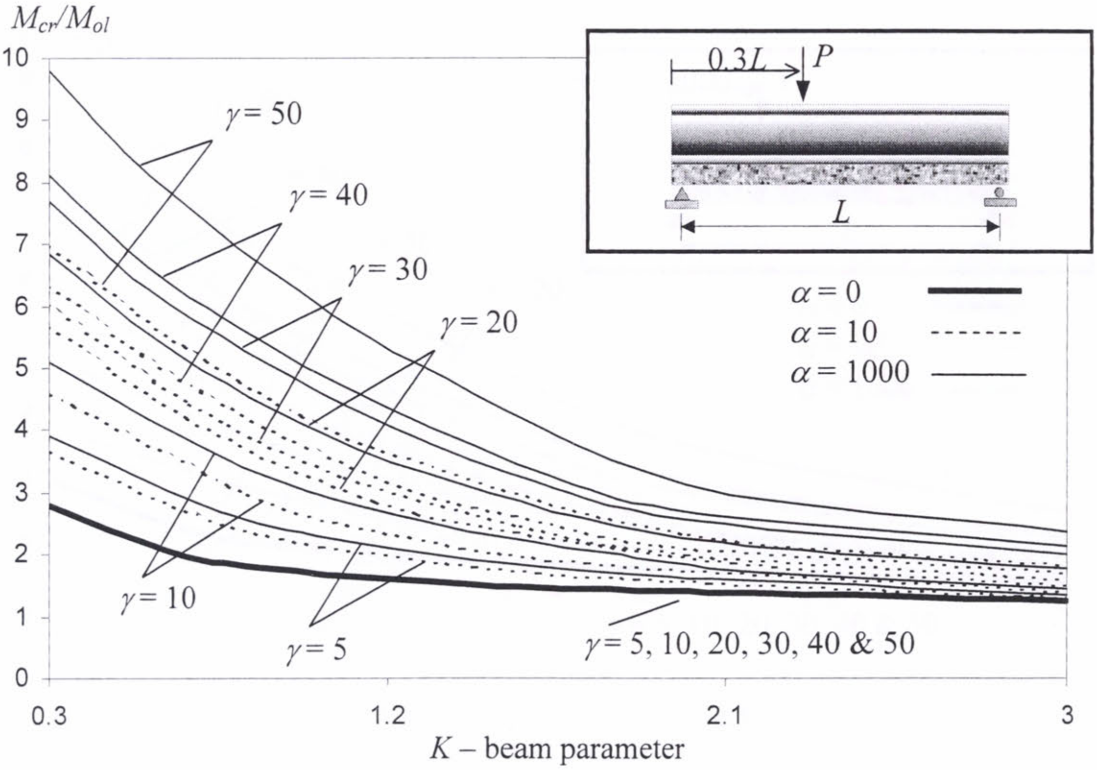
Mcr/Mol
0.3L
P
L
α = 0
α = 10
α = 1000
γ = 50
γ = 40
γ = 30
γ = 20
γ = 10
γ = 5
γ = 5, 10, 20, 30, 40 & 50
K – beam parameter
0
1
2
3
4
5
6
7
8
9
10
0.3
1.2
2.1
3

e)

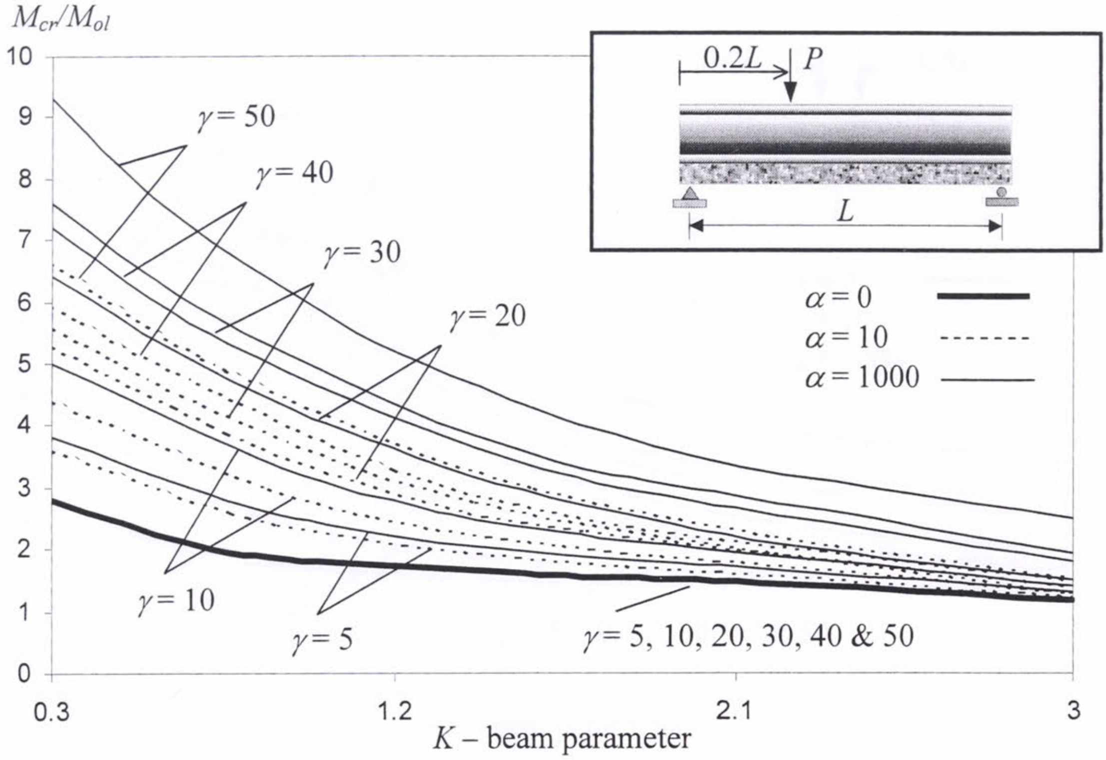

f)

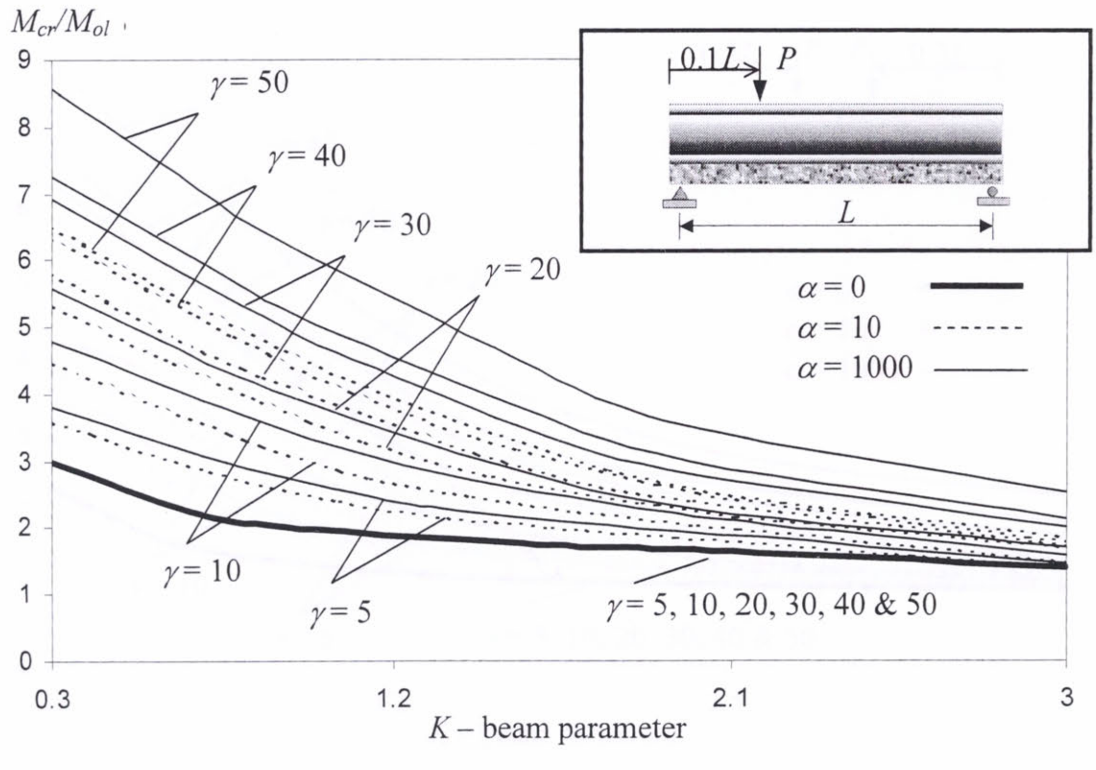

Figure 4.7 Buckling curves for transverse loads
(uniformly distributed load and one point concentrated load)

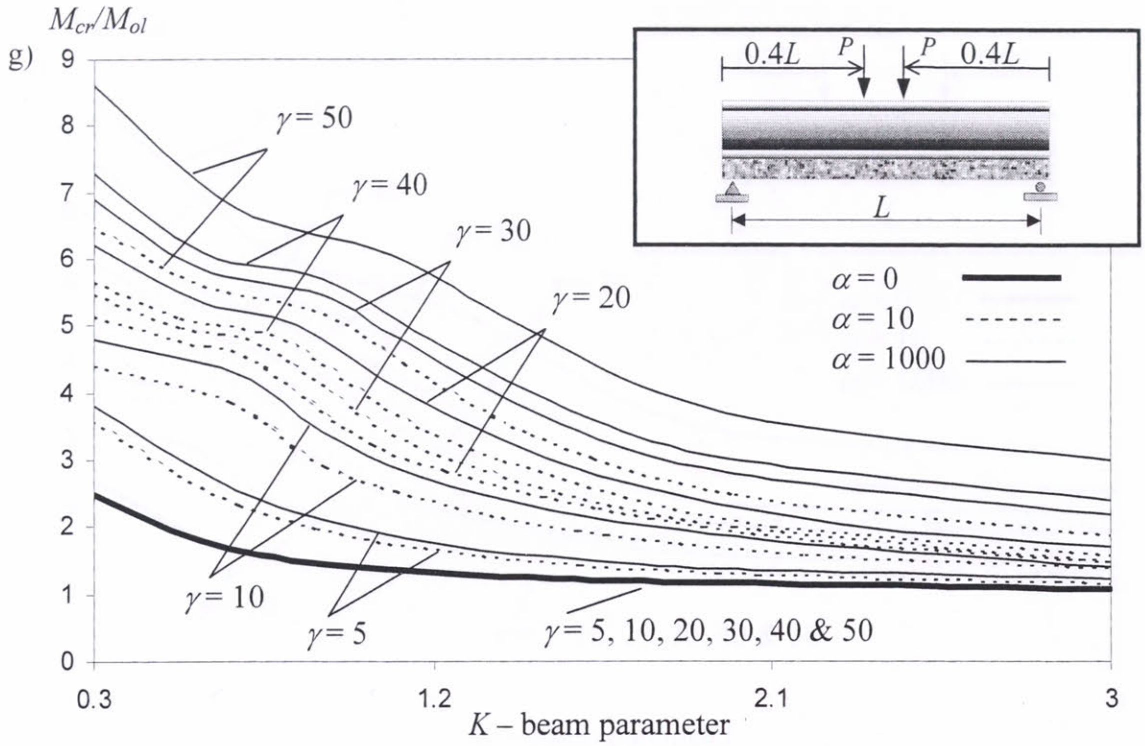
M_{cr}/M_{ol}
g)
0.4L
P
P
0.4L
L
α = 0
α = 10
α = 1000
γ = 50
γ = 40
γ = 30
γ = 20
γ = 10
γ = 5
γ = 5, 10, 20, 30, 40 & 50
9
8
7
6
5
4
3
2
1
0
0.3
1.2
2.1
3
K – beam parameter

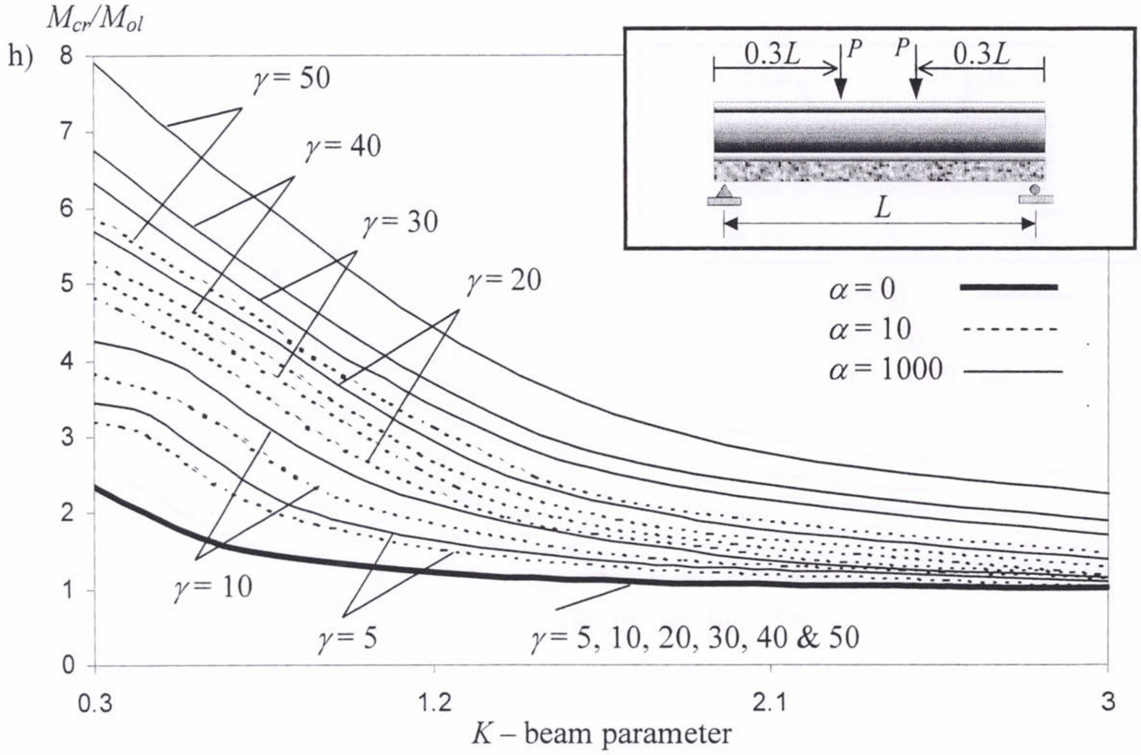
M_{cr}/M_{ol}
h)
0.3L
P
P
0.3L
L
α = 0
α = 10
α = 1000
γ = 50
γ = 40
γ = 30
γ = 20
γ = 10
γ = 5
γ = 5, 10, 20, 30, 40 & 50
8
7
6
5
4
3
2
1
0
0.3
1.2
2.1
3
K – beam parameter

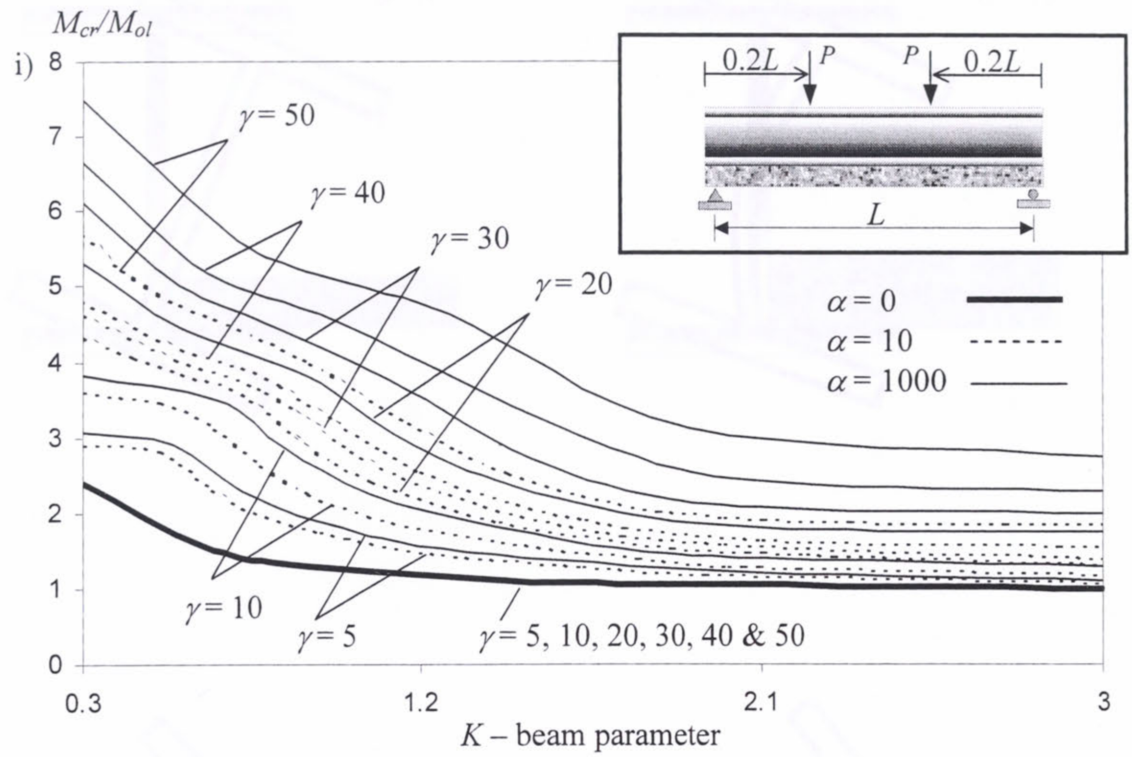

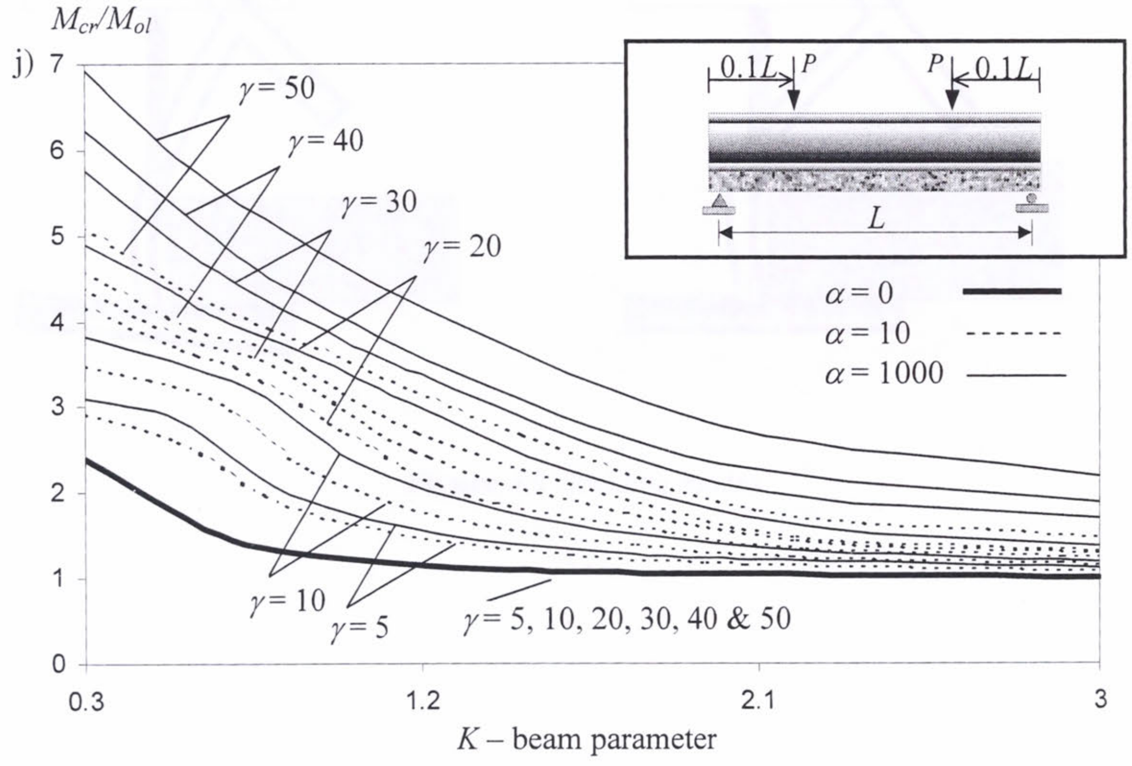

Figure 4.8 Buckling curves for transverse loads (two point concentrated load)

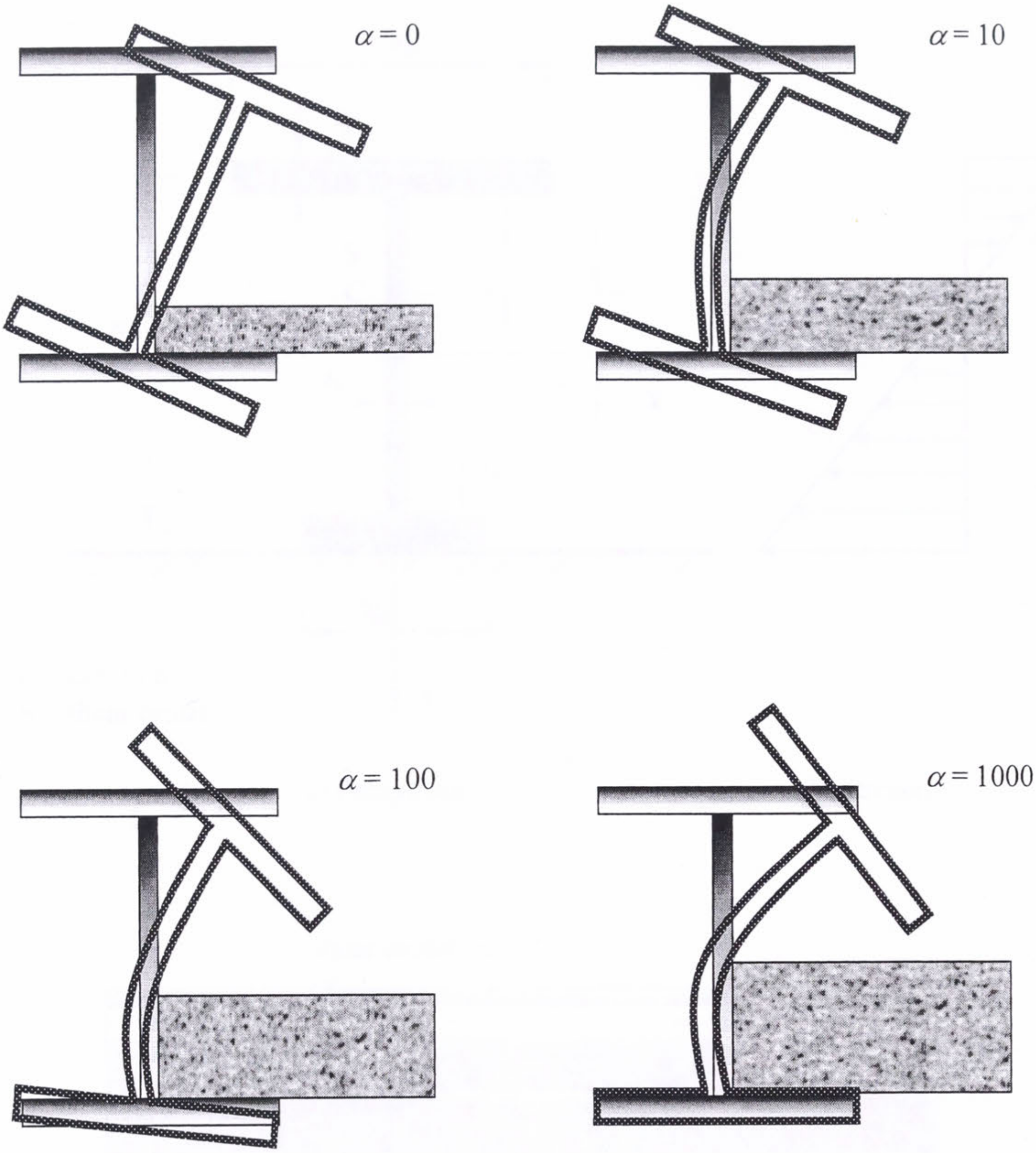

Figure 4.9 Buckling modes

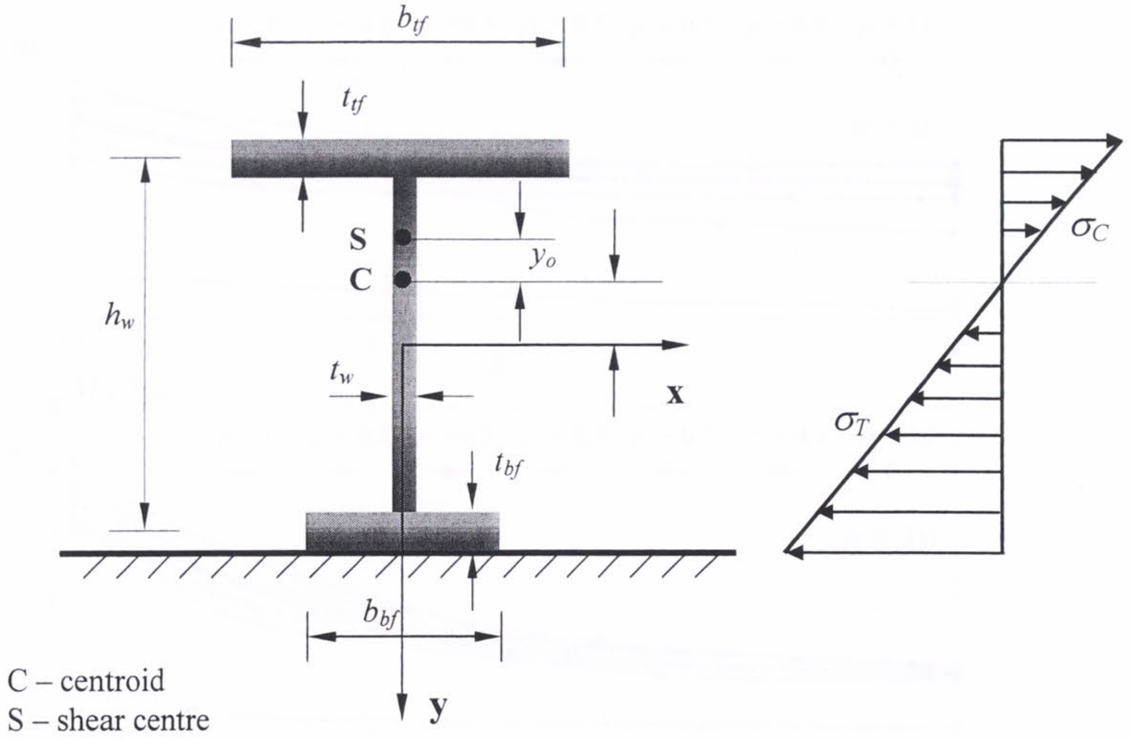

(a) dimensions (b) stresses

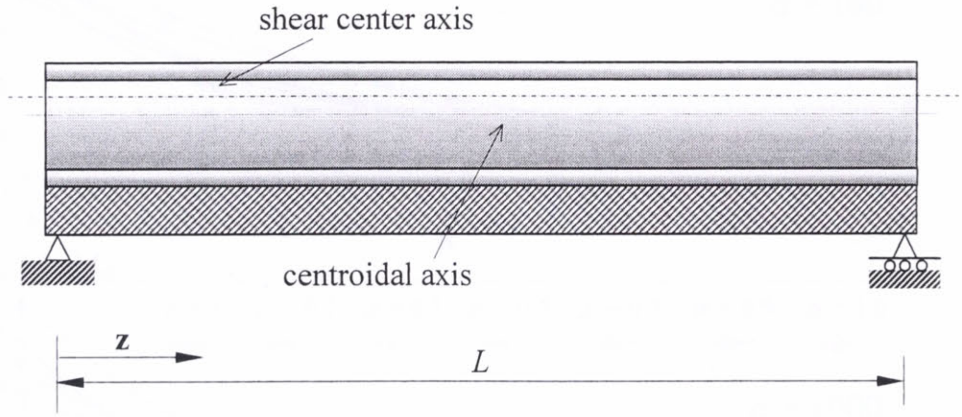

c) beam elevation

Figure 4.10 Monosymmetric simply supported continuously restrained I-beam

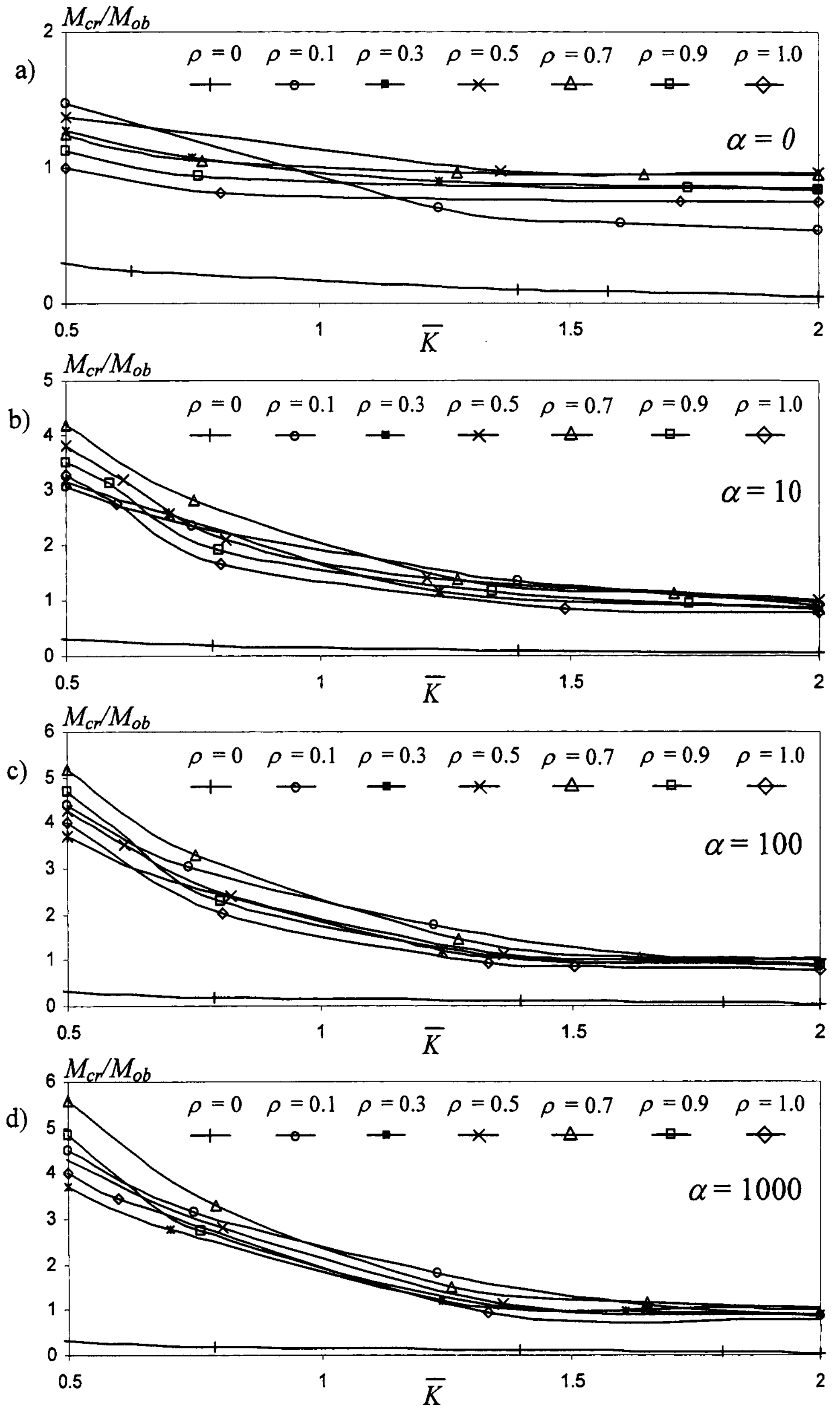

Figure 4.11 Elastic critical moments of restrained monosymmetric I-beams under uniform moment ($\beta = -1$)

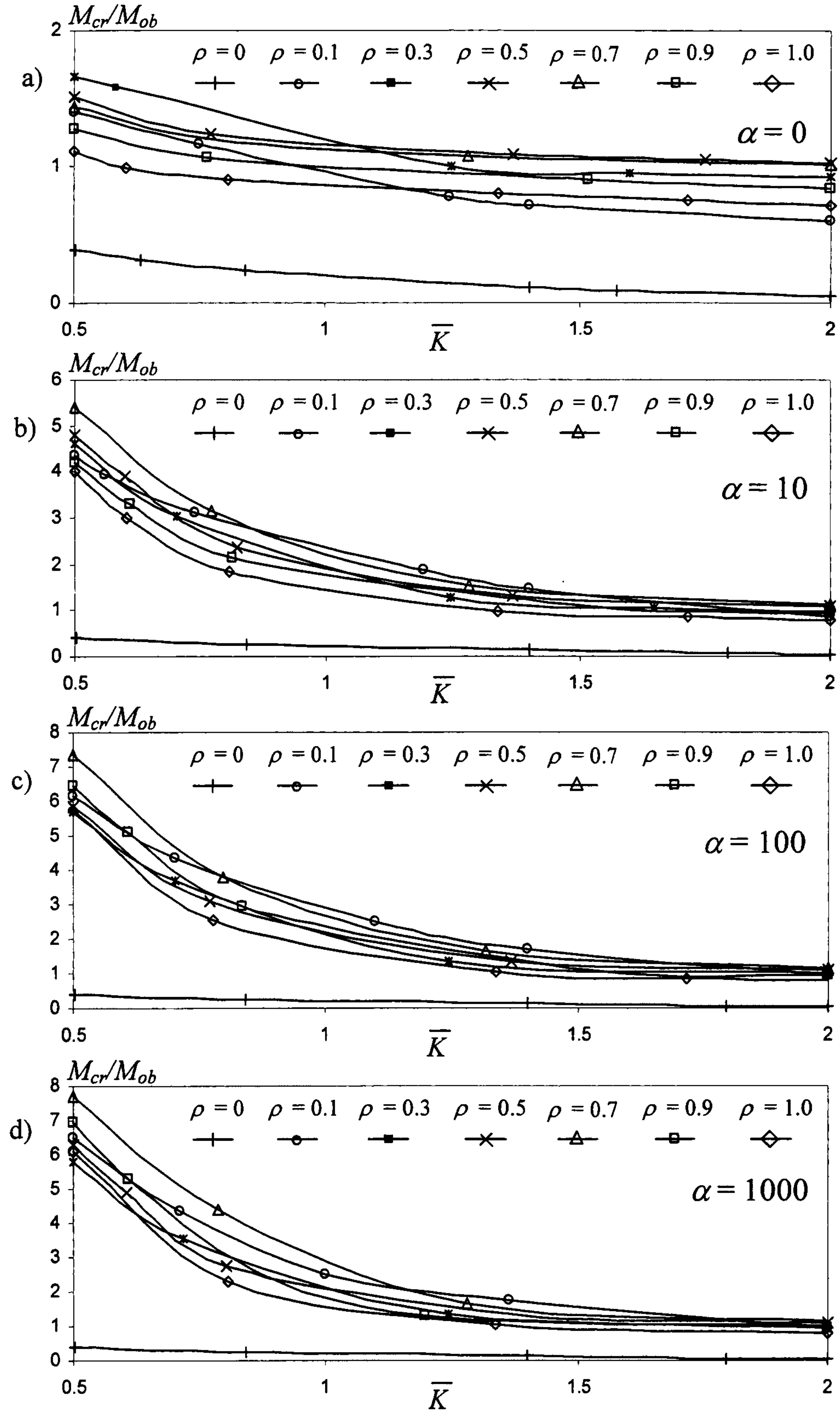

Figure 4.12 Elastic critical moments of restrained monosymmetric I-beams under uniformly distributed load

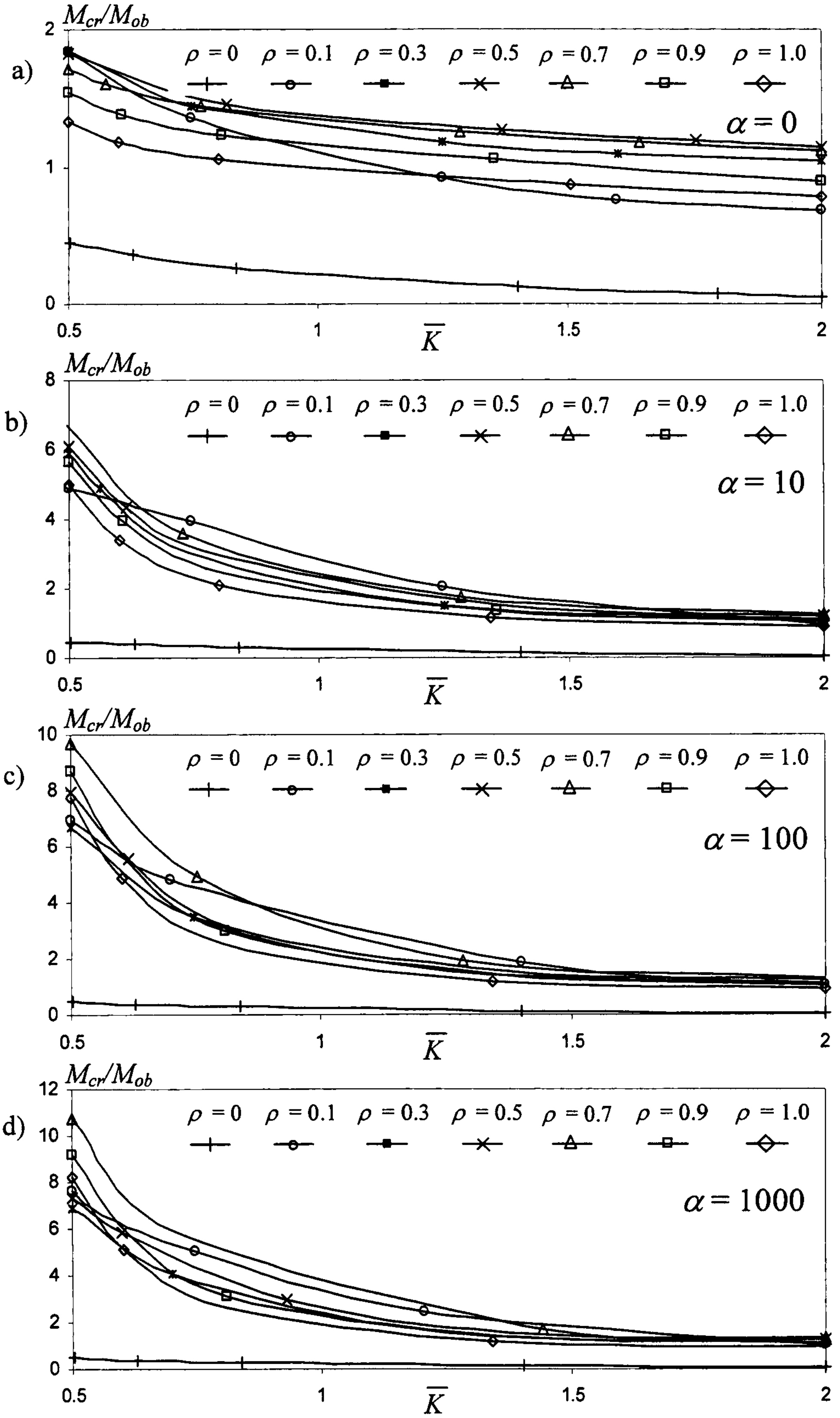

Figure 4.13 Elastic critical moments of restrained monosymmetric I-beams under central point load

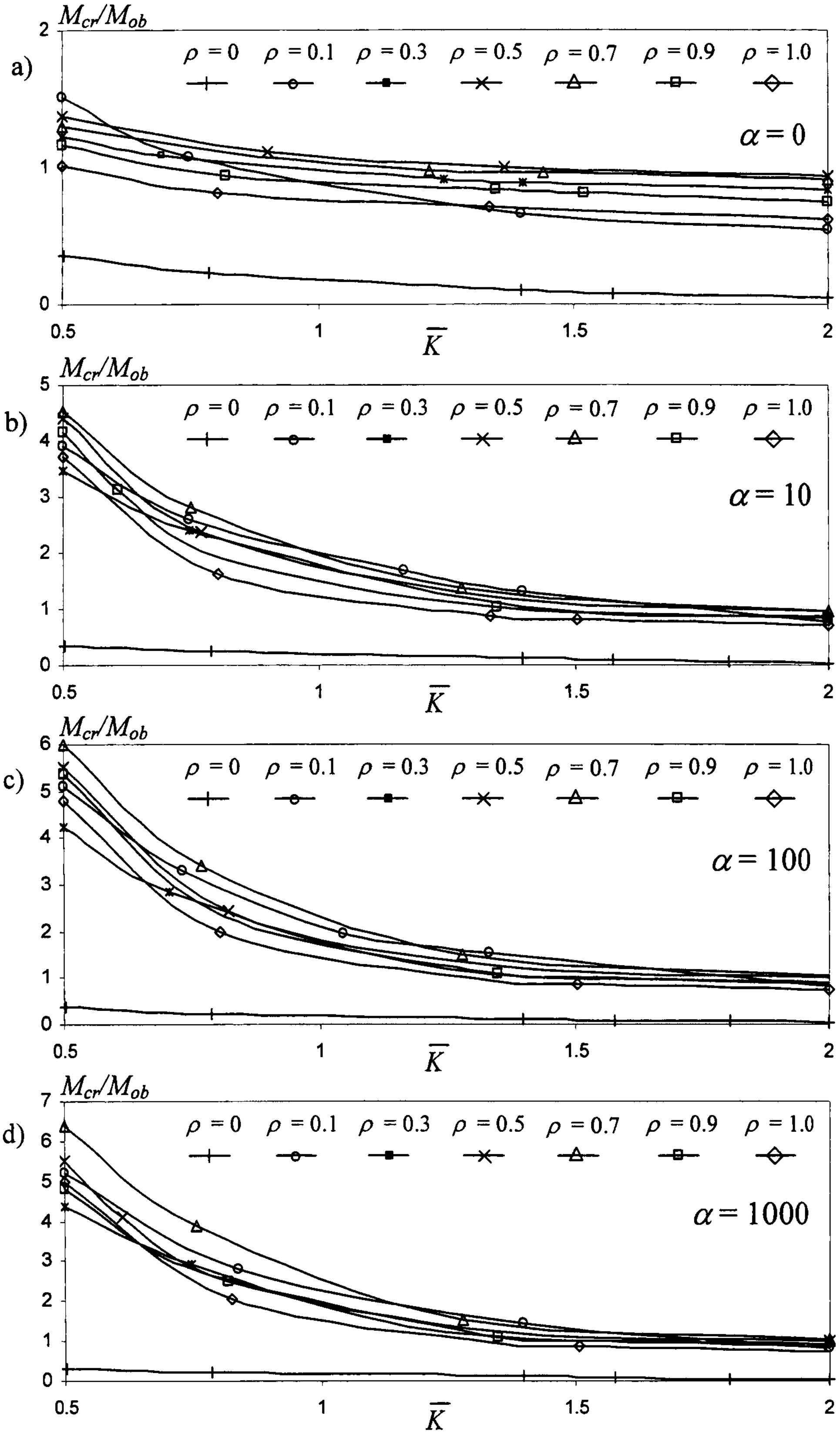

Figure 4.14 Elastic critical moments of restrained monosymmetric I-beams under two point load (acting at 0.25L from support)

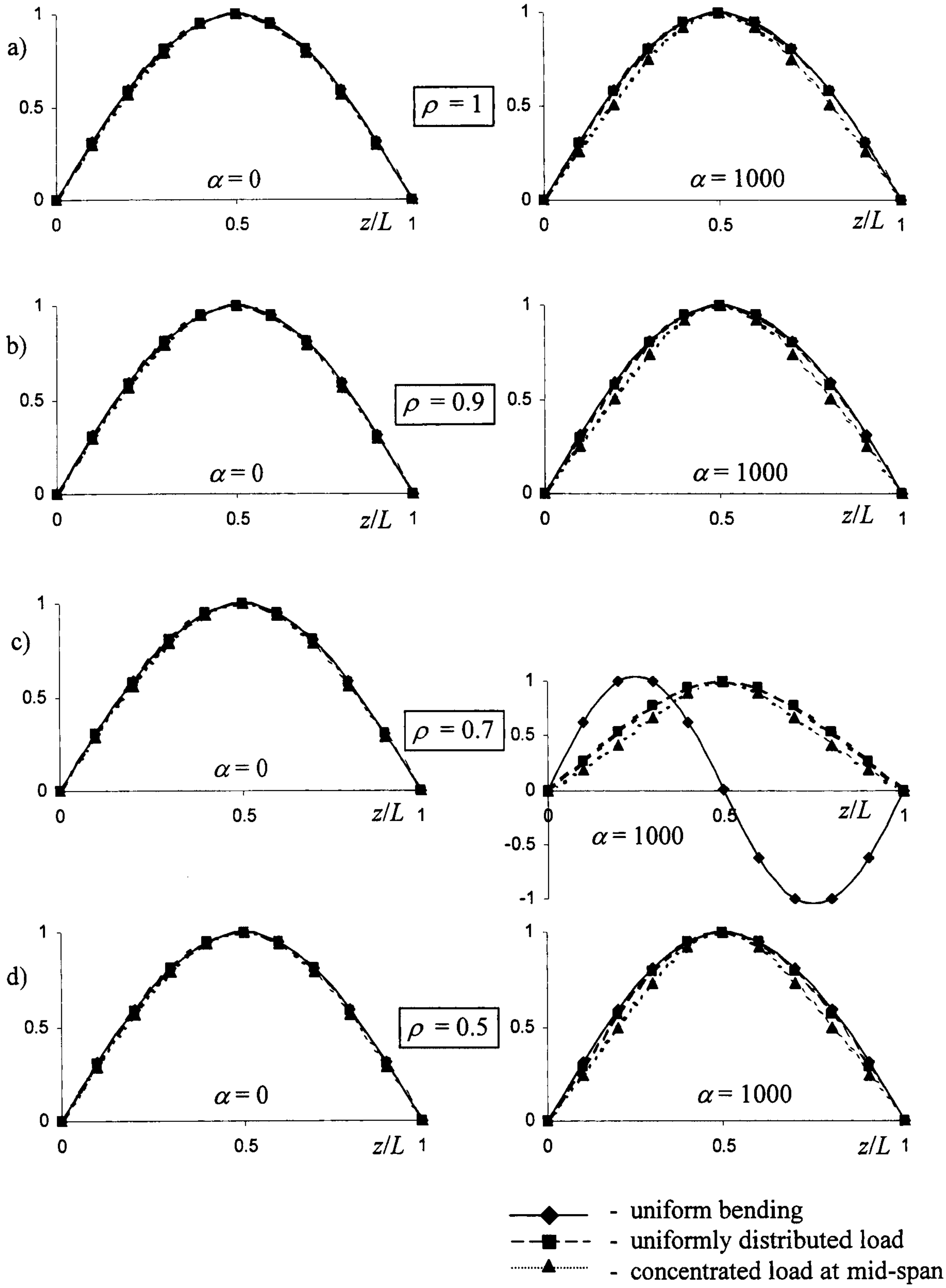
a)
b)
c)
d)
$\rho = 1$
$\rho = 0.9$
$\rho = 0.7$
$\rho = 0.5$
$\alpha = 0$
$\alpha = 1000$
z/L
0
0.5
1
-0.5
-1
- uniform bending
- uniformly distributed load
- concentrated load at mid-span

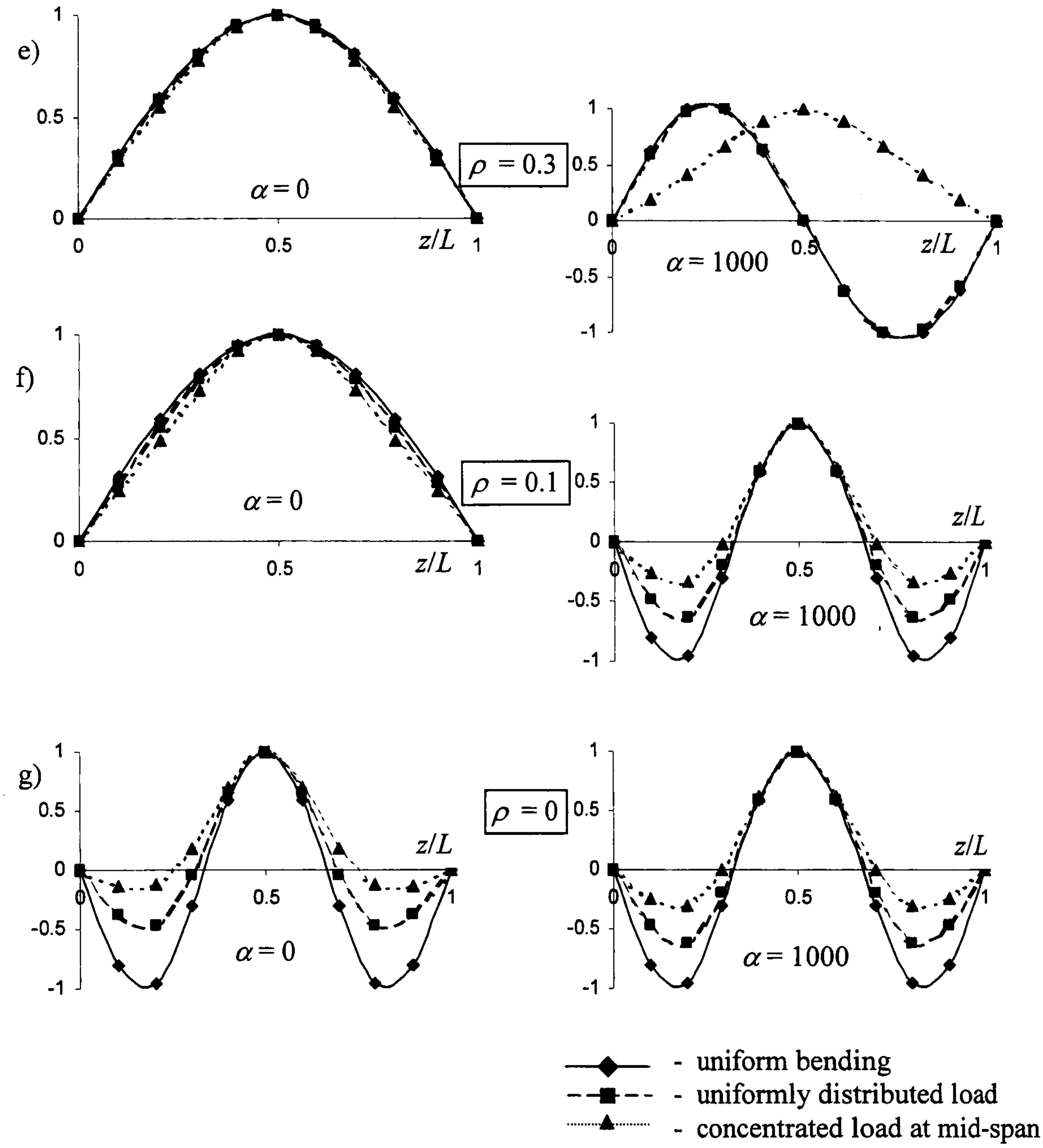

Figure 4.15 Normalised buckling mode shapes of restrained monosymmetric I-beams with $\alpha = 0$ and $\alpha = 1000$; compression flange lateral displacement

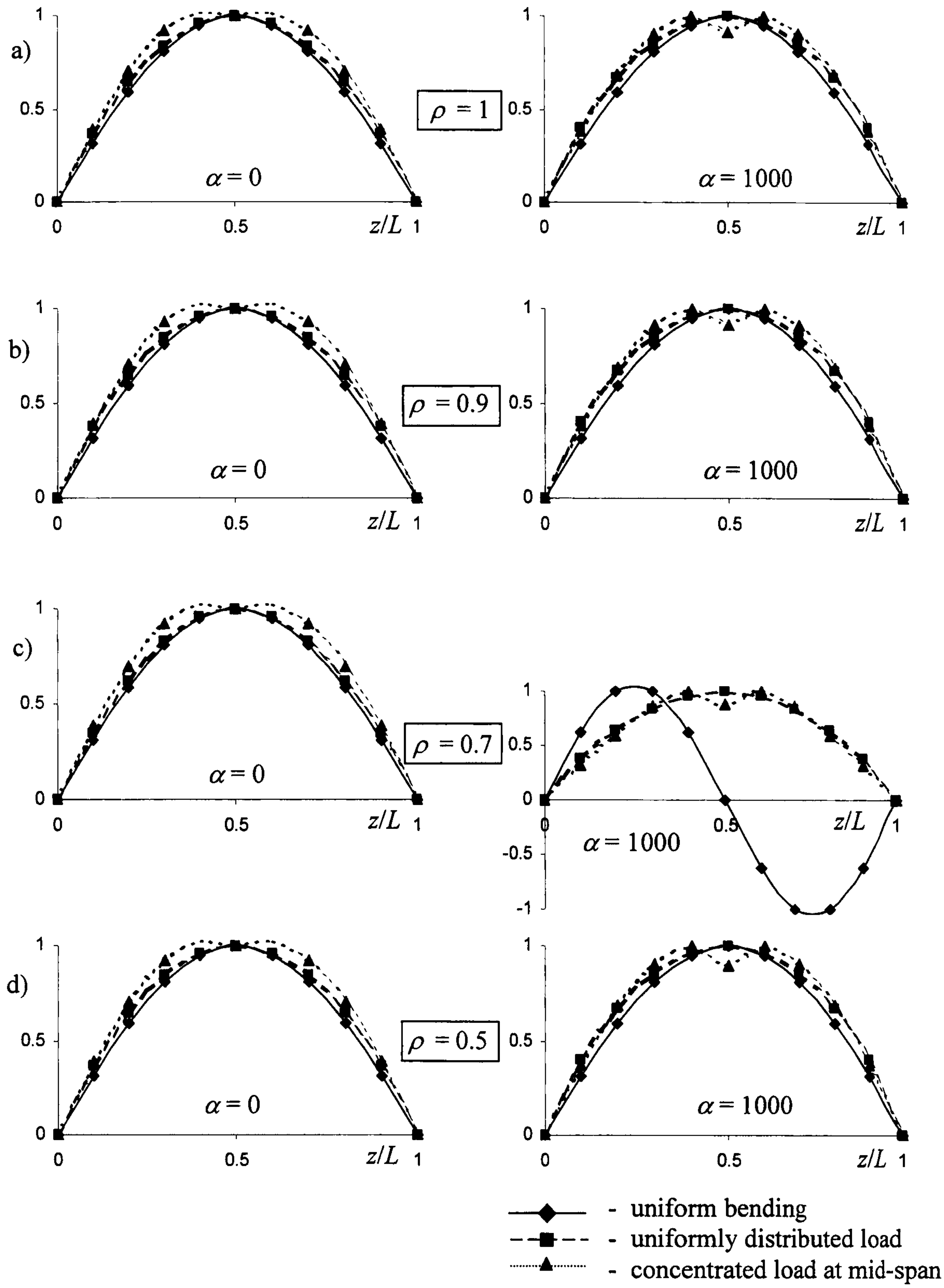
a)
b)
c)
d)
$\rho = 1$
$\rho = 0.9$
$\rho = 0.7$
$\rho = 0.5$
$\alpha = 0$
$\alpha = 1000$
z/L
- uniform bending
- uniformly distributed load
- concentrated load at mid-span

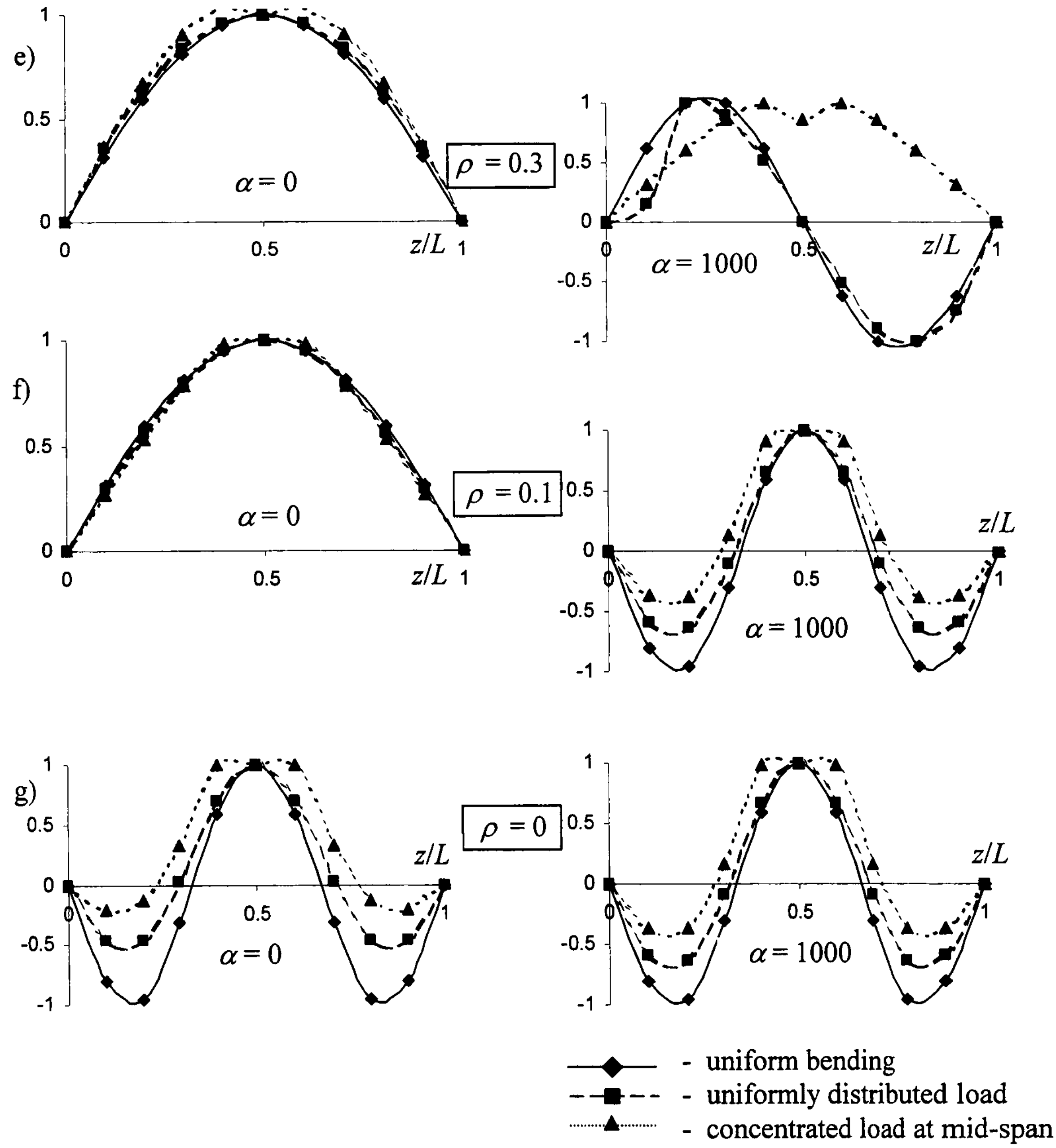

Figure 4.16 Normalised buckling mode shapes of restrained monosymmetric I-beams with $\alpha = 0$ and $\alpha = 1000$; compression flange twist

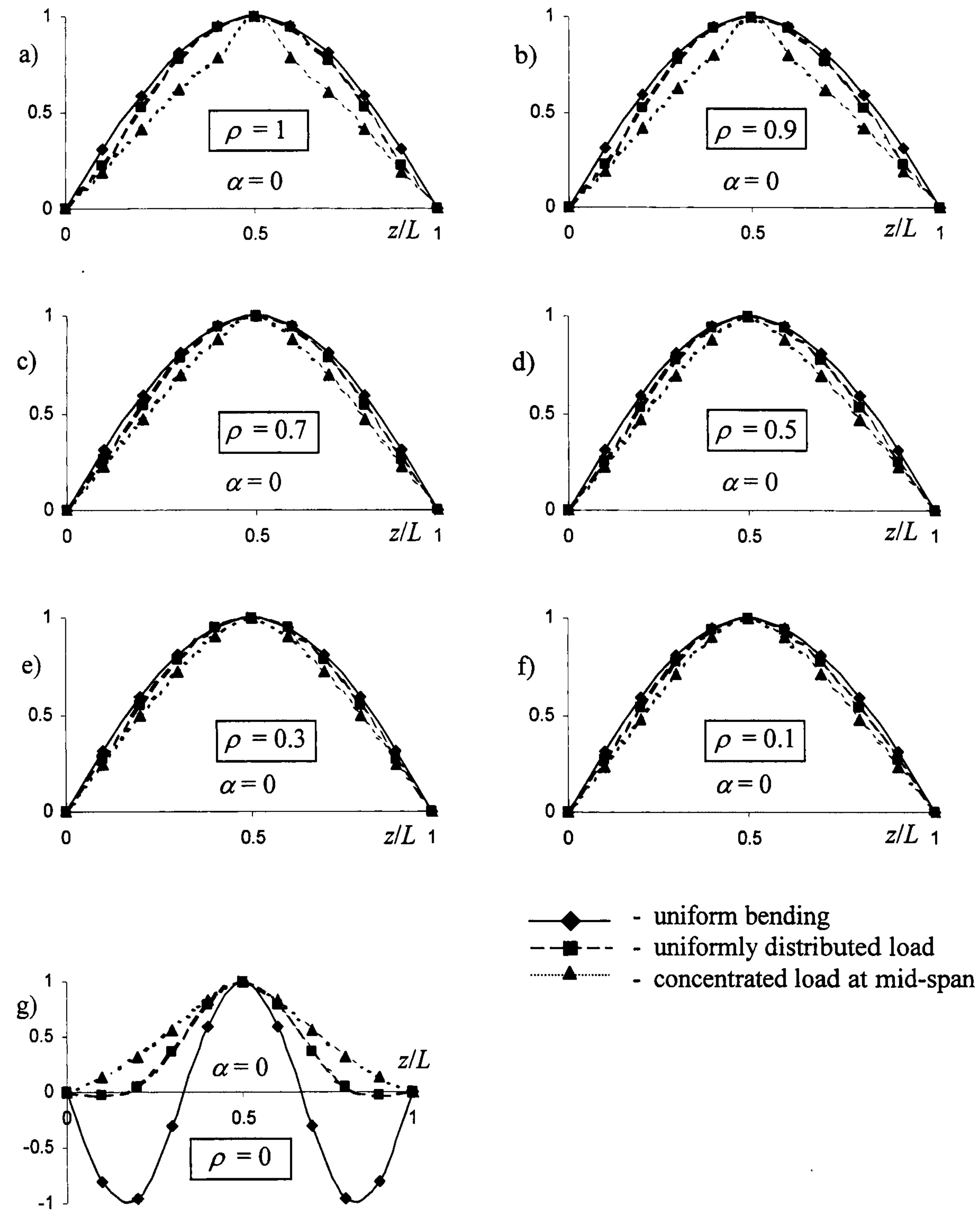

Figure 4.17 Normalised buckling mode shapes of restrained monosymmetric I-beams with $\alpha = 0$ and $\alpha = 1000$; tension flange twist

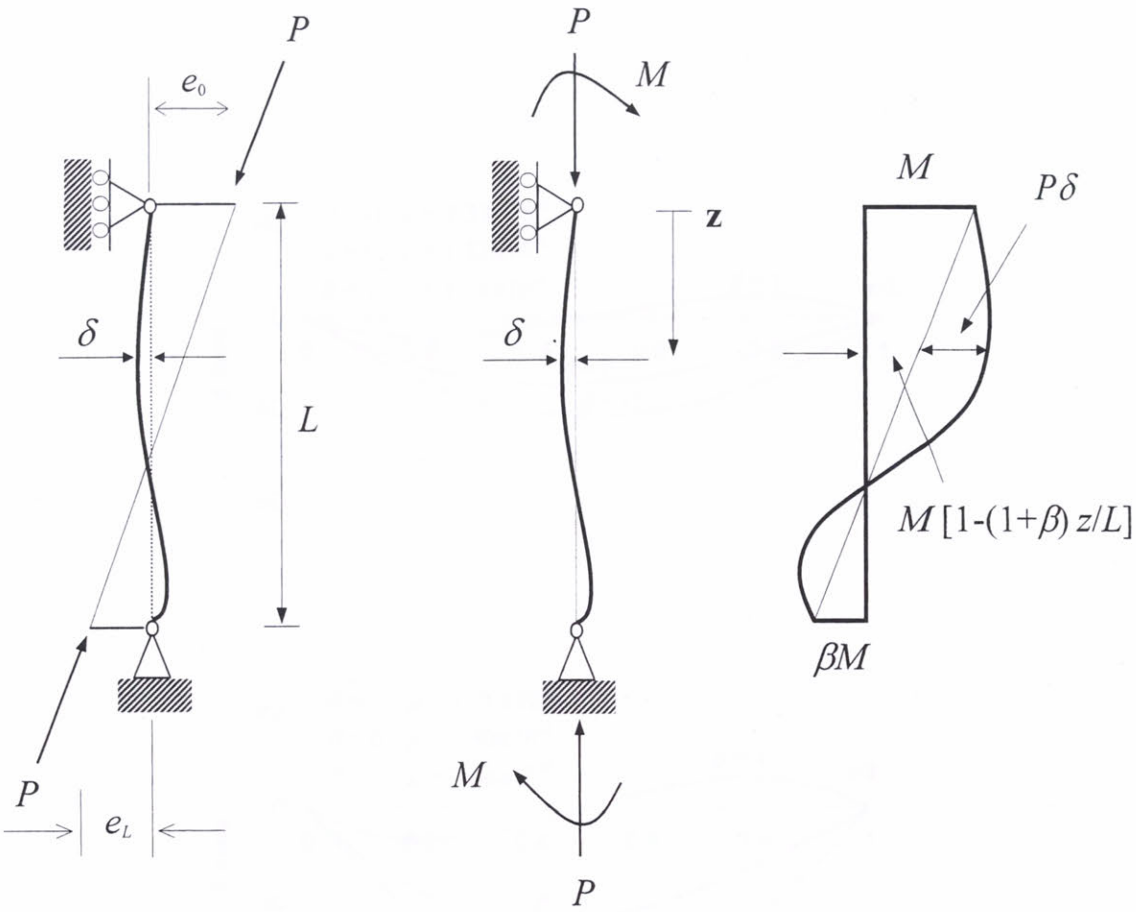

Figure 4.18 In-plane bending moment distribution in a beam-column

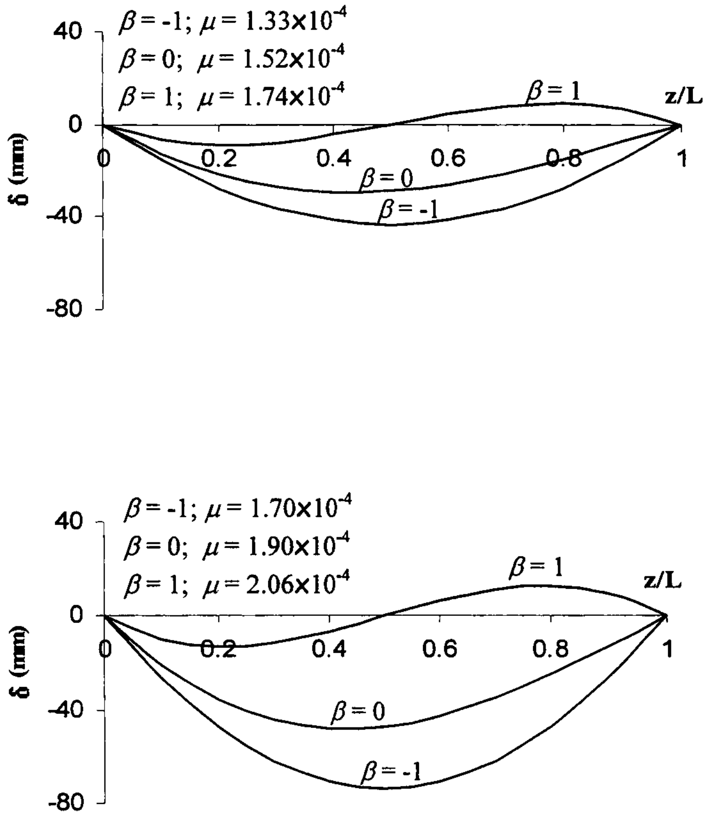

Figure 4.19 In-plane deformations

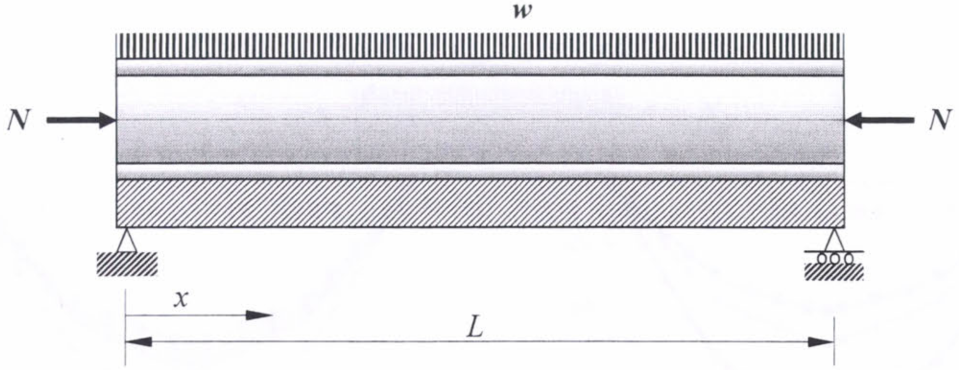

a) Continuously restrained I-section beam-column

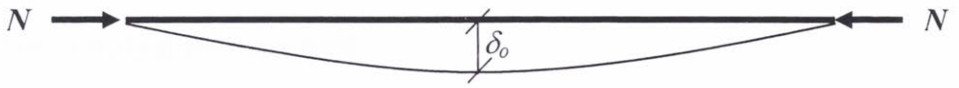

b) Beam-column deflection due to axial force

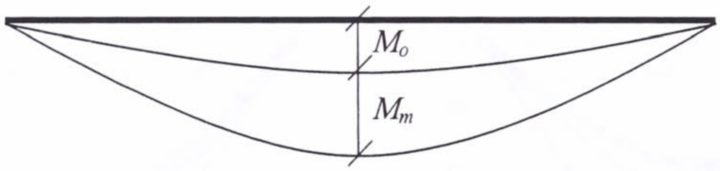

$M_m = \dfrac{wL^2}{8}$ - primary moment $\quad\quad$ $M_o = N\delta_o$ - secondary moment

c) Bending moment diagram due to axial force and transversely applied load

Figure 4.20 In-plane deformations and bending moment distribution in a beam-column

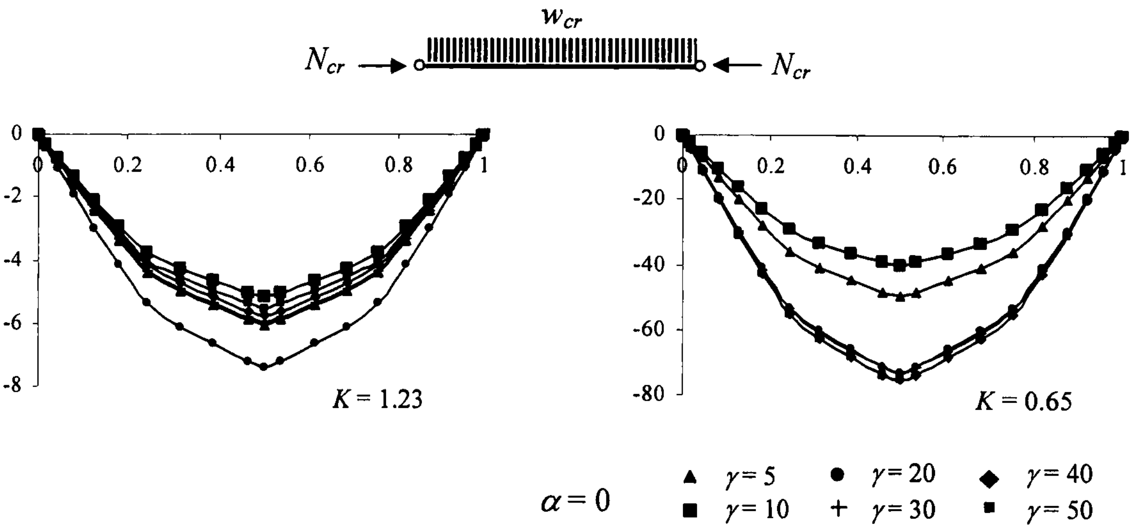

b) uniformly distributed load

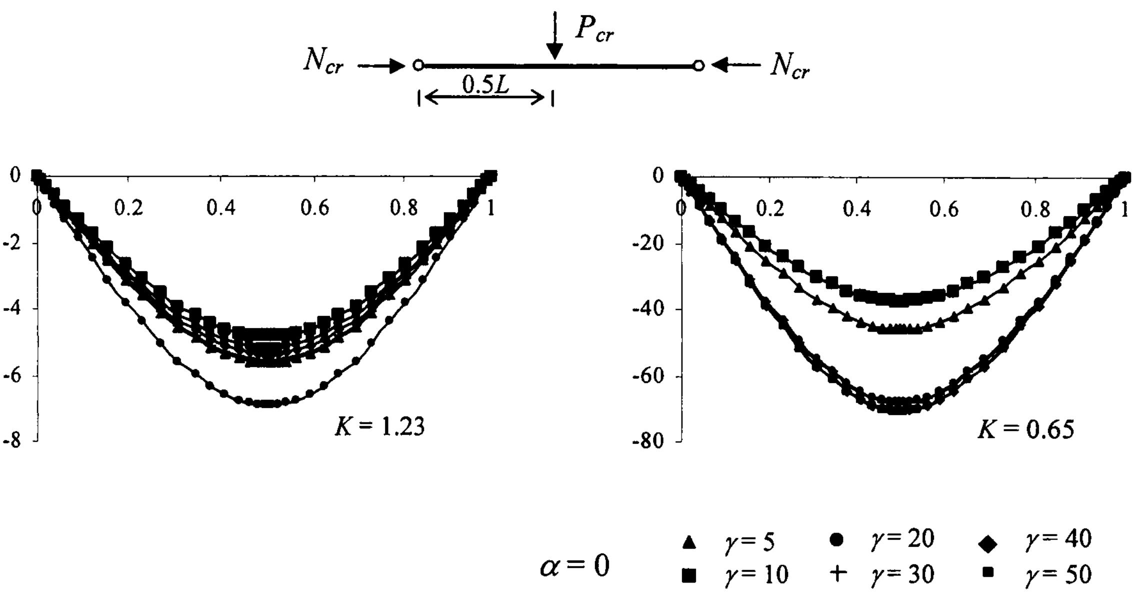

b) central concentrated load

Figure 4.21 In-plane deformations

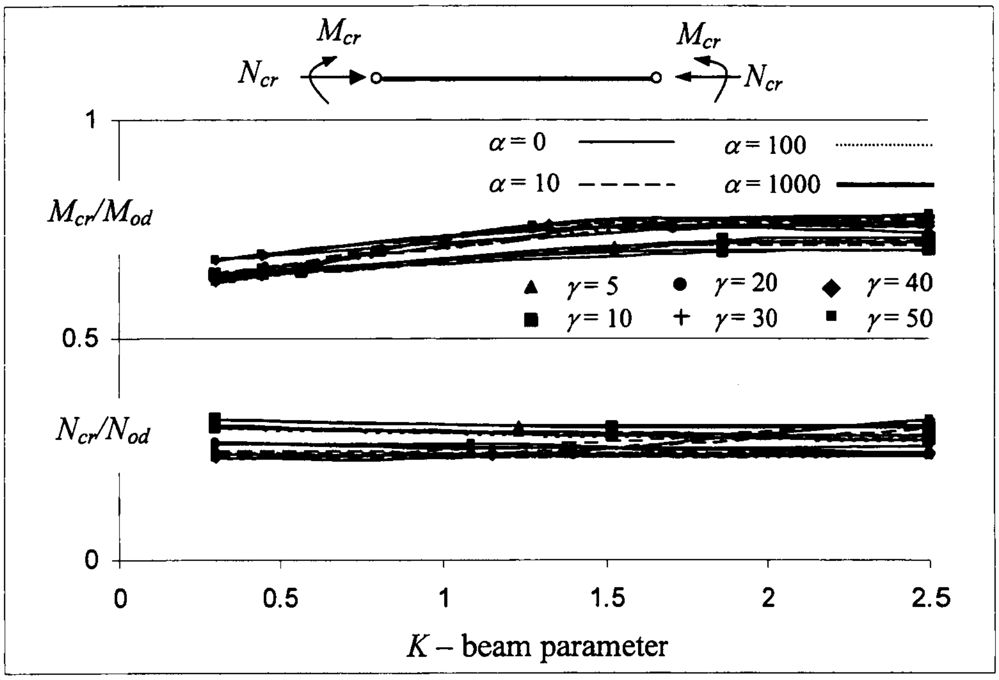

Figure 4.22 Buckling curves for beam-columns under uniform bending

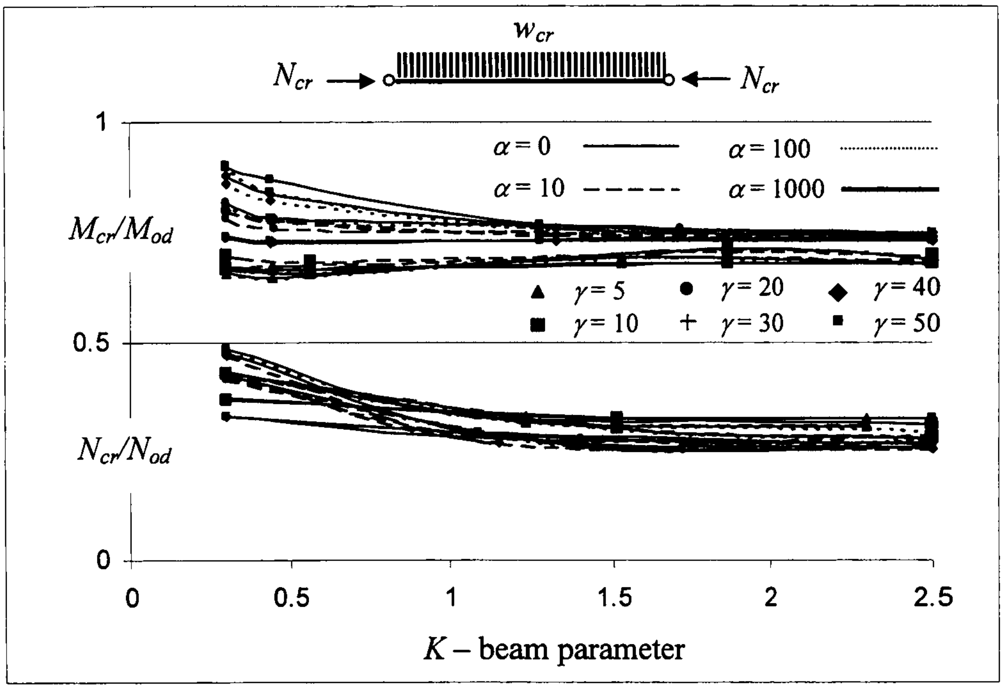

Figure 4.23 Buckling curves for beam-columns under uniformly distributed load

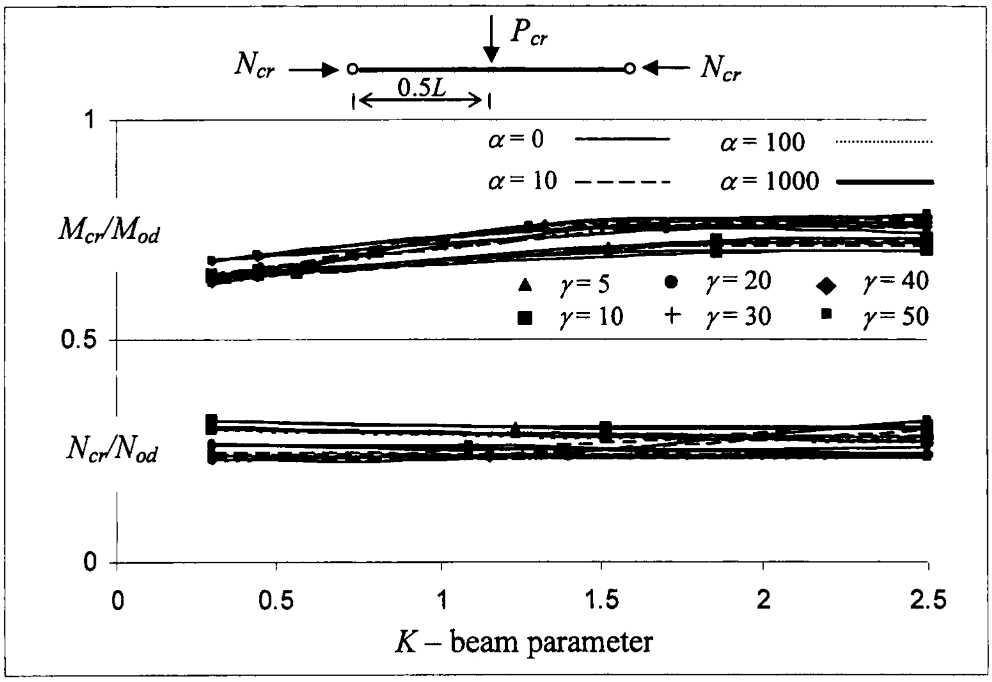

Figure 4.24 Buckling curves for beam-columns under central point load

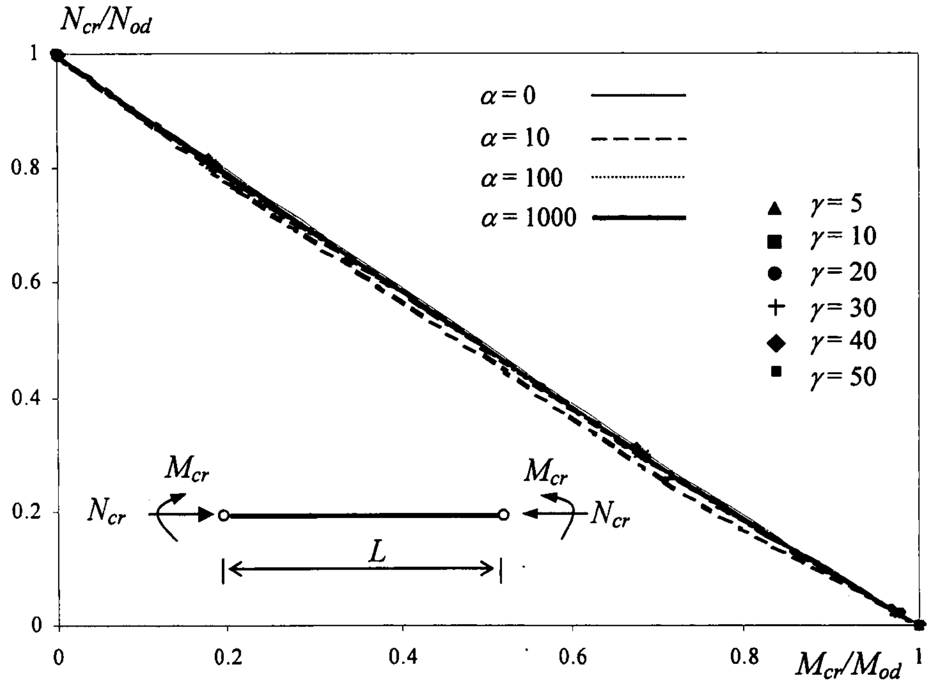

Figure 4.25 Interaction curves for uniform bending

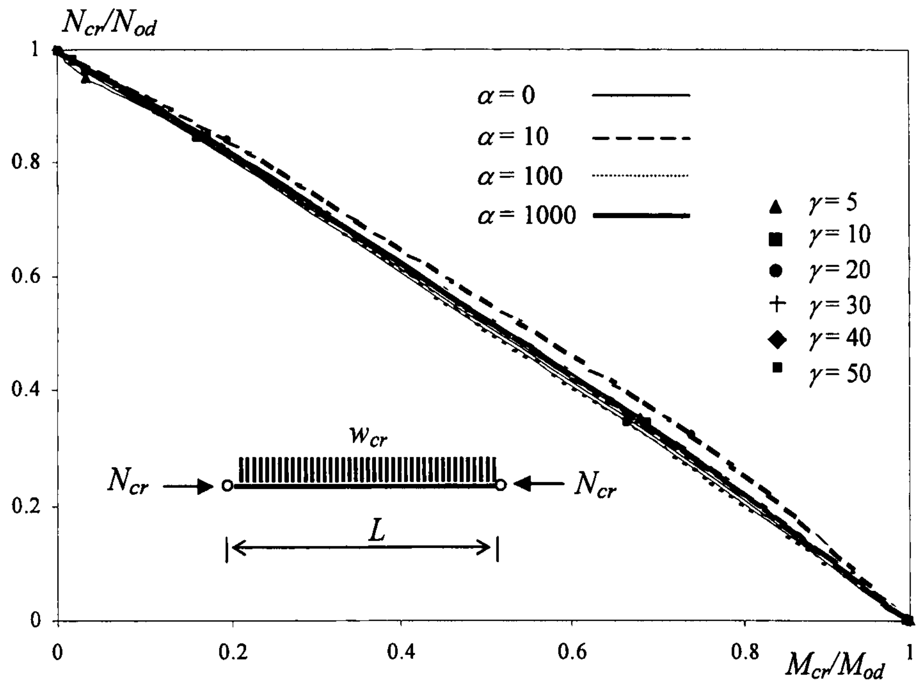

Figure 4.26 Interaction curves for uniformly distributed load

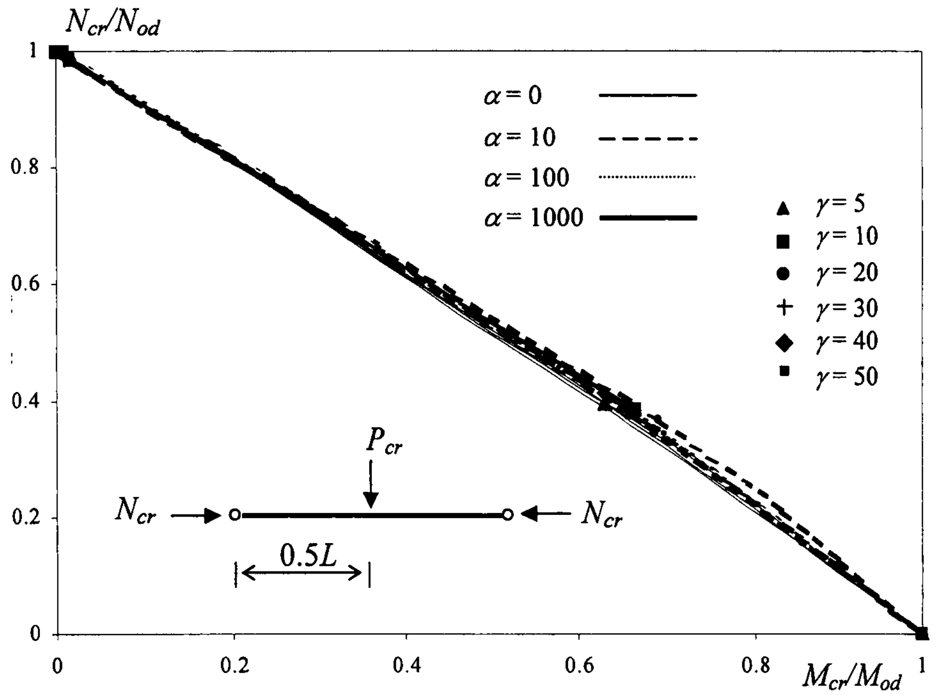

Figure 4.27 Interaction curves for central concentrated load

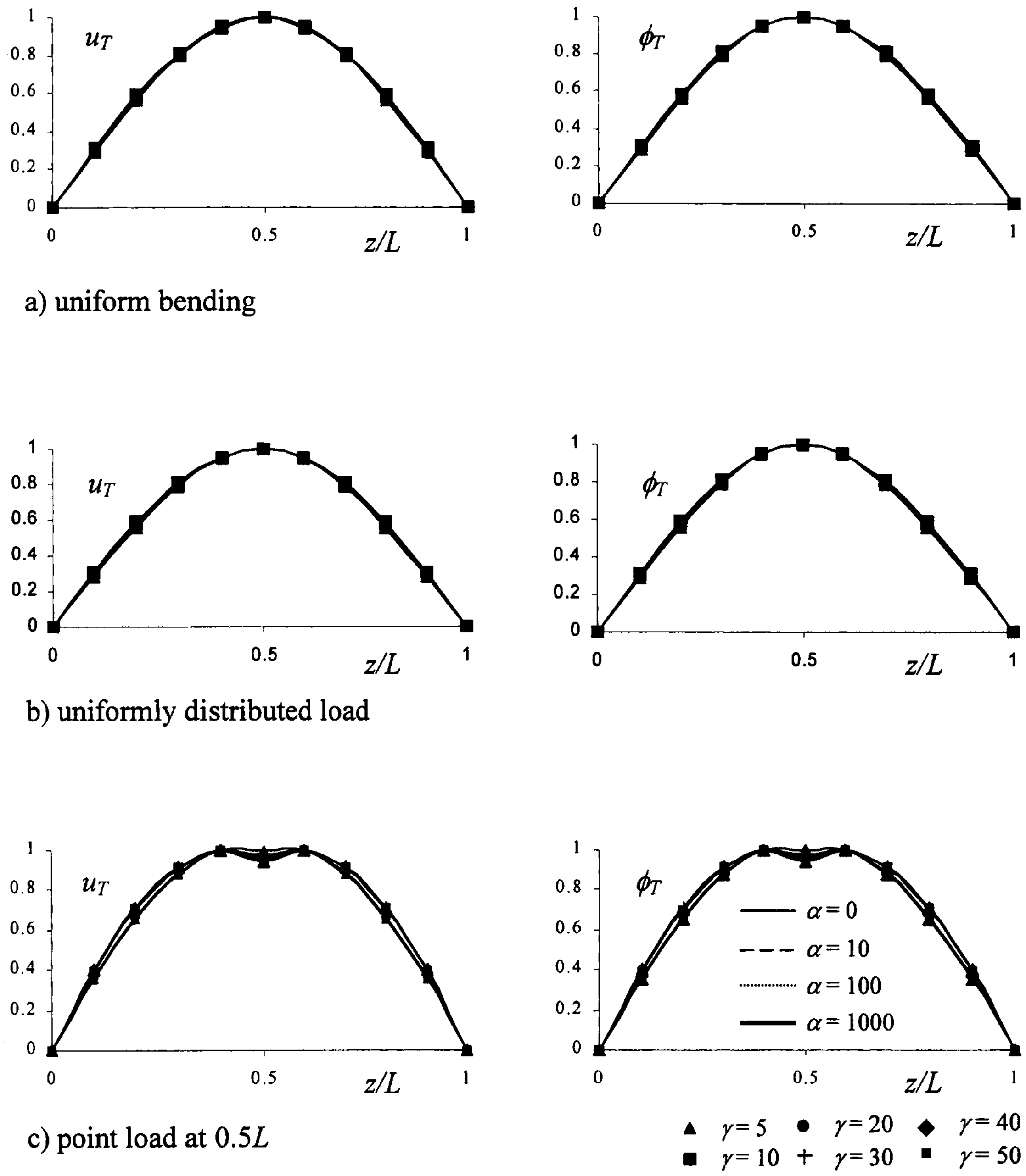

Figure 4.28 Normalised buckling modes: a) – c) compression flange lateral displacement, u_T; d) – f) and compression flange twist, ϕ_T

Chapter 5

INELASTIC RESTRAINED DISTORTIONAL BUCKLING OF I-SECTION MEMBERS

TABLE OF CONTENTS

5.1 INTRODUCTION

The inelastic lateral-distortional buckling of continuously restrained doubly symmetric and monosymmetric welded I-section beams and beam-columns subjected to uniform bending, compression and transverse loading is considered in this chapter. The numerical procedure adopted is an energy-based method that leads to the incremental and iterative solution of a third-order eigenproblem, with very rapid solutions being obtained. The basic features of the analysis were introduced in Chapter 4, in which the Rayleigh-Ritz method of analysis was applied to elastic restrained distortional buckling (RDB) of I-section members.

As was described in Chapter 4, there are number of variables that affect the elastic distortional buckling load of unrestrained I-section members, and this increases dramatically when elastic restraints and inelasticity are included in the problem. Although the elastic lateral-distortional buckling of simply supported unrestrained beams under various loading provisions is well documented, as discussed in Chapters 2 and 4, research investigations into both elastic and inelastic RDB are rather limited and still far from complete.

The scenario of continuous restraint, which prevents complete lateral displacement and rotation, and provides quantifiable twist restraint, is often met in practice. Some commonplace structural configurations such as a half-through girder bridge (Fig. 1.3, Chapter 1), a rafter with a standing-seam sheeting system (Fig. 1.4), and a composite bridge girder near an internal support (Fig. 1.5) or in a composite beam-to-column connection are examples of such behaviour. Previous studies have shown that the buckling mode of unrestrained doubly symmetric I-beams is essentially lateral-torsional (Trahair & Bradford 1998), but this is not the case for continuously restrained I-section members, especially with elastic torsional restraint ($\alpha > 0$) applied at the level of tension flange, as demonstrated in Chapter 4. The effects of elastic restraints, particularly against twist rotation, can lead to buckling modes in which the effect of distortion is quite severe.

The strength of unrestrained I-section beams is usually reduced below the elastic buckling value due to premature yielding as a result of combined effects of the stresses caused by the applied load and of the residual stresses which are established during the cooling of welded steel member. Since yielding occurs before the ultimate moment is reached, significant portions of the beam are inelastic when buckling commences, the effective moduli of the yielded and strain-hardened portions of the member are reduced below their elastic values, with consequent reductions in the stiffness, which contribute towards reducing the resistance to lateral buckling. Inelasticity is particularly significant in fabricated I-section members because the welding process results in levels of residual stresses that are typically higher than those in hot-rolled beams. It is generally acknowledged that the influence of welding residual stresses on beam buckling capacity is more severe that that of residual stresses induced by hot-rolled procedures (Kitipornchai & Wong-Chung 1987).

When a beam has a more general loading than that of equal and opposite end moments, the in-plane bending moment varies along the beam, and so when yielding occurs its distribution also varies (Fig 5.1). The analysis of the inelastic buckling of beams under transverse loading is more complicated than for beams under uniform bending due to spatial non-uniformity of the elastic core of the beam as it is both monosymmetric and tapered. Because of this, the beam acts as if non-uniform, and the equilibrium equations become more complicated. However, the variations of the residual stresses across the flanges are nearly uniform in welded beams, and so once flange yielding is initiated, it spreads quickly through the flange with little increase in moment. This causes large reductions in the inelastic buckling moments of stocky beams (Trahair & Bradford 1998).

Research work on inelastic lateral buckling of unrestrained I-sections has been reasonably plentiful. The first such study by the finite element method that considered cross-sectional distortion appears to be that of Bradford (1986a). While this model, which was based on an earlier elastic formulation (Bradford & Trahair 1981) appears to be valid for including distortion when the flanges are either free or fully fixed, it was argued (Bradford & Ronagh 1997a) that the elastic 12 degree of freedom line element used in Bradford and Trahair (1981) can not account accurately for elastic restraint against twist rotation, and a 16 degree of freedom elastic model was proposed (Bradford

& Ronagh 1997a). Recently Lee (2001) developed a beam-type line element with 16 degrees of freedom to study the inelastic lateral-distortional buckling of simply supported unrestrained and restrained beams under transverse loading. However, Lee's investigation was limited to hot-rolled I-sections only. So far, no detailed study appears to have been undertaken of the influences of the welding residual stresses on the inelastic RDB of I-section beams and beam-columns under transverse loading and the author has found no reported systematic study.

Thus, in the following sections the energy-based method of the elastic distortional buckling of continuously restrained I-section members is extended into the inelastic domain. The modified method accounts for residual stresses appropriate for welded I-sections (Fig. 5.2), by adopting so called 'tendon force concept' model first developed by Cambridge group (Dwight & Moxham 1969; Young & Schulz 1977; Dwight 1981). Thus, the model developed in this chapter combines the effects of cross-sectional distortion, and of inelasticity. The method is then validated by comparisons with inelastic buckling results for both unrestrained and restrained I-section beams. Following studies of the accuracy of the buckling solutions, the method is used to demonstrate the interaction between distortion and yielding of I-section beams under a variety of loading configurations. The energy method is then employed to study the relationship between elastic distortional buckling and yielding for an I-section beam-column restrained by concrete medium at the tension flange level and some results are reported. Conclusions are drawn that address the influence of geometry, residual stresses, member length and restraint stiffness for the inelastic RDB.

5.2 RESIDUAL STRESSES

The prediction of the inelastic buckling load depends on the beam cross-section, the variation in yield stress, the assumptions made when calculating the moduli for the various rigidities and on the magnitude and distribution of residual stresses. It is well known that residual stresses are introduced in members as a result of welding and flame cutting processes, and that these stresses may influence the load carrying capacity of thin-walled members, particularly those that contain slender component plates

(Kitiponchai & Wong-Chung 1987). The magnitudes and distributions of residual stress in steel members vary considerably with the cooling and straightening process. Due to the welding process, the residual stresses (and strains) at the flange-web junctions are assumed to be at yield in tension. The shrinking after welding of the late cooling regions of a member induces residual compressive stresses in the early cooling regions, and these are balanced by equilibrating tensile stresses in the late cooling regions. The flange-web junctions are least exposed to cooling influences, and so these are regions of residual tensile stress. On the other hand, the exposed flange tips cool more rapidly, hence these are regions of residual compressive stress.

By making use of the heat input incurred during the welding process, as well as equilibrium of the unloaded section, it is possible to determine the distribution and magnitude of the stresses around the section. The residual stresses caused by welding have been studied extensively at Cambridge University (Dwight & Moxham 1969; Young & Schulz 1977; Dwight 1981), and recommendations for their magnitude and distribution have been given by Kitipornchai and Wong-Chung (1987). The residual stress model for an I-section member, presented by Kitipornchai and Wong-Chung (1987), is illustrated in Fig. 5.3. The model assumes that tension blocks stressed to yield stress, f_y occur at the cuts and welds, accompanied by adjacent compression blocks such that the plate is in longitudinal equilibrium. The expressions for the size of these blocks are empirical, and depend on the plate thickness, weld size and welding process efficiency. The assumed residual stress pattern consists of a fully yielded tensile stress block of width $2c_f$ in the flange at the weld, and a constant residual compressive stress, σ_{rc} at the outer edges to maintain equilibrium. The half-width c_f of the tensile stress block is given by

$$c_f = \frac{F}{(\sigma_y + \sigma_{rc})(2t_F + t_W)} \tag{5. 1}$$

in which the tendon force, F is expressed as a function of the area of the added weld metal, A_w, and the welding process constant, B from the equation

$$F = BA_w. \tag{5. 2}$$

For manual arc welding, a value of the constant B = 8,000 N/mm^2 is generally recommended (Dwight 1981). t_F and t_W are the thicknesses of the flange and web plates, respectively. It is assumed that this zone of influence will extend by an equal amount c_f into the web.

In calculating the residual strains, tension blocks occurring at the welds, as shown in Fig. 5.3, are assumed to be stressed to yield stress and the compressive residual stress, σ_{rc} is given as

$$\sigma_{rc} = \frac{F}{b_F\left(t_F + 0.5t_W\right)}. \tag{5. 3}$$

Because of the presence of residual stresses in the member, yielding will be initiated at the most highly strained regions and then spread through the cross-section. At high moments, the strain-hardening strain, ε_h will be exceeded, and so some regions will have stresses greater than the yield stress, f_y. The applied stress anywhere in the section, σ may then be found from

$$\sigma(x,y) = \int_{\varepsilon_r}^{\varepsilon} E_{st}\,\mathrm{d}\varepsilon_a + E\varepsilon_r(x,y) \tag{5. 4}$$

where ε_a is the strain due to applied load, ε_r is the residual strain, assumed herein to be σ_r/E, E is Young's modulus and E_{st} is the tangent modulus. Of course, ε_a and ε_r vary around the cross-section. Hence a doubly symmetric I-section will behave as a monosymmetric I-section because different parts of the section have different material properties. High compressive residual stresses will result in early yielding at the compressive flange tips with subsequent significant reductions in the minor axis flexural and warping rigidities, and an increased destabilising effect of monosymmetry.

5.3 THEORY

5.3.1 General

The energy method developed in Chapter 4 is modified herein to incorporate inelasticity and residual stresses to analyse the inelastic buckling of simply supported beams and beam-columns under transverse loading. The approach is to undertake an in-plane analysis of a straight member under a monotonically increasing load factor, λ and at the given load factor to perform an out-of-plane buckling analysis. The load factor is then increased until buckling occurs, with the stiffness and stability matrices in the out-of-plane analysis being dependent nonlinearly on the value of λ. Since the simply supported member is statically determinate, the bending moment and shear force at a cross-section can be determined from simple statics, but the extent of yielding over a cross-section and along the member depends nonlinearly on λ. In the buckling analysis, yielding and strain hardening regions of the member are assigned a tangent modulus equal to that of the strain-hardening modulus of the steel, which is consistent with the dislocation model of yielding used in other studies (Bradford & Trahair 1985; Bradford 1986a). It should be pointed out that this study is concerned with bifurcation buckling, and is not reliant explicitly on a plasticity model that allows for unloading. The ensuing realisation of a 'nonlinear elastic' modelling of inelastic buckling has its basis on the infinitesimal buckling deformations that depart from an initially straight and unbuckled primary equilibrium path at bifurcation, and which justifies the uncoupling of the in-plane and out-of-plane analysis.

The first step in the in-plane analysis is to determine the relationship between the in-plane bending moment and/or axial force acting at a section with the curvature and/or strain of the beam/column, and then to find the positions in the cross-section of the elastic, yielded and strain-hardened boundaries. This then allows the variations with bending moment and axial force of the out-of-plane buckling section properties to be determined.

The stress-strain curve assumed for the structural steel is a tri-linear idealisation, shown in Fig. 5.4, with a plastic plateau and a constant tangent modulus $E_{st} = E/33$. For this, the yield stress, f_y was taken to be 250 MPa with a yield strain, ε_y of 0.00125. The strain hardening, ε_h was taken as $11\varepsilon_y$. These are commonly accepted values. Compressive stresses and deformations are taken as positive, and positive bending causes tensile stresses in the bottom fibres of the composite section.

5.3.2 In-plane analysis

The energy method requires a calculation of the distribution of strains applied to the member prior to invoking the bifurcation analysis. This involves use of the Cambridge residual stress model for the welded beam, described in section 5.2, and application of an initial strain and curvature consistent with externally applied load. The applied stress anywhere in the section, σ may then be found from Eqn. 5.4. By defining ε_{oi} as the strain at the top of the section and κ as the curvature, as illustrated in Fig. 5.5, the strain at any point y below the top surface of the section can be expressed as

$$\varepsilon = \varepsilon_{oi} + \varepsilon_r - y\kappa . \tag{5. 5}$$

The axial force, N and moment, M at the given value of strain and curvature are then obtained by numerical integration over the cross-section as shown in Eqns. 5.6 and 5.7

$$N = \int_A \sigma(x,y)\mathrm{d}A \tag{5. 6}$$

$$M = \int_A \sigma(x,y)y\,\mathrm{d}A \tag{5. 7}$$

where $N = 0$ satisfies pure bending condition. σ (x,y) is the stress calculated at strain, ε and obtained from the relevant constitutive relationship as

$$\sigma = \begin{cases} E\varepsilon & \varepsilon < \varepsilon_y \\ \dfrac{|\varepsilon|}{\varepsilon}\sigma_y & \varepsilon_y \le |\varepsilon| \le \varepsilon_h \\ E_{st}\varepsilon & \varepsilon > \varepsilon_h \end{cases} . \tag{5. 8}$$

The bending moment, axial and shear force distributions in the member are determined at each Gauss point along the length of the member prior to the buckling analysis. The loose form of the externally applied actions, M_a, N_a and V_a is

$$
\begin{aligned}
N_a(z/L) &= \lambda N_o \sum_{i=0}^{3} a_i (z/L)^i \\
M_a(z/L) &= \lambda M_o \sum_{i=0}^{3} b_i (z/L)^i \\
V_a(z/L) &= \lambda \frac{M_o}{L} \sum_{i=1}^{3} i b_i (z/L)^{i-1}
\end{aligned}
\tag{5. 9}
$$

with [0, L] being a length domain, λ is the buckling load factor, and the coefficients a_i (i = 0,..,3) and b_i (i = 0,..,3) define the axial, moment and shear field respectively.

The integrations in Eqns. 5.6 and 5.7 are carried out numerically by subdividing the flanges and web into a number of rectangles that distinguish elastic, yielded and strain-hardened regions around the section, as shown in Fig. 5.6, and using a trapezoidal integration technique.

The value of y in Eqn. 5.5 is adjusted iteratively by employing the Newton-Raphson procedure, as described in Bradford (1997c) and shown graphically in Fig. 5.7. For the purpose of this study, actions, M_a and N_a, are applied to the section and compared with the internal stress resultants. The incremental versions of Eqns. 5.6 and 5.7 are written as

$$
\begin{aligned}
\delta M &= -\int_A \delta\sigma(\varepsilon) y \, \mathrm{d}A \\
\delta N &= \int_A \delta\sigma(\varepsilon) \mathrm{d}A
\end{aligned}
\tag{5. 10}
$$

in which

$$
\sigma(\varepsilon) = E(\varepsilon)\varepsilon \tag{5. 11}
$$

and $E(\varepsilon)$ is the relevant elastic modulus (E, E_{st} or 0) from Eqn. 5.8.

The incremental strain $\delta\varepsilon$ may be obtained from Eqn. 5.5, noting that ε_r is constant, as

$$\delta\varepsilon = \delta\varepsilon_{oi} - y\delta\kappa\,. \tag{5.12}$$

Combining Eqns. 5.10 and 5.12 results in the matrix expression

$$\begin{Bmatrix}\delta M\\ \delta N\end{Bmatrix} = \begin{bmatrix}\int E(\varepsilon)y^2\,\mathrm{d}A & -\int E(\varepsilon)y\,\mathrm{d}A\\ -\int E(\varepsilon)y\,\mathrm{d}A & \int E(\varepsilon)\,\mathrm{d}A\end{bmatrix}\begin{Bmatrix}\delta\kappa\\ \delta\varepsilon_{oi}\end{Bmatrix} \tag{5.13}$$

or

$$\delta\bar{R} = \bar{T}(\varepsilon)\delta\bar{r}_i \tag{5.14}$$

where $\delta\bar{R}$ is the vector of incremental actions; $\delta\bar{r}$ is the vector of generalised incremental displacements; and $\bar{T}(\varepsilon)$ is the tangent stiffness matrix.

The process is repeated n times until the normalised Euclidean norm

$$\left\|\delta M^{(n)}/M, \delta N^{(n)}/N\right\| \le c \tag{5.15}$$

between two successive values of externally applied actions is less than some predetermined accuracy, c and the final strains are determined from the values

$$\begin{aligned}\varepsilon_{oi} &= \varepsilon_{oi}^{(n)}\\ \kappa &= \kappa^{(n)}\end{aligned}\,. \tag{5.16}$$

Arrays relating curvature, κ and strain, ε to applied bending moment, M_a and axial force, N_a respectively are thus obtained at each Gaussian station along the beam length. Thus at any value of moment in the beam corresponding to λ, values of κ and ε are obtained. This strain distribution is used for the ensuing buckling calculations.

5.3.3 Out-of-plane-analysis

The method of analysis that is deployed in the present study for inelastic restrained lateral-distortional buckling is a modification of that presented in Chapter 4. In a same manner, the energy-based buckling analysis assumes that the deformations of the cross-section are the lateral deformation and twist rotations of the top flange u_T and ϕ_T respectively, and the twist rotation ϕ_B of the bottom flange. These buckling freedoms, which deflect and twist as Fourier sine series with n harmonics, are consistent with the restraint conditions assumed for the half–through girder (Fig. 4.3, Chapter 4). The flanges are assumed to be rigid bars whose minor axis flexural and torsional rigidities are based on tangent modulus theory (Trahair & Bradford 1998). The web on the other hand is treated as a plate whose orthotropic property matrix is assembled from Haaijer's inelastic model (1957). The torsion constants of the flanges, which combine the elastic and inelastic values, are adopted as suggested in Bradford (1990d). These models have been shown to predict inelastic beam buckling (Bradford 1987) and inelastic plate buckling (Dawe & Kulak 1984) accurately. Furthermore, it is assumed that the beam is simply supported and that the web is unstiffened, except at its ends where load-bearing stiffeners are assumed to provide simple support with respect to out-of-plane buckling.

The strain energy U_F stored in the flanges during buckling can then be written as

$$U_F = \frac{1}{2}\int_0^L \bar{\varepsilon}_F^T \overline{D}_F \bar{\varepsilon}_F \mathrm{d}z \tag{5. 17}$$

where $\overline{D}_F$ is the appropriate flange property matrix given by

$$\overline{D}_F = \begin{bmatrix} EI_T & 0 & 0 \\ 0 & GJ_T & 0 \\ 0 & 0 & GJ_B \end{bmatrix} \tag{5. 18}$$

For elastic-yielded-strain hardened buckling, the property matrix at each Gauss point along the beam length is a function of the applied strain ε in Eqn. 5.5. Since the flanges are treated as rectangular 'beams', tangent modulus theory is used with the shear modulus being that derived by Lay (1965). Two quasi-elastic flange sections are engendered based on the value of the applied strain, ε (Eqn. 5.5) which depends on the applied curvature, κ and on the residual strain, ε_r. When the value of ε at a particular point in the cross-section is less than the yield strain ε_y, the full thickness t_T or t_B is used to generate the quasi-elastic flange sections. However, the points where ε exceeds ε_y, the thickness of the quasi-elastic sections are based on the strain-hardening modular ratio as t_T/h' or t_B/h' and property matrix appropriate for inelastic buckling must be used. The use of the strain-hardening modular ratio h' to generate the quasi-elastic sections has been used by a few researchers (Nethercot 1973a; Trahair 1993; Bradford 1987) who have shown that it produces accurate predictions of inelastic lateral buckling. This has its basis in the dislocation theory of yielding.

The top and bottom flange minor axis flexural rigidities used to calculate the membrane strain energy stored during buckling of the flanges can be obtained numerically as

$$EI_T = 2E\int_0^{b_t/2} x^2 \mathrm{d}A_T \tag{5. 19}$$

$$EI_B = 2E\int_0^{b_b/2} x^2 \mathrm{d}A_B \tag{5. 20}$$

noting that the differential areas $\mathrm{d}A_T$ and $\mathrm{d}A_B$ depend on the applied curvature, κ and the residual strain, ε_r.

For regions of the quasi-elastic sections where there is no reduction in the thickness due to inelasticity, the elastic shear modulus, G is used to calculate the torsional strain energy stored during buckling of the flanges, where

$$G = \frac{E}{2(1+\nu)}. \tag{5. 21}$$

However, the shear modulus used in the inelastic zones of the quasi-elastic flange sections is based on the inelastic value G_{st} derived by Lay (1965) as

$$G_{st} = \frac{4EE_{st}}{4E_{st}(1+\nu)+E}. \tag{5. 22}$$

Combining the elastic and inelastic values, the torsion constants of the flanges can be obtained from the approximation of Booker and Kitipornchai (1971) so that

$$GJ_T = [G - \beta_T(G - G_{st})]J_T \tag{5. 23}$$

and

$$GJ_B = [G - \beta_B(G - G_{st})]J_B \tag{5.24}$$

where β_T and β_B are ratios of the inelastic to total areas of the full top and bottom flanges respectively, and J_T and J_B are the torsion constants of each flange.

The generalized strain vector in Eqn. 5.17, given as

$$\bar{\varepsilon}_F = \langle u_{T},_{zz}, \phi_{T},_{z}, \phi_{B},_{z} \rangle^T, \tag{5.25}$$

can be obtained by suitable differentiation of the Fourier sine series function, which defines the lateral deformation u_T and twist ϕ_T of the top flange, and twist ϕ_B of the bottom flange, given as

$$\bar{u} = \bar{q}\sum_{i=1}^{n} \sin i\pi z / L. \tag{5.26}$$

In Eqn. 5.26, $\bar{q}$ represents the vector of the maximum amplitudes of the buckling displacements, and n is a positive integer representing the number of harmonics into which the beam buckles. The vector $\bar{\varepsilon}_F$ then takes the following form

$$\bar{\varepsilon}_F = \bar{B}_F \langle q_1, q_2, q_3 \rangle^T. \tag{5.27}$$

Thus by substituting equations 5.18 and 5.25 into Eqn. 5.17, the increase in strain energy due to lateral deflection and twist during buckling can be formulated as

$$U_F = \frac{1}{2}\bar{q}^T \bar{k}_F \bar{q} \tag{5.28}$$

where $\bar{q} = \langle q_1, q_2, q_3 \rangle^T$ and the flange stiffness matrix, $\bar{k}_F$ can be written in matrix form as

$$\bar{k}_F = \int_0^L \bar{B}_F^T \bar{D}_F \bar{B}_F \, \mathrm{d}z. \tag{5.29}$$

The strain energy, U_W stored during buckling of the flexible plate web may be obtained from

$$U_W = \frac{1}{2}\int_0^L \int_{-h_w/2}^{h_w/2} \bar{\varepsilon}_w^T \overline{D}_W \bar{\varepsilon}_w \mathrm{d}y\mathrm{d}z \tag{5.30}$$

where the generalized web strain vector, $\bar{\varepsilon}_w$, since the web is modelled as a 'plate', is given by

$$\bar{\varepsilon}_w = \langle u_{w,zz},\ u_{w,yy},\ -2u_{w,yz} \rangle^T . \tag{5.31}$$

The generalised web strain vector, $\bar{\varepsilon}_w$ in Eqn 5.31 may be obtained by suitable differentiation of the cubic curve function that describes the web deformation during buckling, given as

$$u_w = h_w \{\alpha_0 + \alpha_1 (y/h_w) + \alpha_2 (y/h_w)^2 + \alpha_3 (y/h_w)^3\} \sum_{i=1}^{n} \sin i\pi z / L . \tag{5.32}$$

The coefficients $\alpha_0, \ldots \alpha_3$ may be obtained by imposing displacement and twist compatibility of the flanges and web at the flange-web junctions as it was shown in Chapter 4. The generalised web strain vector, $\bar{\varepsilon}_w$ can then be written as

$$\bar{\varepsilon}_w = \overline{B}_W \langle \alpha_1, \alpha_2, \alpha_3, \alpha_4 \rangle^T = \overline{B}_W \overline{C} \bar{q} \tag{5.33}$$

where

$$\overline{C} = \begin{bmatrix} 1/2h_w & -1/8 & 1/8 \\ 3/2h_w & 1/4 & 1/4 \\ 0 & 1/2 & -1/2 \\ -2/h_w & -1 & -1 \end{bmatrix} . \tag{5.34}$$

The web property matrix in Eqn. 5.30, applicable to isotropic plate buckling, may be written as

$$\overline{D}_W = \frac{t_W{}^3}{12}\begin{bmatrix} D_{11} & D_{12} & 0 \\ D_{21} & D_{22} & 0 \\ 0 & 0 & D_{33} \end{bmatrix}. \tag{5. 35}$$

For isotropic elastic buckling (ie. in regions of the web where the applied strain, ε is less than ε_y), the rigidities given by Timoshenko and Woinowsky-Krieger (1959) are used, so that

$$\begin{aligned} D_{11} &= D_{22} = E/\left(1-\nu^2\right) \\ D_{12} &= D_{21} = \nu D_{11} \\ D_{33} &= G \end{aligned} \quad . \tag{5. 36}$$

However, when ε exceeds ε_y, property matrices appropriate for inelastic buckling must be used. For inelastic buckling (ie. in regions of the web where ε exceeds ε_y), rigidities based on plasticity theory must be used. In this study, the rigidities employed by Bradford (1988b) have been used. These approximate rigidities, which are based on a derivation from the flow theory of plasticity given by Haaijer (1957), are given as

$$\begin{aligned} D_{11} &= E_{st}/\left(1-\nu_1\nu_2\right) \\ D_{22} &= 4EE_{st}/\left[\left(3E_{st}+E\right)\left(1-\nu_1\nu_2\right)\right] \\ D_{12} &= D_{21} = \left\{\frac{2E_{st}}{3E_{st}+E}\right\}\left\{(2\nu-1)E_{st}+E\right\}/\left(1-\nu_1\nu_2\right). \\ D_{33} &= G_{st} \\ \nu_1\nu_2 &= \frac{\left\{(2\nu-1)E_{st}+E\right\}}{E\left(3E_{st}+E\right)} \end{aligned} \tag{5. 37}$$

Thus by substituting equations 5.33 and 5.35 into Eqn. 5.30, the strain energy stored in the web can be expressed as

$$U_W = \frac{1}{2}\vec{q}^T\overline{k}_W\vec{q} \tag{5. 38}$$

where the web stiffness matrix $\overline{k}_W$ is given as

$$\overline{k}_W = \overline{C}^T\left(\int_0^L\int_{-h_w/2}^{h_w/2}\overline{B}_W^T\overline{D}_W\overline{B}_W\,\mathrm{d}y\mathrm{d}z\right)\overline{C}. \tag{5. 39}$$

The integrals in the above equation are calculated by Gaussian quadrature and pre- and post-multiplication by $\overline{C}^T$ and $\overline{C}$ is facilitated by computer. Finally, the total strain energy, U stored during buckling can be expressed as

$$U = \frac{1}{2}\bar{q}^T \overline{K}\bar{q} \tag{5.40}$$

where the stiffness matrix $\overline{K}$ is given by

$$\overline{K} = \bar{k}_F + \bar{k}_W \,. \tag{5.41}$$

Note that $\overline{K}$ is not a matrix of constants (as predicted by linear elastic theories), since it depends on the applied curvature, κ and residual strain, ε_r.

5.3.4 Work done during buckling

The reference bending moment and axial force distribution within each element are determined prior to the buckling analysis and this enables the reference moments and axial forces at each Gauss point along the length of the element to be specified. The reference bending moment, M_a and axial force, N_a given in Eqn. 5.9 are scaled proportionally by a load factor, λ until buckling occurs. For a given moment gradient loading configuration, and in the absence of axial loading, this increase is proportional, irrespective of the extent of plasticity developed within the beam. However, the same does not hold true for the beam-column analysis, where this increase is not proportional, since for every given constant value of the axial force a beam buckling curve can be plotted.

During buckling, the stresses applied in the beam, which depend on the strain ε, undergo displacements which result in work V being done. This work may be written as

$$V = V_F + V_W \tag{5.42}$$

where V_F is the work done by the stresses in the flanges and V_W is the work done by the stresses in the web.

The contribution V_F in the flanges may be written as

$$V_F = \frac{1}{2}\int_A \sigma(\varepsilon)\int_0^L \left\{u_{T,z}^2 + v_{T,z}^2 + v_{B,z}^2\right\} \mathrm{d}z\mathrm{d}A \tag{5.43}$$

where A is the area of the flanges, $\sigma(\varepsilon)$ is the stress in the flange obtained from Eqn. 5.11, and where the vertical displacements v_T and v_B of the straight flanges are given by

$$v_T = x\phi_T \tag{5.44}$$

and

$$v_B = x\phi_B\,. \tag{5.45}$$

The terms in Eqn. 5.39 may be calculated by appropriate differentiation of Eqn. 5.24 so that the former equation can be written in matrix format as

$$V_F = \frac{1}{2}\int_A\int_0^L \bar{q}^T \overline{B}_F^T \sigma(\varepsilon) \overline{B}_F \bar{q}\,\mathrm{d}z\mathrm{d}A = \frac{1}{2}\bar{q}^T \bar{s}_F \bar{q} \tag{5.46}$$

where the flange stability matrix $\bar{s}_F$ is given as

$$\bar{s}_F = \int_A\int_0^L \overline{B}_F^T \sigma(\varepsilon) \overline{B}_F\,\mathrm{d}z\mathrm{d}A\,. \tag{5.47}$$

The contribution V_w to Eqn. 5.42 from the web may be written as

$$V_W = \frac{1}{2}\int_A\int_0^L \left\{u_{w,z}\ u_{w,y}\right\} \begin{bmatrix} \sigma(\varepsilon) & \tau(\varepsilon) \\ \tau(\varepsilon) & 0 \end{bmatrix} \left\{u_{w,z}\ u_{w,y}\right\}^T \mathrm{d}z\mathrm{d}A \tag{5.48}$$

where A is the area of the web, and $\sigma(\varepsilon)$ and $\tau(\varepsilon)$ are applied normal and shear stresses respectively in the web, which depend on the strain, ε, defined in Eqn. 5.5. Upon differentiation of Eqn. 5.31, work done during buckling in the web plate may be expressed as

$$V_W = \frac{1}{2}\bar{q}^T \bar{s}_W \bar{q} \tag{5. 49}$$

where the web stability matrix, $\bar{s}_W$ is

$$\bar{s}_W = \bar{C}^T \left(\int_A \int_0^L \bar{B}_w^T \bar{\sigma}(\varepsilon) \bar{B}_w \, \mathrm{d}z\mathrm{d}A \right) \bar{C} \tag{5. 50}$$

and

$$\bar{\sigma}(\varepsilon) = \begin{bmatrix} \sigma(\varepsilon) & \tau(\varepsilon) \\ \tau(\varepsilon) & 0 \end{bmatrix}. \tag{5. 51}$$

Finally, the total work done during buckling can be written as

$$V = \frac{1}{2}\bar{q}^T \bar{S} \bar{q} \tag{5. 52}$$

where the stability matrix, $\bar{S}$ can be written as

$$\bar{S} = \bar{s}_F + \bar{s}_W \,. \tag{5. 53}$$

As with the stiffness matrix, $\bar{K}$ the stability matrix, $\bar{S}$ depends nonlinearly on the strain ε, owing to the nonlinearity introduced in Eqn. 5.8.

The method also allows for an elastic restraint matrix, $\bar{R}$ to be included. This matrix is constant, and the assembly procedure has been shown in Chapter 4. However, the stability matrix, $\bar{S}$ as well as the stiffness matrix, $\bar{K}$ developed as above from tangent modulus and isotropic plate theory, are functions of the strain ε. The familiar eigenproblem then takes the following form:

$$\left[\bar{K}(\varepsilon) + \bar{R} - \lambda \bar{S}(\varepsilon)\right]\bar{\Delta} = \bar{0} \tag{5. 54}$$

where $\bar{\Delta}$ is the vector of buckling degrees of freedom.

The integrations in the equations for the element stiffness and stability matrices $\overline{K}$, $\overline{R}$ and $\overline{S}$ respectively for out-of-plane buckling, are determined by Gaussian quadrature. The integrations with respect to z along the element length, L are carried out using twenty-point Gaussian quadrature.

5.4 METHOD OF SOLUTION

For the inelastic RDB analysis, $\overline{K}$ and $\overline{S}$ in Eqn. 5.54 must be recalculated at incremented values of the load factor, λ because of changes in the inelastic properties and stresses. Because the member is determinate, this increase is proportional, irrespective of the extent of plasticity developed within the beam. The load factor, λ is increased monotonically, and the stiffness and stability matrices in Eqn. 5.54 are calculated at the value of λ by numerical integration over the cross-section as described in the previous section. The load factor increments are kept reasonably small so that the lowest critical load factor is not missed. Thus the determinant

$$\left|\overline{K}(\varepsilon)+\overline{R}-\lambda\overline{S}(\varepsilon)\right|=\left|\overline{A}(\lambda)\right|=0 \tag{5. 55}$$

is calculated, and if it is non-zero, then an increment in λ is applied and the determinant recalculated, until the determinant changes sign. In this model, which is based on the approach adopted by Pifko and Isakson (1969) and Smith *et al.* (2000), the matrix $\overline{A}(\lambda)$ is reduced to upper triangular form by Gaussian elimination without row interchanges. The determinant, which must necessarily vanish at buckling, is calculated by multiplying the diagonal elements of the reduced matrix, and the number of eigenvalues less than the trial loading level λ is equal to the number of negative diagonal elements in this reduced matrix. The range in which the loading level λ produces only one eigenvalue is then sought, and once this has been bracketed, the method of bisections is used to converge on the critical load factor, λ_{cr} for which the determinant vanishes. The load factor increments are kept reasonably small so that the lowest critical load factor is not missed. The critical moment and axial force are then determined from Eqns. 5.6 and 5.7. When the critical moment and axial force are found, a standard eigenvector routine (Garbow *et al.* 1977) is invoked to calculate the buckled shape. Since the matrices are of order $3n$, the solution process is rapid. The flow chart diagram that summarises the procedure described above is shown in Fig. 5.8.

5.5 ACCURACY OF SOLUTION

5.5.1 Convergence studies

Convergence studies have been carried out to determine the number of terms in the Fourier sine series function, employed in this study to describe the buckling displacements of deformed I-section, and required for accurate solutions. It has been shown in Chapter 4 that the number of terms required to achieve amply accurate solution depends on the loading. The convergence study is expanded in this chapter to assess the influences of the material imperfections, such as yielding and residual stresses.

The convergence of the energy method solution for a doubly symmetric I-beam under variety of loading conditions and with a different degree of tension flange twist restraint (ie. $\alpha = 0$ and $\alpha = 1000$) is demonstrated in Fig. 5.9. Figure 5.9a illustrates convergence characteristics for a stressed relived section, whilst Fig. 5.9b includes residual stresses. Since tabulated or closed form solutions are unavailable for inelastic RDB for I-section beams under moment gradient, the results plotted in Fig. 5.9 are compared with those derived when a large number of Fourier sine series terms, n is used (ie. n = 20). This large value of n was selected once the converged solution was identified (ie. zero percentage relative difference between successive terms). It is evident form Fig. 5.9 that solutions for $n \geq 9$ where within 0.1% for both stress relieved and welded I-beams.

5.5.2 Model verification

RDB solutions for I-section beams under moment gradient are unavailable in the literature, so the energy method developed herein was first verified by comparisons with inelastic lateral (non-distortional) buckling solutions for a simply supported, unrestrained, stress relieved beam subjected to transverse loading as given by

Kitipornchai and Trahair (1975). To account for the welded residual stresses the energy method for inelastic buckling is further verified with the inelastic lateral (non-distortional) buckling solutions obtained independently by Kitipornchai and Wong-Chung (1987) and Bradford (1988b), for welded monosymmetric beams.

The method developed in this chapter is lateral-distortional and therefore it is necessary to suppress the web distortion so that the lateral-distortional buckling mode becomes a lateral-torsional one. In order to model rigid web behaviour, distortion of the web in the energy method of this chapter was suppressed by expressing the strain energy due to out-of-plane plate flexure of the web, $u_{w,yy}$ as

$$U_{wF} = \frac{1}{2}\gamma_r \int_0^L \int_{-h_w/2}^{h_w/2} \overline{D}_W \; u_{w,yy}^2 \, \mathrm{d}y\mathrm{d}z \tag{5.56}$$

and allowing γ_r to approach infinity; where $\overline{D}_W$ is the relevant web rigidity applicable to elastic-plastic buckling and defined in 5.35. For the purpose of these comparisons, the tension flange was also allowed to displace laterally and to twist. Thus, the section modelled is a bare steel section.

Figure 5.10 shows the comparison between the model presented herein and the results of Kitipornchai and Trahair (1975). The geometries and material properties for the beams are also given in Fig. 5.10. It can be seen that the results are in a very good agreement for the stressed relieved 10UB29 section. Because the energy solution and the method by Kitipornchai and Trahair (1975) treat the inelasticity in a different way, the agreement indicates that the energy method would be expected to produce accurate prediction of inelastic buckling.

The results of the buckling study, where they are compared with the corresponding results reported by Kitipornchai and Wong-Chung (1987) and Bradford (1988b), are shown in Figs. 5.11 and 5.12. The geometries and material properties for the beams are also given in Figs. 5.11 and 5.12. Figure 5.11 compares the dimensionless inelastic lateral buckling moments M_{Icr}/M_P as a function of the modified slenderness $\lambda_r = \sqrt{M_P/M_{ob}}$ for the three widths of the flange residual stress block, where M_{ob} is the elastic lateral buckling moment, and M_P is the full plastic moment. The comparison between M_{Icr}/M_P and λ_r given in Fig. 5.12 is for beams with two different degrees of monosymmetry. The comparison between the three models of lateral buckling is reasonably close, as is evident from Figs. 5.11 and 5.12.

The developed method for predicting the inelastic RDB load is also compared herein with results for welded continuously restrained doubly symmetric I-beams obtained by Bradford (1998a). The numerical investigations presented by Bradford (1998a) were limited to only one beam cross-section subjected to uniform bending and with the magnitude of the elastic twist restraint, α varying from 0 to 1000. The stiffness of the torsional restraint per unit length, k_z has been expressed in the non-dimensional form as

$$\alpha = \frac{k_z L^2}{GJ} \tag{5.57}$$

where GJ is the Saint Venant torsional rigidity. The geometry of the simply supported beam studied is given in Fig. 5.13. In this study (Bradford 1998a) the dimensionless inelastic RDB moment is plotted as a function of the dimensionless length L/h_w for α = 0 (no twist restraint), 10 and 1000. The trend of the bucking curves is similar to that of local buckling, where even for zero twist restraint the inelastic buckling moment tends to asymptote, rather than decrease sharply as would occur for lateral-torsional buckling. For α = 10 there are two harmonics represented, while three harmonics are exhibited for α = 1000. It can be seen that there is a good agreement between the two solutions over the range of dimensionless beam lengths L/h_w for which the calculations were performed. This provides verification of the inelastic RDB energy method. Figure 5.13 also illustrates the comparison of the present model with over-conservative U-frame method solutions. A detailed description of the U-frame method is given in Chapter 3.

5.6 BUCKLING STUDY

5.6.1 Buckling strength of I-section beams

5.6.1.1 General

Conventionally, the buckling of plain steel beams is usually represented by so-called 'beam-curves', in which the relationship between the length of the member and its critical load is plotted on a Cartesian coordinate system. A typical length versus critical moment curve is shown in Fig. 5.14 for a simply supported unrestrained steel beam subjected to uniform bending (β = -1). The curve consists of three main parts: a) classical elastic buckling; b) buckling in the inelastic range and; c) the buckling behaviour of a very short member for which it is assumed that all fibres have been strained into the strain-hardening range. The strain hardening and the elastic curves are hyperbolas, which do not intersect. The curve for inelastic bucking provides a transition between these two extreme idealizations. A number of studies available in the literature have indicated that the critical buckling moment for an unrestrained I-beam has a profound dependence on the model of the residual stresses, thus altering the shape of the conventional 'beam-curve' shown in Fig. 5.14. This influence of the residual stresses results from their dependence on the geometric proportions of the beam cross-section (Trahair & Bradford 1998). Inelasticity is particularly significant in fabricated beams (Bradford 1988b) because the welding process results in levels of residual stresses that are considerably higher than those in hot-rolled beams.

So far, no detailed study has been made of the influences of the welding residual stresses on the I-section steel beams under transverse loading and restrained continuously against lateral displacement and minor axis twist at its tension flange. Thus this section seeks to examine the influence of the residual stress pattern and continuous elastic twist restraint on the behaviour of such structural configurations.

5.6.1.2 Doubly symmetric I-beams

The effects of continuous elastic restraint on the inelastic RDB of I-section beams have been investigated. In this study, the cross-sections with welded model of residual stresses were adopted, with the beam subjected to continuous translational, minor axis rotational and twist rotational (torsional) restraint applied at the tension flange. The stiffness of the torsional restraint, k_z has been expressed in the non-dimensional form, as shown in Eqn. 5.57.

Bradford (1998a) showed that the modified method of 'design by buckling analysis' (Trahair & Bradford 1998) may be used in accordance with the AS4100 (1998) to calculate the inelastic bending capacity, M_{Icr} for the limit state of RDB. For a beam subjected to uniform bending, this strength was determined by Bradford (1998a) from the modified AS4100 design equation given as

$$M_{Icr} = \alpha_s M_P \tag{5. 58}$$

where

$$\alpha_s = 0.8\left\{\sqrt{\left(\frac{M_P}{M_E}\right)^2 + 3} - \left(\frac{M_P}{M_E}\right)\right\} \tag{5. 59}$$

in which the multiplier 0.8 replaces AS4100 value of 0.6, as shown above. In this equation, M_P represents the plastic section moment and M_E is the elastic RDB moment derived as discussed in Chapter 4. Figure 5.15 shows the comparison between the model developed in this chapter and the results of Bradford (1998a) for I-section beams in uniform bending for different values of the elastic twist restraint, α (ie. α = 0, 10, 100 and 1000). Figure 5.15 plots the dimensionless inelastic lateral buckling moments M_{Icr}/M_P as a function of the beam slenderness, L/h_w. It can be seen that the results are in a good agreement for the welded residual stress pattern with c_f = 20 mm. This study has been extended to evaluate the effectiveness of the modified AS4100 approach, given by Eqns. 5.58 and 5.59, when moment gradient is included. Figures 5.16-5.20 show the comparison of the energy method developed in this study and the AS4100 'design by buckling analysis' method, both conventional and modified. The geometry and material properties of the simply supported beams studied are same as those used by Bradford (1998a) and given in Fig. 5.14. In part a) of each of Figs. 5.16-5.20 the energy method results are compared with the conventional AS4100 approach (ie. multiplier in Eqn. 5.59 is 0.6), whilst part b) plots the results of the energy method versus modified AS4100 method, given in Eqns. 5.58 and 5.59. It can be seen from Figs. 5.16-5.20 that the results, for the two methods considered, are almost in complete agreement, slightly less so for very short beams.

The results of the buckling study are further shown in Figs. 5.21-5.30, where the effects of different widths of the flange tensile residual stress block, $2c_f$ are investigated. The inelastic buckling moment M_{Icr}/M_P is plotted against the modified slenderness $\lambda_r = \sqrt{M_P/M_E}$ for $c_f = 0$ (no residual stress), 20, 40 and 60. It can be seen that the magnitude and shape of the residual stress pattern have marked influences on the inelastic buckling moments due to their effects on the geometry of the yielded zones in the cross section. The reductions in the buckling moment due to inelastic behaviour are severe. For stress-relieved beams with no residual stresses ($c_f = 0$), the inelastic buckling capacities reduce sharply when the compression flange is fully yielded. The reductions in buckling strength from the $c_f = 0$ case are of the order of 20%, 40% and 40-60% of the section's fully plastic moment, M_P for $c_f = 20$, 40 and 60 mm respectively.

The presence of welding residual stresses results in premature yielding of the tension flange and some stress relief in the compression flange at the early loading stages. However, as soon as the compression flange yields, stiffnesses reduce rapidly, causing a sudden drop in the inelastic buckling moment. The inelastic buckling of a beam is governed primarily by the stiffness of the compression flange. Theoretical results indicate that a welded beam buckles inelastically when the regions of compressive residual stress in the compression flange become fully yielded (Kitipornchai & Wong-Chung 1987). The remaining elastic core in the tensile stress block contributes little to beam stability.

In following study, in the modelling of the beam the geometry is embodied in a knowledge of the distortional restraint parameter, γ, proposed in Chapter 4, and the beam parameter K. Figures 5.31-5.35 illustrate plots of the inelastic distortional buckling moment, M_{Icr} normalized with elastic lateral-torsional (non-distortional) buckling moment, M_{ob}, generally deployed for plain steel sections (AS4100 1998) in uniform bending, and defined as

$$M_{ob} = \sqrt{\left(\frac{\pi^2 EI_y}{L^2}\right)\left(GJ + \frac{\pi^2 EI_w}{L^2}\right)} \tag{5. 60}$$

where EI_y and EI_w represent minor axis flexural rigidity and warping rigidity respectively. The inelastic RDB moment values are derived from the numerical model as a function of the dimensionless twist restraint $\alpha = 0$ (no twist restraint), 10, 100 and 1000 (or ∞) for the dimensionless beam parameter, K defined by AS4100 (1998) for doubly symmetric I-sections as

$$K = \sqrt{\frac{\pi^2 EI_y}{GJL^2}} \,. \tag{5. 61}$$

The values of the beam parameter, K range from 0.3 to 3.0. Low values of K represent slender members with stocky sections, while high values describe the beams with short span and stocky cross section. Figures 5.31-5.35 show the variation of the dimensionless buckling moment M_{Icr}/M_{ob} with the beam parameter, K for different loading configurations. The welding residual stress patterns are calculated based on Kitiponchai and Wong-Chung's (1987) suggestions presented in section 5.2. The trends in curves shown for different loading configurations are very similar and in some way comparable to those exhibited by local buckling and elastic RDB presented in Chapter 4. As would be expected, the buckling mode of the beam is lateral-torsional when beam is subjected to translational restraint only (ie. $\alpha = 0$). When the dimensionless torsional parameter, α is greater than 10 the buckling mode becomes a lateral-distortional one. The severity of the web distortion is emphasized when α is very high (α = 1000 or ∞). The illustration of the cross-sectional deformation due to variation in magnitude of α is shown in Fig. 4.9 (Chapter 4).

Figures 5.36-5.44 plot the longitudinal distribution of normalised buckling mode shapes of the lateral displacements, u_T and the flange twist, ϕ_T for the compression/top flange and the angle twist, ϕ_B for the tension/bottom flange. These curves are derived from the energy method presented in section 5.6 by solving for the eigenvectors in the Eqn. 5.54 after converged critical buckling value, λ_{cr} has been identified. The beam slenderness, L/h_w values were varied between 3 and 120 and the widths adopted for the tensile residual stress block, c_f were 0, 20, 40 and 60. In Fig. 5.36, in which the longitudinal distribution of lateral displacements, u_T for uniformly distributed load is plotted, only one harmonic is needed for beams with $\alpha = 0$, while for $\alpha = 1000$ two harmonics are needed. In the case where the longitudinal distribution of the compression flange twist, ϕ_T is plotted for both $\alpha = 0$ and $\alpha = 1000$, as shown in Fig. 5.37, at least three harmonics are required. This figure also illustrates significant variation in the shape of the buckling modes for different values of c_f when $\alpha = 1000$, while greater consistency for a given weld size, c_f can be observed for $\alpha = 0$. In Fig. 5.38 the tension flange twist restraint, ϕ_B is obviously shown only for $\alpha = 0$, and it can be observed that at least three sine half-waves are describing this buckling mode. Similar behaviour is observed for loading cases different to that of uniform bending, as evident from Figs. 5.39-5.44, especially so for symmetrical transverse loading. Plots of buckling mode shapes for asymmetrical point loading, such as a point load at the quarter span, show a larger number of harmonics is needed to represent the longitudinal distribution for u_T, when $\alpha = 1000$ and for ϕ_T when $\alpha = 0$ or 1000. The same holds true for the angle twist, ϕ_B for the tension/bottom flange when $\alpha = 0$.

5.6.1.3 Monosymmetric I-beams

Kitipornchai and Wong-Chung (1987) studied the inelastic lateral buckling of unrestrained monosymmetric I-beams in uniform bending and demonstrated that the assumed magnitude of the residual stresses greatly affects the buckling strength. Bradford (1988a) studied the inelastic buckling of unrestrained fabricated monosymmetric I-beams in uniform bending for which the slender web is free to distort. Inelastic lateral buckling of unrestrained fabricated monosymmetric I-beams under moment gradient was also studied using the Cambridge residual stress model by Bradford (1988b). Those studies showed that the relationship between the inelastic critical moment and slenderness was the same for lateral and distortional buckling, except for extremely stocky beams. It was also demonstrated that this relationship can be used to predict the inelastic distortional buckling moment.

The energy method described in the theory (section 5.3) has been employed herein to study the inelastic RDB of monosymmetric beams with its larger flange in compression or tension. In this subsection, the beam is fully restrained against lateral translation and elastically restrained against torsion applied at the level of the tension/bottom flange, as depicted in Fig. 4.3 (Chapter 4). The torsional/twist restraint, k_z has been represented as the dimensionless parameter, α as shown in Eqn. 5.57. The loading configurations considered in this chapter are uniform bending and transverse uniformly distributed and concentrated loads. The material properties of the cross-section used are same as in the previous subsection. Residual stresses were determined in accordance with Kitipornchai and Wong-Chung's (1987) recommendations, presented in section 5.2. It was shown by Kitipornchai and Wong-Chung (1987) that there is little variation in the flange tension block half-width, c_f when the flange width is reduced, but this is not so when the flange thickness is reduced.

Varying degrees of the beam monosymmetry parameter, ρ are obtained by arbitrarily reducing either the thickness or the width of the flanges, while keeping the web dimensions unchanged. The degree of beam monosymmetry, ρ is defined as

$$\rho = \frac{I_{y(compression)}}{I_{y(compression)} + I_{y(tension)}} = \frac{I_{y(compression)}}{I_y}, \qquad (5.62)$$

where $I_{y(compression)}$, $I_{y(tension)}$ and I_y are the second moments of area about the y-axis of the top flange, the bottom flange, and the whole section respectively. In this study, values of ρ for steel I-sections are varied between 0 and 1. However, the cross-sections with ρ value of 0 and 1 are not typical T-sections, but two-flanged sections with very narrow compression and tension flanges respectively. Thus, 0 and 1 represent rounded figures within a tolerance of 0.2%.

The results for the inelastic RDB of simply supported beams in uniform bending, under transverse uniformly distributed and concentrated loads, and with varying degree of welded residual stresses, are shown in Figs. 5.45-5.47. The values of the dimensionless torsional (twist) parameter, α considered herein are 0 and 1000. In these figures, the critical buckling moment (either elastic, M_E and M_{ob} or inelastic, M_{Icr}) is normalised with respect to the plastic moment M_P, as a function of dimensionless slenderness $\sqrt{M_P / M_{ob}}$, where M_{ob} is the conventional elastic critical moment for a plain monosymmetric steel I-beam in uniform bending and assuming rigidity of the cross-section, as defined in Eqn 4.49 (Chapter 4). Values of parameter c_f, defined in section 5.2, were 0 (no residual stresses), 15 and 20 mm, and two different magnitudes of dimensionless twist restraint parameter, α were investigated (ie. 0 and 1000). In addition to the inelastic buckling curves, the elastic buckling curves for restrained I-beams (ie. $\alpha = 0$ and 1000) and for bare steel sections with both rigid and flexible webs are also plotted in these figures. In Figs. 5.45-5.47 part a) illustrates buckling curves for the monosymmetry parameter $\rho = 0.7$ and part b) for $\rho = 0.3$. These figures clearly demonstrate that the inelastic buckling behaviour of I-section members is dependent on the topology of the residual stresses. The reduction of the buckling moment due to yielding of the cross-section is much higher for larger values of the tension stress block, c_f. For instance, the reductions in buckling strength from the $c_f = 0$ case are of the order of 5% and 10% of the section's fully plastic moment, M_P for $c_f = 15$ and 20 mm respectively. It is also evident that the capacity of I-beams with a smaller compression flange ($\rho = 0.3$) is well reduced when compared to those with larger flange in compression ($\rho = 0.7$), especially so for uniform bending. In addition, Figs. 5.45-5.47 illustrate a significant increase in buckling capacity when the twist restraint parameter, α is increased to 1000.

In Figs. 5.53-5.55 the inelastic RDB moment, M_{Icr} normalised with respect to the elastic critical moment, M_{ob} for the plain monosymmetric steel I-beam as defined in Eqn. 4.49 (Chapter 4), is shown for a range of the beam monosymmetry parameter, ρ (ie. $\rho = 0$ to 1). The results are plotted for the dimensionless beam parameter, $\overline{K}$ defined in AS4100 (1998) for simply supported monosymmetric steel I-sections as

$$\overline{K} = \sqrt{\frac{\pi^2 E I_y h^2}{4GJL^2}}\,. \tag{5. 63}$$

The results (Figs. 5.53-5.55) also show the favourable effects of the elastic translational and minor axis rotational restraints (ie. $\alpha = 0$, 10, 100, 1000) applied at the tension flange of a simply supported beam, as normally employed in half-through girder bridges. The increase in the buckling capacity is most evident for low values of the beam parameter, $\overline{K}$, which define very long beams with a stocky cross-section, and especially so for large values of α (ie. 100 and 1000). Lesser increase in buckling capacity due to the continuous twist restraint, α are evident for large values of $\overline{K}$, which define short beams with slender cross-sections. It was anticipated that yielding, as already verified in Figs. 5.45-5.47, significantly influences the buckling capacity of such beams. Furthermore, very little increase in the buckling capacity is observed for I-beams with the degree of monosymmetry, ρ of 0, which represents I-sections with very narrow compression flange. The rigid restraint (ie. α = 1000) does not cause any increase in capacity for such beams.

As would be expected, under a condition of restraint in which only translational and lateral rotation of the bottom flange are prevented, but for which twist rotation is free to occur during buckling (ie. α = 0), the RDB buckling is not accompanied by cross-sectional distortion and the distortional and lateral-torsional buckling moments are identical. As the dimensionless torsional (twist) restraint parameter, α increases, the effects of distortion are more evident and the inelastic RDB moment is less than the corresponding inelastic lateral-torsional buckling moment.

Figures 5.53-5.55 show the longitudinal distribution of the normalised buckling mode shapes for the lateral displacement, u_T and the angle of twist, ϕ_T for the compression/top flange and the angle of twist, ϕ_B for the tension/bottom flange. It is evident that as the values of ρ decrease from 1 to 0, and therefore the compression flange becomes stockier, the deflected shape changes from a half-sine wave to a full-sine wave and a two full-sine waves. Therefore, as the value of ρ approaches 0, the u and ϕ buckled shapes are more complicated functions and require more terms, n in the Fourier series to describe them closely.

5.6.2 Buckling strength of I-section beam-columns

5.6.2.1 General

The ultimate strength of a slender, laterally unsupported, stress-relieved beam-column is usually governed by elastic lateral (flexural)-torsional buckling, while the strength of a stocky beam-column is generally reduced below the elastic buckling value due to yielding. However, the strength of a welded beam-column with continuous lateral support is dependent on the combined effects of the stresses caused by the applied loads and the residual stresses which are established during the fabrication procedures. Thus, the effective moduli of the yielded and strain-hardened portions of the member are reduced below its elastic value with consequent reductions in the stiffnesses, which contribute towards the resistance to buckling. In addition, because of the restraint provided at the tension flange level, cross-sectional distortion is more pronounced and this buckling mode is classified as RDB. The complexity of the problem is attributed to numerous parameters, such as member slenderness, cross-sectional properties, restraints, residual stress pattern, continuity, and two- or three-dimensional behaviour of the beam-column.

In this study, a modified version of the energy method of analysis presented in section 5.3 has been employed to study the inelastic RDB of simply supported doubly symmetric I-section beam-columns. For the purpose of this investigation, beam-columns are assumed to be provided with lateral restraints such as a full lateral translational restraint and elastic twist (torsional) restraint applied at the level of the tension flange, as illustrated in Fig. 4.20 (Chapter 4). Loading configurations include uniform axial load combined with uniform bending and transverse uniformly distributed and point loads. The idealised residual stress pattern consists of a fully yielded tensile stress block of width $2c_f$ in the flange at the weld (Eqn. 5.1), and a constant residual compressive stress σ_{cr} at the outer edges to maintain equilibrium. Tensile stress block of width c_f extends into the web away from the weld.

The in-plane analysis of a beam-column is somewhat different to the in-plane analysis of a beam subjected to moment gradient, described in section 5.3, because of additional moment caused by the axial force (P-δ effect). The numerical procedure, adopted in this study, which takes into account the non-linearity due to P-δ effect, is described in detail in section 4.5.4.2 (Chapter 4) and for the sake of brevity is not repeated herein. However, the inelastic behaviour adds another dimension of non-linearity to the problem since the major axis flexural rigidity, EI_x is not constant due to yielding of the cross-section caused by the combined effects of residual stresses and applied load. The inelastic in-plane analysis of the beam-column to determine stress resultants is therefore more complicated than an elastic in-plane analysis of a beam.

The details of the buckling analysis are those given in sections 5.3.3 and 5.3.4. It is worthwhile noting that although this procedure assumes a proportional increase in both bending and axial stresses, the same cannot be applied to the inelastic buckling analysis of beam-columns. Thus, in the analyses of this section the reference bending moment, M_a given in Eqn. 5.9, is scaled proportionally by a load factor, λ until buckling occurs, for a given constant value of the axial force. The modified energy method has then been employed to investigate the effects of residual stresses and continuous lateral restraint on the inelastic RDB of beam-columns under variety of loading regimes.

5.6.2.2 Numerical studies

Figures 5.57 and 5.58 show the inelastic critical buckling moment, M_{Icr} of a simply supported beam-column, normalised with the elastic buckling load, M_{ob} and the first yield moment, M_Y respectively, plotted versus the beam slenderness, L/r_x. Two different loading configurations are compared; uniform bending and uniformly distributed load. The cross-sectional geometry is shown in the same figures and the residual stress pattern used herein is based on the recommendations given in section 5.2. In part a) of each of Figs. 5.57 and 5.58 the buckling moment, M_{Icr} is plotted for a constant axial load $N = 0.1N_Y$, where N_Y is the section capacity in compression, and in part b) is plotted for $N = 0.2N_Y$. Although the axial load in b) is only slightly higher that the load in a), it is worthwhile noting that the reductions in buckling capacity for short beams are rather significant (≈20%). Also, the trends exhibited in these graphs are somewhat analogous to those for local buckling, especially so for the twist restraint parameter, $\alpha = 1000$. For both loading conditions the inelastic buckling moment tends to asymptote, rather than decrease sharply as would occur for lateral-torsional buckling.

The inelastic load-moment interaction diagrams obtained from the energy method are shown in Figs. 5.58-5.60. In these, the inelastic RDB moment, M_{Icr} for a given beam-column, is normalised with the inelastic RDB moment, M_{od} for a beam, and plotted versus the inelastic RDB axial load, N_{Icr} for the beam-column, normalised in a similar manner with the inelastic RDB axial load, N_{od} for a column. The interaction curves are plotted for a wide range of the dimensionless distortional parameter, γ, proposed in Chapter 4 (ie. $\gamma = 5$ to 50). It was shown in Chapter 4 that for a particular loading configuration the interaction curves are identical for a range of γ, α and K values. Thus, it was suggested in Chapter 4 that the similar trend exhibited in the buckling curves can be simplified to the linear interaction equation given as

$$\frac{M_{cr}}{M_{od}} + \frac{N_{cr}}{N_{od}} = 1.0\,. \tag{5. 64}$$

Loading configurations considered herein are uniform bending (Fig. 5.58), uniformly distributed load (Fig. 5.59) and a concentrated point load at the mid-span (Fig 5.60). Varying degrees of the twist restraint parameter, α are also included, and each of the values (0, 10, 100 & 1000) are considered in separate graphs (a-d). The geometry of the member was selected in order for the dimensionless beam parameter, K to approach 1 (ie. within a tolerance of 0.1%) for each of the γ values. Figures 5.61-5.63 plot the same interaction curves as a function of the dimensionless twist restraint parameter, α for a single value of the distortional parameter, γ.

It is evident from Figs. 5.56-5.61 that the inelastic buckling characteristics of continuously restrained beam-columns are somewhat different from those presented in Chapter 4. When the critical buckling load and moment are plotted in this way, it can be seen that there are very minor discrepancies between the elastic solutions and inelastic solutions for $\alpha \geq 10$. Therefore, the use of the linear elastic load-moment interaction Eqn. 5.64 may lead to satisfactory approximations for the inelastic RDB of beam-columns in uniform bending and when subjected to uniformly distributed load, provided the elastic quantities M_{cr}/M_{od} and N_{cr}/N_{od} are replaced with their inelastic equivalents M_{Icr}/M_{od} and N_{Icr}/N_{od}. For $\alpha = 0$ the inelastic curves are a little higher than the elastic values and with the shape of parabola.

However, the inelastic solutions for a concentrated point load at the mid-span are a little lower when compared with their elastic counterparts for $\alpha \geq 10$. The greatest reductions below the elastic curves, for this loading case, occur when $\gamma = 50$. Furthermore, it is worthwhile emphasising that these solutions are derived for the beam parameter $K \approx 1$ and are not applicable to the entire range of the beam parameter as was the case in Chapter 4 with the elastic curves.

5.7 SUMMARY

An energy method of solution has been presented for the study of inelastic RDB of I-section members under uniform bending, transverse loading and compression. The method incorporates the residual stresses induced by the process of fabrication, described by the so-called Cambridge residual stress model, to include the effects of inelasticity. The literature review has indicated that welded beams are more susceptible to buckling than their hot-rolled section counterparts. When restraint against twist rotation is applied to the cross-section along the beam length, the member is not free to twist during buckling and cross-sectional distortion must necessarily accompany the buckling deformation. This effect is difficult to quantify, and depends on such factors as the topology of the cross-sectional profile, the level of residual stress, the beam length and the stiffness of the torsional restraint.

Thus the Ritz-based energy method has been developed in this chapter for determining the inelastic RDB buckling loads for simply supported I-section members without transverse stiffeners along the span, subjected to transverse loading, and which includes cross-sectional distortion during the bifurcation of equilibrium. The solution is obtained efficiently, since the stiffness matrices are only of order $3n$. Generally, very few Fourier terms were required to obtain accurate solutions, indicating the accuracy and economy of the numerical procedure presented. By a simple modification of the buckling model, the results have been validated against results reported for inelastic lateral-torsional buckling that does not involve distortion of the cross-section during buckling nor continuous elastic restraint against lateral displacement and twist. Comparison studies were also undertaken for inelastic RDB of a continuously restrained I-beam in uniform bending. The solutions were found to be in close agreement with the independent predictions.

The application of the model was demonstrated for the inelastic RDB of doubly symmetric beams, monosymmetric beams and beam-columns. The nominal buckling load obtained from the modified 'design by buckling analysis' in AS4100 has been compared with inelastic RDB solutions obtained from the current model. Overall, the energy method has demonstrated an excellent agreement with the proposed method.

There are a number of variables that affect the elastic RDB load, and this increases considerably when elastic restraints and inelasticity are incorporated. However, the distortional buckling parameter, γ identified in Chapter 4 allows the high multiplicity of buckling curves associated with inelastic distortional instability to be reduced to only few. Provided that the designer can make some assessment of the level of welding residual stress present in the member, the inelastic buckling moment may be calculated to acceptable accuracy from a simple design curve that depends on the inelastic RDB moment and the elastic critical (non-distortional) buckling moment for unrestrained I-beam, the latter being obtained from solutions presented in design codes.

The influences of the degree of beam monosymmetry, ρ, torsional twist restraint, α and the width of the tensile stress block in the flange, $2c_f$ have been examined. It was shown that the inelastic buckling capacities decrease by reducing ρ and with increasing c_f values. The numerical studies have also demonstrated the favourable effects of the elastic translational and minor axis rotational restraints applied at the tension flange of a simply supported beam, as normally employed in half-through girder bridges.

The energy method was then employed to study the inelastic lateral buckling of isolated beam-columns under different loading configurations, and demonstrated that the inelastic RDB load-moment interaction curves are a little variable when compared with corresponding elastic curves. It was concluded that the linear elastic load-moment interaction equation may lead to satisfactory approximations for the inelastic RDB of beam-columns in uniform bending and when subjected to uniformly distributed load, for $\alpha \geq 10$ provided the elastic quantities M_{cr}/M_{od} and N_{cr}/N_{od} are replaced with their inelastic equivalents M_{Icr}/M_{od} and N_{Icr}/N_{od}.

It was found that the effects of the residual stresses cause significant variations in the inelastic RDB strength. The changes in the residual stress system lead to variations in the yielded regions in the cross-section, and resulting variations in the section rigidities. These variations cause quite considerable changes in the inelastic critical buckling moments. It may thus be concluded that the process of fabrication of I-section members may have an adverse effect on their strength for the limit state of RDB. As residual stresses exist in all welded steel I-sections, it is concluded that these should be carefully quantified and designed for.

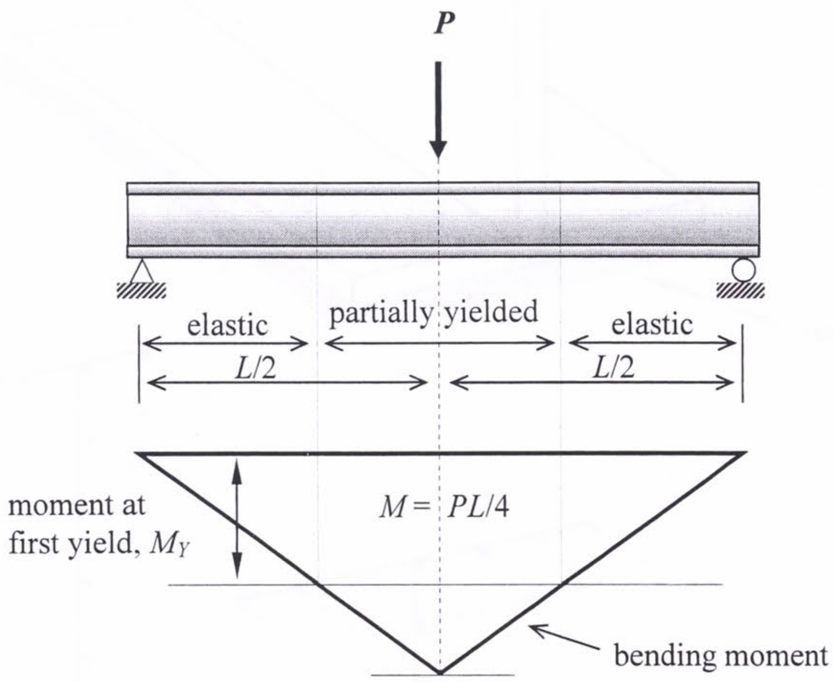

Figure 5.1 Inelastic I-beam

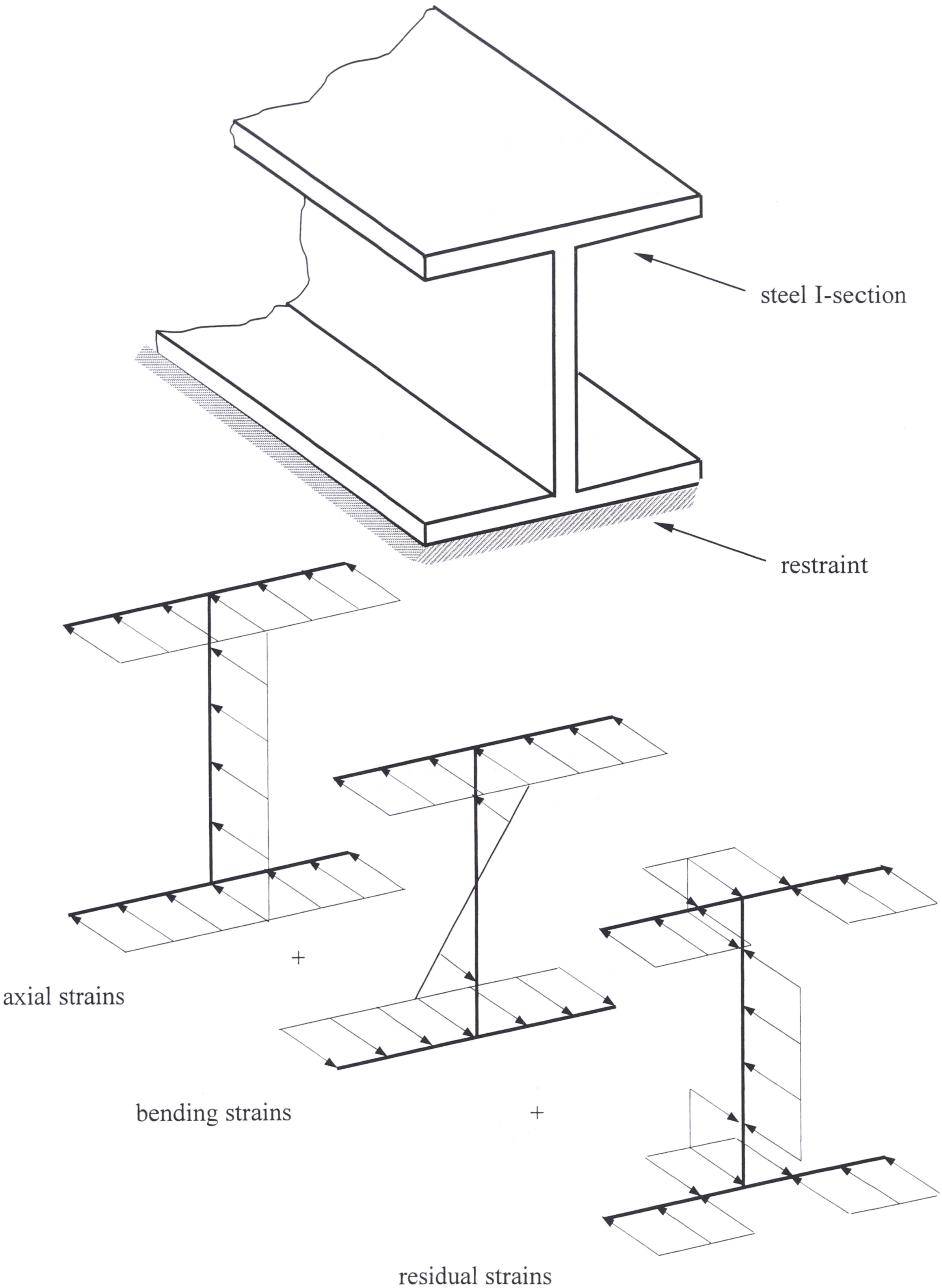

Figure 5.2 Strain distribution in a steel beam-column

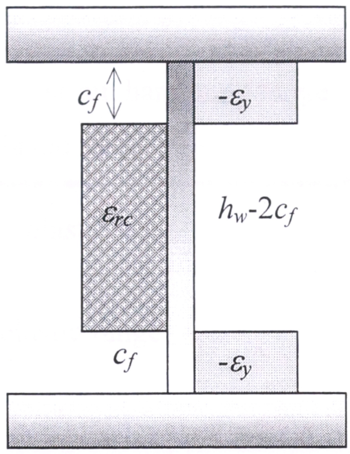

a) web residual strain, ε_r distribution

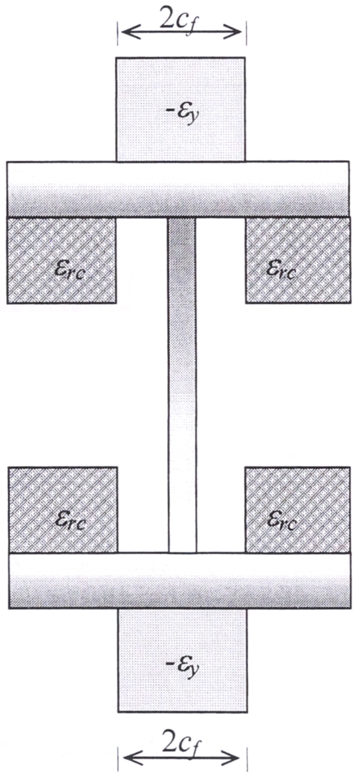

b) top and bottom flange residual strain, ε_r distribution

Figure 5.3 Residual strain distribution

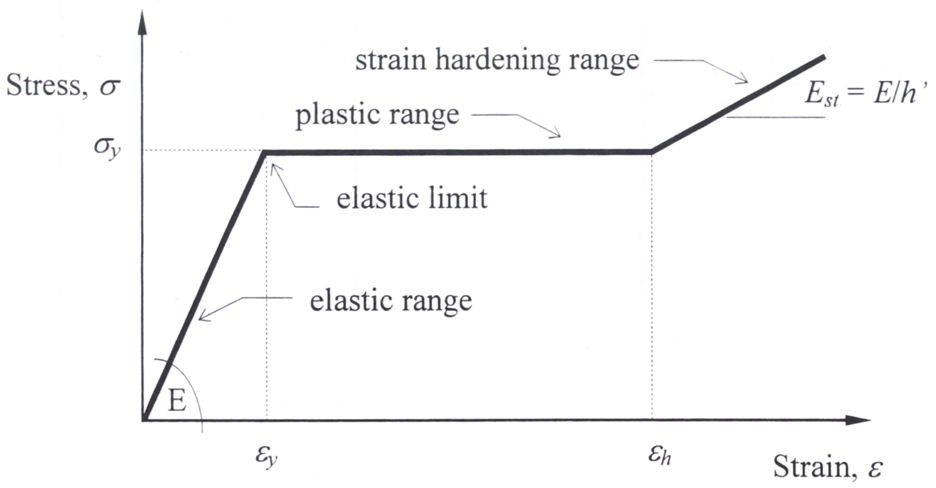

Figure 5.4 Stress-strain curve for structural steel

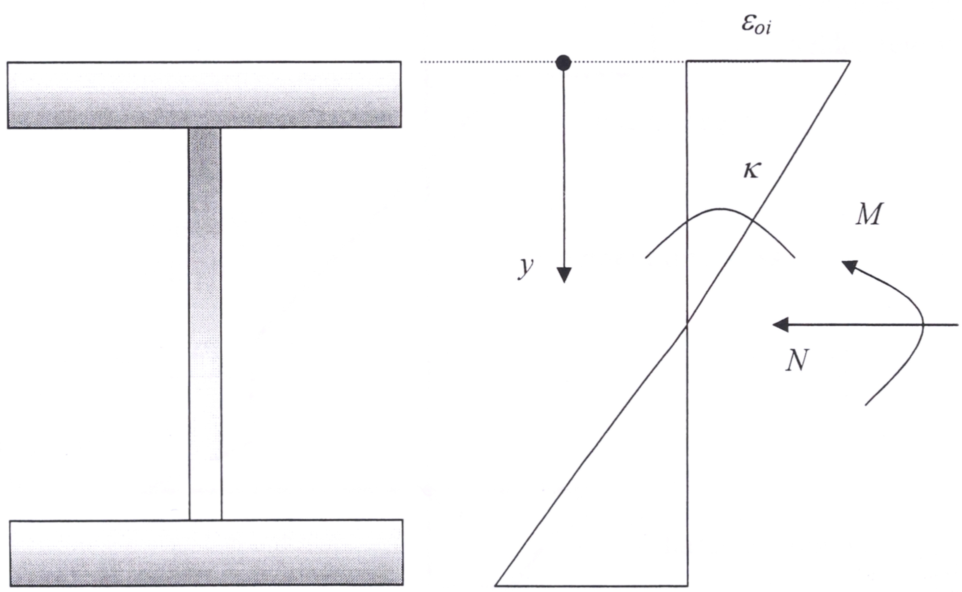

Figure 5.5 Strain distribution due to applied load, ε_a

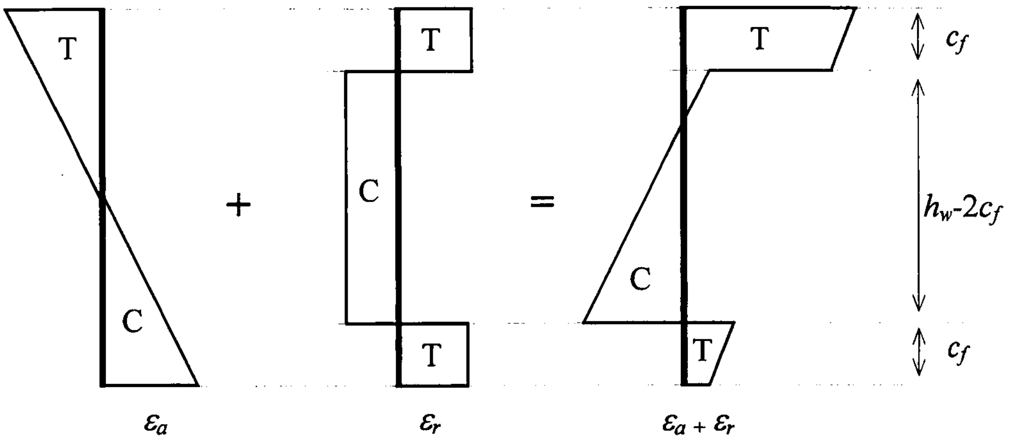

*T – tension; C - compression

a) Web applied and residual strains

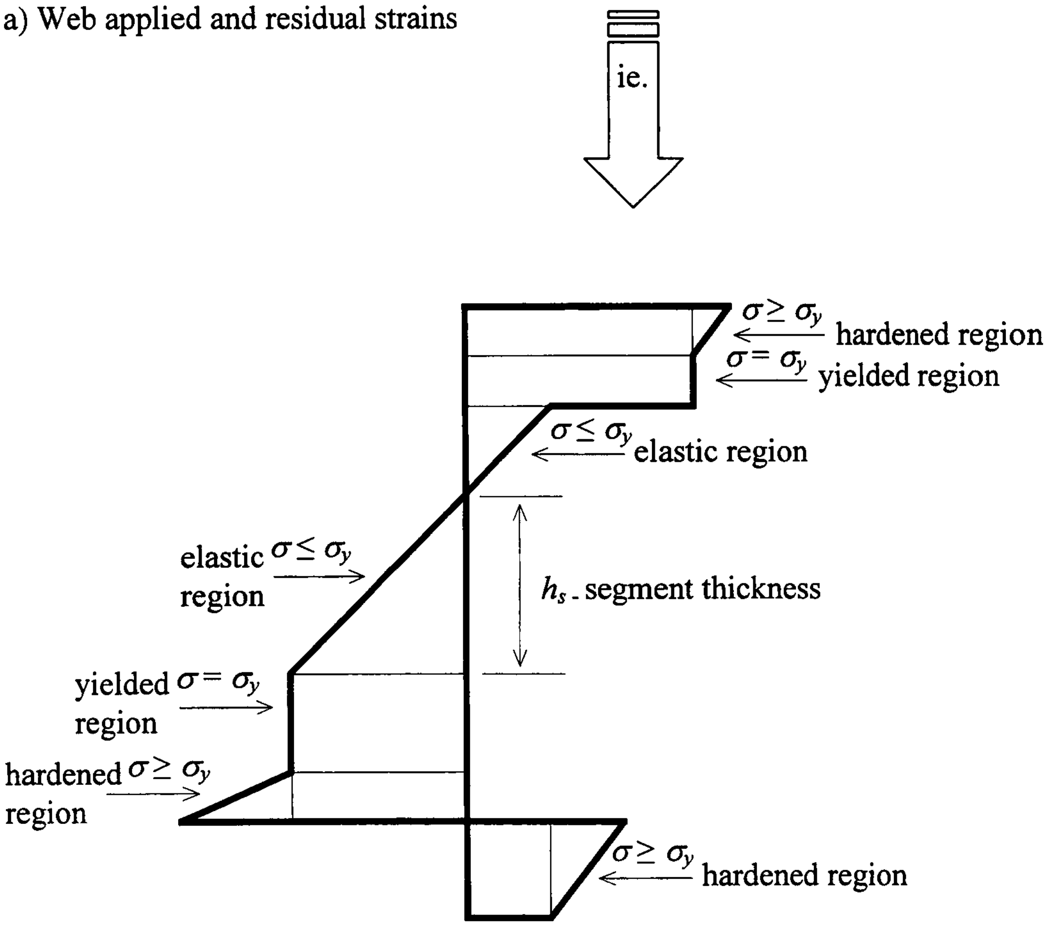

b) Web stress distribution

Figure 5.6 Web strain and stress distribution

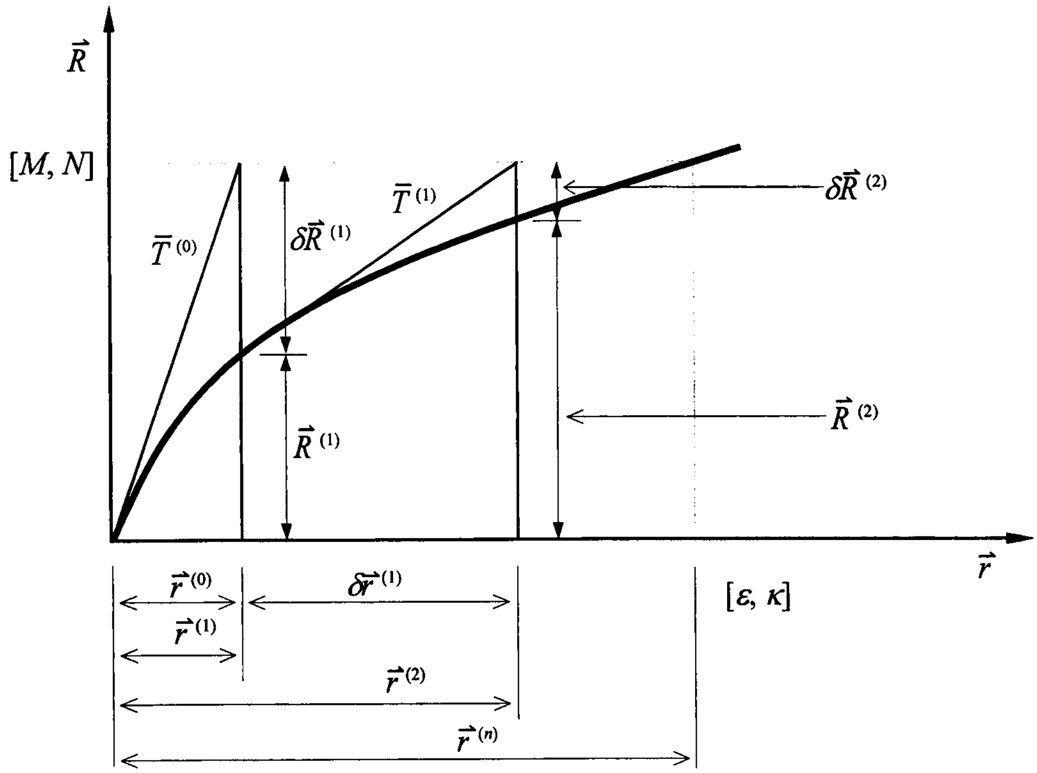

Figure 5.7 Newton-Raphson procedure

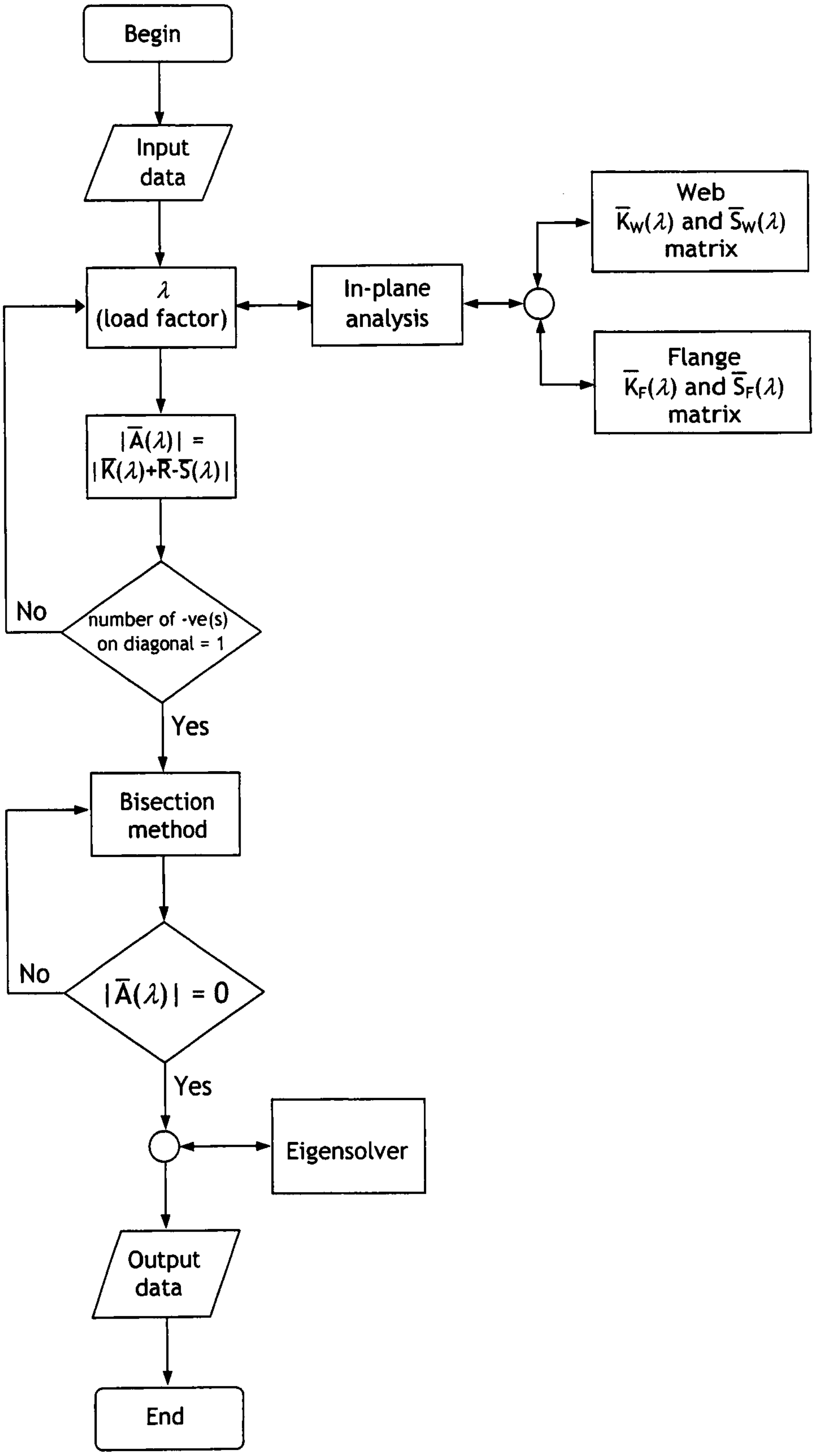

Figure 5.8 Flow-chart diagram for in-plane and buckling analysis

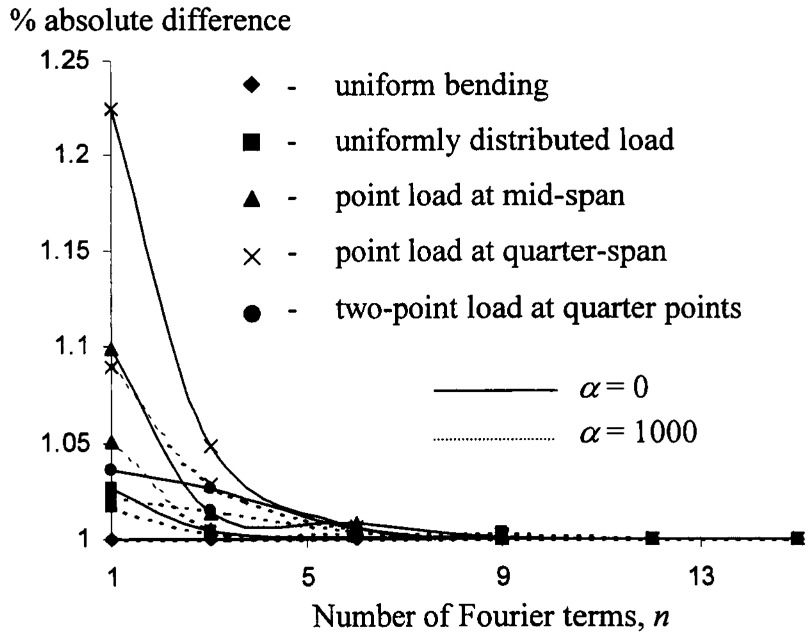

a) without residual stresses

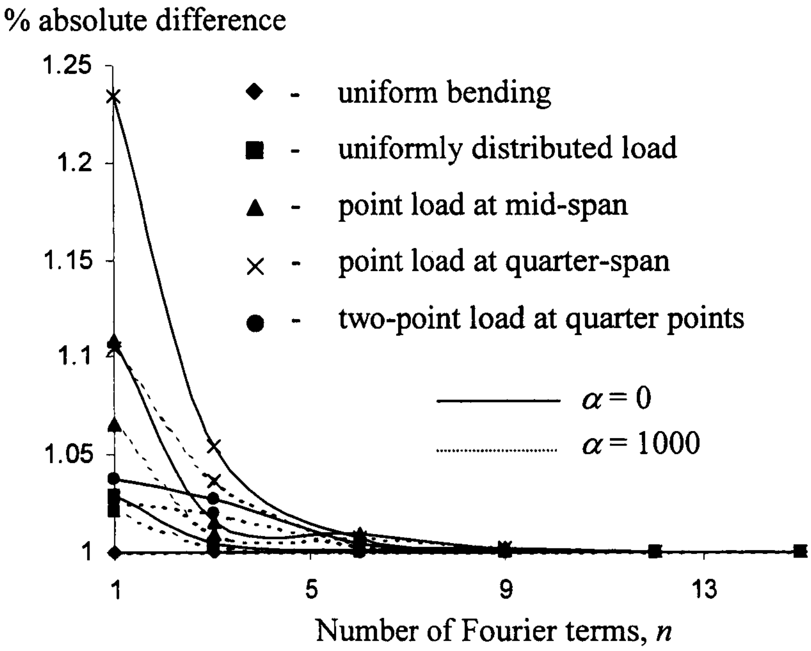

b) with residual stresses

Figure 5.9 Convergence of the model

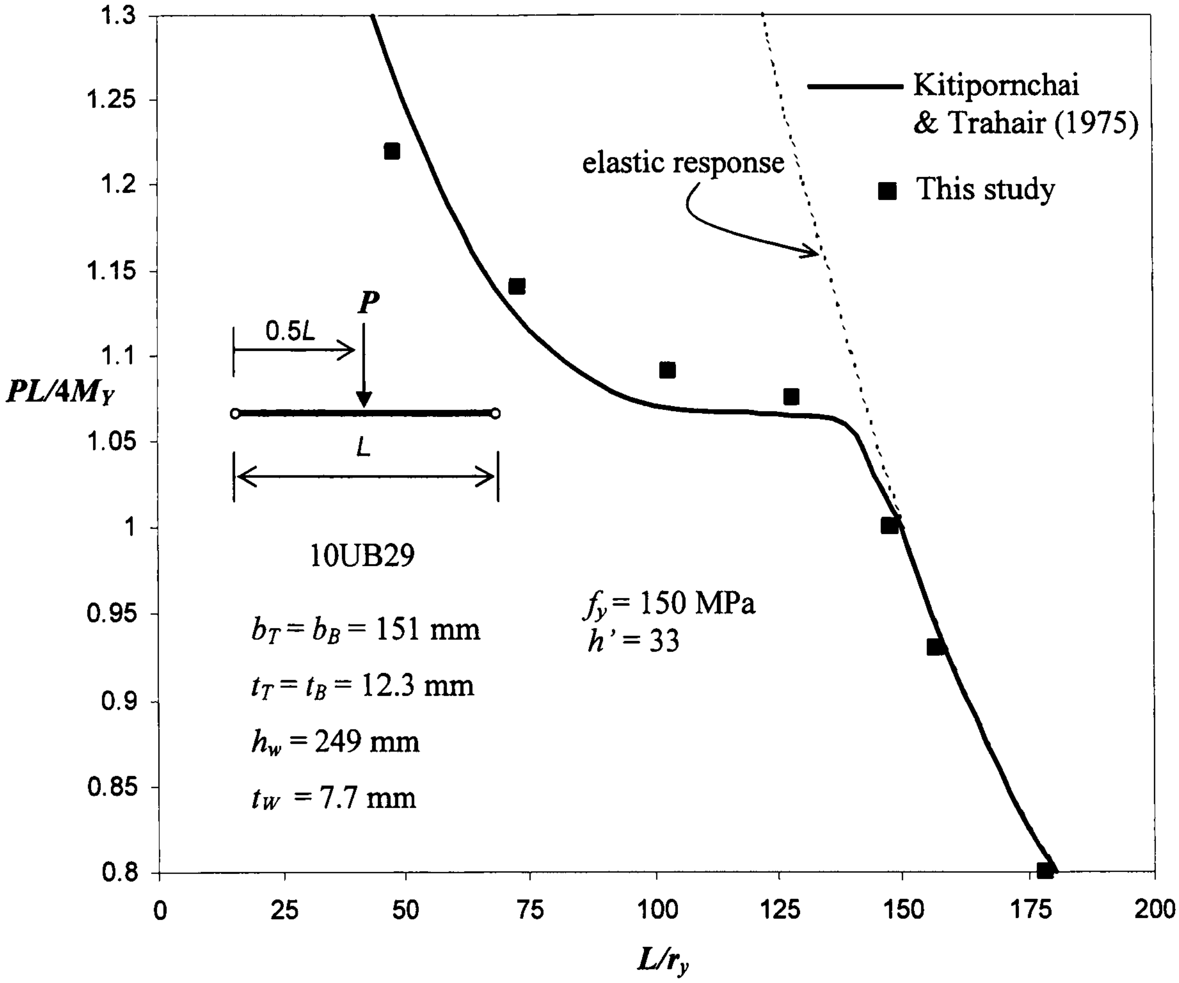

Figure 5.10 Comparison of solutions for stress-relieved beams (inelastic lateral buckling)

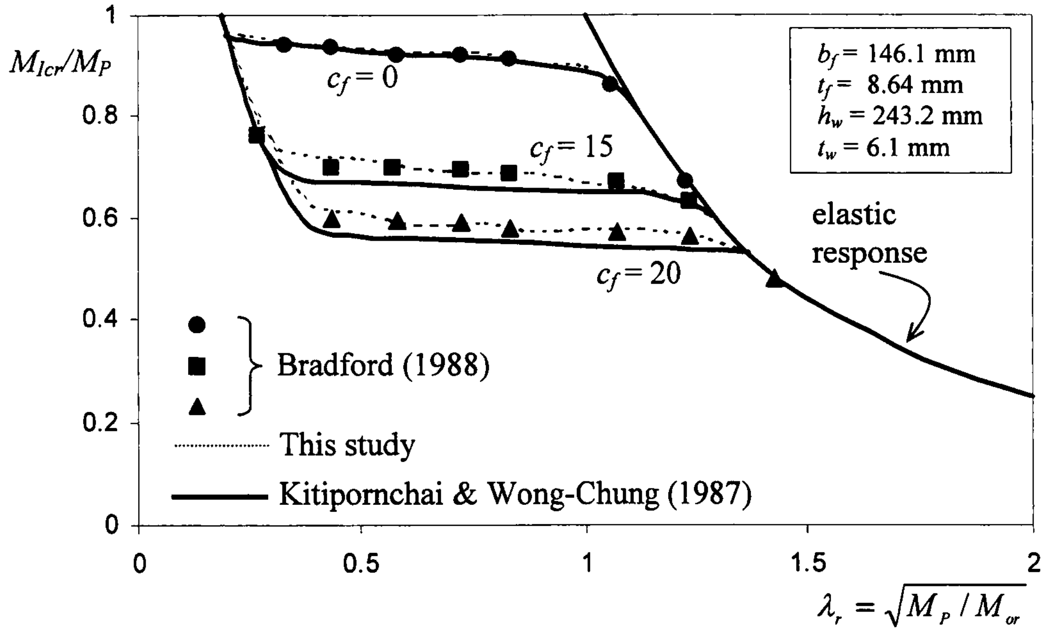

Figure 5.11 Comparison study for different residual stress distributions

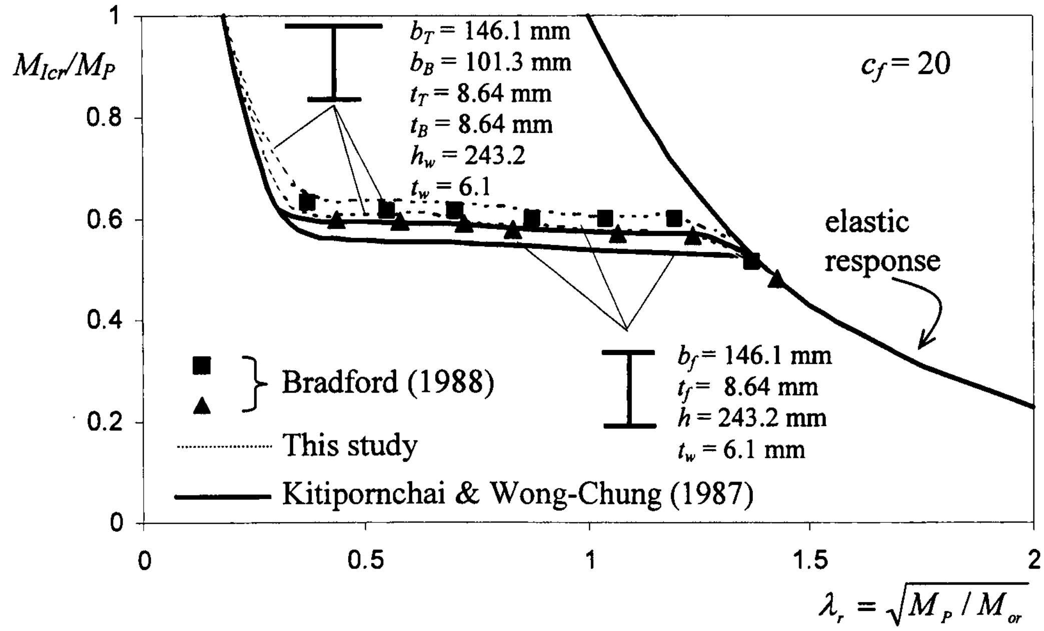

Figure 5.12 Comparison study for different monosymmetric beams

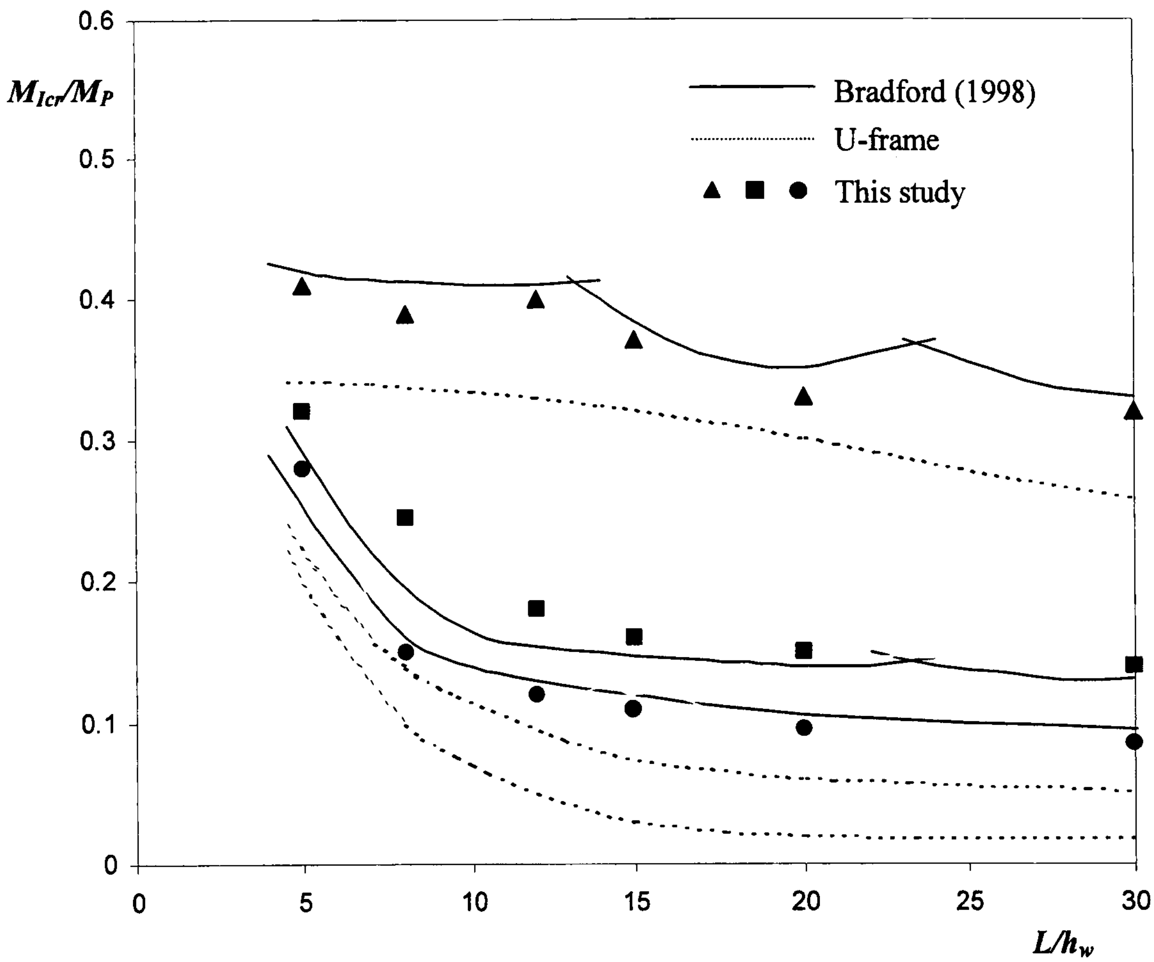

Section Geometry:	
h_w	– 1500 mm
t_w	– 10 mm
b_f	– 300 mm
t_f	– 30 mm

Material Properties:	
E	– 200 GPa
v	– 0.3
f_y	– 250 MPa
E_{st}	– E/33
ε_h	– 11ε_y
$2c_f$	– 40 mm

Figure 5.13 Comparison study for inelastic buckling moment versus beam length

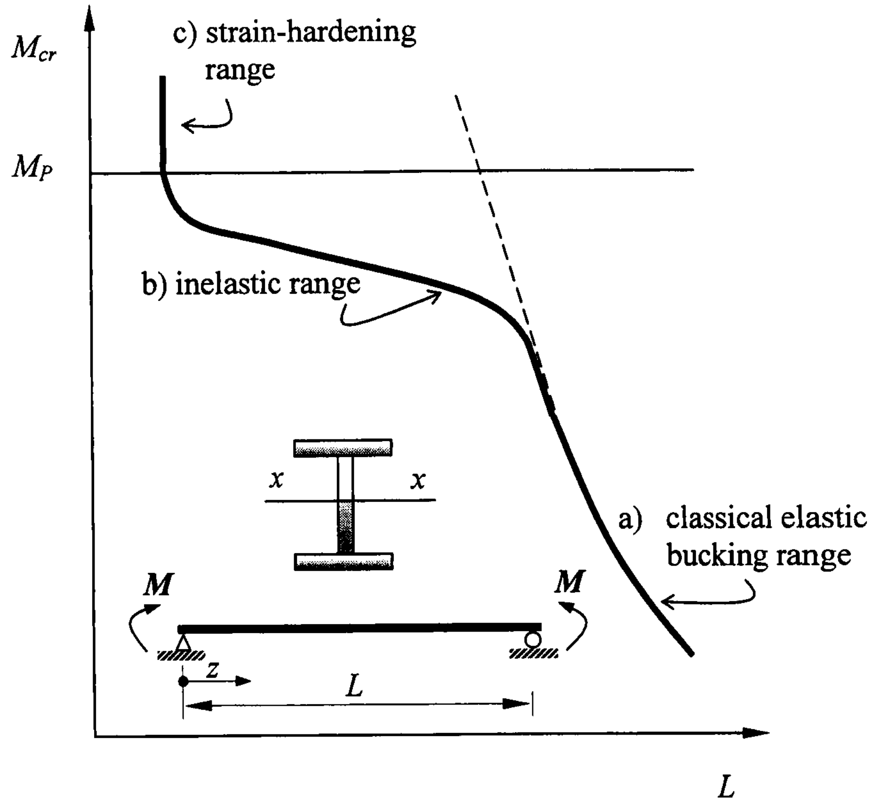

Figure 5.14 Typical beam buckling curves

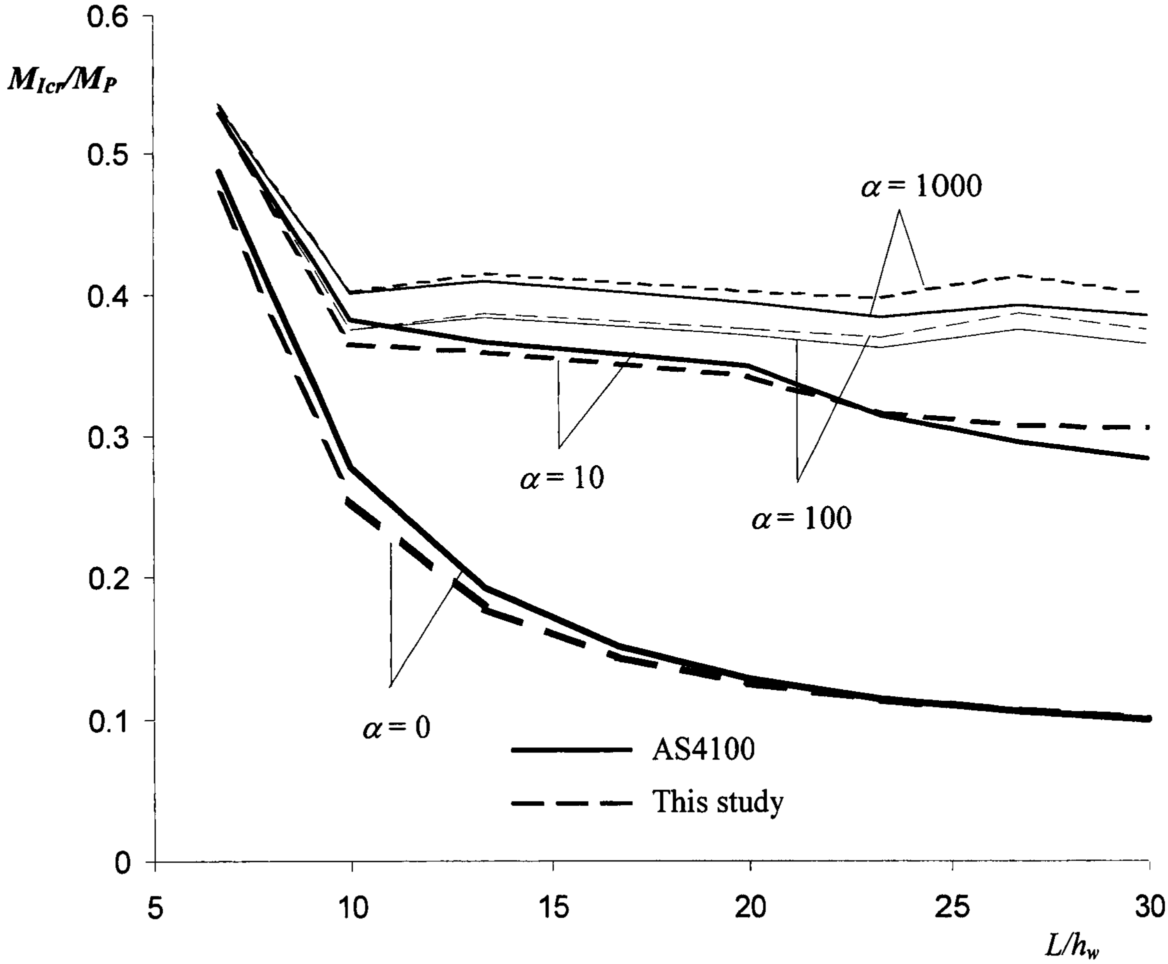

Section Geometry:	
h_w	– 1500 mm
t_w	– 10 mm
b_f	– 300 mm
t_f	– 30 mm

Material Properties:	
E	– 200 GPa
v	– 0.3
f_y	– 250 MPa
E_{st}	– E/33
ε_h	– 11ε_y
$2c_f$	– 40 mm

Figure 5.15 Modified AS4100 approach ('design rule by buckling analysis') vs numerical analysis

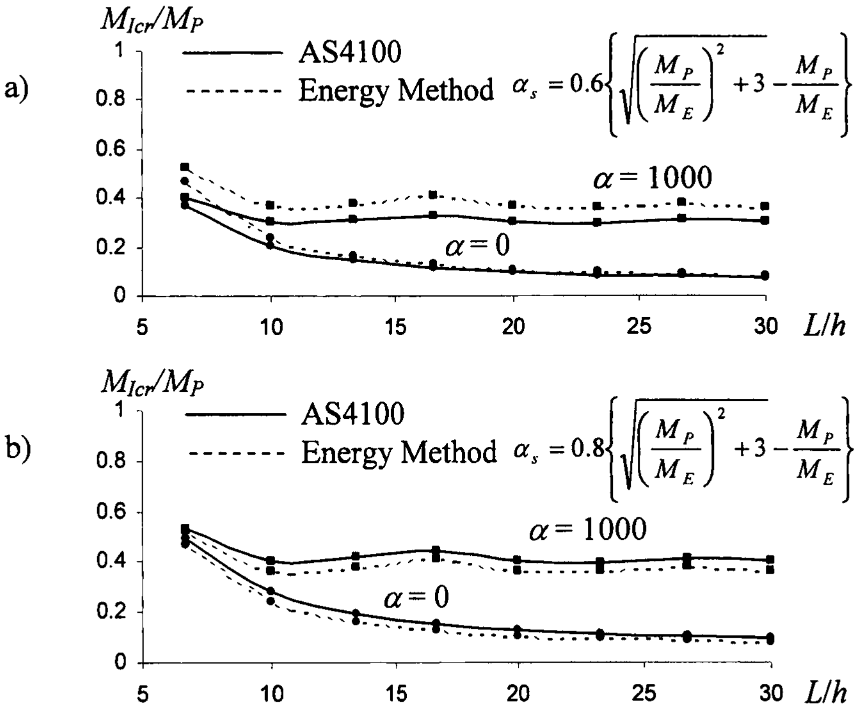

Figure 5.16 Inelastic buckling moment versus beam length for a doubly symmetric I-section beam in uniform bending: a) α_s as per AS4100; b) modified α_s

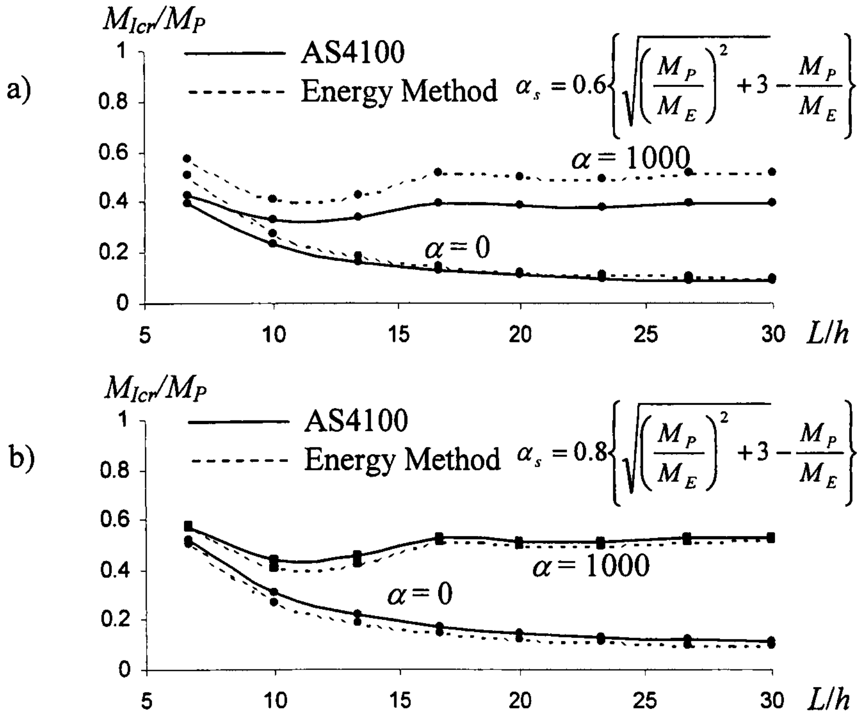

Figure 5.17 Inelastic buckling moment versus beam length for a doubly symmetric I-section beam under uniformly distributed load: a) α_s as per AS4100; b) modified α_s

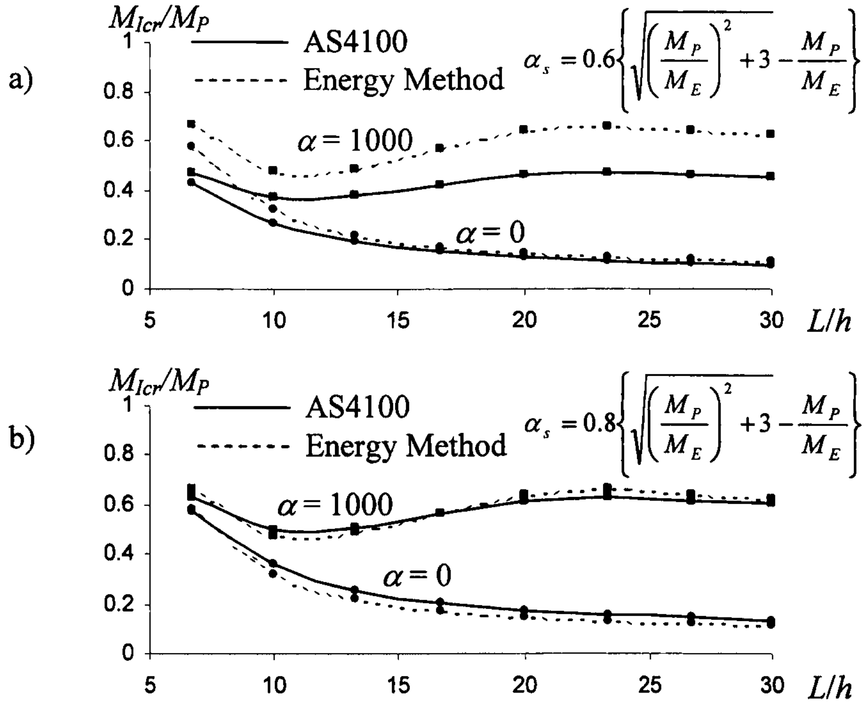

Figure 5.18 Inelastic buckling moment versus beam length for a doubly symmetric I-section beam under point load at mid-span: a) α_s as per AS4100; b) modified α_s

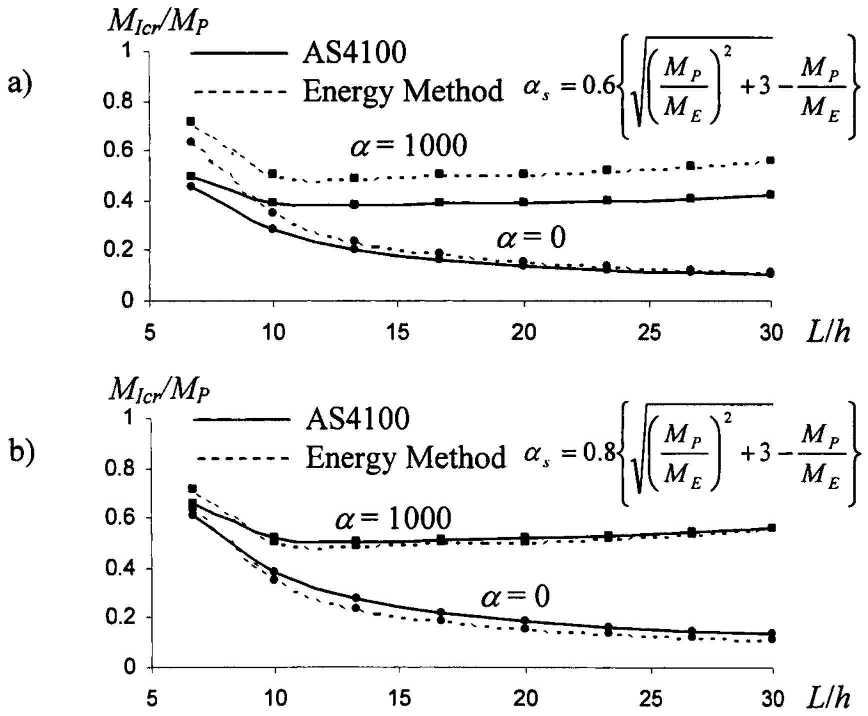

Figure 5.19 Inelastic buckling moment versus beam length for a doubly symmetric I-section beam under point load at quarter span: a) α_s as per AS4100; b) modified α_s

a)

b)

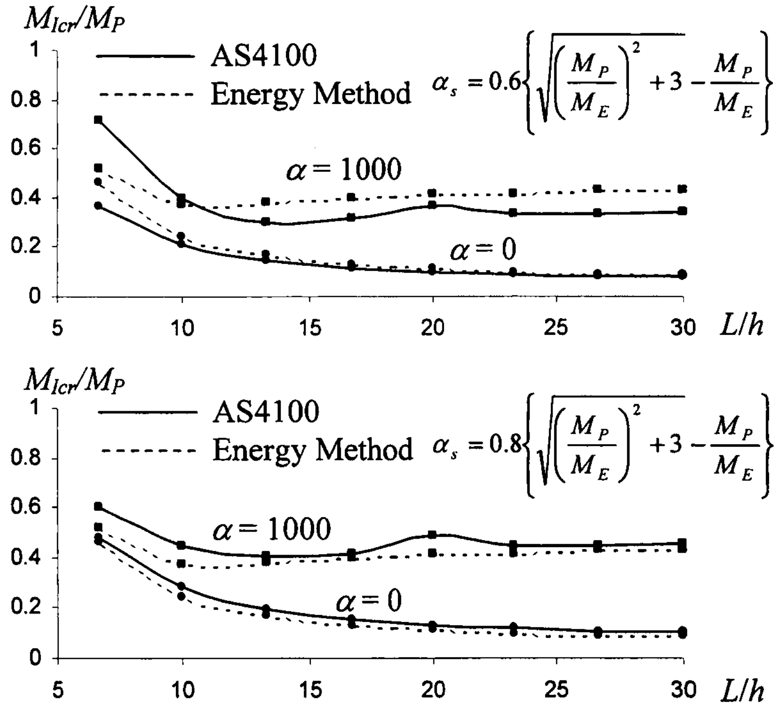

Figure 5.20 Inelastic buckling moment versus beam length for a doubly symmetric I-section beam under two-point load at quarter span: a) α_s as per AS4100; b) modified α_s

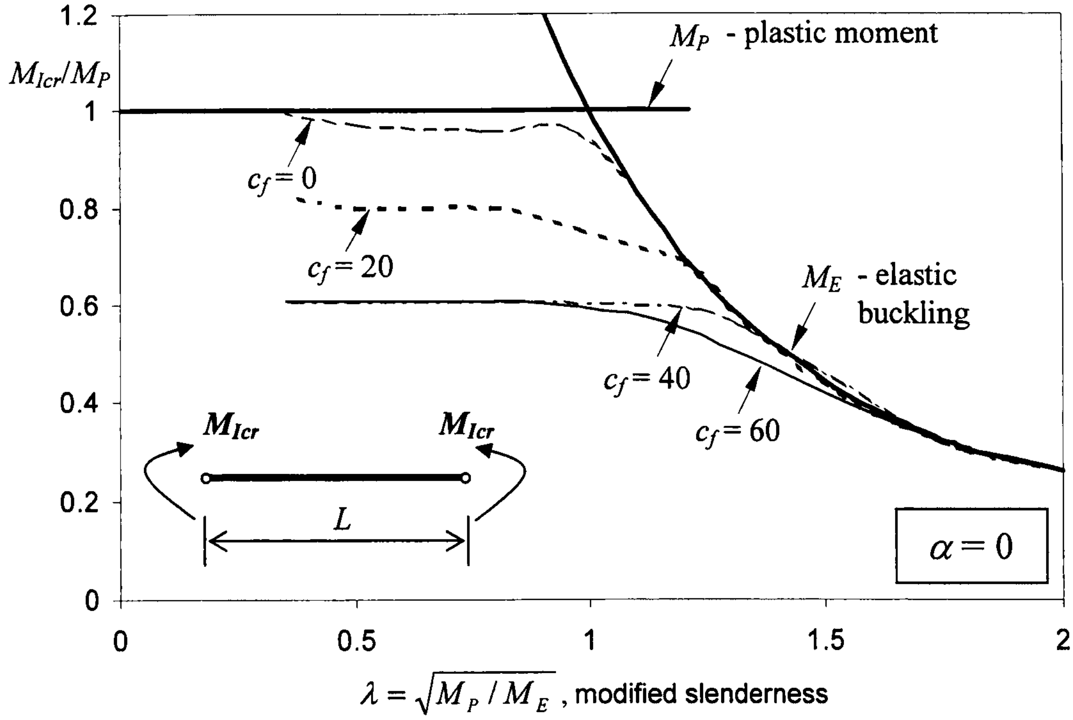

Figure 5.21 Inelastic buckling moments of I-section beam in uniform bending; $\alpha = 0$

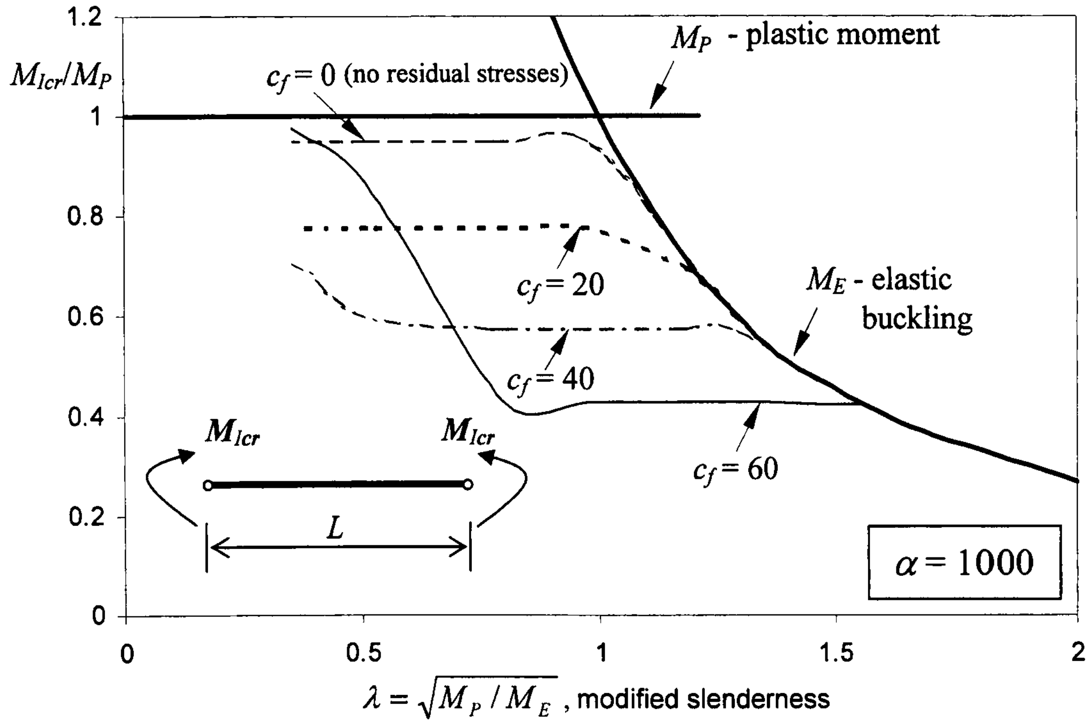

Figure 5.22 Inelastic buckling moments of I-section beam in uniform bending; $\alpha = 1000$

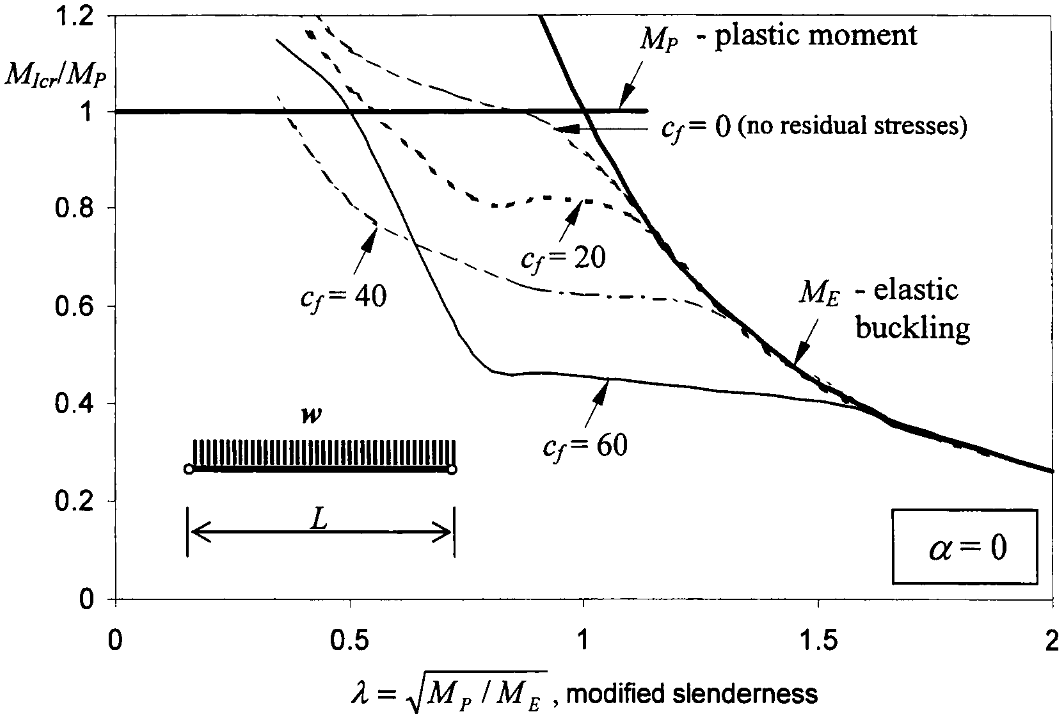

Figure 5.23 Inelastic buckling moments of I-section beam under uniformly distributed load; $\alpha = 0$

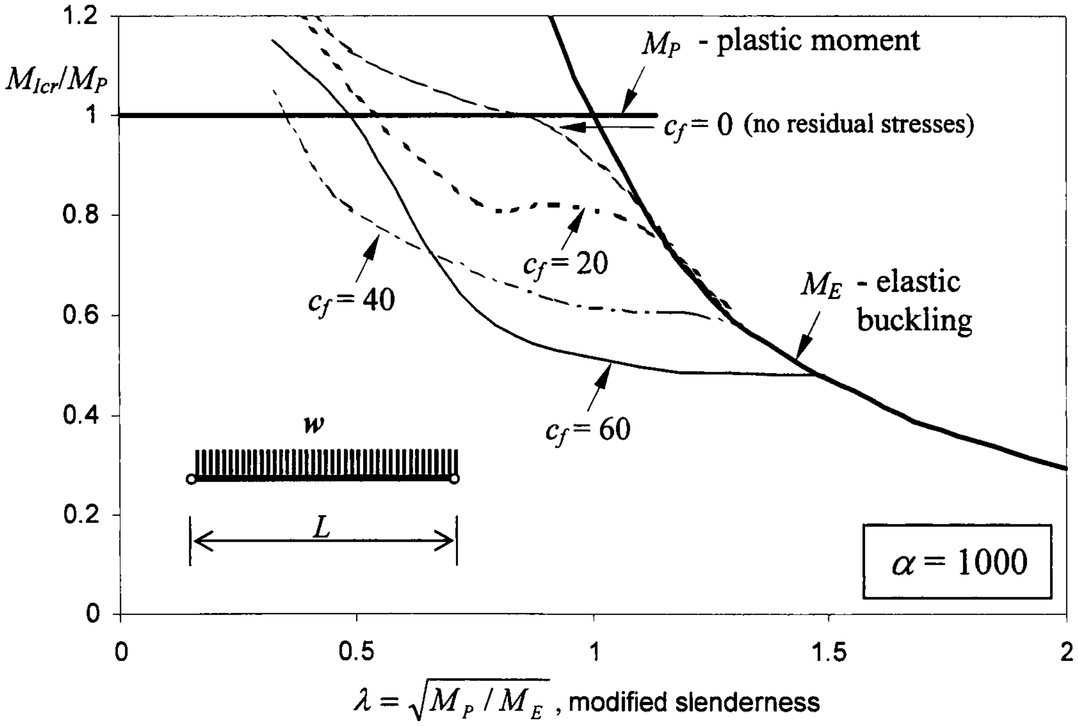

Figure 5.24 Inelastic buckling moments of I-section beam under uniformly distributed load; $\alpha = 1000$

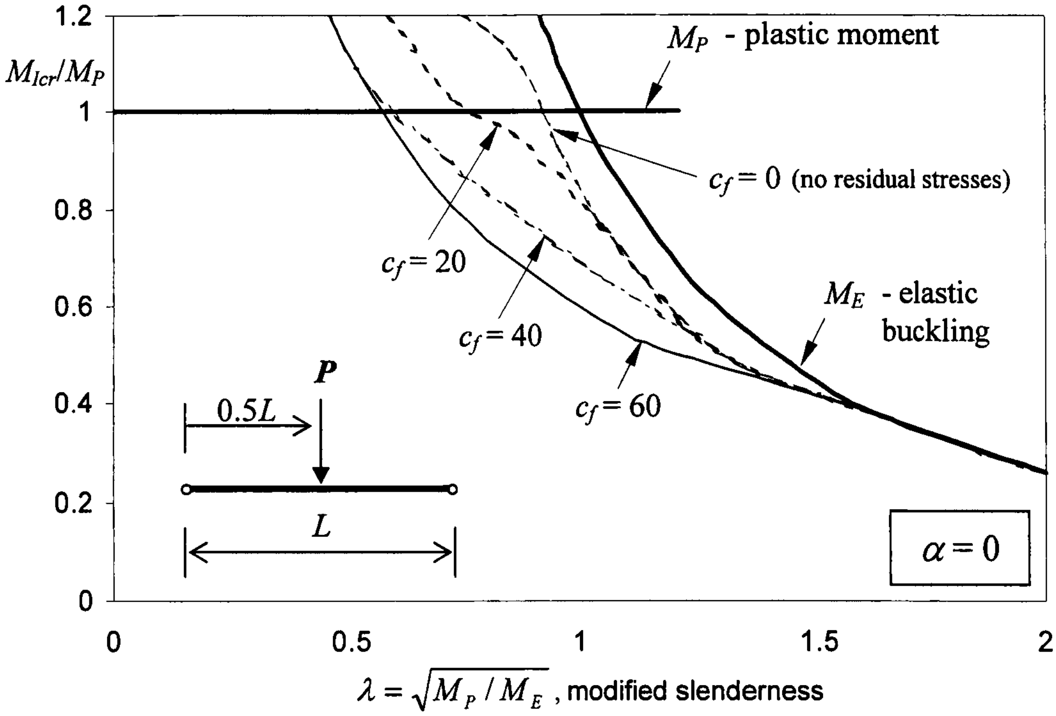

Figure 5.25 Inelastic buckling moments of I-section beam under central point load; $\alpha = 0$

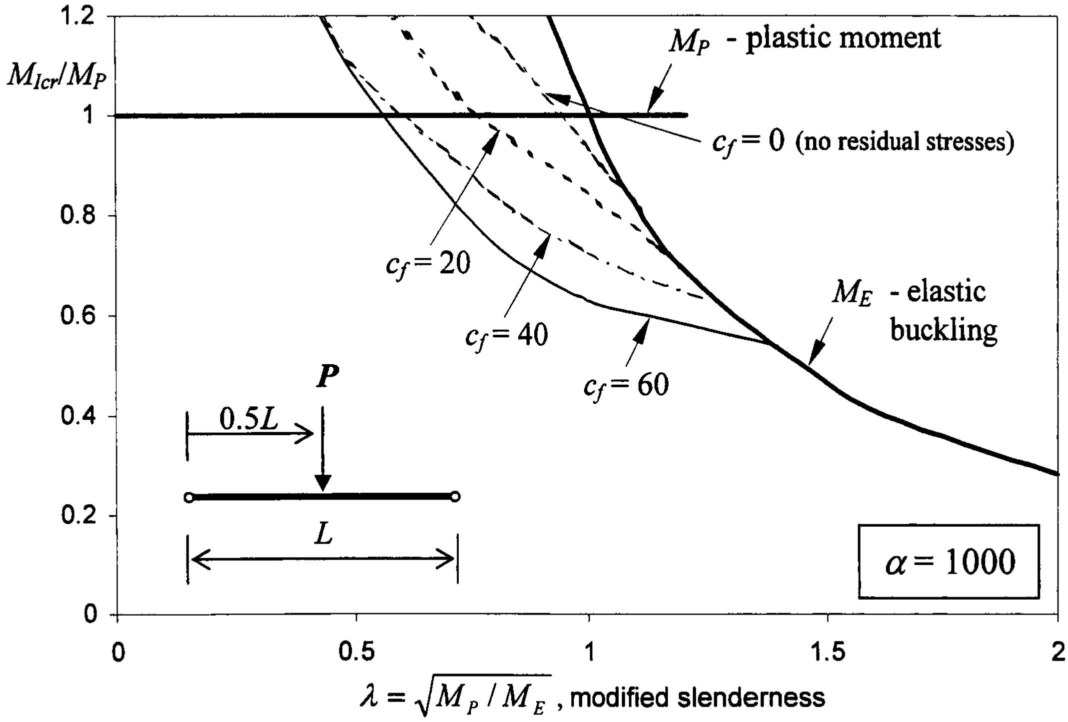

Figure 5.26 Inelastic buckling moments of I-section beam under central point load; $\alpha = 1000$

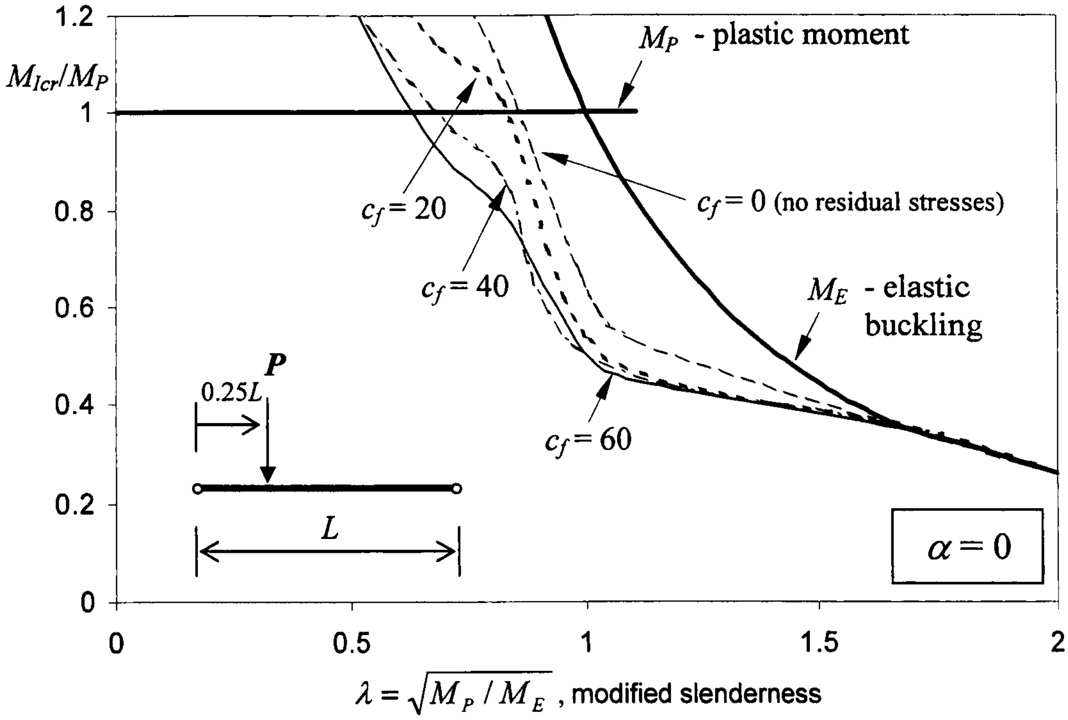

Figure 5.27 Inelastic buckling moments of I-section beam under point load at quarter span; $\alpha = 0$

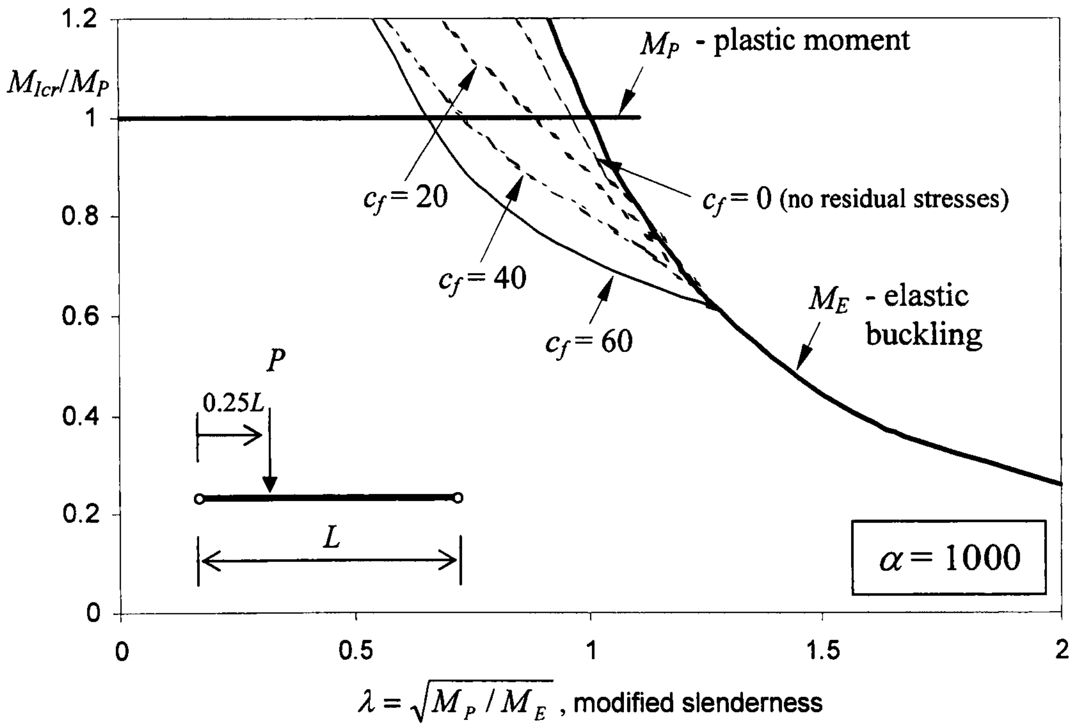

Figure 5.28 Inelastic buckling moments of I-section beam under point load at quarter span; $\alpha = 1000$

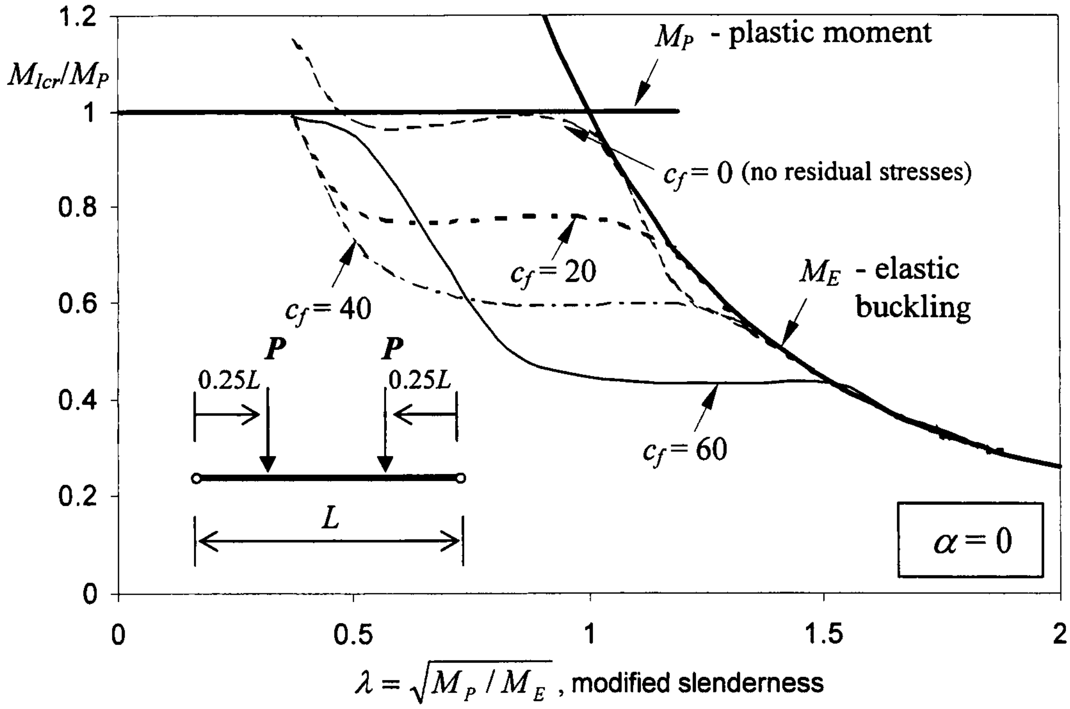

Figure 5.29 Inelastic buckling moments of I-section beam under two-point load at quarter span; $\alpha = 0$

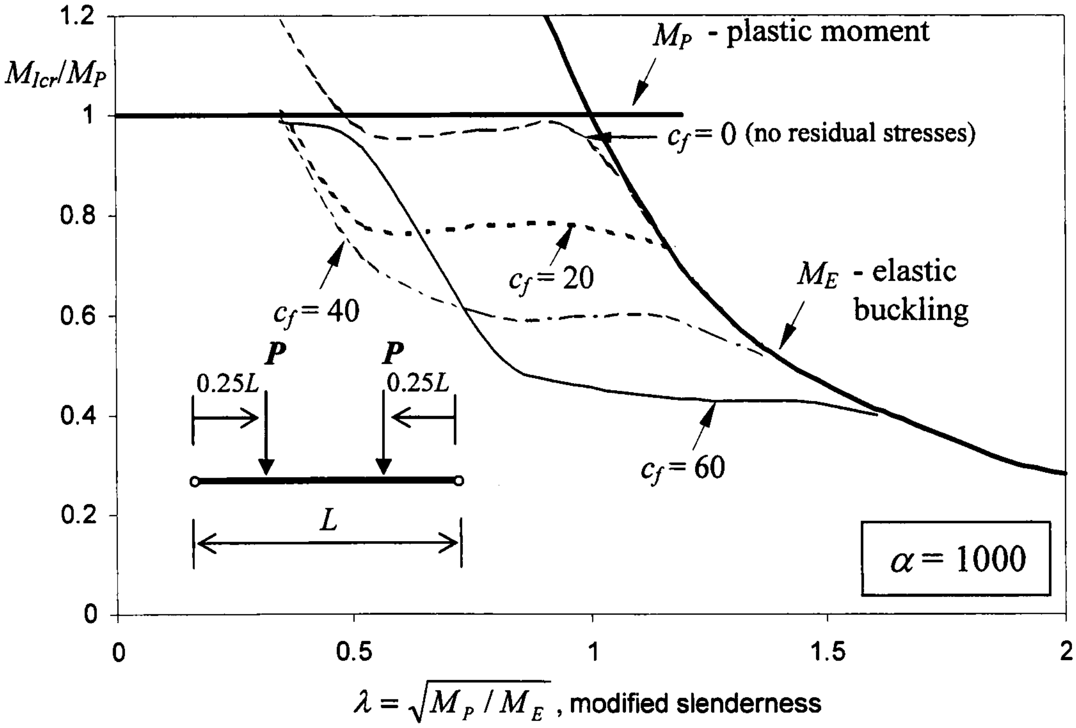

Figure 5.30 Inelastic buckling moments of I-section beam under two-point load at quarter span; $\alpha = 1000$

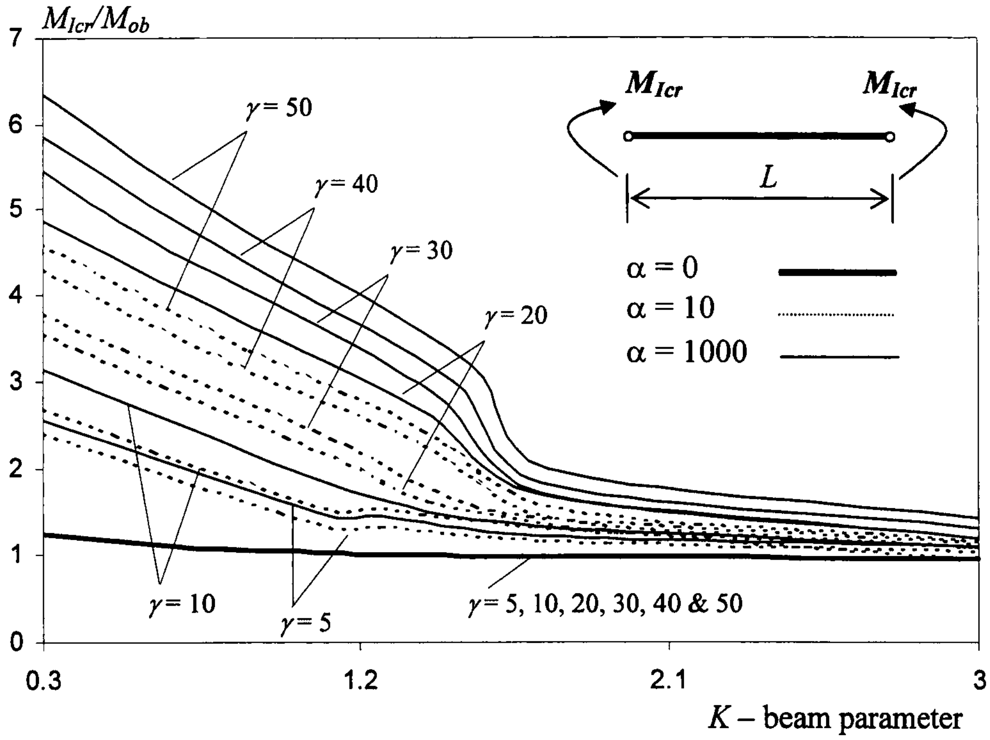

Figure 5.31 Buckling curves for I-section beam in uniform bending

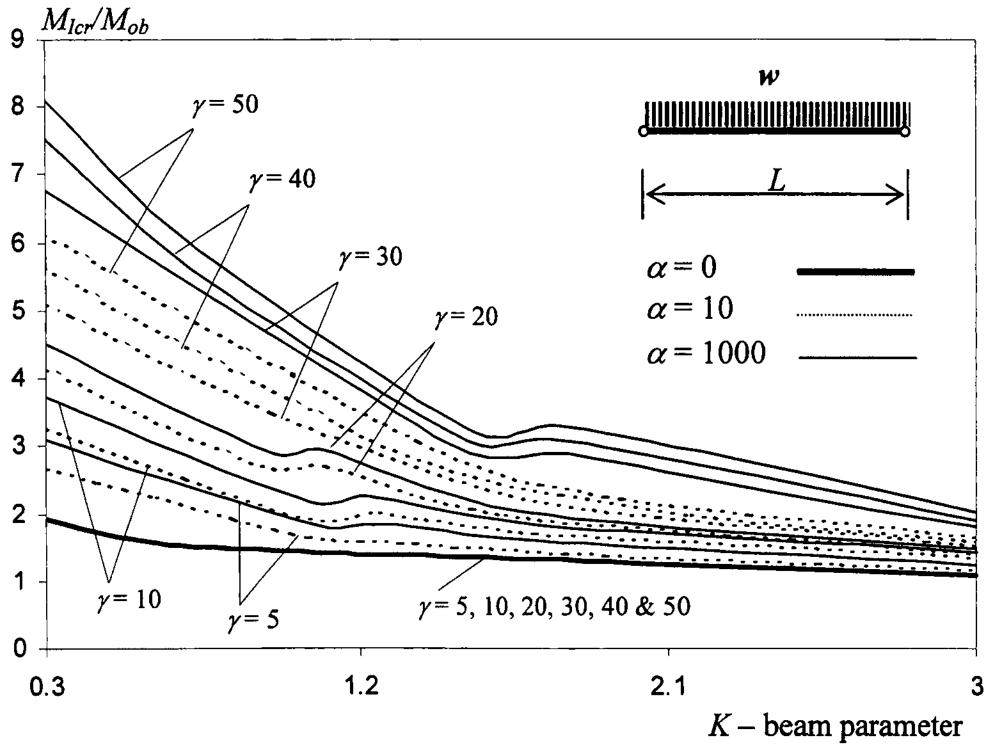

Figure 5.32 Buckling curves for I-section beam under uniformly distributed load

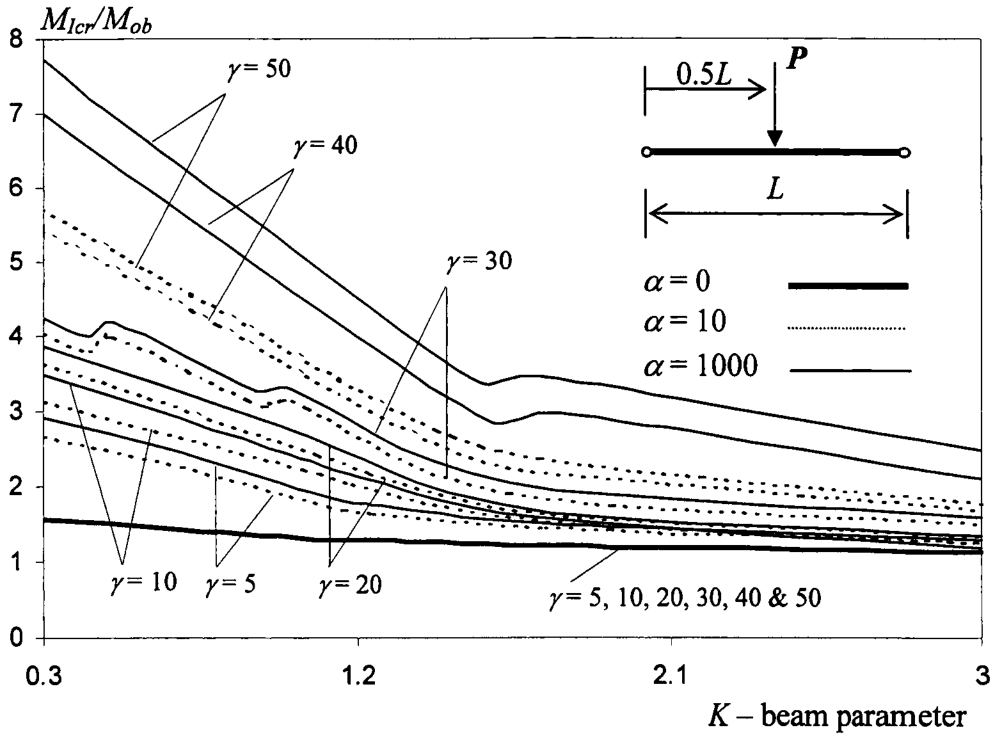

Figure 5.33 Buckling curves for I-section beam under point load at mid-span

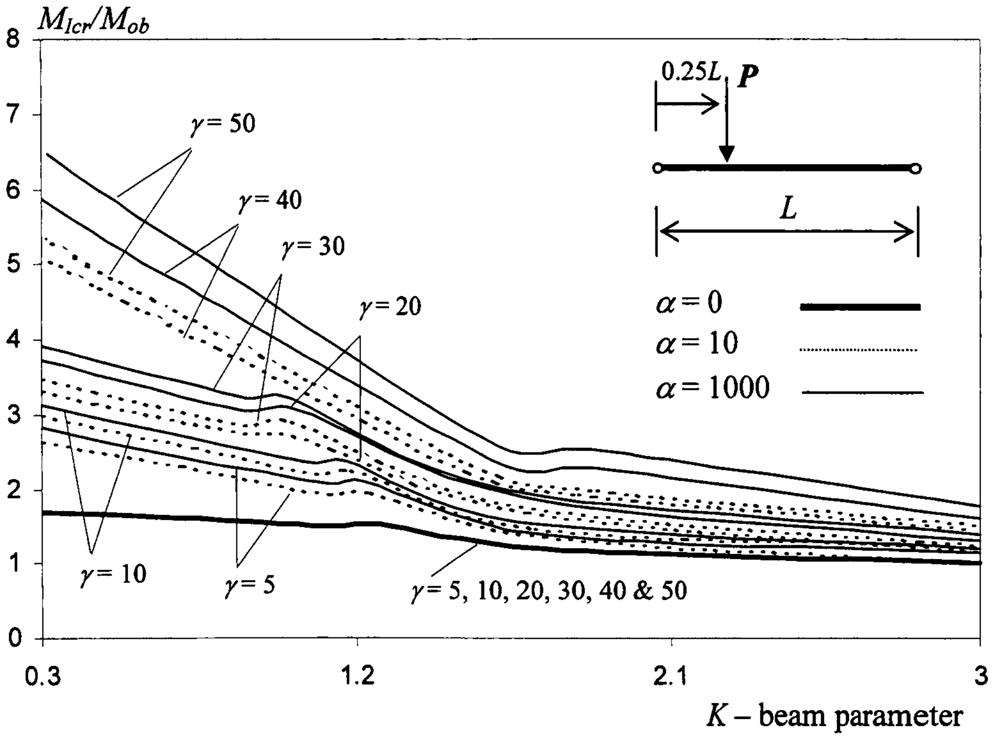

Figure 5.34 Buckling curves for I-section beam under point load at quarter span

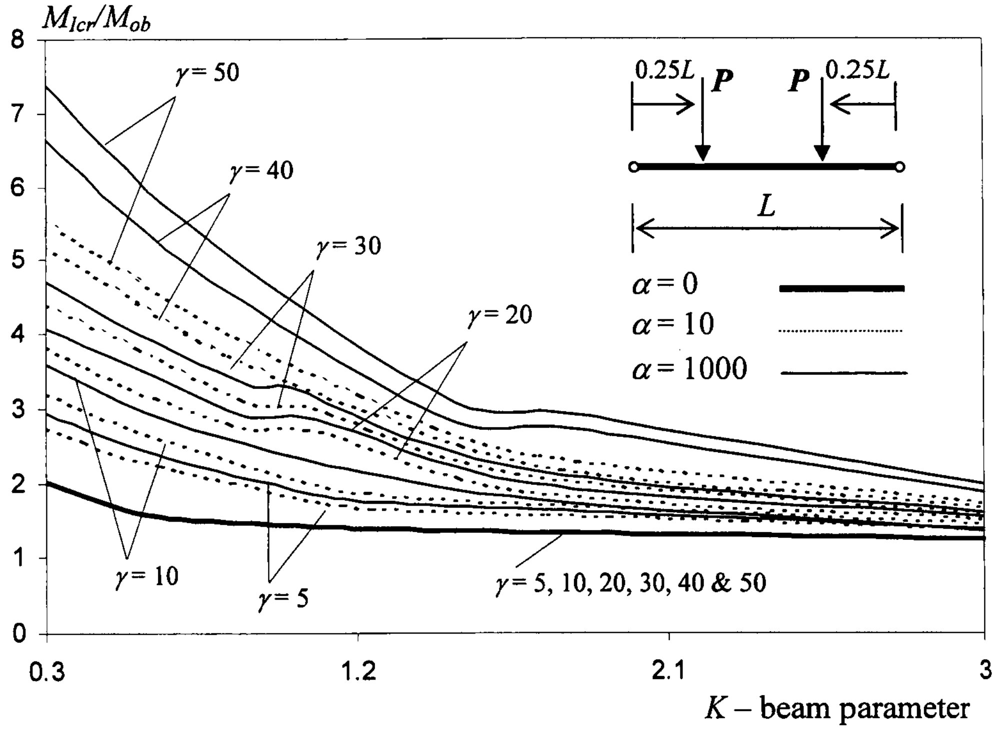

Figure 5.35 Buckling curves for I-section beam under two-point load at quarter span

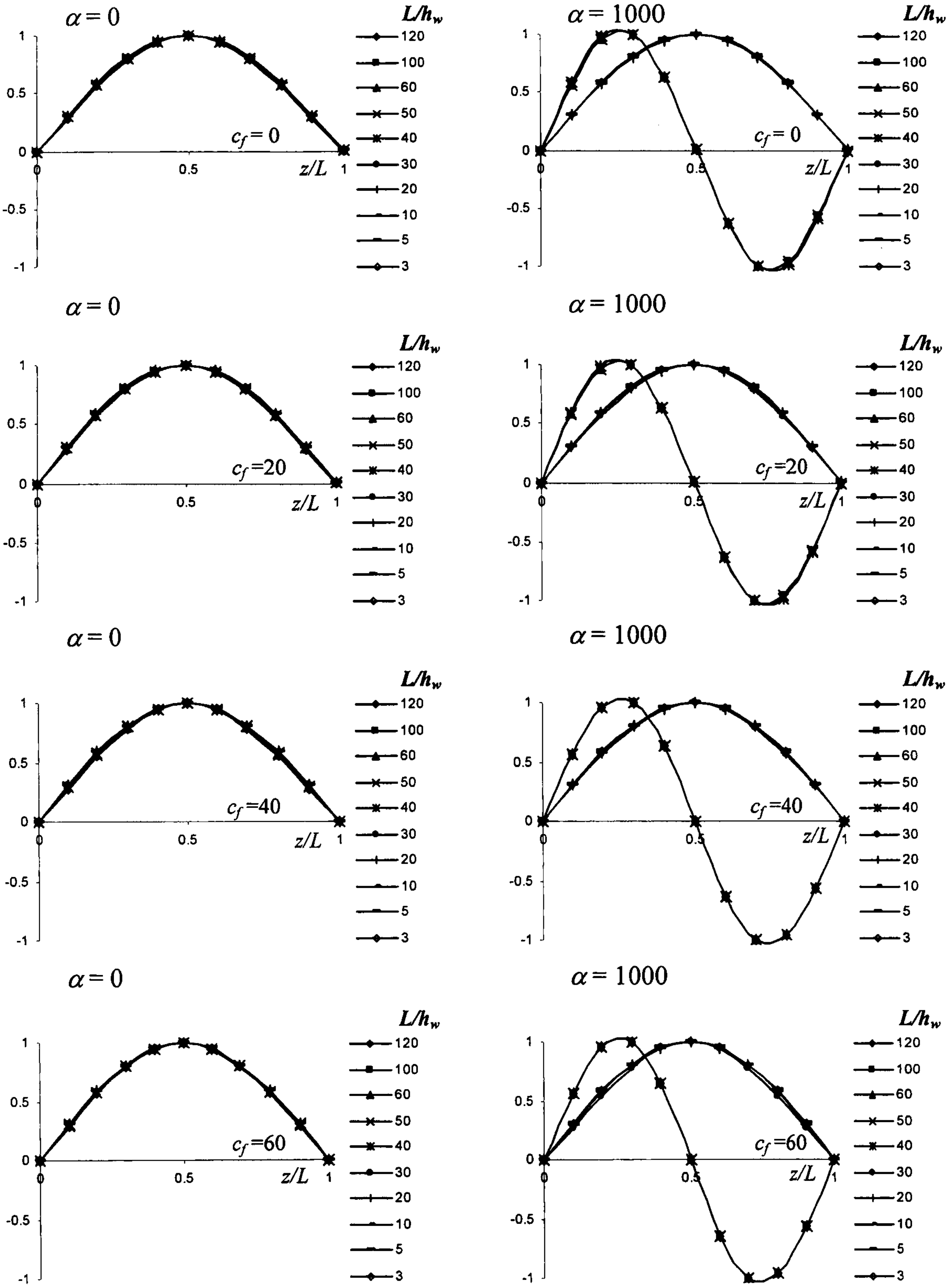

Figure 5.36 Normalised buckling mode shapes of restrained doubly symmetric I-section beams under transverse loading (uniformly distributed load) with $\alpha = 0$ and $\alpha = 1000$; compression flange lateral displacement

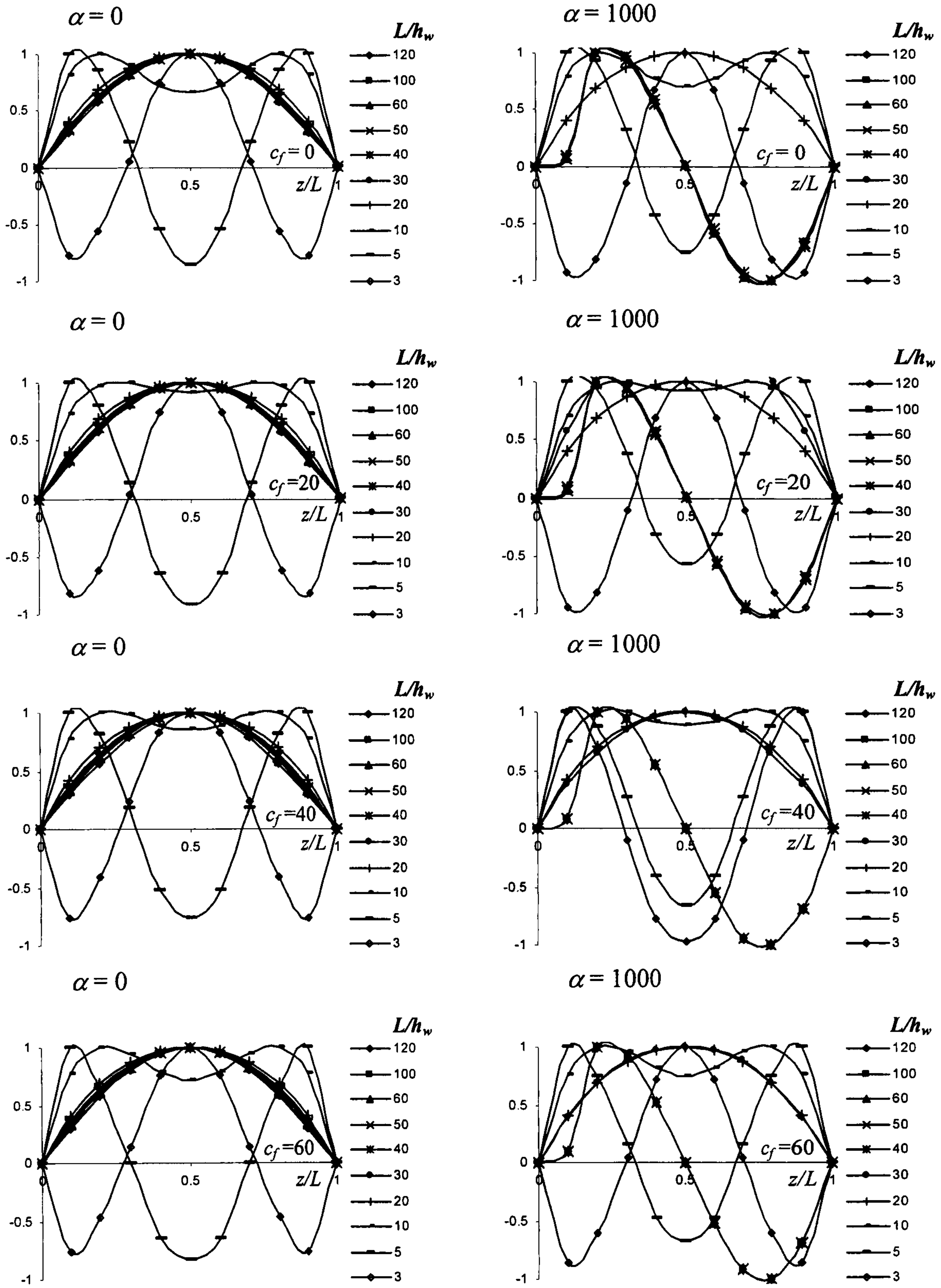

Figure 5.37 Normalised buckling mode shapes of restrained doubly symmetric I-section beams under transverse loading (uniformly distributed load) with $\alpha = 0$ and $\alpha = 1000$; compression flange twist

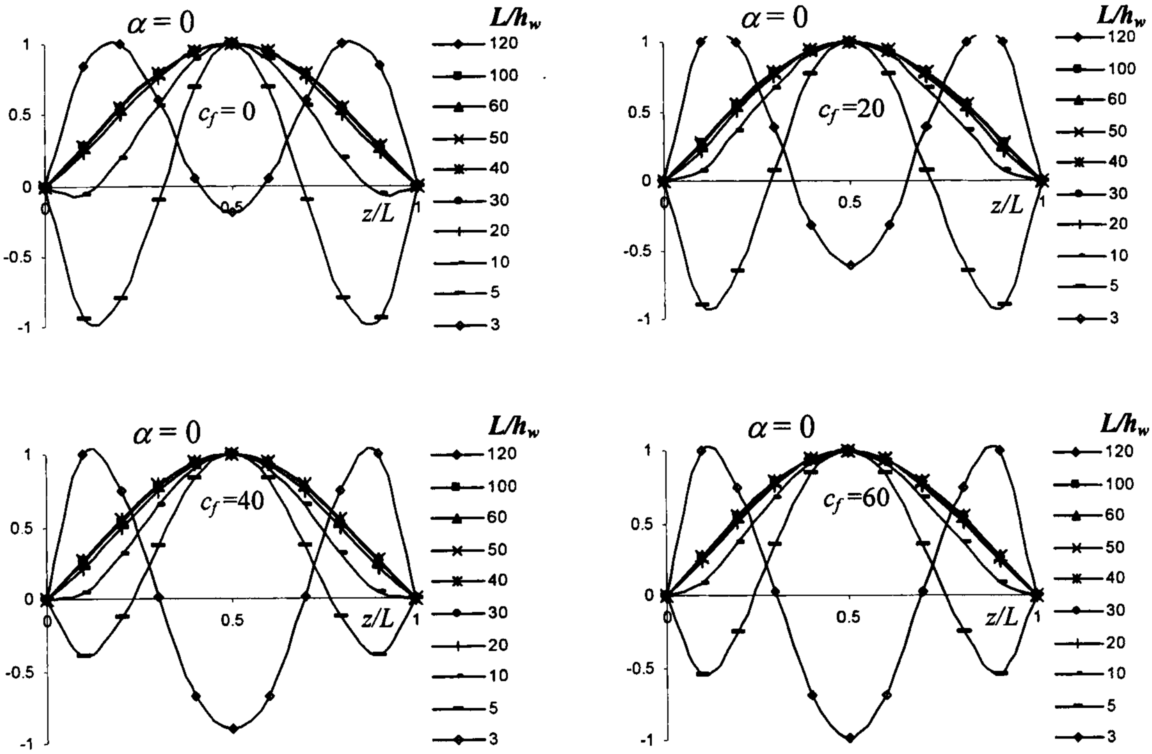

Figure 5.38 Normalised buckling mode shapes of restrained doubly symmetric I-section beams under transverse loading (uniformly distributed load) with $\alpha = 0$; tension flange twist

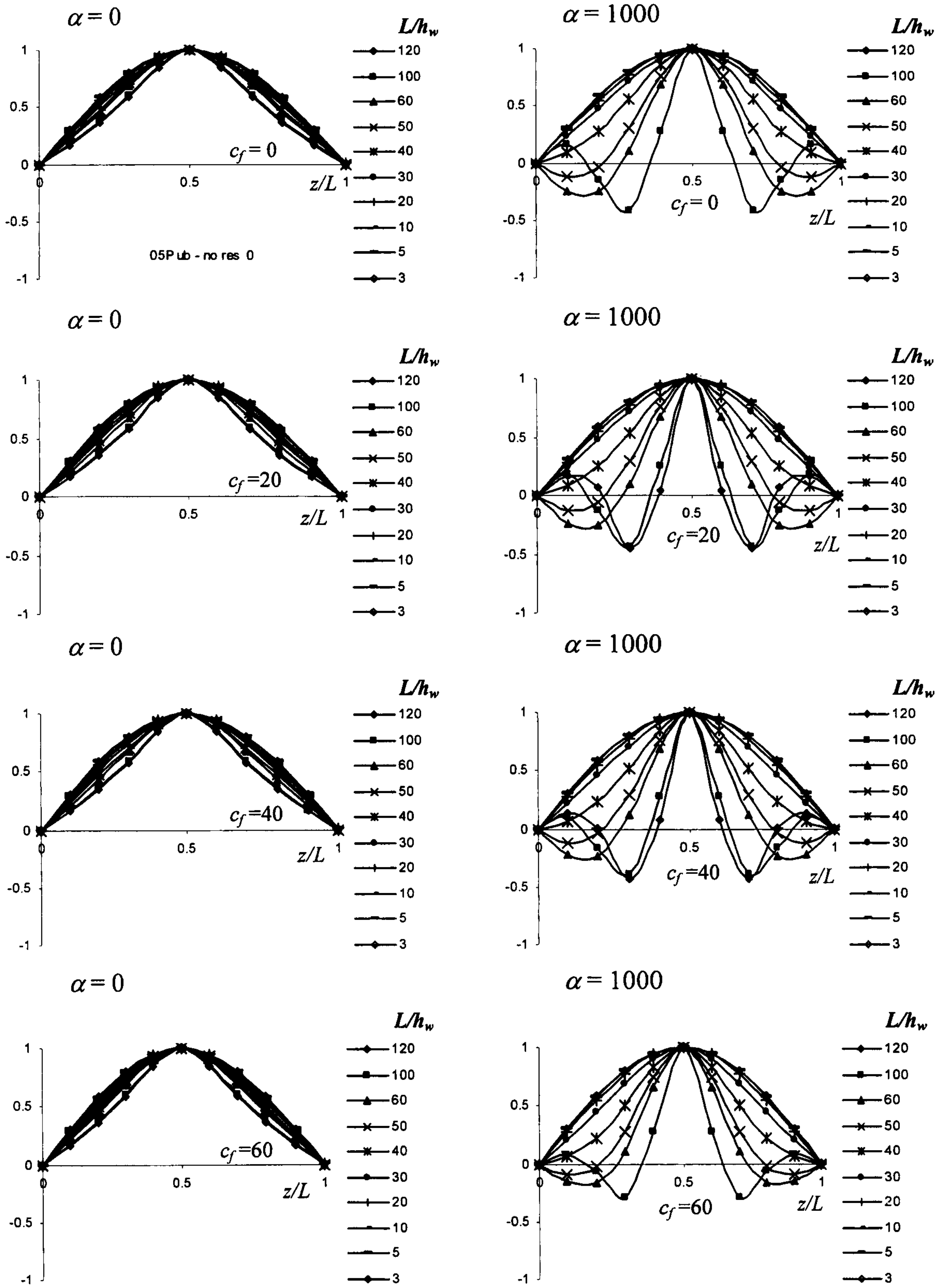

Figure 5.39 Normalised buckling mode shapes of restrained doubly symmetric I-section beams under transverse loading (point load at mid-span) with $\alpha = 0$ and $\alpha = 1000$; compression flange lateral displacement

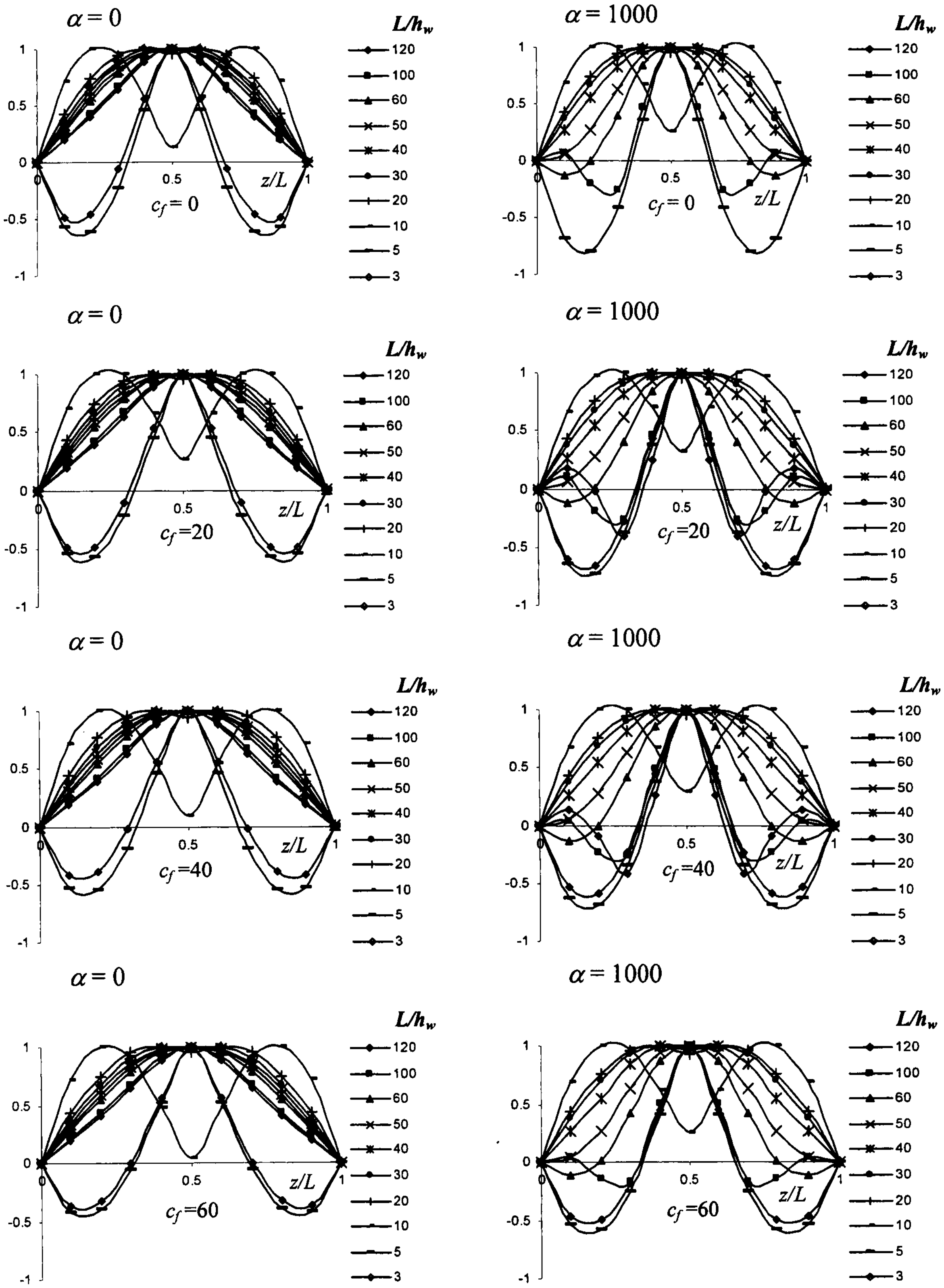

Figure 5.40 Normalised buckling mode shapes of restrained doubly symmetric I-section beams under transverse loading (point load at mid-span) with $\alpha = 0$ and $\alpha = 1000$; compression flange twist

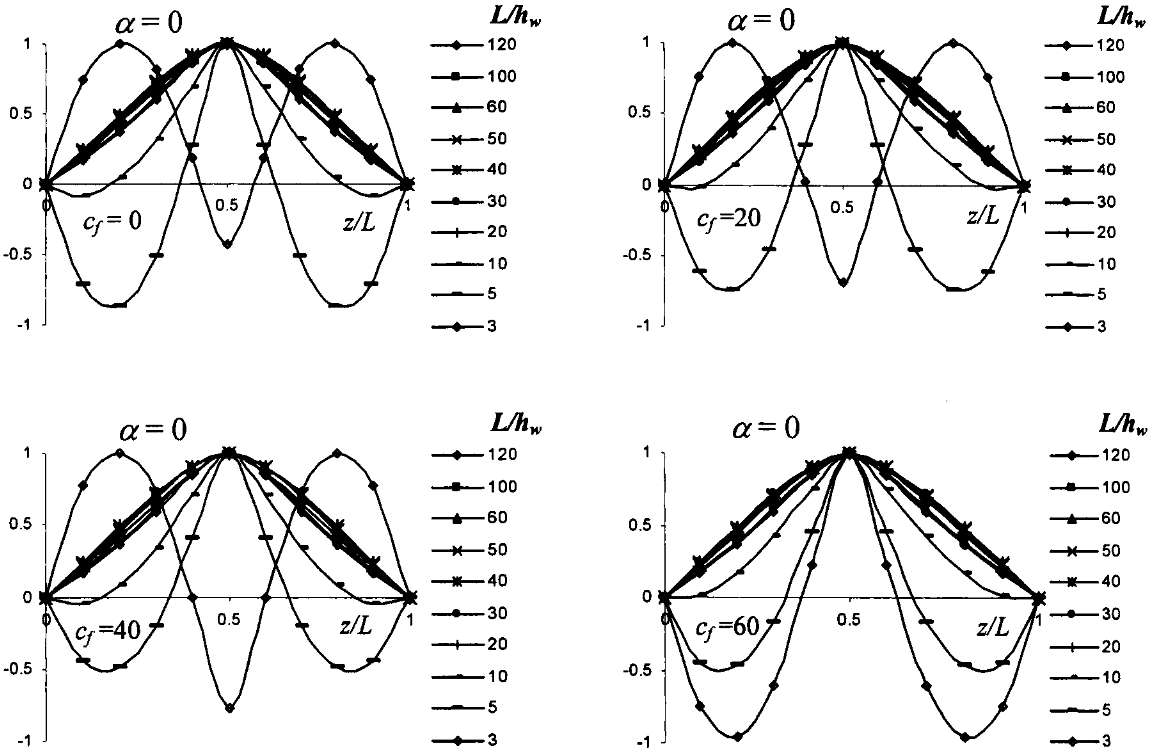

Figure 5.41 Normalised buckling mode shapes of restrained doubly symmetric I-section beams under transverse loading (point load at mid-span) with $\alpha = 0$; tension flange twist

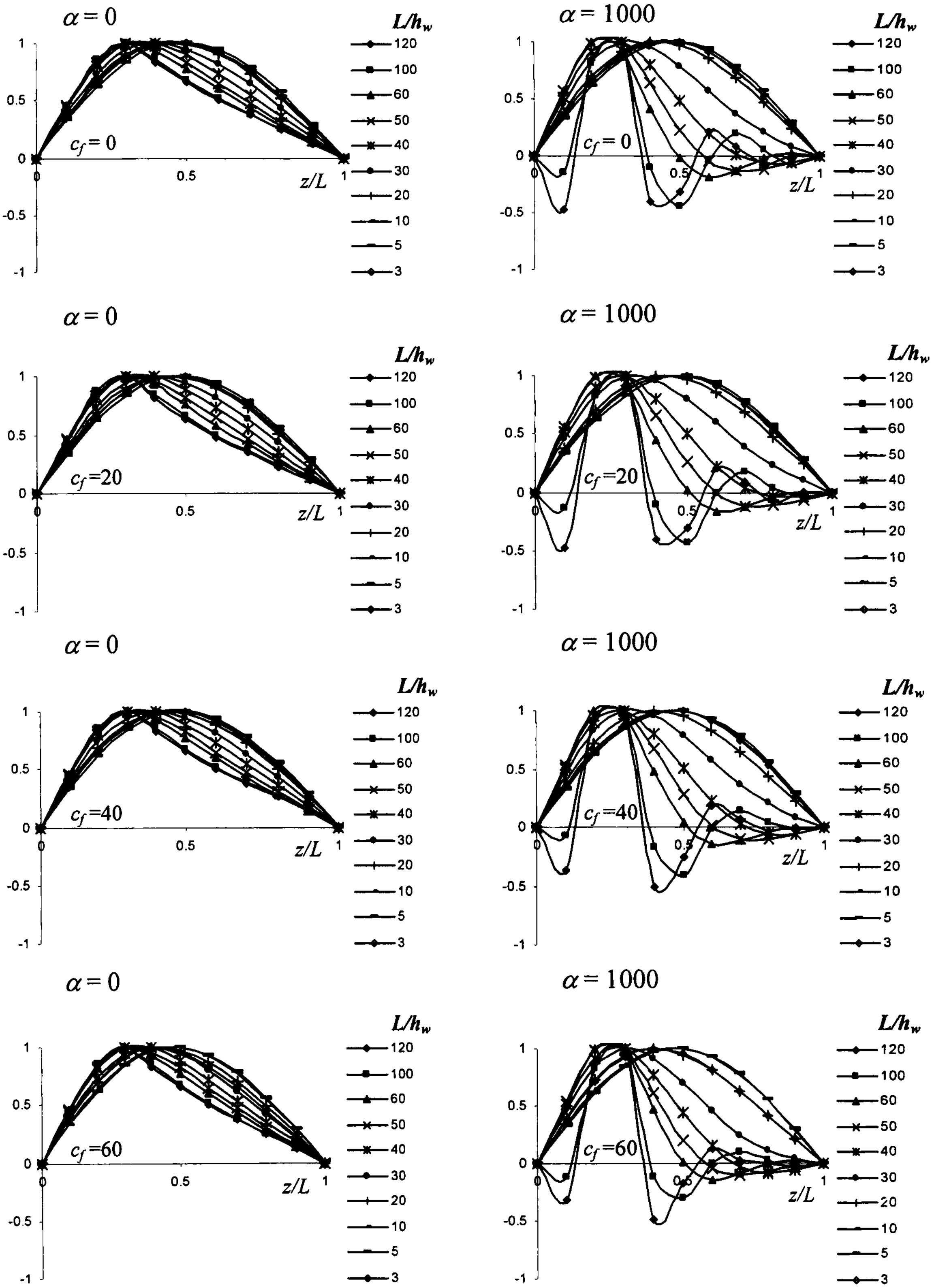

Figure 5.42 Normalised buckling mode shapes of restrained doubly symmetric I-section beams under transverse loading (point load at quarter span) with $\alpha = 0$ and $\alpha = 1000$; compression flange lateral displacement

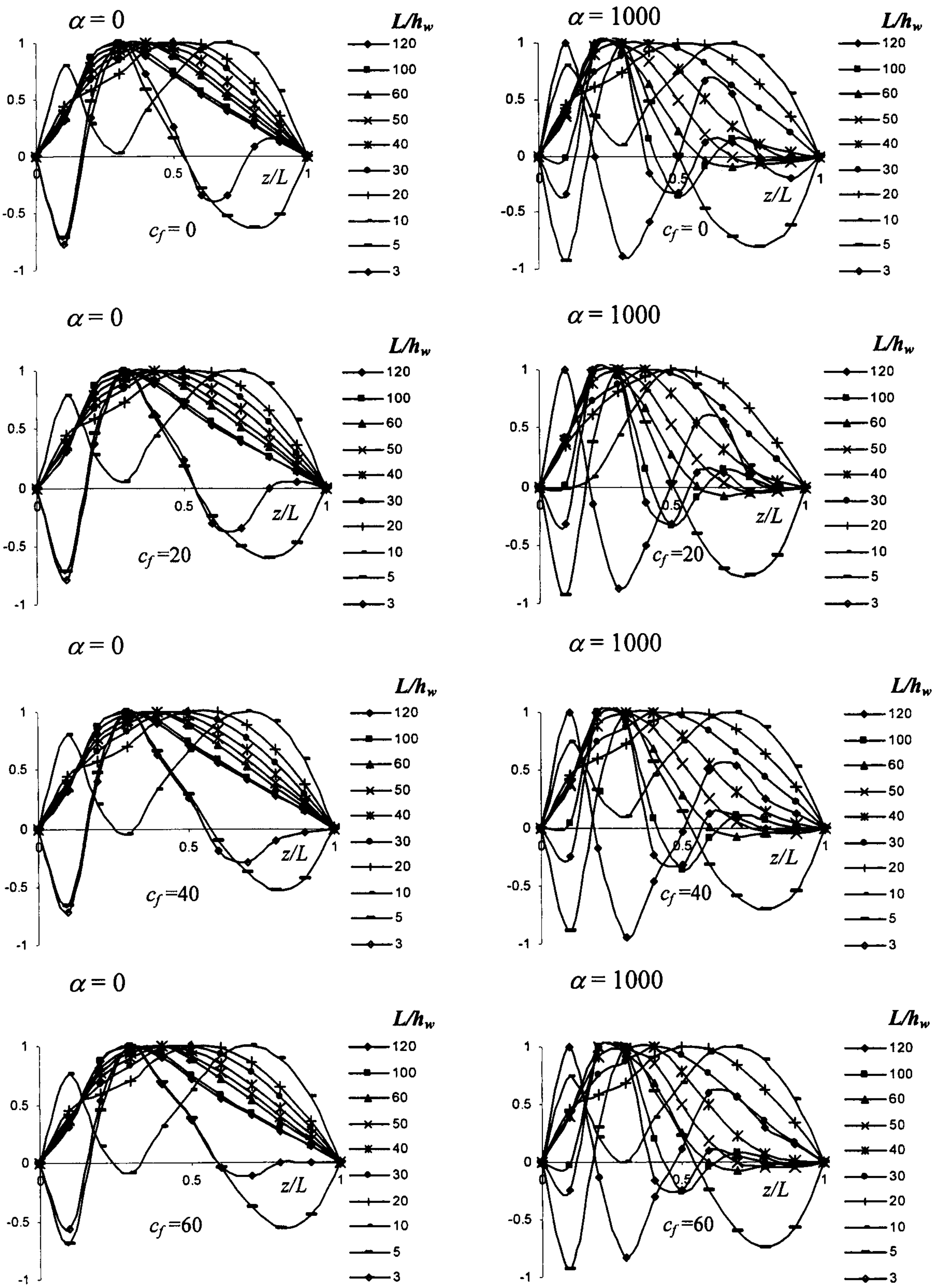

Figure 5.43 Normalised buckling mode shapes of restrainea aouoly symmetric I-section beams under transverse loading (point load at quarter span) with $\alpha = 0$ and $\alpha = 1000$; compression flange twist

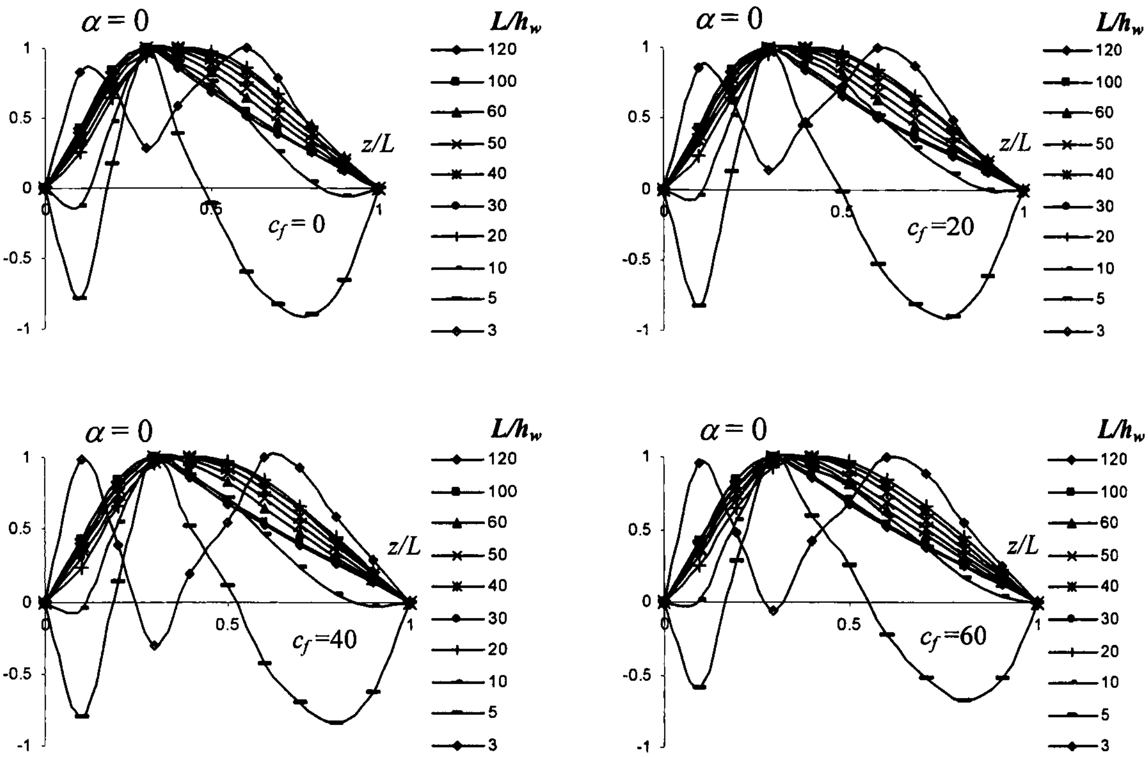

Figure 5.44 Normalised buckling mode shapes of restrained doubly symmetric I-section beams under transverse loading (point load at quarter span) with $\alpha = 0$; tension flange twist

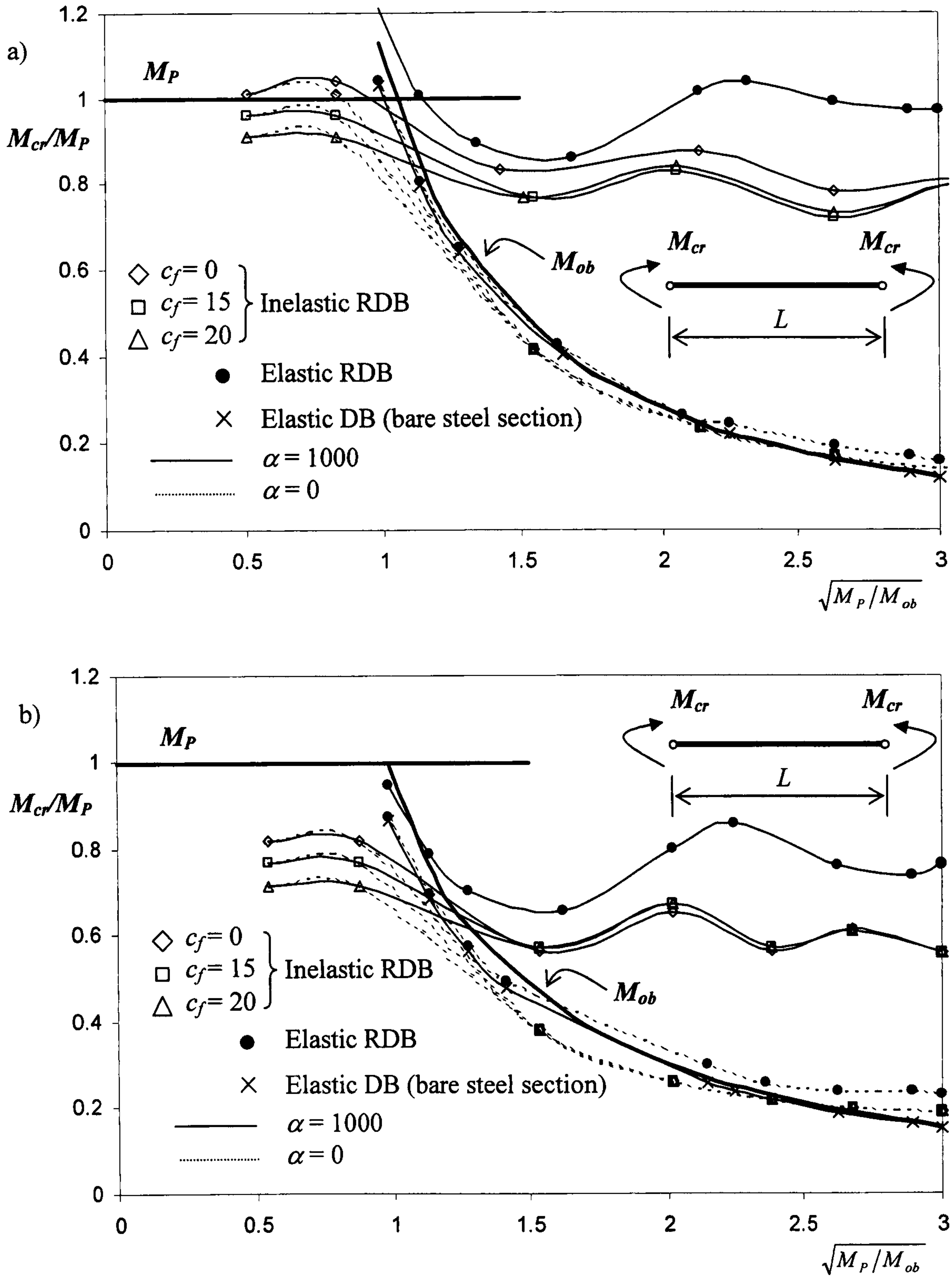

Figure 5.45 Buckling curves for monosymmetric I-beams in uniform bending: a) $\rho = 0.7$; b) $\rho = 0.3$

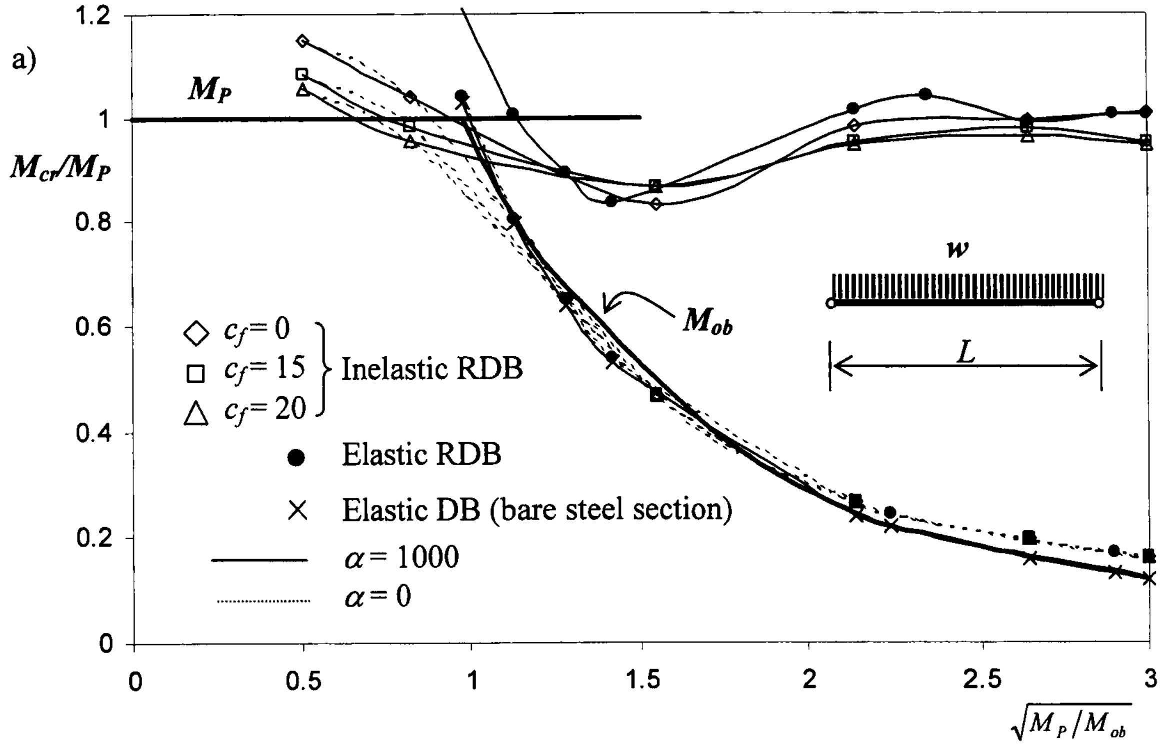

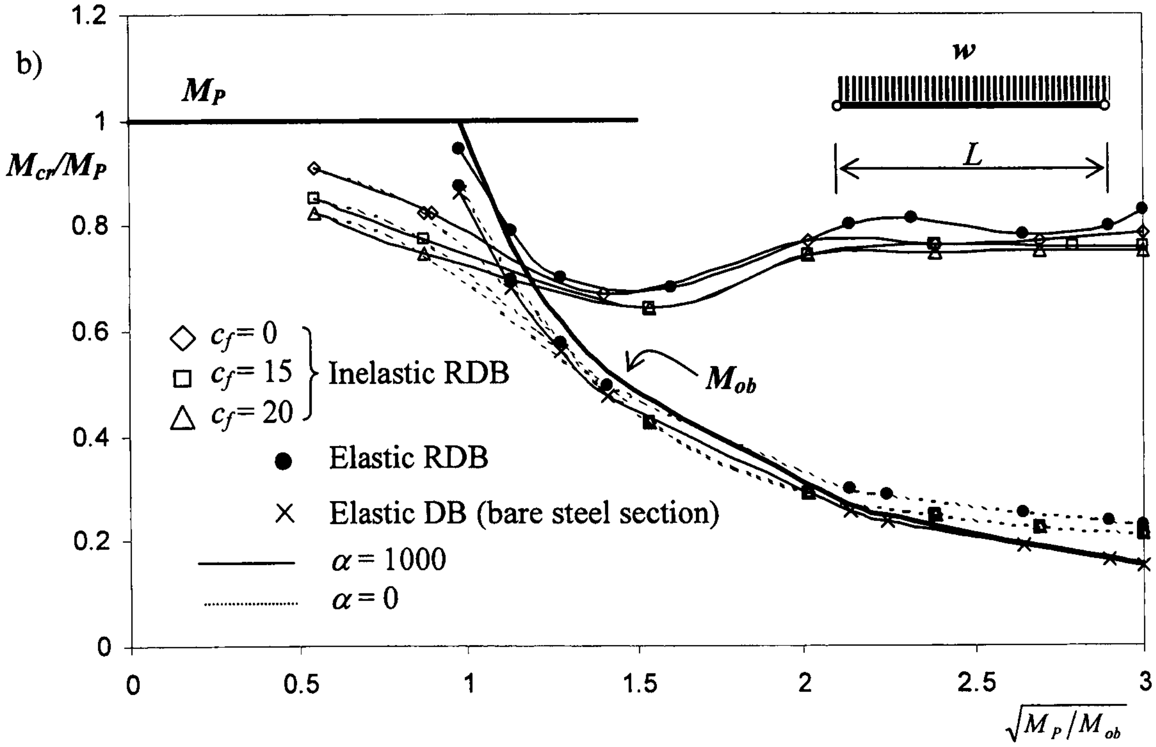

Figure 5.46 Buckling curves for monosymmetric I-beams under uniformly distributed load: a) $\rho = 0.7$; b) $\rho = 0.3$

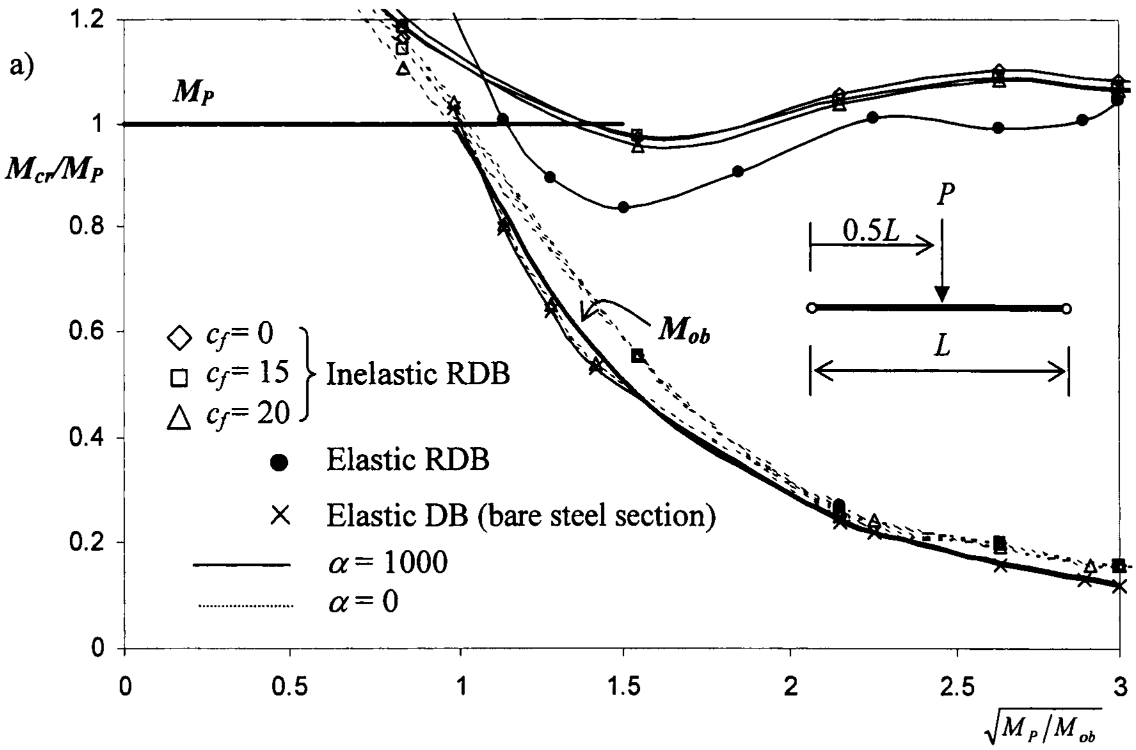

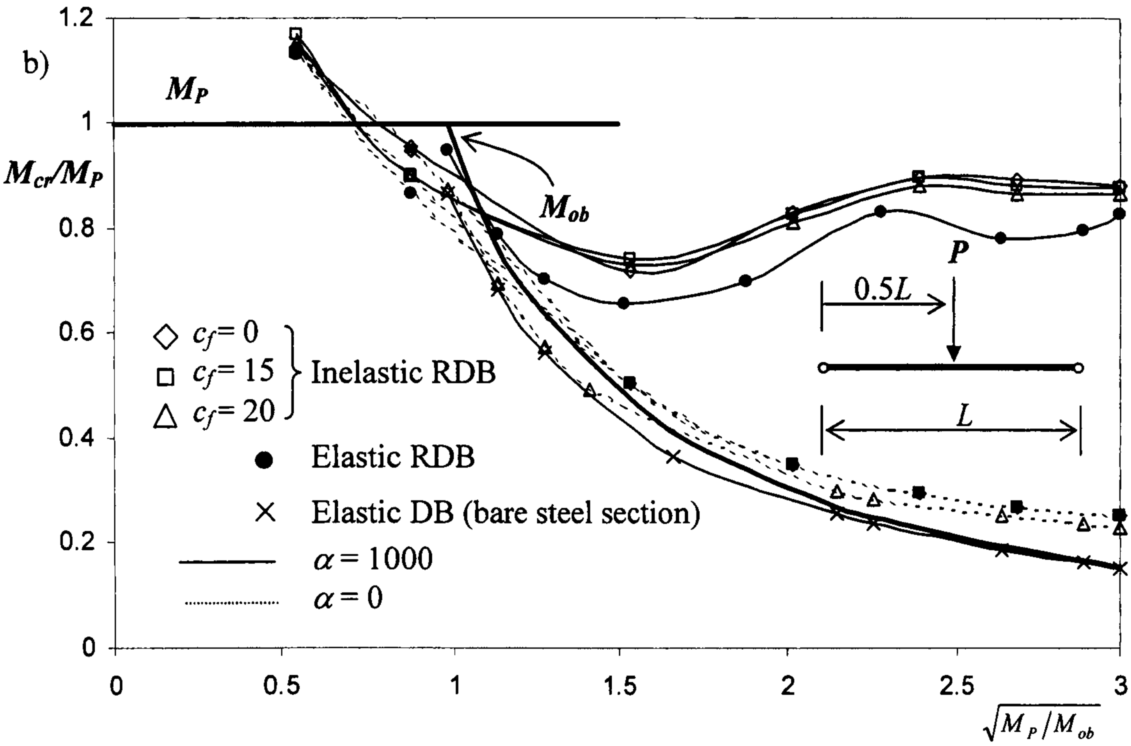

Figure 5.47 Buckling curves for monosymmetric I-beams under central point load: a) $\rho = 0.7$; b) $\rho = 0.3$

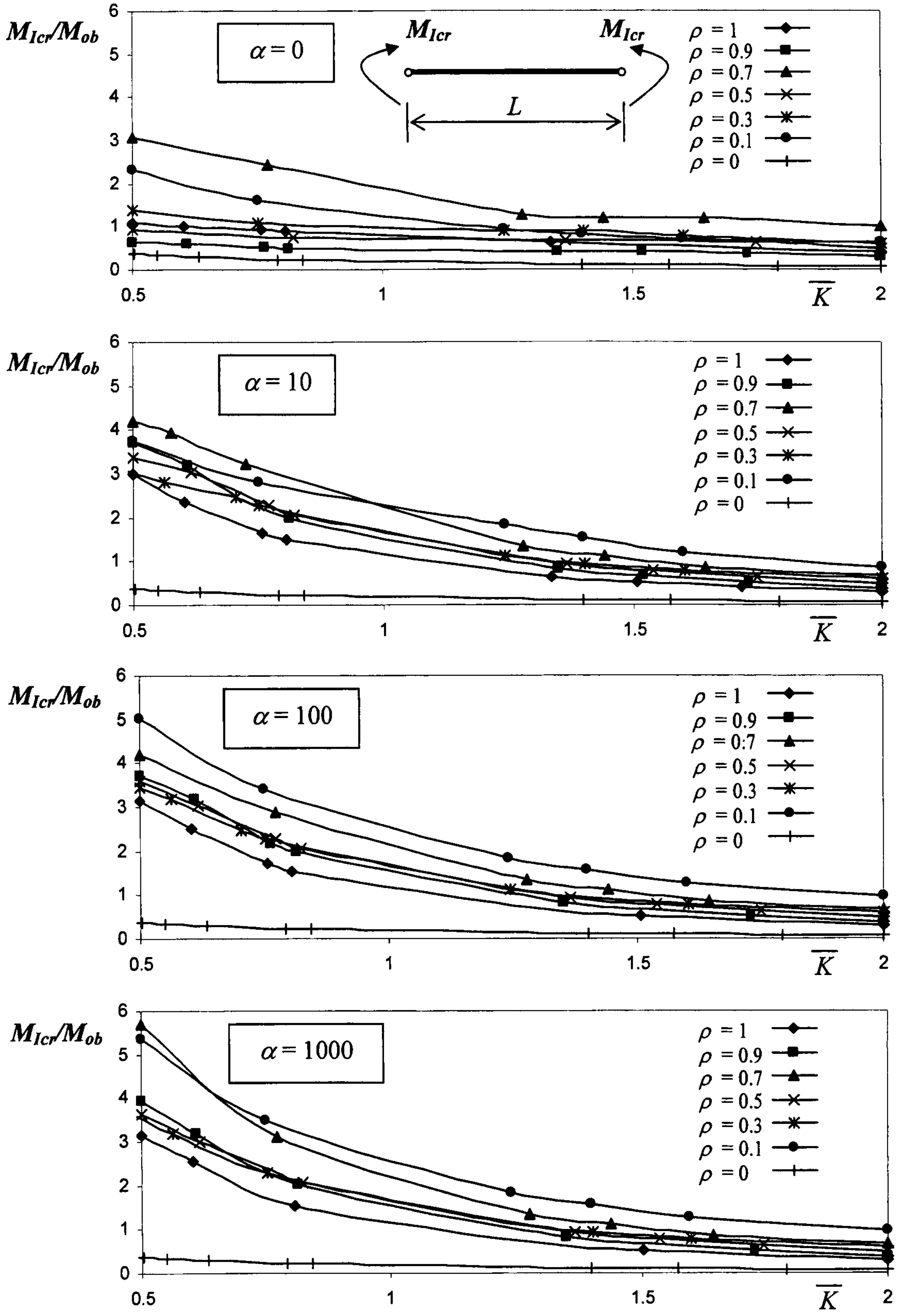

Figure 5.48 Inelastic critical moments of restrained monosymmetric I-beams in uniform bending

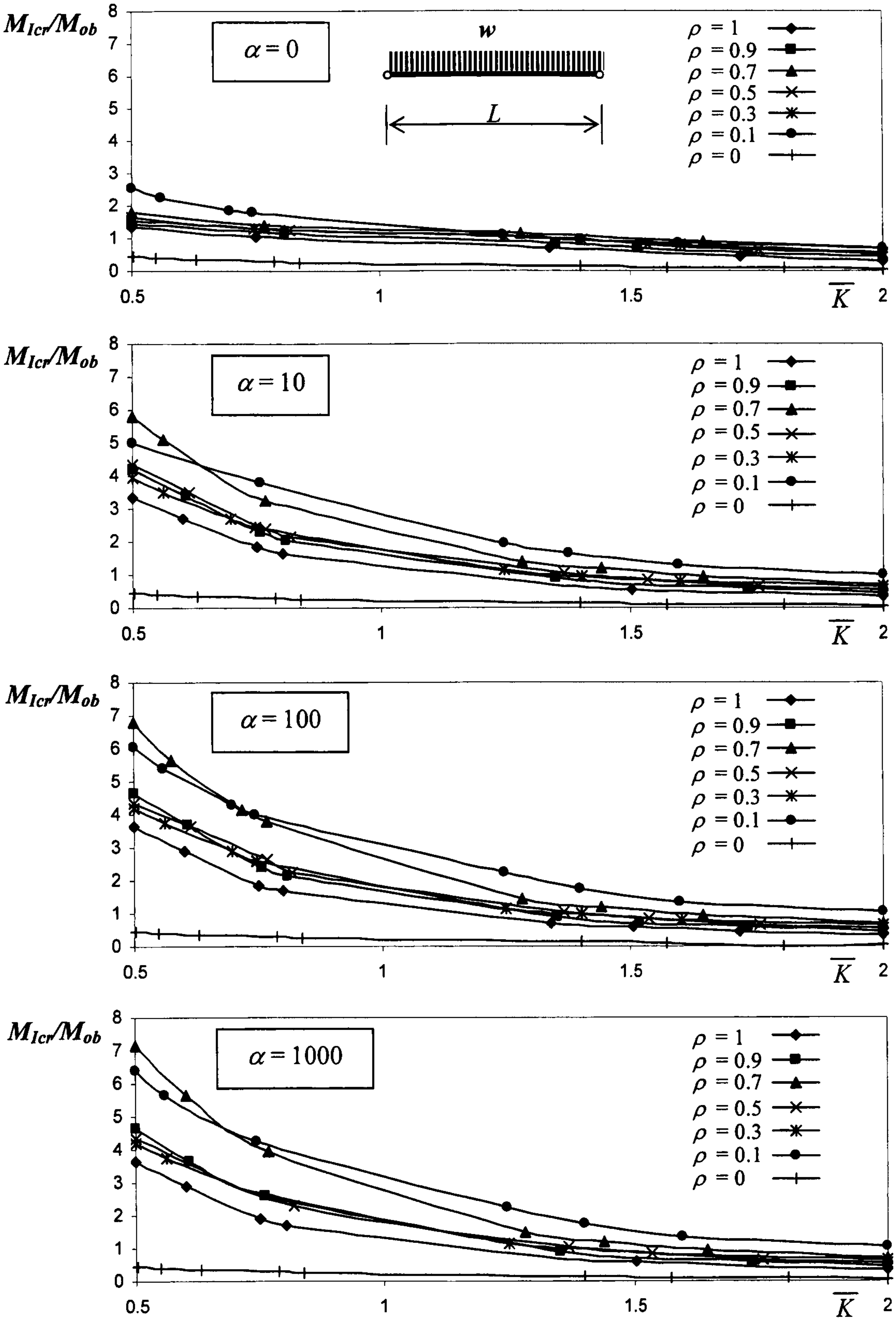

Figure 5.49 Inelastic critical moments of restrained monosymmetric I-beams under uniformly distributed load

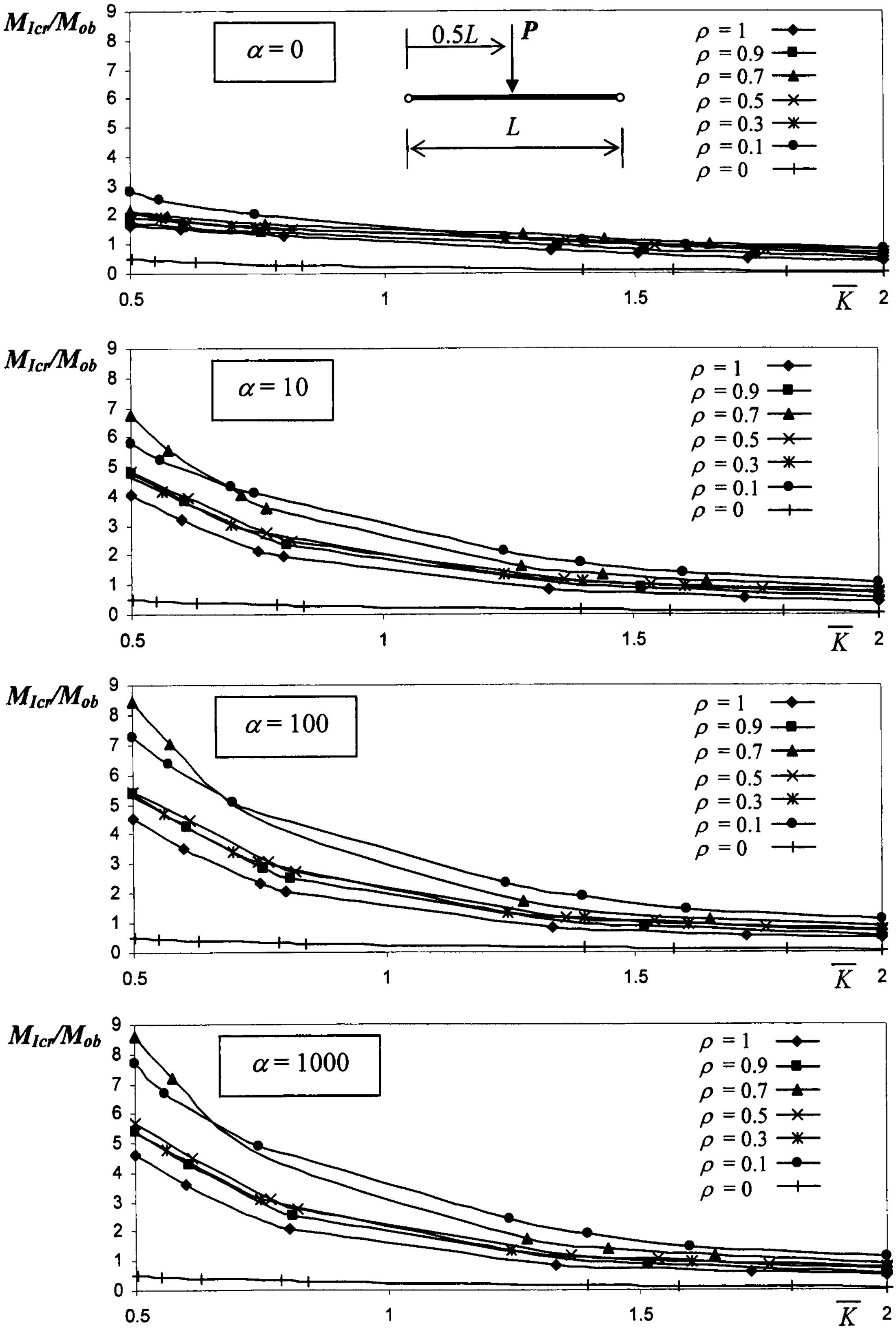

Figure 5.50 Inelastic critical moments of restrained monosymmetric I-beams under point load at mid-span

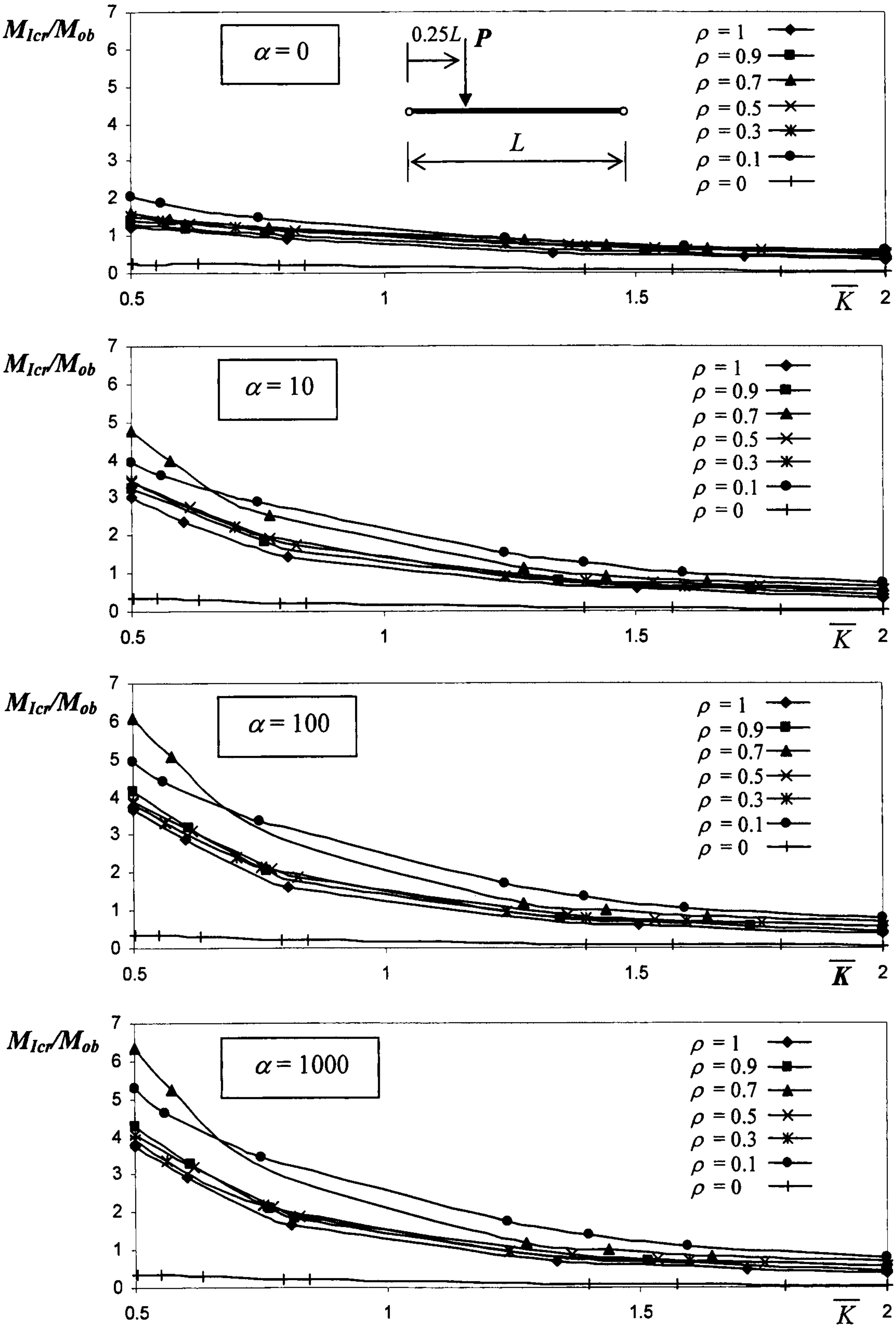

Figure 5.51 Inelastic critical moments of restrained monosymmetric I-beams under point load at quarter span

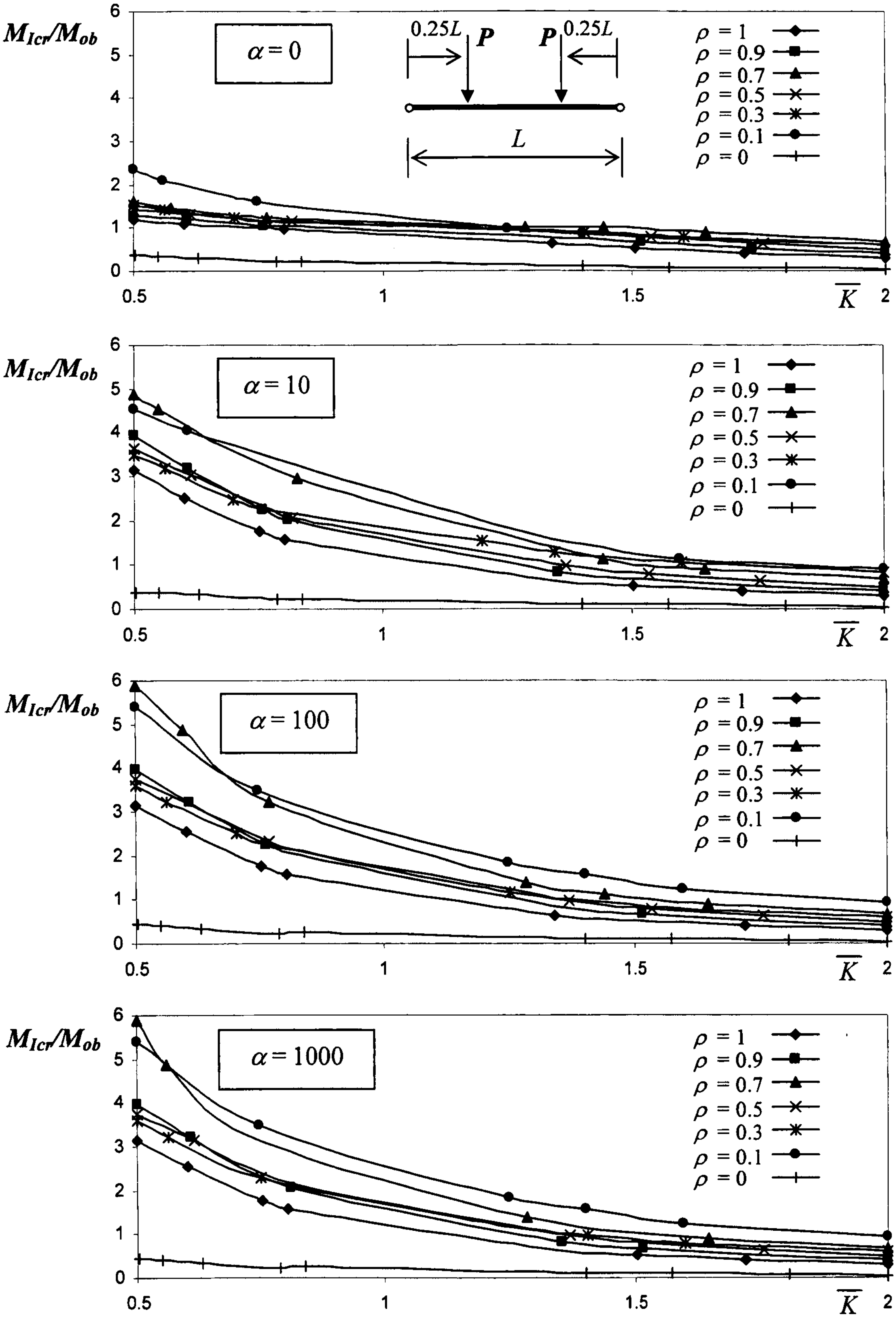

Figure 5.52 Inelastic critical moments of restrained monosymmetric I-beams under two-point loads at quarter span

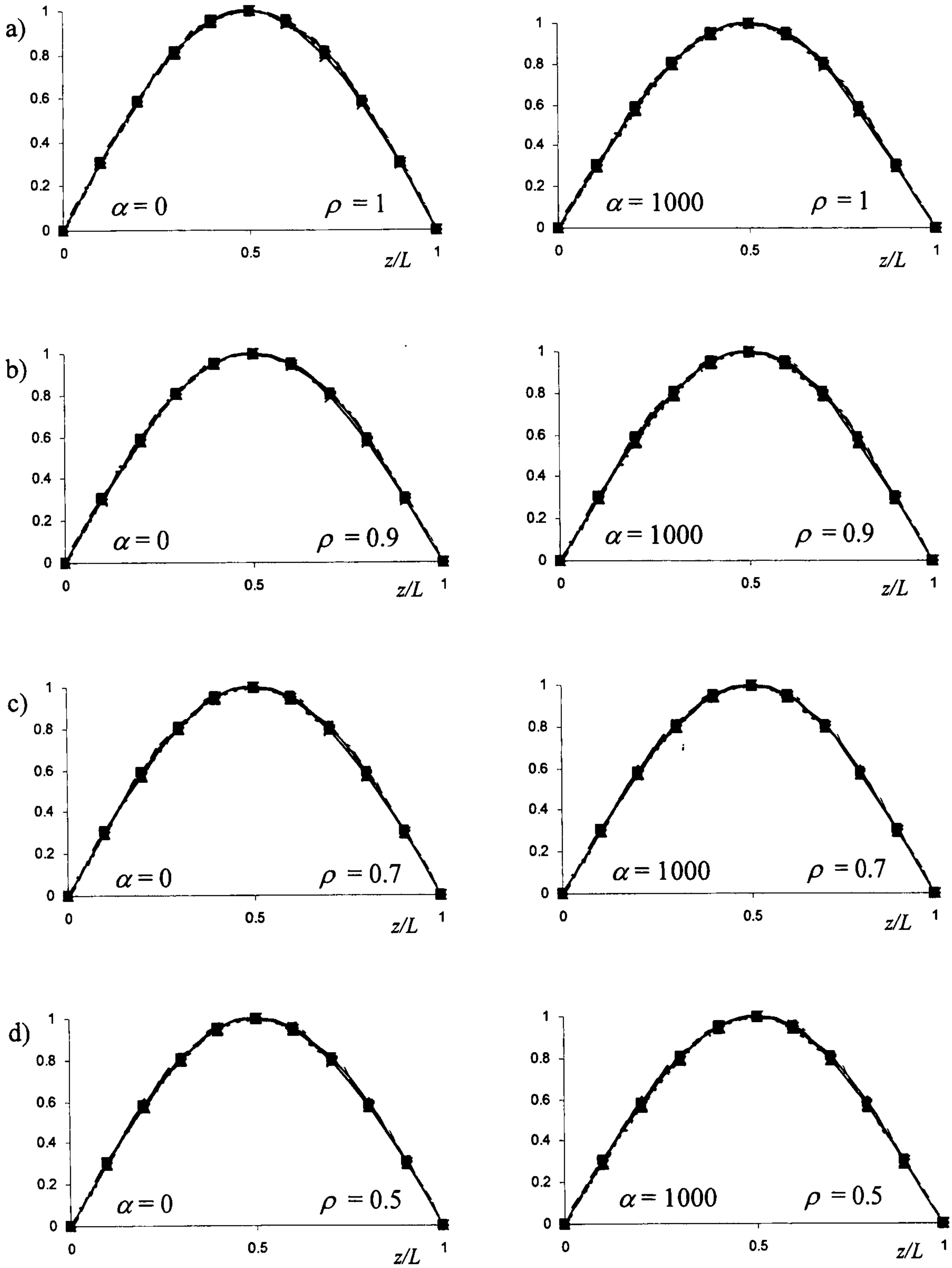
a)
$\alpha = 0$
$\rho = 1$
$\alpha = 1000$
$\rho = 1$
b)
$\alpha = 0$
$\rho = 0.9$
$\alpha = 1000$
$\rho = 0.9$
c)
$\alpha = 0$
$\rho = 0.7$
$\alpha = 1000$
$\rho = 0.7$
d)
$\alpha = 0$
$\rho = 0.5$
$\alpha = 1000$
$\rho = 0.5$
z/L
0
0.5
1
0.2
0.4
0.6
0.8

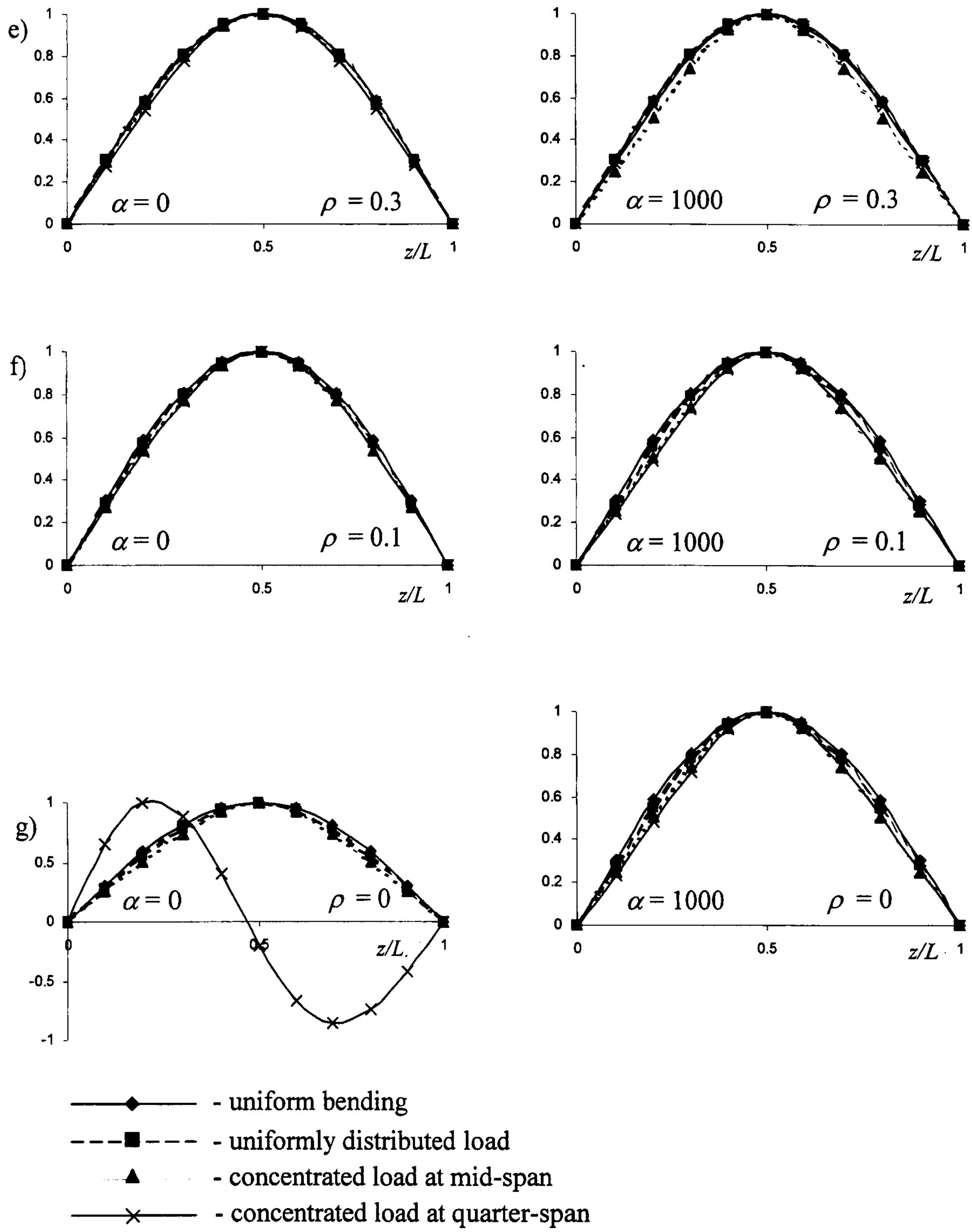

Figure 5.53 Normalised buckling mode shapes of restrained monosymmetric I beams with $\alpha = 0$ and $\alpha = 1000$; compression flange displacement

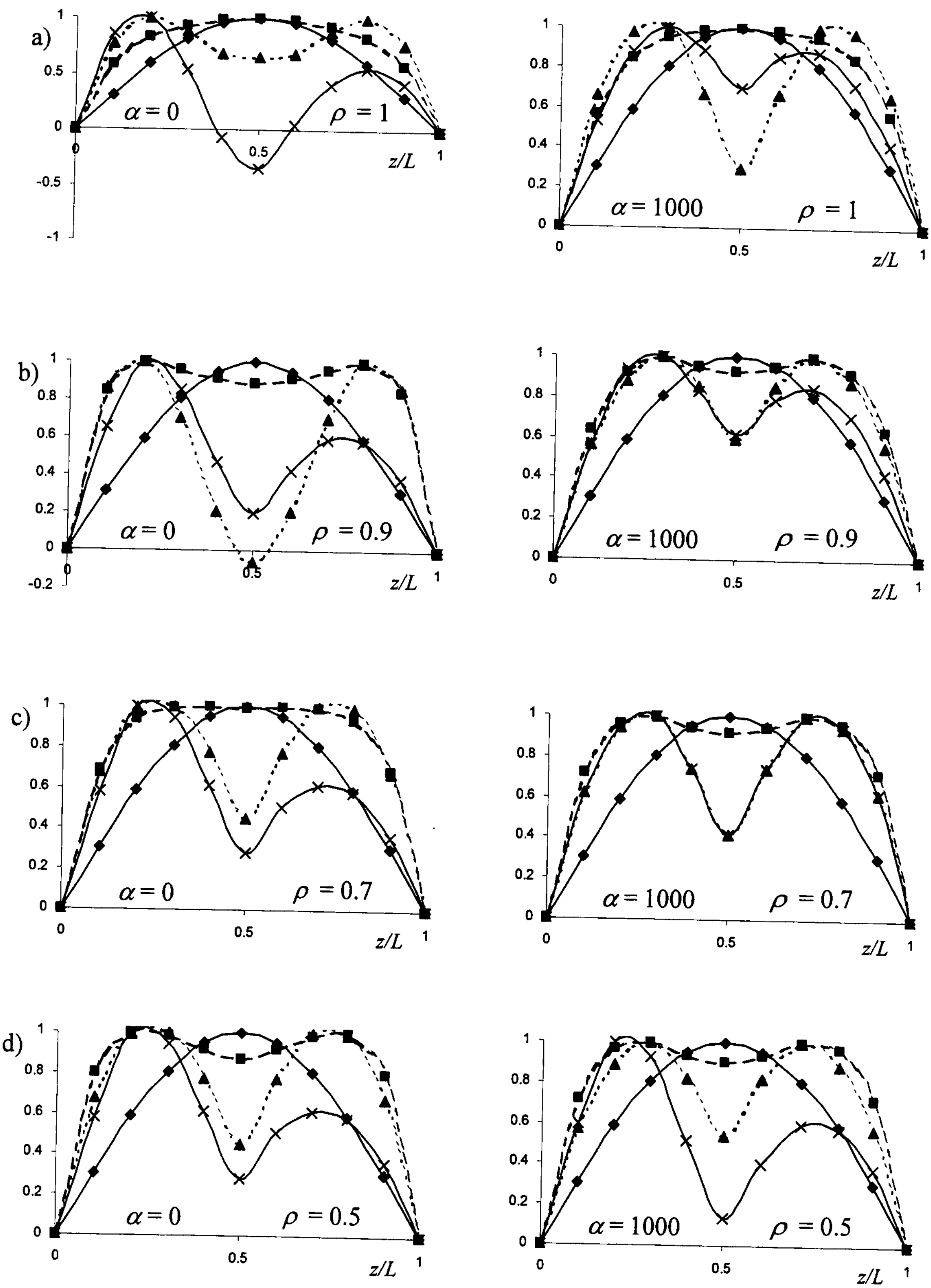
a)
α = 0
ρ = 1
z/L
α = 1000
ρ = 1
z/L
b)
α = 0
ρ = 0.9
z/L
α = 1000
ρ = 0.9
z/L
c)
α = 0
ρ = 0.7
z/L
α = 1000
ρ = 0.7
z/L
d)
α = 0
ρ = 0.5
z/L
α = 1000
ρ = 0.5
z/L

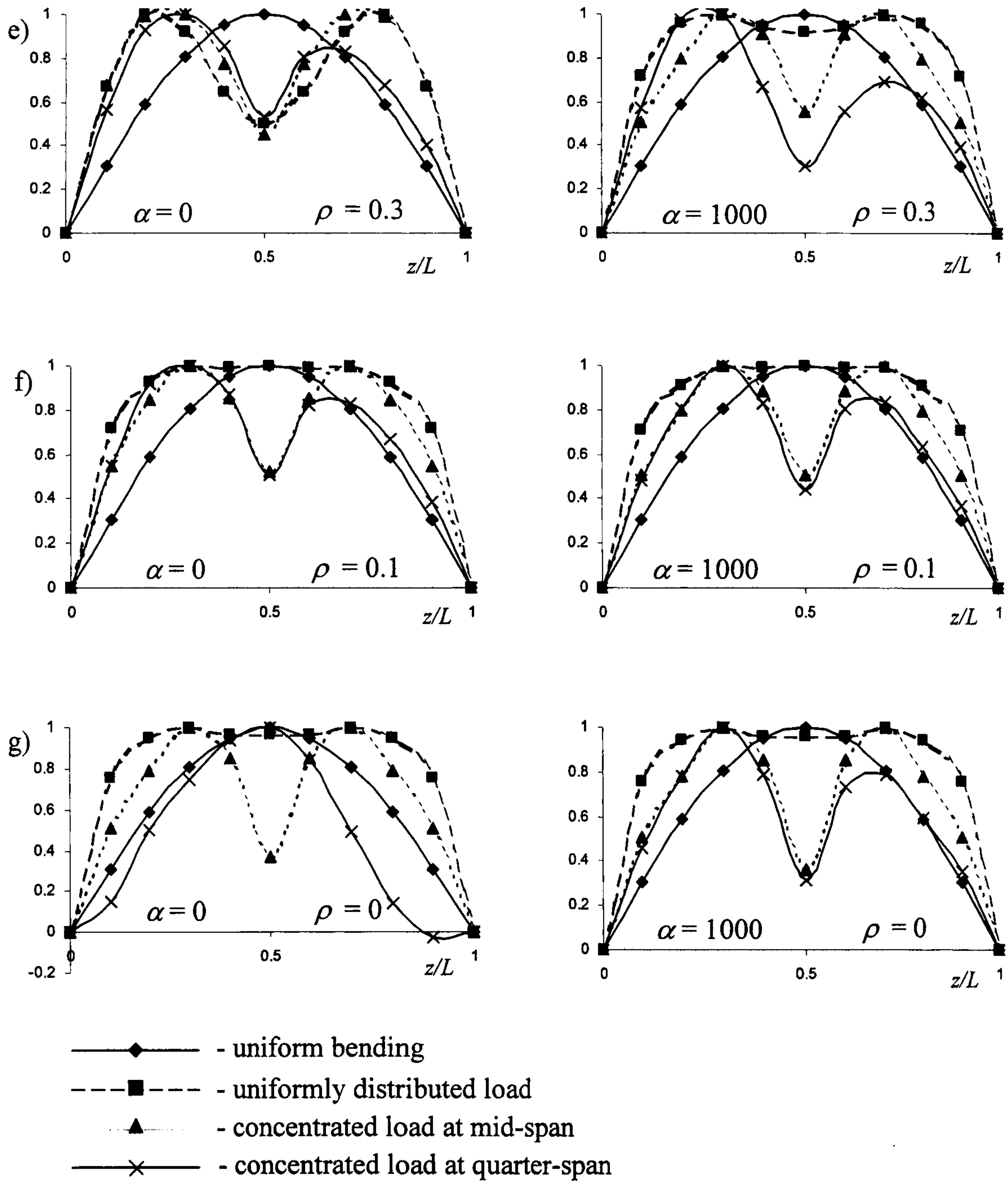

Figure 5.54 Normalised buckling mode shapes of restrained monosymmetric I beams with $\alpha = 0$ and $\alpha = 1000$; compression flange twist

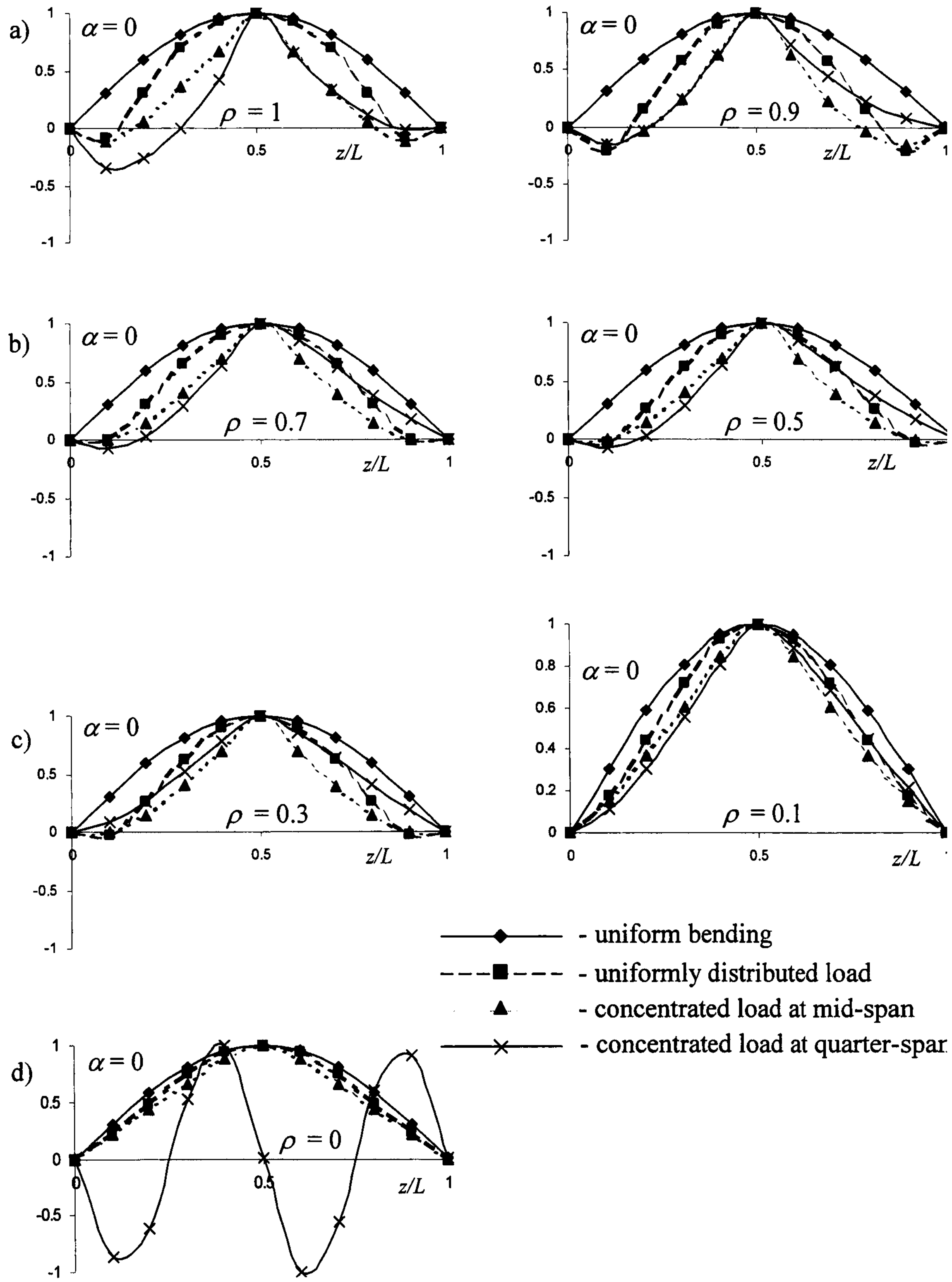

Figure 5.55 Normalised buckling mode shapes of restrained monosymmetric I-beams with $\alpha = 0$; tension flange twist

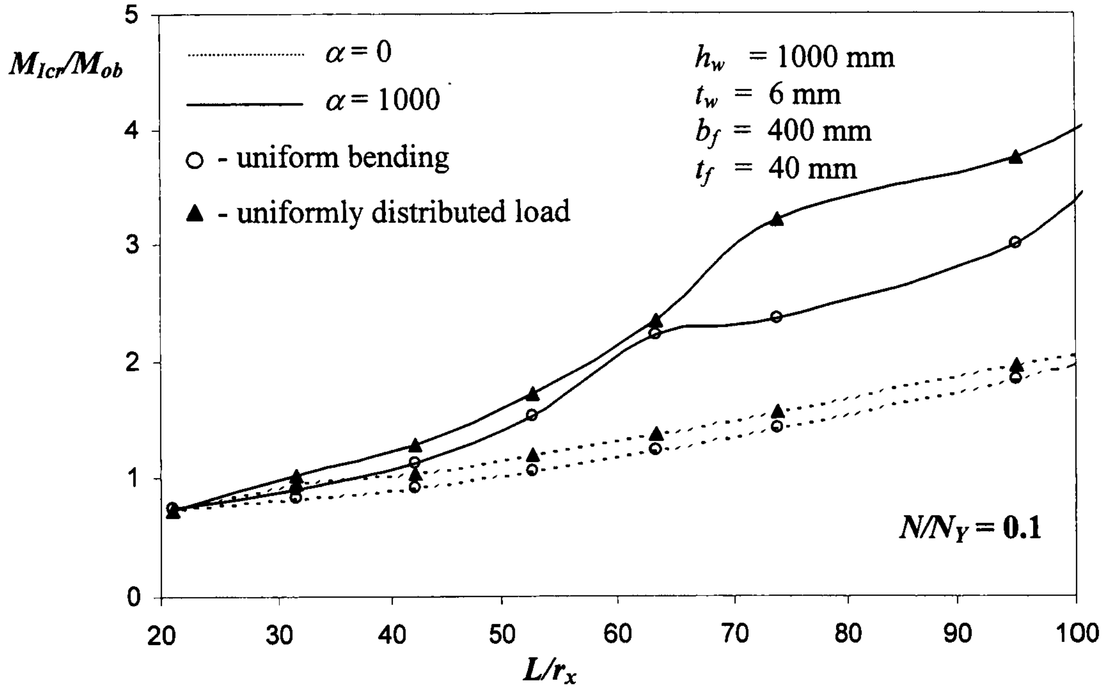

a) $N/N_Y = 0.1$

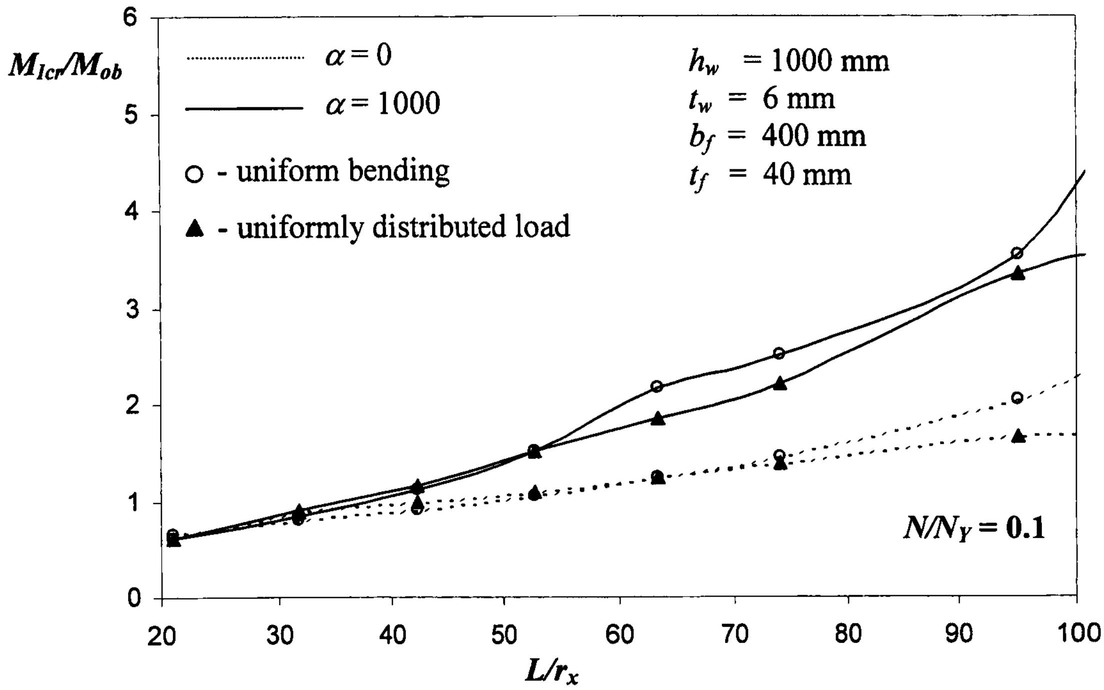

b) $N/N_Y = 0.1$

Figure 5.56 Inelastic buckling of beam-columns

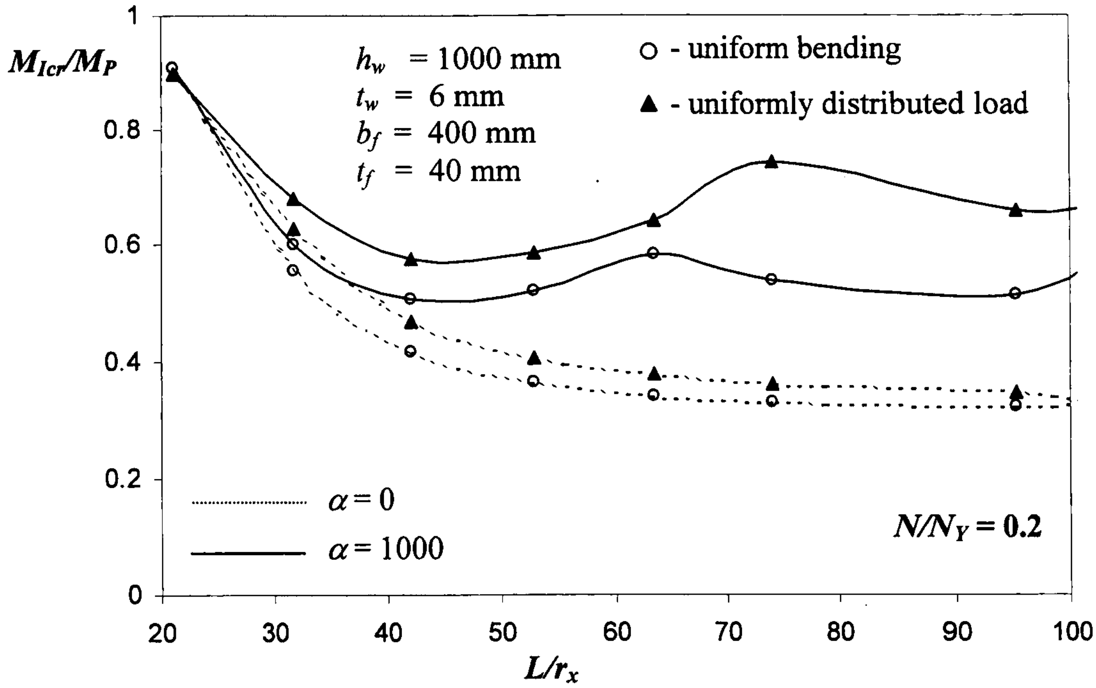

a) $N/N_Y = 0.2$

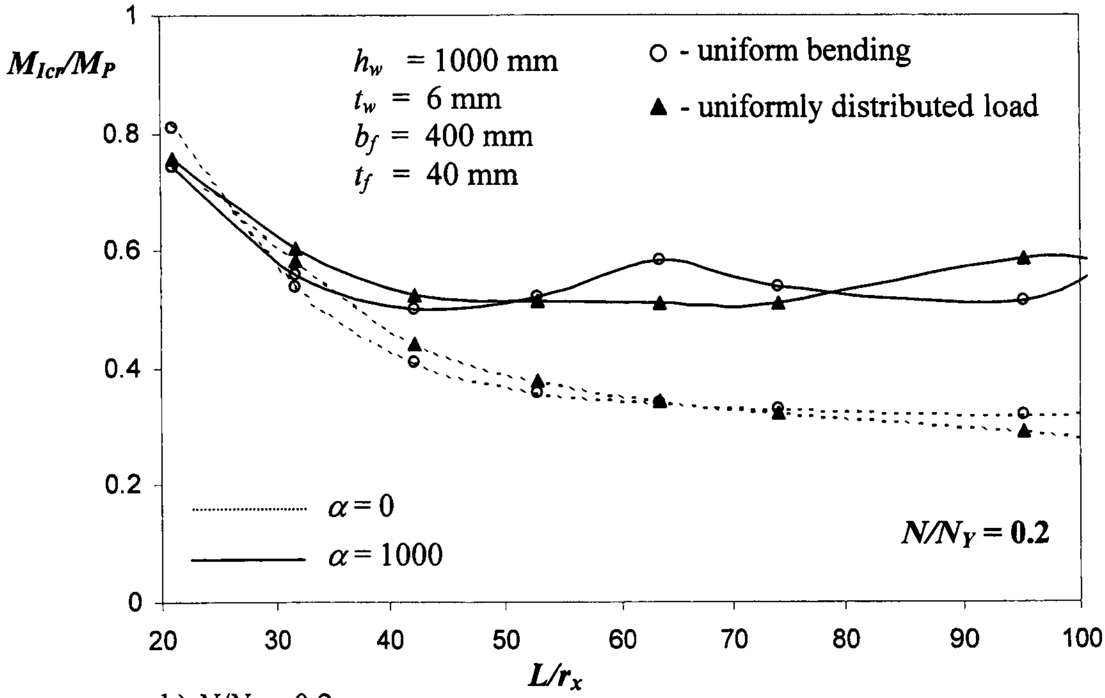

b) $N/N_Y = 0.2$

Figure 5.57 Inelastic buckling of beam-columns

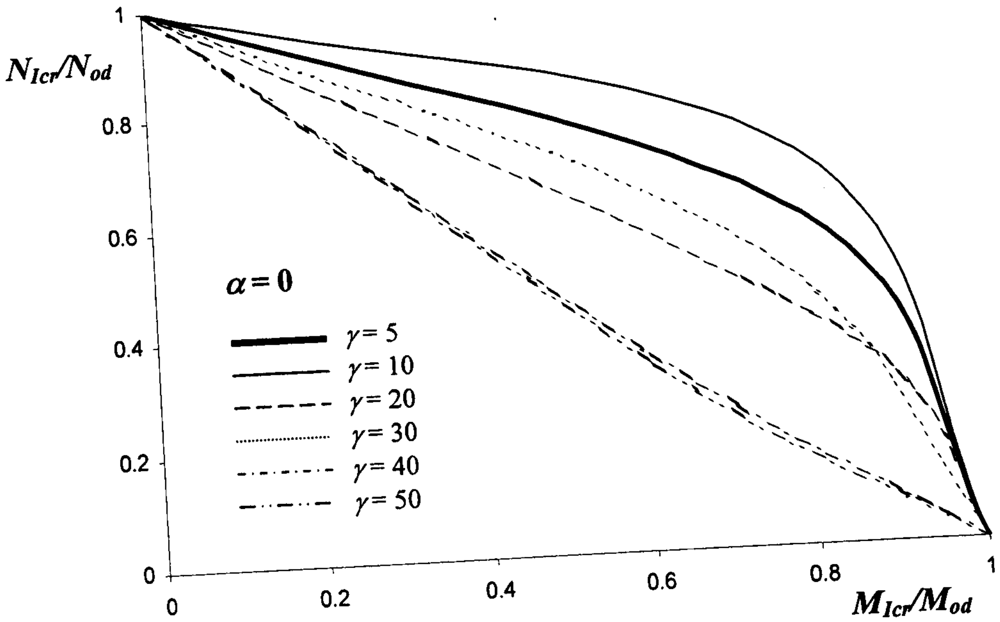

a) $\alpha = 0$

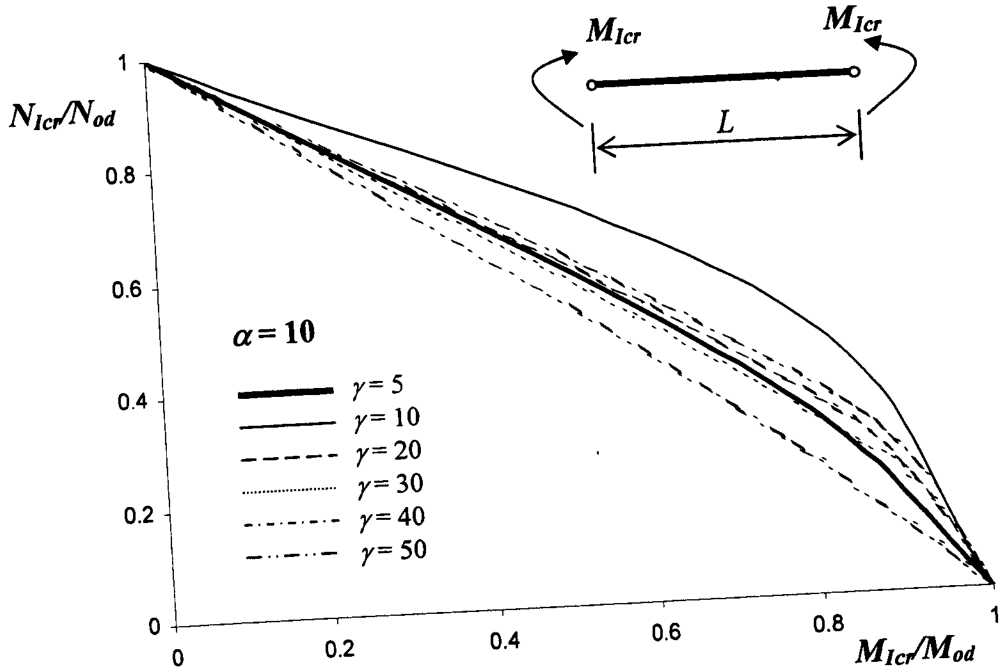

b) $\alpha = 10$

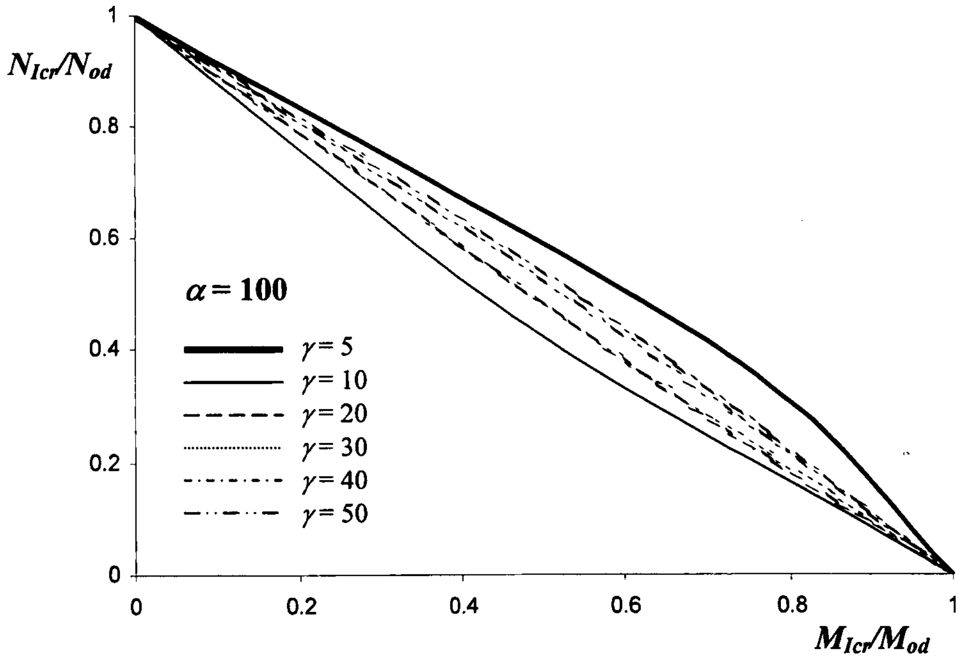

c) $\alpha = 100$

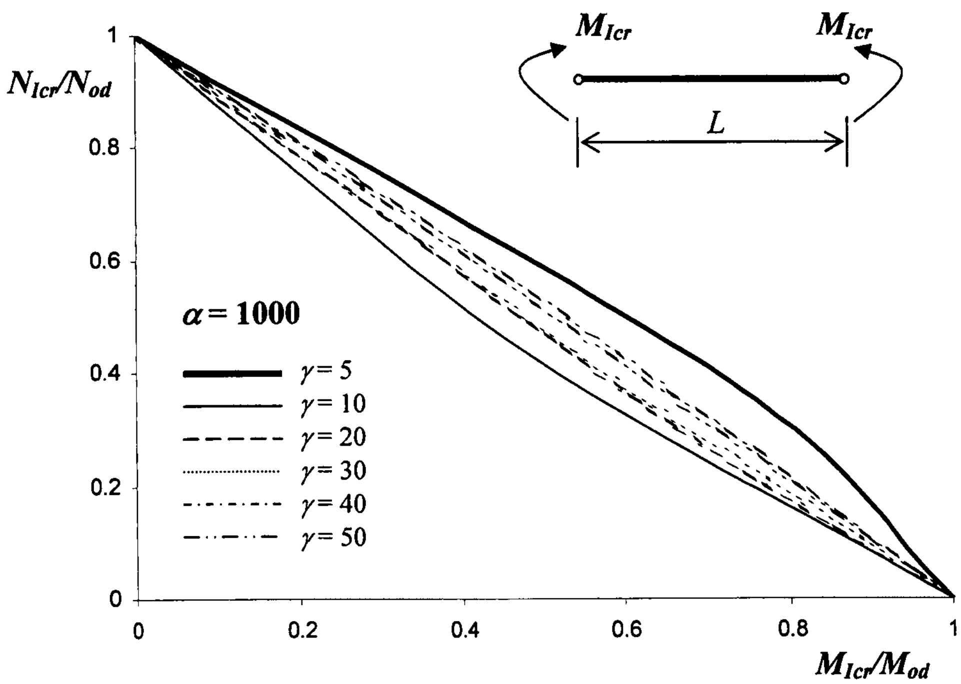

d) $\alpha = 1000$

Figure 5.58 Interaction buckling curves for I-section beam-columns in uniform bending

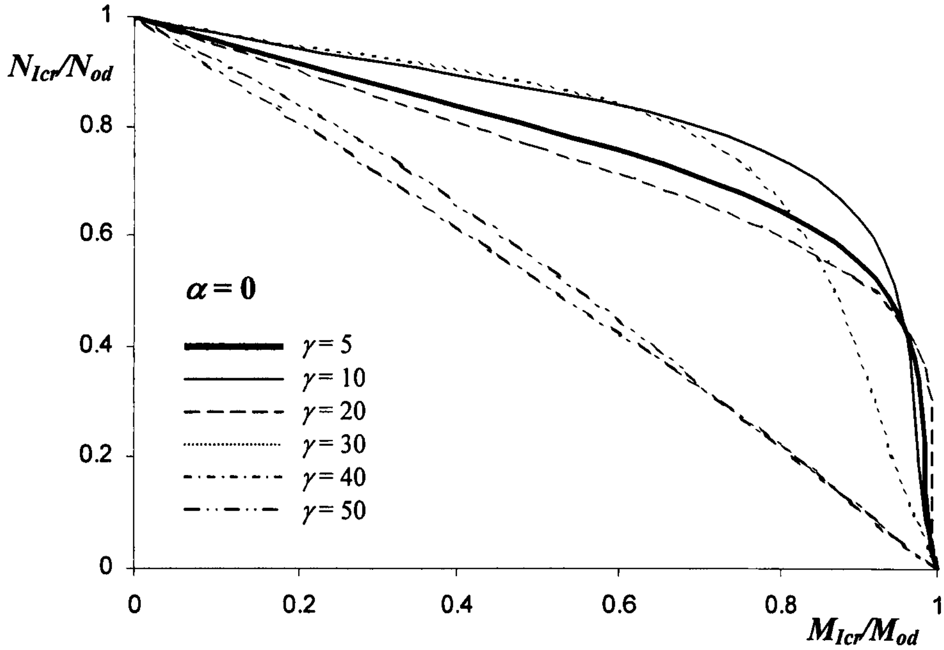

a) $\alpha = 0$

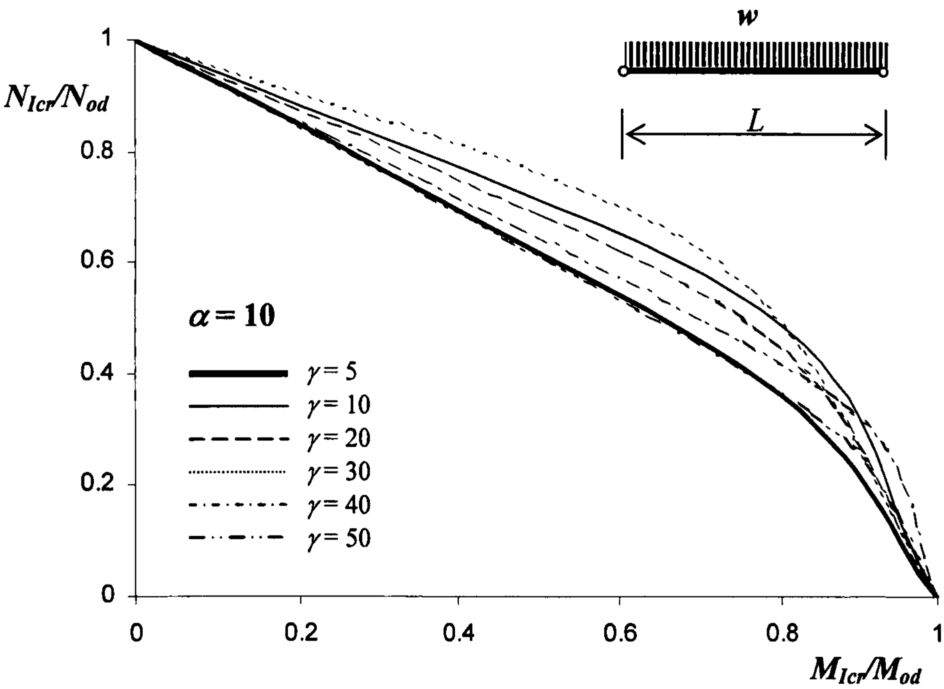

b) $\alpha = 10$

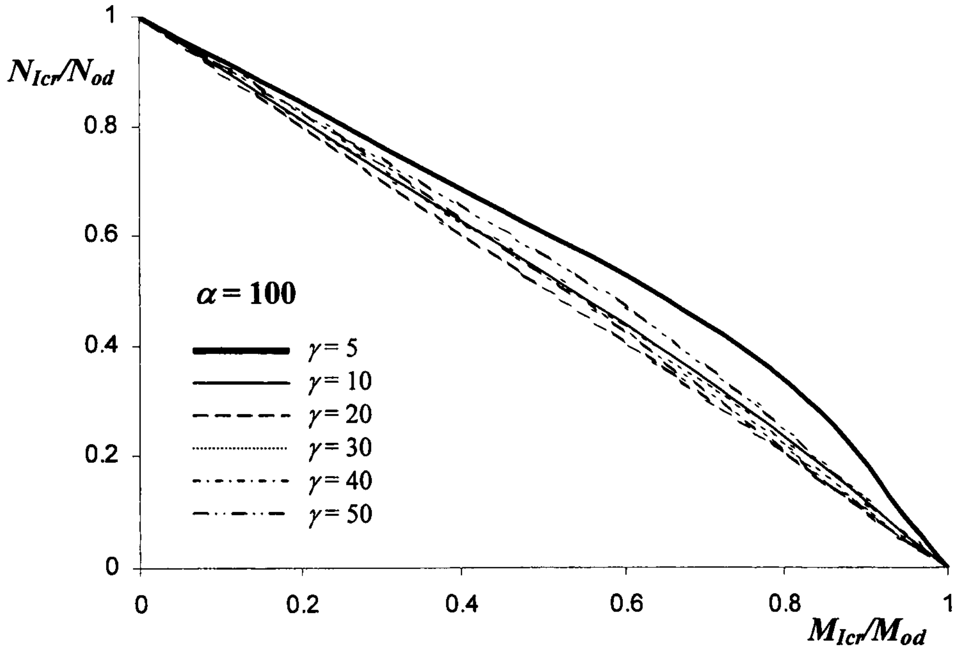

c) $\alpha = 100$

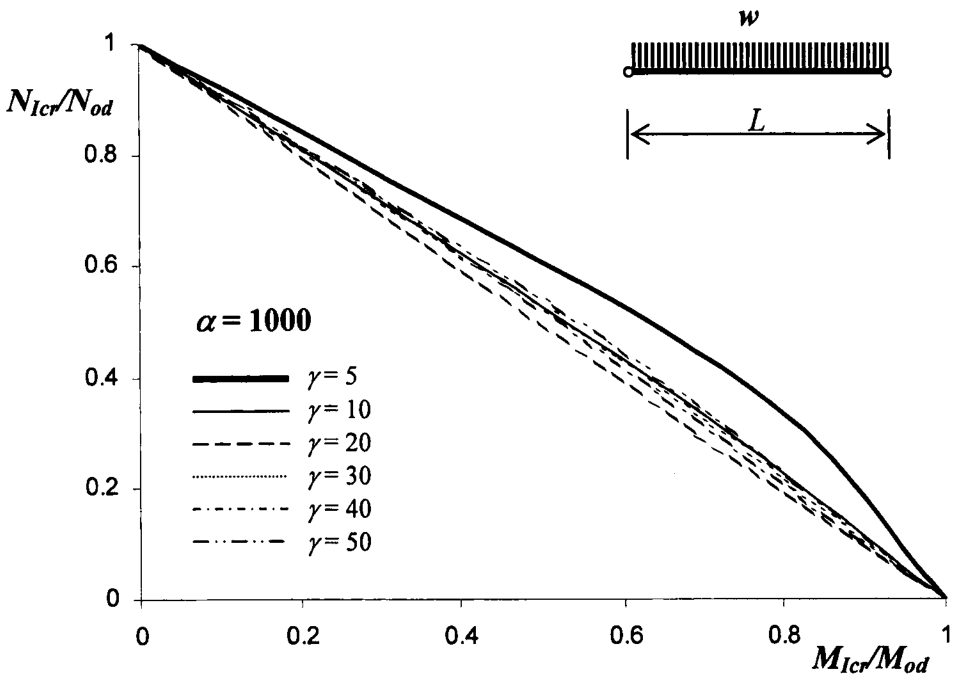

d) $\alpha = 1000$

Figure 5.59 Interaction buckling curves for I-section beam-columns under uniformly distributed load

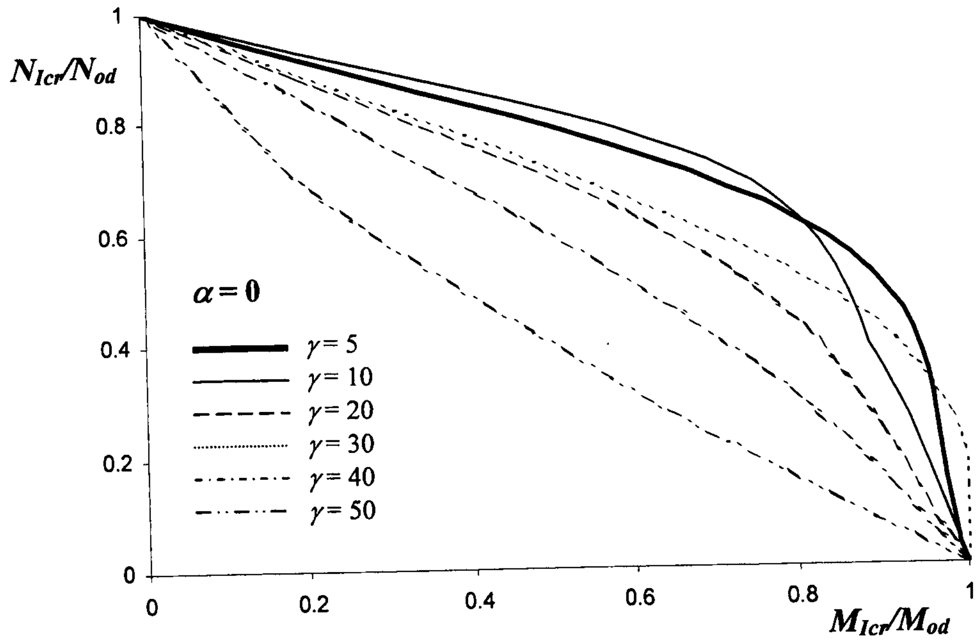

a) $\alpha = 0$

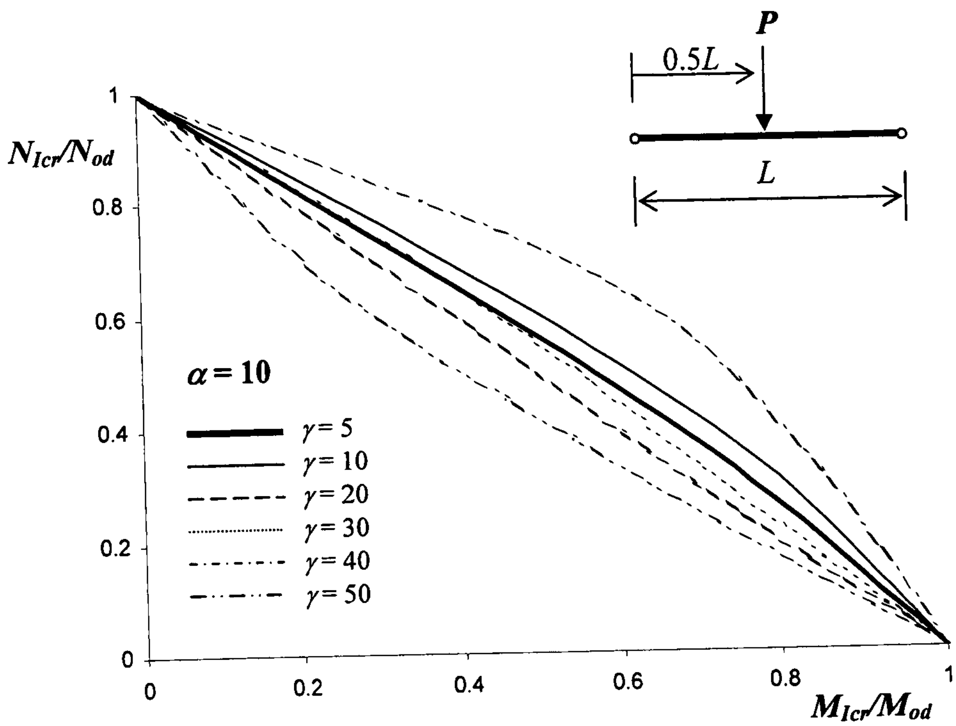

b) $\alpha = 10$

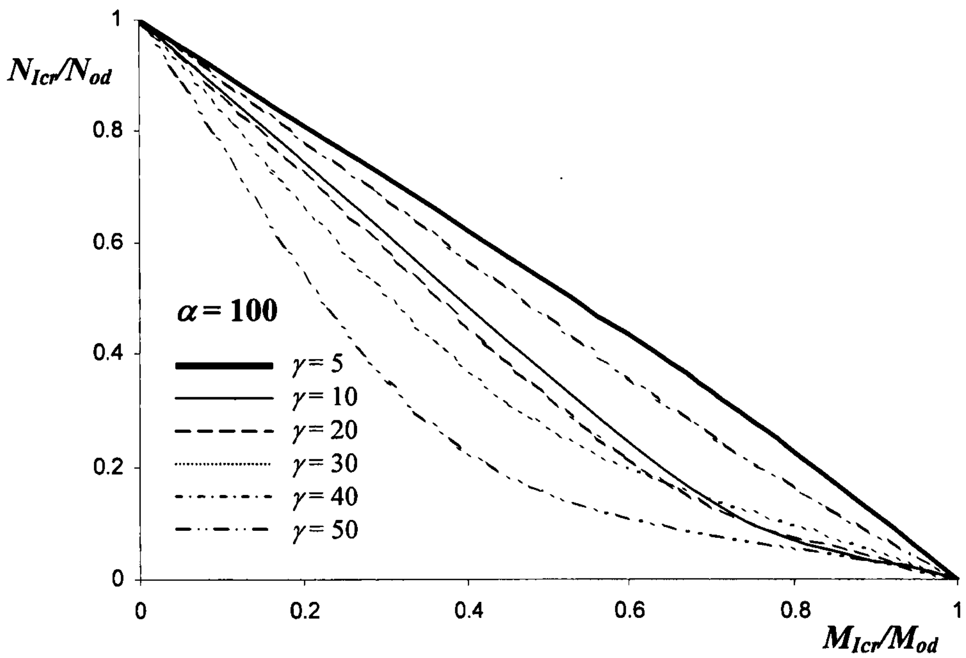

c) $\alpha = 100$

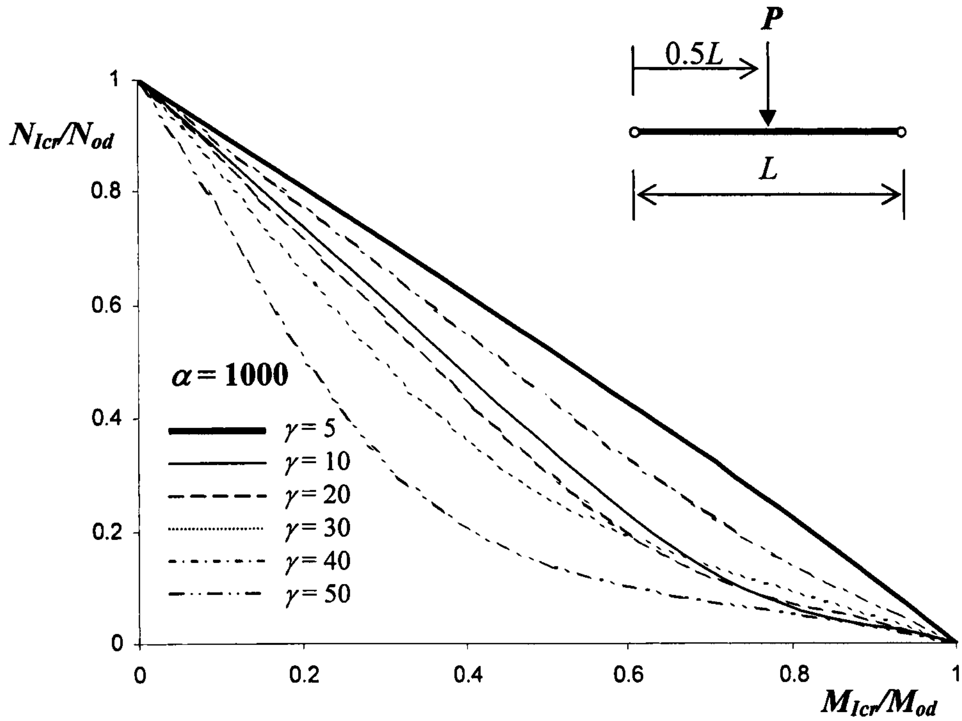

d) $\alpha = 1000$

Figure 5.60 Interaction buckling curves for I-section beam-columns under point load at mid-span

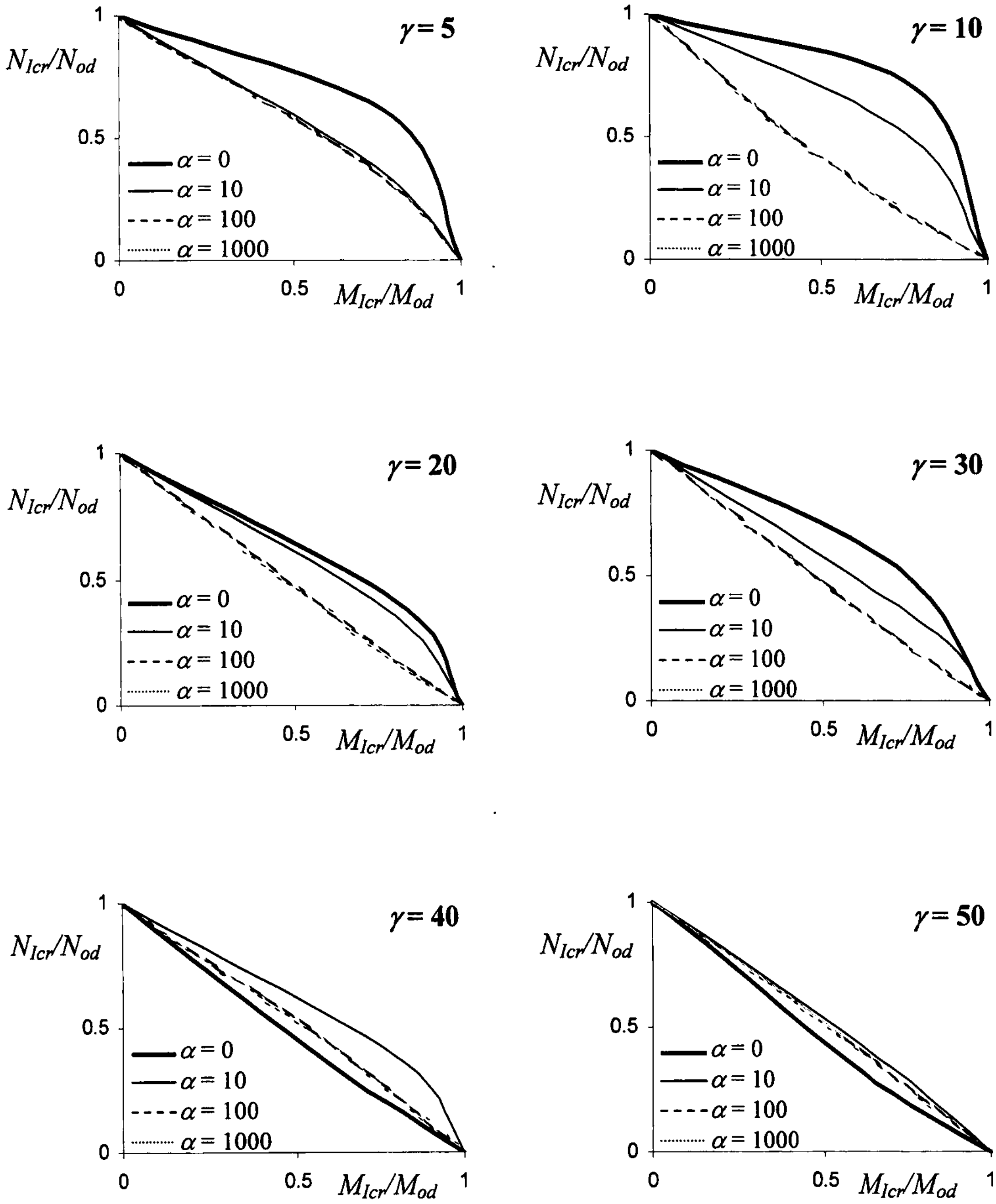

Figure 5.61 Interaction buckling curves for I-section beam-columns in uniform bending

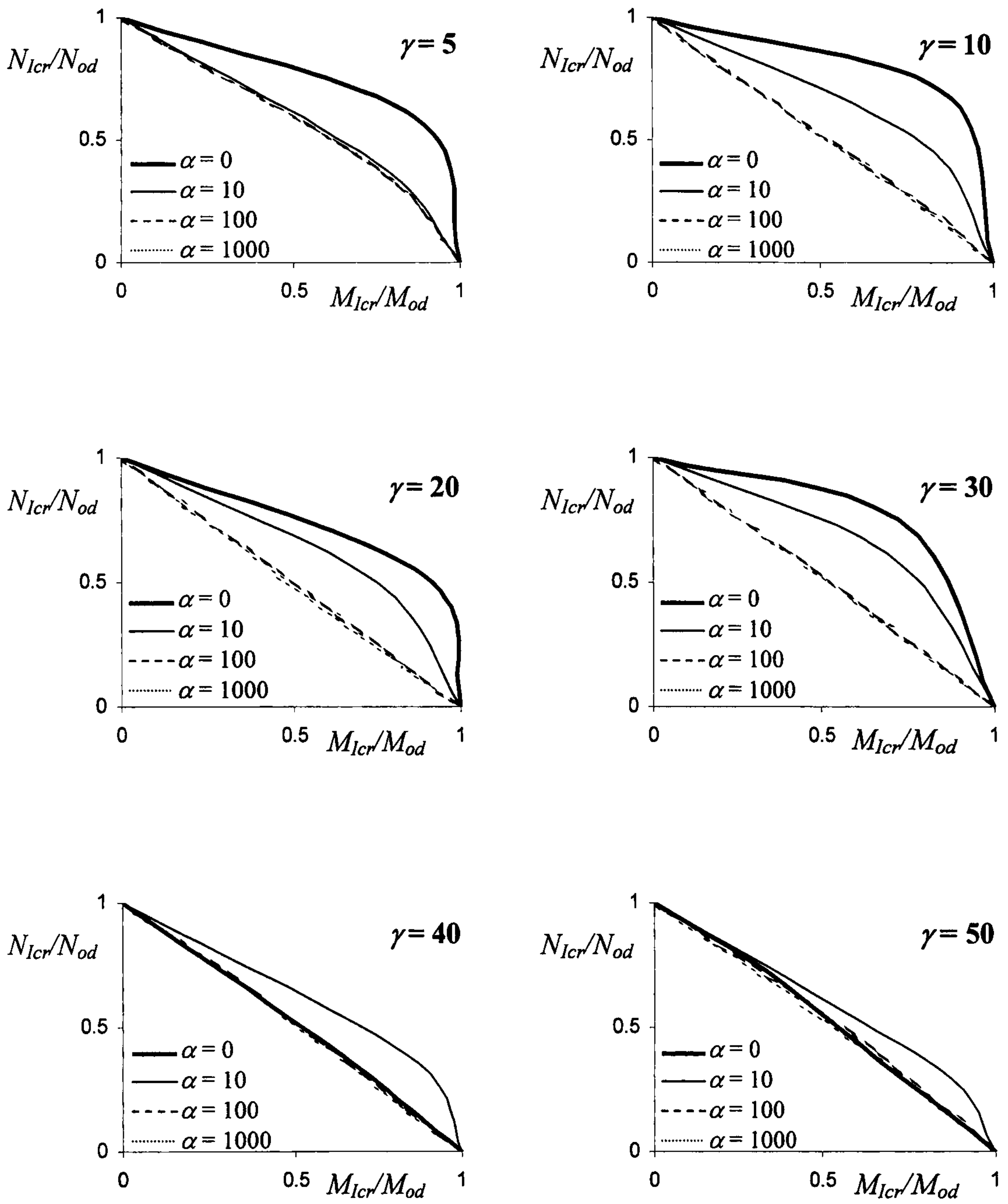

Figure 5.62 Interaction buckling curves for I-section beam-columns under uniformly distributed load

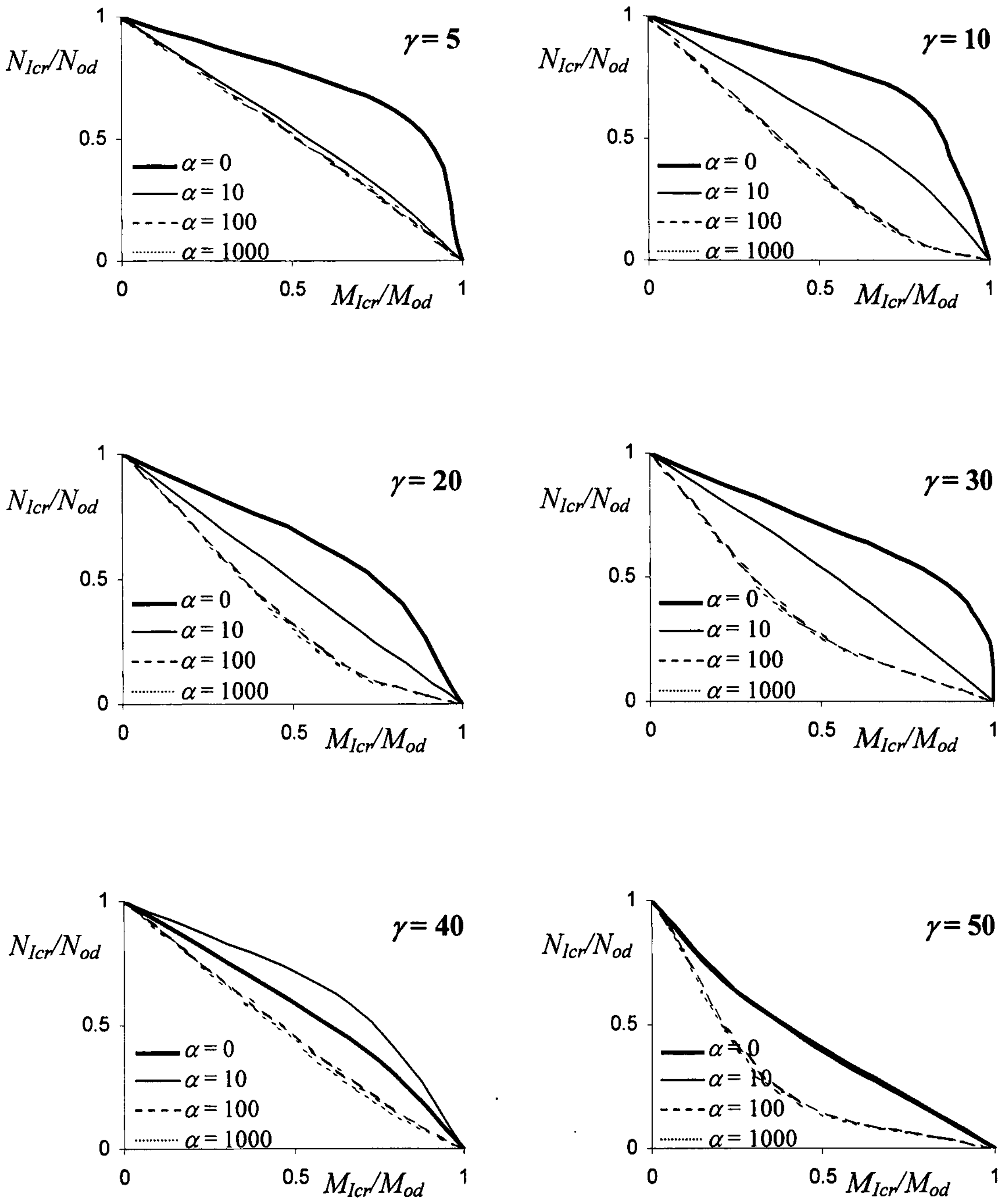

Figure 5.63 Interaction buckling curves for I-section beam-columns under point load at mid-span

Thesis Topic:

BUCKLING MODES IN CONTINUOUS COMPOSITE BEAMS

Vol. 2

By:

ZORA VRCELJ

A thesis Submitted as Partial Fulfilment of The Requirements For The Degree of

DOCTOR OF PHILOSOPHY

October 2004

SCHOOL OF CIVIL AND ENVIRONMENTAL ENGINEERING
THE UNIVERSITY OF NEW SOUTH WALES

VOLUME II

TABLE OF CONTENTS

VOLUME 2

Chapter 6 Bubble Augmented Harmonic Semi-Analytical Finite Strip Method

Chapter 7 Elastic Bubble Based Spline Finite Strip Method

Chapter 8 Inelastic Bubble Based Spline Finite Strip Method

Chapter 9 Concluding Remarks

REFERENCES

APPENDIX

Chapter 6

BUBBLE AUGMENTED HARMONIC SEMI-ANALYTICAL FINITE STRIP METHOD

TABLE OF CONTENTS

6.1 INTRODUCTION

Over the last three decades considerable progress has been made in the applications of numerical procedures for the analysis of basic structural elements, as well as highly refined structures in different disciplines of engineering. For instance, the efficient analysis of plate structures is of essential importance in many branches of engineering, and continues to be an area of active research. Moreover, an understanding of elastic buckling (ie. stresses and buckling modes) is vital to understanding the behaviour and design of thin-walled structures.

While the governing differential equations for particular modes of plate buckling analysis are well-established (Allen & Bulson 1980), it is in general not possible to obtain analytical solutions of the equations in closed form, except for simple geometries. Hence, numerical solutions are required for practical problems. Amongst these numerical procedures, by far the most popular method in use for plate analysis is the finite element method (Zienkewicz & Taylor 2000). Its supremacy lies in its generality and its ability to easily deal with complex geometries and loading configurations. However, the full generality of the method is not required when the geometry of the problem is regular, as is commonly the case for many practical structures, for instance bridges and buildings. In such cases, the efficiency of the analysis can be improved by adopting alternative approximation schemes that explicitly account for the regularity of the structure. One simple and economical technique that is suitable in such cases is the finite strip method, as shown in Fig. 6.1.

Finite strips have now been used for the analysis of plates and shells for some thirty years. The finite strip method, developed by Cheung (1976), is a semi-analytical finite-element method and involves longitudinal subdivision of a thin-walled member into a series of strips of finite width (Fig. 6.2). In many cases this now well-known method provides a significant reduction of the degrees of freedom of a strip as only one set of cross-sectional degrees of freedom are required. The method in essence transforms a three-dimensional problem to a two-dimensional one, and if only flexural buckling deformations are considered it becomes a one-dimensional problem. The method is similar to the finite element method except that Fourier series terms are used to define the displacement functions in the longitudinal direction.

The method was initially developed by analysing thin rectangular plates with two opposite edges simply supported. In this case, the global equations uncouple into a number of smaller systems of equations owing to certain orthogonality relationships resulting from the selected displacement functions. This leads to a reduction in storage requirements for the global equations and an increase in computational efficiency when compared with the finite element method. Later research work enabled other boundary conditions to be incorporated. However, in all other cases uncoupling of the equations does not occur, and the method loses some of its efficiency. A more serious problem is that the shape functions used in the finite strip method do not satisfy free edge boundary conditions, which frequently arise in practice. Although the finite strip method is less general than the finite-element method, it can significantly reduce the structural discretization and can fully describe the space deformation configuration of plate structures.

In the usual finite strip methods, stiffness and stability matrices operate conventionally on nodal degrees of freedom, which are necessary for the assembly of the strips for a given topology. Azhari and Bradford (1994b) included so-called bubble functions, which represent nodeless but additional strip degrees of freedom in the form of higher order orthogonal polynomials, into the expressions for the transverse buckling displacements, and have demonstrated great computational saving in this augmentation of the finite strip method based on complex arithmetic. These extra modes are associated with internal or nodeless degrees of freedom. By their nature, bubble modes have no effect on the displacements across the edges of a finite strip, and so the 'bubble strip' is more involved than would otherwise be required. The method was employed by Bradford and Azhari (1997) to investigate the local buckling behaviour of isotropic plates with different boundary conditions along all edges under both axial and biaxial compression, and the buckling of stiffened plates under compression. Hitherto, these serendipity type bubble strips have only been used for buckling modes that involve plate flexure such as local buckling. A more comprehensive survey of literature on the bubble functions is included in Chapter 2.

The conventional semi-analytical finite strip method that uses a single Fourier term, originally formulated by Hancock (1978) in a very simple and convenient fashion for elastic unified buckling, has been modified herein and augmented with bubble functions for the transverse buckling displacements. This chapter aims to explore an improvement in the efficiency and efficacy of the semi-analytical finite strip method through the use of bubble functions in the transverse buckling displacements in terms of strip discretization. It therefore considers flexural as well as membrane terms in bifurcative buckling. The developed numerical approach is applied to both plates and their assemblies and buckling modes at different wavelengths are examined, which include local, lateral-distortional and lateral-torsional modes.

6.2 THEORY

6.2.1 General

Finite strip analysis identifies three distinctive buckling modes: local, distortional and lateral-torsional, as illustrated in Fig. 1.1. Local buckling occurs at wavelengths close to or less than the width of the elements, whereas longer wavelengths indicate a different mode of behaviour. In local buckling, nodes at fold lines rotate only, if they are translating then the buckling mode is no longer local but either lateral-distortional or lateral-torsional, as explained in Chapter 1. This chapter considers the issue of improving computationally a unified buckling analysis for all of these three categories using bubble functions.

6.2.2 Displacements

In order to generate the serendipity 'bubble strip' for the semi-analytical finite strip method for buckling problems, a new set of transverse functions will be adopted in addition to the usual cubic function. Hence the particular functions describing the flexural and membrane buckling displacements and shown in Fig. 6.3, are given by

$$w = \langle 1, \eta, \eta^2, \eta^3, X_B \rangle N_n \langle a_1, a_2, a_3, a_4, a_5 \rangle^T$$
$$u = \langle 1, \eta \rangle N_n' / k_n \langle a_3', a_4' \rangle^T \qquad (6.1)$$
$$v = \langle 1, \eta \rangle N_n \langle a_1', a_2' \rangle^T$$

where X_B is bubble polynomial given as the Legendre polynomial:

$$X_B = \sum_{i=2}^{\infty} A \frac{\eta^i}{2^{2i}} (1-\eta)^i \qquad (6.2)$$

and

$$N_n = \sin k_n x$$
$$k_n = n\pi/L \qquad (6.3)$$
$$\eta = y/b$$

where n is the number of buckling half wavelengths over the length L of the strip, and where primes denote differentiation with respect to x. The multiplier A in Eqn 6.2 is arbitrary and may be taken as unity. The stiffness and stability matrices of a strip were obtained herein by using the bubble function of order 10 ($i = 5$), written as

$$X_B = A\frac{\eta^2}{16}(1-\eta)^2 + B\frac{\eta^3}{64}(1-\eta)^3 + C\frac{\eta^4}{256}(1-\eta)^4 + D\frac{\eta^5}{1024}(1-\eta)^5 . \qquad (6.4)$$

The flexural and membrane displacement fields are shown in Fig. 6.3.

Equation 6.1 can be arranged more compactly in a standard matrix form to include both the flexural and membrane displacements and the resulting set of equations can be represented in matrix form by

$$\vec{u} = \overline{M}\,\vec{a} \qquad (6.5)$$

where

$$\vec{u} = \langle w, u, v \rangle^T \qquad (6.6)$$

$$\vec{a} = \langle \vec{a}_F, \vec{a}_B, \vec{a}_M \rangle \tag{6. 7}$$

and the kernel freedoms are

$$\begin{aligned}
\vec{a}_F &= \langle a_1, a_2, a_3, a_4 \rangle^T \\
\vec{a}_B &= \langle a_5 \rangle^T \\
\vec{a}_M &= \langle a_1^{'}, a_2^{'}, a_3^{'}, a_4^{'} \rangle^T
\end{aligned} \quad . \tag{6. 8}$$

The kernel freedom a_5 is associated with the bubble displacement. By appropriate differentiation and substitution for x and y in Eqn. 6.5, the assemblable vector $\vec{\delta}$ can be related to the vector $\vec{a}$ in the usual way to produce

$$\vec{\delta} = \overline{C}\vec{a} \tag{6. 9}$$

from which the vector of nodal displacements is represented by

$$\vec{u} = \overline{MC}^{-1}\vec{\delta} \, . \tag{6. 10}$$

The displacement matrices $\overline{M}$ and $\overline{C}^{-1}$ are given in the Appendix 6.1. The vector of assemblable freedoms is then given by

$$\vec{\delta} = \langle \delta_F, \delta_B, \delta_M \rangle^T \tag{6. 11}$$

and contains the flexural and membrane nodal line displacements

$$\vec{\delta}_F = \langle w_1, \theta_1, w_2, \theta \rangle^T \tag{6. 12}$$

and

$$\vec{\delta}_M = \langle u_1, v_1, u_2, v_2 \rangle^T \tag{6. 13}$$

respectively, and bubble nodeless or internal displacement,

$$\vec{\delta}_B = \langle \psi_B \rangle^T \, . \tag{6. 14}$$

For a symmetric bubble, the bubble freedom is defined as

$$\psi_B = X_{B(\eta=1/2)}. \tag{6. 15}$$

6.2.3 Strains

The generalised linear strain vector $\vec{\varepsilon}_L$ can be obtained by appropriate differentiation of Eqn. 6.10, so that

$$\vec{\varepsilon}_L = \langle \rho_x \quad \rho_y \quad \rho_{xy} \quad \varepsilon_x \quad \varepsilon_y \quad \varepsilon_{xy} \rangle^T = \begin{bmatrix} \partial^2/\partial x^2 & 0 & 0 \\ \partial^2/\partial y^2 & 0 & 0 \\ -2\partial^2/\partial x \partial y & 0 & 0 \\ 0 & \partial/\partial x & 0 \\ 0 & 0 & \partial/\partial y \\ 0 & \partial/\partial y & \partial/\partial x \end{bmatrix} \langle w \quad u \quad v \rangle^T \tag{6. 16}$$

or

$$\vec{\varepsilon}_L = \overline{B}\,\overline{C}^{-1}\vec{\delta}. \tag{6. 17}$$

The nonlinear component

$$\vec{\varepsilon}_N = \tfrac{1}{2}\left[(\partial w/\partial x)^2 + (\partial u/\partial x)^2 + (\partial v/\partial x)^2\right] \tag{6. 18}$$

of the longitudinal strain $\vec{\varepsilon}_N$ is used to calculate the geometric or stability matrix of a strip. It can be obtained from Eqn. 6.10, so that

$$\vec{\varepsilon}_N = \tfrac{1}{2}\vec{H}^T\vec{H} \tag{6. 19}$$

where

$$\begin{aligned} \vec{H} &= \langle \partial w/\partial x, \partial u/\partial x, \partial v/\partial x \rangle^T \\ &= \overline{B}^{*}\overline{C}^{-1}\vec{\delta} \end{aligned}. \tag{6. 20}$$

The matrices $\overline{B}$ and $\overline{B}^{*}$ are shown in the Appendices 6.2 and 6.3.

6.2.4 Stresses

The generalised stresses (consisting of bending and torsional moments, and axial and shear stresses) are related to the generalised strains through the elastic properties of the strip. These material properties are contained in the property or elasticity matrix $\overline{D}$, so that

$$\bar{\sigma} = \overline{D}\bar{\varepsilon}_L \tag{6. 21}$$

where

$$\bar{\sigma} = \left\langle \bar{\sigma}_F, \bar{\sigma}_M \right\rangle^T \tag{6. 22}$$

in which

$$\bar{\sigma}_F = \left\langle M_x, M_y, M_{xy} \right\rangle^T \tag{6. 23}$$

and

$$\bar{\sigma}_M = \left\langle \sigma_x, \sigma_y, \tau_{xy} \right\rangle^T \tag{6. 24}$$

are the flexural and membrane generalised stresses respectively.

In the present formulation, the property matrix is derived using the orthotropic plate theory set out in Timoshenko and Woinowsky-Krieger (1959), and is given in the Appendix 6.4.

6.2.5 Stiffness and Stability Matrices for a Strip

During buckling, the strip deflects and twists. The stiffness matrix $\bar{k}$ of a strip is derived from the increase in strain energy due to buckling as

$$U = 1/2 \int_V \bar{\varepsilon}_L{}^T \bar{\sigma}\, \mathrm{d}V = 1/2\, \bar{\delta}^T \bar{k} \bar{\delta}\,. \tag{6. 25}$$

Substitution for $\bar{\varepsilon}_L$ and $\bar{\sigma}_L$ from Eqn. 6.17 and from Eqn. 6.21, and knowing that Eqn. 6.24 holds for all $\vec{\delta}$, results in

$$\bar{k} = \bar{C}^{-T}\left(\int_V \bar{B}^T \bar{D}\bar{B}\,\mathrm{d}V\right)\bar{C}^{-1}. \tag{6.26}$$

The potential energy resulting from the longitudinal in-plane forces can be calculated using the following equation

$$V = 1/2\int_V \sigma\varepsilon_N \mathrm{d}V = 1/2\vec{\delta}^T\,\bar{g}\vec{\delta} \tag{6.27}$$

where

$$\sigma = \sigma_1 + (\sigma_2 - \sigma_1)\eta. \tag{6.28}$$

Substitution for $\bar{\varepsilon}_N$ from Eqn. 6.18 and knowing that Eqn. 6.26 holds for all $\vec{\delta}$, results in

$$\bar{g} = \bar{C}^{-T}\left(\int_V \bar{B}^{*T}\sigma\bar{B}^{*}\mathrm{d}V\right)\bar{C}^{-1}. \tag{6.29}$$

An explicit form for the stiffness matrix derived by the described analysis, but without a bubble term, is given in Cheung (1976). The stability matrix for flexural displacements appears to have been presented first by Przemieniecki (1973) and the stability matrix for the membrane displacements appears to have been presented first by Plank and Wittrick (1974). The kernel stiffness and stability matrices $\bar{k}_e$ and $\bar{g}_e$ are given in the equations

$$\begin{aligned}\bar{k} &= \bar{C}^{-T}\bar{k}_e\bar{C}^{-1}\\ \bar{g} &= \bar{C}^{-T}\bar{g}_e\bar{C}^{-1}\end{aligned} \tag{6.30}$$

with pre and post-multiplication being effected by computer.

6.2.6 Buckling Solution

The individual stiffness and stability matrices of a strip were computed with respect to the local coordinate system (x, y, z). However, since all adjoining strips do not lie in the same plane, as shown in Fig. 6.4, it is necessary to transform the stiffness and stability matrices to the global coordinate system (X, Y and Z) as shown in the Appendix 6.5. A transformation matrix $\overline{R}$ such that

$$\vec{\delta} = \overline{R}\vec{\Delta}_e \tag{6. 31}$$

can be used to relate the displacements of the nodal lines in the global directions $\vec{\Delta}_e$ to the displacements of the nodal lines in the local directions $\vec{\delta}$. Hence, the global stiffness and stability matrices $\overline{K}$ and $\overline{G}$ for a plate assembly can be simply assembled from the transformed matrices $\overline{k}_e$ and $\overline{g}_e$ for each strip by the principle of contragredience, where

$$\overline{k}_e = \overline{R}^T \overline{k}\overline{R} \tag{6. 32}$$

and

$$\overline{g}_e = \overline{R}^T \overline{g}\overline{R}\,. \tag{6. 33}$$

Following the usual procedure as set out in Zienkiewicz and Taylor (2000), the stiffness and stability matrices for the finite strip are assembled in order to obtain the global stiffness and stability matrices $\overline{K}$ and $\overline{G}$ respectively. Either the Timoshenko's energy method or the Rayleigh Ritz method may be invoked to solve the buckling equation, which may be written in the familiar form

$$\overline{K}\vec{\Delta} - \lambda\overline{G}\vec{\Delta} = \vec{0} \tag{6. 34}$$

where $\vec{\Delta}$ is the vector of buckling global degrees of freedom that include both flexural and membrane terms. The buckling load factor λ, as well as the buckling mode shape $\vec{\Delta}$, may be extracted from Eqn. 6.33 by using standard eigenvalue routines.

6.3 NUMERICAL ANALYSES

6.3.1 General

The numerical studies presented in this section are intended, in addition to ascertaining the accuracy of the method, to investigate the discretization that is necessary when a bubble term is included, and the ramifications on potential minimisation of the size (and storage required) of the stiffness and stability matrices.

6.3.2 Plates

Simply supported plates with different transverse end conditions under uniform in-plane compression and bending were analysed, as illustrated in Fig. 6.5. The accuracy and convergence of the solutions with increasing the number of bubble strips is compared with the results derived by the conventional finite strip method by suppression of the bubble term, and some available exact solutions.

The familiar local buckling coefficient k, as defined by Allen and Bulson (1980), is calculated as

$$k = \left(\frac{b}{t}\right)^2 \sigma_{cr} \frac{12(1-\nu^2)}{\pi^2 E} \tag{6. 35}$$

where b and t are the plate width and thickness respectively. The local buckling coefficients of simply supported, clamped, clamped-free and simply supported-free rectangular plates under uniaxial loads are compared with some available exact results and results as derived by the conventional semi-analytical finite strip method in Table 6.1. The results clearly indicate that when one bubble strip is used, the error is less than 0.05% while for two bubble strips the error is in general less than 0.01%.

Simply supported and built-in flat plates under uniform in-plane bending were analysed, and the accuracy and convergence of the solutions with an increasing number of strips is shown in Table 6.2. The worst case for convergence is that of a plate in uniform bending with built-in edges, but for which only three strips are needed to produce an error of less that 0.1%.

In order to show the effect of a bubble function of a higher order (ie. $i > 4$) on the accuracy of the method, plates in uniform bending were studied with the coefficients B, C, and D being different from 0. It can be seen in Table 6.2 (when $B = 1$) that although there is some minor variation of the solution with B, the overall results are fairly insensitive to this parameter. Because of this, B, C and D were taken as 0 in the remaining studies.

The results show that by implementation of the bubble function in the semi-analytical finite strip method, it is possible to obtain results very close to the exact solution by subdividing the plates into one or two strips. This contrasts with the conventional finite strip treatment, for which it is necessary to subdivide the plate into eight strips in some cases in order to produce results of comparable accuracy to the bubble treatment.

6.3.3 Plate Assemblies

The extension of the finite strip analysis from a single flat plate to a prismatic member has been investigated for plate assemblies such as I-sections, T-sections, channels, square hollow sections (SHS) and cruciform sections. The section geometries are shown in Figs. 6.6 and 6.7, and the results derived by bubble strip treatment have been compared with the results obtained by the conventional semi-analytical finite strip method of analysis.

For this study, square hollow sections and cruciform sections in uniform compression were divided into 8 and 16 equal width longitudinal strips, as shown in Fig. 6.6. The results for the SHS, summarised in Table 6.3, clearly show that improvement is significant only for local buckling modes of thin-walled sections whose L/b ratio is less than 7. Once this ratio is exceeded, and the buckling mode changes from one of local buckling to one of flexural buckling, there is no significant improvement in terms of computational savings. Similar behaviour was observed in case of a cruciform section that buckles in a local, distortional and flexural torsional modes, where it is clear that the computational savings are significant only for the L/h_w ratio being less than 1, as shown in Table 6.4.

For the subject analysis, channel section and I and T-beam sections were subjected to uniform bending stresses. The I-beams were divided into six strips (two equal width strips in each flange and two in the web) and nine strips (four in the compression flange, three in the web and two in the tension flange), as shown in Fig. 6.7. The T-section was first divided into two equal width strips across the flange and two equal width strips across the web, and then into four strips across the flange and three strips across the web, as illustrated in Fig. 6.7. As shown in the same figure, the channel section was subdivided first into five and then nine longitudinal strips (four in the compression flange, two in the tension flange and three in the web).

For the channel section, similar behaviour to that observed in the analysis of SHS and cruciform sections under in-plane compressive stresses is evident from the results given in Table 6.5. From this table, it is clear that the improvement measured in terms of strip discretization is significant only for very short members where the buckling mode is local rather than overall buckling. The results summarised in Tables 6.6 and 6.7, for I and T- sections respectively, where membrane deformations are predominant in the overall buckling mode, clearly show that augmentation of bubble function does not lead to significant improvement as gauged by strip discretization.

6.4 SUMMARY

A numerical model based on the harmonic-based semi-analytical finite strip method and augmented with bubble functions has been described. The numerical analyses undertaken have demonstrated the accuracy and versatility of the present approach for predicting elastic local buckling loads for simply supported thin-walled plates with different transverse end supports under in-plane compression and bending. The results were compared with those published elsewhere, and significant improvement in terms of discretization was observed. It was found that in some cases only one bubble strip for each flat was needed to model the topology, compared with several needed with conventional finite strips, in order to achieve comparable accuracy.

It was also shown that augmentation of bubble terms, in modelling plate assemblies where membrane actions are significant (such as I and T-beam sections), does not improve the efficiency of the finite strip method when measured by the topological discretization. Similarly, there was no significant improvement in convergence for members where overall buckling precedes local buckling.

6.5 APPENDICES

6.4.1 Displacement Matrices

$$\bar{u} = \overline{M}\ \overline{C}^{-1}$$

where

$$\bar{u} = \begin{bmatrix} w \\ \hline u \\ v \end{bmatrix},$$

$$\overline{M} = \left[\begin{array}{cccc:c:cccc} N_n & \eta N_n & \eta^2 N_n & \eta^3 N_n & \mathrm{X}_B N_n & 0 & 0 & 0 & 0 \\ \hdashline 0 & 0 & 0 & 0 & 0 & 0 & 0 & N_n'/k_n & \eta N_n'/k_n \\ 0 & 0 & 0 & 0 & 0 & N_n & \eta N_n & 0 & 0 \end{array}\right],$$

$$\overline{C}^{-1} = \left[\begin{array}{cccc:c:cccc} 1 & 0 & 0 & 0 & 0 & 0 & 0 & 0 & 0 \\ 0 & b & 0 & 0 & 0 & 0 & 0 & 0 & 0 \\ -3 & -2b & 3 & -b & 0 & 0 & 0 & 0 & 0 \\ 2 & b & -2 & b & 0 & 0 & 0 & 0 & 0 \\ \hdashline 0 & 0 & 0 & 0 & B^* & 0 & 0 & 0 & 0 \\ \hdashline 0 & 0 & 0 & 0 & 0 & -1 & 0 & 1 & 0 \\ 0 & 0 & 0 & 0 & 0 & 1 & 0 & 0 & 0 \\ 0 & 0 & 0 & 0 & 0 & 0 & -1 & 0 & 1 \\ 0 & 0 & 0 & 0 & 0 & 0 & 1 & 0 & 0 \end{array}\right] \begin{bmatrix} w_1 \\ \theta_1 \\ w_2 \\ \theta_2 \\ \hline \psi_B \\ \hline u_1 \\ v_1 \\ u_2 \\ v_2 \end{bmatrix}$$

and

$$B^* = 1048576/(4096A + 256B + 16C + D).$$

6.4.2 Linear Strain Matrix

$$\vec{\varepsilon}_L = \overline{B}\vec{a}$$

where

$$\vec{\varepsilon}_L = \begin{bmatrix} \rho_x \\ \rho_y \\ \rho_{xy} \\ \hdashline \varepsilon_x \\ \varepsilon_y \\ \varepsilon_{xy} \end{bmatrix},$$

$$\overline{B} = \left[\begin{array}{cccc:c:cccc} 0 & 0 & 2N_n/b^2 & 6\eta N_n/b^2 & X_B'' N_n & 0 & 0 & 0 & 0 \\ N_n'' & \eta N_n'' & \eta^2 N_n'' & \eta^3 N_n'' & X_B N_n'' & 0 & 0 & 0 & 0 \\ 0 & -2N_n'/b & -4\eta N_n'/b & -6\eta^2 N_n' & -2X_B' N_n' & 0 & 0 & 0 & 0 \\ \hdashline 0 & 0 & 0 & 0 & 0 & 0 & 0 & N_n''/k_n & \eta N_n''/k_n \\ 0 & 0 & 0 & 0 & 0 & 0 & N_n/b & 0 & 0 \\ 0 & 0 & 0 & 0 & 0 & N_n' & \eta N_n' & 0 & N_n'/bk_n \end{array}\right]$$

and

$$\vec{a} = \begin{bmatrix} a_1 \\ a_2 \\ a_3 \\ a_4 \\ \hdashline a_5 \\ \hdashline a_1' \\ a_2' \\ a_3' \\ a_4' \end{bmatrix}.$$

6.4.3 Nonlinear Strain Matrix

$$\vec{H} = \overline{B}^{*}\,\vec{a}$$

$$\begin{bmatrix} \partial w/\partial x \\ \hdashline \partial u/\partial x \\ \partial v/\partial x \end{bmatrix} = \left[\begin{array}{cccc:c:cccc} N_n' & \eta N_n' & \eta^2 N_n' & \eta^3 N_n' & X_B N_n' & 0 & 0 & 0 & 0 \\ \hdashline 0 & 0 & 0 & 0 & 0 & 0 & 0 & N_n''/k_n & \eta N_n''/k_n \\ 0 & 0 & 0 & 0 & 0 & N_n' & \eta N_n' & 0 & 0 \end{array}\right] \begin{bmatrix} a_1 \\ a_2 \\ a_3 \\ a_4 \\ \hdashline a_5 \\ \hdashline a_1' \\ a_2' \\ a_3' \\ a_4' \end{bmatrix}$$

$$\varepsilon_N = \vec{H}^T \vec{H} = \vec{a}^T \overline{B}^{*T} \overline{B}^{*} \vec{a}$$

6.4.4 Orthotropic Property Matrix

a) Flexural Stiffness

$$\begin{bmatrix} M_x \\ M_y \\ M_{xy} \end{bmatrix} = \begin{bmatrix} D_x & D_1 & 0 \\ D_1 & D_y & 0 \\ 0 & 0 & D_{xy} \end{bmatrix} \begin{bmatrix} \dfrac{\partial^2 w}{\partial x^2} \\ \dfrac{\partial^2 w}{\partial y^2} \\ -\dfrac{2\partial^2 w}{\partial x \partial y} \end{bmatrix}$$

$$D_x = E_x t^3 / 12(1 - \nu_x \nu_y)$$
$$D_y = E_y t^3 / 12(1 - \nu_x \nu_y)$$
$$D_1 = \nu_x E_y t^3 / 12(1 - \nu_x \nu_y) = \nu_y E_x t^3 / 12(1 - \nu_x \nu_y)$$
$$D_{xy} = G t^3 / 12$$

b) Membrane Stiffness

$$\begin{bmatrix} \sigma_x \\ \sigma_y \\ \sigma_{xy} \end{bmatrix} = \begin{bmatrix} E_1 & E_{12} & 0 \\ E_{12} & E_2 & 0 \\ 0 & 0 & G \end{bmatrix} \begin{bmatrix} \dfrac{\partial u}{\partial x} \\ \dfrac{\partial v}{\partial y} \\ \dfrac{\partial u}{\partial y} + \dfrac{\partial v}{\partial x} \end{bmatrix}$$

$$E_1 = E_x / (1 - \nu_x \nu_y)$$
$$E_{12} = E_y / (1 - \nu_x \nu_y)$$
$$E_2 = \nu_x E_y / (1 - \nu_x \nu_y) = \nu_y E_x / (1 - \nu_x \nu_y)$$

6.4.5 Transformation Matrix

$$\bar{\delta} = \overline{R}\bar{\Delta}$$

$$\begin{bmatrix} w_1 \\ \theta_1 \\ w_2 \\ \theta_2 \\ \hline \psi_B \\ \hline u_1 \\ v_1 \\ u_2 \\ v_2 \end{bmatrix} = \left[\begin{array}{cccc:c:cccc} -\sin\beta & \cos\beta & 0 & 0 & 0 & 0 & 0 & 0 & 0 \\ 0 & 0 & 0 & 1 & 0 & 0 & 0 & 0 & 0 \\ 0 & 0 & 0 & 0 & 0 & -\sin\beta & \cos\beta & 0 & 0 \\ 0 & 0 & 0 & 0 & 0 & 0 & 0 & 0 & 1 \\ \hdashline 0 & 0 & 0 & 0 & 1 & 0 & 0 & 0 & 0 \\ \hdashline 1 & 0 & 0 & 0 & 0 & 0 & 0 & 0 & 0 \\ 0 & \cos\beta & \sin\beta & 0 & 0 & 0 & 0 & 0 & 0 \\ 0 & 0 & 0 & 0 & 0 & 1 & 0 & 0 & 0 \\ 0 & 0 & 0 & 0 & 0 & 0 & \cos\beta & \sin\beta & 0 \end{array}\right] \begin{bmatrix} U_1 \\ V_1 \\ W_1 \\ \Theta_1 \\ \hline \Psi_B \\ \hline U_2 \\ V_2 \\ W_2 \\ \Theta_2 \end{bmatrix}$$

Table 6.1 Convergence and comparison studies for rectangular plates in uniform compression

Number of Strips	Support conditions	*L/b*	FSM	Bubble augmented FSM	
1			4.2584720	4.0006595	
2			4.0085293	4.0001552	
4	s-s*	1.0	4.0004449	4.0000000	
8			4.0001341	4.0000000	4.0 (exact)
1			5403.68533	8.60578	
2			8.92522	8.60461	
4	c-c*	1.0	8.62514	8.60447	
8			8.60571	8.60447	
1			1.75160	1.65322	
2			1.66097	1.65269	
4		1.0	1.65318	1.65252	
8			1.65256	1.65250	
1			1.38783	1.31529	
2			1.32057	1.31513	
4	c-f*	1.4	1.31548	1.31509	
8			1.31511	1.31508	
1			1.35196	1.29279	
2			1.29693	1.29265	
4		1.8	1.29292	1.29263	
8			1.29265	1.29263	
1			1.41477	1.40298	
2			1.40341	1.40166	
4		1.0	1.40175	1.40166	
8			1.40161	1.40166	
1			0.92942	0.92248	
2			0.92279	0.92200	
4	s-f*	1.4	0.92205	0.92199	
8			0.92199	0.92199	
1			0.73009	0.72550	
2			0.72571	0.72527	
4		1.8	0.72530	0.72526	
8			0.72526	0.72526	

* s – Simply Supported; c – Clamped End; f – Free End

Table 6.2 Convergence and comparison studies for rectangular plates in uniform bending

Number of Strips	Support Conditions	*L/b*	FSM	Azhari (1993)	Bubble Augmented FSM (A = 1)	Bubble Augmented FSM (A = 1, B =1)
1			27.41166		27.29264	27.27258
2	s-s*		25.45224		23.94958	23.94649
4		0.665	23.96627		23.88388	23.88427
8	23.9 (exact)		23.88751	23.9	23.88267	23.88306
1			9789.2509		9789.67566	48.85403
2	c-c*		57.41010		40.21886	40.21626
4		0.470	40.36065		39.56880	39.57059
8	39.6 (exact)		39.61263	39.6	39.56192	39.56229

* s – Simply Supported; c – Clamped End

Table 6.3 Square hollow section in uniform compression

Length	Cross-section	8 Strips		16 Strips	
		FSM	Bubble augmented FSM	FSM	Bubble augmented FSM
610	SHS 200×200×3	859.20	847.21	847.61	846.84
1220		2854.36	2815.27	2815.09	2812.60
1830		4983.02	4955.40	4924.16	4923.05
3660		3605.39	3603.12	3591.30	3591.12
7320		3197.64	3196.32	3188.52	3188.48
9000		3018.16	3017.02	3009.77	3009.78
12000		2699.58	2698.77	2692.43	2692.43
15000		2407.67	2407.07	2401.46	2401.45
30000		1463.53	1463.39	1459.97	1460.00
610	SHS 200×200×6	3331.62	3286.36	3286.27	3283.18
1220		9313.88	9202.25	9190.16	9183.13
1830		7534.19	7526.50	7482.94	7482.39
3660		6363.14	6360.71	6342.69	6342.49
7320		4870.90	4869.69	4857.86	4857.88
9000		4300.61	4299.90	4289.61	4289.67
12000		3503.19	3502.70	3494.43	3494.47
15000		2926.56	2926.20	2919.43	2919.37
30000		1560.02	1560.04	1556.40	1556.44
610	SHS 200×200×12	11936.30	11785.60	11763.68	11701.70
1220		14020.81	14007.32	13900.29	12203.73
1830		12487.11	12481.56	12426.99	12022.87
3660		9658.38	9655.91	9629.97	9629.50
7320		5967.09	5966.81	5952.27	5952.45
9000		5001.97	5001.62	4989.69	4989.76
12000		3854.95	3854.71	3845.67	3845.68
15000		3124.39	3124.39	3117.14	3117.09
30000		1590.48	1590.49	1586.87	1586.81

Table 6.4 Cruciform section in uniform compression

L/h_w	8 Strips		16 Strips	
	FSM	**Bubble augmented FSM**	**FSM**	**Bubble augmented FSM**
0.2	634.23	633.42	633.46	633.39
0.4	302.11	301.94	301.95	301.93
0.6	241.00	240.93	240.93	240.93
0.8	219.67	219.63	219.64	219.63
1.0	209.81	209.79	209.78	209.79
1.2	204.45	204.44	204.45	204.44
1.4	201.23	201.22	201.21	201.22
1.6	199.15	199.13	199.13	199.10
3.2	194.01	194.01	194.01	194.01
7.2	192.64	192.65	192.64	192.65
15.0	58.76	58.75	58.48	58.48
30.0	14.71	14.71	14.65	14.65

Table 6.5 Channel section in uniform bending

b_f/h	b_f	L	5 Strips		9 Strips	
			FSM	**Bubble augmented FSM**	**FSM**	**Bubble augmented FSM**
0.2	40.6	610	439.2976	426.0596	426.0015	425.3791
0.4	81.2		92.3002	92.2350	92.2271	92.2263
0.6	121.8		29.2400	29.2220	29.2221	29.2206
0.8	162.4		13.1986	13.1874	13.1880	13.1870
1.0	203.0		7.3975	7.3892	7.3895	7.3890
0.2	40.6	3660	34.2706	34.2687	33.9818	33.9811
0.4	81.2		131.6604	131.6536	130.1891	130.1886
0.6	121.8		222.9886	222.9627	220.5845	220.5780
0.8	162.4		157.1548	157.1158	156.1252	156.1172
1.0	203.0		90.9630	90.9312	90.5467	90.5474
0.2	40.6	9000	8.1454	8.1455	8.1006	8.1006
0.4	81.2		24.7154	24.7158	24.4846	24.4838
0.6	121.8		49.9584	49.9582	49.3982	49.3984
0.8	162.4		78.5539	78.5542	77.6234	77.6223
1.0	203.0		92.9877	92.9772	91.9441	91.9473
0.2	40.6	12000	5.5740	5.5738	5.5480	5.5478
0.4	81.2		15.1743	15.1746	15.0472	15.0468
0.6	121.8		29.5382	29.5377	29.2253	29.2248
0.8	162.4		47.5523	47.5508	46.9940	46.9941
1.0	203.0		64.3121	64.3079	63.5443	63.5440
0.2	40.6	15000	4.2463	4.2462	4.2285	4.2286
0.4	81.2		10.6645	10.6649	10.5844	10.5842
0.6	121.8		19.9326	19.9325	19.7346	19.7345
0.8	162.4		31.8339	31.8335	31.4727	31.4733
1.0	203.0		44.8359	44.8362	44.2979	44.2997

Table 6.6 I-section in uniform bending

b_f/b_w	L/h_w	6 Strips		9 Strips	
		FSM	**Bubble augmented FSM**	**FSM**	**Bubble augmented FSM**
0.1 $b_f = 100$	0.25	969.98	967.00	896.19	895.70
	0.5	537.92	537.44	495.56	495.43
	1.0	408.58	406.20	385.56	385.40
	2.0	167.19	167.08	163.76	163.74
	4.0	51.15	51.14	50.41	50.40
	8.0	18.54	18.54	18.34	18.34
	16.0	8.14	8.14	8.08	8.08
	32.0	3.92	3.92	3.89	3.89
0.3 $b_f = 300$	0.25	695.26	690.39	685.76	685.14
	0.5	448.91	447.17	441.01	440.86
	1.0	457.86	454.17	442.61	442.40
	2.0	794.64	787.73	764.51	764.00
	4.0	589.77	589.51	577.15	577.13
	8.0	160.20	160.20	157.40	157.40
	16.0	46.06	46.06	45.36	45.36
	32.0	16.08	16.08	15.90	15.90
0.6 $b_f = 600$	0.25	393.00	387.35	381.70	380.92
	0.5	182.12	180.52	178.66	178.46
	1.0	151.48	150.78	150.57	150.50
	2.0	226.71	226.01	226.05	225.99
	4.0	565.98	564.48	564.45	564.33
	8.0	730.05	729.98	716.03	716.03
	16.0	191.77	191.77	188.38	188.38
	32.0	53.18	53.18	52.33	52.33

Table 6.7 T-section in Uniform Bending

L/h_w	4 Strips		7 Strips	
	FSM	Bubble augmented FSM	FSM	Bubble augmented FSM
0.1	6331.324	5874.616	3538.844	3267.616
0.2	2046.563	1979.780	1310.669	1248.462
0.3	1283.103	1272.453	875.158	847.562
0.4	1065.186	1064.565	745.223	728.239
0.5	1023.095	1020.702	722.253	709.121
1.0	1599.430	1560.295	1153.271	1139.471
2.0	2682.745	2659.080	2639.276	2622.657
3.0	2405.250	2401.237	2088.082	2086.613
4.0	1449.999	1449.619	1236.574	1236.409
5.0	948.857	948.780	808.891	808.850
6.0	669.135	669.098	570.401	570.389
7.0	498.180	498.141	424.557	424.558
8.0	386.056	386.055	328.875	328.863
9.0	308.461	308.443	262.546	262.545
10.0	252.357	252.347	214.581	214.579

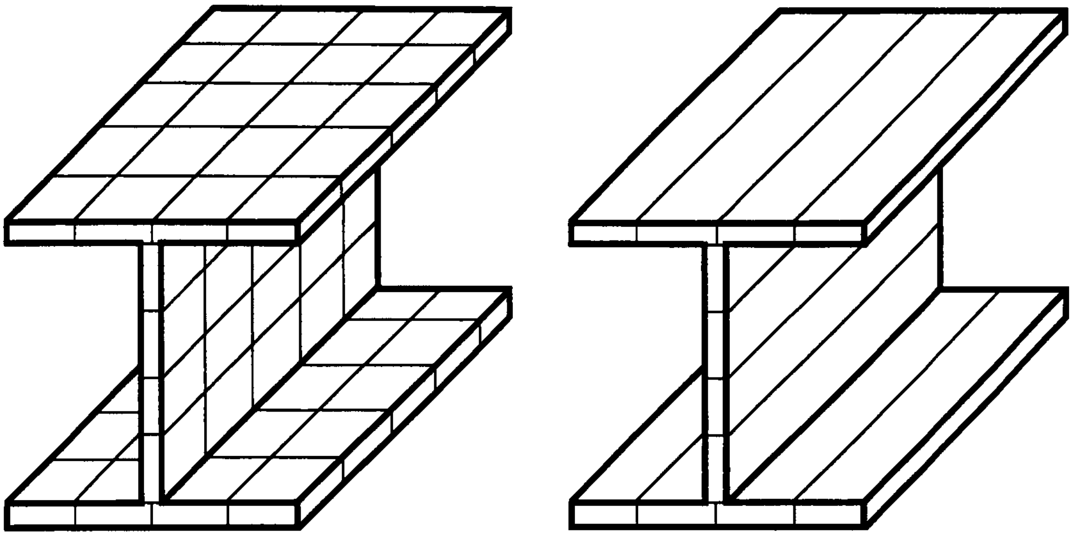

i) finite element division ii) finite strip division

Figure 6.1 Typical member division

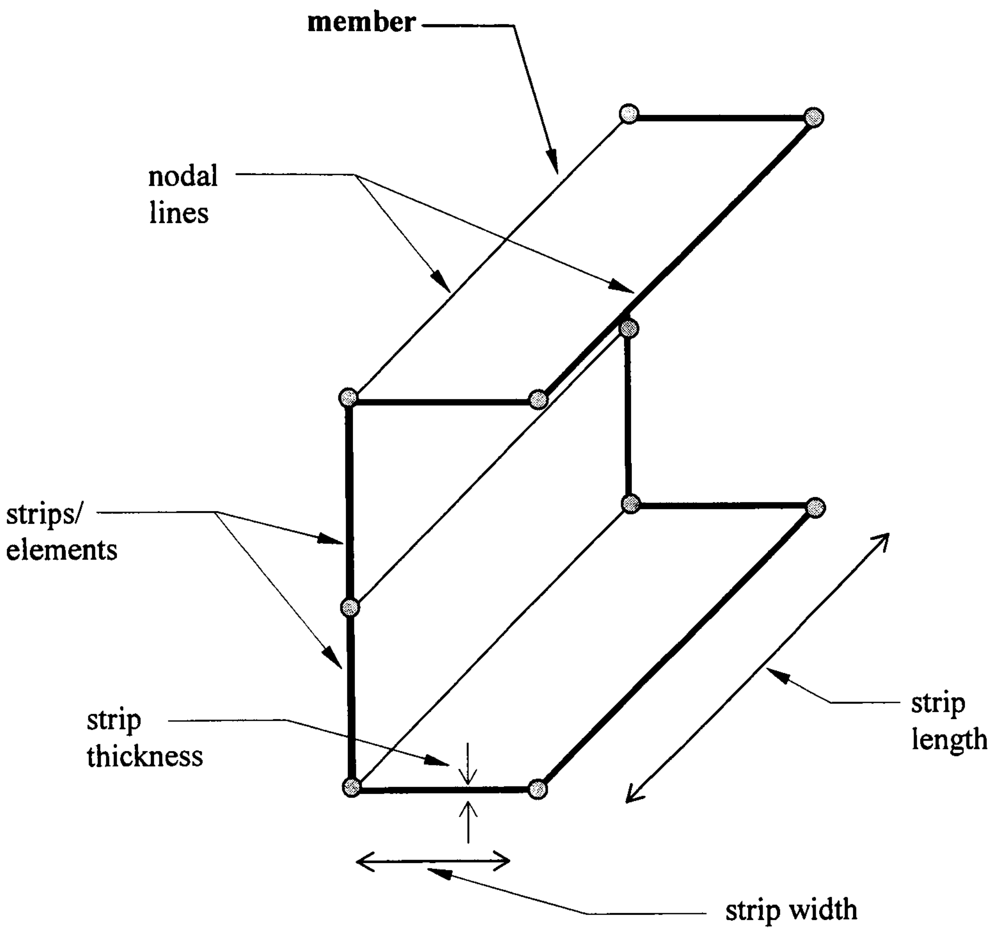

Figure 6.2 Notation

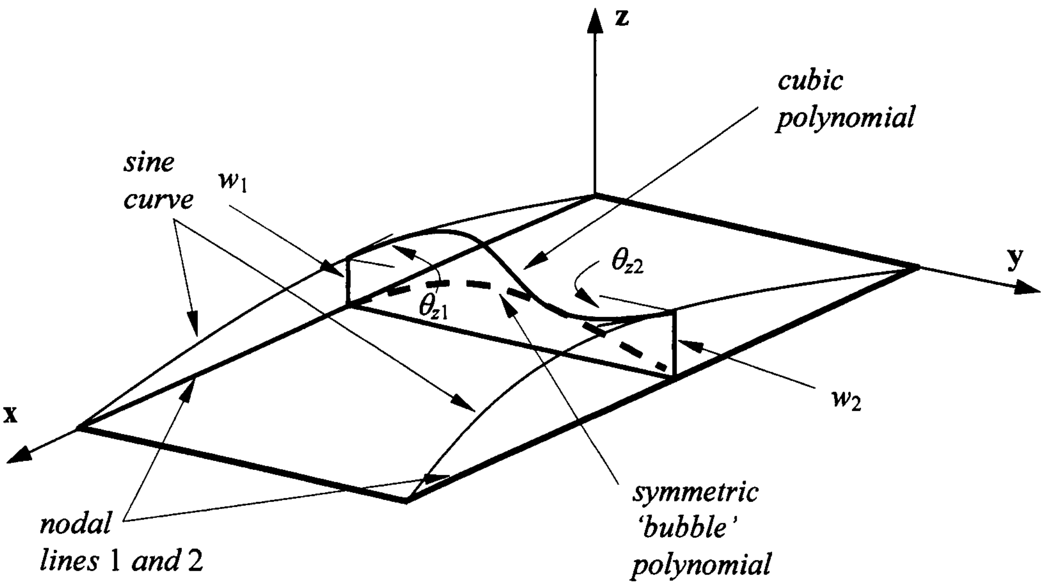

a) flexural (out-of-plane) displacements

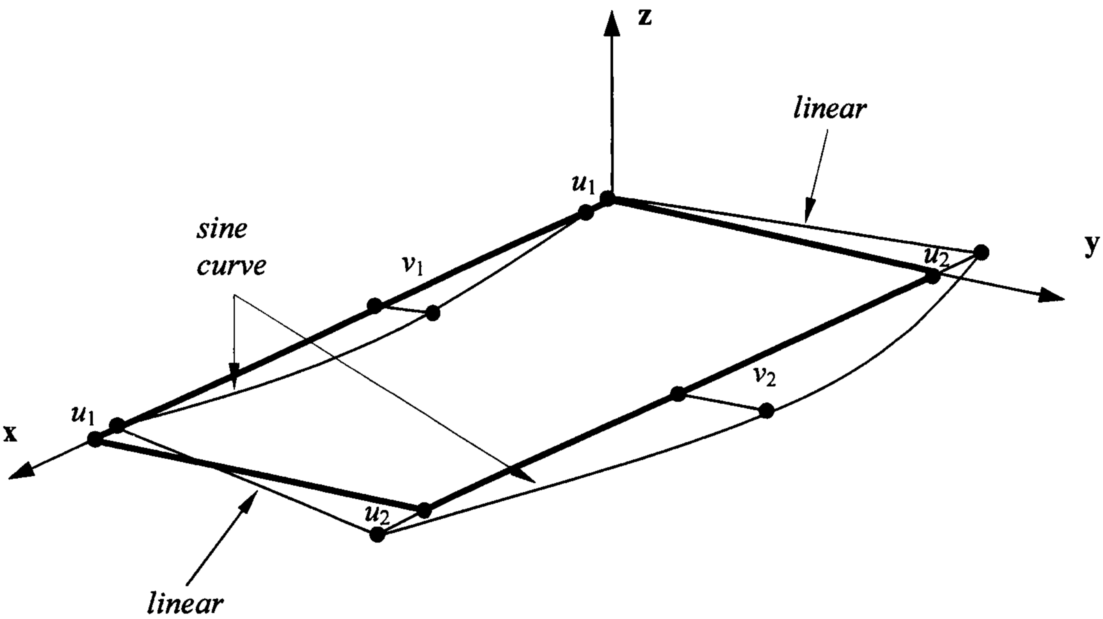

b) membrane (in-plane) displacements

Figure 6.3 Strip displacements fields

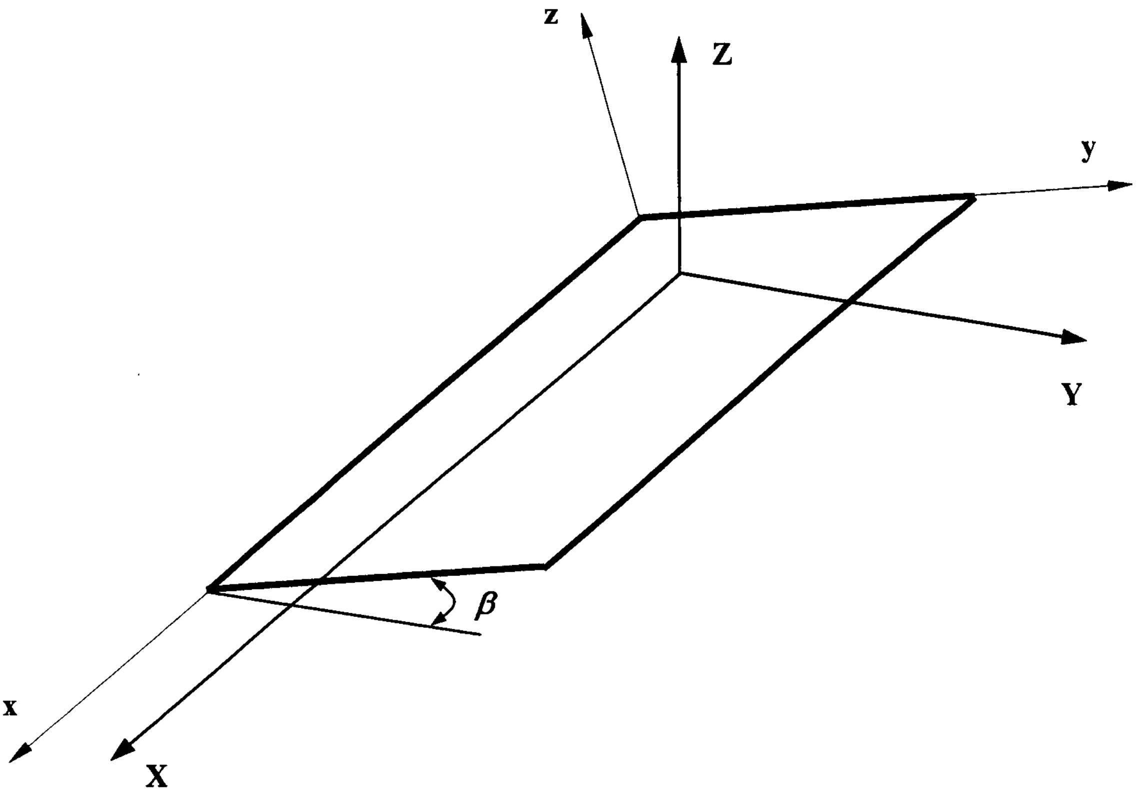

Figure 6.4 Strip orientation relative to global axes

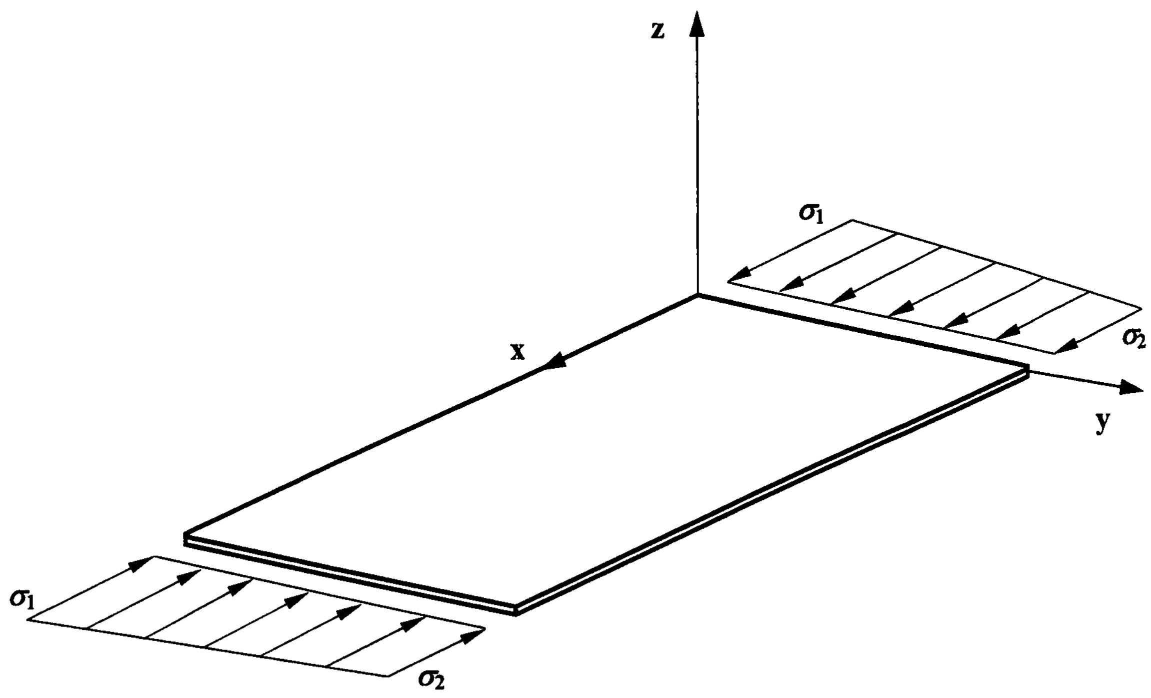

Figure 6.5 Longitudinal stress distribution in a strip

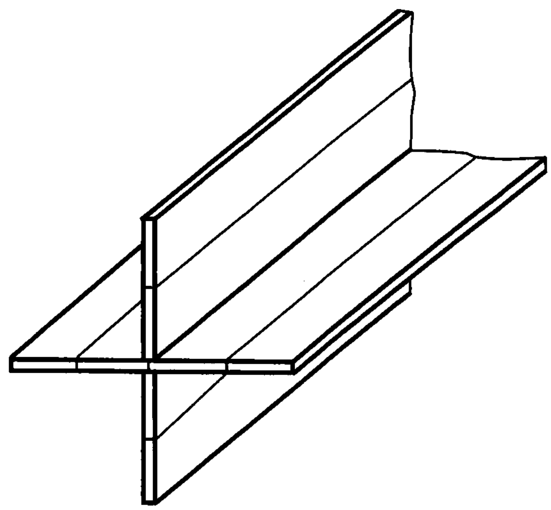

a) cruciform section

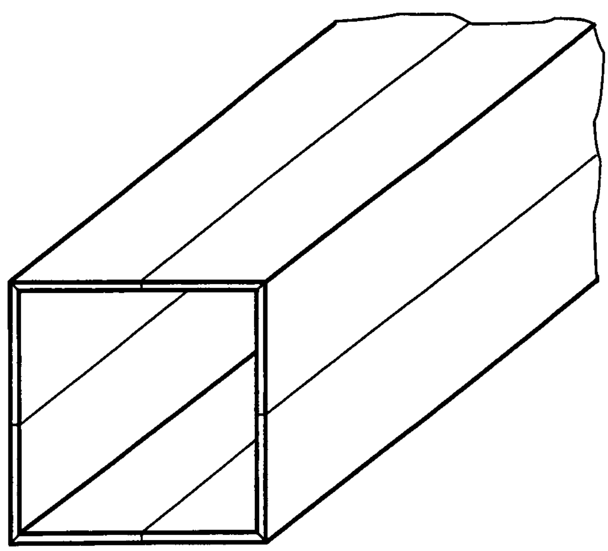

b) square hollow section

Figure 6.6 Finite strips subdivisions for members under pure compression

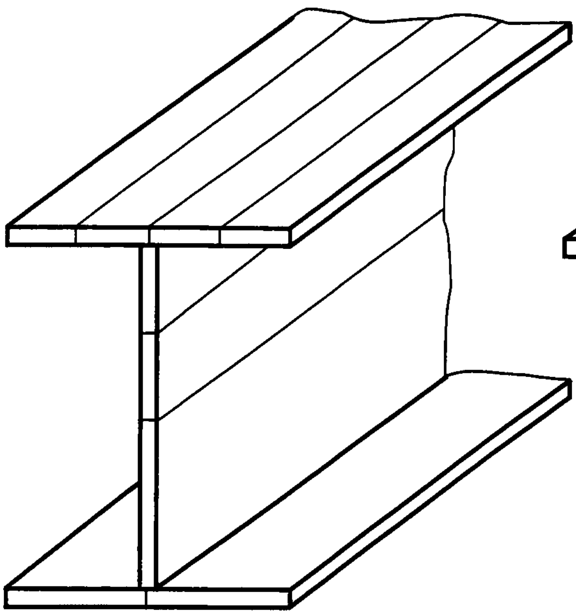

a) I - section

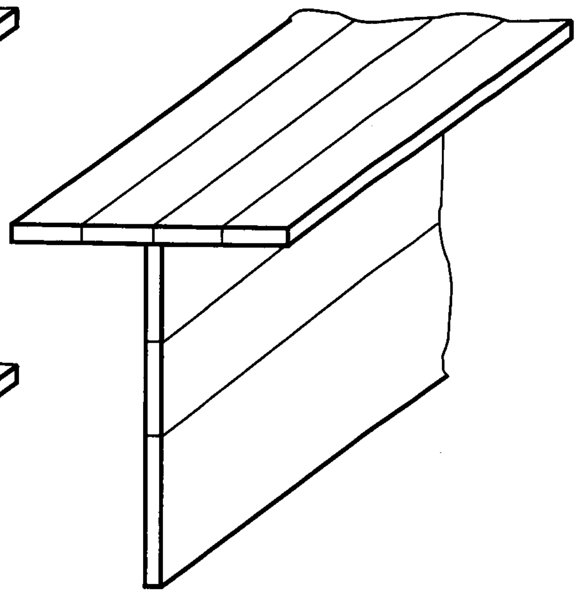

b) T - section

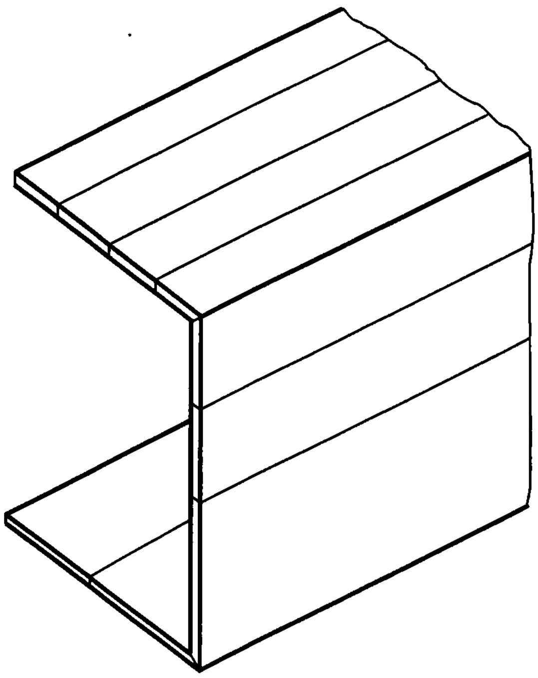

d) channel

Figure 6.7 Finite strips subdivisions for members under pure bending

Chapter 7

ELASTIC BUBBLE BASED SPLINE FINITE STRIP METHOD OF ANALYSIS

TABLE OF CONTENTS

7.1 INTRODUCTION

This chapter presents the development of a bubble-augmented spline finite strip method for the elastic buckling analysis of thin plates and assemblies of folded plates. The method admits local, distortional and lateral buckling modes. The usual cubic transverse variation of the buckling displacements is augmented with bubble terms that comprise of symmetric Legendre polynomials, while B_3-spline functions are used to represent the longitudinal variation of the buckling displacements. A new and simple method for the implementation of the longitudinal boundary conditions, including the incorporation of internal supports, is developed. Because the procedure follows that of standard displacement formulations, it is theoretically simple, and computer implementation of the method is straightforward since it does not require any amended schemes to handle the local splines that are needed near the boundaries or interior supports to represent particular boundary conditions. The accuracy and validity of the method are investigated through the analysis of a representative set of local and overall buckling problems, and the high degree of efficacy of the method is demonstrated.

In the subsequent sections, the strip formulation is discussed in detail, and numerical assessments of the method are carried out when applied to local, distortional and lateral buckling. The investigations include convergence studies with varying convergence criteria, strip subdivision of the structural topology and longitudinal subsections within the strips, so as to determine reliable convergence criteria and required discretisation for the elastic bubble augmented spline finite strip method. Following the convergence and accuracy studies, the method is then employed to study the local buckling behaviour of isolated plates with different boundary conditions and with the longitudinally applied stress varying in both transverse and longitudinal direction. In addition to the compression and bending, the plates are also subjected to equilibriating in-plane shear. The elastic buckling modes of a single span and two-span continuous composite tee-beam subjected to moment gradient are then investigated.

7.2 SPLINE FINITE STRIP METHOD OF ANALYSIS

The spline finite strip method possesses some of the advantages of both the semi-analytical finite strip method and the finite element method. It is similar to the semi-analytical method as the topology of the structure is still discretised into longitudinal strips and the rank of the problem is still reduced one-fold. However, the longitudinal harmonic series is replaced by a linear combination of local B_3-splines while still retaining the use of the transverse interpolation polynomials. Many undesirable features of the conventional finite strip method (Cheung 1976), such as its deficiency in handling concentrated loads, and its inability to allow for a variety of loading configurations (especially shear) and boundary conditions that were discussed in Chapter 6, were successfully overcome with the use of B_3-splines.

The spline finite strip method developed by Cheung *et al.* (1982) possesses some outstanding attributes. For example, the longitudinal variation of displacements in this method uses a series of B_3-splines that are simple piecewise cubic polynomials with C_2 continuity throughout, while for finite element interpolation, quintic polynomials are required to establish the same order of continuity. The use of the lower order polynomials in the spline interpolation simplifies the computation, reduces the risk of unstable calculations in the numerical algorithms and improves the poor approximation and loss of accuracy that sometimes occurs in higher order polynomial interpolation. To achieve the same continuity conditions for the conventional finite element treatment, it is necessary to have three times as many unknowns at the nodes (Zhu & Cheung 1989) and hence the number of freedoms in the finite element method may often be excessive. The ramifications of the large number of degrees of freedom in nonlinear finite element analysis can include both numerical instability and computational inefficiency.

Spline functions have been applied to the solution of a broad range of linear and nonlinear engineering problems. Notwithstanding the scope and efficiency of the spline finite strip, the main difficulty in its solution of nonlinear and some linear problems is even today the high computer cost, although the method is significantly superior to the finite element method in its computational efficiency. In the context of the spline finite strip method, the folded plate structure is discretised by using n strips along the x-axis and m sections along the y-axis, so that there are $n \times m$ subdomains and $(m+3) \times (n+1)$ nodes to be included in the computation. Because of this, the spline finite strip method requires many more degrees of freedom than the conventional harmonic based semi-analytical finite strip method, and this has detracted from its popularity in some applications. However, Azhari *et al.* (2000) included so-called bubble functions into the expressions for the transverse buckling displacements, and confirmed significant computational saving in this formulation of spline finite strip method could be achieved. Nevertheless, their study deals with plain and stiffened plates only, and does not consider plate assemblies such as I-sections and the like.

Another difficulty in the use of the spline finite strip method is the introduction of a complex amended scheme of local splines in the vicinity of the boundary supports and at any internal supports. Specifically, the incorporation of arbitrary boundary conditions within the procedure lacks a general formulation. A new theoretical model that is presented herein allows for node restraints to be defined and prescribed in much the same way as in a conventional finite element formulation.

7.3 METHOD OF ANALYSIS

7.3.1 General

In the bubble-based spline finite strip analysis, each component flat of the plate structure is treated as an assemblage of longitudinal strips subjected to membrane stresses σ_x, σ_y and τ_{xy}, as shown in Fig. 7.1. These are increased monotonically by a buckling load factor λ for a proportional loading scheme. The standard finite element techniques given in Zienkiewicz and Taylor (2000), which are based on the principle of minimum total potential energy, have been followed in this analysis in order to obtain flexural (F) and membrane (M) stiffness and stability matrices $\bar{k}_F, \bar{g}_F, \bar{k}_M, \bar{g}_M$ respectively, for the bubble based spline finite strip.

A thin walled folded-plate structural member is discretised transversely into a finite number of strips using n nodal lines, which are further partitioned longitudinally into m sections using $m+3$ section knots (Fig. 7.2), so that there are $n \times m$ subdomains. For a local buckling analysis, each section knot has two out-of-plane displacements (a flexural displacement and a rotation), two in-plane displacements (a transverse and a longitudinal displacement) and a single flexural bubble displacement intermediate to two section knots in the transverse direction. Consequently, the total number of degrees of freedom for a plate assembly is $(4n+ns) \times (m+3)$, where n and ns are the total number of nodal lines and finite strips, respectively, in a bubble based spline finite strip analysis.

7.3.2 B_3-Spline Function

The local buckling displacements are based on the summation of $m+3$ local B_3-splines by

$$\begin{aligned} f(x) &= \sum_{i=-1}^{m+1} \alpha_i \psi_i(x) \\ &= \alpha_{-1}\psi_{-1}(x) + \alpha_0\psi_0(x) + \alpha_1\psi_1(x) + \ldots + \alpha_i\psi_i(x) + \ldots + \alpha_{m+1}\psi_{m+1}(x) \end{aligned} \tag{7. 1}$$

where $\psi_i(x)$ represents a local B_3-spline and α_i are undetermined coefficients (Fig. 7.3).

The basic B_3-spline function is adopted here (Prenter 1975; de Boor 1978) because of its localised nature and hence its ability to reduce the computing time by bandwidth minimisation, which is illustrated schematically in Fig. 7.5. The length of the plate strip L is divided into m sections of equal length. A typical local B_3-spline function of equal length is defined as

$$\psi_i(x) = \frac{1}{6h^3} \begin{cases} 0, & x < x_{i-2} \\ (x - x_{i-2})^3 & x_{i-2} \le x \le x_{i-1} \\ h^3 + 3h^2(x - x_{i-1})^2 + 3h(x - x_{i-1})^2 - 3(x - x_{i-1}) & x_{i-1} \le x \le x_i \\ h^3 + 3h^2(x_{i+1} - x)^2 + 3h(x_{i+1} - x)^2 - 3(x_{i+1} - x) & x_i \le x \le x_{i+1} \\ (x_{i+2} - x)^3 & x_{i+1} \le x \le x_{i+2} \\ 0 & x_{i+2} \le x \end{cases} \tag{7. 2}$$

where $h = (x_{i-1} - x_{i-2}) = (x_i - x_{i-1}) = (x_{i+1} - x_i) = (x_{i+2} - x_{i+1})$.

Each of the local spline functions ψ_i has a non-zero value over four consecutive sections, with its centre at a section knot located at $x = x_i$. A linear combination of $m+3$

local B_3-splines is required longitudinally to fully define displacement functions for the strip (with m sections). The locations at x_{i-2}, x_{i-1}, x_i etc. are termed section knots. Figure 7.3 shows a single local function, while Fig. 7.4 shows the combination of local functions (with unit α_i) contributing to the variation of $f(x)$ in Eqn. 7.1. The values of the spline function $\psi_i(x)$ and its first and second derivatives at the section knots are well-known, and are given in Table 7.1.

7.3.3 Bubble Functions

In the usual finite strip methods, stiffness and stability matrices operate conventionally on nodal degrees of freedom that are necessary for the assembly of the strips for a given topology. A strip may have extra modes, that vanish on the boundaries, which represent additional strip degrees of freedom. These extra modes are called bubble functions and they are associated with internal or nodeless degrees of freedom, as shown in Fig. 7.6. By their nature, bubble modes have no effect on the displacements along the edges of a finite strip.

In order to generate the bubble augmentation of the conventional finite strip, a new set of transverse functions has been adopted in addition to the usual cubic function. The general polynomial bubble strip may contain symmetric and/or anti-symmetric bubble shapes. Since the buckling modes are generally symmetric for local buckling, greater accuracy is achieved by using symmetric bubble shapes. The general symmetric polynomial bubble displacement that belongs to the family of Legendre polynomials, N_5, can be expressed in terms of non-dimensional coordinates by

$$N_5 = \frac{A}{2^{2n}}\eta^n(1-\eta)^n \qquad n = 2,3,\ldots \tag{7. 3}$$

in which $\eta = y/b$ and where b is the width of the strip. The multiplier A in Eqn. 7.3 is arbitrary, since N_5 is associated with a degree of freedom, and is taken here without loss of generality to be unity.

7.4 DISPLACEMENTS

7.4.1 Flexural Displacements

The flexural displacement function w over the domain Ω for buckling displacements normal to the plane of a spline strip can be represented as the product of the B_3-spline functions with m+3 nodes in the x direction (the longitudinal direction) and conventional cubic beam functions augmented by the bubble function in the y direction (the transverse direction), that is

$$\begin{aligned} w &= \left(N_3\psi_{-1}\gamma_{-1} + N_3\psi_o\gamma_o + \ldots + N_3\psi_{m+1}\gamma_{m+1}\right)_i \\ &+ \left(N_4\psi_{-1}\delta_{-1} + N_4\psi_o\delta_o + \ldots + N_4\psi_{m+1}\delta_{m+1}\right)_i \\ &+ \left(N_3\psi_{-1}\gamma_{-1} + N_3\psi_o\gamma_o + \ldots + N_3\psi_{m+1}\gamma_{m+1}\right)_j \\ &+ \left(N_4\psi_{-1}\delta_{-1} + N_4\psi_o\delta_o + \ldots + N_4\psi_{m+1}\delta_{m+1}\right)_j \\ &+ \left(N_5\psi_{-1}\omega_{-1} + N_5\psi_o\omega_o + \ldots + N_5\psi_{m+1}\omega_{m+1}\right)_B \end{aligned} \tag{7. 4}$$

or more concisely in matrix format as

$$w = \lfloor\langle M_3\rangle\langle M_4\rangle\langle M_3\rangle\langle M_4\rangle\langle M_5\rangle\rfloor_F \langle \bar{\gamma}_i \quad \bar{\delta}_i \quad \bar{\gamma}_j \quad \bar{\delta}_j \quad \bar{\omega}_B\rangle^T \tag{7. 5}$$

where $\langle M_3\rangle = N_{3_{i,j}}\bar{\psi}_{\gamma_{i,j}}, \langle M_4\rangle = N_{4_{i,j}}\bar{\psi}_{\delta_{i,j}}$ and $\langle M_5\rangle = N_5\bar{\psi}_{\omega_B}$, in which the subscript F denotes flexural displacements, $N_{3i,j}$ and $N_{4i,j}$ are the transverse cubic functions of y given by

$$\begin{aligned} N_{3,i} &= 1 - 3\eta^2 + 2\eta^3 \\ N_{4,i} &= \eta\left(1 - 2\eta + \eta^2\right) \\ N_{3,j} &= 3\eta^2 - 2\eta^3 \\ N_{4,j} &= \eta\left(\eta^2 - 1\right) \end{aligned} \tag{7. 6}$$

and where N_5 is the bubble function defined in Eqn. 7.3. The subscripts i and j indicate a freedom that is evaluated at nodal lines i and j respectively. The vectors $\bar{\psi}_{\gamma i}, \bar{\psi}_{\delta i}, \bar{\psi}_{\gamma j}, \bar{\psi}_{\delta j}$ and $\bar{\psi}_{\omega B}$ are the B_3-spline representations for the displacement w and rotation θ of nodal lines i and j respectively, and the bubble displacement w_B is evaluated mid-way between two strip nodal lines, as depicted in Fig. 7.8.

In Eqn. 7.5, $\bar{\gamma}_i,...\bar{\delta}_j$ are vectors of displacement coefficients, and are defined as

$$\begin{aligned}
\bar{\gamma}_i &= \left\langle \gamma_{i-1}, \gamma_{i0}, \gamma_{i1} ..., \gamma_{i\,m-2}, \gamma_{i\,m-1}, \gamma_{i\,m}, \gamma_{i\,m+1} \right\rangle^T \\
\bar{\delta}_i &= \left\langle \delta_{i-1}, \delta_{i0}, \delta_{i1} ..., \delta_{i\,m-2}, \delta_{i\,m-1}, \delta_{i\,m}, \delta_{i\,m+1} \right\rangle^T \\
\bar{\gamma}_j &= \left\langle \gamma_{j-1}, \gamma_{j0}, \gamma_{j1} ..., \gamma_{j\,m-2}, \gamma_{j\,m-1}, \gamma_{j\,m}, \gamma_{j\,m+1} \right\rangle^T \\
\bar{\delta}_j &= \left\langle \delta_{j-1}, \delta_{j0}, \delta_{j1} ..., \delta_{j\,m-2}, \delta_{j\,m-1}, \delta_{j\,m}, \delta_{j\,m+1} \right\rangle^T
\end{aligned} \qquad (7.7)$$

and $\bar{\omega}_B$ is the vector of displacement coefficients related to the bubble functions and is given as

$$\bar{\omega}_B = \left\langle \omega_{B-1}, \omega_{B0}, \omega_{B1} ..., \omega_{B\,m-2}, \omega_{B\,m-1}, \omega_{B\,m}, \omega_{B\,m+1} \right\rangle^T . \qquad (7.8)$$

Since the displacement field of the present strip is expressed in terms of kernel or coefficient degrees of freedom, these degrees of freedom have to be transformed into nodal degrees of freedom defined at the section knots, prior to the assembly of the strips, in order to satisfy the compatibility and equilibrium conditions.

7.4.2 Membrane Displacements

The in-plane buckling displacement functions u and v of a spline strip are also expressed as the product of the transverse polynomials and longitudinal B_3-splines as

$$\begin{aligned}
u &= \left(N_1\psi_{-1}\alpha_{-1} + N_1\psi_o\alpha_o + ... + N_1\psi_{m+1}\alpha_{m+1}\right)_i \\
&\quad + \left(N_2\psi_{-1}\alpha_{-1} + N_2\psi_o\alpha_o + ... + N_2\psi_{m+1}\alpha_{m+1}\right)_j
\end{aligned} \qquad (7.9)$$

$$\begin{aligned}
v &= \left(N_1\psi_{-1}\beta_{-1} + N_1\psi_o\beta_o + ... + N_1\psi_{m+1}\beta_{m+1}\right)_i \\
&\quad + \left(N_2\psi_{-1}\beta_{-1} + N_2\psi_o\beta_o + ... + N_2\psi_{m+1}\beta_{m+1}\right)_j .
\end{aligned} \qquad (7.10)$$

These displacements have the kernel coefficients

$$\begin{aligned}
\bar{\alpha}_i &= \left\langle \alpha_{i-1}, \alpha_{i0}, \alpha_{i1} ..., \alpha_{i\,m-2}, \alpha_{i\,m-1}, \alpha_{i\,m}, \alpha_{i\,m+1} \right\rangle^T \\
\bar{\alpha}_j &= \left\langle \alpha_{j-1}, \alpha_{j0}, \alpha_{j1} ..., \alpha_{j\,m-2}, \alpha_{j\,m-1}, \alpha_{j\,m}, \alpha_{j\,m+1} \right\rangle^T
\end{aligned} \qquad (7.11)$$

and

$$\vec{\beta}_i = \langle \beta_{i-1}, \beta_{i0}, \beta_{i1} ..., \beta_{i\,m-2}, \beta_{i\,m-1}, \beta_{i\,m}, \beta_{i\,m+1} \rangle^T$$
$$\vec{\beta}_j = \langle \beta_{j-1}, \beta_{j0}, \beta_{j1} ..., \beta_{j\,m-2}, \beta_{j\,m-1}, \beta_{j\,m}, \beta_{j\,m+1} \rangle^T \tag{7. 12}$$

respectively, so that there are $4(m+3)$ freedoms associated with defining u and v. Equation 7.9 can be written more concisely in matrix format as

$$u = \lfloor \langle M \rangle_1, \langle M \rangle_2 \rfloor_M \langle \vec{\alpha}_i \quad \vec{\alpha}_j \rangle^T \tag{7. 13}$$

and Eqn. 7.10 can be written similarly as

$$v = \lfloor \langle M \rangle_1, \langle M \rangle_2 \rfloor_M \langle \vec{\beta}_i \quad \vec{\beta}_j \rangle^T \tag{7. 14}$$

in which the subscript M denotes membrane displacements and where

$$\langle M \rangle_1 = \langle N_1 \psi_{-1}, N_1 \psi_o, N_1 \psi_1, ..., N_1 \psi_{m+1} \rangle$$
$$\langle M \rangle_2 = \langle N_2 \psi_{-1}, N_2 \psi_o, N_2 \psi_1, ..., N_2 \psi_{m+1} \rangle \tag{7. 15}$$

$N_1 = (1-\eta)$ and $N_2 = \eta$ are the linear transverse interpolation polynomials which are the same as those used in the semi-analytical finite strip method, and which do not include a Legendre bubble polynomial. Each of the vectors $\bar{\psi}_{\gamma i}, \bar{\psi}_{\delta i}, \bar{\psi}_{\gamma j}, \bar{\psi}_{\delta j}$ and $\bar{\psi}_{\omega B}$ has $m+3$ local B_3-splines as defined in Eqn. 7.1, while $\vec{\alpha}_i, .., \vec{\beta}_j$ are the vectors of displacement coefficients also corresponding to α_i in Eqn. 7.1. The boundary conditions for the membrane displacements of a strip are slightly different from those for the flexural displacements, and they are specified in Table 7.2.

7.4.3 Modification for Boundary and Interior Supports

When the membrane displacement functions u and v are included with the flexural deformations, the vector of strip displacement coefficients can be defined as

$$\vec{\Delta}_s = \langle \alpha_i \quad \beta_i \quad \gamma_i \quad \delta_i \quad \omega_B \quad \alpha_j \quad \beta_j \quad \gamma_j \quad \delta_j \rangle^T \tag{7. 16}$$

or as

$$\bar{\Delta}_s = \left\langle \bar{\Delta}_{si}\, \bar{\Delta}_B\, \bar{\Delta}_{sj} \right\rangle^T . \tag{7. 17}$$

The vector $\bar{\Delta}_s$ contains freedoms that must necessarily lie outside of the ends of the strip due to the specification of spline functions near these ends, but these freedoms can be evaluated simply by specifying the buckling freedoms at each end of the strip only. Consider, for example the vector $\bar{\alpha}_i$. The displacement u is defined from

$$\bar{u}^*{}_i = \bar{T}^* \bar{\alpha}_i \tag{7. 18}$$

where

$$\bar{u}^*{}_i = \left\{ u_0', u_0, u_1, u_2, .., u_{m-1}, u_m, u_m' \right\}_i \tag{7. 19}$$

in which a prime denotes differentiation with respect to x, and where $\bar{T}^*$ is the $(m+3) \times (m+3)$ matrix given as

$$\bar{T}^* = \begin{bmatrix} \frac{-1}{2h} & 0 & \frac{1}{2h} & & & & \\ \frac{1}{6} & \frac{2}{3} & \frac{1}{6} & & zero & & \\ & \frac{1}{6} & \frac{2}{3} & \frac{1}{6} & & & \\ & & \cdots & \cdots & \cdots & & \\ & & & \frac{1}{6} & \frac{2}{3} & \frac{1}{6} & \\ & zero & & & \frac{1}{6} & \frac{2}{3} & \frac{1}{6} \\ & & & & \frac{-1}{2h} & 0 & \frac{1}{2h} \end{bmatrix} . \tag{7. 20}$$

Instead of defining cumbersomely the spline coefficients α_0 and α_m at the ends of the strip, and α_{-1} and α_{m+1} outside of the strip, the displacement and rotation freedoms can be used at the ends, ie. u_0, u_0' (x=0) and u_L, u_L' (x=L). Within the strip, there are m-1 interior or kernel displacement coefficients that are also transformed in the vector of nodal (knot) degrees of freedom, ie. u_1, u_2,..,u_m, u_{m-1}. In this way displacement coefficients are transformed into actual physical freedoms. These can be easily specified as in conventional finite element programs as either fixed or free, and eliminated within the program appropriately. This can also be done in the same fashion for the freedoms associated with v, w, θ and w_B. Hence the transformation given by

$$\vec{\Delta}^{*} = \lfloor \bar{T}^{*} \quad \bar{T}^{*} \quad \bar{T}^{*} \quad \bar{T}^{*} \quad \bar{T}^{*} \quad \bar{T}^{*} \quad \bar{T}^{*} \quad \bar{T}^{*} \quad \bar{T}^{*} \rfloor \vec{\Delta}_s \tag{7.21}$$

or

$$\vec{\Delta}_s = \bar{T}^{-1}\vec{\Delta}^{*} \tag{7.22}$$

may be effected, where the $9(m+3)$ by 1 column vector contains the freedoms specified for both nodal lines (i and j) and for u, v and w and θ and their slopes with respect to x, for each section knot. Consequently, Eqns. 7.5, 7.13 and 7.14 can be then combined into matrix format as

$$\vec{u} = \langle u \quad v \quad w \rangle^{T} = \bar{\psi}\vec{\Delta}_s \tag{7.23}$$

where $\bar{\psi}$ is the interpolation polynomial matrix given as

$$\bar{\psi} = \begin{bmatrix} \langle M \rangle_1 & & & & & \langle M \rangle_2 & & & \\ & \langle M \rangle_1 & & & & & \langle M \rangle_2 & & \\ & & \langle M \rangle_3 & \langle M \rangle_4 & \langle M \rangle_5 & & & \langle M \rangle_3 & \langle M \rangle_4 \end{bmatrix}. \tag{7.24}$$

Eqn. 7.13 can thus be written concisely as

$$\vec{u} = \bar{\psi}\bar{T}^{-1}\vec{\Delta}^{*}. \tag{7.25}$$

The vector $\vec{\Delta}^{*}$ contains the freedoms that may be prescribed as, say, $0 \equiv$ fixed or $1 \equiv$ free accordingly, as in conventional finite element formulations. Constraint conditions within the strip, as shown in Fig. 7.9, as well as at the ends can then be easily invoked.

7.4.4 Flexural Stiffness and Stability Matrices

The flexural strain energy of a plate strip resulting from buckling deformation U_F is given by the familiar expression

$$U_F = \int_V \vec{\sigma}_F^T \vec{\varepsilon}_F \mathrm{d}V \tag{7.26}$$

where V is the volume of the strip and $\vec{\sigma}_F$ and $\vec{\varepsilon}_F$ are the vectors of the generalised internal moments and infinitesimal buckling curvatures respectively. These are given by the well-known expressions

$$\vec{\sigma}_F = \langle M_x, M_y, M_{xy} \rangle^T \tag{7.27}$$

and

$$\vec{\varepsilon}_F = \langle \rho_x, \rho_y, \rho_{xy} \rangle^T \tag{7.28}$$

in which

$$\rho_x = w,_{xx}^2, \ \rho_y = w,_{yy}^2, \ \rho_{xy} = -2w,_{xy}^2. \tag{7.29}$$

In Eqn. 7.27, M_x, M_y and M_{xy} are the bending moments and twisting moment per unit width of the plate shown in Fig. 7.10, resulting from the plate flexural buckling deformations. Upon differentiating Eqn. 7.4, $\vec{\varepsilon}_F$ may be written as

$$\vec{\varepsilon}_F = \overline{B}_F \vec{\delta}_F \tag{7.30}$$

where $\overline{B}_F$ is a flexural strain matrix obtained by appropriate differentiation of Eqn. 7.4 using Eqn. 7.29, and $\vec{\delta}_F$ is a vector of flexural strip degrees of freedom. The property matrix $\overline{D}_F$, based on the orthotropic plate theory derived by Timoshenko and Woinowsky-Krieger (1959), is represented by

$$\vec{\sigma}_F = \overline{D}_F \vec{\varepsilon}_F \tag{7.31}$$

where

$$\overline{D}_F = \begin{bmatrix} D_1 & D_2 & 0 \\ D_3 & D_4 & 0 \\ 0 & 0 & D_9 \end{bmatrix} \tag{7.32}$$

$$D_1 = D_4 = \frac{\nu E t^3}{12(1-\nu^2)}, \qquad D_2 = D_3 = \frac{E t^3}{12(1-\nu^2)}, \qquad D_9 = \frac{G t^3}{12} \tag{7. 33}$$

in which E, ν and G are the appropriate isotropic elastic material properties, and t is the thickness of the plate.

The total strain energy of the strip associated with flexural buckling can thus be expressed in the form

$$U_F = \frac{1}{2} \bar{\delta}_F{}^T \bar{k}_F \bar{\delta}_F \tag{7. 34}$$

in which $\bar{k}_F$ is the flexural stiffness matrix which may be obtained from

$$\bar{k}_F = \int_V \bar{B}_F{}^T \bar{D}_F \bar{B}_F \mathrm{d}V \,. \tag{7. 35}$$

The increase in potential energy of the in-plane stresses resulting from the flexural buckling deformations is chosen to be the same as that employed by Plank and Wittrick (1974), and is given by

$$V_F = -\frac{1}{2} \lambda \int_0^L \int_0^b \left\{ \sigma_x (w,_x)^2 + \sigma_y (w,_y)^2 + 2\tau (w,_x)(w,_y) \right\} t \,\mathrm{d}\,y \,\mathrm{d}\,x \tag{7. 36}$$

where

$$\sigma_x = \sigma_1 + (\sigma_2 - \sigma_1)\eta \tag{7. 37}$$

is the linear stress variation across the strip ends and λ is the buckling load factor under proportional loading. Hence by appropriate substitution, the stability matrix may be obtained by

$$V_F = -\frac{1}{2} \bar{\delta}_F{}^T \lambda \bar{g}_F \bar{\delta}_F \tag{7. 38}$$

where

$$\bar{g}_F = \bar{g}_{F1} + \bar{g}_{F2} + \bar{g}_{F3} \tag{7.39}$$

$$\bar{g}_{F1} = \int_V \left(\bar{\psi},_x \bar{N}_F{}^T\right)\sigma_x\left(\bar{N}_F\bar{\psi},_x^T\right)\mathrm{d}V$$

$$\bar{g}_{F2} = \int_V \left(\bar{\psi}\bar{N}_F,_y{}^T\right)\sigma_y\left(\bar{N}_F,_y\bar{\psi}^T\right)\mathrm{d}V \tag{7.40}$$

$$\bar{g}_{F3} = \int_V \left(\bar{\psi}\bar{N}_F,_y{}^T\right)2\tau\left(\bar{N}_F\bar{\psi},_x^T\right)\mathrm{d}V$$

in which $\bar{N}_F = \langle N_1, \ldots, N_4, N_s\rangle^T$. The three components of the matrix $\bar{g}_F$ in Eqn. 7.40 contain contributions from the longitudinal compressive stress, transverse compressive stress and shear stress respectively. The elements of these matrices, before the appropriate integration has been performed, are given in Appendix 7.10.

7.4.5 Membrane Stiffness and Stability Matrices

In the method presented by Azhari *et al.* (2000), linear interpolation polynomials are assumed in the transverse direction, so that the membrane buckling displacements do not need to utilise the bubble polynomial. Because of this, the membrane stiffness and stability matrices for a spline strip are the same as those presented by Lau and Hancock (1986). The derivation of the membrane stiffness and stability matrices is based on the same principles as those applied for the flexural deformations described in the previous paragraphs.

The membrane strain energy, U_M, of a plate strip resulting from the buckling deformations is given by

$$U_M = \frac{1}{2}\int_0^L\int_0^b \bar{\sigma}_M^T\,\bar{\varepsilon}_M\,t\,\mathrm{d}y\,\mathrm{d}x \tag{7.41}$$

where

$$\bar{\sigma}_M = \langle \sigma_x \quad \sigma_y \quad \tau_{xy}\rangle^T \tag{7.42}$$

$$\bar{\varepsilon}_M = \langle u,_x \quad v,_y \quad u,_y + v,_x \rangle^T \tag{7.43}$$

in which σ_x, σ_y and τ_{xy} are the infinitesimal buckling membrane stresses, as shown in Fig. 7.11, resulting from in-plane buckling deformations. The vector $\bar{\sigma}_M$ can be related to the vector $\bar{\varepsilon}_M$ by

$$\langle \sigma_x \quad \sigma_y \quad \tau_{xy} \rangle^T = \begin{bmatrix} S_1 & S_2 & 0 \\ S_3 & S_4 & 0 \\ 0 & 0 & S_9 \end{bmatrix} \langle u,_x \quad v,_y \quad u,_y + v,_x \rangle^T \tag{7.44}$$

where

$$S_1 = \frac{E_x}{(1 - \nu_x \nu_y)}, \quad S_4 = \frac{E_y}{(1 - \nu_x \nu_y)}, \quad S_2 = S_3 = \nu_x S_1, \quad S_9 = G. \tag{7.45}$$

Eqn. 7.44 can be expressed as

$$\bar{\sigma}_M = \overline{D}_M \bar{\varepsilon}_M \tag{7.46}$$

where $\overline{D}_M$ is the property matrix appropriate for membrane displacements.

The increase in the potential energy of the membrane forces resulting from in-plane buckling deformations was derived by Plank and Wittrick (1974) to be

$$V_M = -\frac{1}{2} \lambda \int_0^L \int_0^b \sigma_x \left\{ (u,_x)^2 + (v,_x)^2 \right\} t \, \mathrm{d}y \, \mathrm{d}x. \tag{7.47}$$

As stated by Plank and Wittrick, there appear to be no in-plane destabilising effects resulting from the stresses σ_y and τ and so they have been ignored in the above equation.

The integrations in Eqns. 7.26, 7.36, 7.41 and 7.47 are carried out herein using four-point Gaussian quadrature, and the elements of the membrane stiffness and stability matrices prior to integration are given in Appendix 7.10.

7.5 TRANSFORMATION TO GLOBAL COORDINATES

The stiffness and stability matrices described in the previous sections were derived in a local coordinate system. Transformation to a global coordinate system is necessary when two adjoining plate strips have different orientations. A plate strip inclined at an angle β to the global axes is shown in Fig. 7.12.

The deformations in the local axis system $\bar{\delta}$ are related to those in the global axes $\bar{\Delta}$ by

$$\bar{\delta} = \bar{R}\bar{\Delta} \tag{7.48}$$

where

$$\begin{aligned} \bar{\delta} &= \langle \bar{u}_i \quad \bar{v}_i \quad \bar{w}_i \quad \bar{\theta}_i \quad \bar{w}_B \quad \bar{u}_j \quad \bar{v}_j \quad \bar{w}_j \quad \bar{\theta}_j \rangle^T \\ \bar{\Delta} &= \langle \bar{U}_i \quad \bar{V}_i \quad \bar{W}_i \quad \bar{\Theta}_i \quad \bar{W}_B \quad \bar{U}_j \quad \bar{V}_j \quad \bar{W}_j \quad \bar{\Theta}_j \rangle^T \end{aligned} \tag{7.49}$$

and where

$$\bar{R} = \begin{bmatrix} \bar{r} & & \\ & \bar{I} & \\ & & \bar{r} \end{bmatrix} \tag{7.50}$$

in which

$$\bar{r} = \begin{bmatrix} \bar{I} & & & \\ & \bar{I}\cos\beta & \bar{I}\sin\beta & \\ & -\bar{I}\sin\beta & \bar{I}\cos\beta & \\ & & & \bar{I} \end{bmatrix} \tag{7.51}$$

and $\bar{I}$ is an identity matrix of size $m3 \times m3$. The strip stiffness and stability matrices, $\bar{k}$ and $\bar{g}$ respectively, can be transformed to the global coordinate system according to the principle of contragredience by

$$\begin{aligned} \bar{K} &= \bar{R}^T \bar{k} \bar{R} \\ \bar{G} &= \bar{R}^T \bar{g} \bar{R} \end{aligned} \tag{7.52}$$

where $\overline{K}$ and $\overline{G}$ are the global stiffness and stability matrices, respectively.

7.6 SOLUTION OF BUCKLING EQUATION

The total potential energy of a deformed structure, Π, under a conservative load system is composed of the internal strain energy U and the potential energy V of the loads. Thus

$$\Pi = U + V \tag{7. 53}$$

or

$$\Pi = \frac{1}{2}\bar{\Delta}^T\left[\overline{K} - \lambda\overline{G}\right]\bar{\Delta}. \tag{7. 54}$$

The principle of minimum total potential energy requires that the first variation of the total potential $\delta\Pi$ vanishes, that is

$$\delta\Pi = \frac{\partial\Pi}{\partial\bar{\Delta}}\delta\bar{\Delta} = 0 \qquad \forall \;\; \delta\bar{\Delta} \tag{7. 55}$$

so that for any arbitrary variation $\delta\bar{\Delta}$ of the buckling deformations,

$$\left[\overline{K} - \lambda\overline{G}\right]\bar{\Delta} = \bar{0}. \tag{7. 56}$$

Bifurcation from the primary equilibrium path occurs when

$$\left|\overline{K} - \lambda\overline{G}\right| = 0 \tag{7. 57}$$

which is the familiar linear buckling eigenproblem. The buckling load is given by the eigenvalue, λ, while the buckling modes are described by the eigenvector $\bar{\Delta}$. In lieu of subroutines in software libraries, an algorithm based on the Sturm sequence property (Garbow *et al.* 1977) and which has proved successful in computing eigenvalues and eigenvectors for many structural problems, has been employed in this analysis.

7.7 CONVERGENCE AND ACCURACY OF SOLUTION

7.7.1 General

In order to assess the performance and efficacy of the new spline finite strip formulation, a number of numerical examples are presented here. These examples consider local and overall buckling, and include the usual documented problem of square and rectangular plates, and plate assemblies. The analysis of square plates is fundamental to all plate compression/bending/shear finite strips. The analytical solutions for a square plate subjected to various types of loading and with various boundary conditions are readily available (Timoshenko & Gere 1970; Allen & Bulson 1980). Although the problems of square plates do not present any specific difficulty with finite strips, the results obtained usually demonstrate the general accuracy and convergence characteristics of the strip, and they also provide a basis of comparison between different strips. Comparisons of the results with theoretical solutions and those of other finite strip analyses have been made to demonstrate the efficiency and accuracy of the present method.

In the present study, square plates with both simply supported and clamped edges and combinations of these have been analysed. Examples of the accuracy of the method, with increasing numbers of spline sections lengthwise, are presented for plates of finite length subjected to compression, bending and shear. The method is also applied to a square stiffened plate subjected to combined compression and shear, and to a rectangular plate with internal supports. The accuracy of the numerical solutions is governed by a number of factors including the number of strips in the transverse direction and the number of subsections in the longitudinal direction. For the present study, the values of Young's modulus and Poisson's ratio have been adopted as 200 GPa and 0.3 respectively.

7.7.2 Square and Rectangular Plates

Plates with simply supported edges subjected to uniform and biaxial compression, bending and shear are shown in Fig. 7.13, while plates with simply supported, clamped and combined boundary conditions, are shown in Fig. 7.14. The local buckling coefficients k given by (Allen & Bulson 1980)

$$k = \sigma_{cr} \frac{12(1-\nu^2)}{\pi^2 E}\left(\frac{b}{t}\right)^2 \tag{7. 58}$$

and computed using the spline finite strip buckling analysis are summarised in Tables 7.3-7.10, where they are compared with the theoretical values (Timoshenko & Gere 1970; Allen & Bulson 1980; Stroud & Anderson 1980; Tham & Szeto 1990; Azhari 1993; Saadatpour *et al.* 1998; Bedair 1997a, Bedair 1997b; Azhari *et al.* 2000). The aspect ratios of the plates studied are also included in the tables.

The plates were each subdivided into a number of longitudinal strips (1, 2 or 3 strips) of equal width for the analysis. For the case of uniaxial compression, the errors are in general less than 0.1% when four spline sections and two strips are used for the simply supported plates, and less than 0.3% when four spline sections and two strips are used for the clamped plate, as shown in Table 7.3. A similar trend is evident for the case of biaxial compression, given in Table 7.4, where only four spline sections and two strips are required to achieve an error less than 0.05%. For the case of shear, the convergence is slower and three spline strips with ten sections are generally required to achieve an error less than 0.5%, as shown in Tables 7.5 and 7.6.

Convergence studies of plates in longitudinal compression, with simply supported and clamped edges, such that three local buckle half-waves formed along the length, showed that five and eight spline sections respectively produced buckling loads with an error of less than 1%. For a simply supported plate in shear with four local buckle half-waves, ten spline sections longitudinally (and three strips) were required to achieve an error of less than 1%.

7.7.3 Stiffened Plates

In many structural engineering applications, the plates are large and slender. Longitudinal stiffeners are then provided primarily to carry part of the compressive force proportional to its area and to reduce the effective width to thickness ratio of the thin plate element, thus increasing its buckling strength. Even in the ultimate limit state design of stiffened plates, the information on the buckling coefficient as well as the optimum rigidity of the stiffener (maximum buckling strength with the smallest stiffener dimensions) is generally needed.

Figures 7.15 and 7.16 show the geometry of a square stiffened panel, simply supported along four edges with one and two longitudinal stiffeners respectively. For the purpose of this investigation the plates were subjected to uniaxial compressive stress, transverse stress and combinations of these. Further, for the case where only one longitudinal stiffener is used, two strips were employed to model the plate, while for the case shown in Fig. 7.16, three strips were utilised. The longitudinal stiffener was modelled by restraining the horizontal, transverse and vertical displacements for the specified nodal line. In this way it is assumed that the stiffener is rigid enough to divide the plate into two and three equal sub-plates respectively.

The solutions for such configurations are readily available (Timoshenko & Gere 1970; Bedair 1997a), and the comparisons with the current method are shown in Table 7.9. The relative percentage difference is calculated as the difference between the buckling coefficient k derived by this method and the k factor given by specified researcher which was nearest to the converged value obtained from the present method. Note that in Table 7.6, this difference is provided for each k factor published elsewhere since only one converged value derived by present analysis is tabulated. These comparisons indicate that when six sections are used the error is less than 0.4% while with ten sections the error is reduced below 0.1%. It is worthwhile nothing that the k factors given by Bedair (1997a) and Timoshenko and Gere (1970) in Tables 7.9 and 7.10 are to two decimal point figures and the comparisons with the k factors obtained by the present method, which have been rounded to four significant figures, might not be precise.

Figure 7.17 illustrates the plate originally analysed by Stroud *et al.* (1980, 1981) using the finite element program EAL and the VIPASA program, which is a smeared stiffener approach. They discretised the plate into 1296 elements with approximately 8000 degrees of freedom, and concluded that the results of the EAL software are the most satisfactory for the general situation. Lau and Hancock (1986), Bedair (1997a) and Azhari *et al.* (2000) have also considered this example as a benchmark with which to verify their models. The numerical analyses carried out in this chapter produced good agreement with the published results, as shown in Fig. 7.18. For the current analysis, one bubble strip was used for the stiffened panel between the stiffeners, and one strip for each stiffener. It was sufficient to use six to eight sections for the buckling load to converge. Therefore, the number of degrees of freedom is approximately 10% of that required by the finite element method.

7.7.4 Rectangular Plates with Internal Supports

The previous section dealt with stiffeners that are oriented longitudinally and their inclusion is straightforward. Adding the stiffeners in the transverse direction in the conventional spline finite strip method requires a complex amended scheme to be introduced. However, the method developed in this study allows for transverse stiffeners to be incorporated in the same way as for the longitudinal direction by simply restraining the displacements of relevant section knots. In this chapter, the internal support that represents the rigid transverse stiffener, was modelled as a simple line support.

Figures 7.19 and 7.20 show a simply supported plate with internal supports that divide the plate into two and three sub-plates respectively, while Fig. 7.21 shows the geometry of a plate simply supported along four edges and stiffened in both the longitudinal and transverse direction. The stiffeners and internal supports in this case divide the plate into nine sub-plates, each with an aspect ratio of unity. The local buckling coefficients k for these geometrical and loading configurations are compared in Table 7.10 with those reported by Bedair (1997b) and Timoshenko and Gere (1970). For the case depicted in Fig. 7.19 the k factor equals 16.0, which corresponds to that for a square sub-plate of width $b/2$ in Eqn. 7.58 and with a local buckling coefficient of 4.0. The buckling coefficient k for the plate shown in Fig. 7.21 and subjected to uniaxial stress only is obtained from that for a sub-plate of width $b/3$ in Eqn. 7.58 and with a local buckling coefficient of 4.0, so that the k factor is $4.0 \times 3 \times 3 = 36.0$. Similarly, for the case in Fig. 7.21 subjected to biaxial stresses (σ_x/σ_y = 1), the k factor is 18.0, which is $3 \times 3 = 9$ times the k factor of 2.0 of the unstiffened plate, as shown in Tables 7.4 and 7.10.

These numerical assessments have demonstrated that in general it is sufficient to use two strips for the plate with one longitudinal stiffener and three strips for the case where two stiffeners are utilised. It is evident from Table 7.10 that in general six sections result in an error less of than 0.1%.

7.7.5 Plate Assemblies

The accuarcy of the method when applied to plate assemblies was demonstrated by studying a T-section in uniform compression with different flange to thickness ratios. In this example, the method is compared in Fig. 7.22 with the results produced by the bubble augmented semi-analytical finite strip analysis, developed and verified extensively in Chapter 6 of this thesis. The T-sections were subdivided in 4 strips, two in the web and two in the flange. The first mode buckling solution of the semi-analytical solution is given in Fig. 7.22, and the spline analysis represents the locus of the lower bounds of the multiple harmonic solution. For clarity, only the first buckling mode of the harmonic semi-analytical solution is shown in Fig. 7.22. The maximum difference between the solutions obtained by the two methods is less than 0.1%.

7.8 NUMERICAL STUDIES

7.8.1 Plates

In circumstances where structures are subjected to combined compressive, bending and shear stresses, there is a requirement in the design process to predict the critical level of these stresses at which buckling will occur. In this study, the local buckling coefficient, k is derived for isolated plates with various boundary conditions and with the end compression (σ_x) varying in the direction of loading (longitudinally) and equilibrated by shear stress, τ along the longitudinal edges. These sorts of stress condition are also found in the skin of an aeroplane wing in bending, and a solution was first formulated by Libove *et al.* (1949) for simply supported plates of uniform thickness. The variation of the end stress, σ_x in the transverse direction is shown in Fig. 7.23, where the stress gradient α varies between 0 and 0.8. The local buckling coefficient, k is plotted on a logorithmic scale versus the plate aspect ratio, L/b for ten different loading configurations, tabulated in Fig. 7.24 as Cases 1-10, which define the stress gradient in longitudinal direction.

Figures 7.25-7.28 show the local buckling coefficients of plates with the in-plane boundary conditions in the sequence of left, bottom, right and top, simply represented as 's-f-s-s', 's-f-s-c', 'c-f-c-s' and 'c-f-c-c'. These types of boundary conditions simulate the framing of the free flange outstand into the web, where one of the longitudinal edges (bottom) is free, and the loaded edges (left and right) are either simply supported (Figs. 7.25-7.26) or clamped (Figs. 7.27-7.28). For the purpose of this study the plates are subjected to uniform end compressive stress (σ_x), which is a typical state of stress in the flange outstand of an I-section loaded either in compression, bending or a combination of the two. The local buckling coefficient is plotted against the plate aspect ratio, L/b for Cases 1-10. The aspect ratio was varied by changing the length of the plate. Figures 7.25-7.28 indicate that, in general, a decrease of plate aspect ratio increases the plate capacity. Buckling modes for those loading configurations are shown in Figs. 7.29-7.32.

Figures 7.33-7.35 show the variation of the local buckling coefficient versus aspect ratio of plates with boundary conditions defined as 's-s-s-s', 's-c-s-c' and 'c-c-c-c'. These types of boundary conditions simulate the framing of the web plate into the flanges. In reality, the conditions of restraint imposed on the web by the flanges vary between simply supported and clamped. Accordingly, the buckling coefficients for real I-section beams are bounded by the simply-supported and clamped curves. Two different loading combinations are considred herein: i) longitudinally varying end stress, σ_x (Cases 1-10) equilibrated by shear stress, τ along the longitudinal edges; and ii) uniform transverse stress, σ_y in addition to longitudinally varying end stress, σ_x, and equilibrium shear along the longitudinal edges. Furthermore, in addition to the stress gradient in the longitudinal direction, the end stress, σ_x is also varied in its transverse direction, as shown in Fig. 7.23, where the stress gradient parameter α ranges from 0 to 0.8. Thus, the results given in the figures need careful interpretation for loading configurations where the positive bending moment changes into a negative bending moment (ie. Case 7 or 8) as this reverses the distribution of tensile and compressive stresses along the plate width. Figures 7.33-7.35 show that loaded edge's boundary conditions affect significantly the local buckling coefficient, especially so when the uniform transverse stress, σ_y is included. It is, however, important to note that the occurrence of elastic local buckling does not represent a true strength limit state, since the webs of plate girders exhibit a significant postbuckling reserve of strength (Trahair & Bradford 1998). Buckling modes for selected loading configurations (Case 2, 6, 8 and 10) are plotted in Figs. 7.36-7.43.

Figures 7.44 and 7.45 show the variation of the local buckling coefficient against the aspect ratio of plates with boundary conditions given as 'c-c-f-c' and 'c-s-f-s' for the loading configuration defined as Case 4, 6, 7 and 8. These types of boundary conditions replicate the framing of the web plate into the flanges in cantilever beams with one loaded edge free. The plotted curves are of similar trend for all loading configurations considered with the minimum occuring at the aspect ratio of 0.5, except for the Case 7 in Fig. 7.45 where the minimum is at L/b of 1.0. Buckling modes for Cases 4 and 6 are plotted in Figs. 7.46-7.49 respectively.

Figures 7.50 and 7.51 show the variation of the local buckling coefficient against the aspect ratio of plates with boundary conditions given as 'c-s-s-s' and 's-c-c-c' for the loading configuration given as Cases 4, 7 and 8. The boundary conditions for this type represent the framing of the web plate into the flanges in propped cantilever beams, in which one of the loaded edges is clamped and another is free. As the figures show, for plates with L/b less than 1.0, the boundary conditions for loaded edges have significant effects on the buckling stress. However, for long plates the boundary conditions for the loaded edges have a minor effect on the buckling stress. Buckling modes for Cases 7 and 8 are plotted in Figs. 7.52-7.55 respectively.

7.8.2 Composite T-section beams

Composite bridge girders with a fabricated joist are not always compact, due to the difficulty in controlling the slenderness of a thin web when the neutral axis is positioned reasonably close to the top/tension flange. Local buckling, which will occur prior to attainment of the full plastic moment in hogging, will clearly be of importance for such fabricated girders. There is both experimental evidence (Hope-Gill & Johnson 1976) and theoretical evidence (Bradford & Johnson 1987) that local buckling will procede lateral-distortional buckling in many composite tee-beams subjected to negative moment. Test results reported by Loh *et al.* (2004), and by others (Climenhaga & Johnson 1972; Johnson & Fan 1991; Johnson & Chen 1993), also confirm that local buckling of the bottom flange is important in semi-continuous composite joints in building. When the component flats of plate assemblies are subjected to in-plane shear in addition to compression and bending, the concept of a local buckling mode in which the line junctions remain straight is still a valid one. However, with shear present, there are no cross-sections that remain undistorted (Wittrick *et al.* 1968; Azhari 1993). There are a number of instances of local instability under combined loading. When the shear loading is combined with large bending moments, such as that which occurs at the internal supports of beams, the strength of the web in shear will be reduced. This reduction is normally represented by an interaction diagram which indicates the combination of bending stresses and shear stresses. Azhari and Bradford (1993) obtained the interaction buckling curves for bending and shear stress for different positions of the neutral axis. Their study showed that the interaction between bending and shear was close to circular, while that between compression and shear is close to parabolic and was independent of the position of the longitudinal stiffener.

The bubble augmented spline finite strip buckling analysis, developed in this chapter, has been applied to study the buckling modes of a single span and two span composite T-section beams subjected to moment gradient. For this study, the beams were subdivided into six strips (two in the web, two in the compression flange, and two in the tension flange). For the analysis, it was assumed that the shear stresses are carried entirely by the steel web and the distribution in the flange was determined from the method set out in Trahair and Bradford (1998) based on thin-walled structural theory.

In practical cases, transformed section analysis incorporating slab reinforcement shows that the neutral axis is positioned reasonably close to the top flange in the negative bending moment region, as shown in Chapter 3 of this thesis, and local buckling is likely to occur prior to the attainment of the yield stress when the web is slender. For the study herein, it was assumed that the neutral axis is located at a height αh below the tension flange, where the stress gradient parameter α is varyied between 0 and 0.8 as shown in Fig. 7.23. Since the stress distribution is linear-elastic, the parameter α for a particular loading case may be determined from standard modular ratio theory (Hall 1986), which accounts for cracking of the concrete and for any reinforcing steel. For the purpose of this study the depth of the neutral axis αh is assumed constant throughout the beam length. It was shown in Chapter 3 that the ratio between the longitudinally varying axial force and bending moment in the steel joist of a composite T-beam is constant for the majority of the beam length.

Figures 7.56-7.59 show the results for the loading configurations of single span I-beams, either simply supported (Fig. 7.56) or fully fixed (Figs. 7.57-7.59) at the end supports. The beams are fully restrained at the level of the tension flange, where the tension flange corresponds to the positive bending moment as shown in Fig. 7.24, in which different loading configurations are tabulated. The figures are plotted for the values of flange width to web depth ratio, b_f/h_w of 0.2, 0.4 and 0.6, web slenderness ratio, h_w/t_w of 100 and 200, and the ratio of flange thickness to web thickness, t_f/t_w of 2 and 4. The critical buckling stress derived by this analysis, and taken as the maximum compressive stress, is plotted versus the beam slenderness ratio, L/h_w for a number of different neutral axis depths defined by the stress gradient parameter, α (α = 0, 0.2, 0.5 and 0.8).

The investigation was then extended to two span beams with an internal support (Figs. 7.60-7.63) for a number of different loading configurations. The curves for all loading cases considered, for both single and two-span beams, exhibit the same characteristics. As the beam length increases the curves rise to peak and away from the peak the buckling stress decreases rapidly with increasing slenderness ratio L/h_w. The curves also show that increasing the web thickness substantially increases the critical buckling stress. This is because local buckling, coupled with the cross-sectional distortion, first occurs in the web, so that its thickness is a governing parameter. It is also shown in the figures that an increase in the flange width to web depth ratio parameter, b_f/h_w leads to improved buckling capacity for the beams with large values of the slenderness ratio, L/h_w and stockier webs (ie. h_w/t_w = 100).

Figure 7.56 shows the results for a simply supported half through bridge girder with a concentrated load at mid-span. It is evident that when the length of the beam decreases, the cross-section starts to distort markedly near the concentrated load, with more pronounced distortion for b_f/h_w equal to 0.2. This local distortion produces something that looks like a local buckle at mid-span, as illustrated in Fig. 7.64. A similar trend can be observed in Figs. 7.58 and 7.59. These analyses demonstrate that cross-sectional deformations may have a marked influence on the buckling behaviour of thin-walled composite T-beams loaded by concentrated forces. A similar behaviour was observed in plain thin-walled steel beams (Van Erp 1989).

Figures 7.64-7.66 show the buckling modes for I-section beams obtained from the eigenvector at the critical buckling stress, as given in Eqn. 7.56, for selected loading configurations (ie. Cases 3, 7 & 11). The flange width to web thickness ratios, b_f/h_w considered herein are 0.2, 0.4 and 0.6 whilst the beam slenderness ratio, L/h_w is 10. Figures 7.67-7.69 show the variation of the cross-sectional deformations along the beam length for Cases 3, 7 and 11 and the beam slenderness ratios, L/h_w of 4, 10 and 16. It is evident from these figures that the RDB mode is a governing mode for I-sections with one flange fully restrained. Figure 7.69 clearly indicates that the deformations can be reasonably large in the vicinity of the internal support. For instance, in Fig. 7.69 the plots display a combined flange-web buckle, coupled with the cross-sectional distortion, and significant relative web deformations, especially so for the point D which is located close to the internal support.

7.8.3 Composite T-section Beams with Longitudinal Stiffener

In many fabricated sections, such as I-section beams and composite T-beams, the web slenderness is very large and the web plate may be subjected to local buckling before the inception of RDB or plasticity of the member. The local buckling (and also post-buckling) performace of a web plate in bending can be improved by the provision of longitudinal stiffeners parallel to the direction of the longitudianl stress. Climenhaga and Johnson (1972) also reported from experiments that the provision of a longitudianl stiffener attached to the web improved the local buckling capacity of composite tee-beams. This provision is allowed in many design codes of practice. The main function of the longitudianl stiffeners, therefore, is to increase the local buckling capacity of the web in bending. Azhari (1993) showed that the maximum slenderness required for attainment of a yield stress σ_y of 250 MPa before buckling lies between 82 and 142.

Since the values of h_w/t_w in fabricated composite beams are usually much greater than these values, the slender web plates are stiffened by longitudinal stiffeners.

The local buckling of a composite T-section with a longitudinal stiffener under the action of moment gradient and shear was studied using the bubble formulation developed in this chapter. The flanges were subdivided into two bubble strips, the stiffeners into one strip, while the web was subdivided into four bubble strips.

In Fig. 7.70, the critical buckling stress is plotted as a function of the longitudinal stiffener position, d_s along the web depth for a number of different stiffener widths, b_s. The figure shows the results for a constant flange and web thickness for two different loading configurations, naimly, Case 3 and Case 7. The critical buckling stress is plotted as a function of the longitudinal stiffener position, d_s along the web depth for a number of different stiffener widths, b_s and for various depths of the neutral axis. The figure indicates that the location of the neutral axis is not of significance for the loading configuration shown in b). However it is important to note that where the positive bending moment changes into a negative bending moment, as for the internal support of the Case 7 in this figure, the distribution of tensile and compressive stresses along the cross-sectional depth is reversed.

The critical buckling stress is then plotted in Fig. 7.71 as a function of the stiffener location, d_s for a number of different web slendernesses, ie. h_w/t_w = 100, 150, 200, 300 and 400, and varying depths of the neutral axis. The optimum position to maximise the stress was found to lie at around $0.5h_w$.

Figure 7.72 plots the critical buckling stress versus the stiffener location parameter, d_s for a number of different stiffener thicknesses (ie. t_s/t_w = 1, 2, 4 and 6) for three different loading configurations and different positions of the neutral axis. A significant increase in the buckling capacity is evident for the sections where a stockier stiffener is employed. Similarly, these figures indicate that the optimum position of the stiffener is at $0.5h$.

The illustrations of the longitudinal and cross-sectional buckling modes for various positions of the longitudinal stiffener are presented in Figs. 7.73 and 7.74 respectively.

It can be seen from the figures that the location of the longitudinal stiffeners governs whether web local buckling, in majority of instances coupled with the RDB, occurs in the upper or lower portion of the web.

7.9 SUMMARY

This chapter has presented a new spline finite strip method suitable for the elastic buckling analysis of general thin-plate structures. The strip is formulated routinely by the displacement approach. Finite strip displacement functions were augmented with bubble functions in order to calculate the elastic buckling stresses of plates and plate assemblies. Numerical tests on the ability of the strip to model local buckles were carried out through the analysis of a representative set of standard problems including square and long plate structures. The applications presented demonstrate the good convergence properties and numerical accuracy of the spline finite strip method in a range of situations. The method is particularly attractive with regard to its versatility in accommodating in proper fashion the full scope of conditions that may be prescribed at the ends of a plate or plate assembly. The approach provides greater versatility than do previous FSMs since this method has allowed for consideration of structures with intermediate supports and with step changes of properties along their length.

The present method gives not only excellent results for the local buckling coefficient, *k*, but the buckling coefficients computed also converge rapidly. In most cases, only a coarse discretisation is required for a practical analysis, and hence the developed spline finite strip method is accurate and efficient. Numerical examples for plates of various boundary, internal support and loading conditions have demonstrated the accuracy and versatility of the method. The simplicity of the semi-analytical fnite strip method is preserved, while the problems of dealing with non-periodic buckling modes, shear and non-simple support are eliminated.

The method was then used to study extensively elastic local and overall buckling modes in I-beams under moment gradient. The study has confirmed that RDB mode is a governing mode for steel I-sections with one flange fully restrained. It has been shown that the deformations can be reasonably large in the vicinity of the internal supports (in the region of the negative bending moment) and near the concentrated forces. The numerical investigations have also demonstrated that variations of the web slenderness parameter, L/h_w have a most pronounced influence on the elastic buckling capacity of composite T-section beams. The bubble augmented spline finite strip method was also employed to study the elastic local buckling and RDB of single span and continuous composite T-sections subjected to moment gradient containing a longitudinal stiffener attached to the web.

7.10 APPENDICES

7.10.1 Flexural Stiffness Matrix

The terms in the symmetrical flexural stiffness matrix are as in the following:

$$
\bar{k}_F = \int_0^L \int_0^b \begin{array}{|c|c|c|c|c|}
\hline
k_{F1,1} & k_{F1,2} & k_{F1,3} & k_{F1,4} & k_{F1,5} \\
\hline
 & k_{F2,2} & k_{F2,3} & k_{F2,4} & k_{F2,5} \\
\hline
 & & k_{F3,3} & k_{F3,4} & k_{F3,5} \\
\hline
\multicolumn{2}{|c|}{\textit{symmetric}} & & k_{F4,4} & k_{F4,5} \\
\hline
 & & & & k_{F5,5} \\
\hline
\end{array} \, dydx
$$

In the above table the symbols are defined as follows:

$$
\begin{aligned}
k_{F\,i,j} = {} & N_i N_j \psi_i'' \psi_j'' D_1 + N_i'' N_j \psi_i \psi_j'' D_2 + N_i N_j'' \psi_i'' \psi_j D_3 \\
& + N_i'' N_j'' \psi_i \psi_j D_4 + 4 N_i' N_j' \psi_i' \psi_j' D_9
\end{aligned}
\tag{7.59}
$$

where

$$
\begin{aligned}
\psi_1 &= \psi_{wi} \\
\psi_2 &= \psi_{\theta i} \\
\psi_3 &= \psi_{wj} \\
\psi_4 &= \psi_{\theta j} \\
\psi_5 &= \psi_{ws}
\end{aligned}
\tag{7.60}
$$

and $D_1, \ldots, D_9$ are defined in Eqn. 7.33.

7.10.2 Flexural Stability Matrix

The terms in the symmetrical flexural stability matrix are as in the following:

$$\bar{g}_F = t\int_0^L\int_0^b \left[\begin{array}{ccccc} g_{F\,1,1} & g_{F\,1,2} & g_{F\,1,3} & g_{F\,1,4} & g_{F\,1,5} \\ & g_{F\,2,2} & g_{F\,2,3} & g_{F\,2,4} & g_{F\,2,5} \\ & & g_{F\,3,3} & g_{F\,3,4} & g_{F\,3,5} \\ \multicolumn{2}{c}{\textbf{\textit{symmetric}}} & & g_{F\,4,4} & g_{F\,4,5} \\ & & & & g_{F\,5,5} \end{array}\right] \mathrm{dydx}$$

$$g_{F\,i,j} = \sigma_x N_i N_j \psi'_i \psi'_j + \sigma_y N'_i N'_j \psi_i \psi_j + 2\tau N'_i N_j \psi_i \psi'_j \tag{7. 61}$$

where

$$\begin{aligned} \psi_1 &= \psi_{wi} \\ \psi_2 &= \psi_{\theta i} \\ \psi_3 &= \psi_{wj} \\ \psi_4 &= \psi_{\theta j} \\ \psi_5 &= \psi_{wB} \end{aligned} \tag{7. 62}$$

and

$$\sigma_x = \sigma_1 + (\sigma_2 - \sigma_1)\eta \tag{7. 63}$$

7.10.3 Membrane Stiffness Matrix

The terms in the symmetrical membrane stiffness matrix are as in the following:

$$\bar{k}_M = t\int_0^L\int_0^b \begin{array}{|c|c|c|c|} \hline k_{M\,1,1} & k_{M\,1,2} & k_{M\,1,3} & k_{M\,1,4} \\ \hline & k_{M\,2,2} & k_{M\,2,3} & k_{M\,2,4} \\ \hline \multicolumn{2}{|c|}{\textit{\textbf{symmetric}}} & k_{M\,3,3} & k_{M\,3,4} \\ \hline & & & k_{M\,4,4} \\ \hline \end{array}\ \mathrm{d}y\mathrm{d}x$$

The subscript M denotes membrane displacements.

$$k_{M\,1,1} = N_1 N_1 \psi_i \psi_j S_1 + N_1' N_1' \psi_i \psi_j S_9$$
$$k_{M\,1,2} = N_1 N_1' \psi_i' \psi_j S_3 + N_1' N_1 \psi_i \psi_j' S_9$$
$$k_{M\,1,3} = N_1 N_2 \psi_i' \psi_j' S_1 + N_1' N_2' \psi_i \psi_j S_9$$
$$k_{M\,1,4} = N_1 N_2' \psi_i' \psi_j S_3 + N_1' N_2 \psi_i \psi_j S_9$$

$$k_{M\,2,2} = N_1' N_1' \psi_i \psi_j S_4 + N_1 N_1 \psi_i' \psi_j' S_9$$
$$k_{M\,2,3} = N_1' N_2 \psi_i \psi_j' S_2 + N_1 N_2' \psi_i' \psi_j S_9 \qquad (7.64)$$
$$k_{M\,2,4} = N_1' N_2' \psi_i \psi_j S_4 + N_1 N_2 \psi_i' \psi_j' S_9$$

$$k_{M\,3,3} = N_2 N_2 \psi_i' \psi_j' S_1 + N_1' N_2' \psi_i \psi_j S_9$$
$$k_{M\,3,4} = N_2 N_2' \psi_i' \psi_j S_3 + N_1' N_2 \psi_i \psi_j' S_9$$

$$k_{M\,3,4} = N_2' N_2' \psi_i \psi_j S_4 + N_1 N_2 \psi_i' \psi_j' S_9$$

where

$$
\begin{aligned}
\psi_1 &= \psi_{ui} \\
\psi_2 &= \psi_{vi} \\
\psi_3 &= \psi_{uj} \\
\psi_4 &= \psi_{vj}
\end{aligned}
\tag{7. 65}
$$

and $S_1,\ldots, S_9$ are defined in Eqn. 7.45.

7.10.4 Membrane Stability Matrix

The terms in the symmetrical membrane stability matrix are as in the following:

$$\bar{g}_M = t\int_0^L\int_0^b \begin{bmatrix} g_{M\,1,1} & - & g_{M\,1,3} & - \\ & g_{M\,2,2} & - & g_{M\,2,4} \\ \multicolumn{2}{c}{\textbf{\textit{symmetric}}} & g_{M\,3,3} & - \\ & & - & g_{M\,4,4} \end{bmatrix} \mathrm{d}y\mathrm{d}x$$

$$\begin{aligned} g_{M\,1,1} &= \sigma_x N_1 N_1 \psi_i' \psi_j' \\ g_{M\,1,3} &= \sigma_x N_1 N_2 \psi_i' \psi_j' \\ g_{M\,2,2} &= \sigma_x N_1 N_1 \psi_i' \psi_j' \\ g_{M\,2,4} &= \sigma_x N_1 N_2 \psi_i' \psi_j' \\ g_{M\,3,3} &= \sigma_x N_2 N_2 \psi_i' \psi_j' \\ g_{M\,4,4} &= \sigma_x N_2 N_2 \psi_i' \psi_j' \end{aligned} \tag{7.66}$$

where

$$\begin{aligned} \psi_1 &= \psi_{ui} \\ \psi_2 &= \psi_{vi} \\ \psi_3 &= \psi_{uj} \\ \psi_4 &= \psi_{vj} \end{aligned} \tag{7.67}$$

and

$$\sigma_x = \sigma_1 + (\sigma_2 - \sigma_1)\eta \tag{7.68}$$

Table 7.1 Values of ψ_i, ψ_i' and ψ_i'' at section knots

	$x < x_{i-2}$	$x = x_{i-2}$	$x = x_{i-1}$	$x = x_i$	$x = x_{i+1}$	$x = x_{i+2}$	$x > x_{i+2}$
$\psi_i(x)$	0	0	1/6	2/3	1/6	0	0
$\psi_i'(x)$	0	0	$1/2h$	0	$-1/2h$	0	0
$\psi_i''(x)$	0	0	$1/h^2$	$-2/h^2$	$1/h^2$	0	0

Table 7.2 Boundary conditions for strip flexural and membrane displacements

Strip Boundary Conditions	**Flexural Displacements**	**Membrane Displacements**	
	w, θ, w_B	u	v
Free End	$f(x_i) \neq 0$ $f'(x_i) \neq 0$	$f(x_i) \neq 0$ $f'(x_i) \neq 0$	$f(x_i) \neq 0$ $f'(x_i) \neq 0$
Simply Supported End 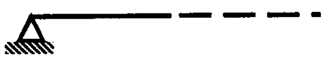	$f(x_i) = 0$ $f'(x_i) \neq 0$	$f(x_i) \neq 0$ $f'(x_i) = 0$	$f(x_i) = 0$ $f'(x_i) \neq 0$
Clamped End 	$f(x_i) = 0$ $f'(x_i) = 0$	$f(x_i) = 0$ $f'(x_i) \neq 0$	$f(x_i) = 0$ $f'(x_i) \neq 0$
Sliding Clamped End 	$f(x_i) \neq 0$ $f'(x_i) = 0$	$f(x_i) = 0$ $f'(x_i) \neq 0$	$f(x_i) \neq 0$ $f'(x_i) = 0$

Table 7.3 Buckling load factors for square plates under uniaxial compression

Support Conditions	Reference	k	This Study: Number of strips	Number of sections	k	% difference
s-s-s-s	Tham & Szeto (1990) Timoshenko & Gere (1961)	**4.00** **4.00**	1	4	**4.0006**	0.02
	Azhari (1993) Azhari *et al.* (2000)	**4.00** **4.00**	2	8	**4.0000**	0.00
c-c-c-c	Tham & Szeto (1990)	**10.08**	2	4	**10.1096**	0.29
	Timoshenko & Gere (1961) Azhari *et al.* (2000)	**10.07** **10.10**	2	10	**10.0871**	0.07
c-s-c-s	Tham & Szeto (1990)	**7.70**	2	4	**7.7118**	0.15
	Timoshenko & Gere (1961) Azhari *et al.* (2000)	**7.69** **7.72**	2	10	**7.7044**	0.06
c-s-c-s*	Azhari *et al.* (2000)	**14.8**	2	8	**14.7506**	0.33
			2	12	**14.7254**	0.50
c-c-c-c*	Azhari *et al.* (2000)	**19.70**	2	10	**19.4375**	1.33

* - triangular stress distribution

Table 7.4 Buckling load factors for square plates under biaxial compression

<table>
<tr><th rowspan="2">Support Conditions</th><th colspan="2">Reference</th><th colspan="3">This Study</th><th rowspan="2">% difference</th></tr>
<tr><th></th><th>k</th><th>Number of strips</th><th>Number of sections</th><th>k</th></tr>
<tr><td rowspan="4">s-s-s-s</td><td>Tham & Szeto (1990)</td><td>2.00</td><td rowspan="2">1</td><td rowspan="2">4</td><td rowspan="2">2.0008</td><td rowspan="2">0.04</td></tr>
<tr><td>Timoshenko & Gere (1961)</td><td>2.00</td></tr>
<tr><td>Azhari (1993)</td><td>2.00</td><td rowspan="2">2</td><td rowspan="2">8</td><td rowspan="2">2.0000</td><td rowspan="2">0.00</td></tr>
<tr><td>Azhari et al. (2000)</td><td>2.00</td></tr>
<tr><td rowspan="3">c-c-c-c</td><td>Tham & Szeto (1990)</td><td>5.31</td><td>2</td><td>6</td><td>5.3260</td><td>0.30</td></tr>
<tr><td>Timoshenko & Gere (1961)</td><td>5.61</td><td rowspan="2">3</td><td rowspan="2">6</td><td rowspan="2">5.3087</td><td rowspan="2">0.02</td></tr>
<tr><td>Azhari et al. (2000)</td><td>5.31</td></tr>
<tr><td rowspan="3">c-s-c-s</td><td>Tham & Szeto (1990)</td><td>3.83</td><td>2</td><td>6</td><td>3.8419</td><td>0.31</td></tr>
<tr><td>Timoshenko & Gere (1961)</td><td>3.83</td><td rowspan="2">3</td><td rowspan="2">4</td><td rowspan="2">3.8309</td><td rowspan="2">0.05</td></tr>
<tr><td>Azhari et al. (2000)</td><td>3.83</td></tr>
</table>

Table 7.5 Buckling load factors for square plates under shear load

Support Conditions	Reference		This Study			% difference
		k	Number of strips	Number of sections	***k***	
s-s-s-s	Tham & Szeto (1990)	**9.33**	2	10	**9.3847**	0.58
	Timoshenko & Gere (1961)	**9.40**	3	10	**9.3323**	0.02
	Azhari *et al.* (2000)	**9.34**				
c-c-c-c	Tham & Szeto (1990)	**14.66**	3	8	**14.6601**	0.00
	Timoshenko & Gere (1961)	**14.58**				
c-s-c-s	Tham & Szeto (1990)	**12.58**	2	10	**12.5997**	0.16
	Timoshenko & Gere (1961)	**12.28**	3	8	**12.5802**	0.00

Table 7.6 Buckling load factors for rectangular plates under shear load

L/b	**Reference**		**This Study**			**% difference**
		k	Number of strips	Number of sections	*k*	
1	Saadatpour *et al.* (1998)	**9.32**	3	10	**9.3323**	0.132
	Allen & Bulson (1980)	**9.34**				0.083
	Azhari *et al.* (2000)	**9.342**				0.104
1.2	Saadatpour *et al.* (1998)	**8.04**	3	10	**7.9898**	0.628
	Allen & Bulson (1980)	**8.00**				0.128
1.4	Saadatpour *et al.* (1998)	**7.29**	3	10	**7.2930**	0.041
	Allen & Bulson (1980)	**7.30**				0.096
1.5	Saadatpour *et al.* (1998)	**7.08**	3	10	**7.0752**	0.068
	Allen & Bulson (1980)	**7.11**				0.492
1.6	Saadatpour *et al.* (1998)	**6.92**	3	10	**6.9124**	0.110
	Allen & Bulson (1980)	**6.91**				0.035
1.8	Saadatpour *et al.* (1998)	**6.70**	3	10	**6.693**	0.105
	Allen & Bulson (1980)	**6.80**				1.599
2	Saadatpour *et al.* (1998)	**6.57**	3	10	**6.5507**	0.295
	Allen & Bulson (1980)	**6.60**				0.753
	Azhari *et al.* (2000)	**6.345**				3.140
2.5	Saadatpour *et al.* (1998)	**6.08**	3	10	**6.0384**	0.689
	Allen & Bulson (1980)	**6.10**				1.020
3	Saadatpour *et al.* (1998)	**5.53**	3	10	**5.8453**	5.394
	Allen & Bulson (1980)	**5.50**				5.907
	Azhari *et al.* (2000)	**5.784**				1.049
4	Saadatpour *et al.* (1998)	**5.80**	3	10	**5.6323**	2.972
	Allen & Bulson (1980)	**5.70**				1.197
	Azhari *et al.* (2000)	**5.604**				0.508
5	Azhari *et al.* (2000)	**5.552**	3	10	**5.5307**	0.385
10	Azhari *et al.* (2000)	**5.380**	3	10	**5.3888**	0.163

Table 7.7 Buckling load factors for rectangular plate in compression with longitudinal edges simply supported and loaded edges clamped

L/b	Reference		This Study			% difference
		k	Number of strips	Number of sections	*k*	
1	Timoshenko & Gere (1961)	**6.72**	2	6	**6.7538**	0.204
			2	10	**6.7444**	0.065
	Azhari (1993)	**6.7, 6.74**				
1.25	Timoshenko & Gere (1961)	**5.69**	2	6	**5.7138**	0.417
			2	10	**5.7055**	0.272
	Azhari (1993)	**5.69, 5.73**				
1.5	Timoshenko & Gere (1961)	**5.35**	2	6	**5.3856**	0.104
			2	10	**5.3759**	0.076
	Azhari (1993)	**5.38, 5.38**				
1.75	Timoshenko & Gere (1961)	**5.20**	2	6	**5.3248**	0.654
			2	10	**5.2935**	0.066
	Azhari (1993)	**5.34, 5.29**				
2	Timoshenko & Gere (1961)	**4.83**	2	6	**4.8775**	0.564
			2	10	**4.8502**	0.004
	Azhari (1993)	**4.93, 4.85**				
2.5	Timoshenko & Gere (1961)	**4.46**	2	6	**4.5526**	0.163
			2	10	**4.5255**	0.762
	Azhari (1993)	**4.65, 4.56**				

Table 7.8 Buckling load factors for rectangular plate in compression with all edges clamped

L/b	Reference	*k*	This Study: Number of strips	Number of sections	*k*	% difference
1	Timoshenko & Gere (1961)	**10.10**	2	6	**6.7538**	0.204
	Azhari (1993)	**10.13** **10.13**	2	10	**6.7444**	0.065
1.25	Timoshenko & Gere (1961)	**9.35**	2	6	**5.7138**	0.417
	Azhari (1993)	**9.48** **9.30**	2	10	**5.7055**	0.272
1.5	Timoshenko & Gere (1961)	**8.45**	2	6	**5.3856**	0.104
	Azhari (1993)	**8.62** **8.41**	2	10	**5.3759**	0.076
1.75	Timoshenko & Gere (1961)	**8.15**	2	6	**5.3248**	0.654
	Azhari (1993)	**8.44** **8.29**	2	10	**5.2935**	0.066
2	Timoshenko & Gere (1961)	**7.89**	2	6	**4.8775**	0.564
	Azhari (1993)	**8.02** **7.89**	2	10	**4.8502**	0.004
2.5	Timoshenko & Gere (1961)	**7.72**	2	6	**4.5526**	0.163
	Azhari (1993)	**7.93** **7.74**	2	10	**4.5255**	0.762

Table 7.9 Buckling load factors for stiffened plates

Loading case	Reference		This Study			% difference
		k	Number of strips	Number of sections	*k*	
Fig. 7.15 (σ_x)	Bedair (1997)	**16.00**	2	6	**16.0176**	0.110
	Timoshenko & Gere (1961)	**16.00**	2	10	**16.0099**	0.062
Fig. 7.16 (σ_x)	Bedair (1997)	**36.00**	3	6	**36.1311**	0.363
	Timoshenko & Gere (1961)	**36.00**	3	10	**36.0319**	0.089
Fig. 7.16 ($\sigma_x + \sigma_y$)	Bedair (1997)	**11.12**	3	6	**11.1162**	0.034
	Timoshenko & Gere (1961)	**11.12**	3	10	**11.1160**	0.036

Table 7.10 Buckling load factors for continuous plate

Loading case	Reference		This Study			% difference
		k	Number of strips	Number of sections	k	
Fig. 7.19 (σ_x)	Bedair (1997)	**16.00**	2	6	**16.0086**	0.110
	Timoshenko & Gere (1961)	**16.00**	2	10	**16.0009**	0.062
Fig. 7.20 (σ_x)	Bedair (1997)	**11.12**	3	6	**11.1291**	0.082
	Timoshenko & Gere (1961)	**11.12**	3	10	**11.1132**	0.061
Fig. 7.21 (σ_x)	Bedair (1997)	**36.00**	3	6	**36.0386**	0.107
	Timoshenko & Gere (1961)	**36.00**	3	10	**36.0221**	0.061
Fig. 7.21 (σ_x+ σ_y)	Bedair (1997)	**18.00**	3	6	**18.0149**	0.083
			3	10	**18.0061**	0.034

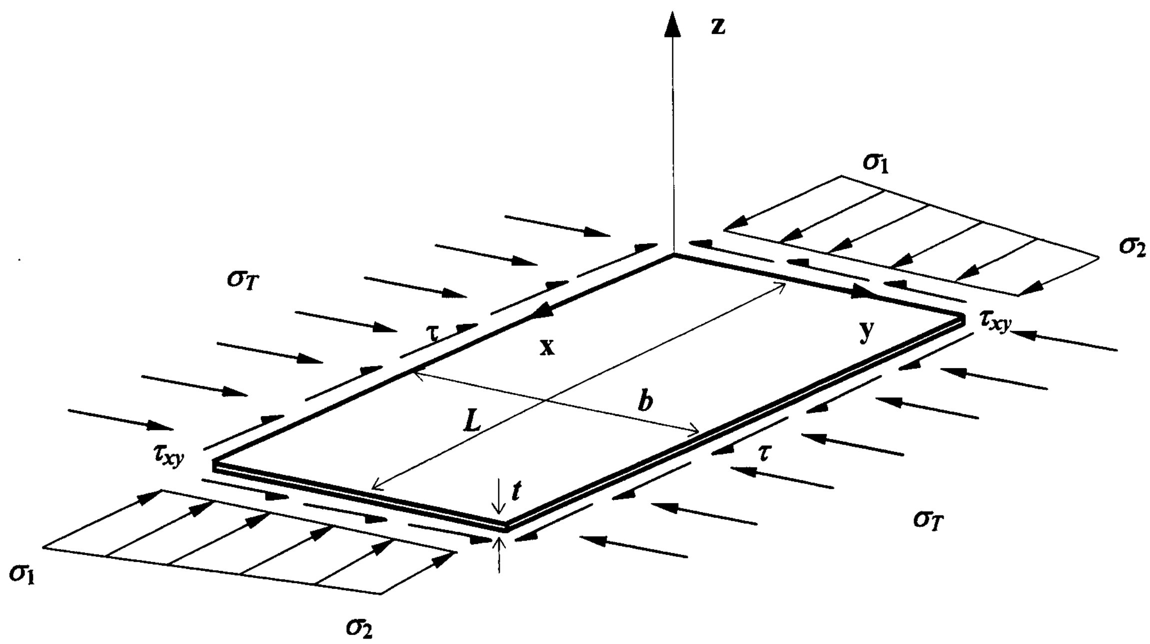

Figure 7.1 The basic state of stress in a strip

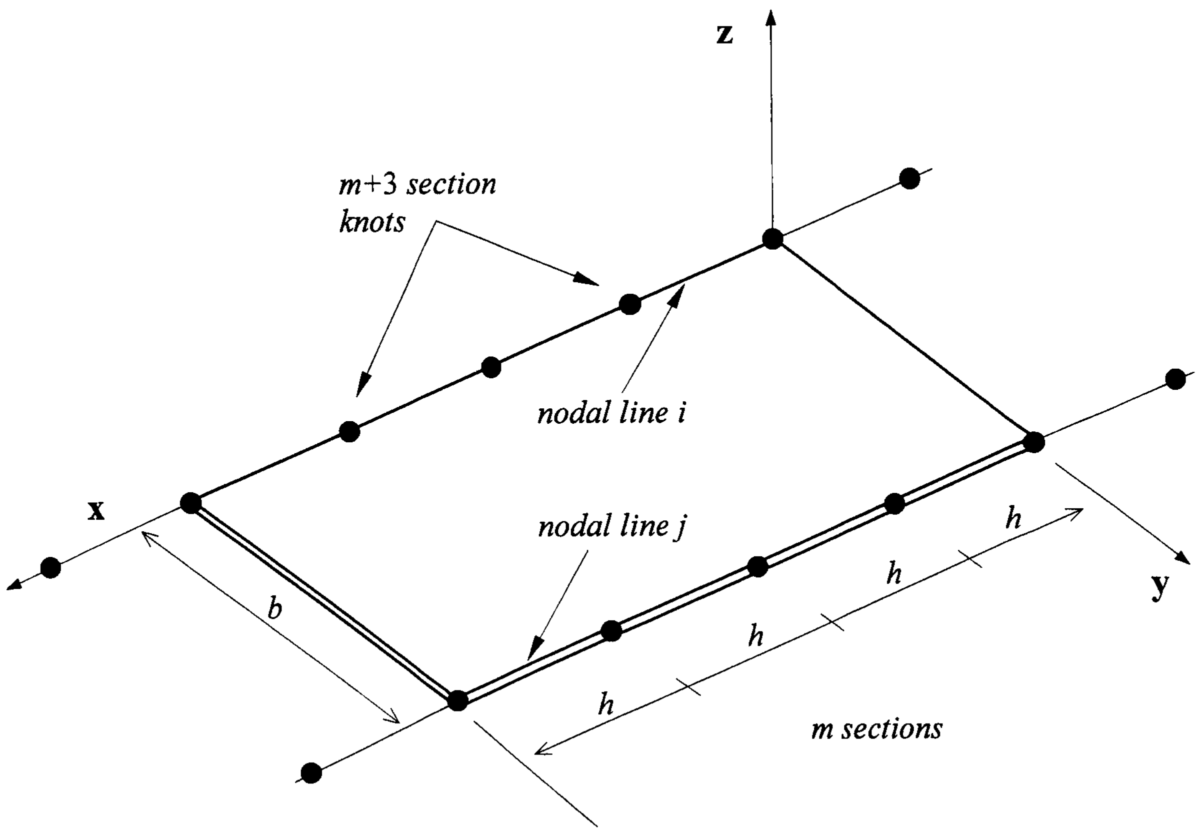

Figure 7.2 A B_3- spline strip

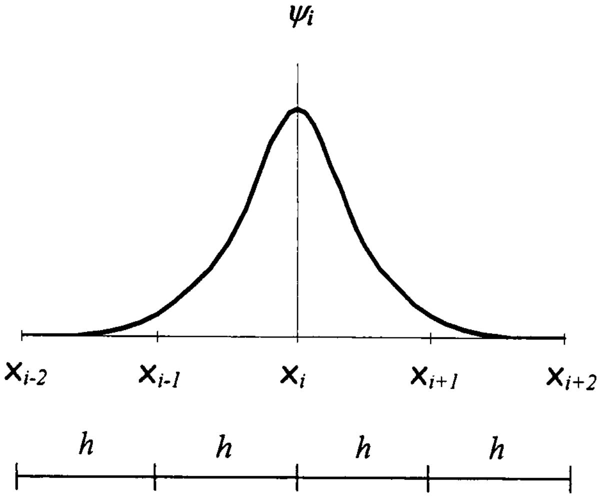

Figure 7.3 A local B_3- spline

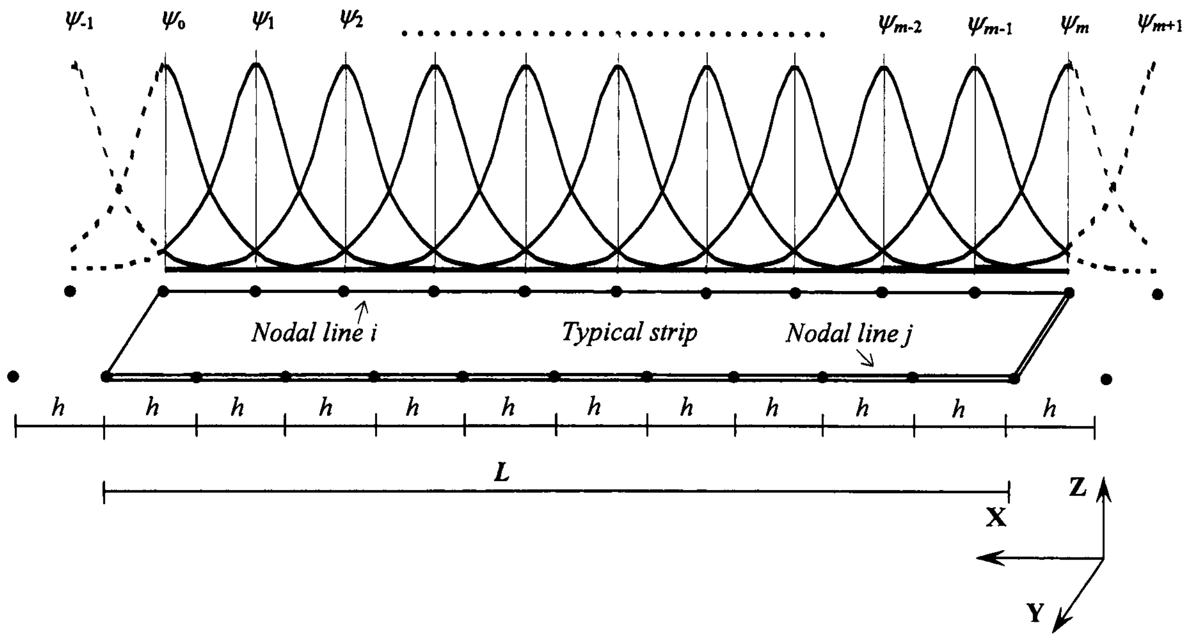

Figure 7.4 A linear combination of local B_3- splines

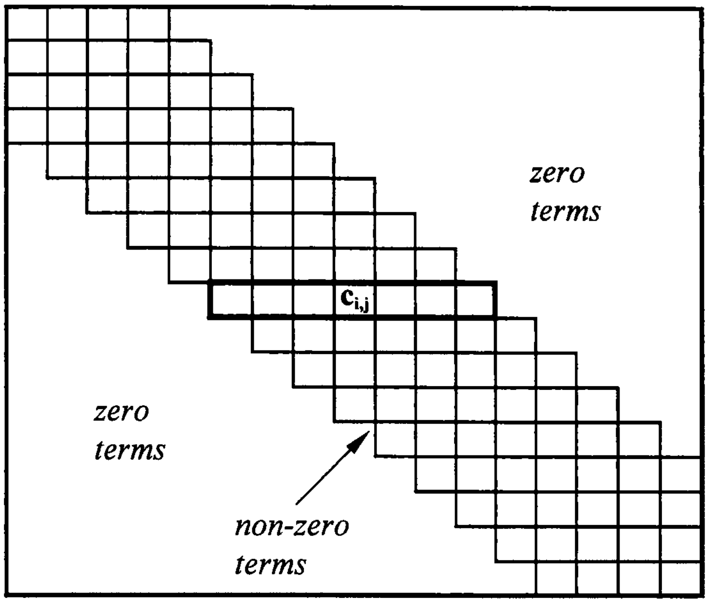

a) A banded coupling matrix

$c_{i,j-3}$	$c_{i,j-2}$	$c_{i,j-1}$	$c_{i,j}$	$c_{i,j+1}$	$c_{i,j+2}$	$c_{i,j+3}$

b) Non-zero terms in coupling matrix

Figure 7.5 Coupling matrix $\overline{C} = \int_0^L \bar{\psi}_i^T \bar{\psi}_j \, dx$

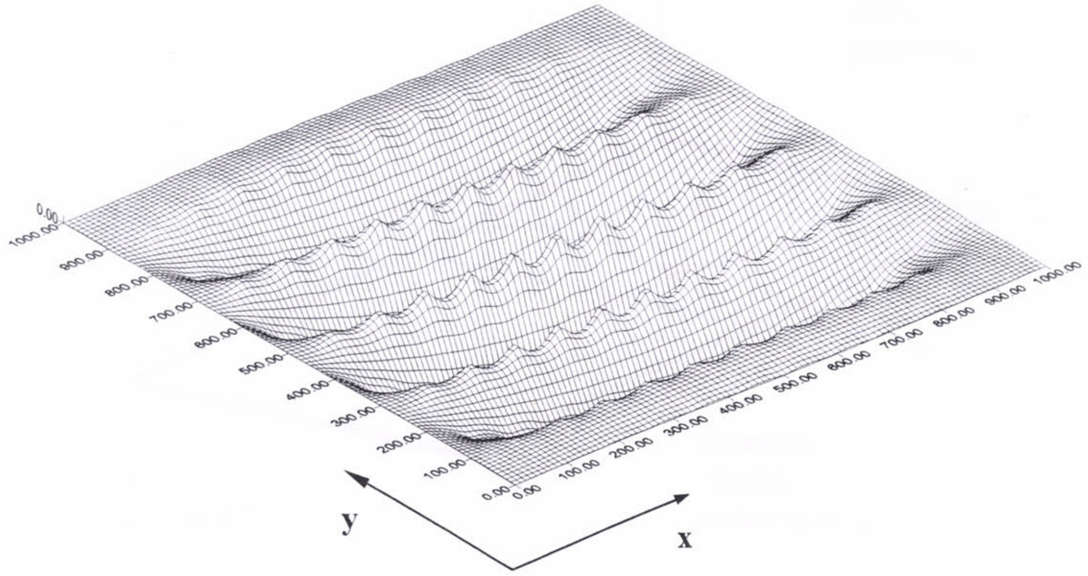

Figure 7.6 Buckling mode for a square plate (s-s-s-s) in uniform compression - bubble displacements included

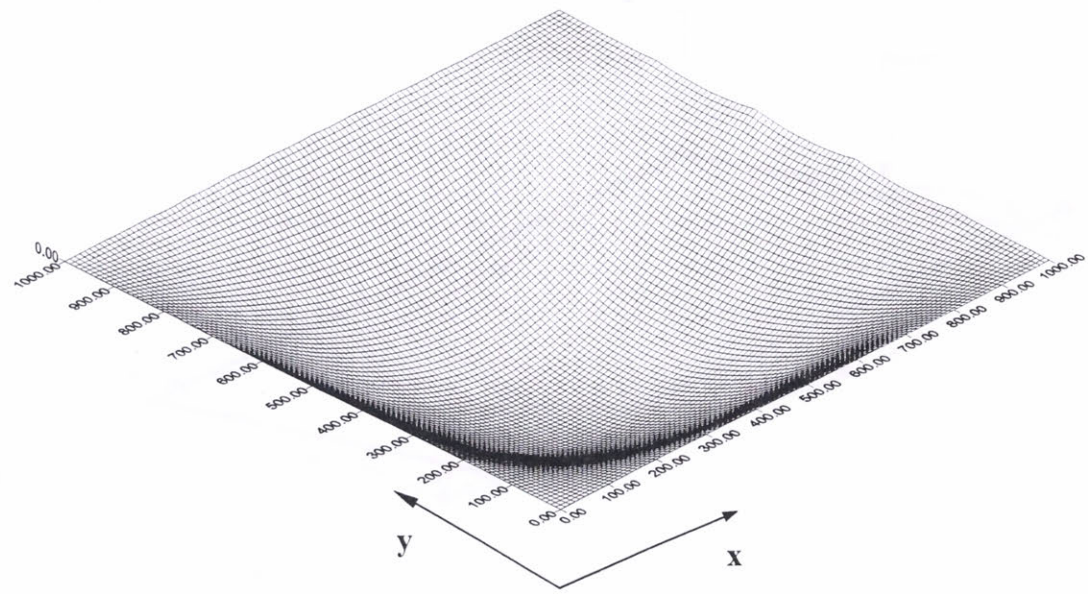

Figure 7.7 Buckling mode for a square plate (s-s-s-s) in uniform compression - bubble displacements excluded

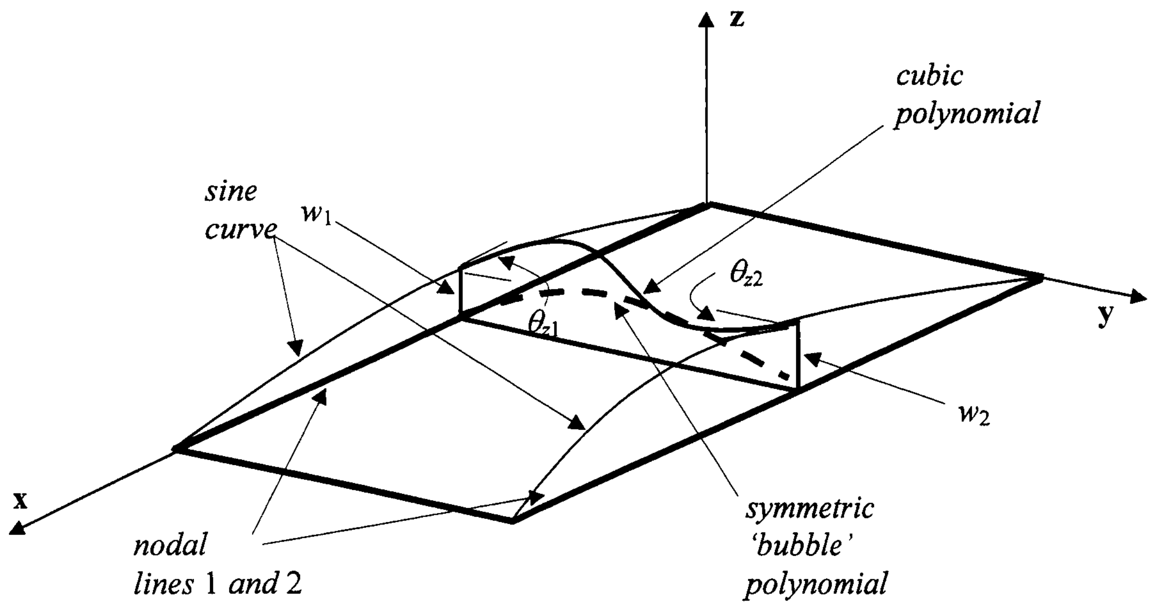

a) flexural (out-of-plane) displacements

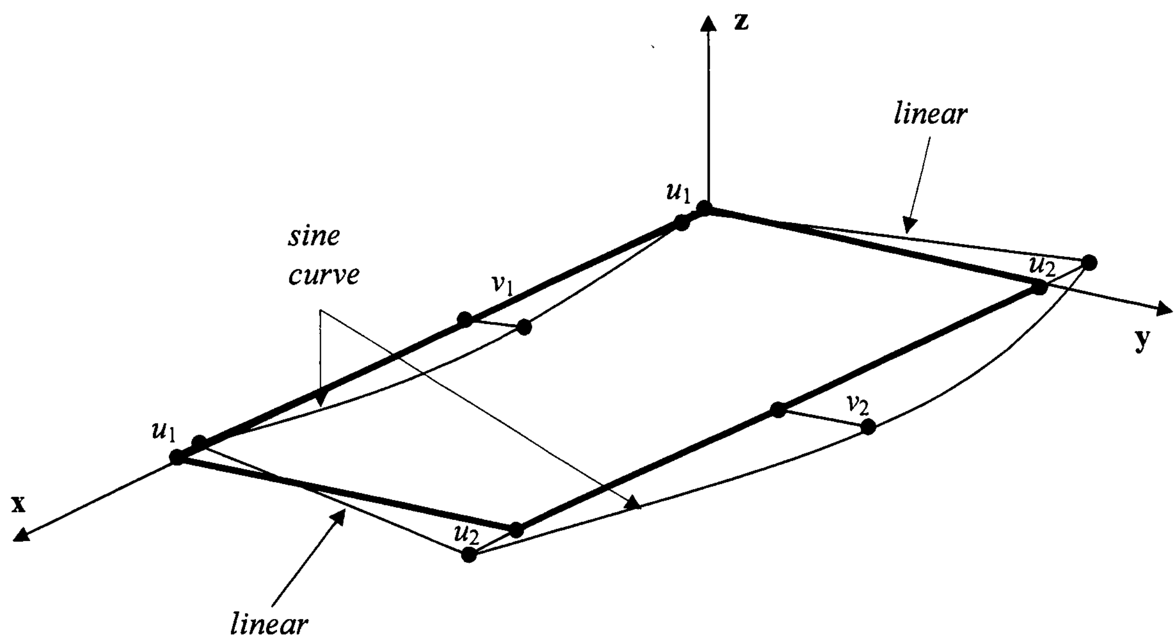

b) membrane (in-plane) displacements

Figure 7.8 Strip displacements fields

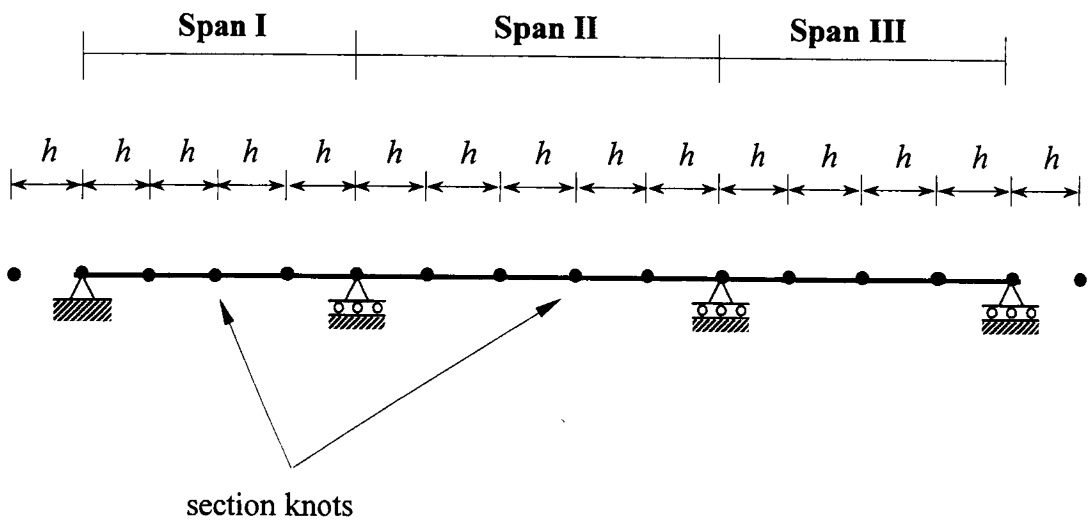

Figure 7.9 A continuous rectangular plate

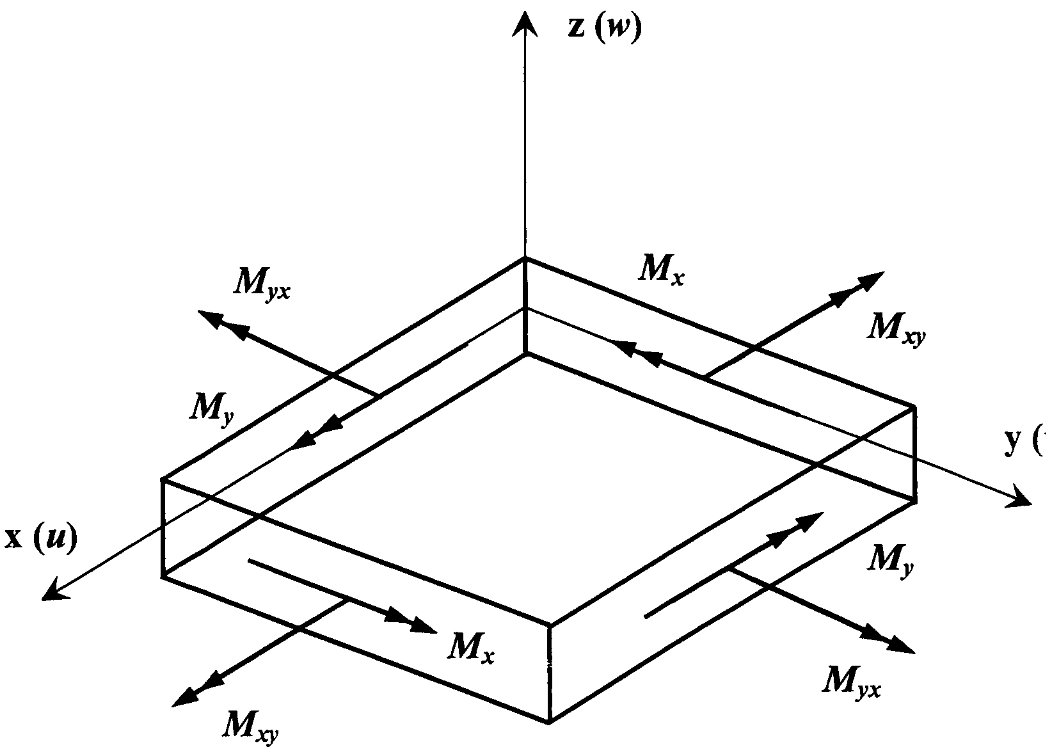

Figure 7.10 Plate bending and twisting moments

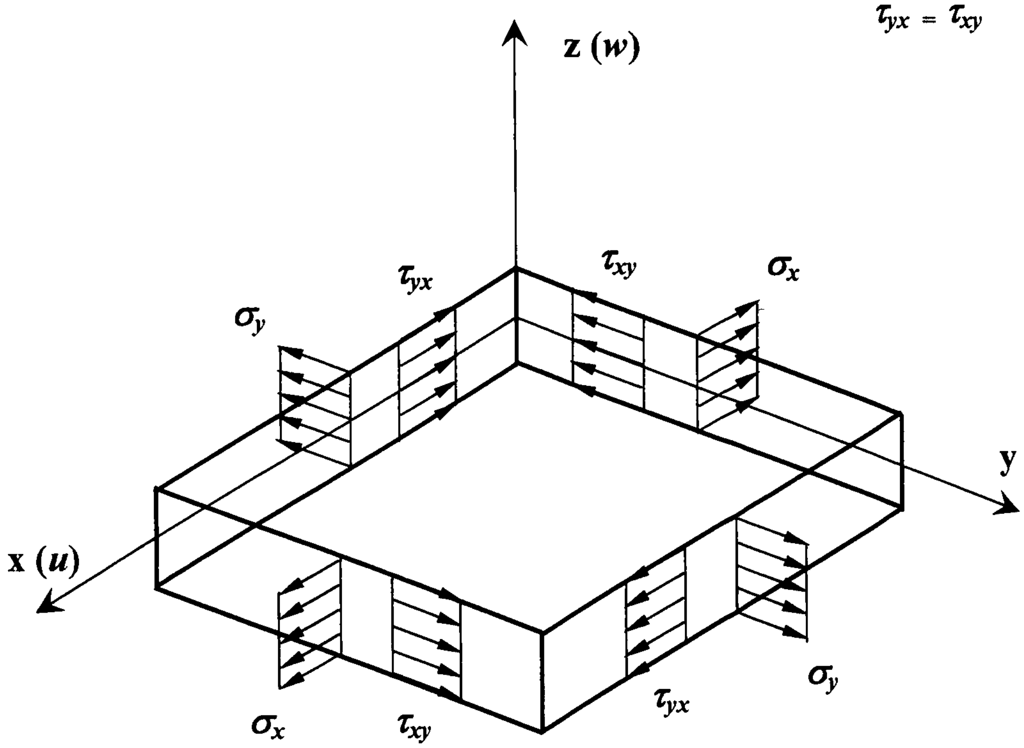

Figure 7.11 Membrane stresses

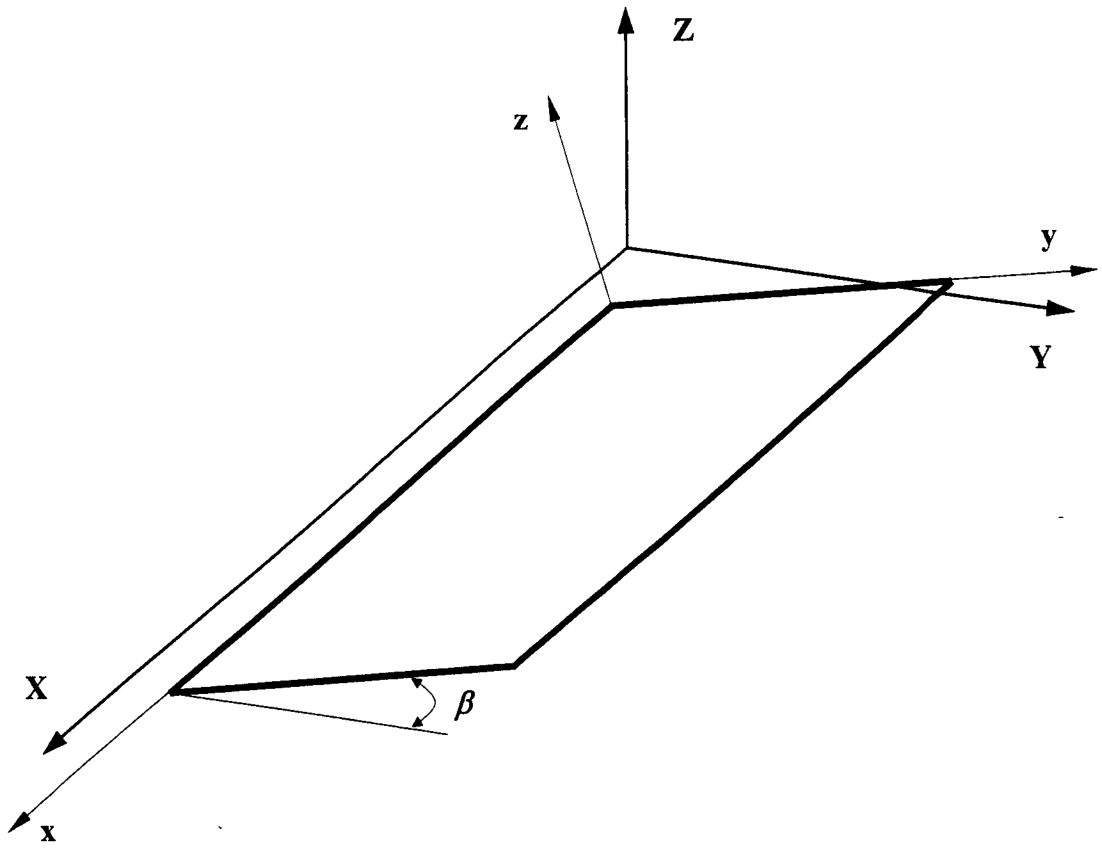

Figure 7.12 Strip orientation relative to global axes

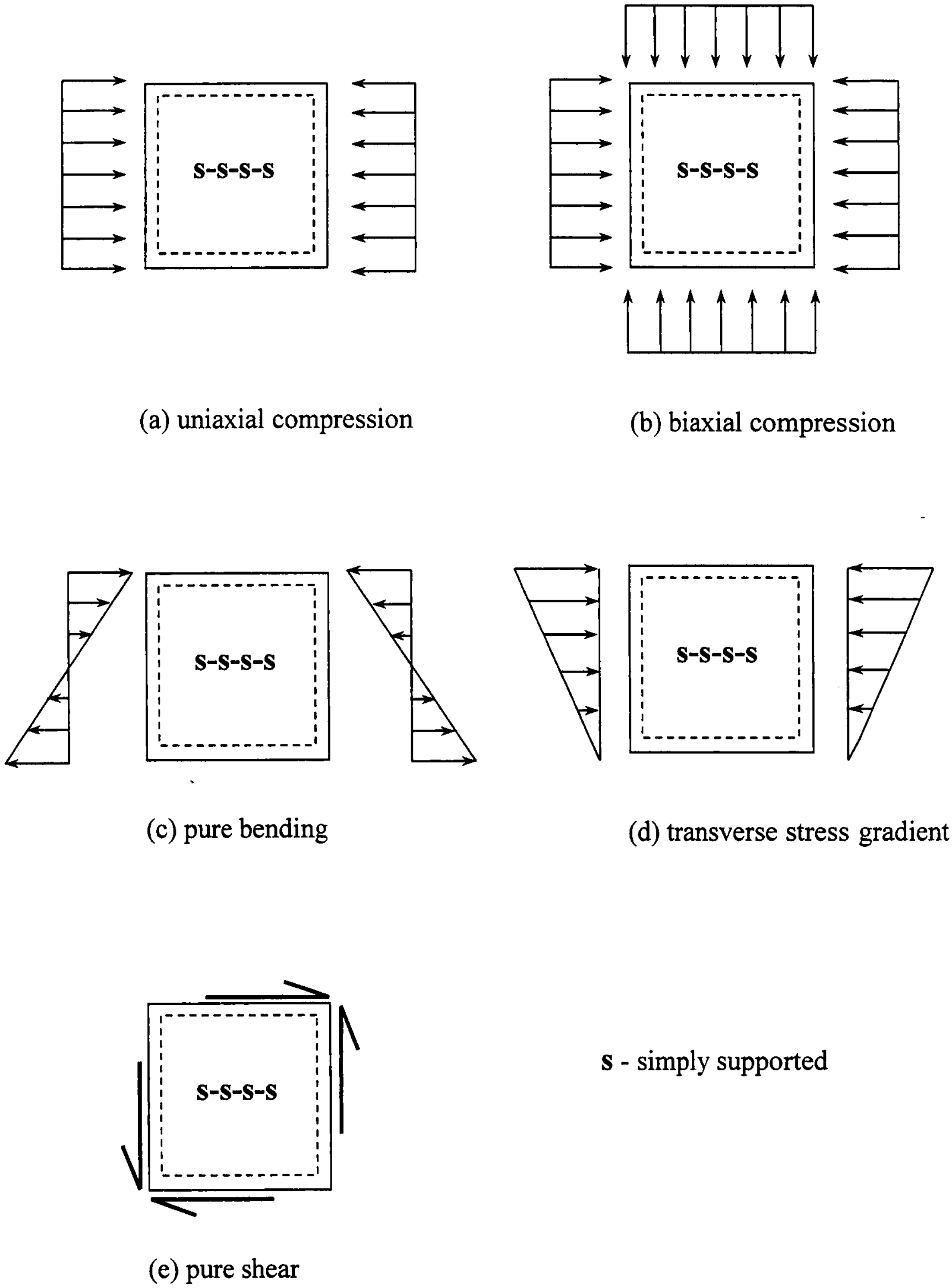

Figure 7.13 Plate loading configurations for simply supported plate

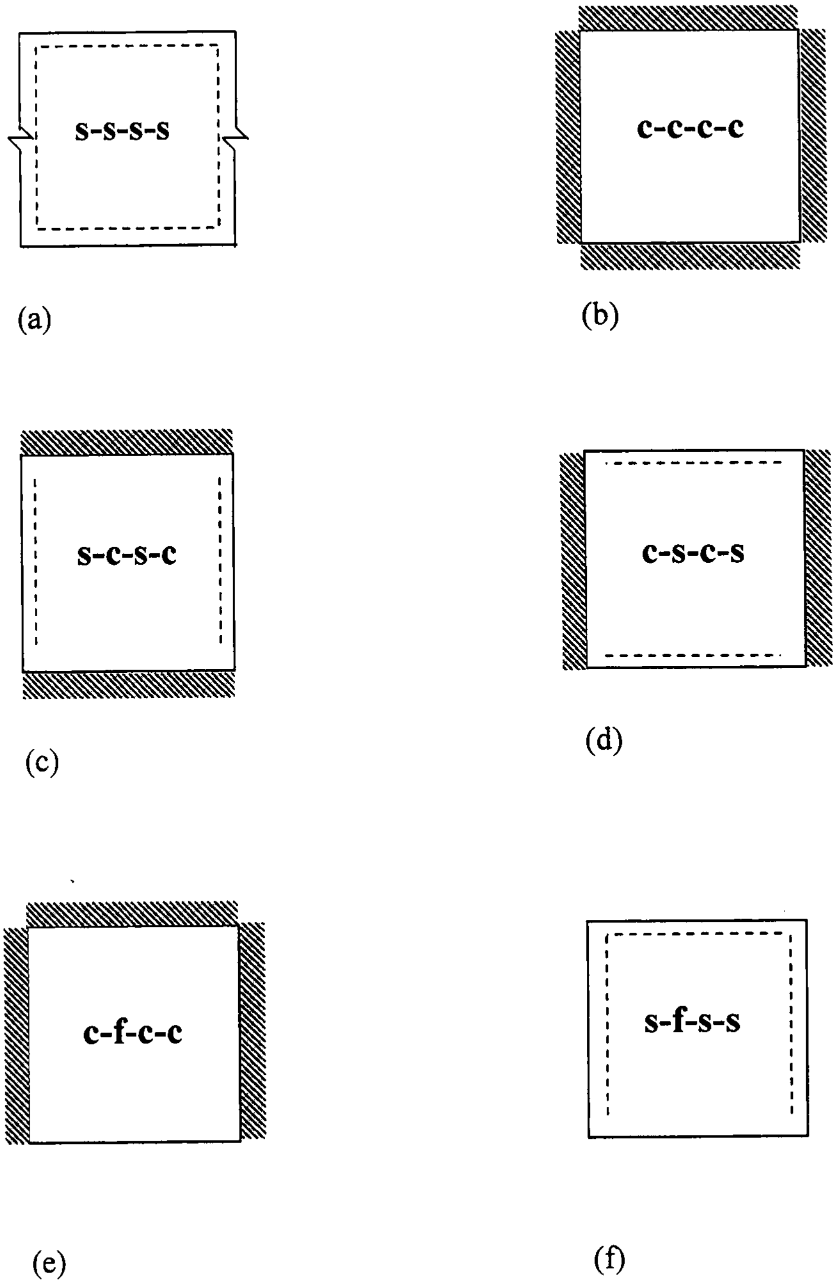

s – simply supported
c – clamped
f – free

Figure 7.14 Plate support configurations

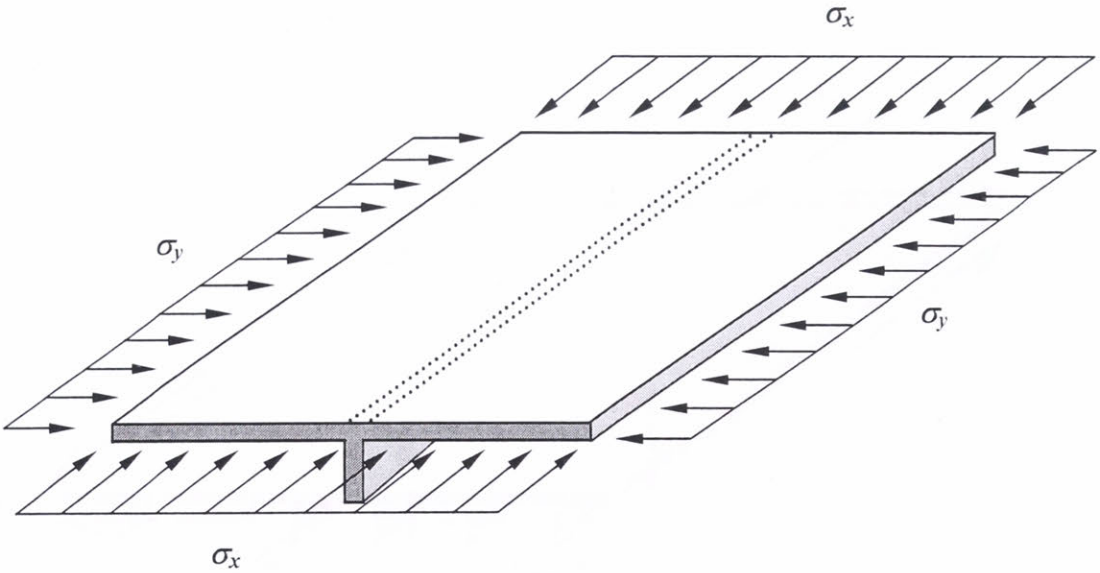

Figure 7.15 Plate with one longitudinal stiffener

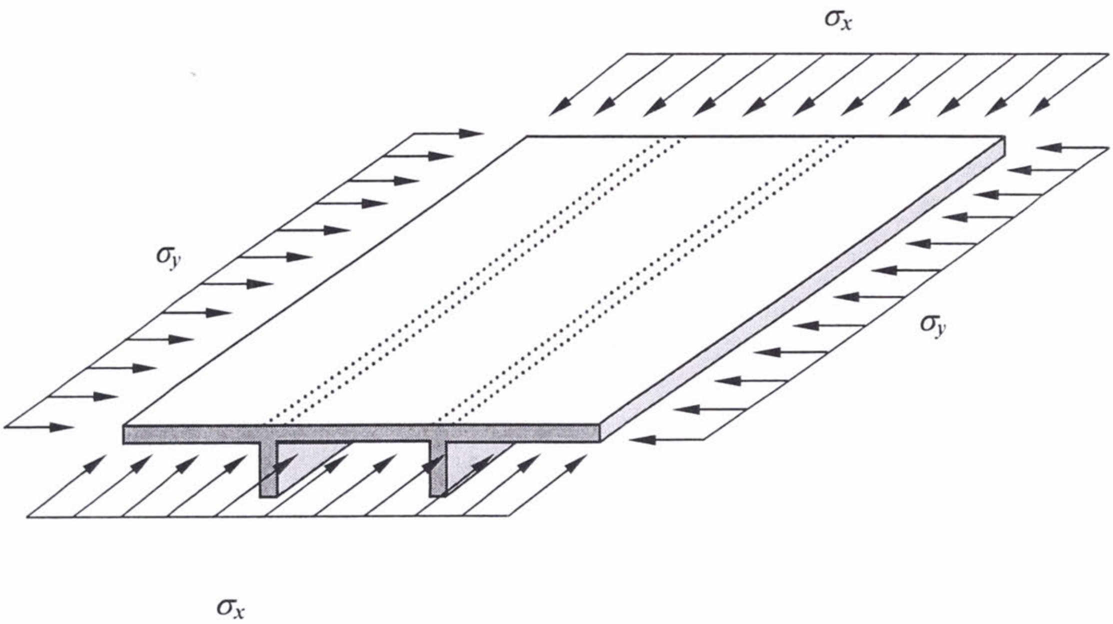

Figure 7.16 Plate with two longitudinal stiffeners

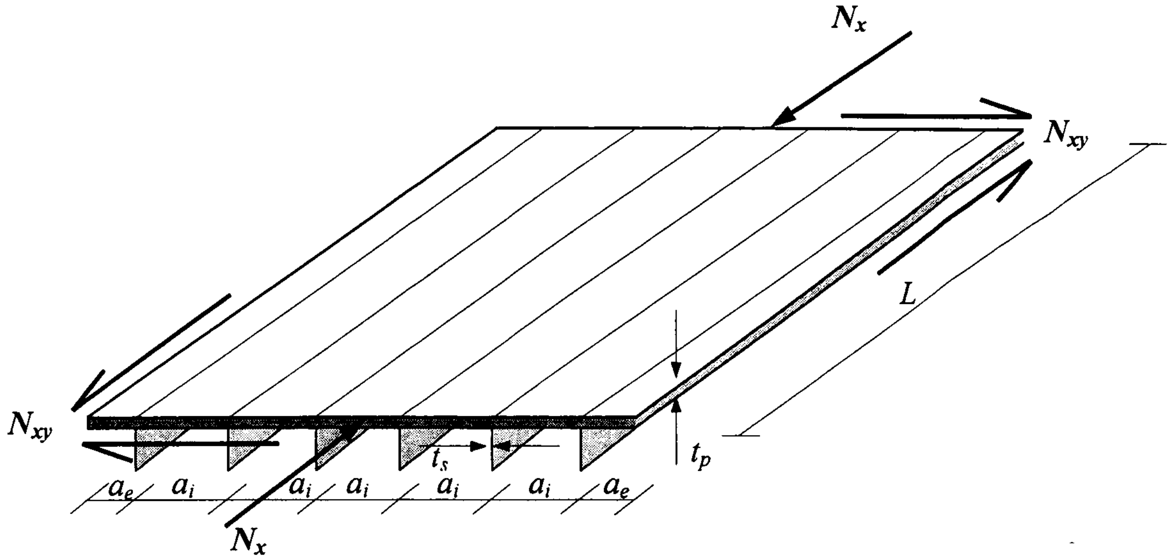

Geometric and material properties:

$L = 762.0$ mm

$a_e = 63.5$ mm

$a_i = 127.0$ mm

$t_p = 2.1336$ mm

$t_s = 1.4732$ mm

Young's Modulus = 72,400 MPa

Poisson's Ratio = 0.32

Figure 7.17 Simply supported square stiffened plate subjected to combined uniaxial and shear stresses

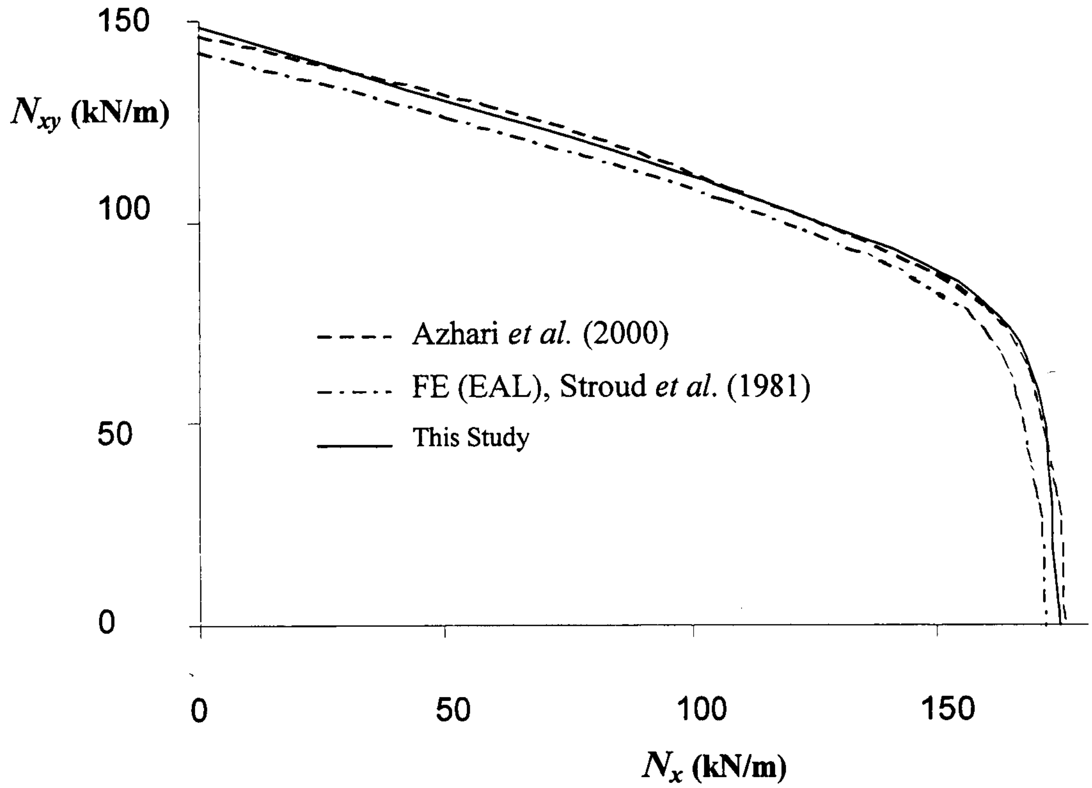

Figure 7.18 Interaction buckling load for square stiffened plate

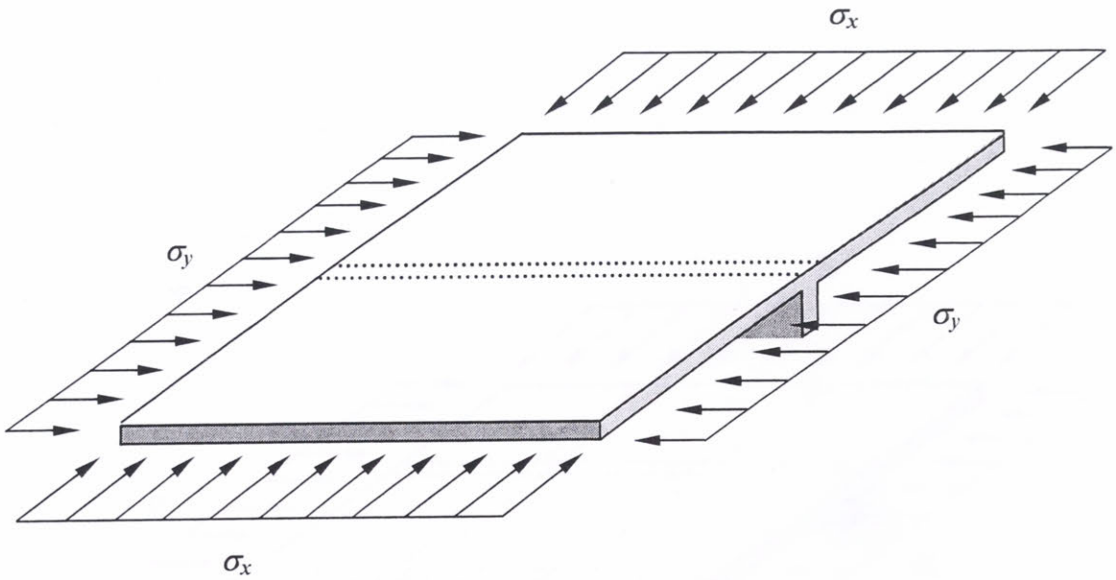

Figure 7.19 Plate with one internal support

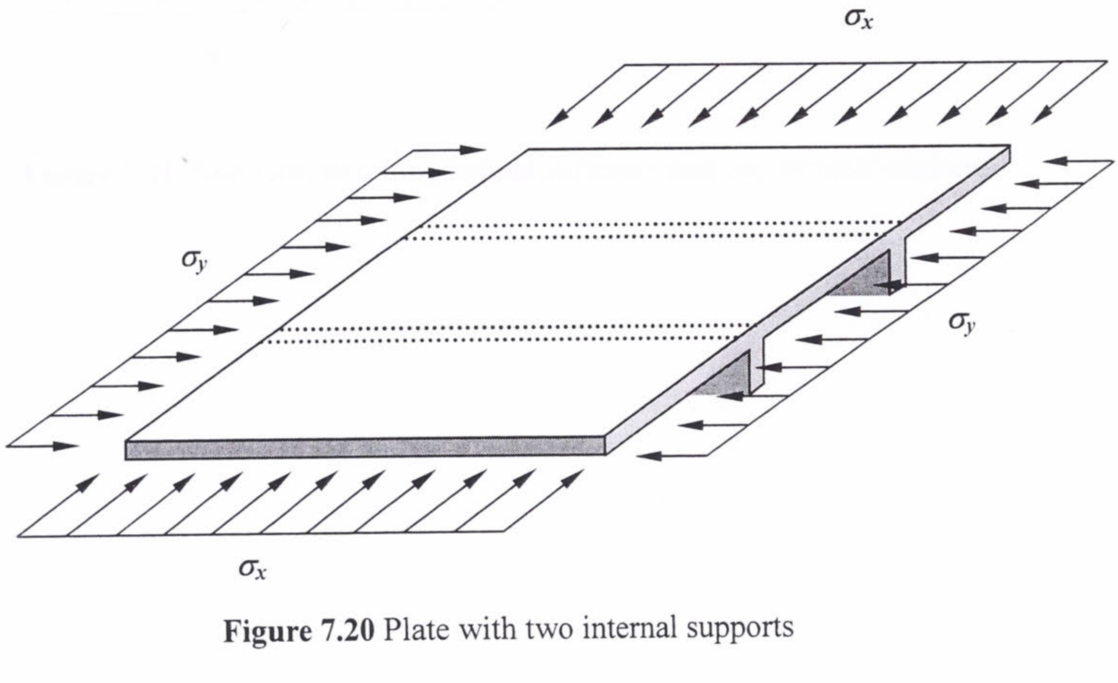

Figure 7.20 Plate with two internal supports

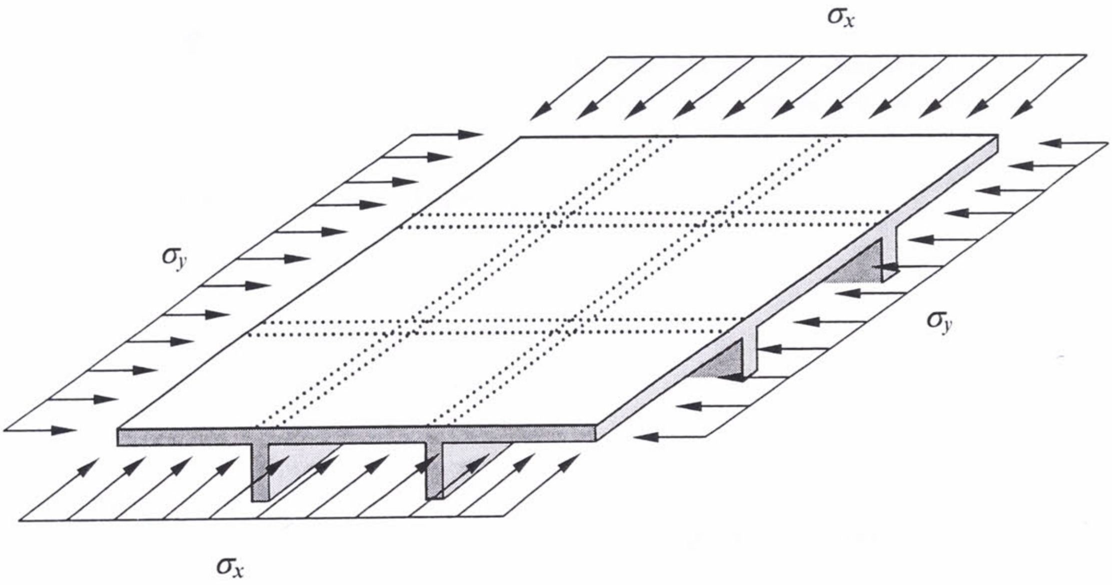

Figure 7.21 Plate with two longitudinal stiffeners and two internal supports

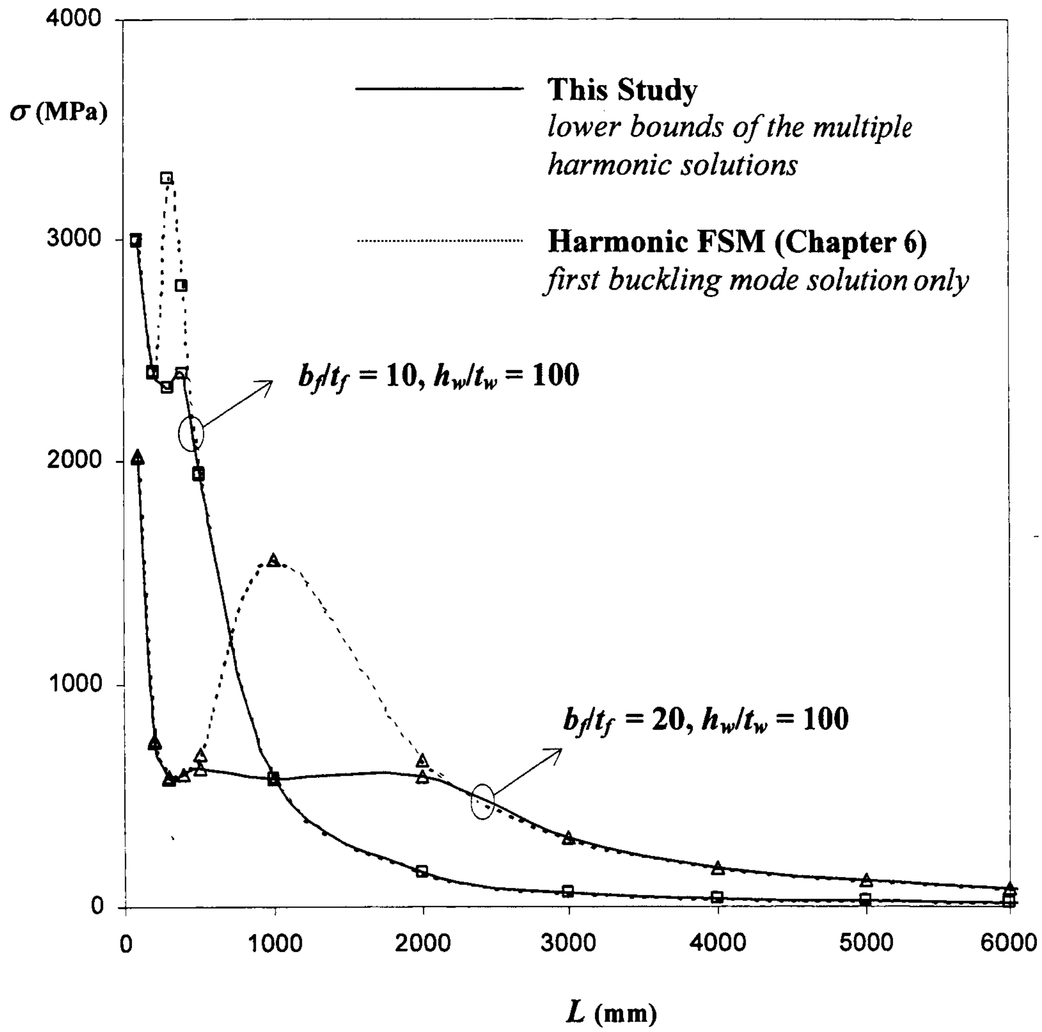

Figure 7. 22 Buckling stress for a T-section in uniform bending

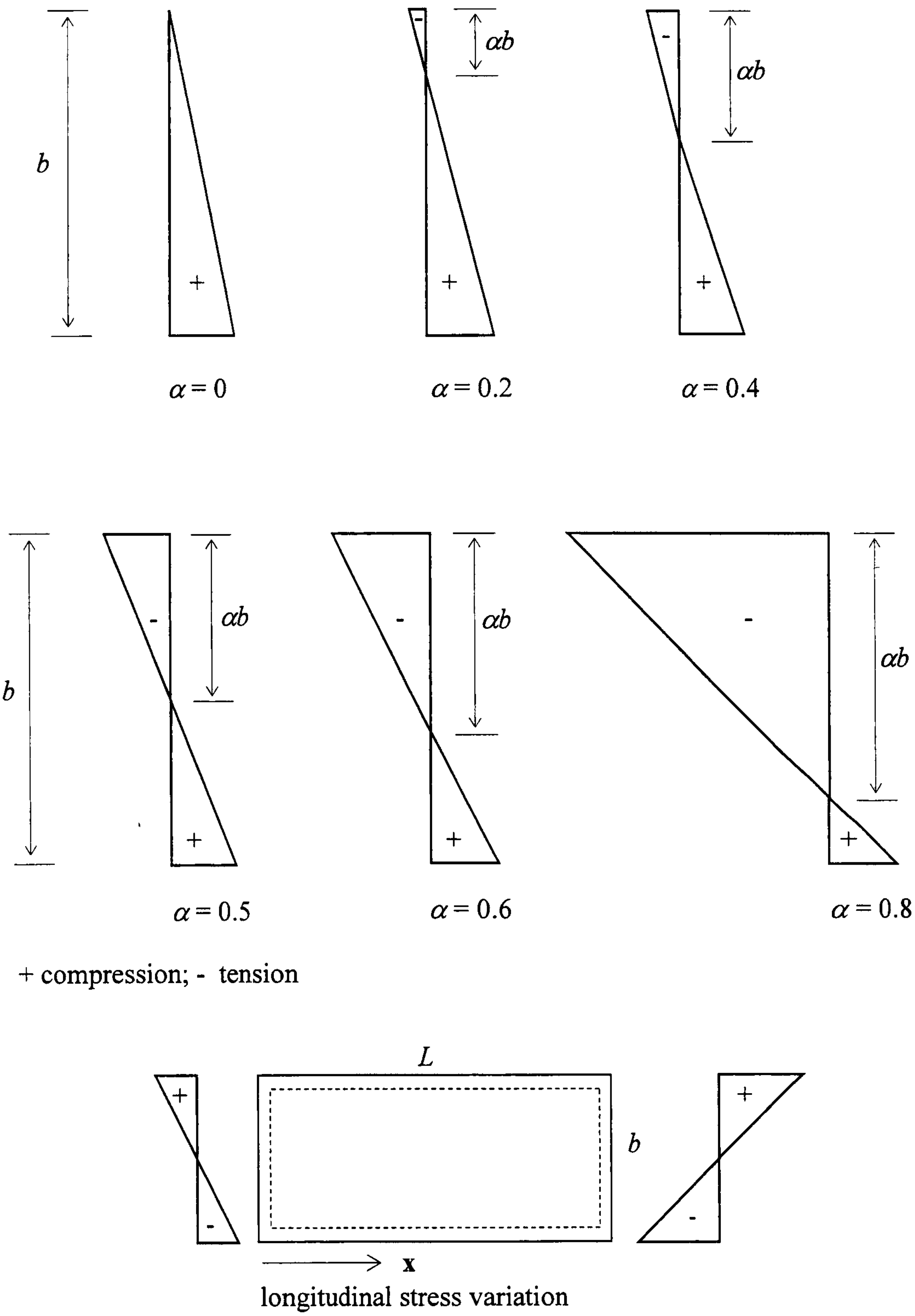

Figure 7.23 Transverse stress distribution

Case	Variation of $M(\xi^*)$ and $V(\xi)$
1	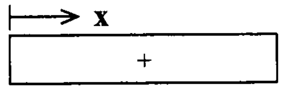 $M(\xi) = 1$ $V(\xi) = 0$
2	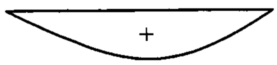 $M(\xi) = 4\xi - 4\xi^2$ $V(\xi) = 4 - 8\xi$
3	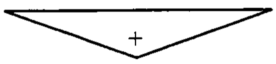 $M(\xi) = 2\xi$ $V(\xi) = 2$ + mirror image
4	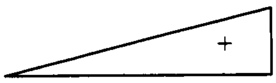 $M(\xi) = \xi$ $V(\xi) = 1$
5	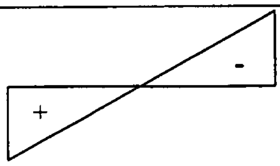 $M(\xi) = 1-2\xi$ $V(\xi) = -2$
6	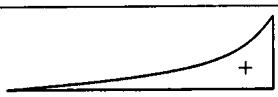 $M(\xi) = \xi^2$ $V(\xi) = 2\xi$

Case	Variation of $M(\xi)$ and $V(\xi)$
7	 $M(\xi) = -3\xi + 4\xi^2$ $V(\xi) = -3 + 8\xi$
8	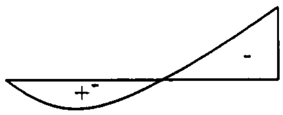 $M(\xi) = (16/3)\xi - (64/9)\xi^2$ $V(\xi) = (16/3) - 2(64/9)\xi$
9	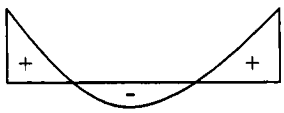 $M(\xi) = 1 - 6\xi + 6\xi^2$ $V(\xi) = -6 + 12\xi$
10	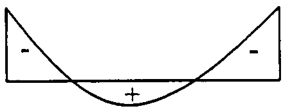 $M(\xi) = -2 + 12\xi - 12\xi^2$ $V(\xi) = 12 - 24\xi$
11	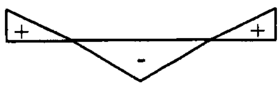 $M(\xi) = 1 - 4\xi$ $V(\xi) = -4$ + mirror image
12	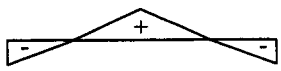 $M(\xi) = -1+4\xi$ $V(\xi) = 4$ + mirror image

$^*\xi = x/L$

Figure 7.24 Variation of $M(\xi)$ and $V(\xi)$ for Cases 1-12

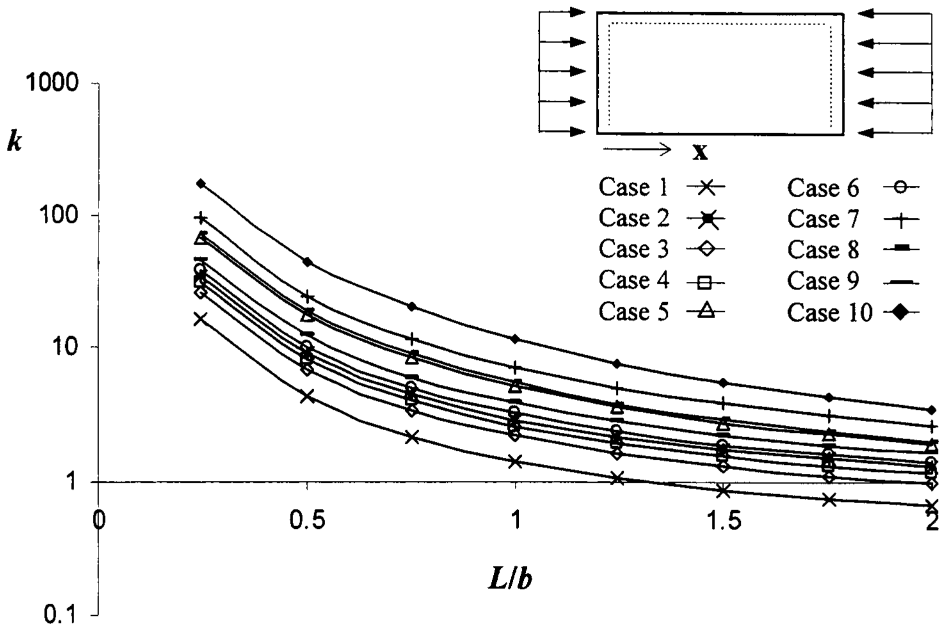

Figure 7.25 Buckling coefficients of s-f-s-s plates subjected to uniform transverse compression stress that varies longitudinally (Cases 1-10)

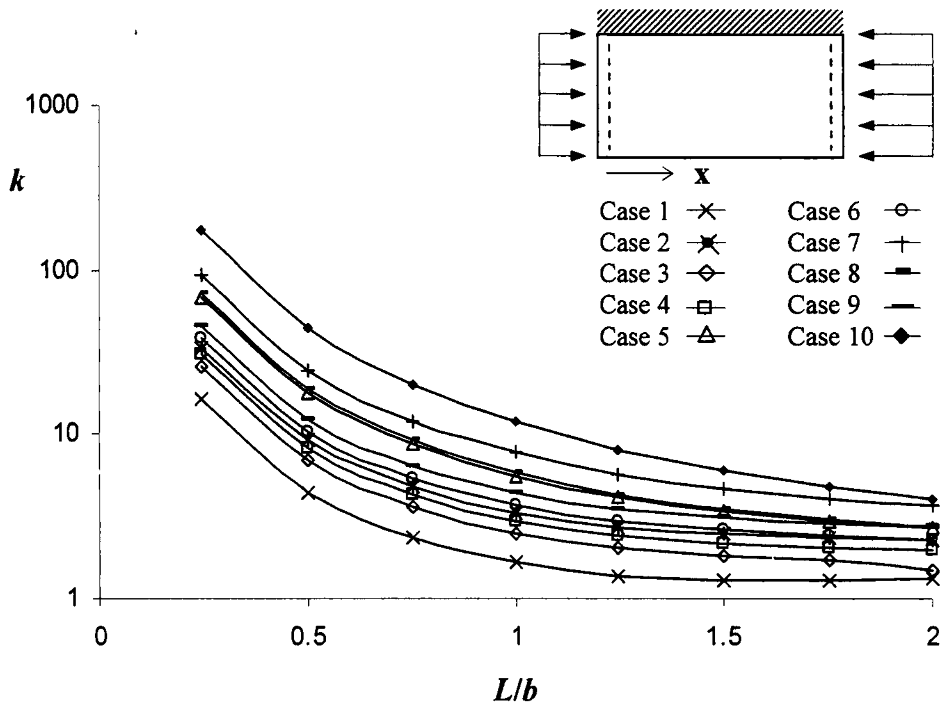

Figure 7.26 Buckling coefficients of s-f-s-c plates subjected to uniform transverse compression stress that varies longitudinally (Cases 1-10)

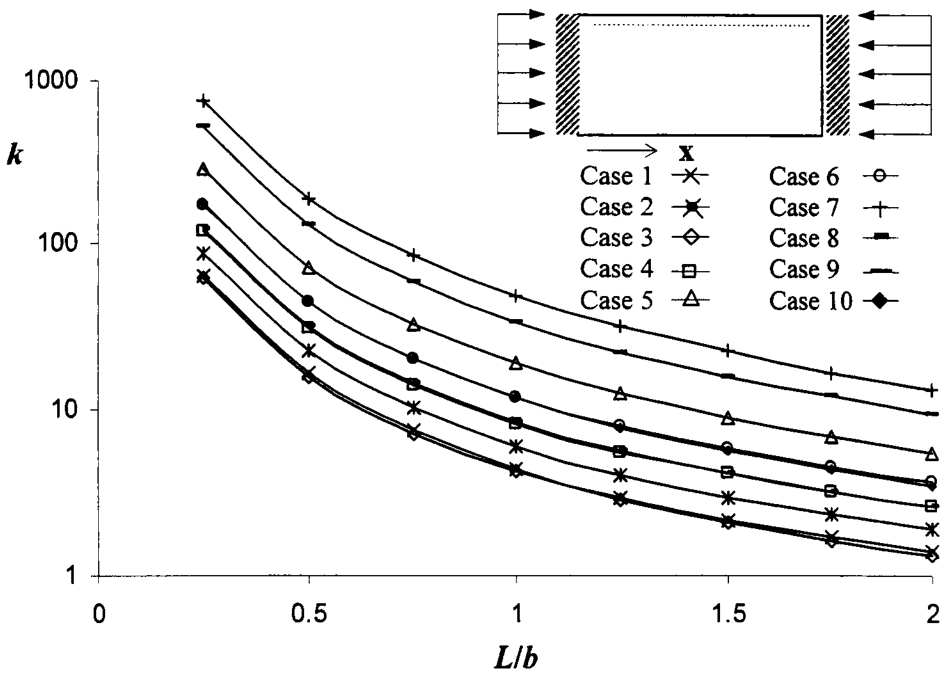

Figure 7.27 Buckling coefficients of c-f-c-s plates subjected to uniform transverse compression stress that varies longitudinally (Cases 1-10)

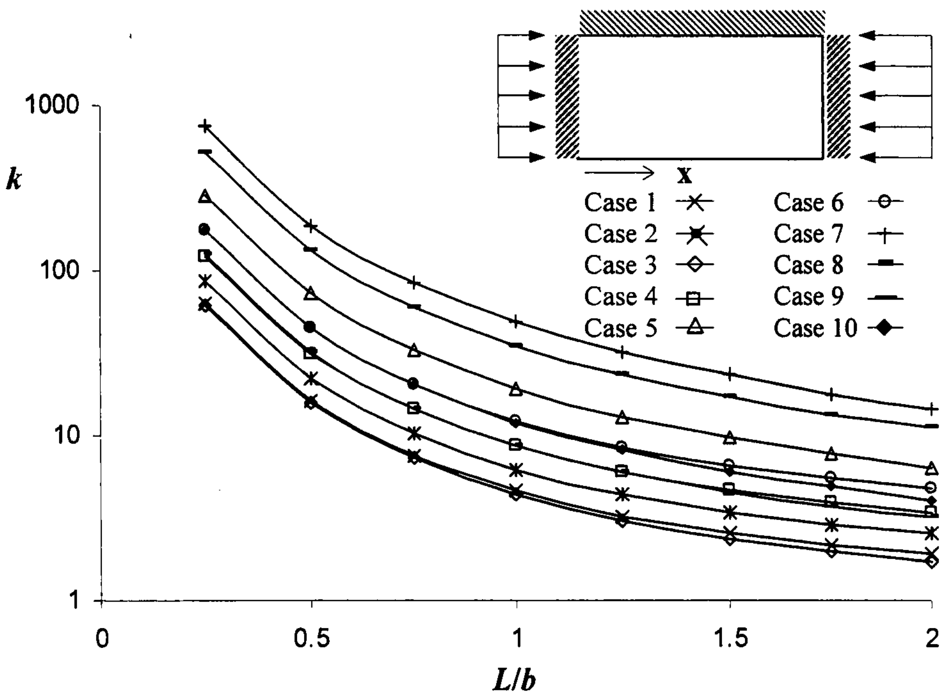

Figure 7.28 Buckling coefficients of c-f-c-c plates subjected to uniform transverse compression stress that varies longitudinally (Cases 1-10)

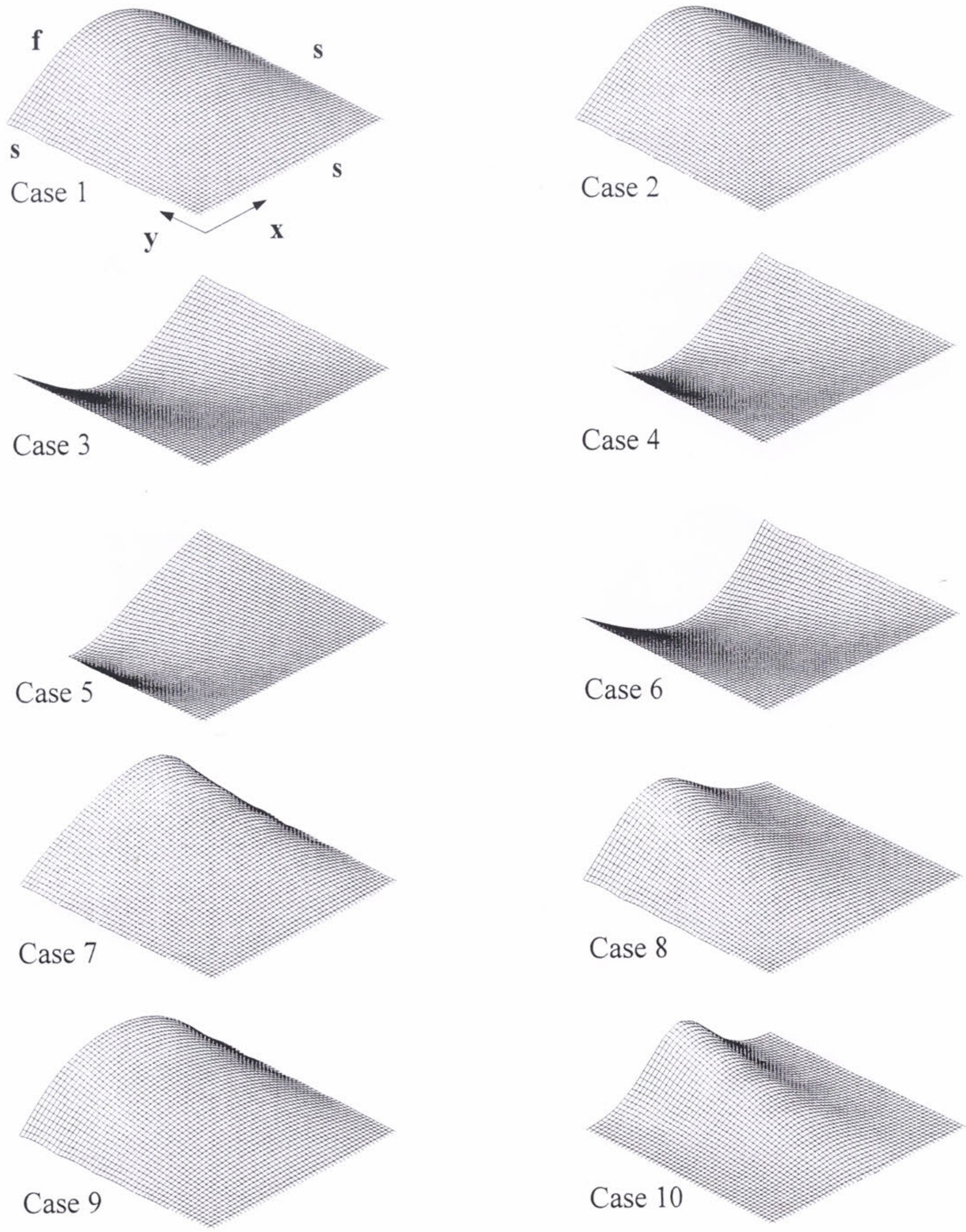

Figure 7.29 Buckling modes for s-f-s-s plates subjected to uniform transverse compression stress that varies longitudinally (Cases 1-10)

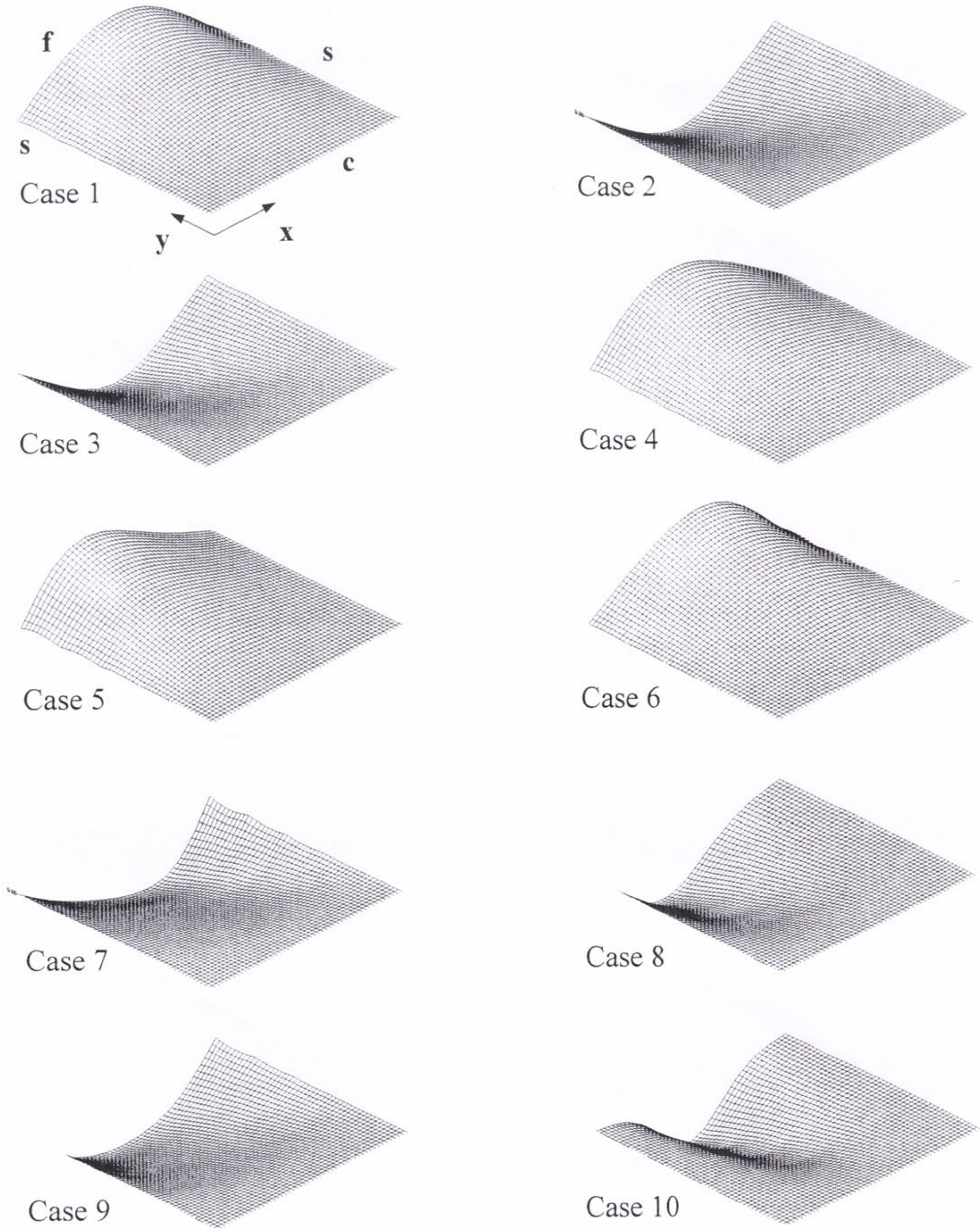

Figure 7.30 Buckling modes for s-f-s-c plates subjected to uniform transverse compression stress that varies longitudinally (Cases 1-10)

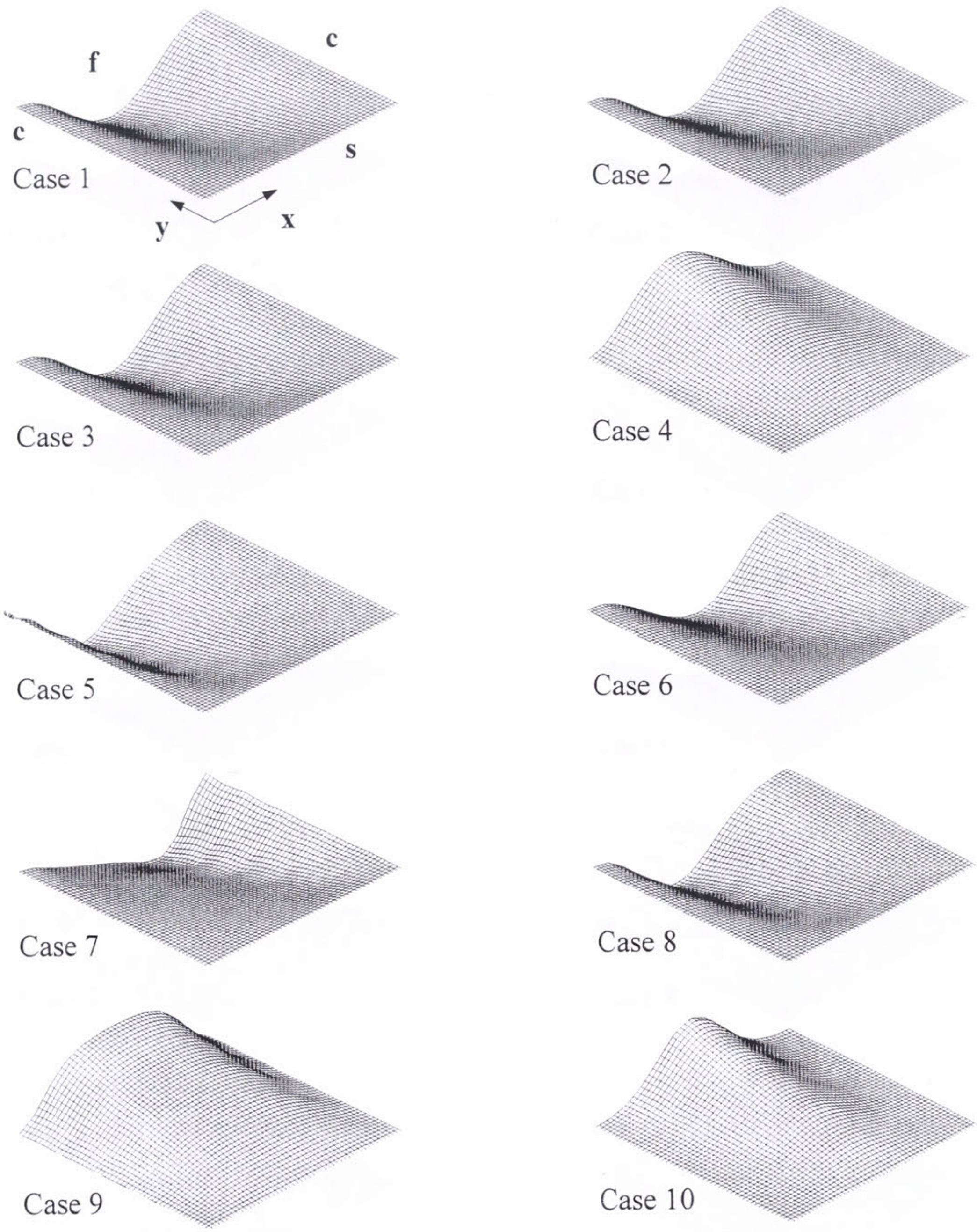

Figure 7.31 Buckling modes for c-f-c-s plates subjected to uniform transverse compression stress that varies longitudinally (Cases 1-10)

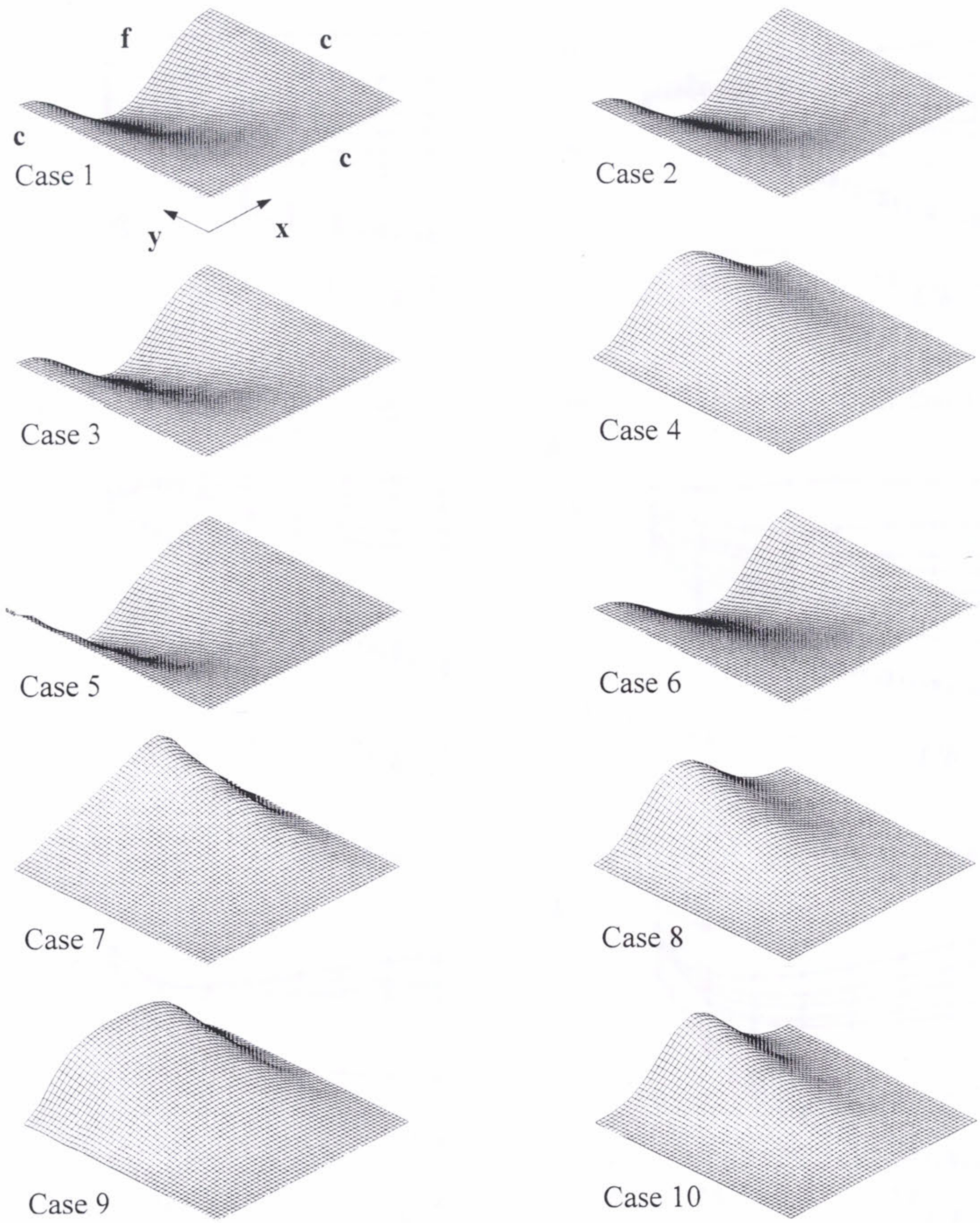

Figure 7.32 Buckling modes for c-f-c-c plates subjected to uniform transverse compression stress that varies longitudinally (Cases 1-10)

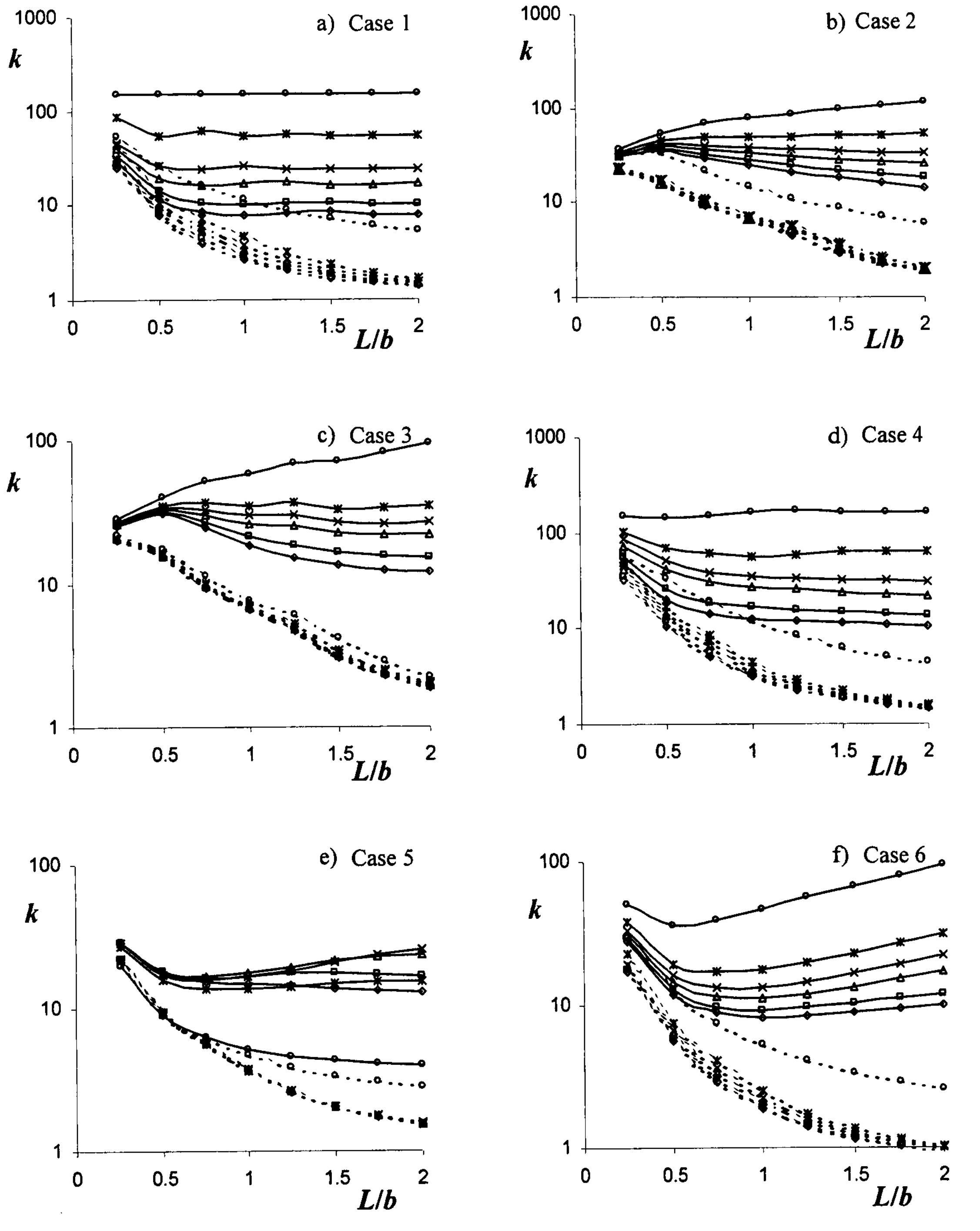
a) Case 1
b) Case 2
c) Case 3
d) Case 4
e) Case 5
f) Case 6
k
L/b
1000
100
10
1
0
0.5
1
1.5
2

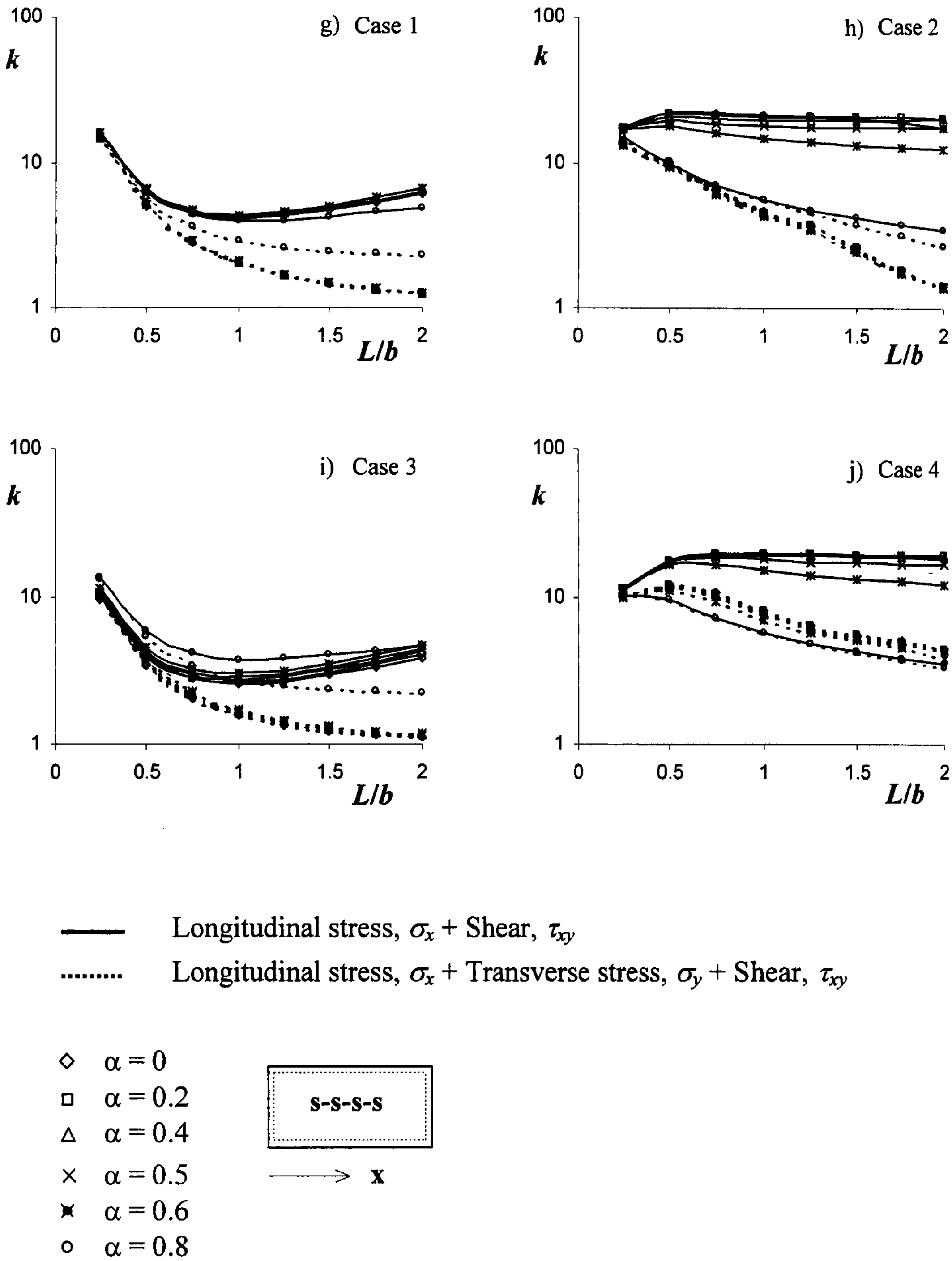

Figure 7.33 Buckling modes for s-s-s-s plates; a) Case 1 to j) Case 10

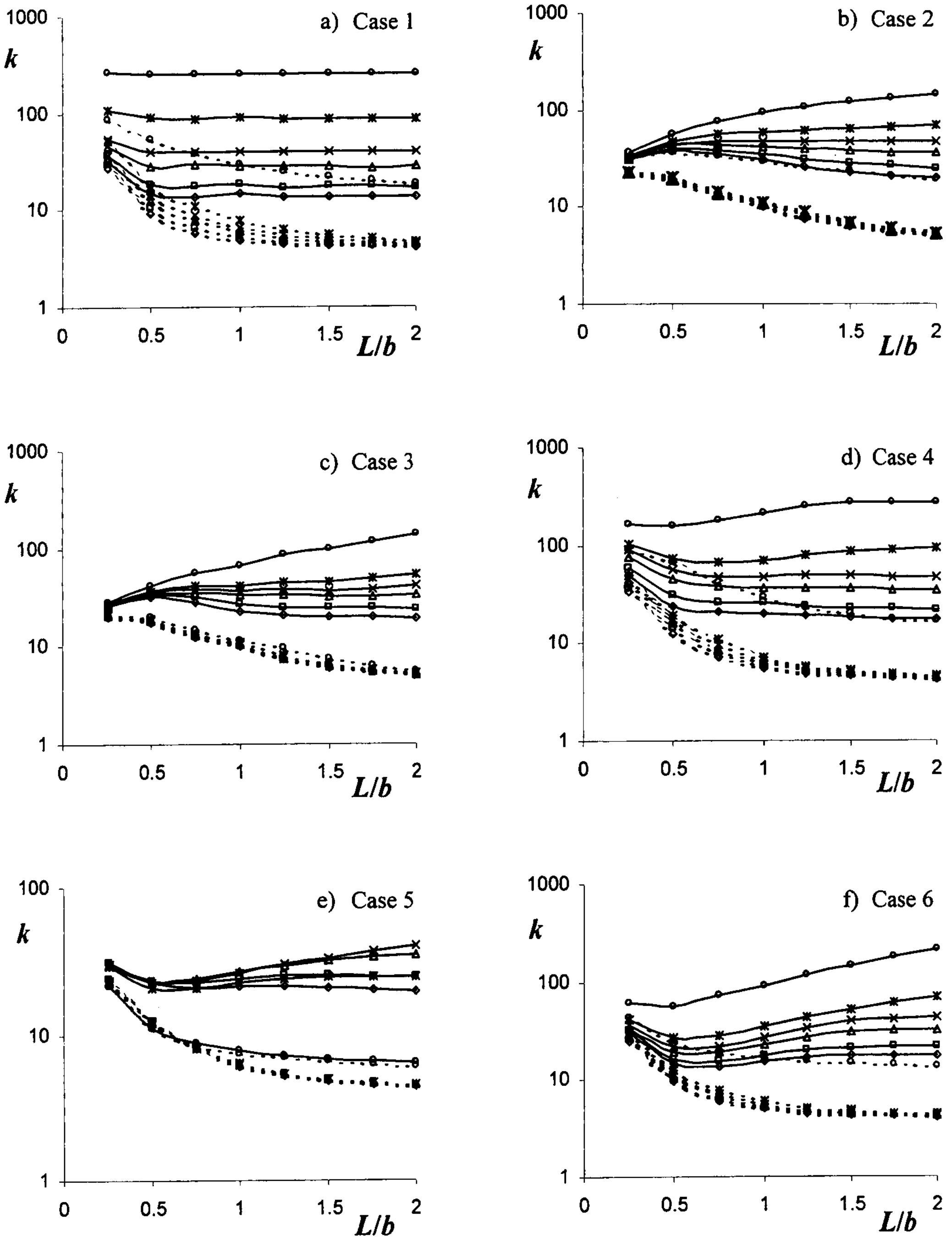

a) Case 1
b) Case 2
c) Case 3
d) Case 4
e) Case 5
f) Case 6
k
L/b
1000
100
10
1
0
0.5
1
1.5
2

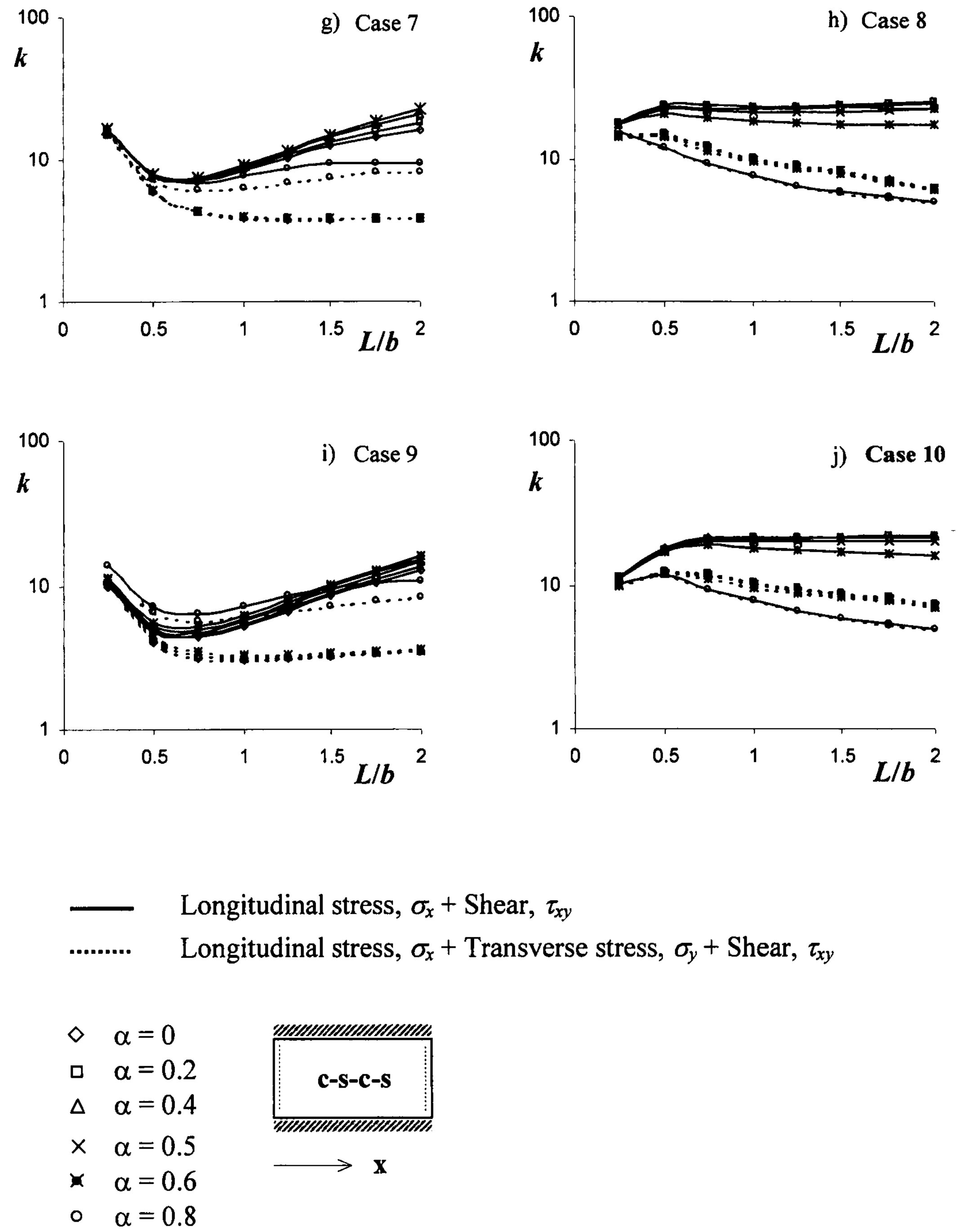

Figure 7.34 Buckling modes for c-s-c-s plates; a) Case 1 to j) Case 10

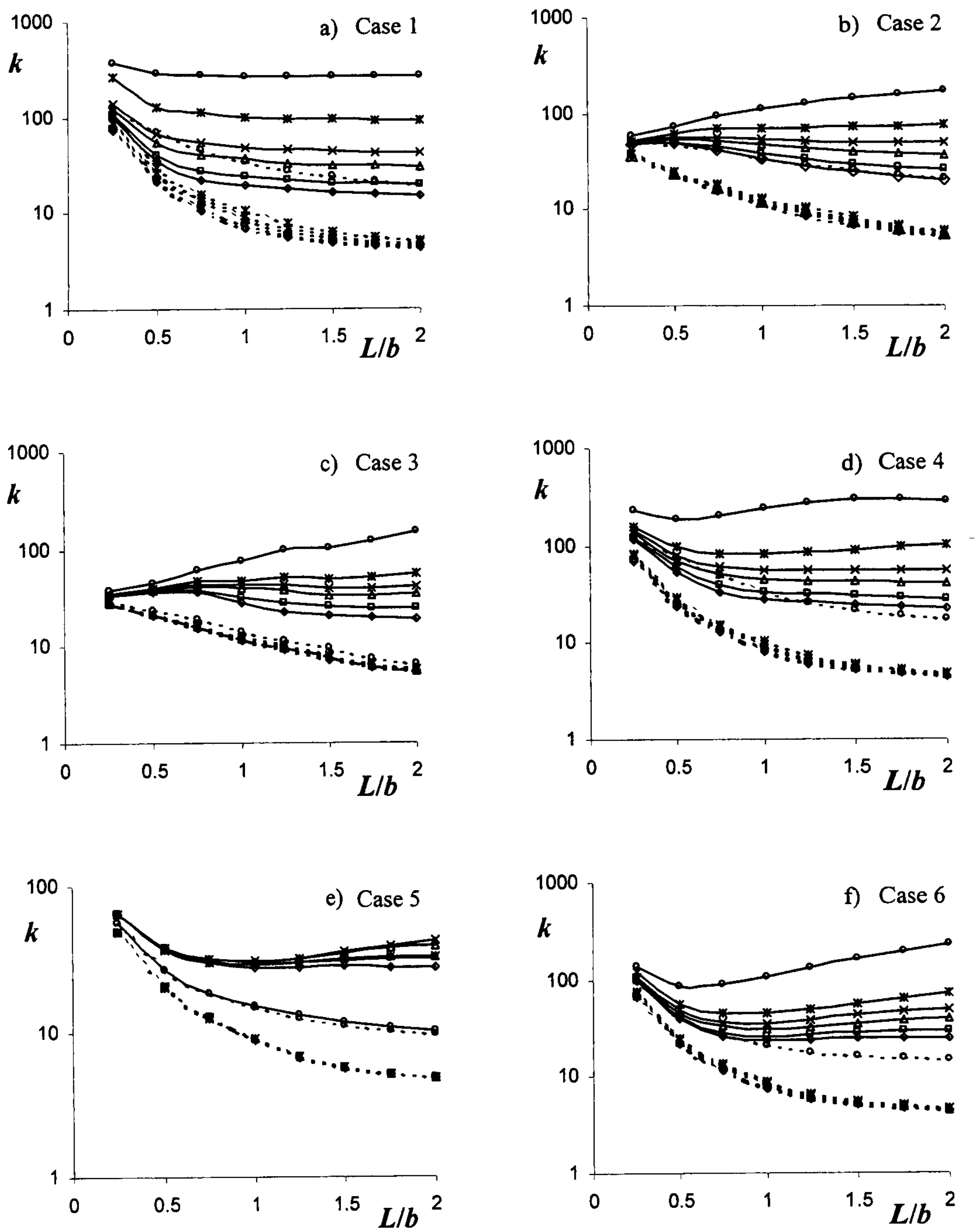
a) Case 1
b) Case 2
c) Case 3
d) Case 4
e) Case 5
f) Case 6
k
L/b
1000
100
10
1
0
0.5
1
1.5
2

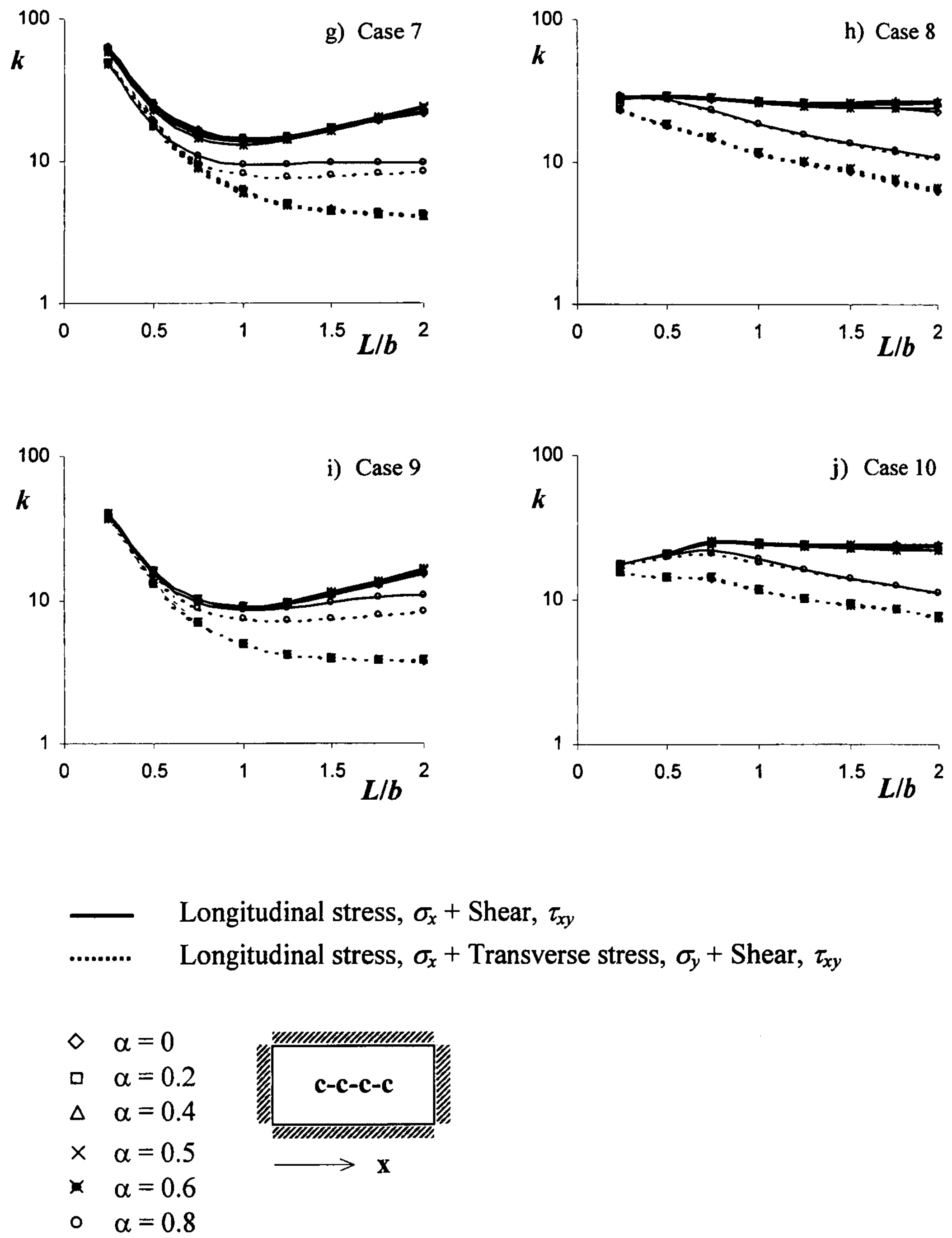

Figure 7.35 Buckling coefficients for c-c-c-c plates; a) Case 1 to j) Case 10

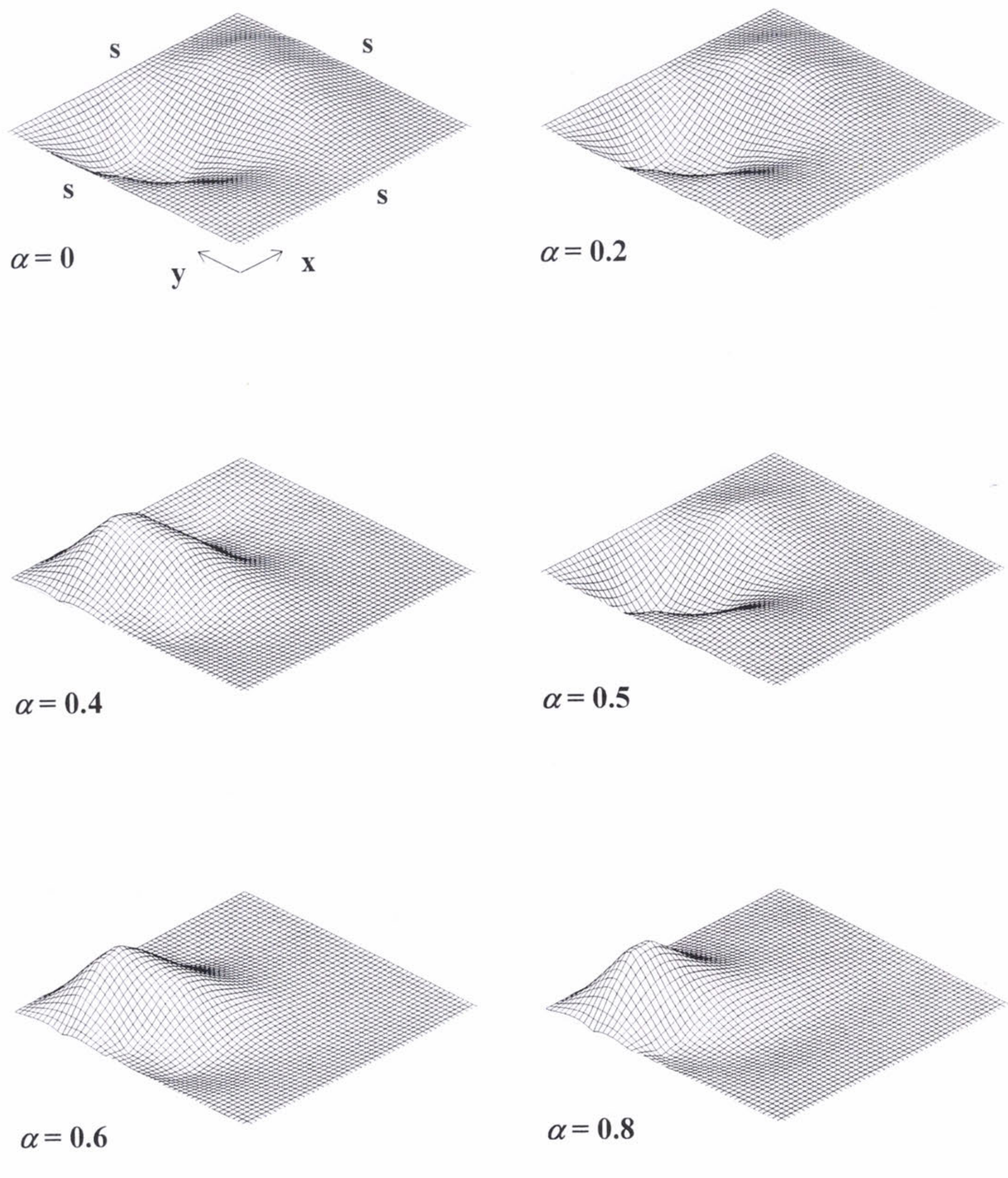

Figure 7.36 Buckling modes for s-s-s-s plates subjected to varying transverse stress; (Cases 2)

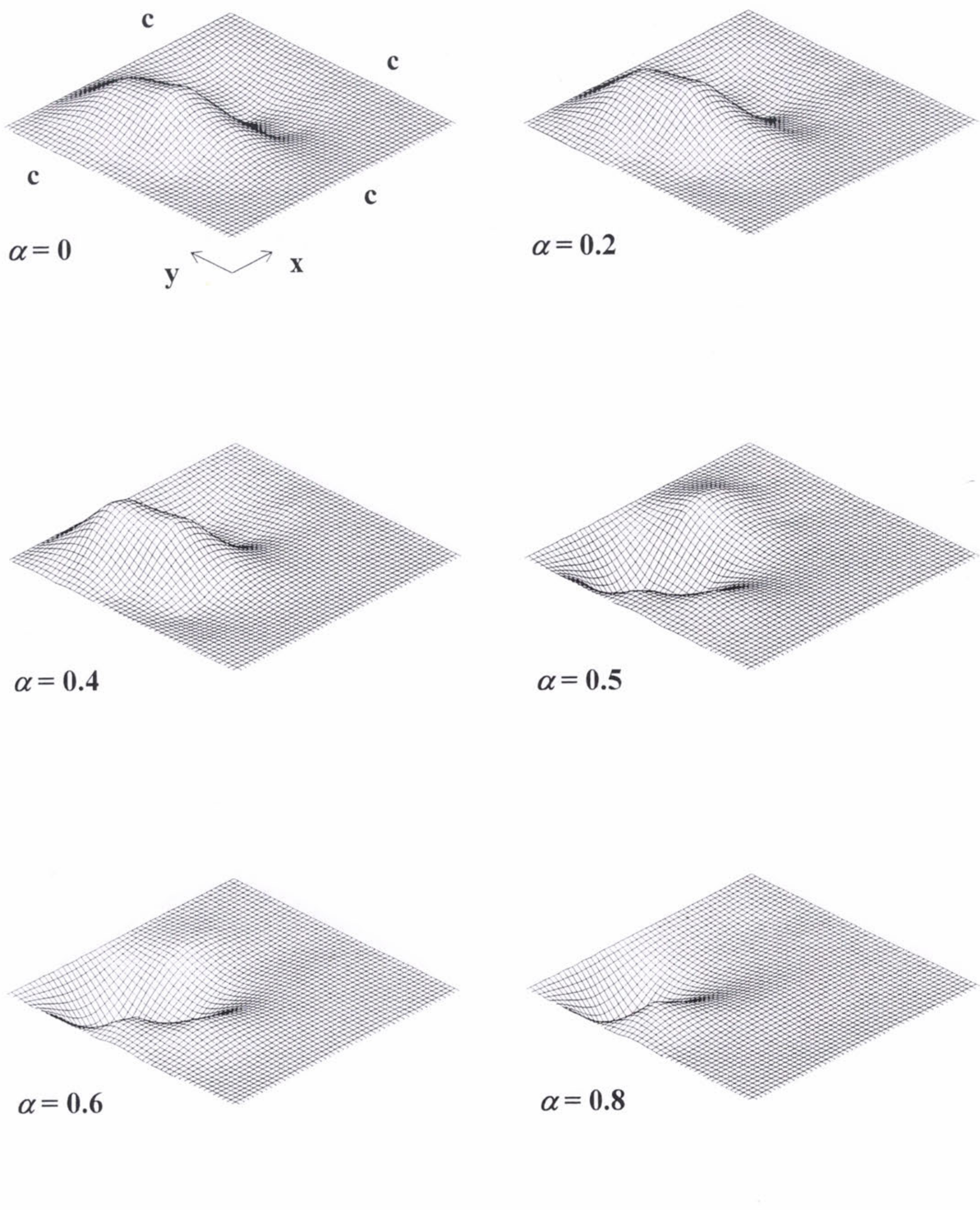

Figure 7.37 Buckling modes for c-c-c-c plates subjected to varying transverse stress (Cases 2)

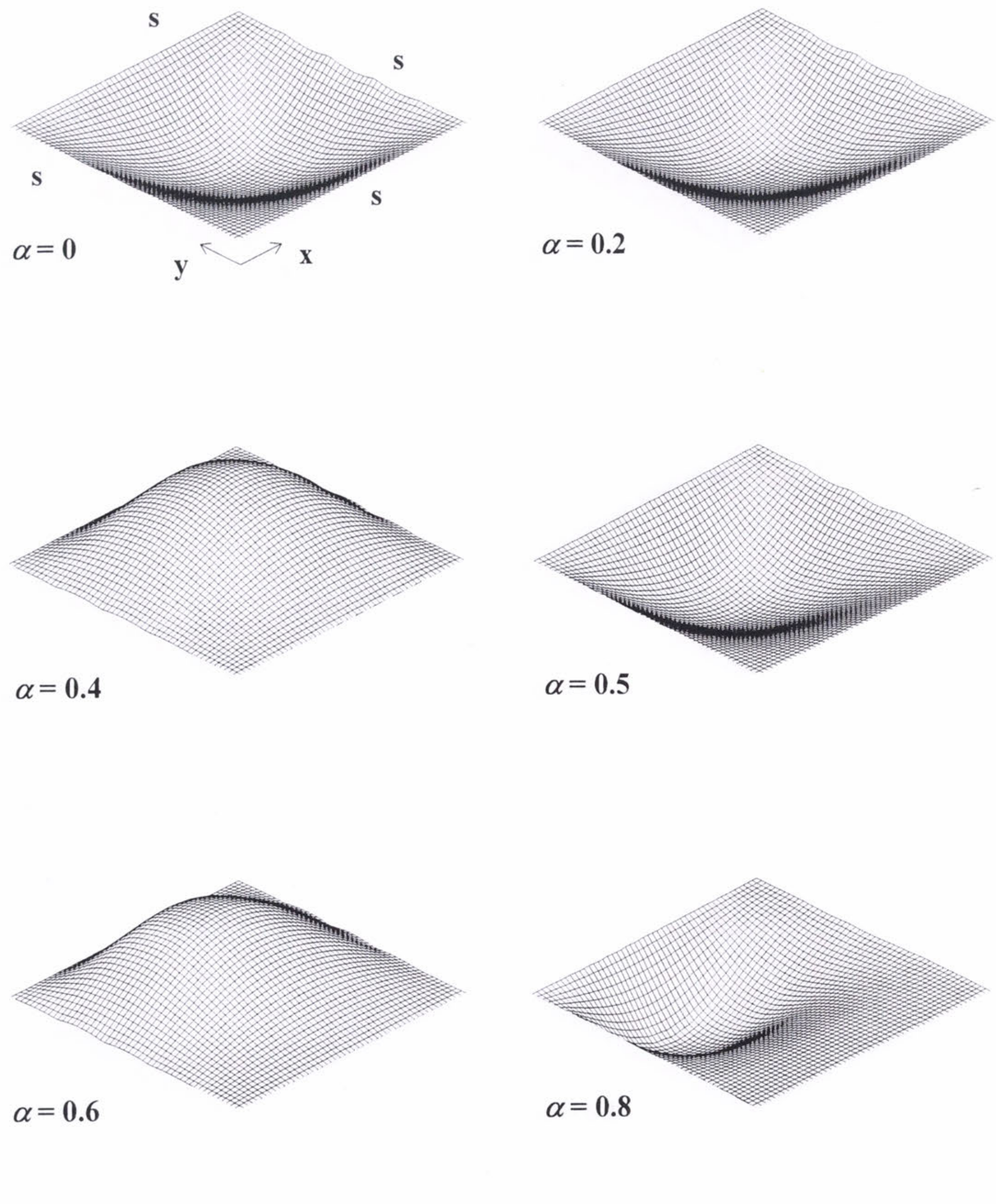

Figure 7.38 Buckling modes for s-s-s-s plates subjected to varying transverse stress; (Cases 6)

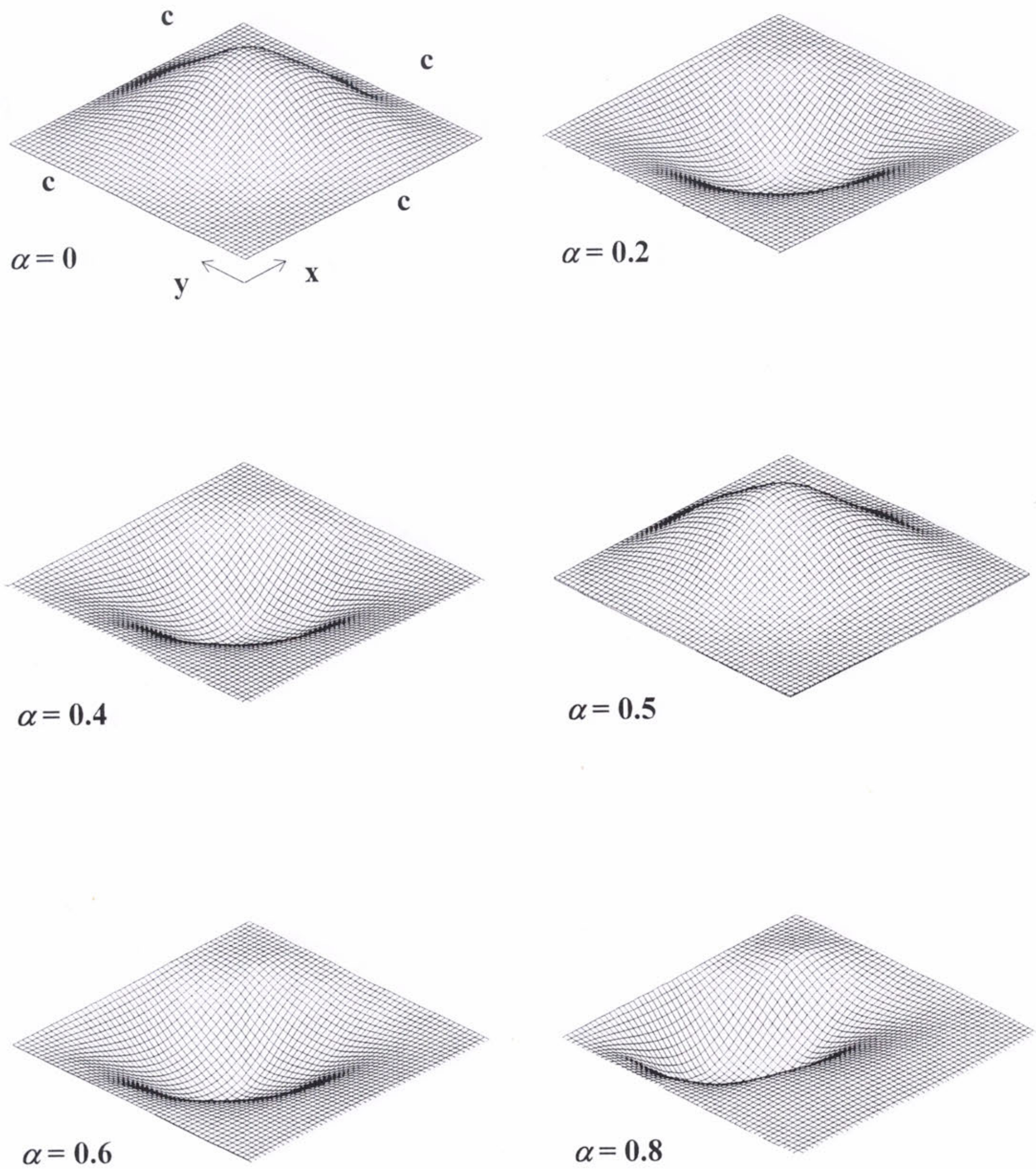

Figure 7.39 Buckling modes for c-c-c-c plates subjected to varying transverse stress; (Cases 6)

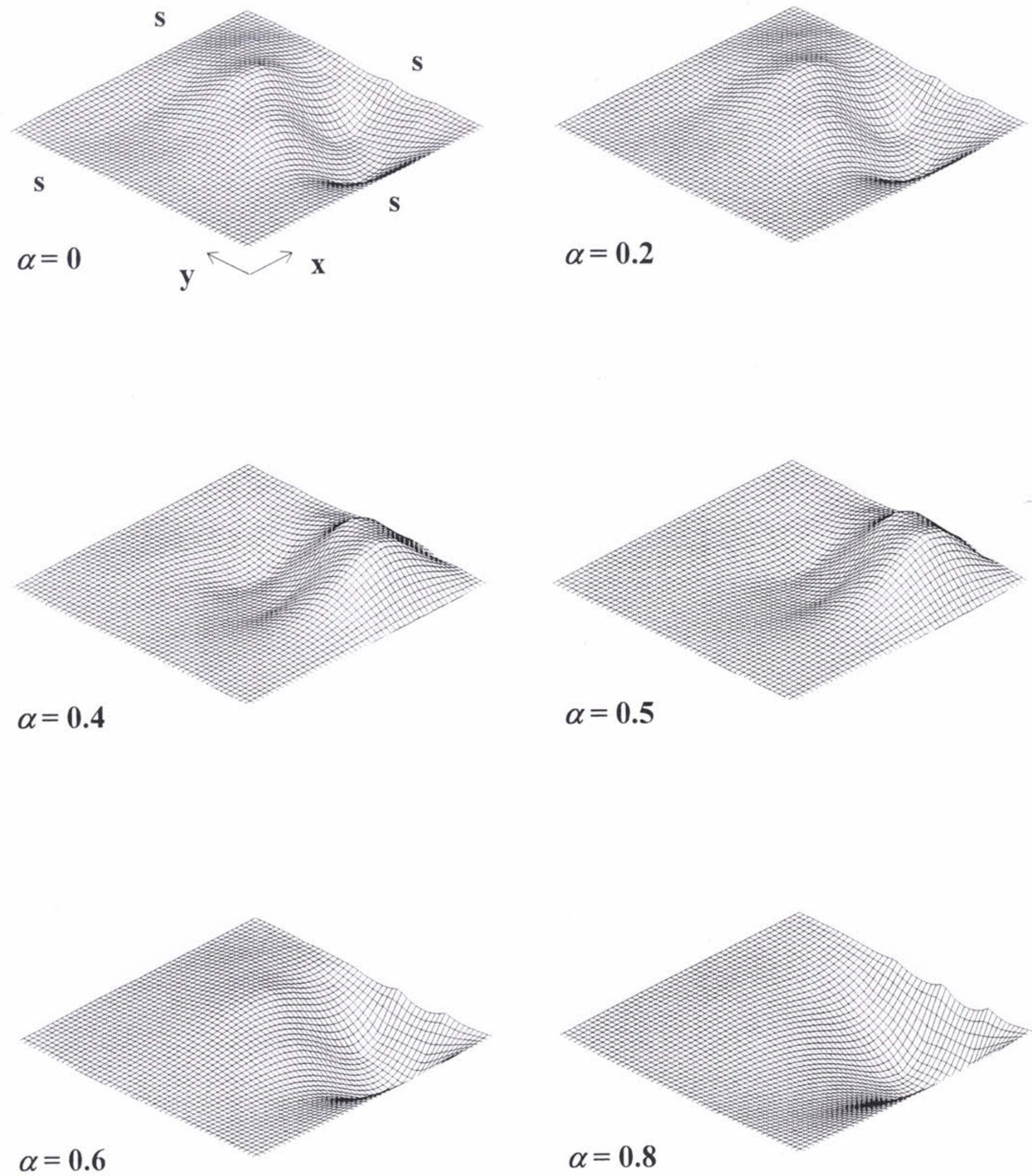

Figure 7.40 Buckling modes for s-s-s-s plates subjected to varying transverse stress; (Cases 8)

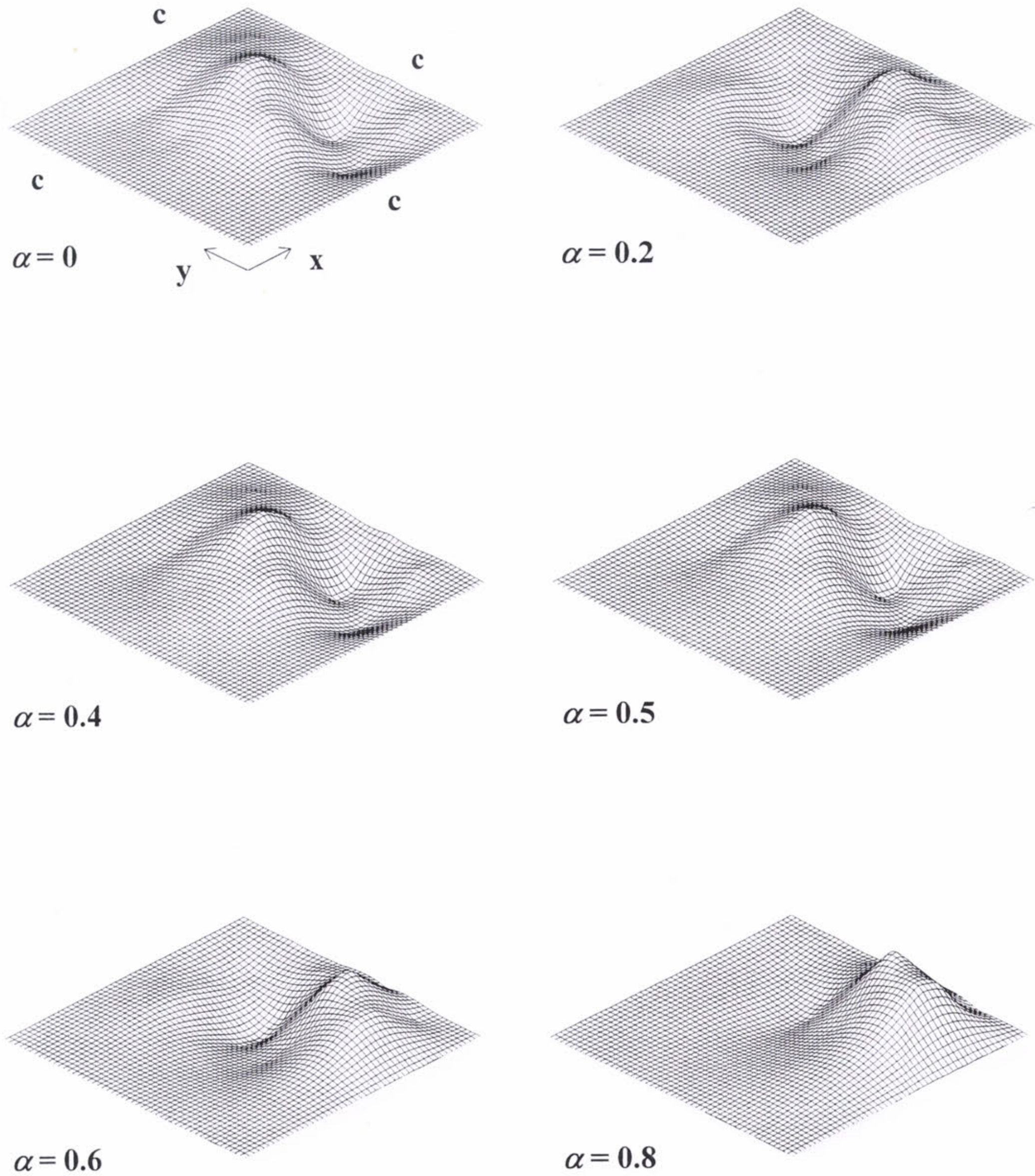

Figure 7.41 Buckling modes for c-c-c-c plates subjected to varying transverse stress; (Cases 8)

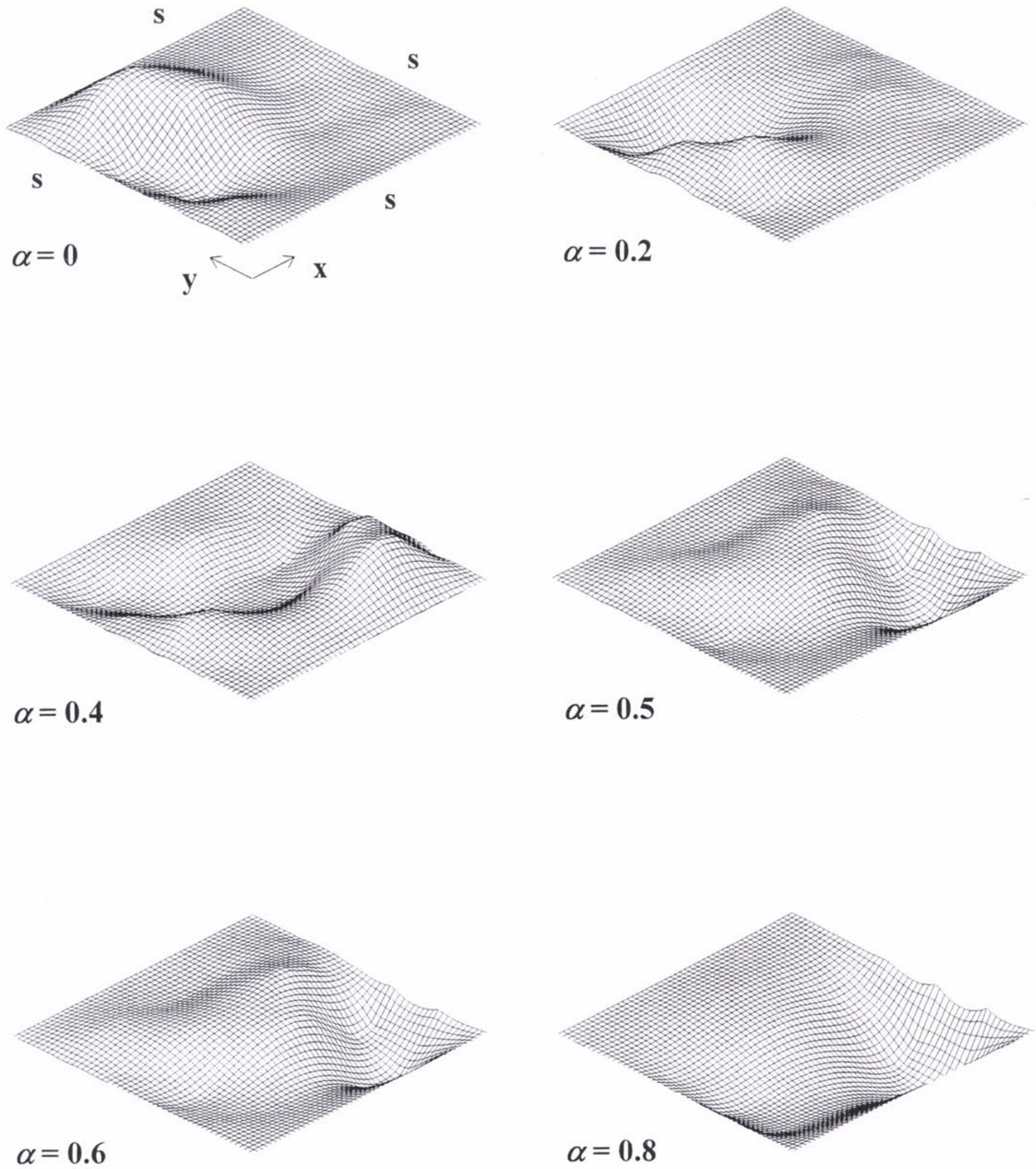

Figure 7.42 Buckling modes for s-s-s-s plates subjected to varying transverse stress (Cases 10)

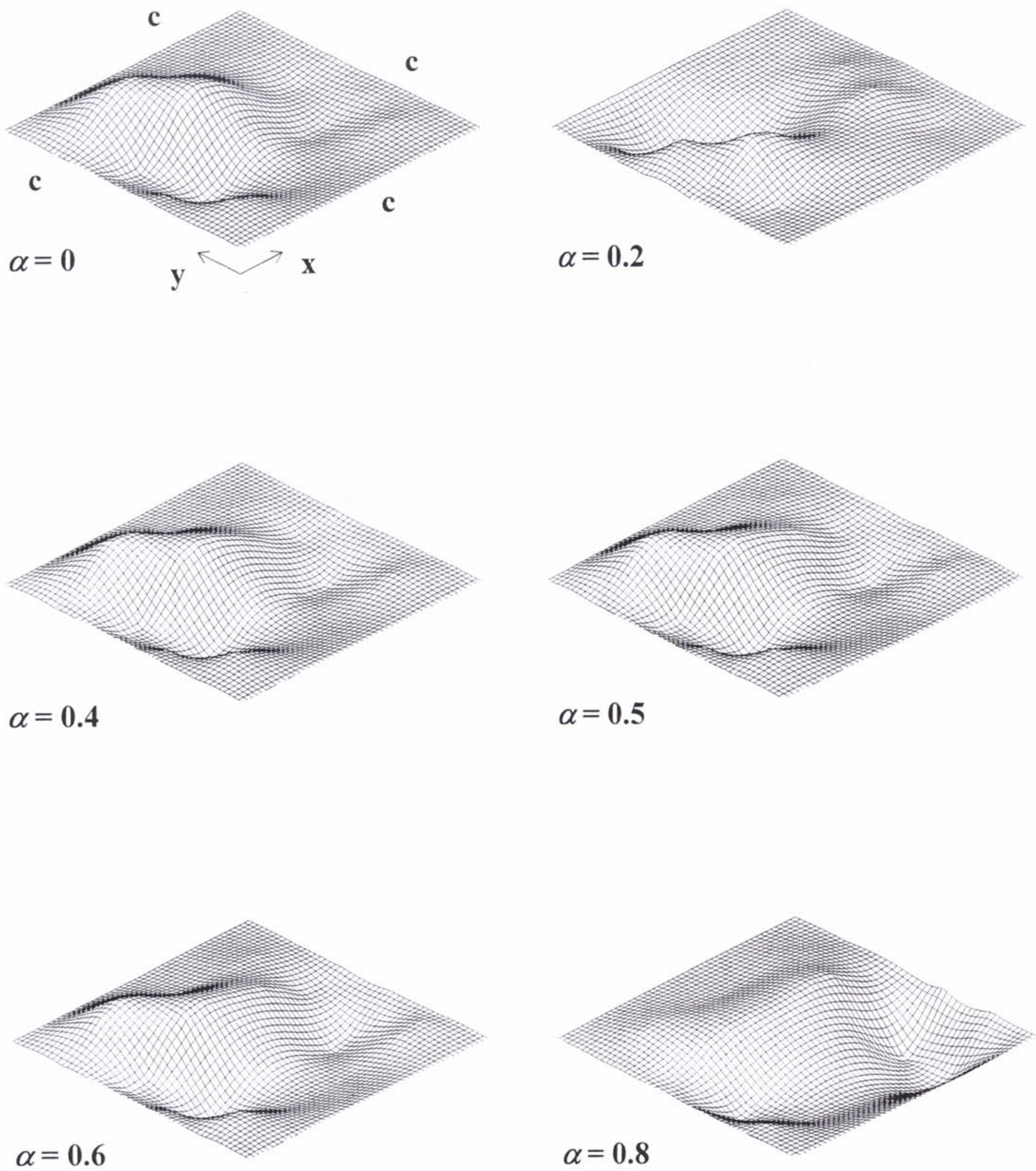

Figure 7.43 Buckling modes for c-c-c-c plates subjected to varying transverse stress; (Cases 10)

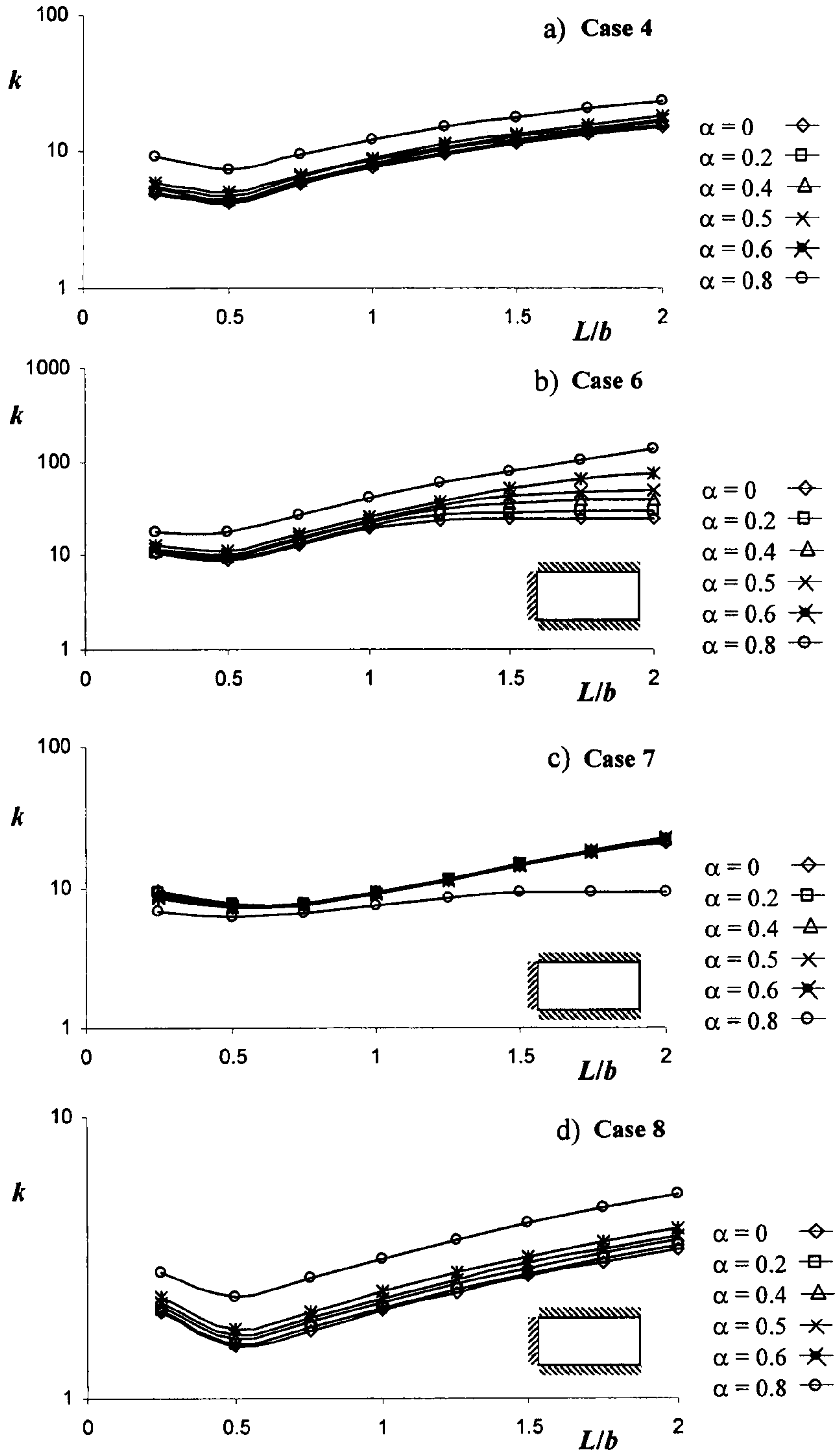

Figure 7.44 Buckling coefficients for c-c-f-c plates subjected to varying transverse stress; (Cases 4,6,7 & 8)

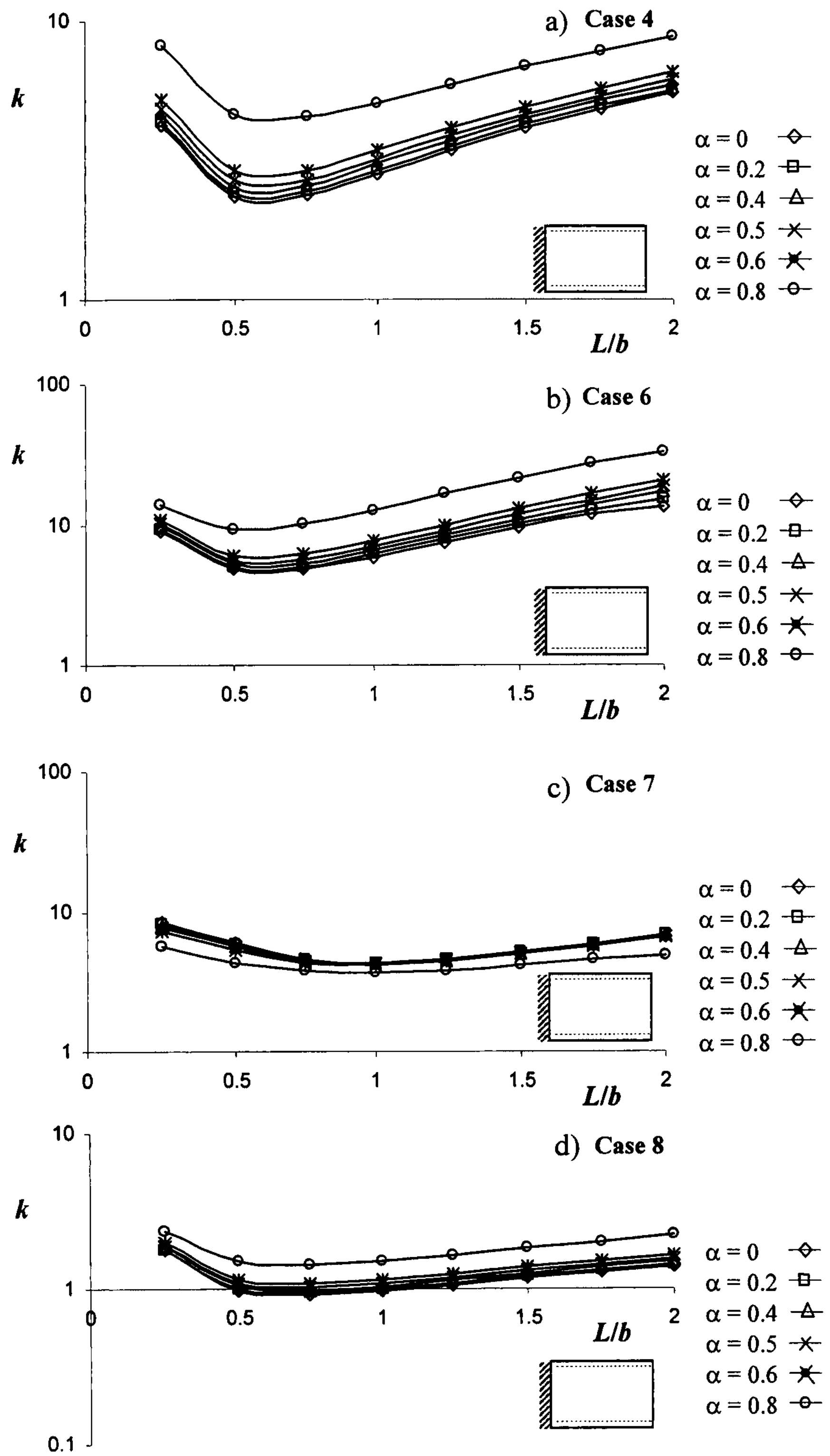

Figure 7.45 Buckling coefficients for c-s-f-s plates subjected to varying transverse stress; (Cases 4,6,7 & 8)

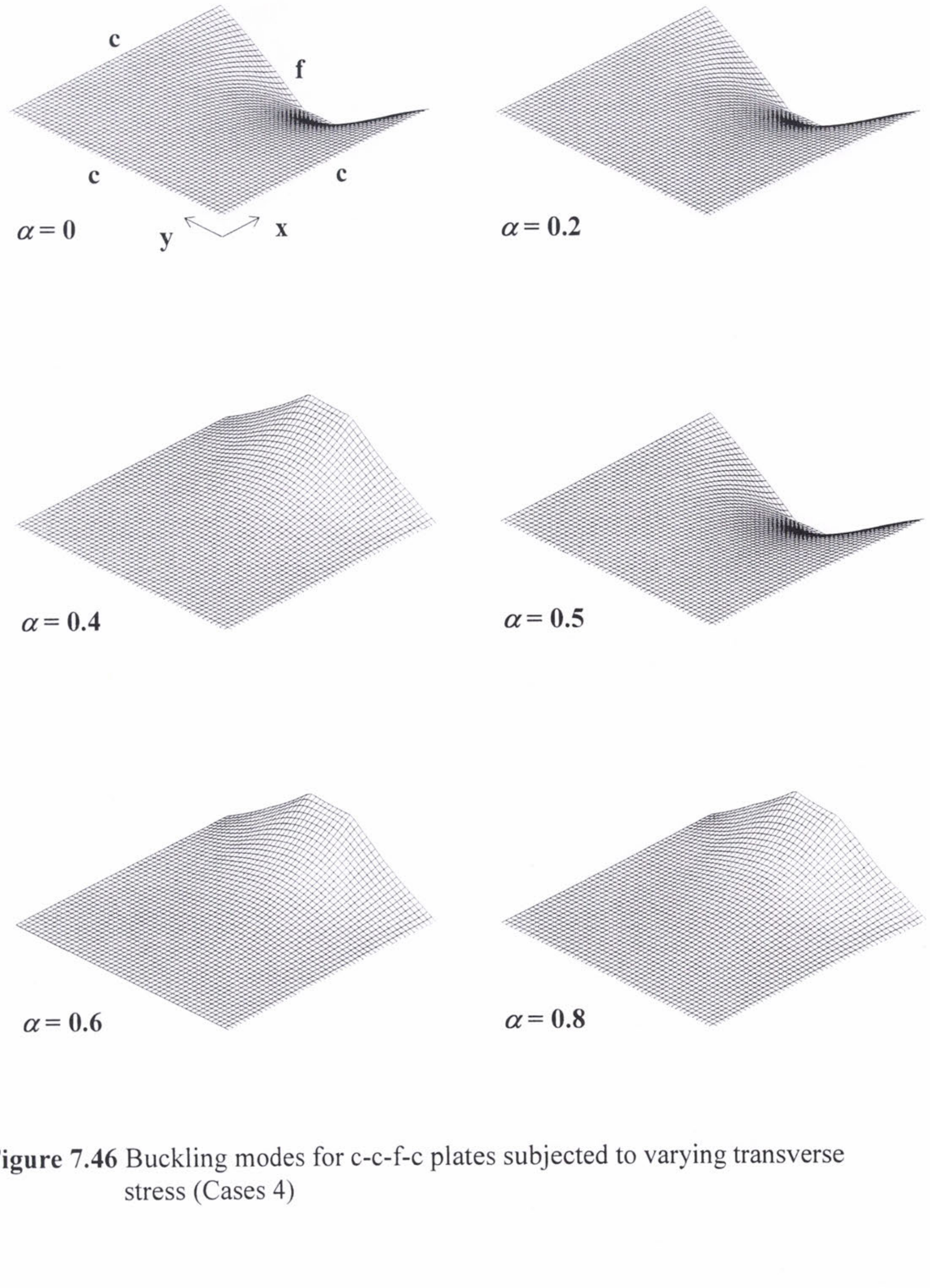

Figure 7.46 Buckling modes for c-c-f-c plates subjected to varying transverse stress (Cases 4)

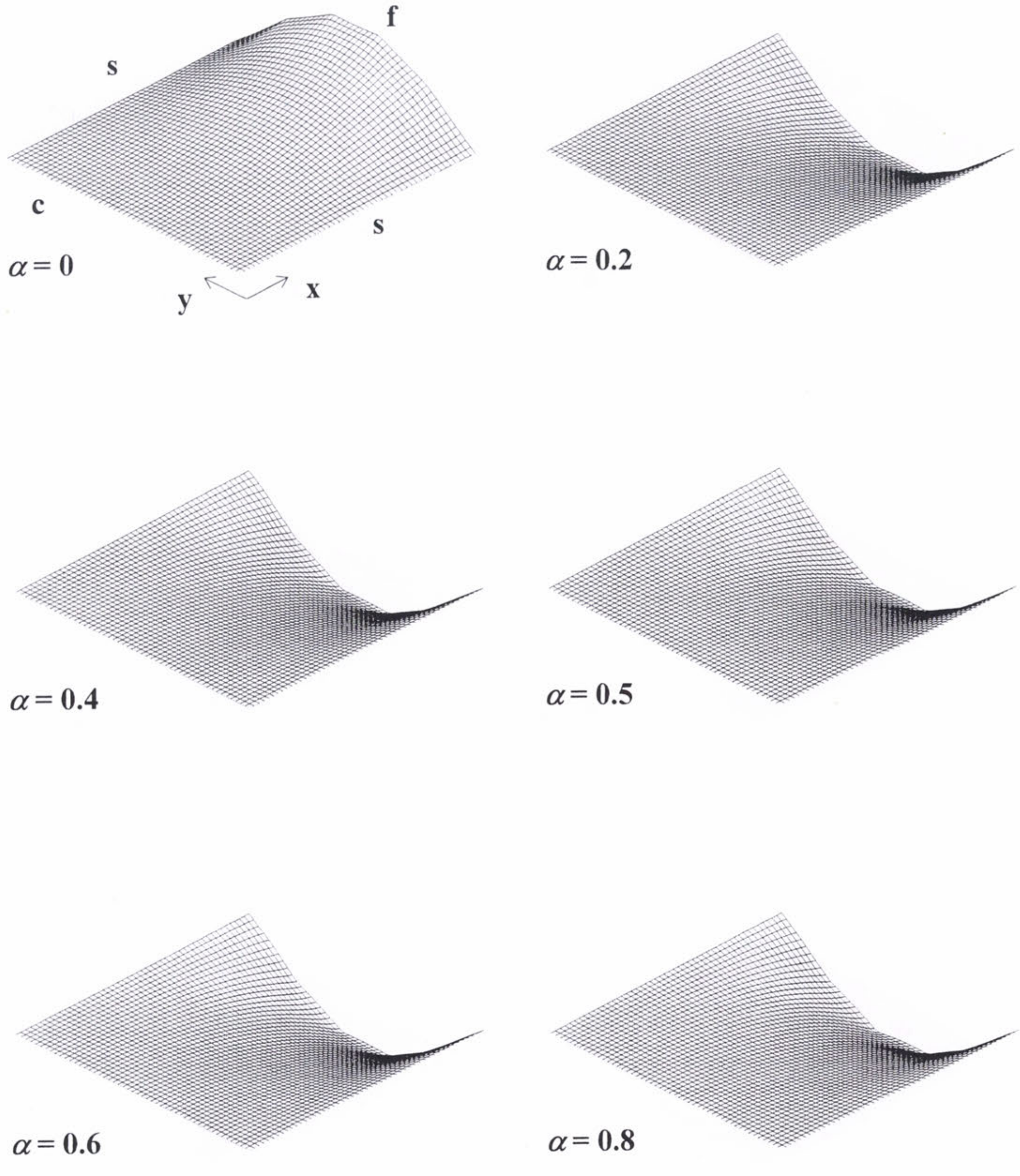

Figure 7.47 Buckling modes for c-s-f-s plates subjected to varying transverse stress (Cases 4)

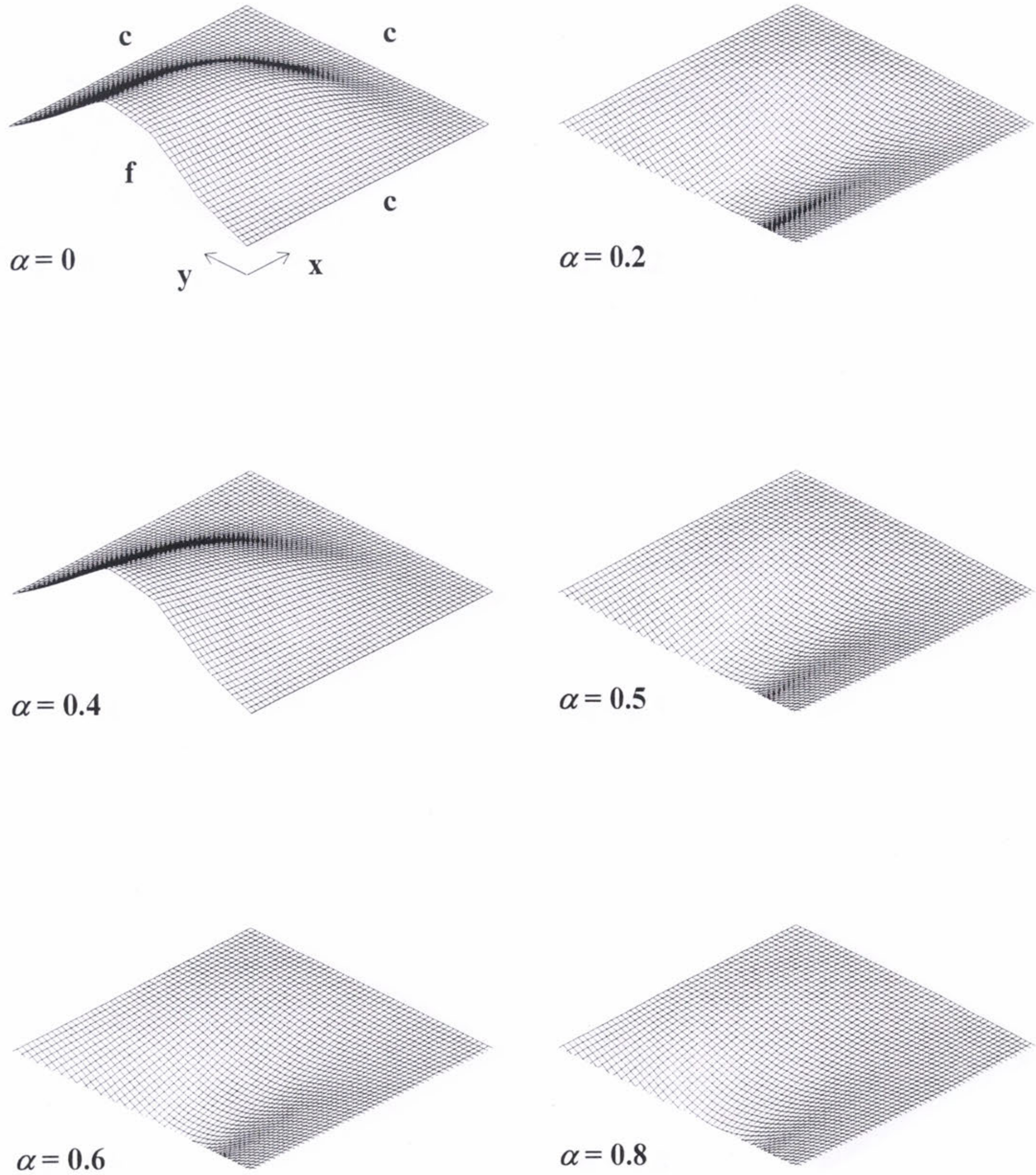

Figure 7.48 Buckling modes for f-c-c-c plates subjected to varying transverse stress (Cases 6)

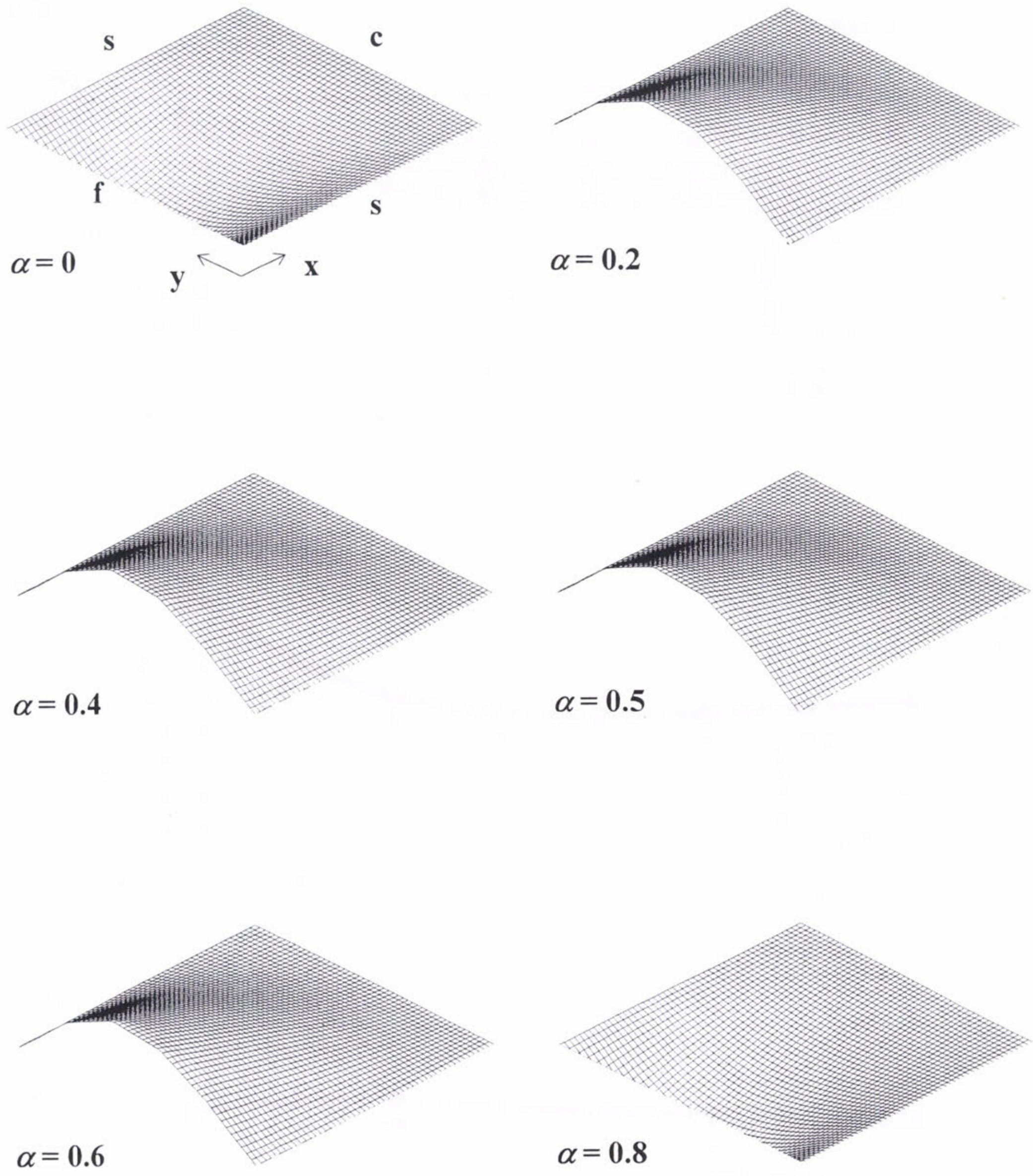

Figure 7.49 Buckling modes for f-s-c-s plates subjected to varying transverse stress (Cases 6)

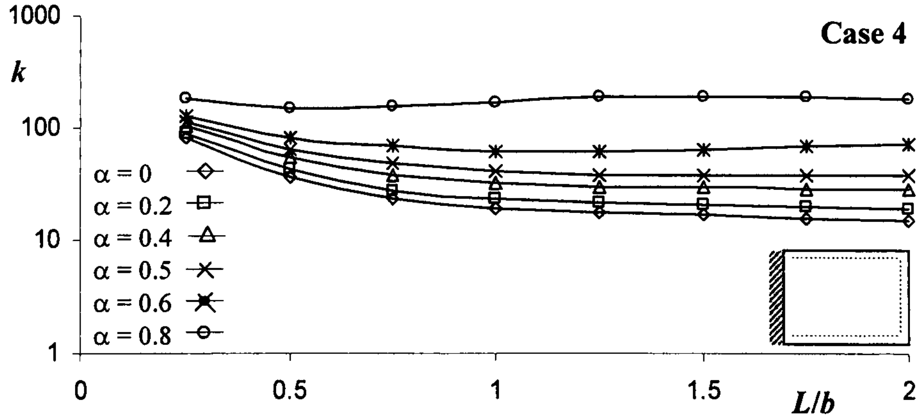

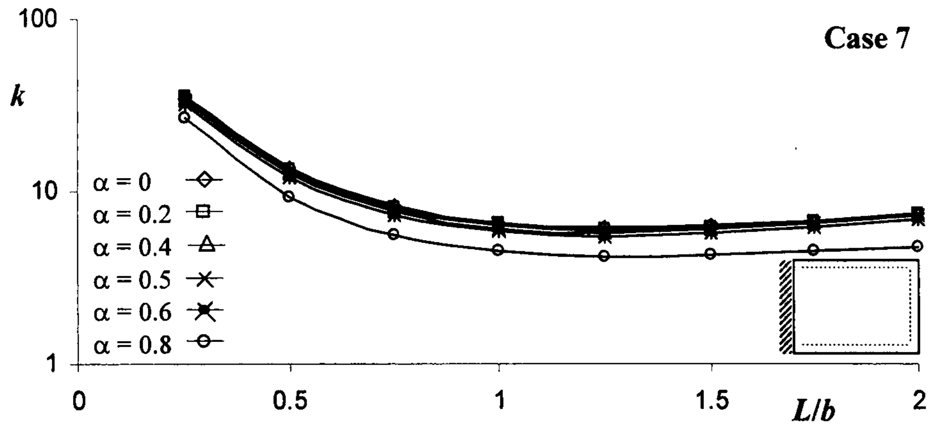

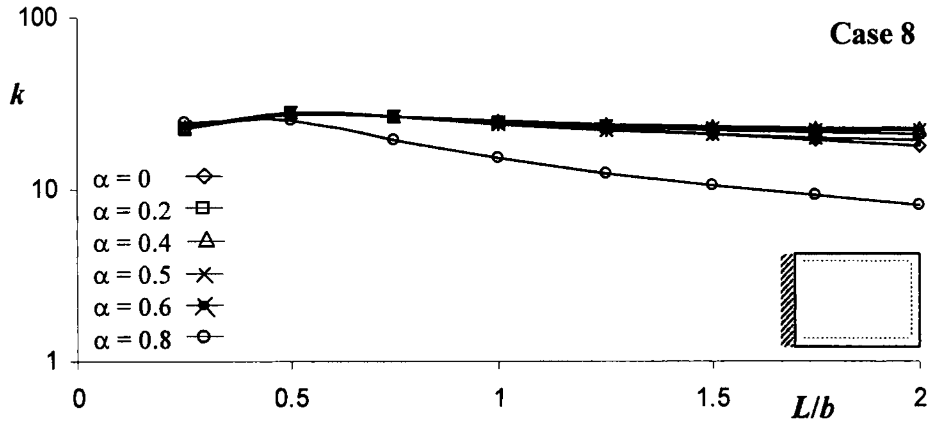

Figure 7.50 Buckling coefficients for c-s-s-s plates subjected to varying transverse stress; (Cases 4, 7 & 8)

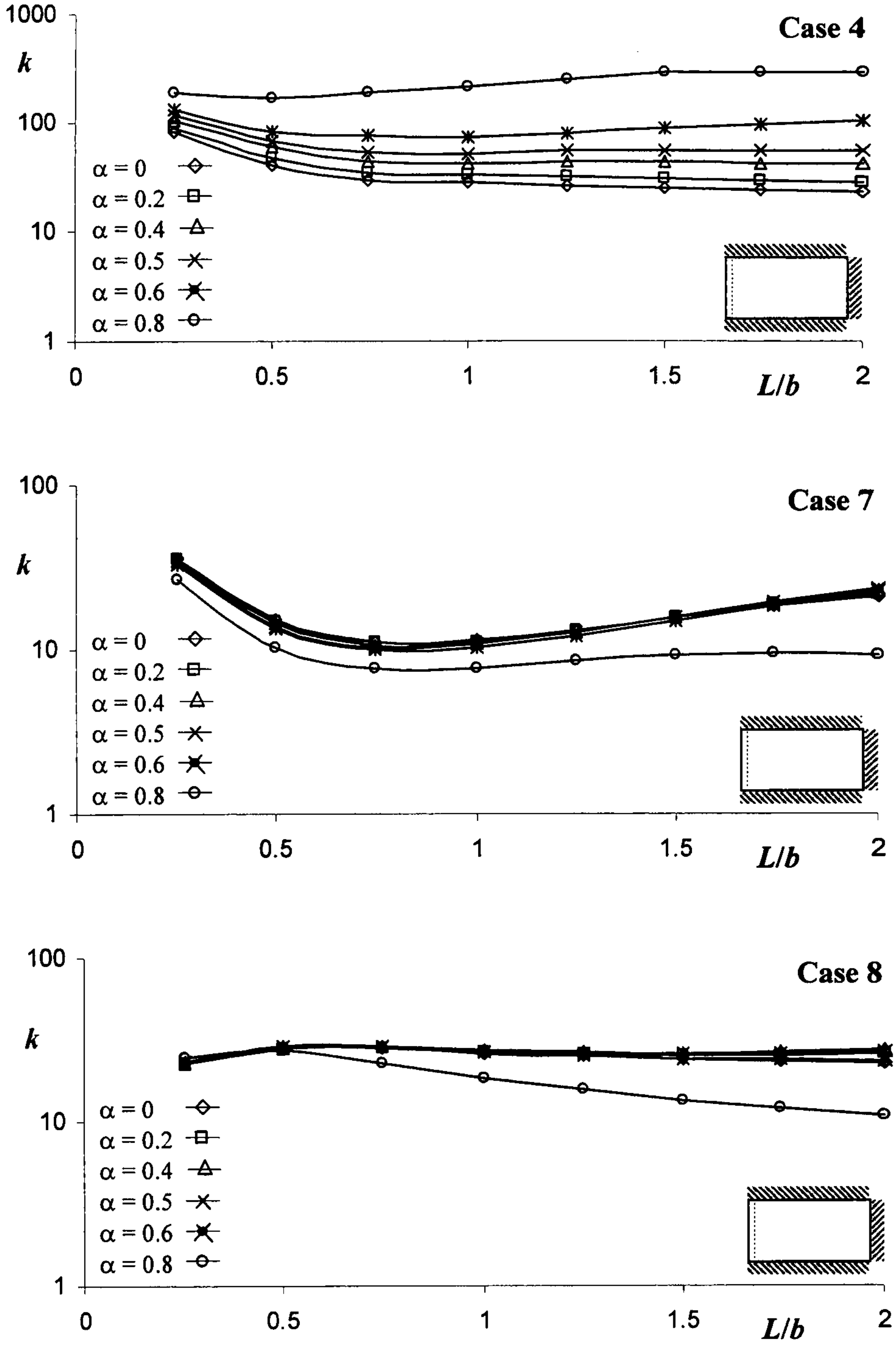

Figure 7.51 Buckling coefficients for s-c-c-c plates subjected to varying transverse stress; (Cases 4, 7 & 8)

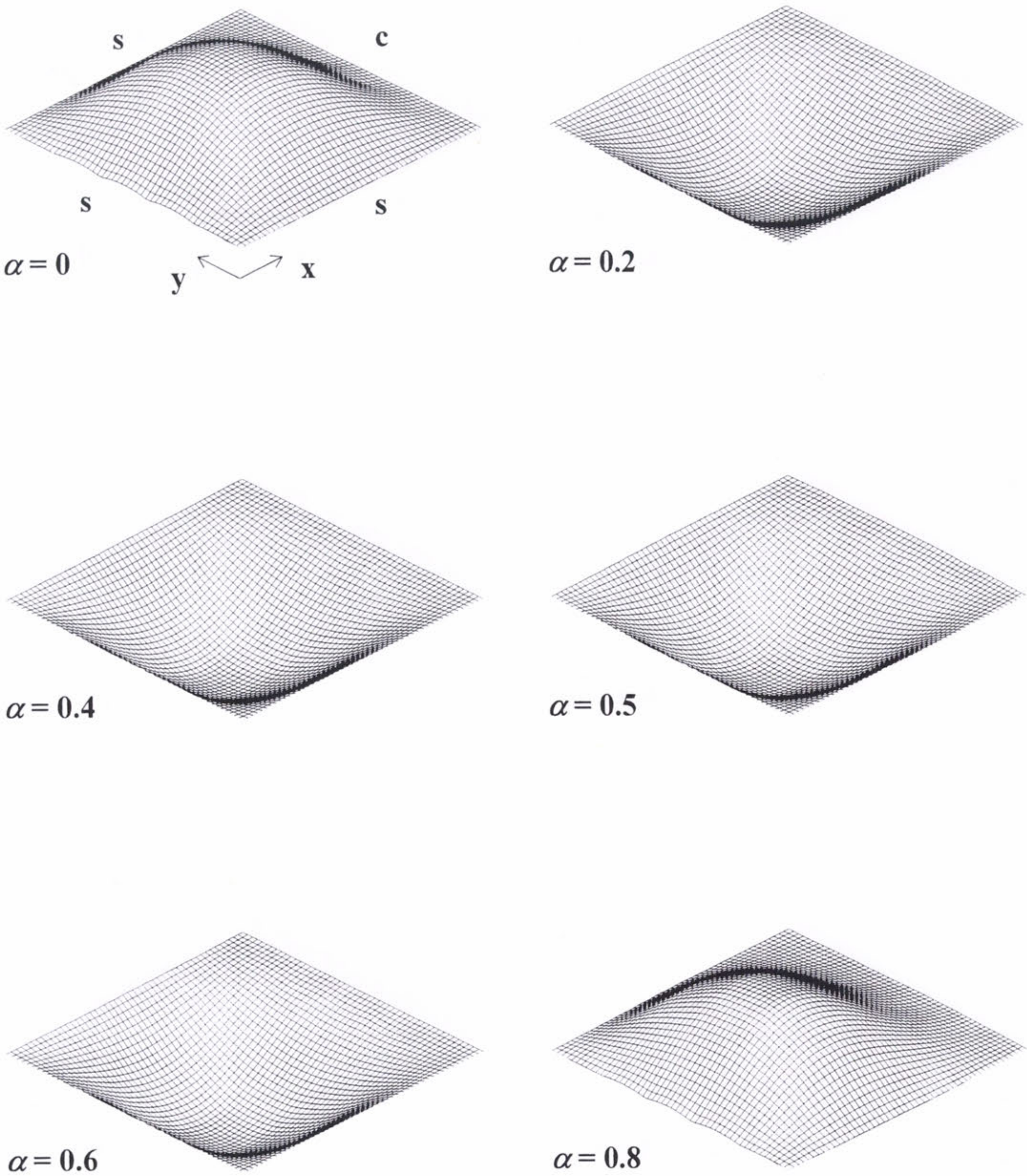

Figure 7.52 Buckling modes for s-s-c-s plates subjected to varying transverse stress (Cases 7)

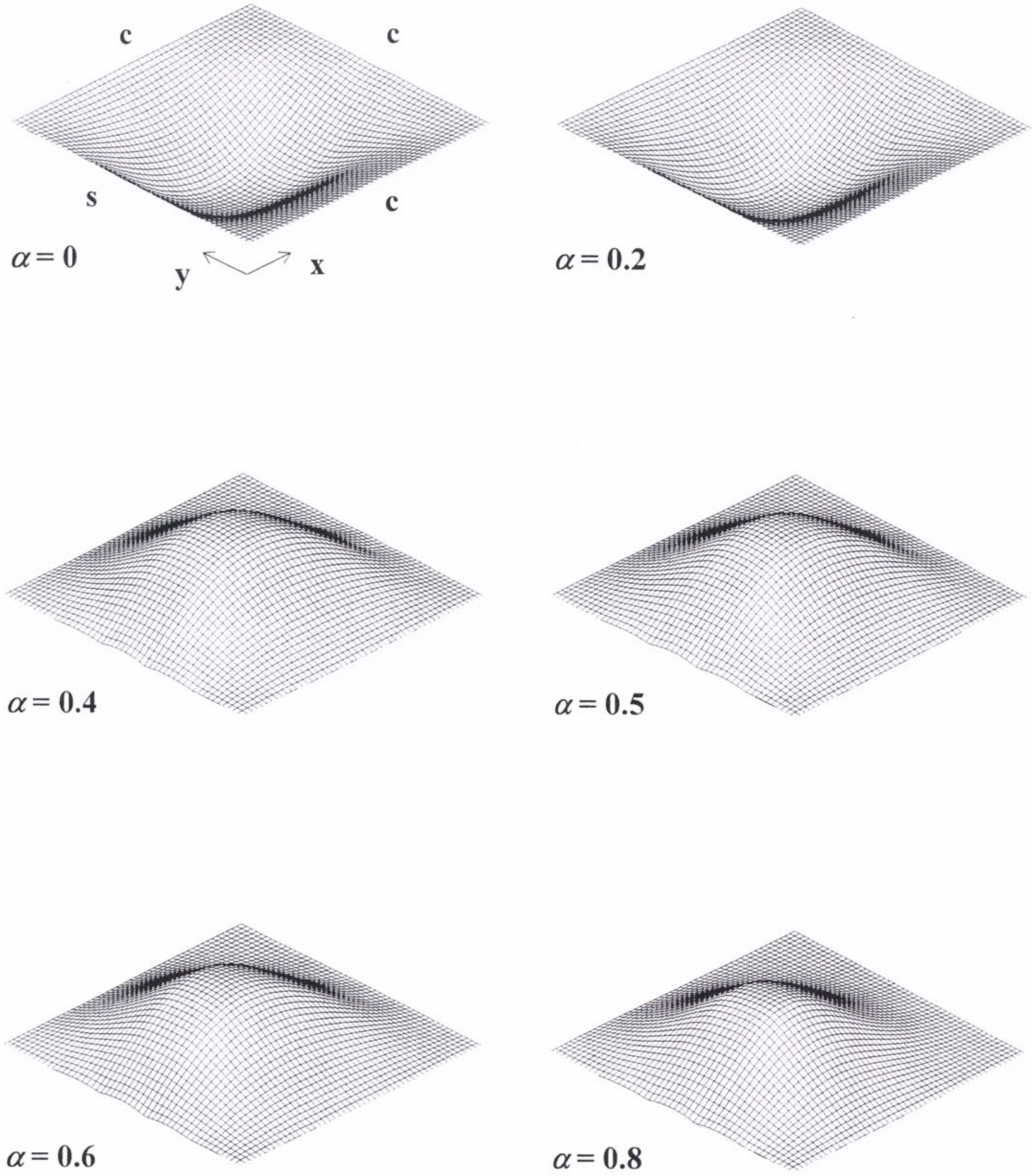

Figure 7.53 Buckling modes for s-c-c-c plates subjected to varying transverse stress (Cases 7)

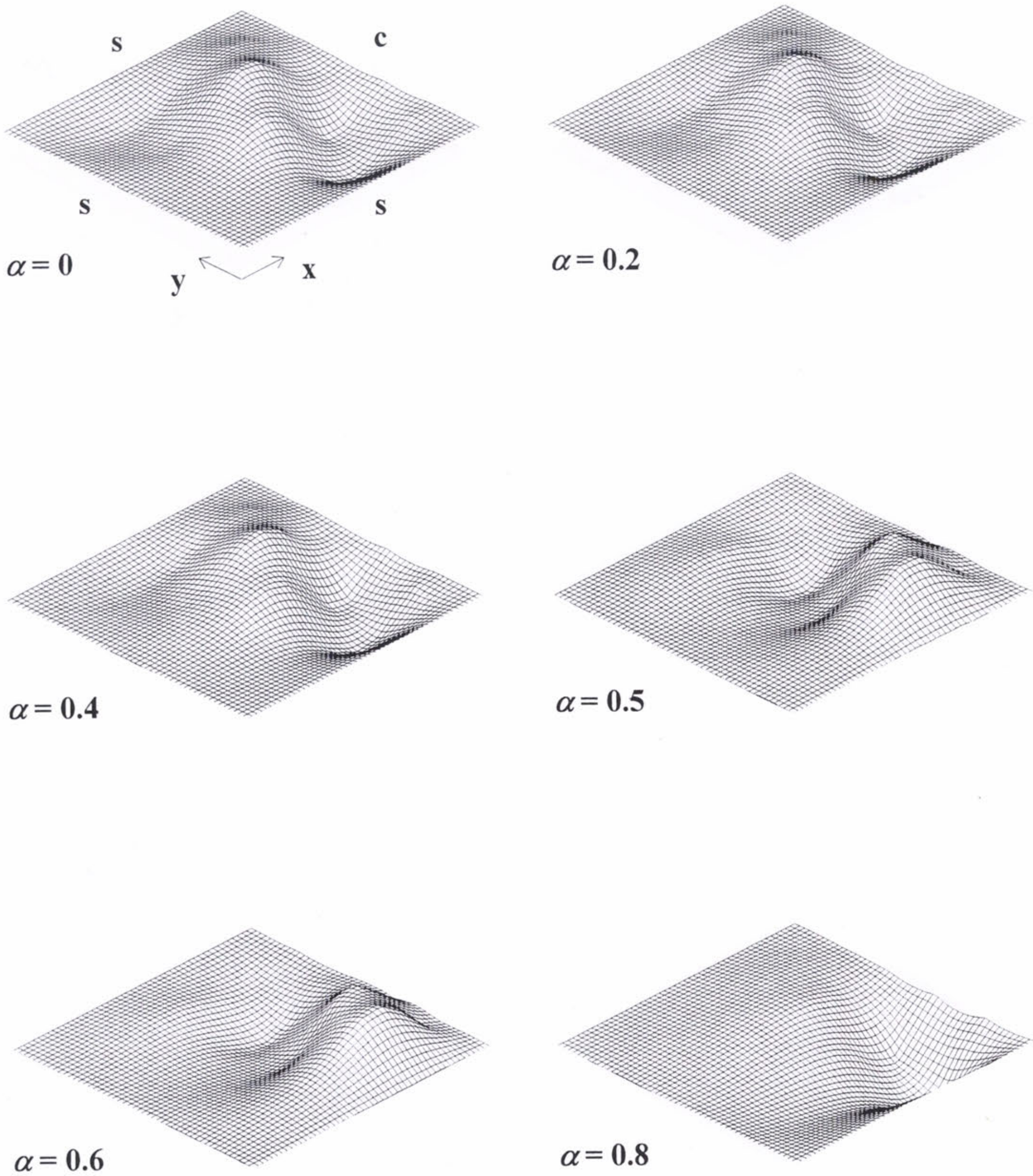

Figure 7.54 Buckling modes for s-s-s-c plates subjected to varying transverse stress (Cases 8)

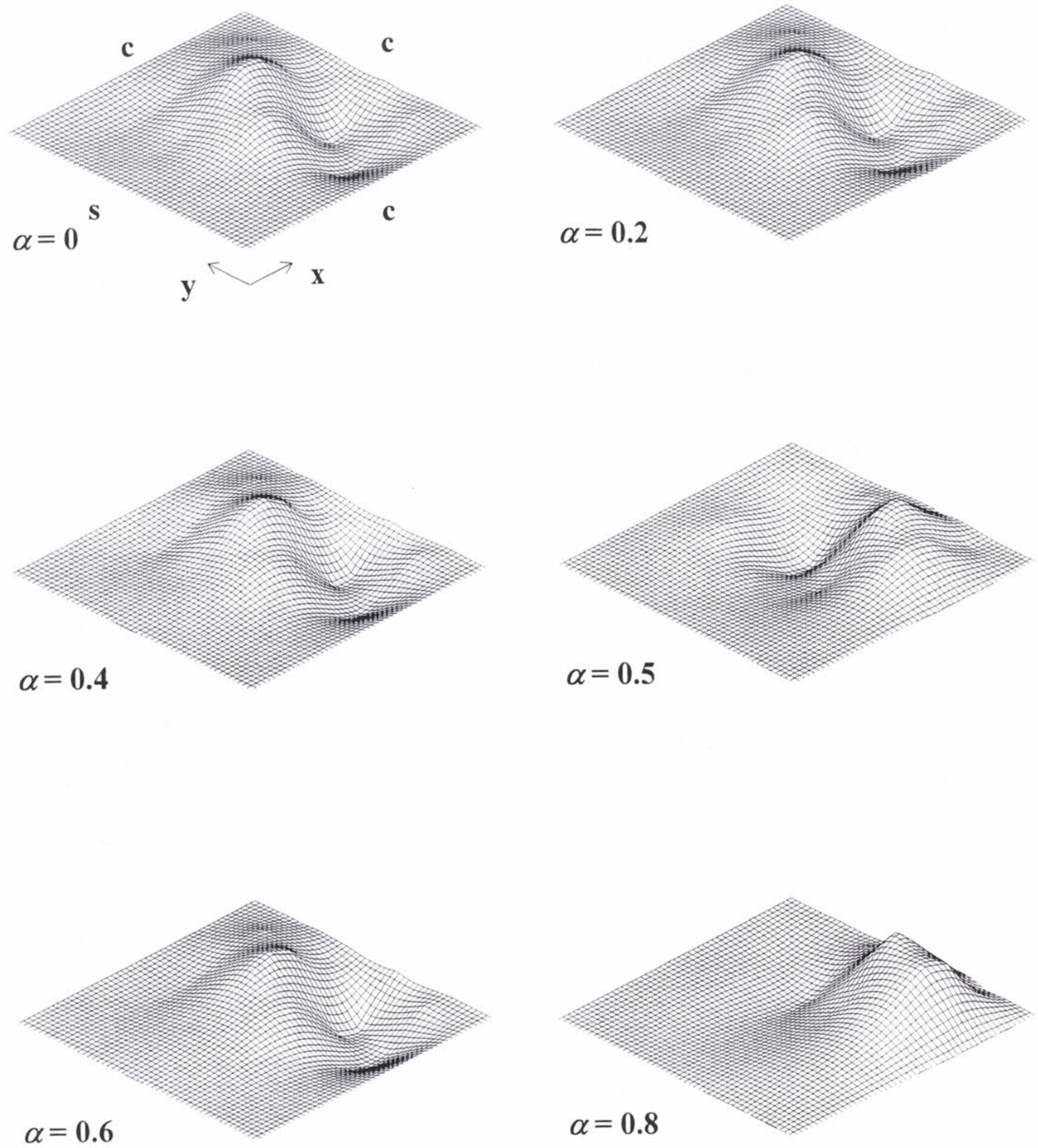

Figure 7.55 Buckling modes for s-c-c-c plates subjected to varying transverse stress (Cases 8)

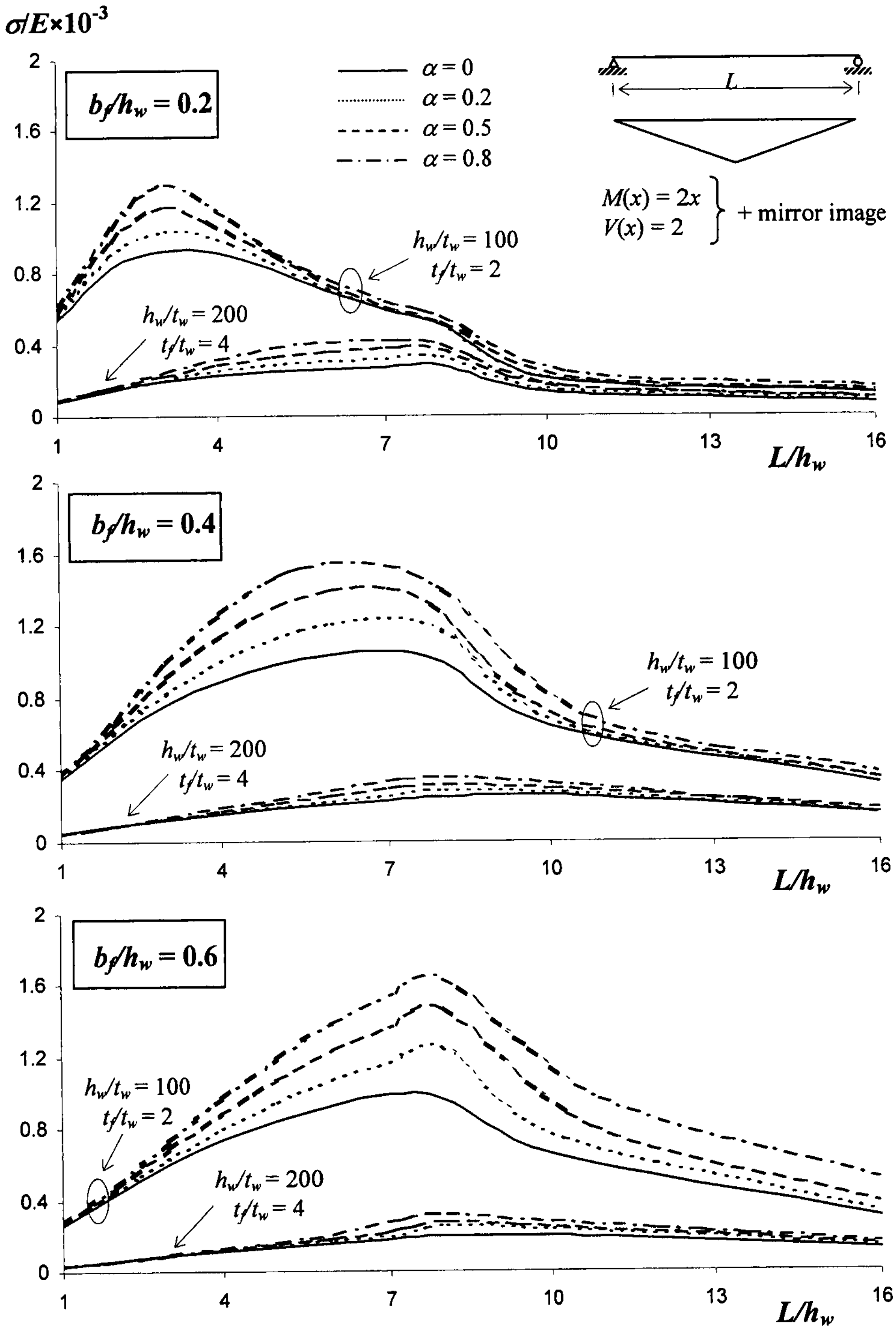

Figure 7.56 Elastic critical buckling stress for composite T-section beams (Case 3)

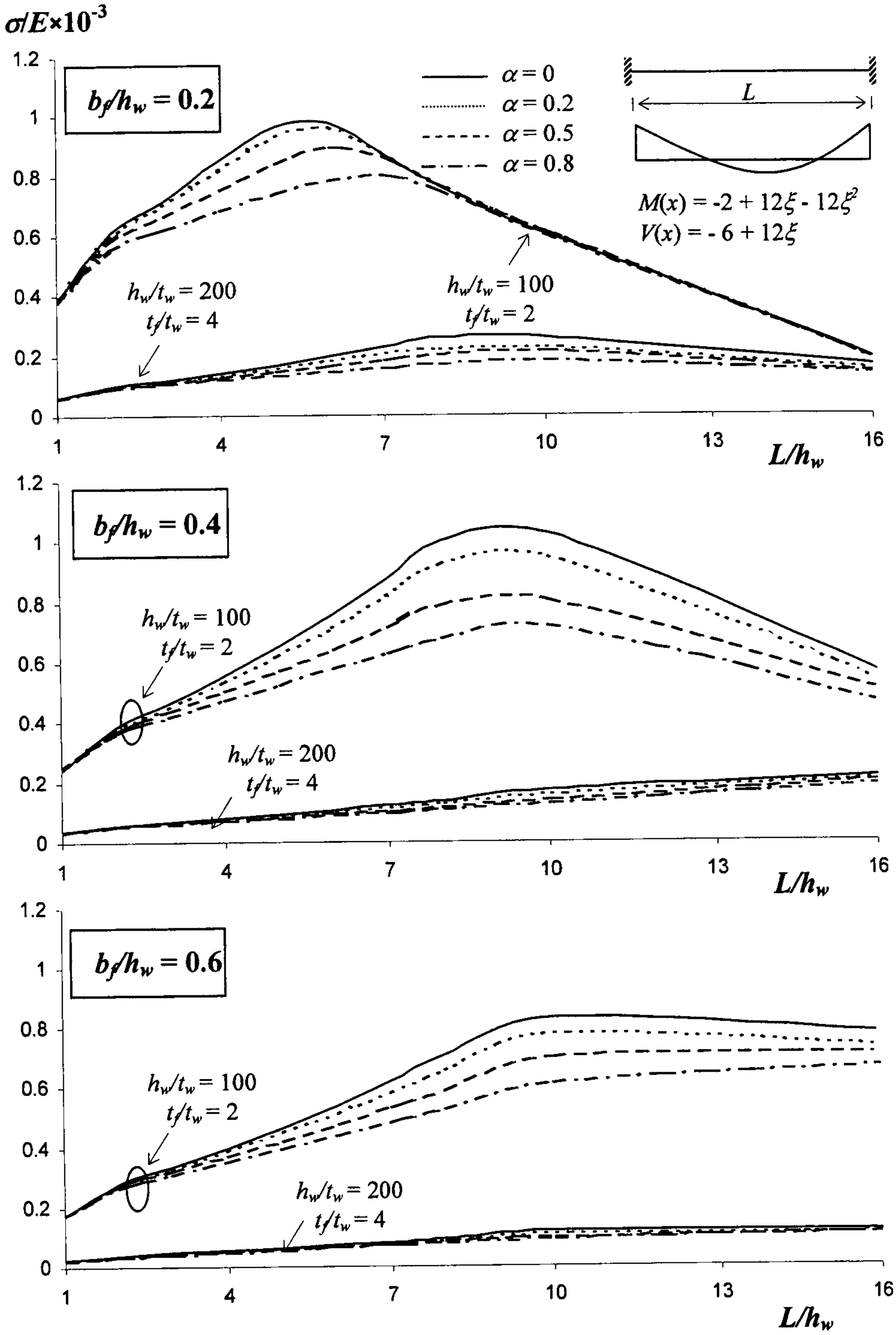

Figure 7.57 Elastic critical buckling stress (Case 10)

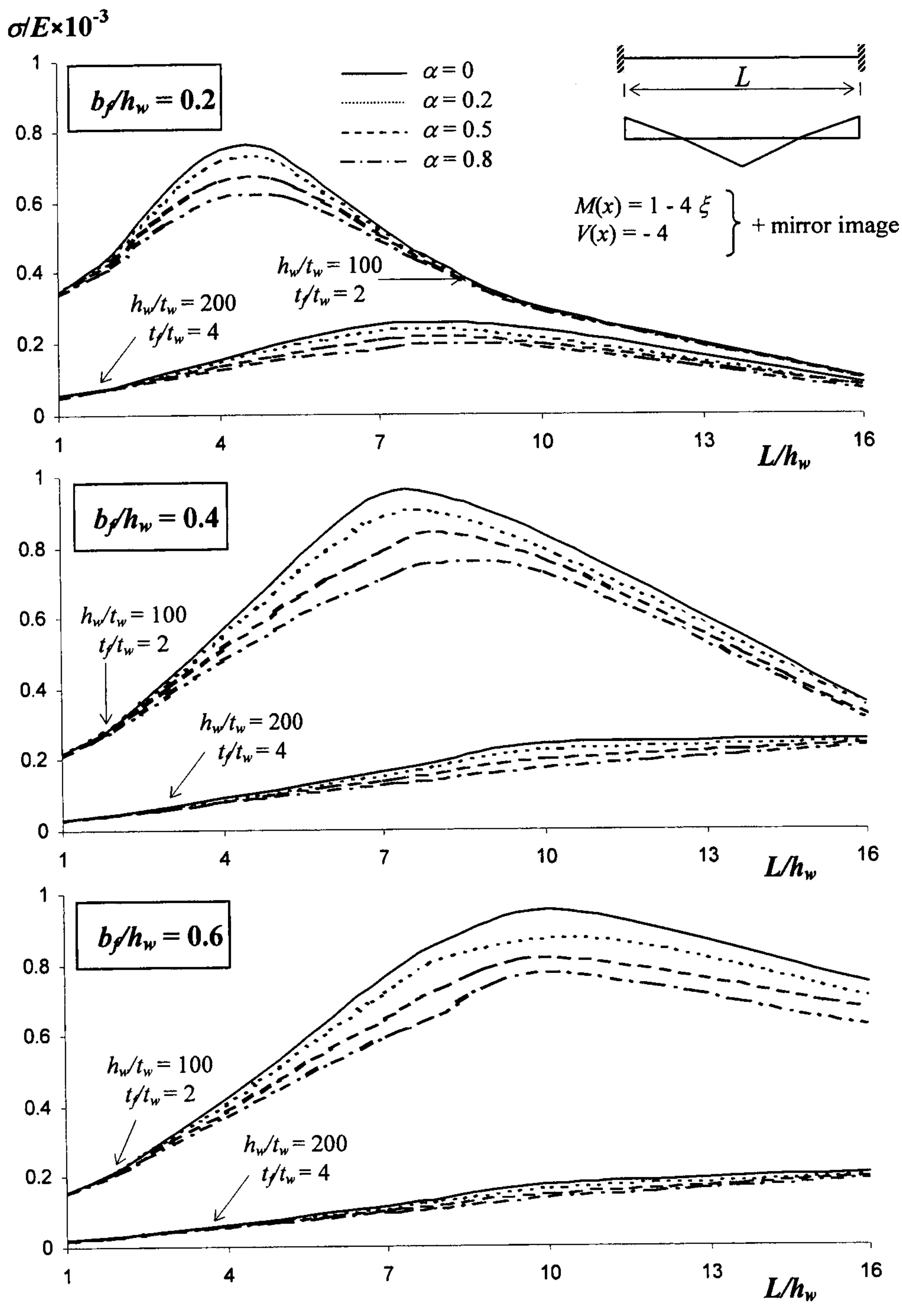

Figure 7.58 Elastic critical buckling stress (Case 11- clamped loaded edges)

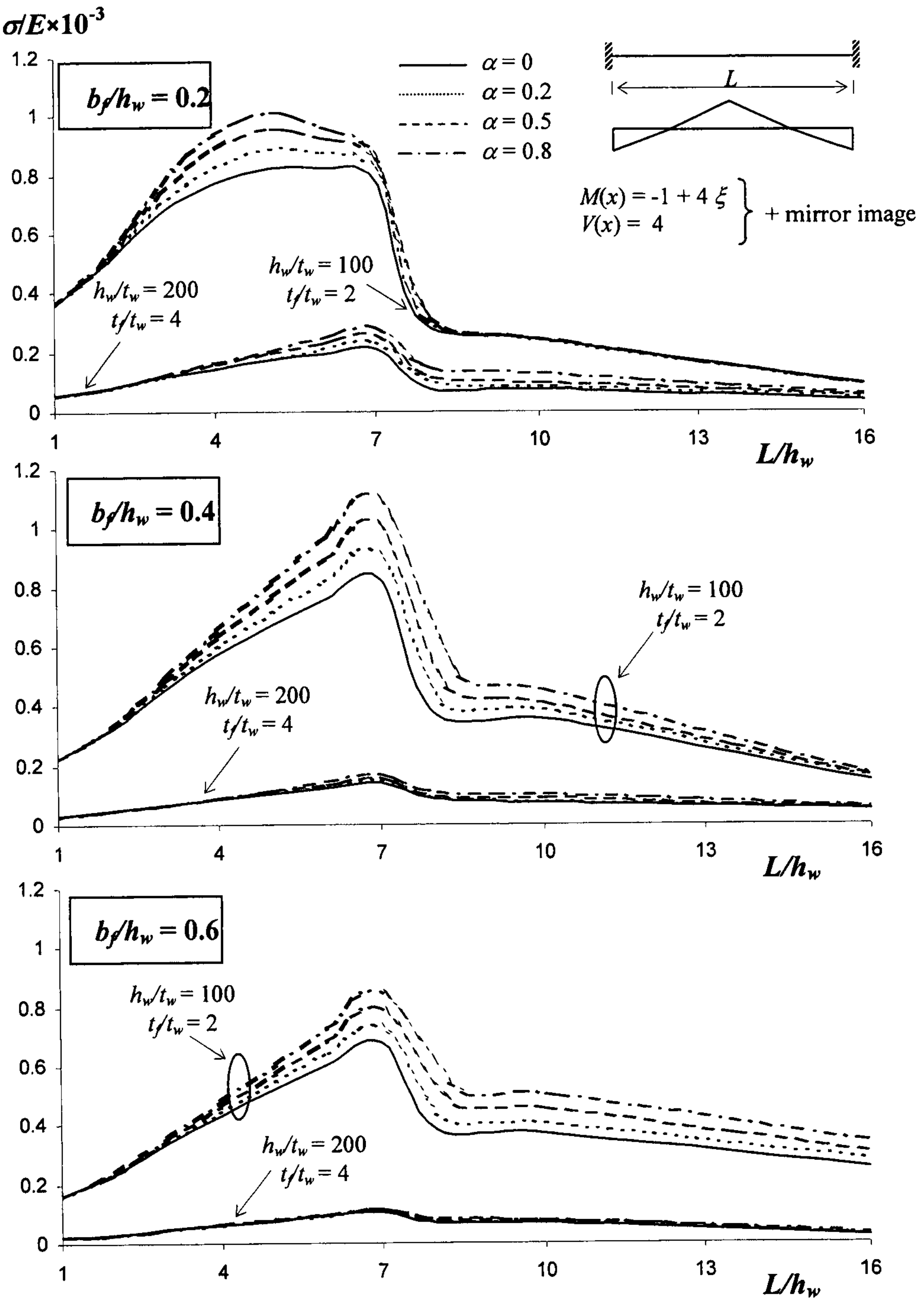

Figure 7.59 Elastic critical buckling stress (Case 12 - clamped loaded edges)

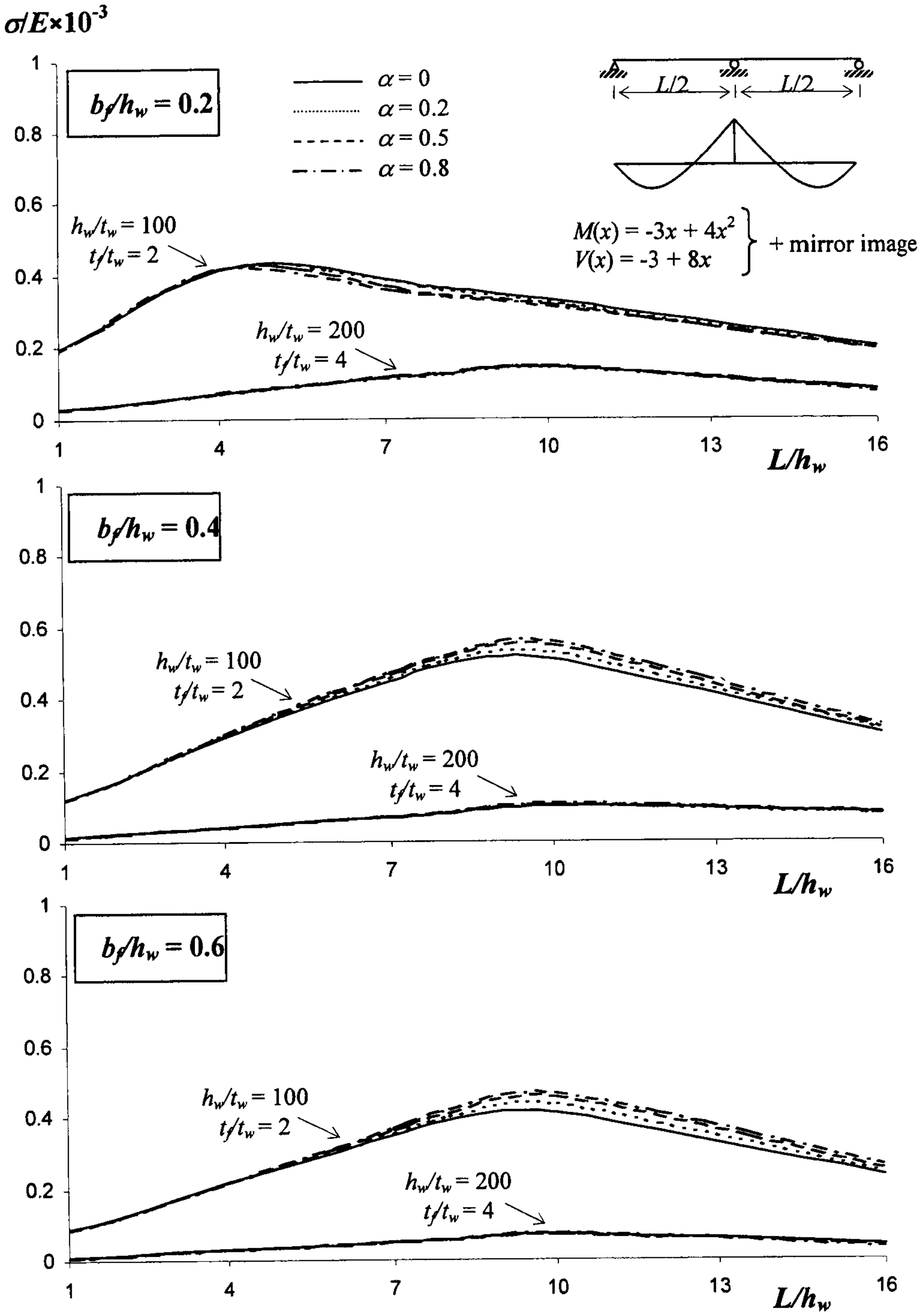

Figure 7.60 Elastic critical buckling stress (Case 7 + mirror image)

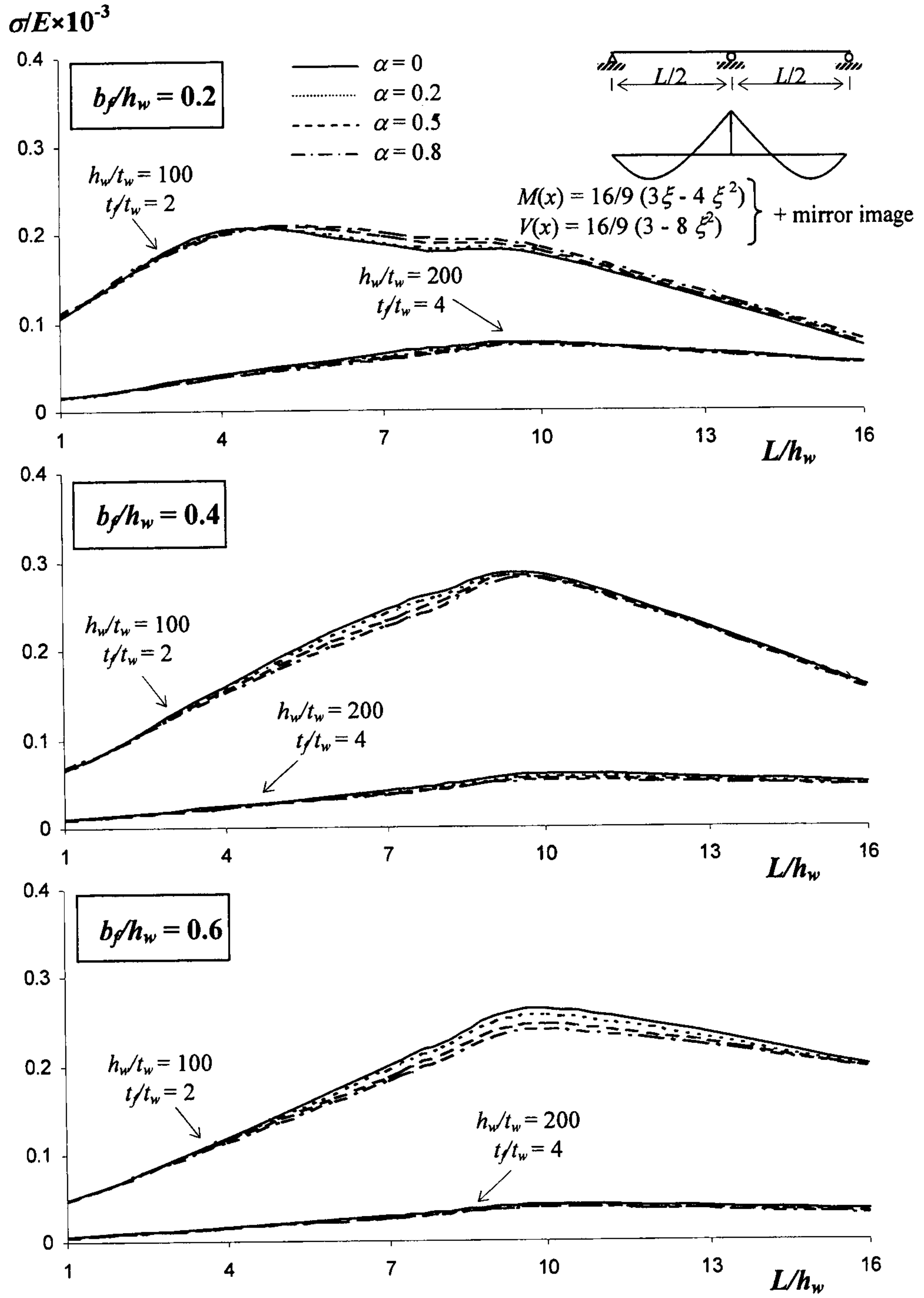

Figure 7.61 Elastic critical buckling stress (Case 8 + mirror image)

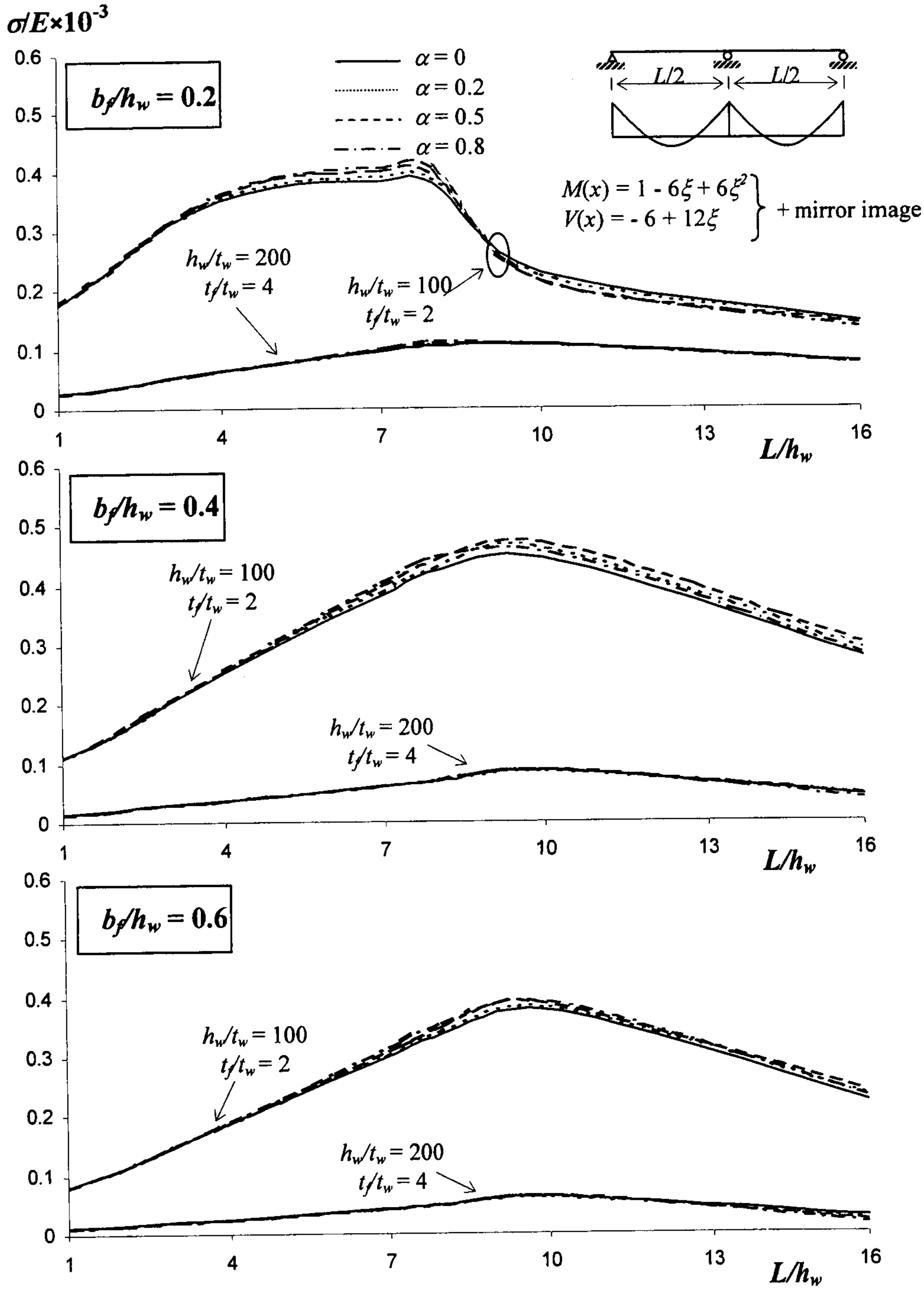

Figure 7.62 Elastic critical buckling stress (Case 9 + mirror image)

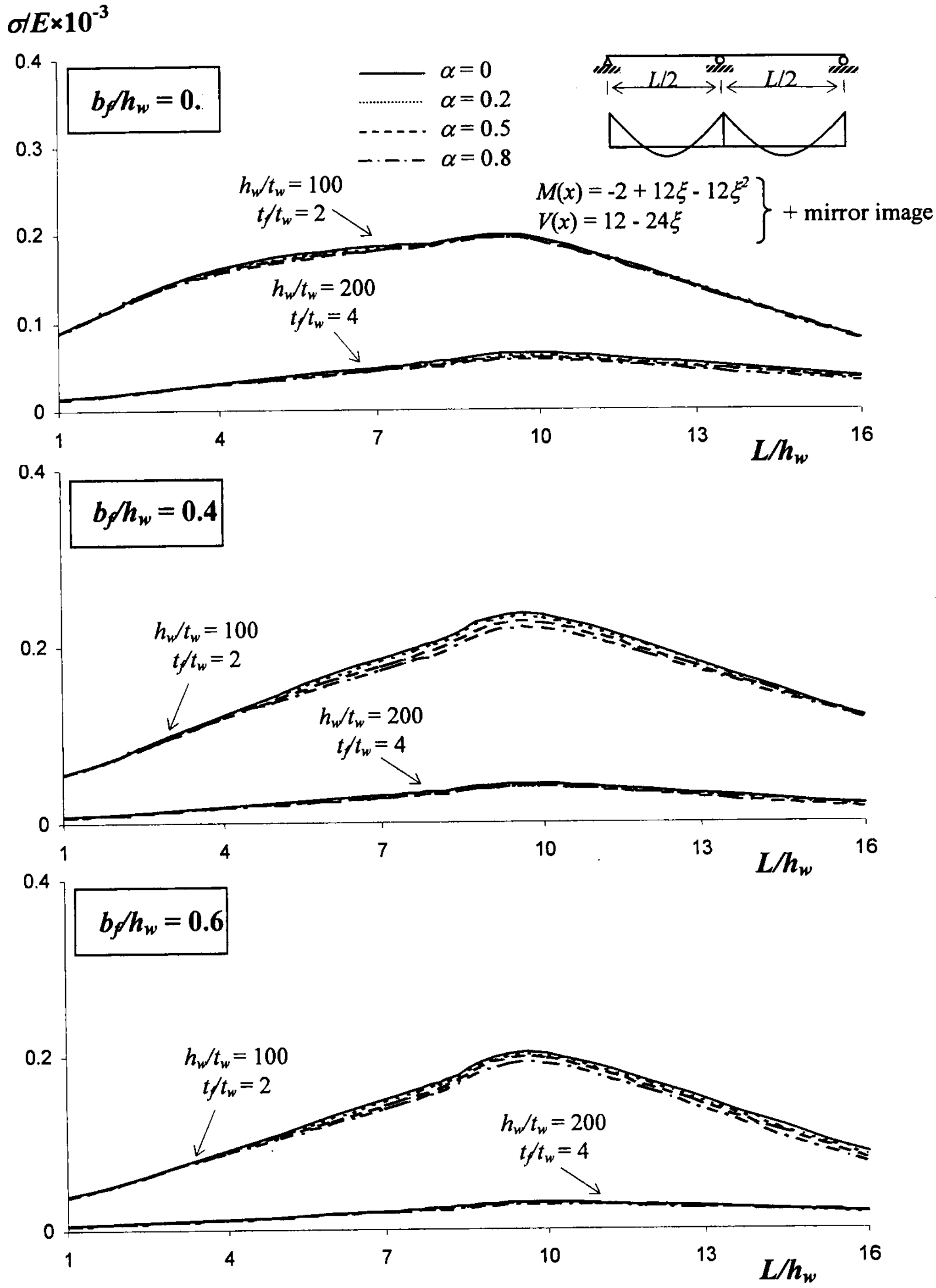

Figure 7.63 Elastic critical buckling stress (Case 10 + mirror image)

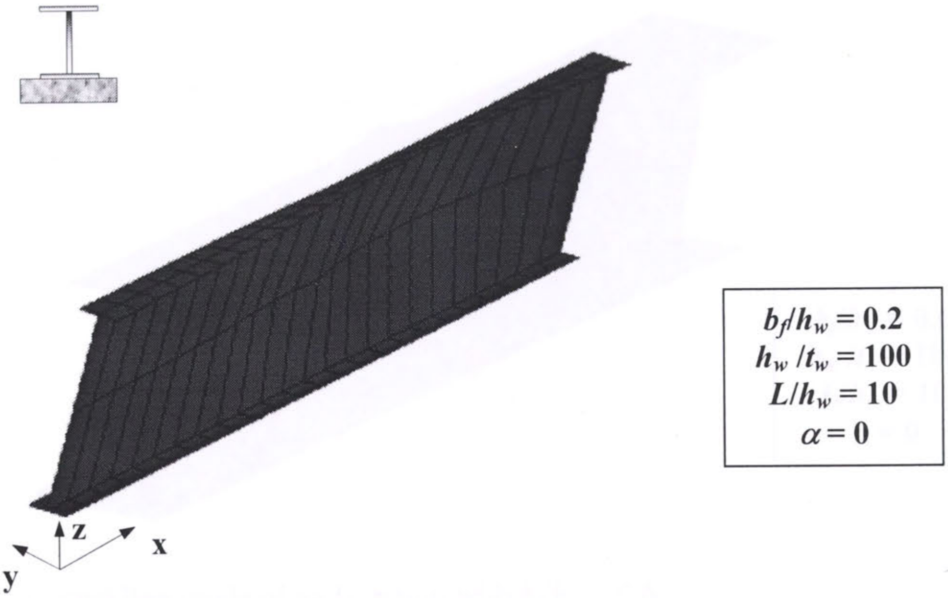

a) buckling mode of an I-section with $b_f/h_w = 0.2$

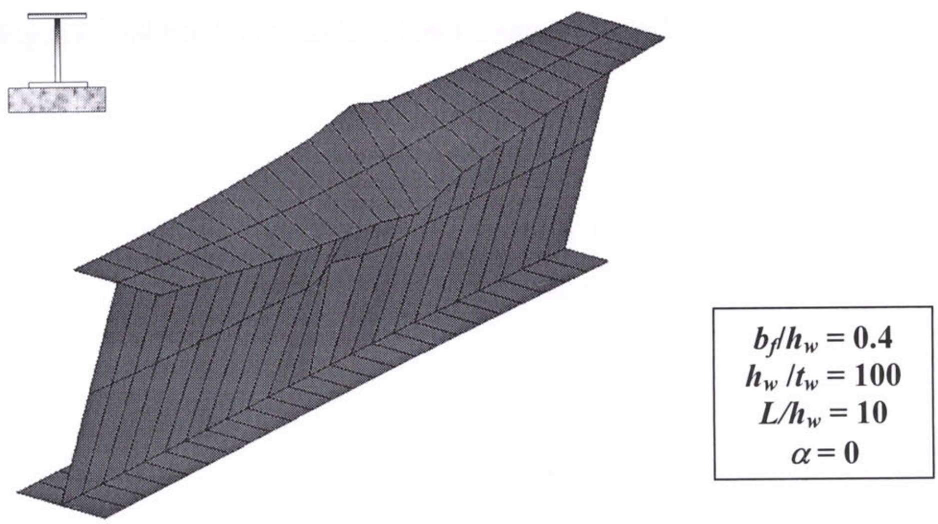

b) buckling mode of an I-section with $b_f/h_w = 0.4$

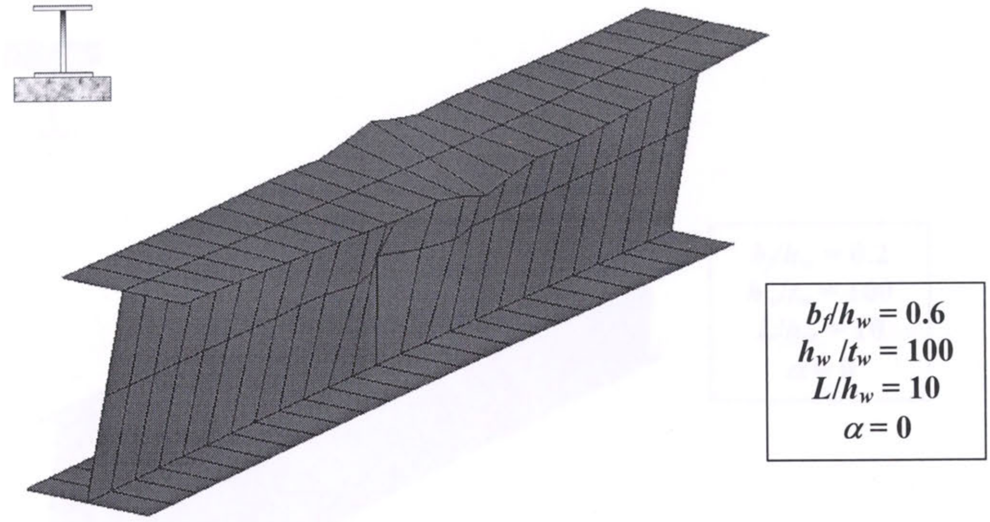

c) buckling mode of an I-section with $b_f/h_w = 0.6$

Figure 7.64 Buckling modes of an I-section (Case 3)

a) buckling mode of an I-section with $b_f/h_w = 0.2$

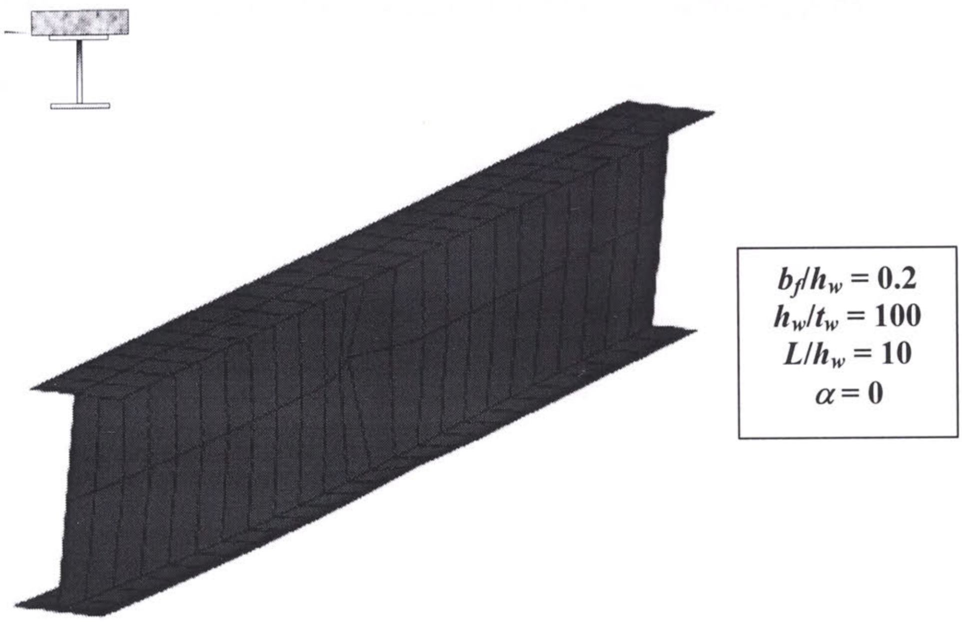

b) buckling mode of an I-section with $b_f/h_w = 0.4$

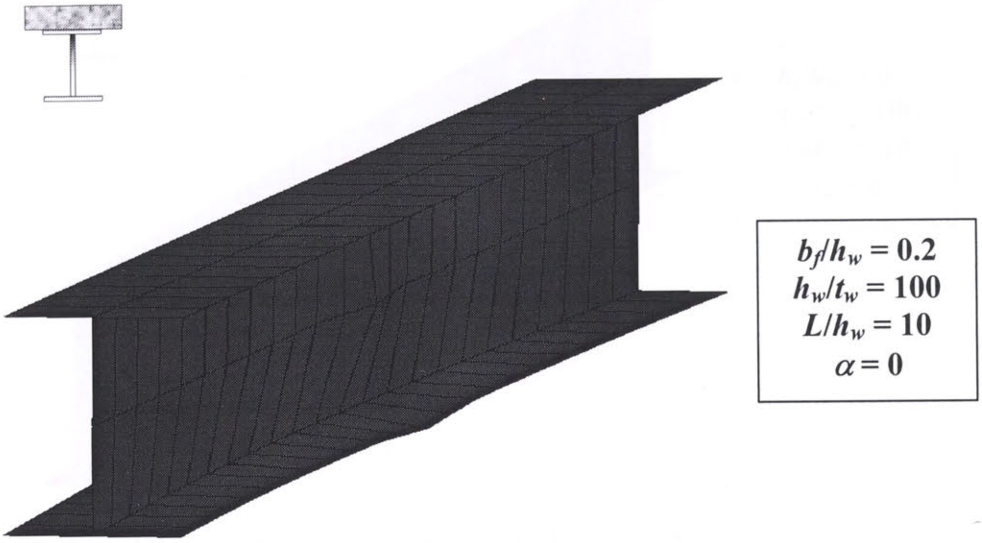

c) buckling mode of an I-section with $b_f/h_w = 0.6$

Figure 7.65 Buckling modes of an I-section (Case 11 – fixed end supports)

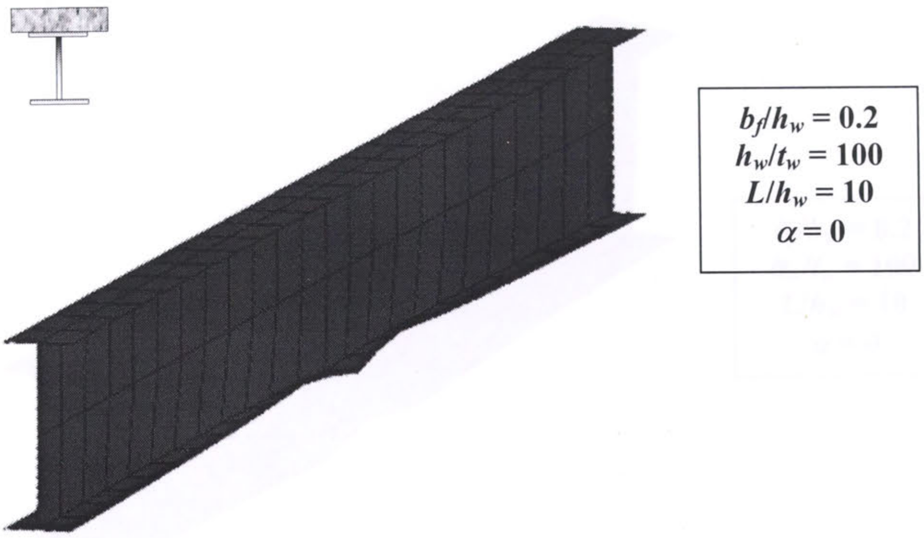

a) buckling mode of an I-section with $b_f/h_w = 0.2$

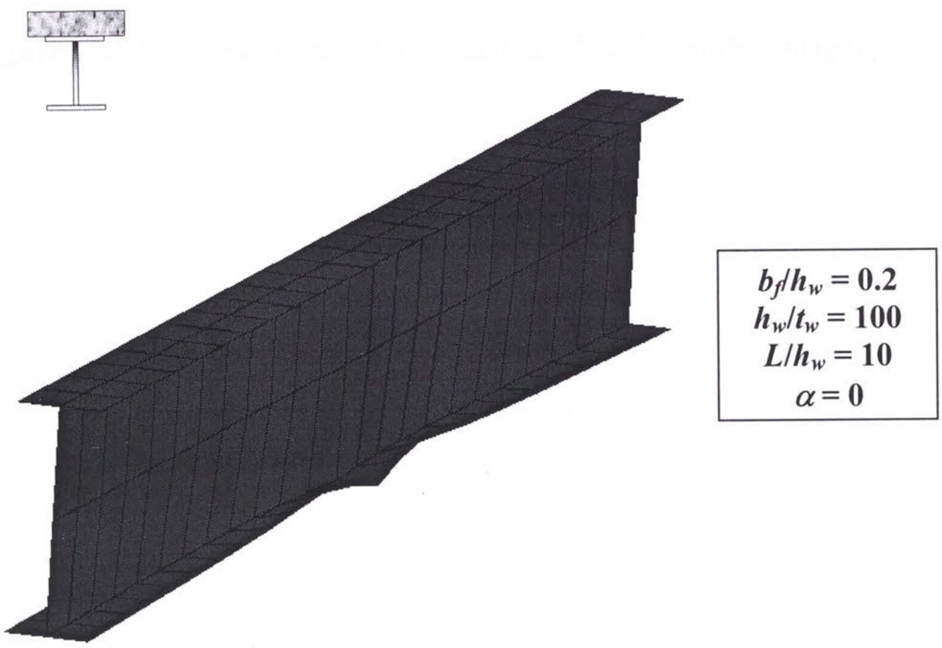

b) buckling mode of an I-section with $b_f/h_w = 0.4$

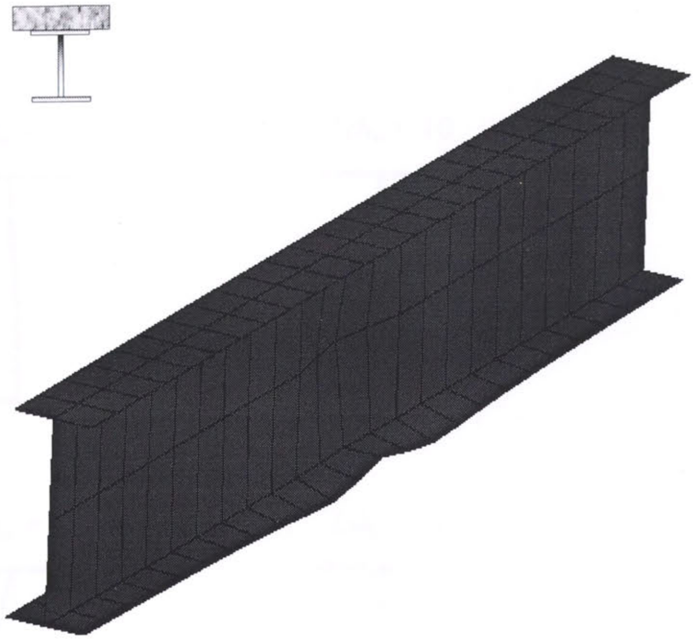

$b_f/h_w = 0.2$
$h_w/t_w = 100$
$L/h_w = 10$
$\alpha = 0$

c) buckling mode of an I-section with $b_f/h_w = 0.6$

Figure 7.66 Buckling modes of an I-section (Case 7 + mirror image)

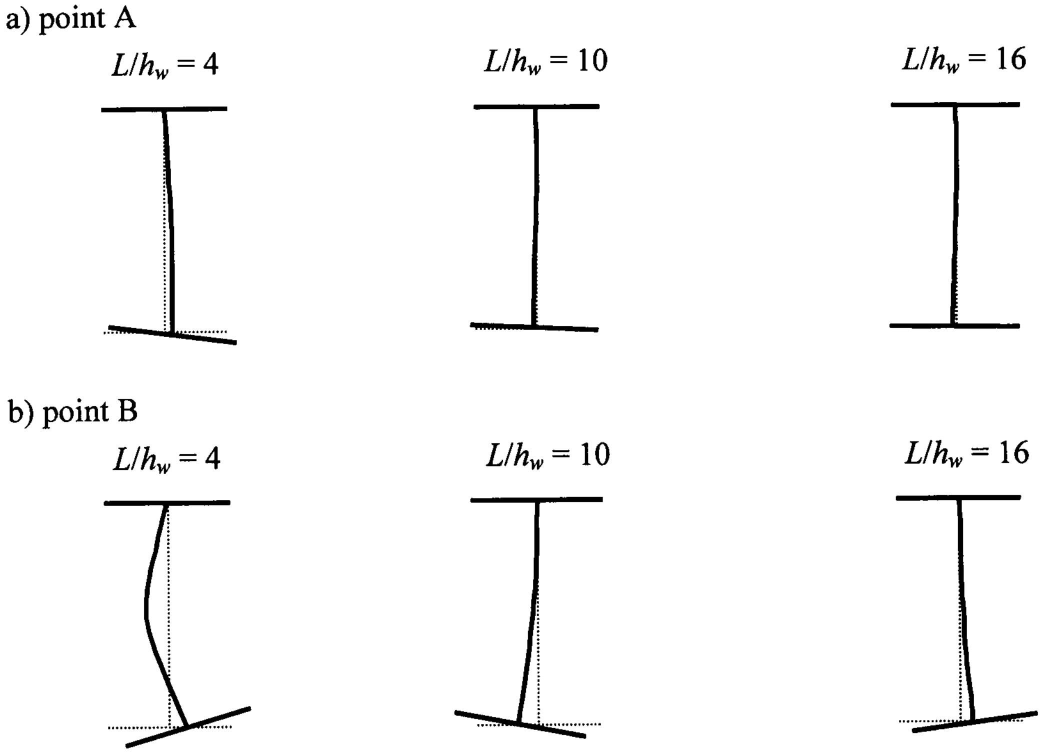

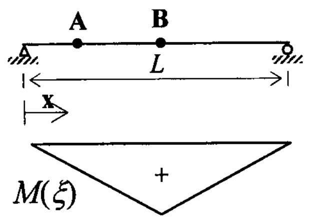

$$\left.\begin{array}{l} M(\xi) = 2\xi \\ V(\xi) = 2 \end{array}\right\} + \text{mirror image}$$

$\xi = L/x$

A at $\xi = 0.208$
B at $\xi = 0.5$

Figure 7.67a Cross-sectional buckling modes of an I-section with $b_f/h_w = 0.2$ (Case 3)

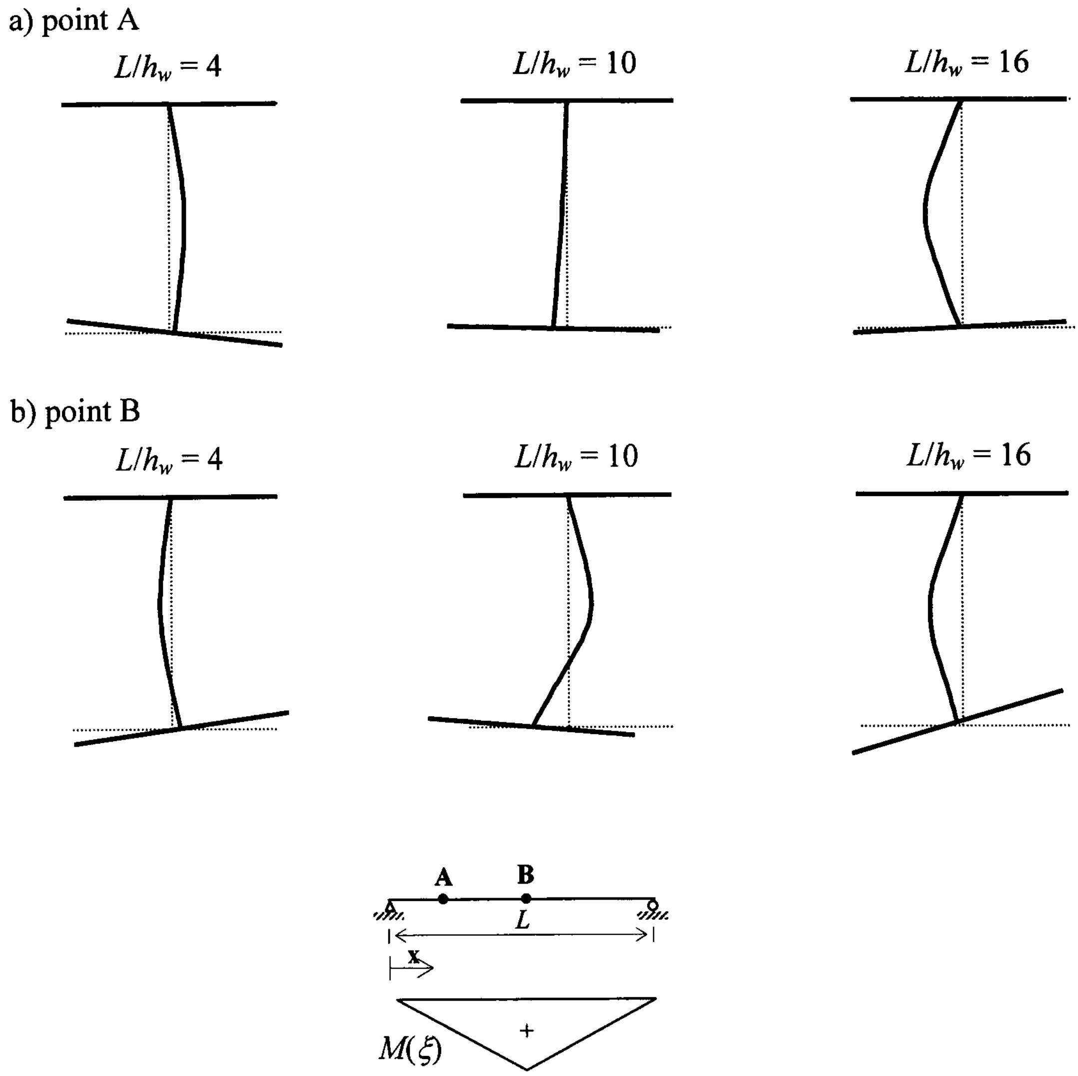

$$\left.\begin{array}{l} M(\xi) = 2\xi \\ V(\xi) = 2 \end{array}\right\} + \text{mirror image}$$

$\xi = L/x$

A at $\xi = 0.208$

B at $\xi = 0.5$

Figure 7.67b Cross-sectional buckling modes of an I-section with $b_f/h_w = 0.4$ (Case 3)

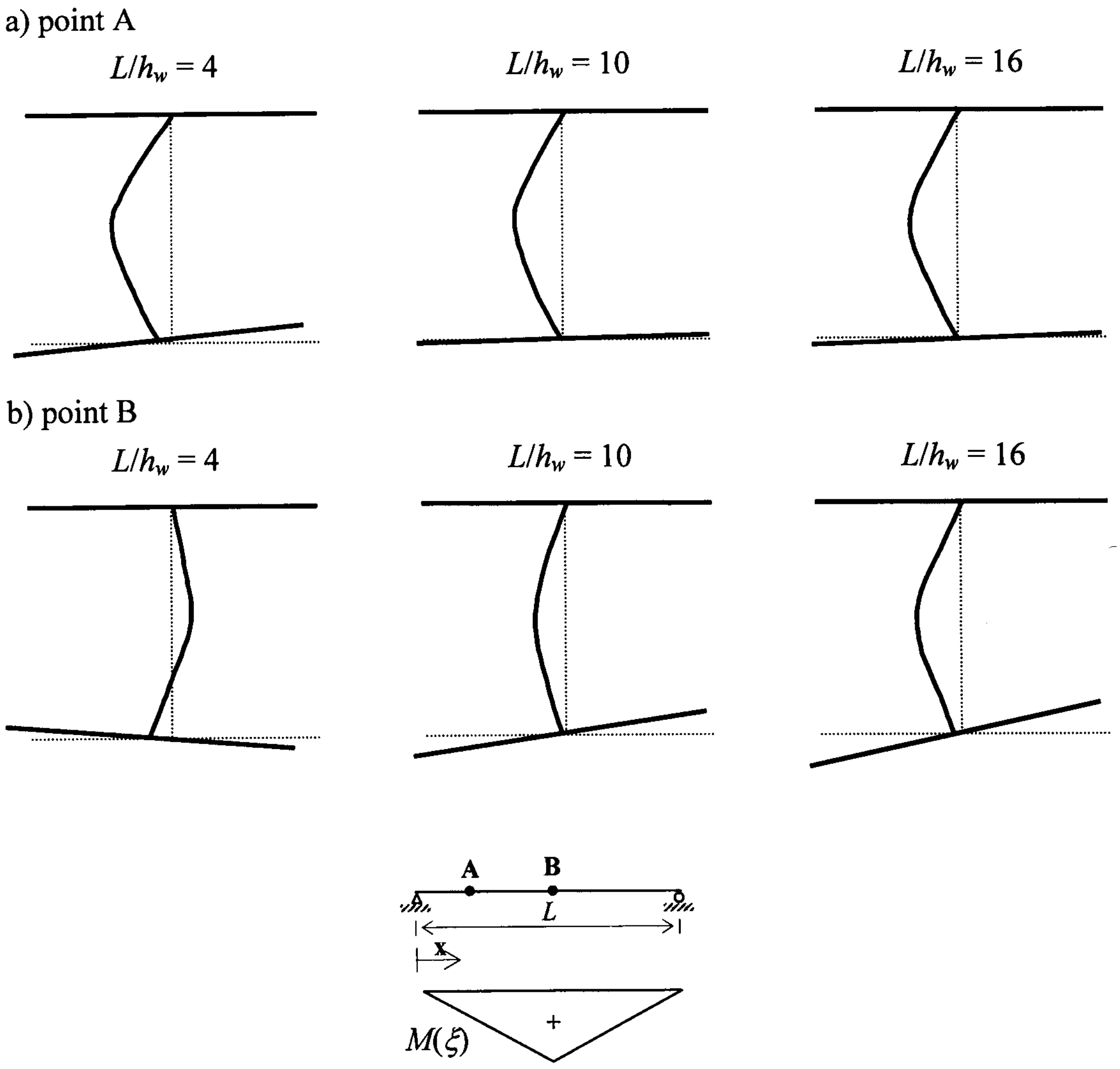

$$\left.\begin{aligned} M(\xi) &= 2\xi \\ V(\xi) &= 2 \end{aligned}\right\} + \text{mirror image}$$

$\xi = L/x$

A at $\xi = 0.208$
B at $\xi = 0.5$

Figure 7.67c Cross-sectional buckling modes of an I-section with $b_f/h_w = 0.6$ (Case 3)

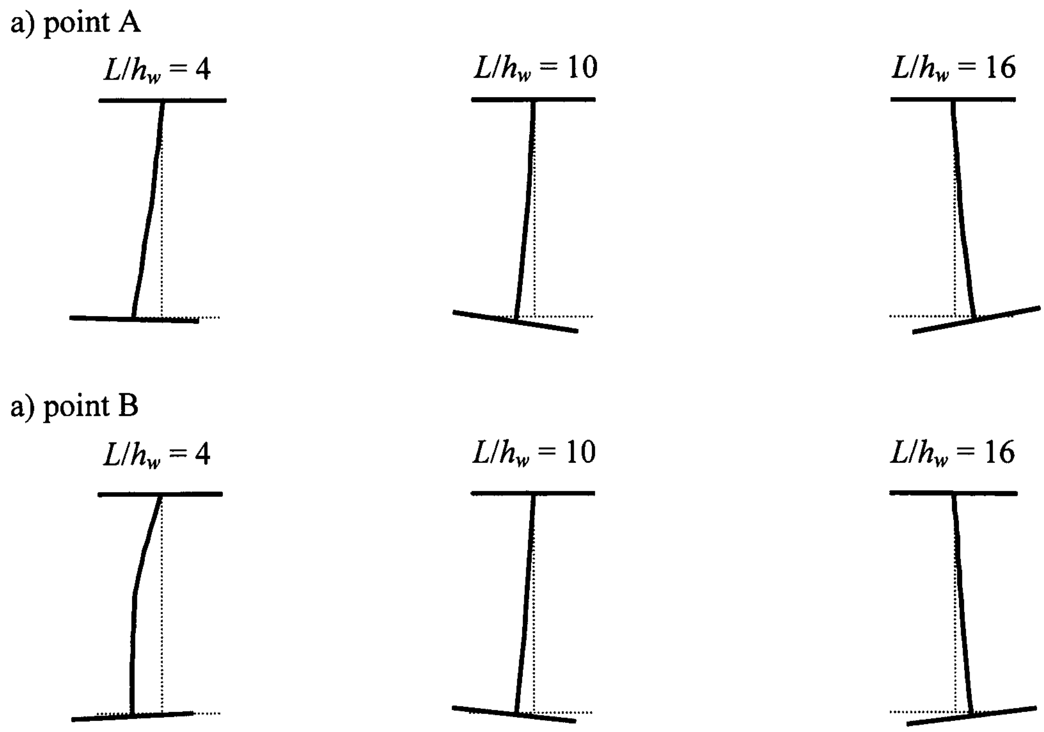

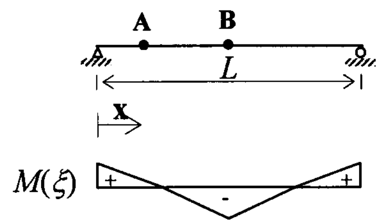

$$\left.\begin{array}{l} M(x) = 1 - 4\xi \\ V(x) = -4 \end{array}\right\} + \text{mirror image}$$

$\xi = L/x$

A at $\xi = 0.208$
B at $\xi = 0.5$

Figure 7.68a Cross-sectional buckling modes of an I-section with $b_f/h_w = 0.2$ (Case 11)

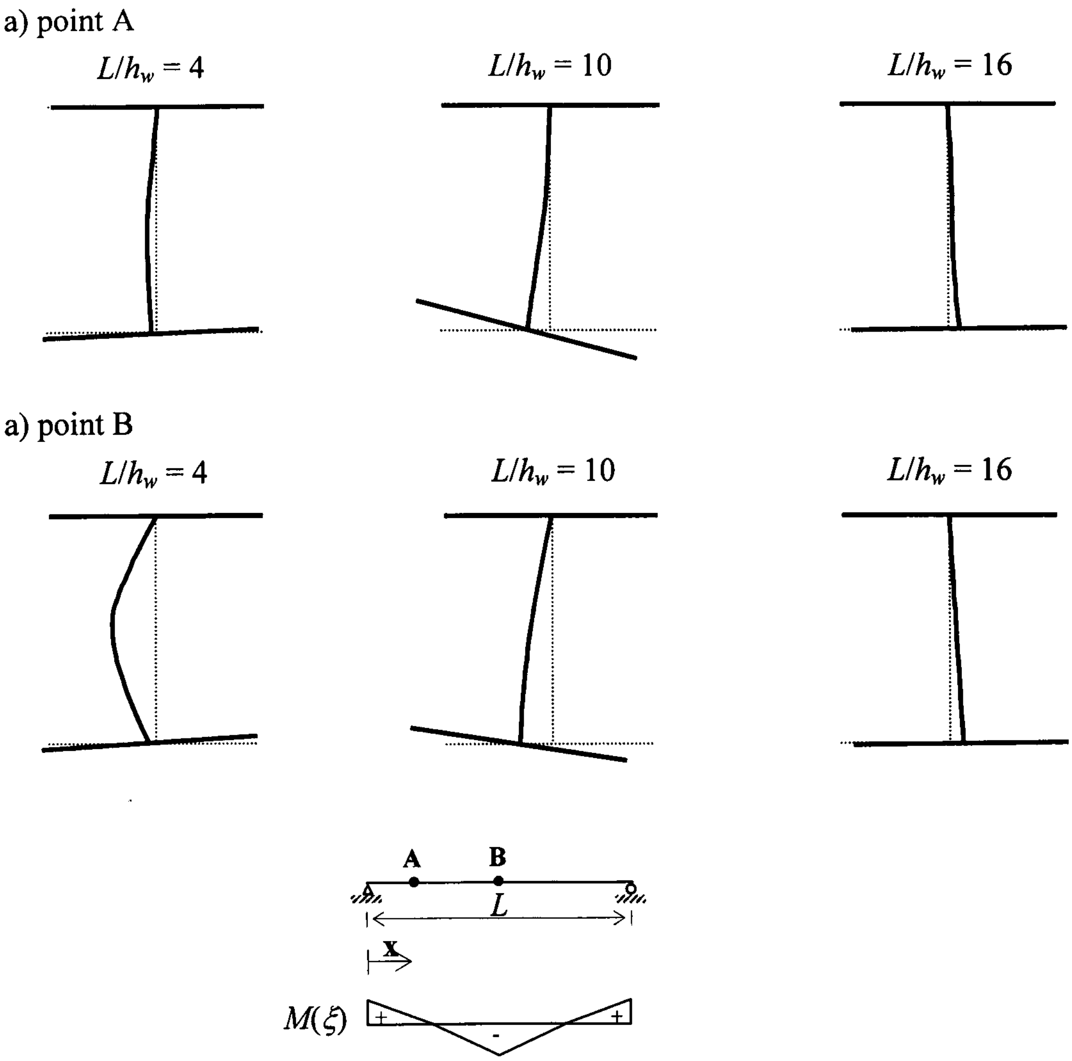

$$\left.\begin{array}{l} M(x) = 1 - 4\xi \\ V(x) = -4 \end{array}\right\} + \text{mirror image}$$

$\xi = L/x$

A at $\xi = 0.208$
B at $\xi = 0.5$

Figure 7.68b Cross-sectional buckling modes of an I-section with $b_f/h_w = 0.4$ (Case 11)

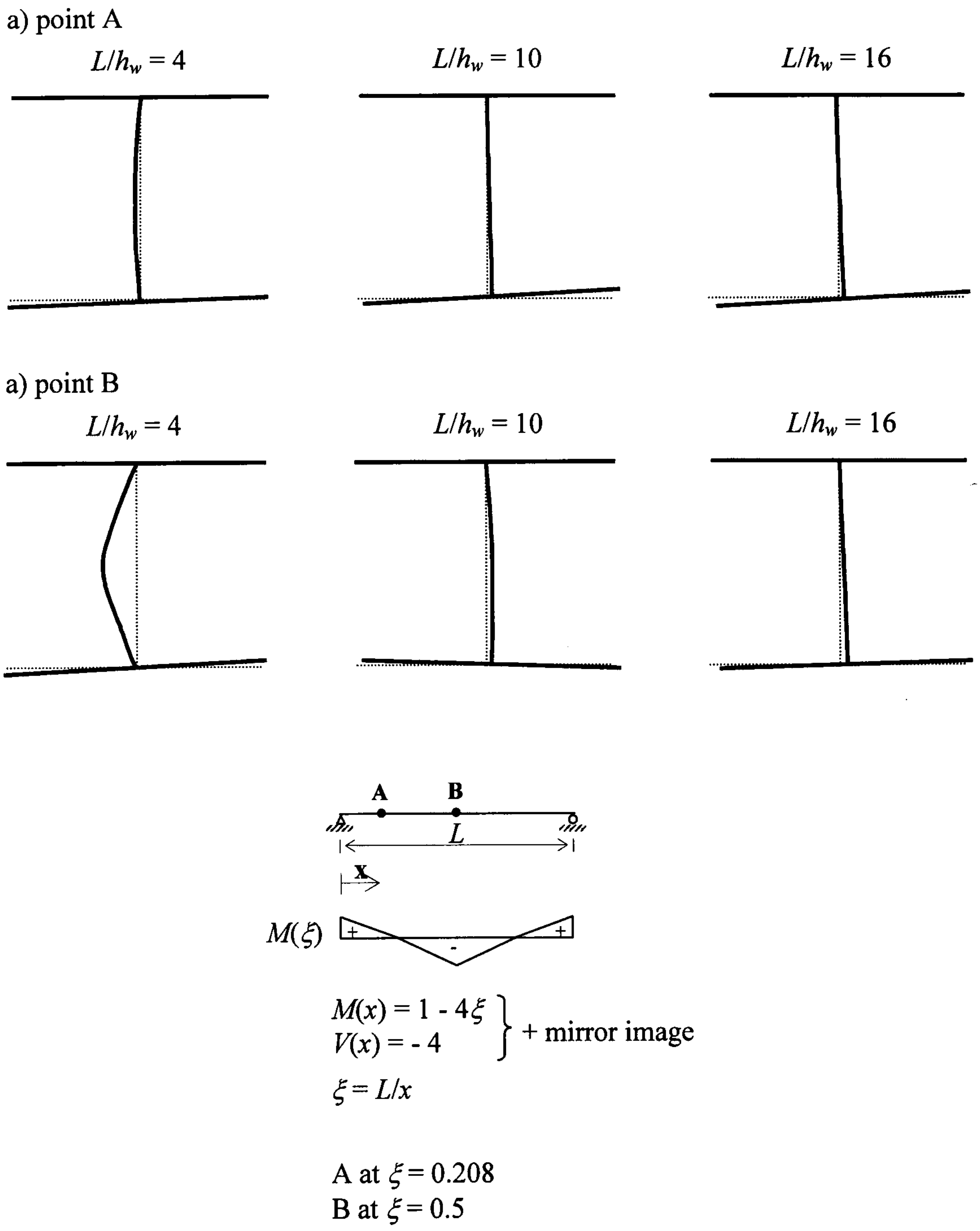

Figure 7.68c Cross-sectional buckling modes of an I-section with $b_f/h_w = 0.6$ (Case 11)

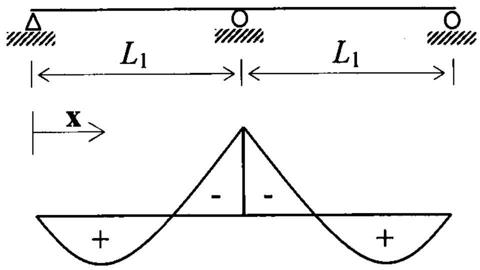

$$\left.\begin{array}{l} M(\xi) = -3\xi + 4\xi^2 \\ V(\xi) = -3 + 8\xi \end{array}\right\} + \text{mirror image}$$

$$\xi = x/L_1$$

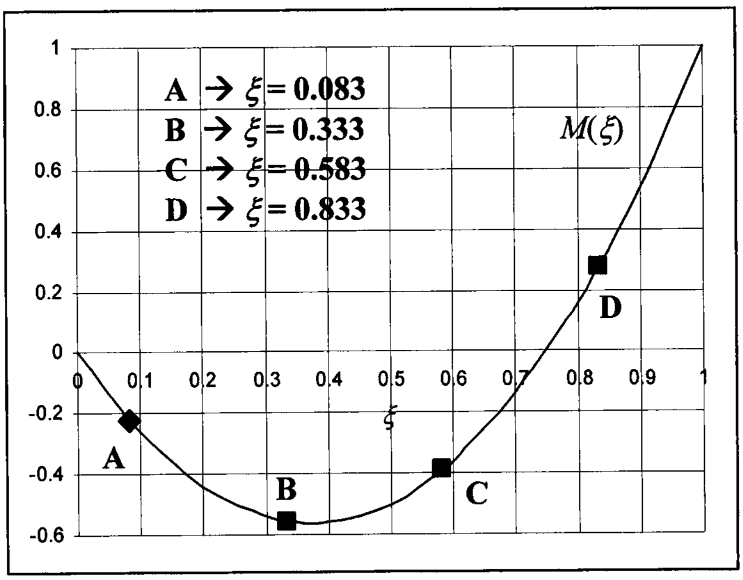

Figure 7.69a $M(\xi)$ at points A, B, C and D for Case 7

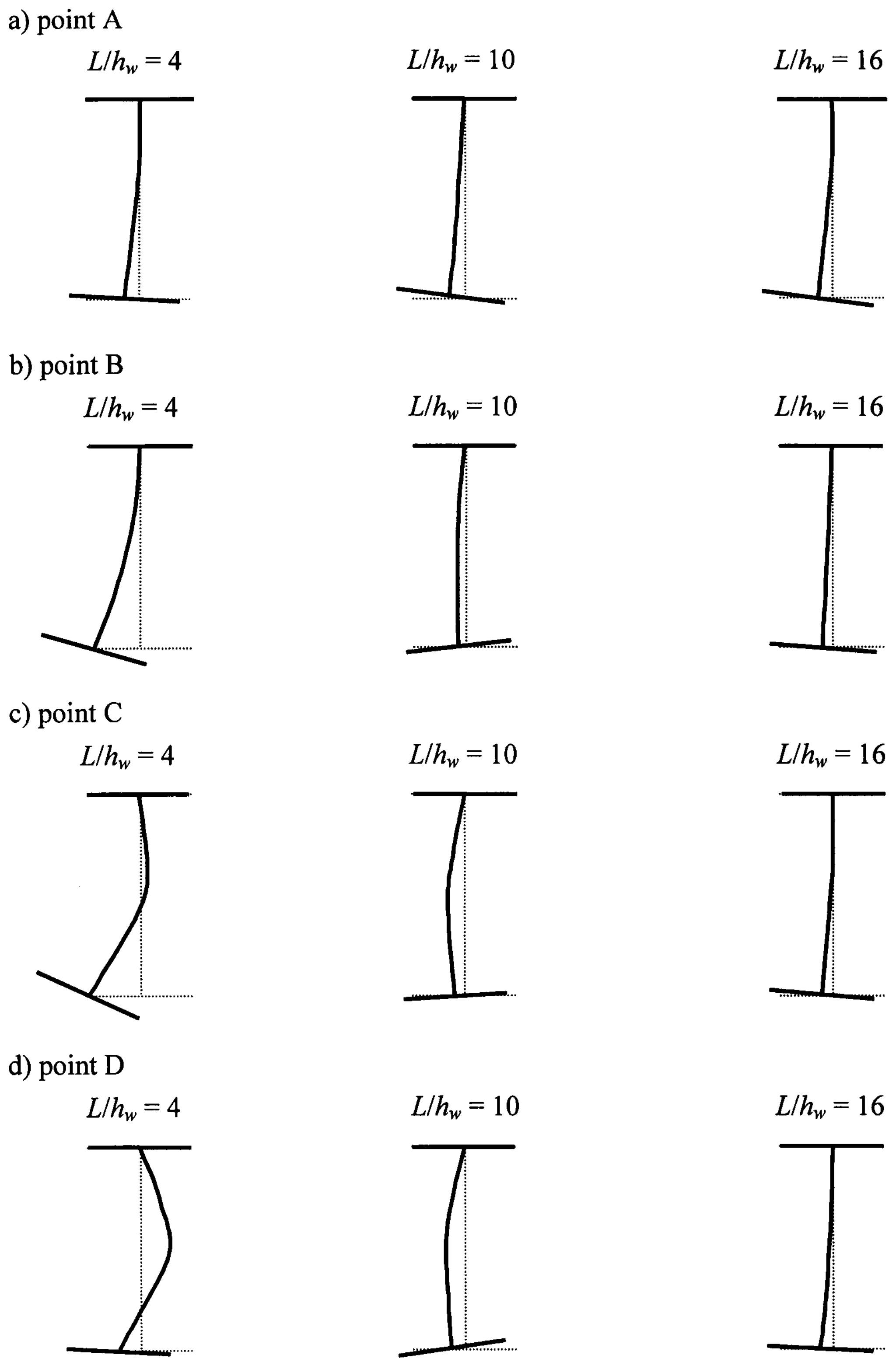

Figure 7.69b Cross-sectional buckling modes of an I-section with $b_f/h_w = 0.2$ (Case 7)

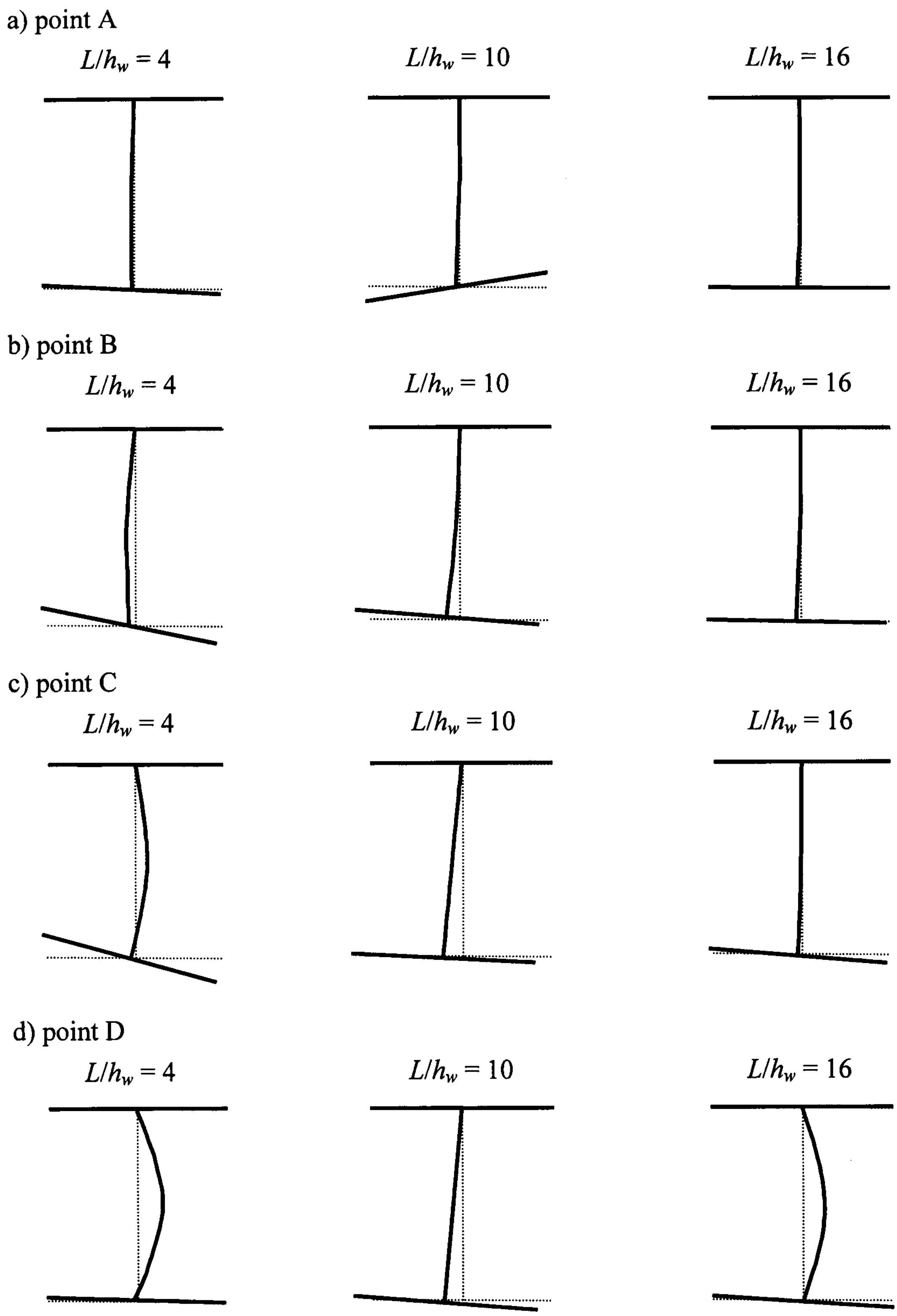

Figure 7.69c Cross-sectional buckling modes of an I-section with $b_f/h_w = 0.4$ (Case 7)

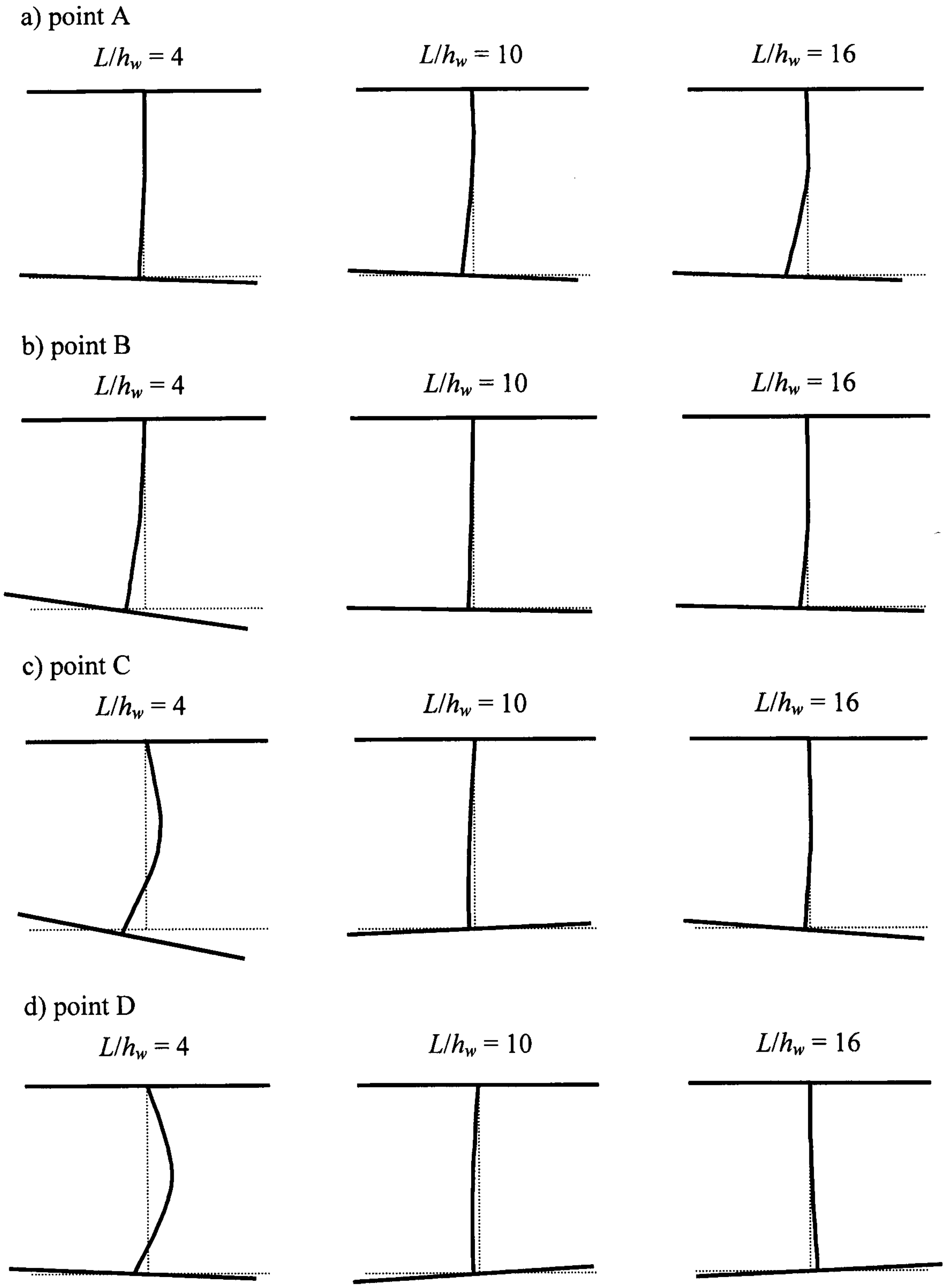

Figure 7.69d Cross-sectional buckling modes of an I-section with $b_f/h_w = 0.6$ (Case 7)

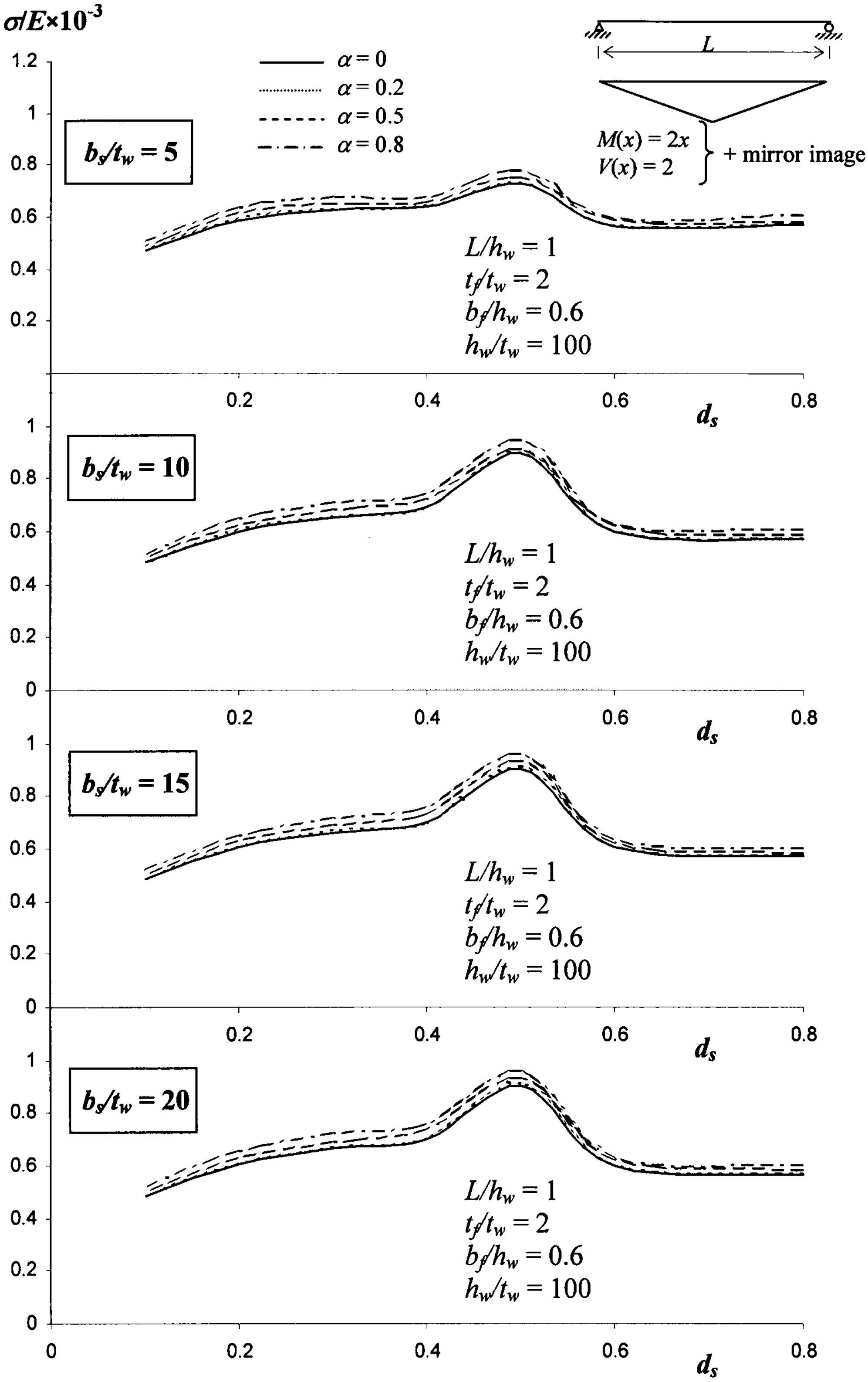

$\sigma/E\times10^{-3}$
$\alpha = 0$
$\alpha = 0.2$
$\alpha = 0.5$
$\alpha = 0.8$
L
$M(x) = 2x$
$V(x) = 2$
+ mirror image
$b_s/t_w = 5$
$b_s/t_w = 10$
$b_s/t_w = 15$
$b_s/t_w = 20$
$L/h_w = 1$
$t_f/t_w = 2$
$b_f/h_w = 0.6$
$h_w/t_w = 100$
d_s
0
0.2
0.4
0.6
0.8
1
1.2

a) Case 3

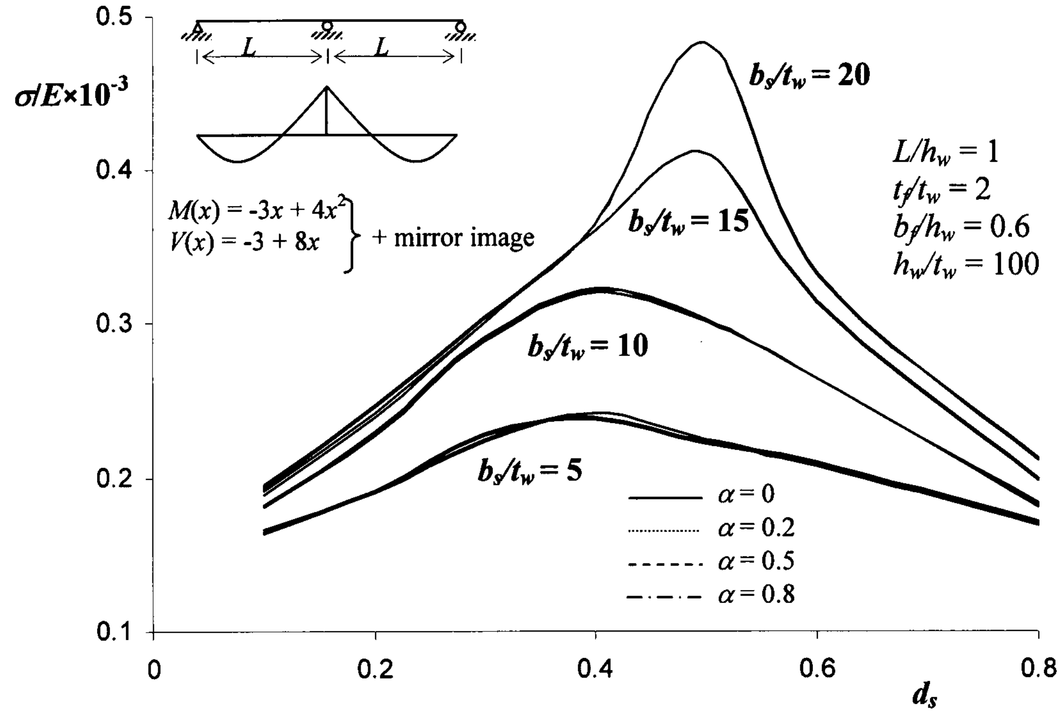

b) Case 7

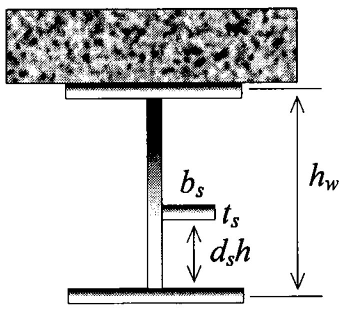

Figure 7.70 Elastic critical buckling stress: a) Case 3; b) Case 7

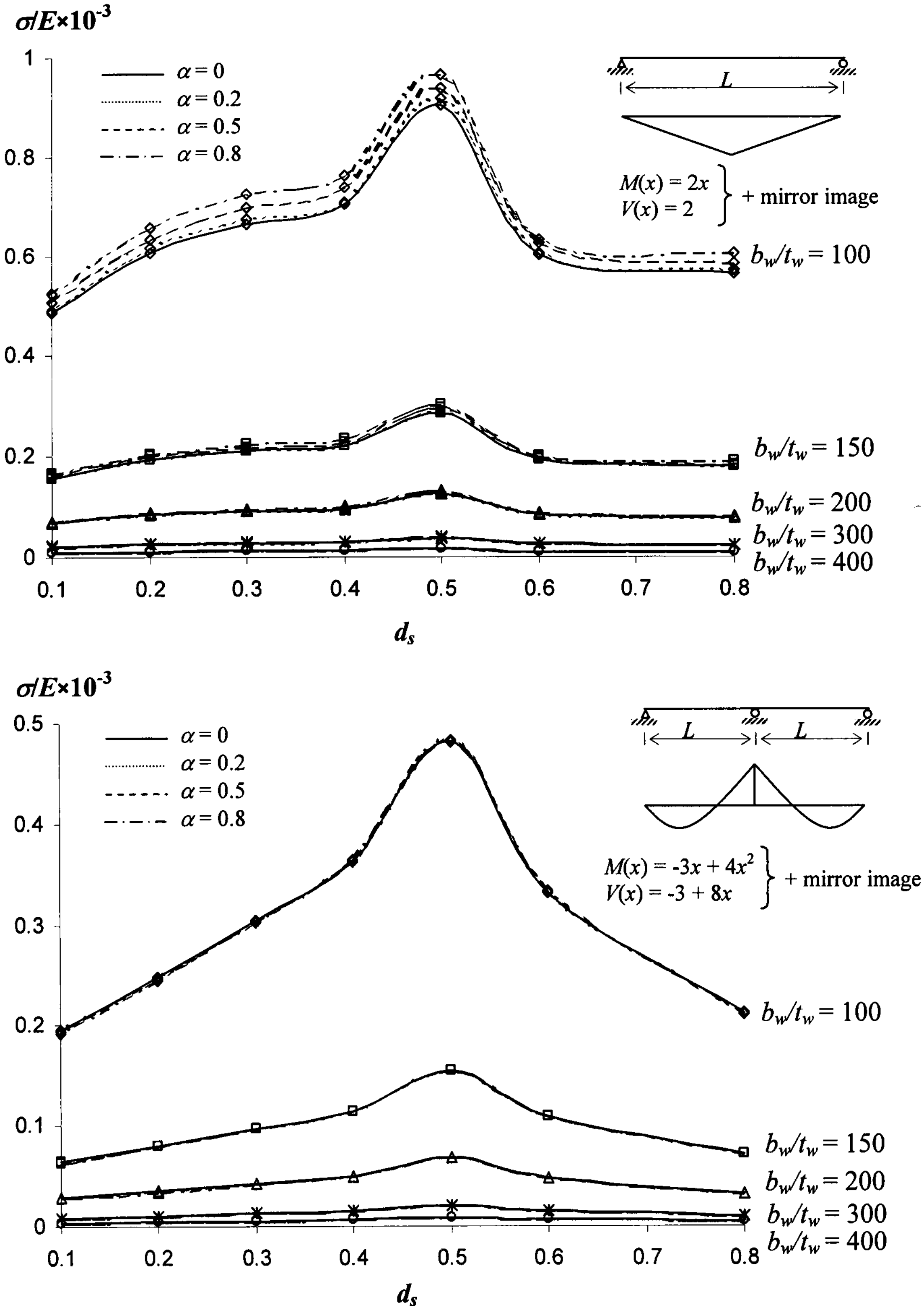

Figure 7.71 Elastic critical web buckling stress: a) Case 3; b) Case 7

a)

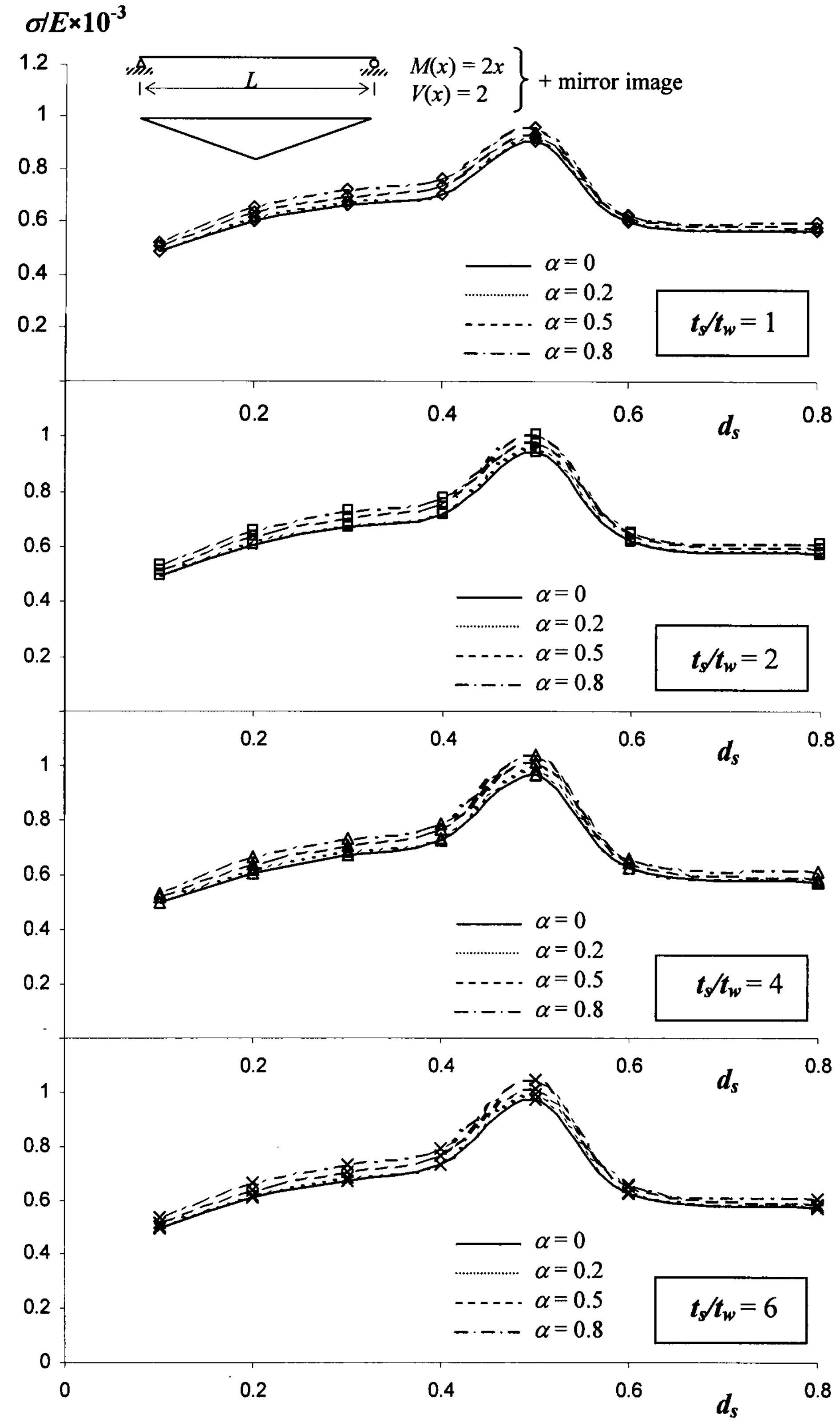
σ/E×10^-3
M(x) = 2x
V(x) = 2
+ mirror image
L
α = 0
α = 0.2
α = 0.5
α = 0.8
t_s/t_w = 1
t_s/t_w = 2
t_s/t_w = 4
t_s/t_w = 6
d_s

a)

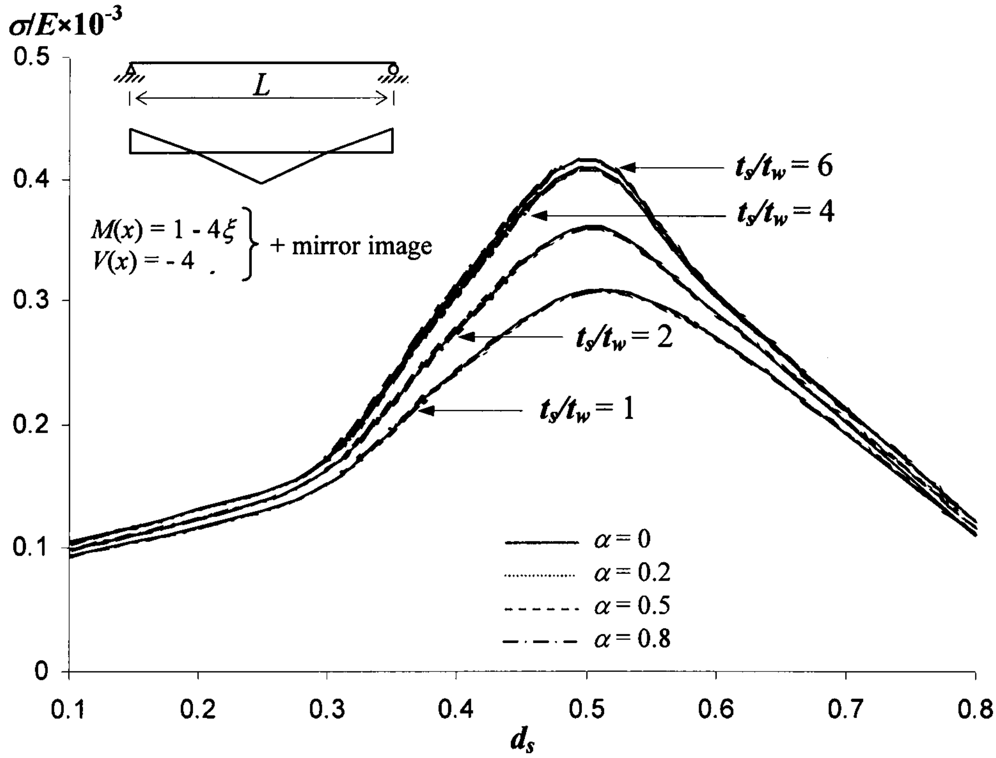

c)

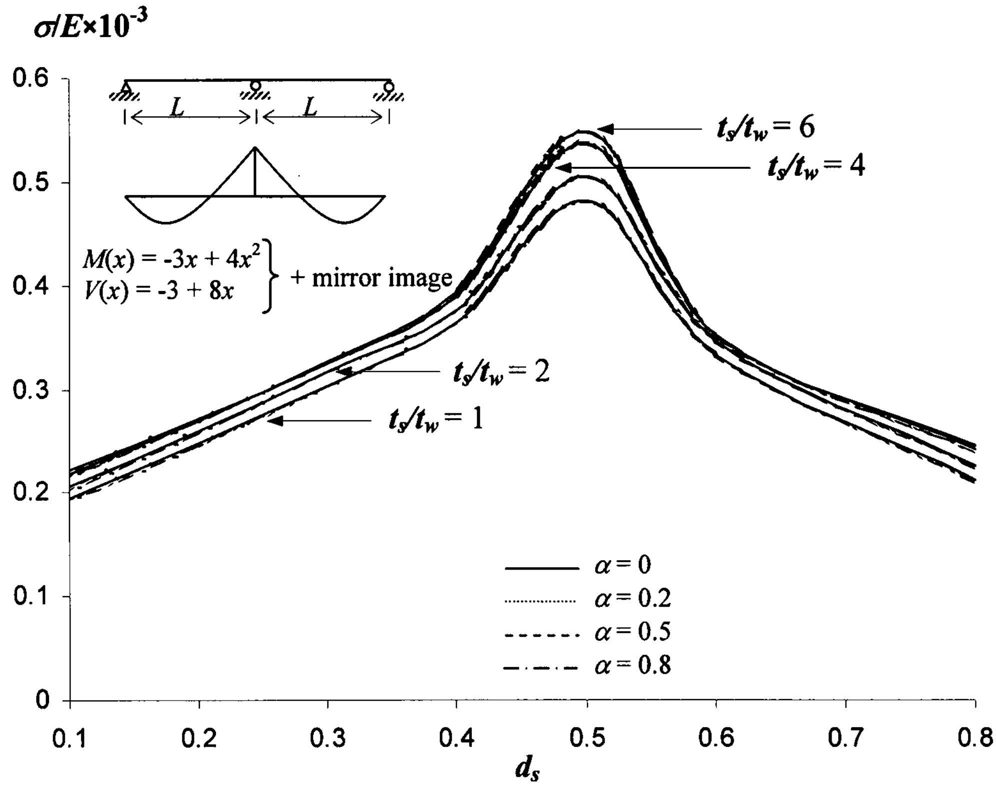

Figure 7.72 Elastic critical buckling stress: a) Case 3; b) Case 11; c) Case 7

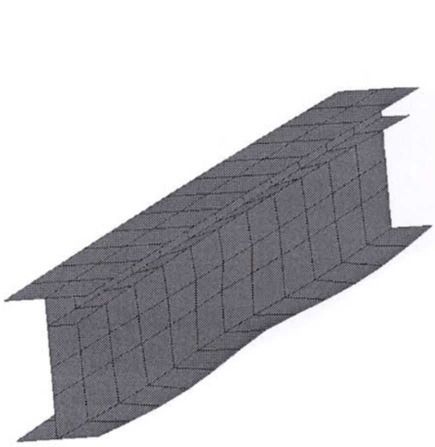

a) $d_s = 0.8$

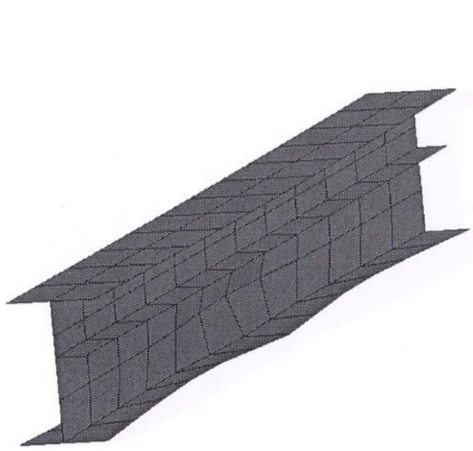

b) $d_s = 0.6$

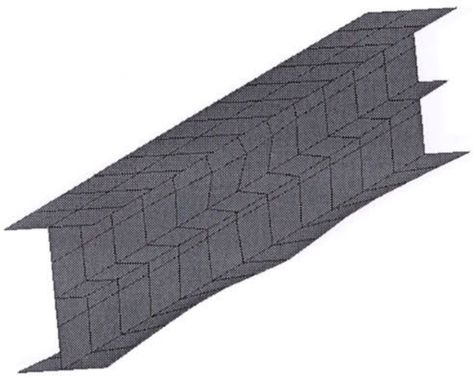

c) $d_s = 0.5$

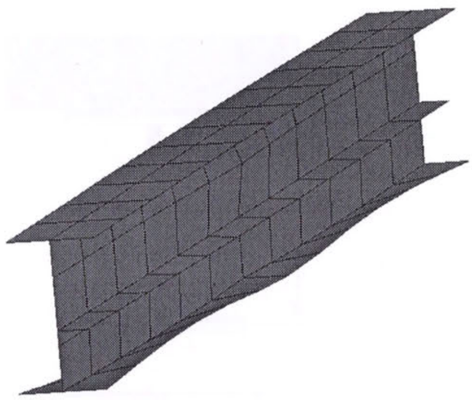

d) $d_s = 0.4$

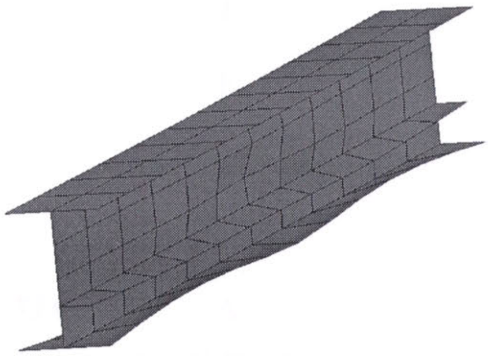

e) $d_s = 0.3$

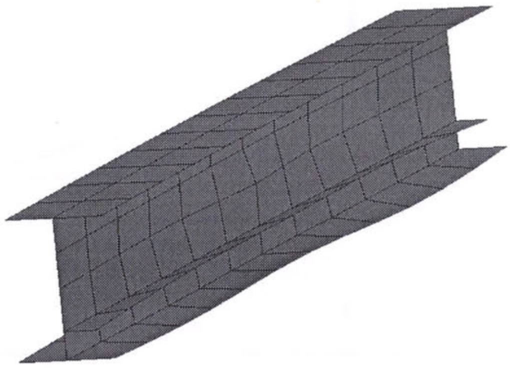

f) $d_s = 0.2$

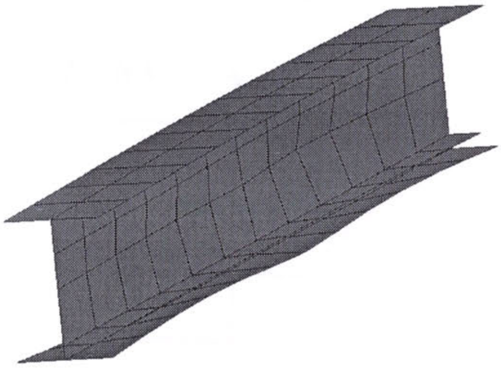

g) $d_s = 0.1$

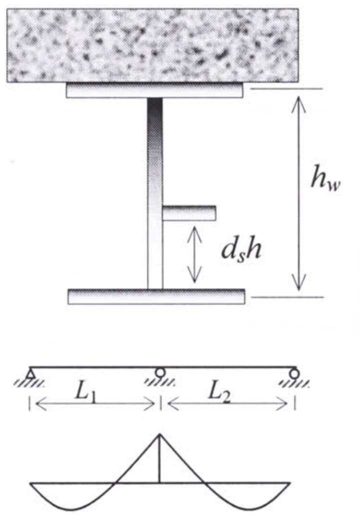

$$\left.\begin{array}{l} M(x) = -3x + 4x^2 \\ V(x) = -3 + 8x \end{array}\right\} + \text{mirror image}$$

$b_f/h = 0.6$, $b_f/t_f = 30$
$t_f/t_w = 2$, $h/t_w = 100$
$L_1/h_w = 1$, $L_1 = L_2$
$\alpha = 0$

Table 7.76 Buckling modes of an I-section with longitudinal stiffener; a) to g) (Case 7 + mirror image)

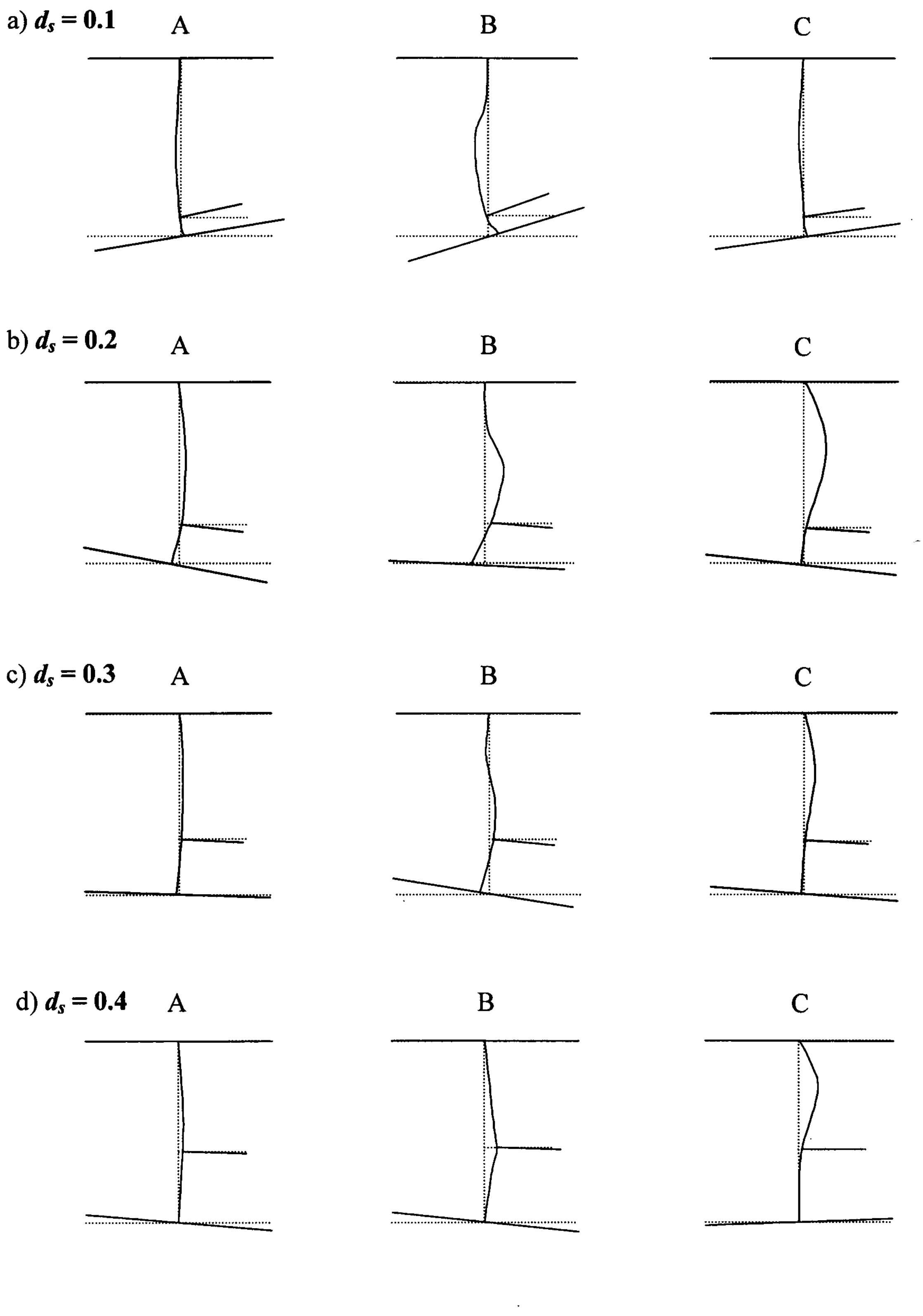

a) $d_s = 0.1$
A
B
C
b) $d_s = 0.2$
A
B
C
c) $d_s = 0.3$
A
B
C
d) $d_s = 0.4$
A
B
C

e) $d_s = 0.5$ A B C

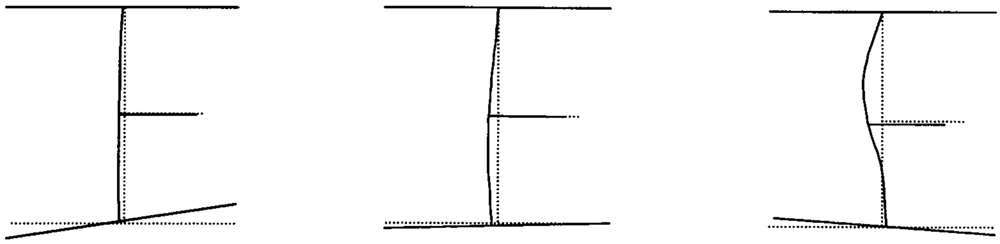

f) $d_s = 0.6$ A B C

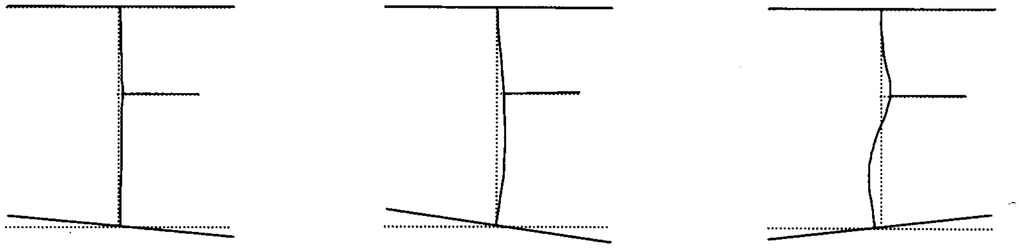

g) $d_s = 0.8$ A B C

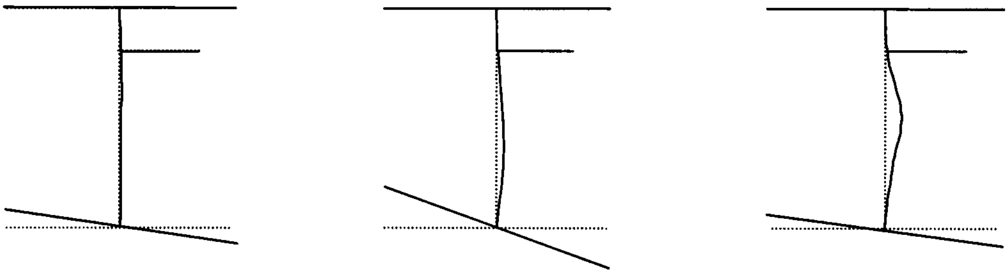

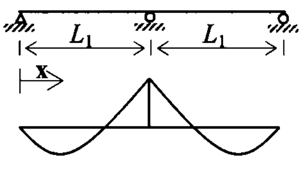

$M(\xi) = -3\xi + 4\xi^2$
$V(\xi) = -3 + 8\xi$ } + mirror image

$\xi = x/L_1$

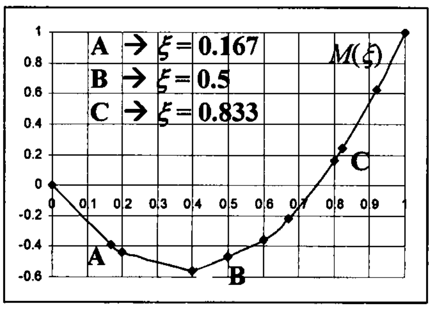

Table 7.74 Buckling modes of an I-section with longitudinal stiffener; a) to g) (Case 7 + mirror image)

Chapter 8

INELASTIC BUBBLE BASED SPLINE FINITE STRIP METHOD OF ANALYSIS

TABLE OF CONTENTS

8.1 INTRODUCTION

In this chapter, a method of inelastic buckling analysis of thin-walled sections is developed to study buckling characteristics of single span and two-span composite T-section beams in the inelastic range of structural response. The method is based on the bubble augmented spline finite strip method, developed in Chapter 7 of this thesis, and confirmed as both accurate and efficient for the elastic buckling analysis of thin-walled structural members and plates. The analysis presented herein takes into account the residual stress distribution and the non-linear stress-strain properties of the material from which the section is made.

The interaction between plastic behaviour and instability is important for steel I-sections with stocky flanges, or for plate girders where the residual stresses represent a significant factor in their design. In such structural configurations, sections may buckle inelastically at a moment which is lower than the elastic buckling moment, as this was demonstrated in Chapter 5 of this thesis. It is also well recognised that the ductility of composite beams in negative bending (Fig. 8.1) is influenced by considerations of the stability of the structural steel (Bradford 1992a). Tests conducted on continous composite beams and on simply supported beams in negative bending (Hope-Gill & Johnson 1976; Climenhaga & Johnson 1972; Johnson & Fan 1991; Johnson & Chen 1993; Loh *et al.* 2004), have verified that the modes of buckling may be local and/or restrained distortional (RDB). There is both theoretical and experimental evidence (Bradford & Johnson 1987) that in uniform composite bridge members, local buckling of the bottom flange at the face of an internal support will always precede RDB. This suggests that the design criterion for such a region could be nominal first yield of the steel, instead of the lower stress (determined by an inappropriate treatment of lateral buckling) which at present governs the design of most unbraced continuous beams. If this criterion were adopted, plasticity would occur earlier than assumed in design, due to the large residual stresses that can occur, particularly in the flanges of welded plate girders.

Plastic design of continuous composite beams has many advantages, however this can only be achieved if buckling is prevented. It is also well recognised that the ability of construction material to deform plastically is economically beneficial, and allows high stress peaks to be levelled out the first time the load to form a plastic hinge is reached. Design procedures based on plasticity have been adopted in most limit states steel structures codes, ie. American LRFD (1998) and Australian Standard AS4100 (1998). The RDB behaviour of continuous composite beams is usually approximated conservatively in design codes as being of a lateral-torsional type. However, studies of buckling in composite I-section bridge girders without intermediate stiffeners (Bradford & Johnson 1987) concluded that the design ultimate buckling loads could be more than doubled in many instances, when the buckling was considered as RDB rather than lateral-torsional.

Inelastic local buckling of plate assemblies has been investigated by a number of researchers. Gradzki and Kowal-Michalska (1985) used deformation theory to study the inelastic local buckling behaviour of thin-walled columns. Dawe and Kulak (1984a, 1984b) and Bradford (1986a) used the material property moduli derived from the flow theory and Lay's (1965) expression for the effective shear modulus to study the inelastic local buckling behaviour of I-sections and composite beams. Plank (1973) modified the finite strip method to allow for non-linear material behaviour in the buckling analysis of plate structures. Lau and Hancock (1986) investigated inelastic buckling of plates and thin-walled members using the spline finite strip method, based on both the deformation theory of plasticity and the flow theory of plasticity. Their analysis took into account strain hardening and residual stresses. Azhari (1993) employed the bubble augmented complex finite strip method to study the inelastic local buckling behaviour of flat plates and plate structures under bending and shear with and without residual stresses.

However, limited research work has been conducted on both elastic and inelastic RDB of single span, two and three-span continuous beams. Hancock and Trahair (1979) considered the elastic lateral-torsional buckling of continuously restrained two and three-span beams subjected to a uniformly distributed load using a line element with 8 buckling degrees of freedom. Bradford and Trahair (1986) studied the inelastic lateral-torsional buckling of restrained continuous beam-columns using a finite element method developed by Bradford (1987) and verified it with an experimental study conducted by Cuk *et al.* (1986). Johnson and Bradford (1983) and Bradford and Johnson (1987) considered composite cross-sections, while Bradford and Gao (1992) investigated the elastic lateral-distortional buckling of continuous composite beams. Lee (2001) studied the inelastic RDB of two and three-span beams under transverse load, fully restrained against translation and elastically against twist at the top flange. Lee's study considered the inelastic RDB buckling of hot-rolled sections only, and it is well recognised that buckling failure modes for hot-rolled sections differ from those of plate girders, as alluded to elsewhere in this thesis.

Therefore, the elastic spline finite strip method of analysis employing bubble functions, presented in Chapter 7, has been modifed herein to account for residual stresses and for material non-linearities. In order to ascertain the validity and accuracy of the method, comparisons are made with independent solutions. The inelastic RDB of simply supported and continuous composite T-section beams under transverse loading and moment gradient is then investigated, and conclusions are drawn that address the influence of geometry, residual stresses, member length, and the rigid restraint provided by the concrete and the degree of reinforcement in the concrete element.

8.2 THEORY

This section extends the bubble augmented spline finite strip method to include the important case of inelastic buckling. The method for solving elastic buckling problems has been set out fully in Chapter 7, and only relevant changes to include inelasticity are presented here. The analysis of continuous beams consists of two parts; the first part is the in-plane analysis using the well-known force or flexibility method to determine the moment and shear force distribution along the member length, whilst the second part is the out-of-plane buckling analysis using the bubble augmented spline finite strip method. The buckling is considered as a bifurcation from a straight pre-buckled configuration, so that the in-plane and buckling analyses are uncoupled.

In elastic buckling analysis, the stiffness matrix is a matrix of constants. The addition of the elastic and geometrical stiffnesses leads to a formulation of the equilibrium equation that may be solved by standard eigenvalue procedures. In inelastic buckling analysis, however, the stiffness matrix should be modified to include the effects of the altered stiffness properties of the material associated with the plastic deformation prior to buckling. This modification is affected by altering the elastic out-of-plane stiffness matrices so that they contain coefficients which depend on the state of plasticity in the plates and therefore on the state of stress. The modification adopted depends on the inelastic plate buckling theory being used.

Engineering theories of plasticity take as their point of departure the stress-strain law for simple tension or compression. In the elastic range, the relation between stress and strain is essentially linear. Beyond the elastic range, two methods of representation are generally employed. In one, the finite relationship is considered between stress and strain, however, the elastic modulus E is replaced by the secant modulus E_s, which depends on the state of stress. The other method is incremental one, which employs the tangent modulus E_t, which also varies with the stress.

The theory involving finite laws is usually called deformation theory, whilst the theory involving infinitesimal laws is usually called flow theory. Both types of theory assume that the plastic law proposed applies during loading, while unloading happens elastically. In order to define the plasticity theories in mathematical forms, the assumption that the principal axes of stress coincide with the principal axes of plastic part of the strain or its increment should be made (Prager 1948; Batdorf 1949).

8.3 IN-PLANE ANALYSIS

8.3.1 General

The first stage in the buckling analysis requires a calculation of the distribution of the strains applied to the member prior to invoking the bifurcation analysis. Firstly, an appropriate residual stress model needs to be selected, and then initial axial strain and curvature are applied as would occur when the member is subjected to axial and bending actions. The residual stresses which occur in welded sections, such as plate girders, are included in this analysis. These residual stresses, as illustrated in Fig. 8.2, are based on a summary of research conducted at Cambridge University (Dwight & Moxham 1969; Young & Schulz 1977; Dwight 1981) and fully described in Chapter 5

(Section 5.2). The constitutive curve for the structural steel is that employed in Chapter 5 of this thesis and shown in Fig. 8.3. The curve represents a trilinear idealisation, with a plastic plateau and a constant strain hardening modulus, E_{st}. The stress-strain curve assumes that the shear force does not influence the yielding of the member, although in theory this could easily be included using Von Mises' yield surface. It has been demonstrated in Chapter 7 that the method can easily handle shear as well as compression and bending.

The I-beam is assumed to be partitioned into a number of finite strips connected to one or more other strips along one or both of their longitudinal edges in the same manner as described in Chapter 7. Figure 8.4 shows the geometry of a typical finite strip which forms part of a plate assembly.

8.3.2 In-plane cross-sectional analysis

The bending moment, shear and axial force distribution in the member are determined at each Gaussian node prior to the buckling analysis. For the purpose of this analysis, the length of the plate strip L is divided into m sections of equal length h, as illustrated in Fig. 7.2, and twenty Gaussian points were assigned within each section. Thus, the total number of Gauss points for a member is $m \times 20$.

An iterative method is then employed to determine the distribution of the bending moment and shear force along the statically indeterminate member because the flexural rigidity, EI_y is initally an unknown quantity. The determination of major axis flexural rigidity $EI_y^{(2)}$ is more complicated than that used in elastic analysis due to the variation of the degree of yielding along the beam. In first iteration, the values of the flexural rigidity $EI_y^{(1)}$ at each node are assumed as elastic. The redundant reactions are then calculated using the force method (Appendix 8.1) and simple statics is employed to determine the moment and shear force distribution along the member as shown in Eqns. 8.16-8.18.

By defining ε^j_{oi} as the strain at the top of the section for a given Gaussian node i, and κ^j as the curvature, as illustrated in Fig. 8.2, the strain at any point z below the top fibre of the section can be expressed as

$$\varepsilon = \varepsilon_{oi}^{(i)} + \varepsilon_r - z\kappa^{(i)} \tag{8. 1}$$

where ε_r is the residual strain. The value of z in Eqn. 8.1 is adjusted iteratively by employing the Newton-Raphson procedure, described in detail in Chapter 5 (Section 5.6.2) and shown graphically in Fig. 5.7. The axial force, $N^{(i)}$ and moment, $M^{(i)}$ at the given value of strain, $\varepsilon_{oi}^{(i)}$ and curvature, $\kappa^{(i)}$ for each Gaussian station are then obtained by numerical integration over the cross-section as shown in Eqns. 8.2 and 8.3 below

$$N^{(i)} = \int_A \sigma(y,z)\mathrm{d}A \tag{8. 2}$$

$$M^{(i)} = \int_A \sigma(y,z)z\,\mathrm{d}A \tag{8. 3}$$

where $N^{(i)} = 0$ satisfies pure bending condition. σ *(y,z)* is the stress calculated at strain, ε and obtained from the relevant constitutive relationship as

$$\sigma(y,z) = \begin{cases} E\varepsilon & \varepsilon < \varepsilon_y \\ \dfrac{|\varepsilon|}{\varepsilon}\sigma_y & \varepsilon_y \le |\varepsilon| \le \varepsilon_h \\ E_{st}\varepsilon & \varepsilon > \varepsilon_h \end{cases}. \tag{8. 4}$$

The integrations in Eqns. 8.2 and 8.3 are carried out numerically by subdividing the flanges and web into a number of rectangles that distinguish elastic, yielded and strain-hardened regions around the section, as shown in Fig. 5.6, and using a trapezoidal integration technique.

The major axis flexural rigidities at each Gaussian station, $EI_y^{(2)}$ are recalculated using secant modulus theory as

$$\kappa^{(i)} = \frac{M^{(i)}}{EI_y^{(2)}} \tag{8. 5}$$

with known value of curvature, $\kappa^{(i)}$ and moment distribution, $M^{(i)}$ along the member. The calculated flexural rigidity values, $EI_y^{(2)}$ are then compared with assumed values of $EI_y^{(1)}$ and if the normalised Euclidean norm

$$\left\| EI_y^{(n)} / EI_y^{(n-1)} \right\| \leq c \tag{8. 6}$$

for the two sets of values, $EI_y^{(2)}$ and $EI_y^{(1)}$, is less than some predetermined accuracy, c these values are accepted. Otherwise, the procedure is repeated n times until the condition in Eqn. 8.6 is satisfied.

8.4 OUT-OF-PLANE ANALYSIS

The elastic bubble augmented spline finite strip method of analysis developed in Chapter 7 is modified herein for the inelastic buckling analysis. The finite strip buckling analysis for inelastic behaviour may be written as

$$\left| \overline{K}(\lambda) - \overline{G}(\lambda) \right| = 0 \tag{8. 7}$$

where $\overline{K}$ and $\overline{G}$ are the stiffness and stability matrices respectively for the member. These may be assembled from the flexural and membrane matrices $\overline{k}_F$, $\overline{k}_M$, $\overline{g}_F$ and $\overline{g}_M$ for each strip, where

$$\overline{k}_F(\lambda) = \int_V \overline{B}_F{}^T \overline{D}_F(\lambda) \overline{B}_F \mathrm{d}V \tag{8. 8}$$

$$\overline{k}_M(\lambda) = \int_V \overline{B}_M{}^T \overline{D}_M(\lambda) \overline{B}_M \mathrm{d}V \tag{8. 9}$$

$$\overline{g}_F(\lambda) = \int_V \vec{\varepsilon}_N{}^T \begin{bmatrix} \sigma_x & \sigma_y \\ \sigma_y & \tau_{xy} \end{bmatrix} \vec{\varepsilon}_N \mathrm{d}V \tag{8. 10}$$

and

$$\bar{g}_M(\lambda) = \int_0^L \int_0^b \bar{\psi}_{,x}^T \bar{N}_M^T \sigma_x(\lambda) \bar{N}_M \bar{\psi}_{,x} \, t \, \mathrm{d}y \, \mathrm{d}x \,. \tag{8. 9}$$

In Eqns. 8.8 and 8.9, $\overline{B}_F$ and $\overline{B}_M$ are the strain matrices, $\overline{D}_F$ and $\overline{D}_M$ are the property matrices, while $\bar{\varepsilon}_N$ in Eqn. 8.10 is the nonlinear strain vector. $\overline{B}_F$, $\overline{B}_M$, and $\bar{\varepsilon}_N$ may be determined from the displacement functions for a strip, which consist of a spline polynomial, $\psi_i(x)$ in the longitudinal direction and a cubic polynomial, N_i in the transverse direction. These have been presented in Chapter 7 and are not reproduced here.

The matrices in Eqns. 8.8-8.11 are in the local coordinate system. It is necessary to transform these matrices to the global coordinate system for folded plate assemblies where the membrane action of a strip will affect the bending action of its adjoining strip. The transformation procedure adopted herein is that presented in Chapter 7 (Section 7.5).

The finite strip treatment presented in this chapter differs from the elastic analysis presented in Chapter 7, since $\overline{D}_F(\lambda)$, $\overline{D}_M(\lambda)$ and σ_x in Eqns. 8.8-8.11 are nonlinear functions of the buckling load factor λ. Unlike the elastic stiffness matrices, the matrices $\overline{K}(\lambda)$ and $\overline{G}(\lambda)$ depend on the stress level. The initial stress $\sigma(y,z)$ at a point on the cross-section of the joist is simply found from Eqn. 8.4. When $\varepsilon < \varepsilon_y$ in the member, the property matrices, $\overline{D}_F(\lambda)$, $\overline{D}_M(\lambda)$ are given from elementary elasticity theory, and have the familiar form of that employed in Chapter 7. However, when $\varepsilon \geq \varepsilon_y$, the rigidities in the property matrices applicable to inelastic buckling must be used. The rigidities employed here are those used in the inelastic buckling study of Dawe and Kulak (1984), and are given in Appendix 8.2.

8.5 SOLUTION OF BUCKLING EQUATION

Using the principle of minimum potential energy, as was done in Chapter 5 of this thesis, the buckling solution of continuous beams can be expressed as

$$\left(\overline{K}(\lambda)-\overline{G}(\lambda)\right)\bar{\Delta}=\overline{A}(\lambda)\bar{\Delta}=\bar{0} \tag{8. 12}$$

where $\overline{K}(\lambda)$ and $\overline{G}(\lambda)$ are the global stiffness and stability matrices respectively and $\bar{\Delta}$ is the vector of buckling deformations (eigenvector).

An incremental and iterative procedure is used to calculate the critical moment at buckling. The in-plane load, which depends on the load factor λ is used in this analysis to determine the distribution of moment, shear force, curvature and elastic and inelastic regions of the cross-section. The procedure has an added degree of complexity since for the given value of λ, the in-plane analysis must firstly iterate to determine the distribution of the bending moment and shear force, as shown in section 8.3.2. The value of λ is increased monotonically until the determinant $\overline{A}(\lambda)$ changes sign. When this occurs, the method of bisections is used to converge on the critical buckling load factor, λ. Thus, a non-trivial solution to Eqn. 8.11 is satisfied in the same fashion as in Chapter 5 (Section 5.4). The buckled shape is then obtained by invoking the eigenvector routines (Garbow *et al.* 1977) at the critical load factor, λ. The complete procedure for the solution of the inelastic buckling problem is set out in the flow chart in Fig. 8.5.

8.6 ACCURACY OF THE METHOD

Extensive verification was carried out by comparing the method with the elastic bubble augmented spline method, developed and verified in Chapter 7 as a vastly accurate and efficient method of analysis. For the purpose of this comparison the elastic buckling load was obtained using a very high value of the yield stress, f_y in absence of residual stresses so that the cross-section remains entirely elastic as was done in Chapter 7.

The validity and accuracy of the spline finite strip method of inelastic buckling analysis described in the previous section were also investigated by comparing the buckling loads and modes computed with the existing theoretical values. For instance, Kitipornchai and Wong-Chung (1987) and Lau (1988) investigated the inelastic buckling of welded monosymmetric I-beams subjcted to uniform bending moment. The welding residual stress distribution adopted in their analysis, based on the 'tendon force concept', is shown in Fig. 8.8. The yield stress was 250 MPa and the stress-strain curve of the material was assumed to be the same as that in Fig. 8.3, only with $E_{st} = 0$. The critical moments, produced by those theoretical studies (Kitipornchai & Wong-Chung 1987; Lau 1988) and the method developed herein, for the T-section in Fig. 8.8 are shown in Fig. 8.9. In Fig. 8.9, M_{cr}, M_E and M_P are the critical moment, elastic critical moment and fully plastic moment respectively. In Lau's analysis, the flange outstand and web plate were subdivided into four and ten strips respectively, and because of symmetry, only four spline sections were required longitudinally for half of the length of a beam. However, in the anlysis developed in this study only two strips were required to model the flange outstand and four strips were used to model the web plate. The computed critical moments are within 10% of those obtained by Kitipornchai and Wong-Chung (1987) and Lau (1988).

8.7 INELASTIC NUMERICAL STUDIES

8.7.1 General

Having establised the validity of the inelastic buckling analysis, the spline finite strip method was applied to study the inelastic buckling behaviour of simply supported and continuous composite beams subjected to transverse loading. Figure 8.10 shows converged number of sections m required for particular beam slenderness and adopted in this study. Because of symmetry, only half of the length of a beam, with appropriate modification for boundary supports and the loading, was analysed. The material has been assumed to have a stress-strain curve as that shown in Fig. 8.3 and the properties f_y = 250 MPa, E = 200 GPa, $E_{st} = E/33$, $\varepsilon_h = 11\varepsilon_y$ and $\nu = 0.3$. The cross-sectional dimensions of the steel I-section investigated herein are illustrated in Fig. 8.11.

8.7.2 Simply supported I-section members

This section considers the inelastic buckling of simply supported beams with transverse loading. For the analysis, the unrestrained flange of the composite steel-concrete beam is subjected to compressive stresses, as would be the case for half-through bridge girders. The assumption was made that the uniform shear stress in the web was $V/(h_w t_w)$, while that in the flanges was a linear distribution (Trahair & Bradford 1998).

Figures 8.12 and 8.13 show the critical buckling moments for simply supported plain steel and steel-concrete composite beams subjected to a concentrated and uniformly distributed load respectively. In the figures, critical buckling moment, M_{cr} is normalised with respect to plastic moment, M_P and is plotted versus modified slenderness $\sqrt{M_P/M_E}$. It is evident from the figures that the buckling behaviour for the cross-section shown in Fig. 8.11, for a range of different slenderness ratios, is elastic. The presence of the residual stresses (c_f = 10 mm) shown in Fig. 8.12-8.13 as a dashed line coinciding with the full line that represents inelastic and/or elastic buckling for the beam, is rather insignificant for such geometry and loading configurations. Nevertheless, the presence of the uniform axial force, which is adopted as 30% of the total yield moment for the steel I-section shown in Fig. 8.11, is quite notable. The figures also show the critical elastic buckling moments for plain steel beams when the assumption that the cross section remains rigid is valid, and the RDB moments for composite steel beams when such assumption is no longer applicable. The RDB values, derived by the analysis method developed in Chapter 4 of this thesis, do not account for any local buckling instability of the cross-sectional plates. The figures, therefore, clearly illustrate significant reductions in the buckling capacity caused by the cross-sectional distortions, such as local buckling, RDB and the combination of the two, in spite of the beneficial effects of the rigid restraint provided by the concrete ($\alpha = \infty$) at the tension flange of the steel I-section.

The results in Figs. 8.14 and 8.15 show the reductions of the beam ultimate load capacity for simply supported steel-concrete composite beams as well as the buckling modes at the mid-span of the beam. In the figures, the normalised load capacity is ploted as a function of beam slenderness, L/h_w. The axial stress is calculated as 50% of the bending stress on the onset of yileding for the given cross-section. Noteworthy reductions in the buckling capacity due to the presence of the uniform axial force in the beam, which inevitably reallocates the neutral axis closer to the restrained flange, are obvious from the graphs. Significant reductions in the ultimate load capacity are also observed due to the residual stresses (c_f = 20) and it is observable that the coupling of local and distortional buckling is a governing failure mode for the cross-sections of this geometry.

8.7.3 Continuous I-section members

Two-span continuos beams with equal span lengths, simply supported and fully fixed at the external supports, and subjected to concentrated load and to a uniformly distributed load, as shown in Figs. 8.15-8.18, are considered in this section. The concentrated load was applied at the mid-point of each span. The figures illustrate the load capacities, w normalised with respect to the beam ultimate load capacity, w_u and plotted as a function of the beam slenderness, L/h_w.

In Chapter 3 an extensive study was undertaken to investigate the influences of the axial stress on the continuous steel-concrete composite beam buckling behaviour. It was concluded that the presence of the axial stresses is of particular significance in propped construction, where the ratio between axial and bending stresses in the compression flange is 0.2-0.3. This ratio is somewhat less for the unpropped construction, where the self-weight of the beam contributes to increased bending stresses. It was further shown that in two-span continuous composite beams the axial force varies longitudinally with prevailing compressive stresses in the vicinity of the internal support, that can be even higher than 20-30% of the bending stress. Therefore in this analysis the axial stress is assumed to vary longitudinally as a sixth order polynomial function, as shown in Fig. 8.1 based on the findings presented in Chapter 3.

The presence of the axial residual stresses in the beam results in a considerable reduction of the ultimate load capacity and contributes to further instability of the cross-section in the negative moment region where the coupling of the local and RDB modes is notable. On the other hand, the presence of the rigid restraint provided by the concrete medium contributes to a ample increase in the capacity when compared to that of a bare steel section beam, as shown in Figs. 8.16-8.19.

Generally, when span ratio is low the governing buckling mode was found to be local buckling, or local buckling coupled with distortional buckling, whilst for high span ratios, owing to the rigid restraint provided at the top flange, the governing buckling mode was found to be distortional.

8.8 SUMMARY

The bubble augumented spline finite strip method of analysis developed in Chapter 7 has been employed to study the inelastic buckling behaviour of single span and two-sapn continuous composite beams with simply supported and fully fixed end supports. The in-plane analysis was performed using the flexibility method of analysis to determine the internal support reactions and simple statics to then determine the distribution of moment and shear force. These action were then used for the out-of-plane buckling analysis. The in-plane analysis is non-linear owing to the redistribution of the bending moments in yielded portions. The rate of convergence and accuracy of the method was demonstrated by comparisons with existing inelastic buckling solutions a T-section in uniform bending. The results also demonstrated that the use of bubble function improved significantly the spline finite strip method in terms of strip subdivision, and led to reduced computation time given the high degree of the iteration involved in this method of analysis.

The method was then applied to investigate inelastic buckling modes of single and two-span continuous composite beams subjected to moment gradient. Buckling mode plots and buckling curves, that depict the effects of the residual stresses and varying axial force, are presented. Significant reductions in the ultimate load capacities are observed for continuous composite beams as a result of the coupling of material non-linearity, local and distorional buckling, residual stresses and the varying axial force. It is concluded that further work is required to asses the interactive nature of the local and RDB modes in such structural configurations.

8.9 APPENDICES

8.9.1 The force method of analysis

The well-known force or flexibility method (Hall & Kabaila 1986) is employed in this chapter to determine the redundant reactions, shear force and bending moment distribution for propped cantilevers, and two and three-span continuous beams. In general, a stiffness method (displacement method) formulation would be preferable for the in-plane analysis, however the force method has been used here for simplicity as the degree of redundancy is small.

Two and three-span continuous beams subjected to concentrated and uniformly distributed loads are considered in this section. The concentrated load is applied at each span some distance away from the support, as shown in Fig. 8.1.

For a single-span propped cantilever and two-span continuous beams, the formulaton is as follows

$$u_1 = u_{10} + X_1 f_{11} \tag{8. 13}$$

where

$u_{10} = \int_0^L \frac{M_o m_1}{EI_x} \mathrm{d}x$, $f_{11} = \int_0^L \frac{m_1 m_1}{EI_x} \mathrm{d}x$ and X_1 represents the redundant reaction. M_o is the bending moment due to applied load on the primary structure and m_1 is the bending moment due to unit value of the redundant action. For instance, for a two-span continuous beams, M_0 and m_1 can be represented as shown in Fig. 8.6.

In a same manner, for a three-span continous beams

$$\begin{aligned} u_1 &= u_{10} + X_1 f_{11} + X_2 f_{12} \\ u_2 &= u_{20} + X_1 f_{21} + X_2 f_{22} \end{aligned} \tag{8. 14}$$

where $u_{20} = \int_0^L \frac{M_o m_1}{EI_x} dx$, $f_{12} = \int_0^L \frac{m_1 m_2}{EI_x} dx$, $f_{21} = \int_0^L \frac{m_2 m_1}{EI_x} dx$, $f_{22} = \int_0^L \frac{m_2 m_2}{EI_x} dx$ and X_1 and X_2 represent unknown reactions. Since there are two redundant systems, m_1 and m_2 represent the moments due to unit values of the redundant actions. Figure 8.7 illustrates the distribution of primary bending moment, M_o and moments, m_1 and m_2 in two redundant systems for the three-span continuous beam.

Equation 8.14 may be expressed in matrix format as:

$$\begin{bmatrix} u_{10} \\ u_{20} \end{bmatrix} + \begin{bmatrix} f_{11} & f_{12} \\ f_{21} & f_{22} \end{bmatrix} \begin{bmatrix} X_1 \\ X_2 \end{bmatrix} = \begin{bmatrix} u_1 \\ u_2 \end{bmatrix} \tag{8. 15}$$

where u_1 and u_2 represent the internal displacement, f_{ij} are flexibility coefficients, and X_1 and X_2 redundant actions. The internal reactions are then determined from the boundary conditions where the internal displacements u_1 and u_2 at the supports are equal to zero. The integrals in Eqns. 8.13 and 8.14 must be performed by Gaussian quadrature, since the value of EI_y depends on the level of loading. X_1 and X_2 represent internal reactions for R_B and R_C respectively (Fig. 8.7). The distribution of the bending moment and shear force along the beam can be determined from simple statics. For instance, for a two-span continuous member subjected to concentrated loads and uniformly distributed load, the bending moment distribution can be described as

$$M(x) = R_1 x - \frac{wx^2}{2} - P_1\langle x - x_1 \rangle + R_B\langle x - L_1 \rangle - P_2\langle x - x_2 \rangle \tag{8. 16}$$

whilst for a three-span continous beam subjected to concentrated loads and uniformly distributed load the distribution is as follows

$$\begin{aligned} M(x) = R_1 x - \frac{wx^2}{2} - P_1\langle x - x_1 \rangle + R_B\langle x - L_1 \rangle - P_2\langle x - x_2 \rangle + R_C\langle x - L_1 - L_2 \rangle - \\ - P_3\langle x - x_3 \rangle \end{aligned} \tag{8. 17}$$

The Macaulay bracket term is taken as zero when the quantity inside the Macaulay bracket is not positive. Similarly, the distribution of the shear force can be calculated as

$$V(x) = \frac{\mathrm{d}M(x)}{\mathrm{d}x}. \tag{8. 18}$$

8.9.2 Property matrices

The membrane displacement property matrix is given by

$$\overline{D}_M = \begin{bmatrix} S_1 & S_2 & 0 \\ S_3 & S_4 & 0 \\ 0 & 0 & G \end{bmatrix}. \tag{8. 19}$$

For isotropic buckling (ie. in regions where the applied strain $\varepsilon < \varepsilon_y$) the elastic material property moduli are given by

$$S_1 = \frac{E}{(1-v^2)}, \quad S_4 = \frac{E}{(1-v^2)}, \quad S_2 = S_3 = vS_1, \quad S_9 = G \tag{8. 20}$$

in which E, v and G are the appropriate isotropic elastic material properties.

For inelastic buckling (ie. in regions where the applied strain $\varepsilon \geq \varepsilon_y$) the inelastic material property moduli are defined as

$$\begin{aligned} S_1 &= E_{st}/(1 - v_1 v_2) \\ S_2 = S_3 &= \left\{\frac{2E_{st}}{3E_{st} + E}\right\}\{(2v-1)E_{st} + E\}/(1 - v_1 v_2) \\ S_4 &= 4EE_{st}/[(3E_{st} + E)(1 - v_1 v_2)] \\ S_9 &= G_{st} \\ v_1 v_2 &= \frac{\{(2v-1)E_{st} + E\}^2}{E(3E_{st} + E)} \\ G_{st} &= \frac{4EE_{st}}{4E_{st}(1+v) + E} \end{aligned} \tag{8. 21}$$

in which E_{st} is the strain hardening modulus in the yielded and strain-hardening regions.

Similarly, flexural displacement property matrix is defined as

$$\overline{D}_F = \frac{t^3}{12}\overline{D}_M \tag{8.22}$$

in which t is the thickness of the plate.

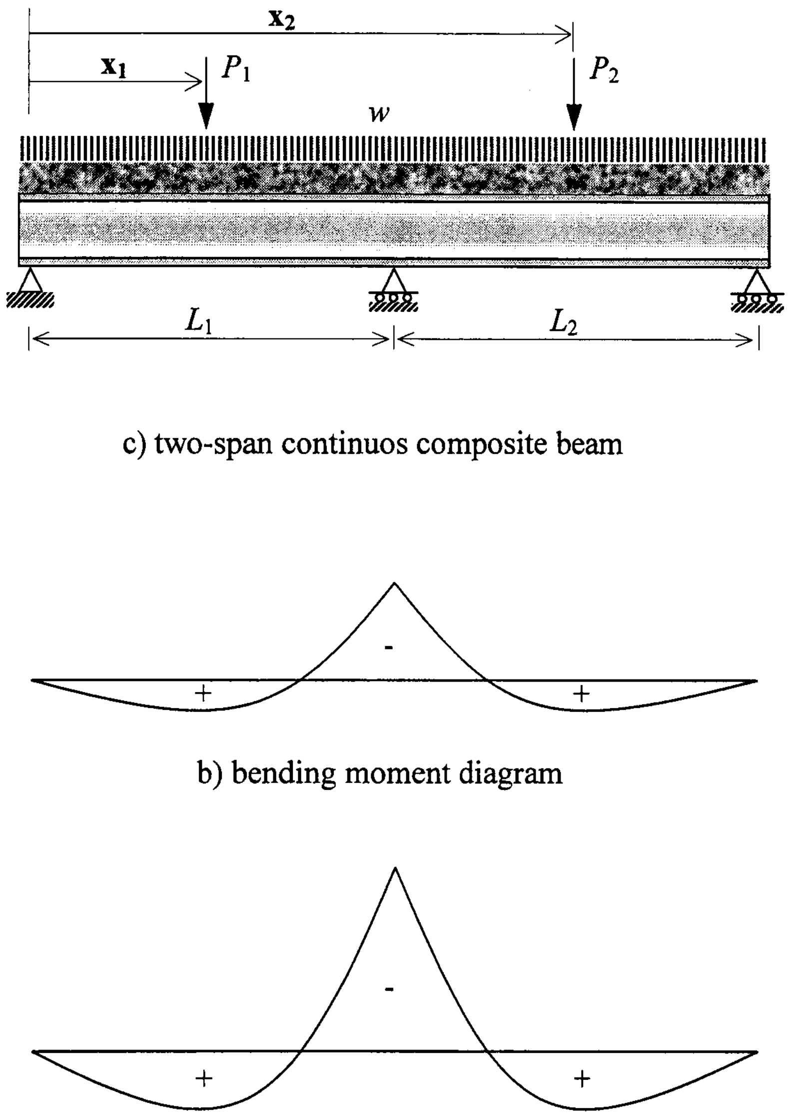

c) two-span continuos composite beam

b) bending moment diagram

c) axial force diagram

Figure 8.1 Continuous composite beam

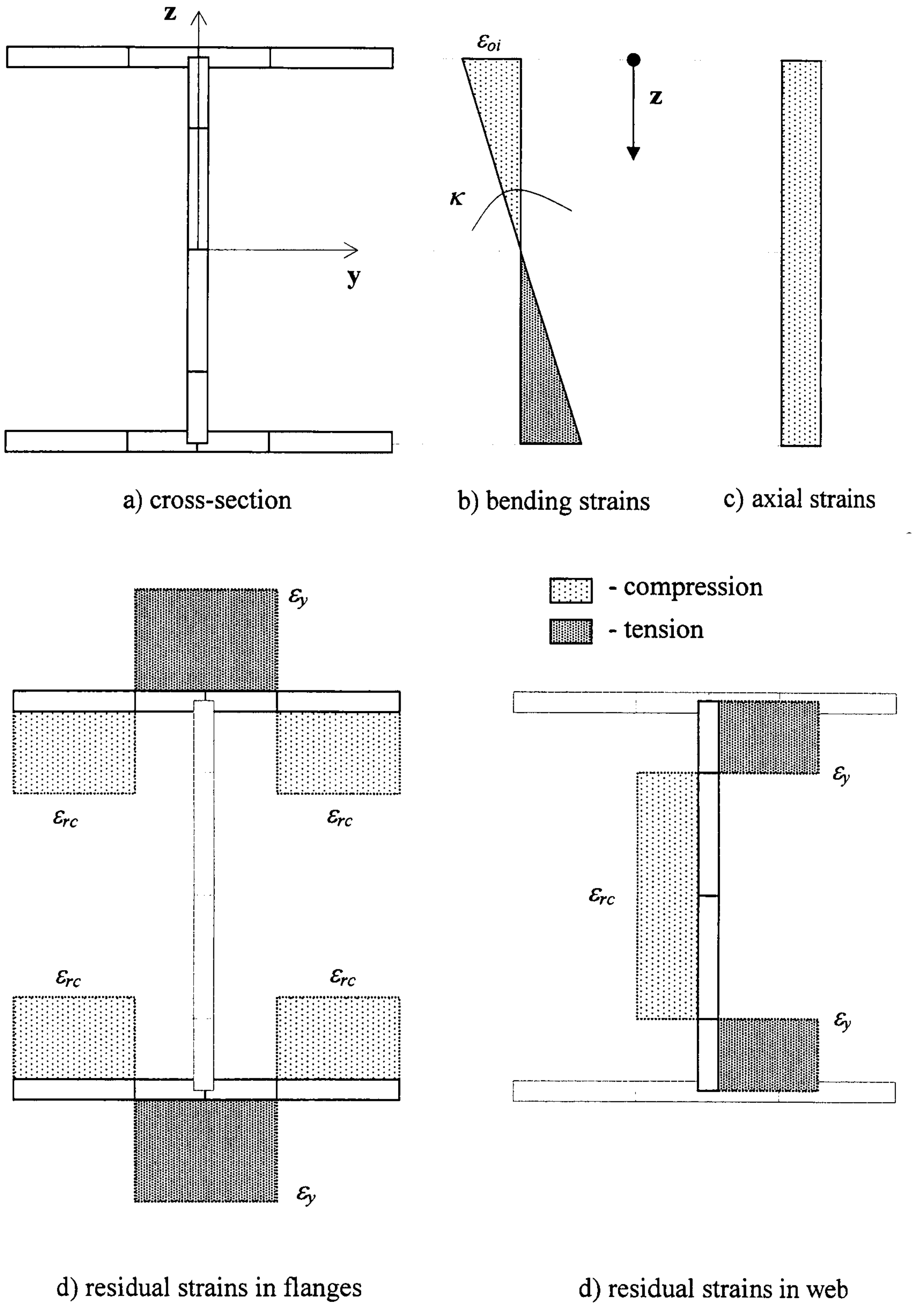

Figure 8.2 Strain distribution in a welded I-section

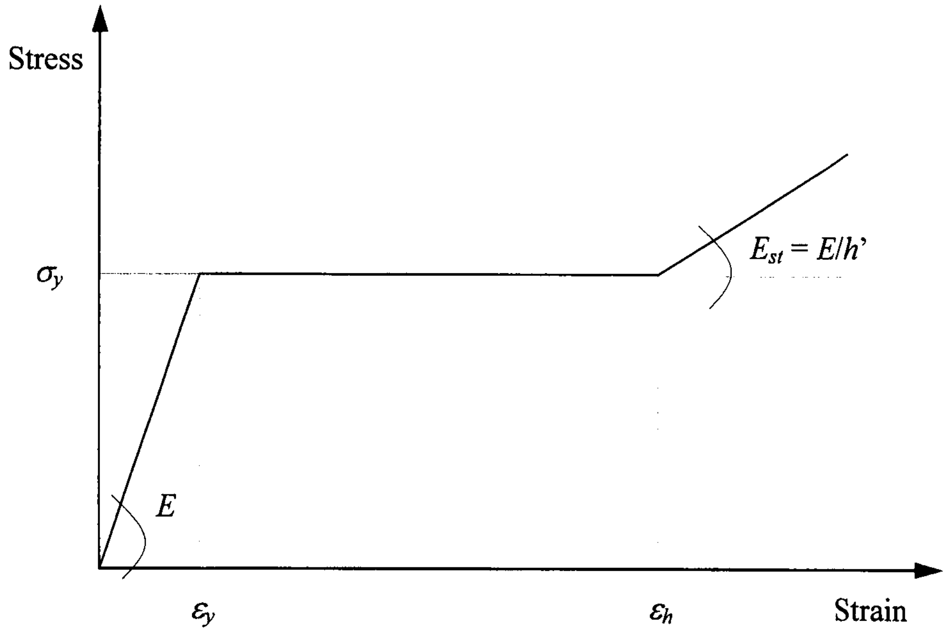

Figure 8.3 Idealised stress-strain curve

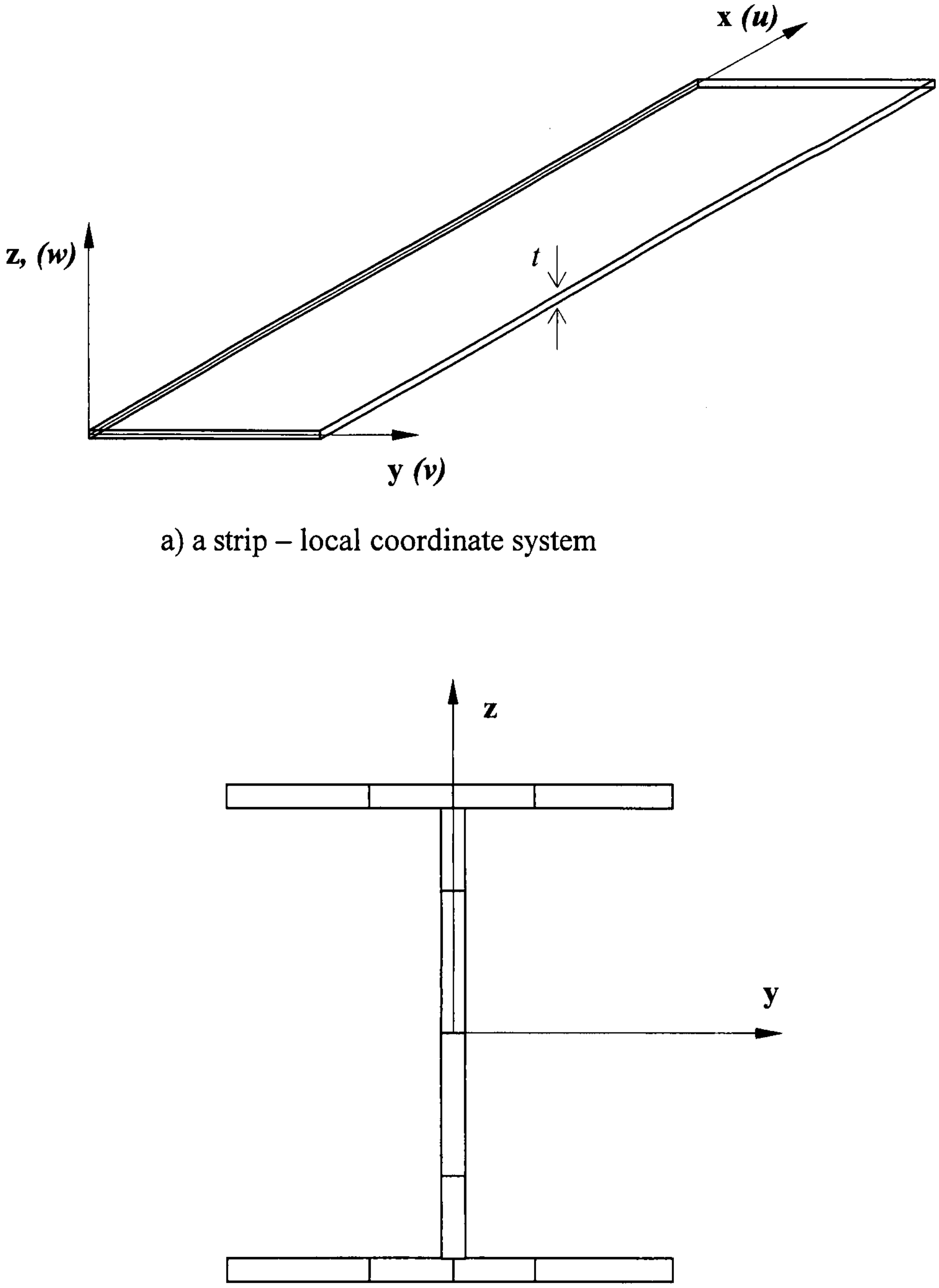

a) a strip – local coordinate system

b) a plate assembly – global coordinate system

Figure 8.4 Strip orientation

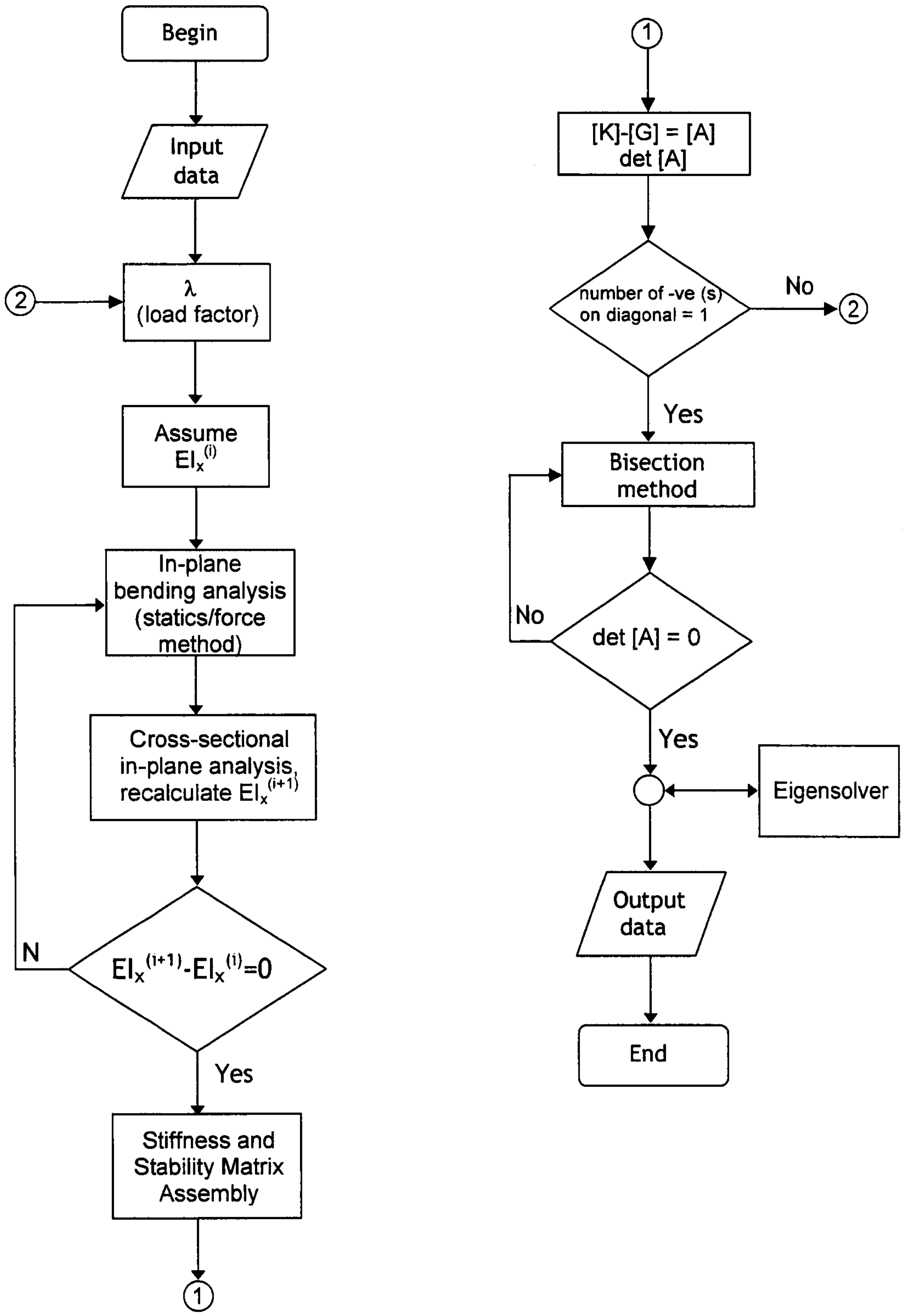

Figure 8.5 Flow-chart for in-plane and buckling analysis

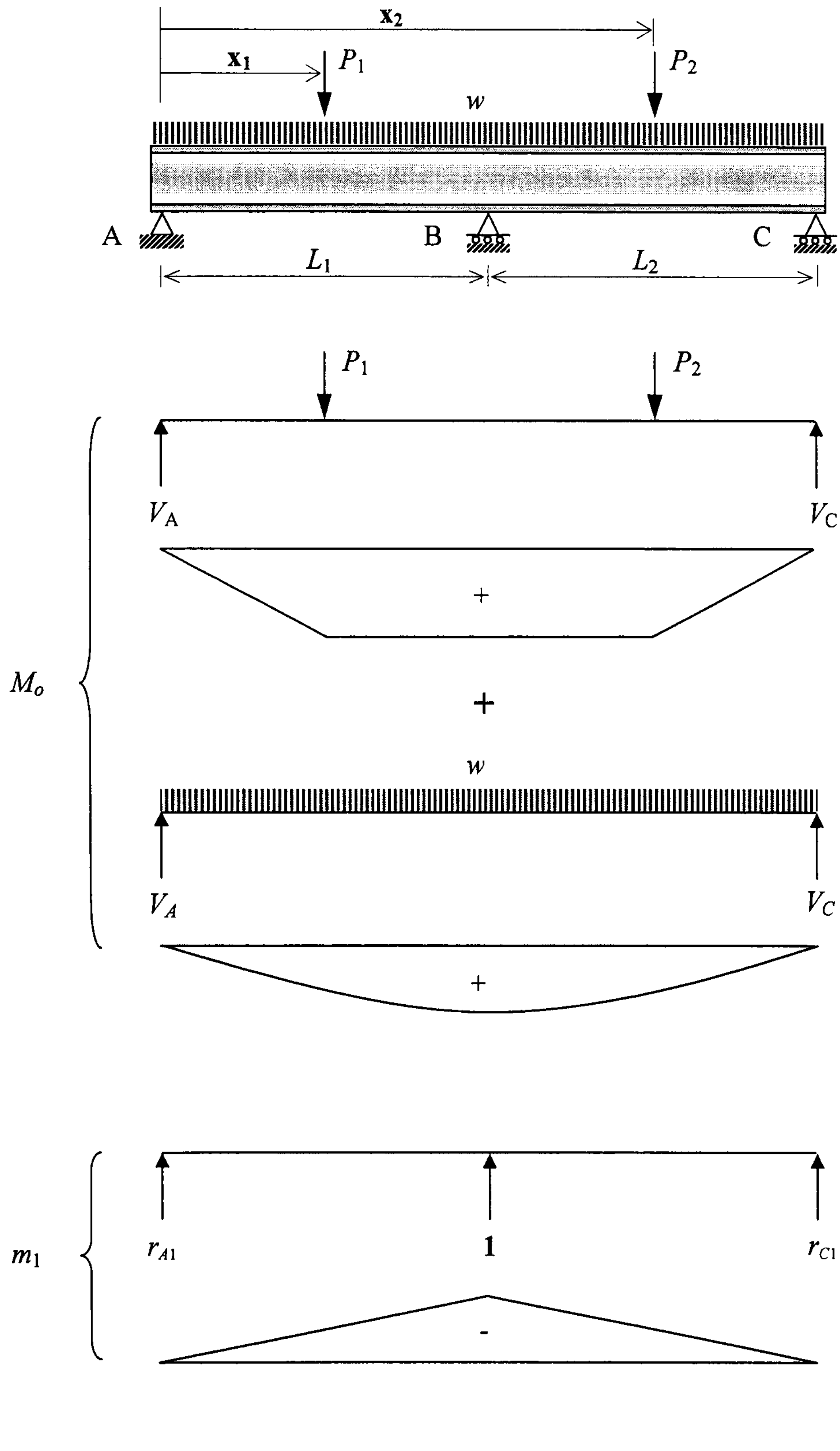

Figure 8.6 Force method (one redundant reaction)

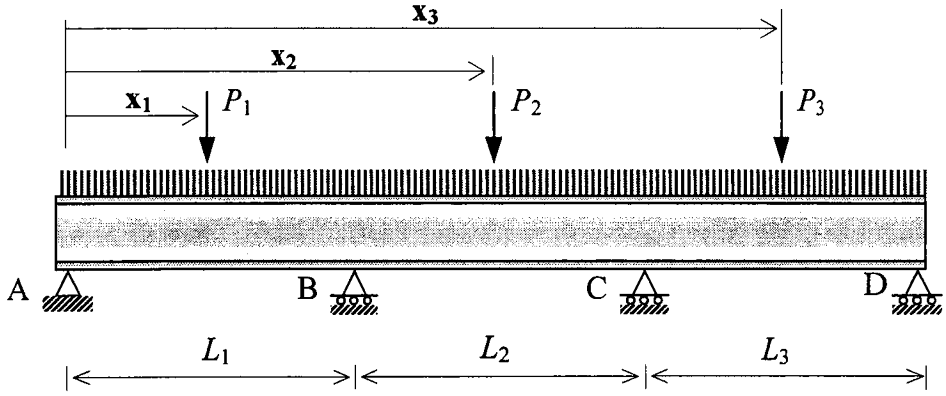

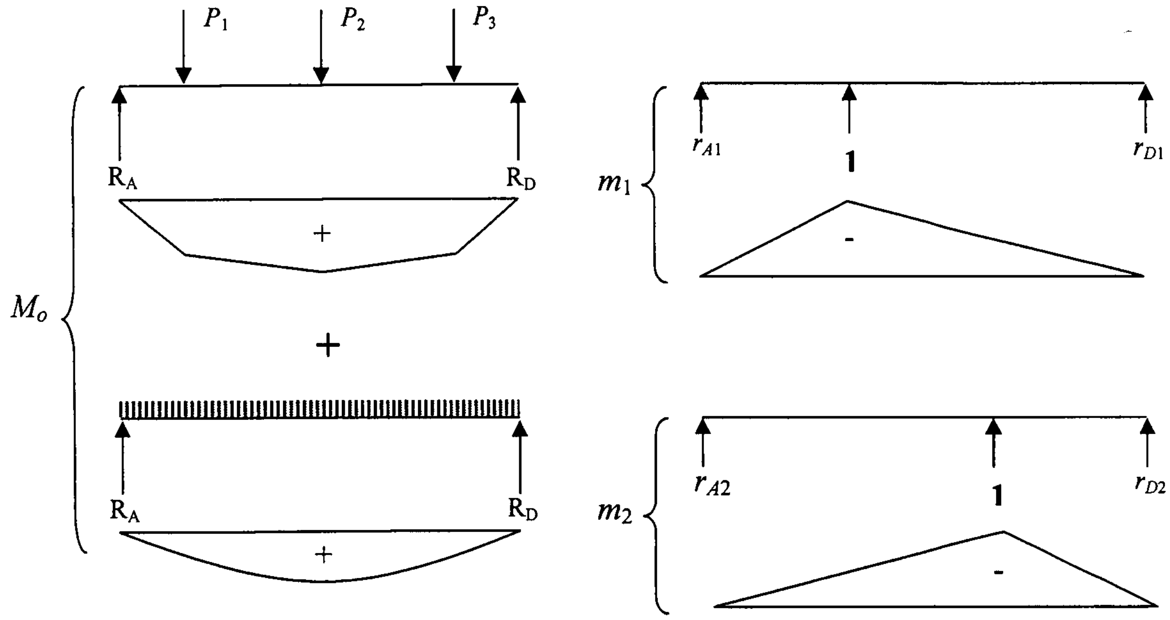

Figure 8.7 Force method (two redundant reactions)

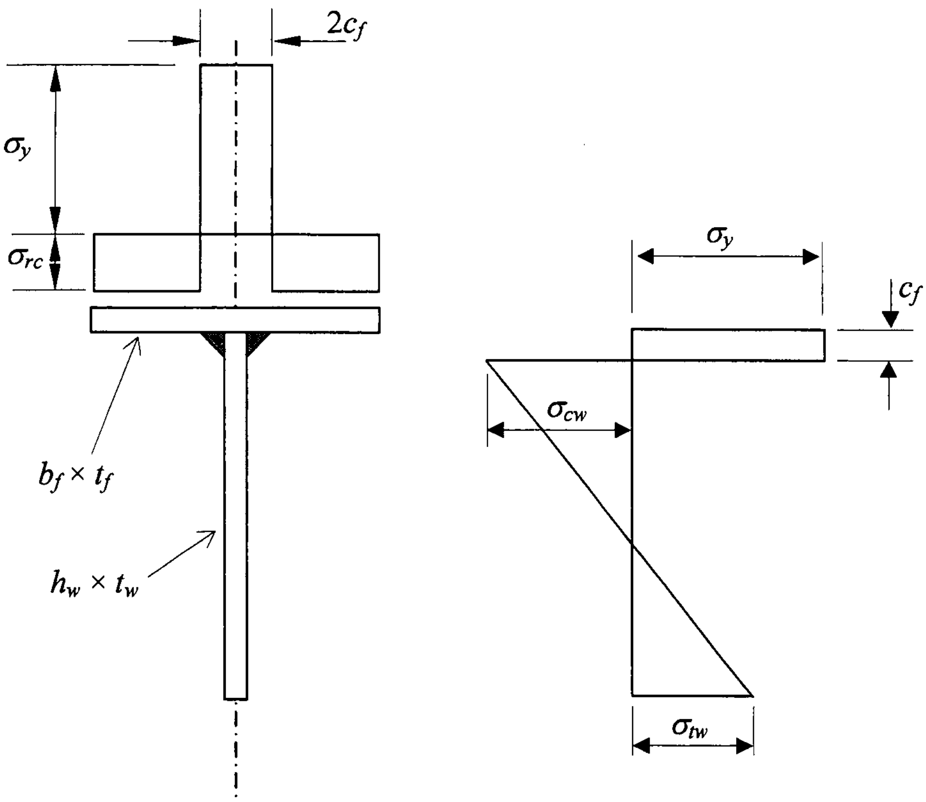

b_f = 146.1 mm
t_f = 8.64 mm
c_f = 20 mm
σ_{cr} = 95.08 MPa

h_w = 243.2 mm
t_w = 6.1 mm
σ_{tw} = 50.82 mm
σ_{cw} = 44.8 mm
σ_y = 250 MPa

Figure 8.8 Dimensions of T-section beam and residual stresses assumed by Kitipornchai and Wong-Chung (1987)

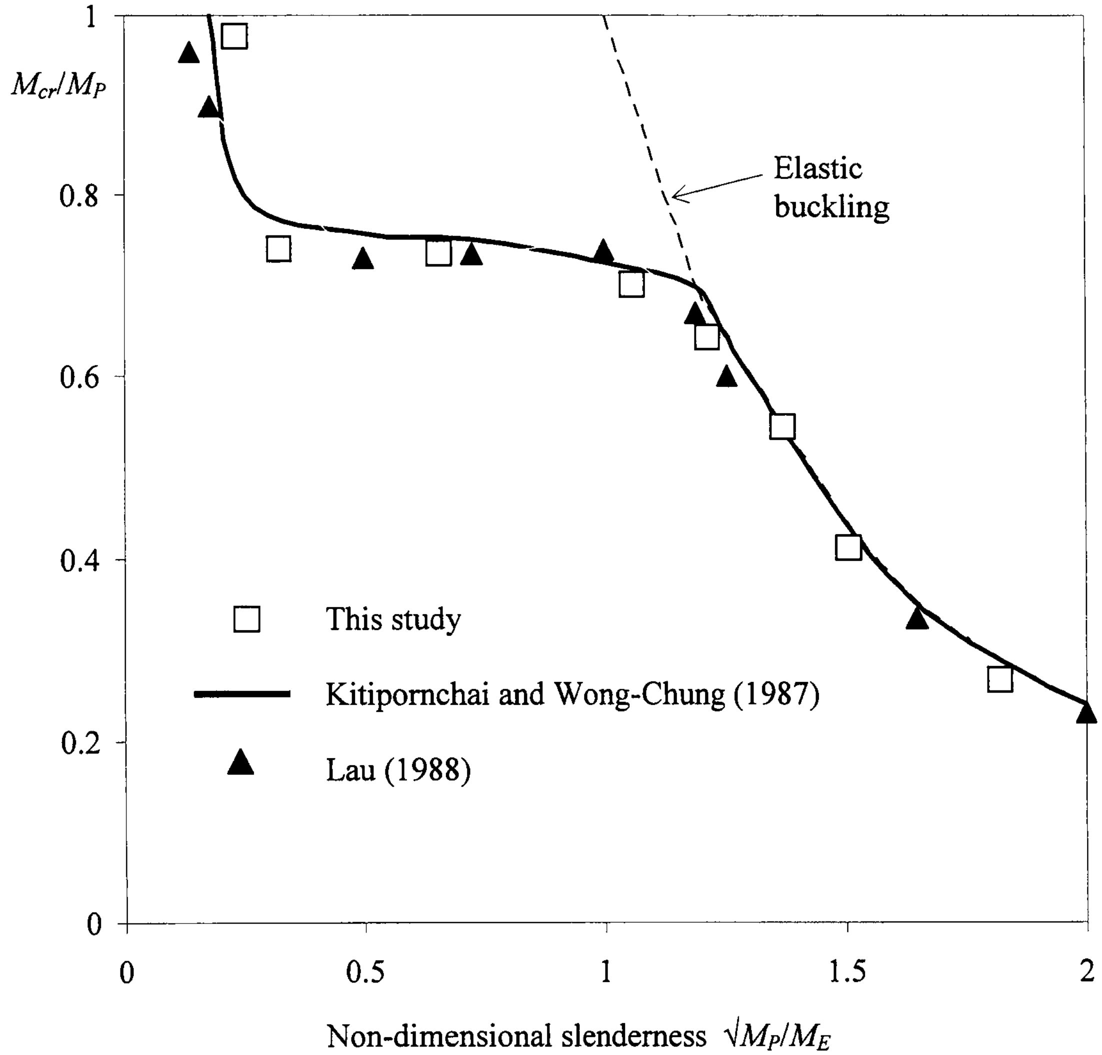

Figure 8.9 Comparison of inelastic buckling moments for T-section beam

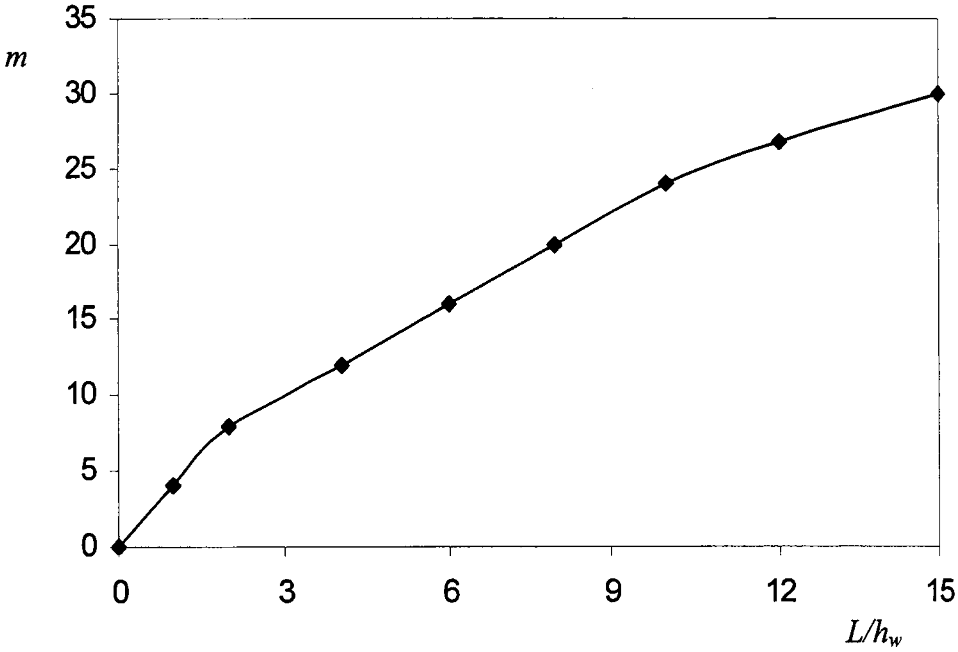

Figure 8.10 Number of sections m employed for a given beam slenderness

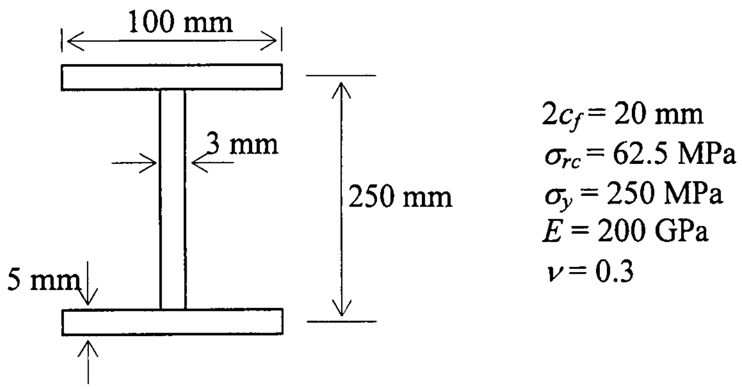

Figure 8.11 Beam I-section geometric and material properties

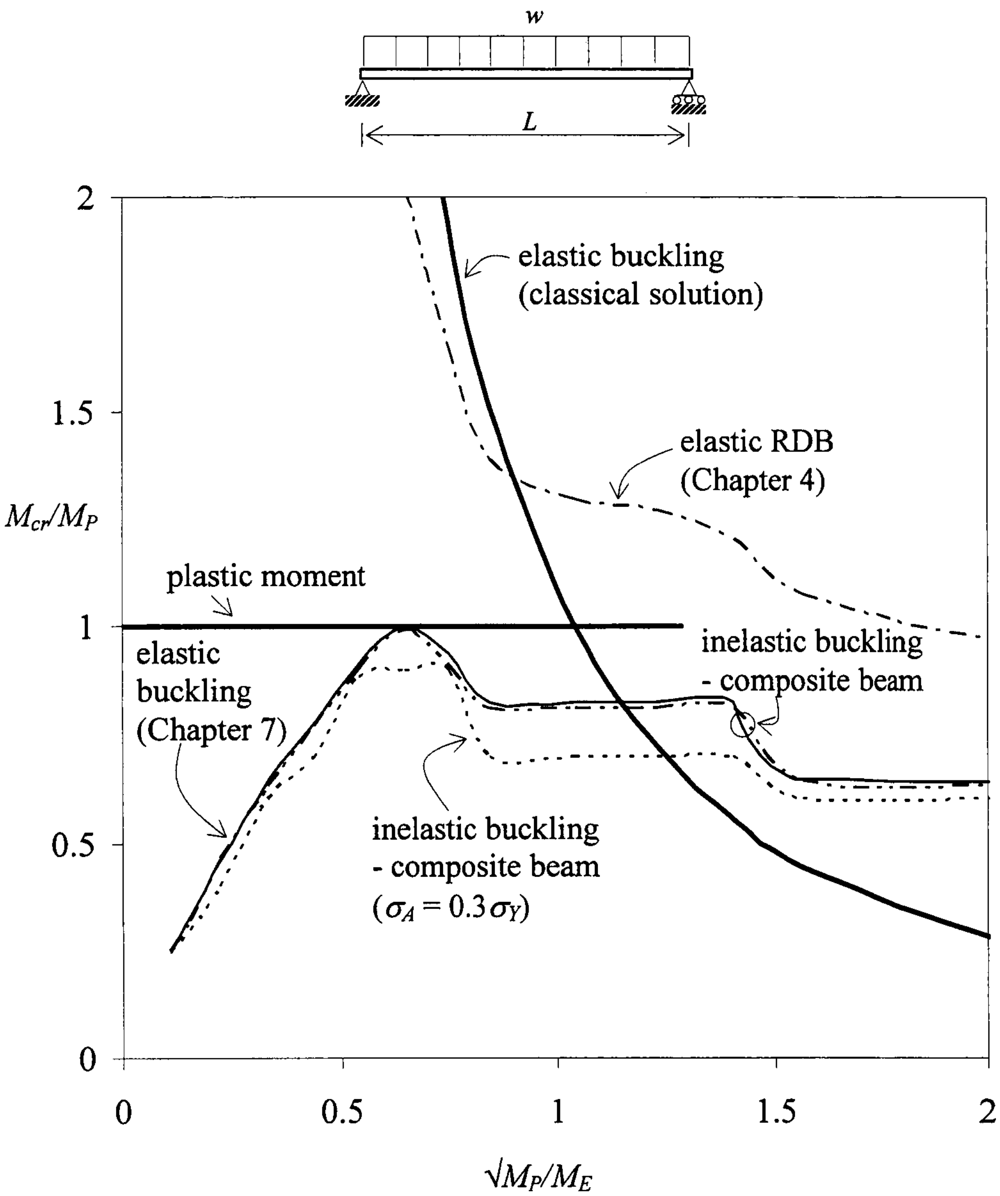

Figure 8.12 Critical buckling moments for simply supported composite beam subjected to uniformly distributed load

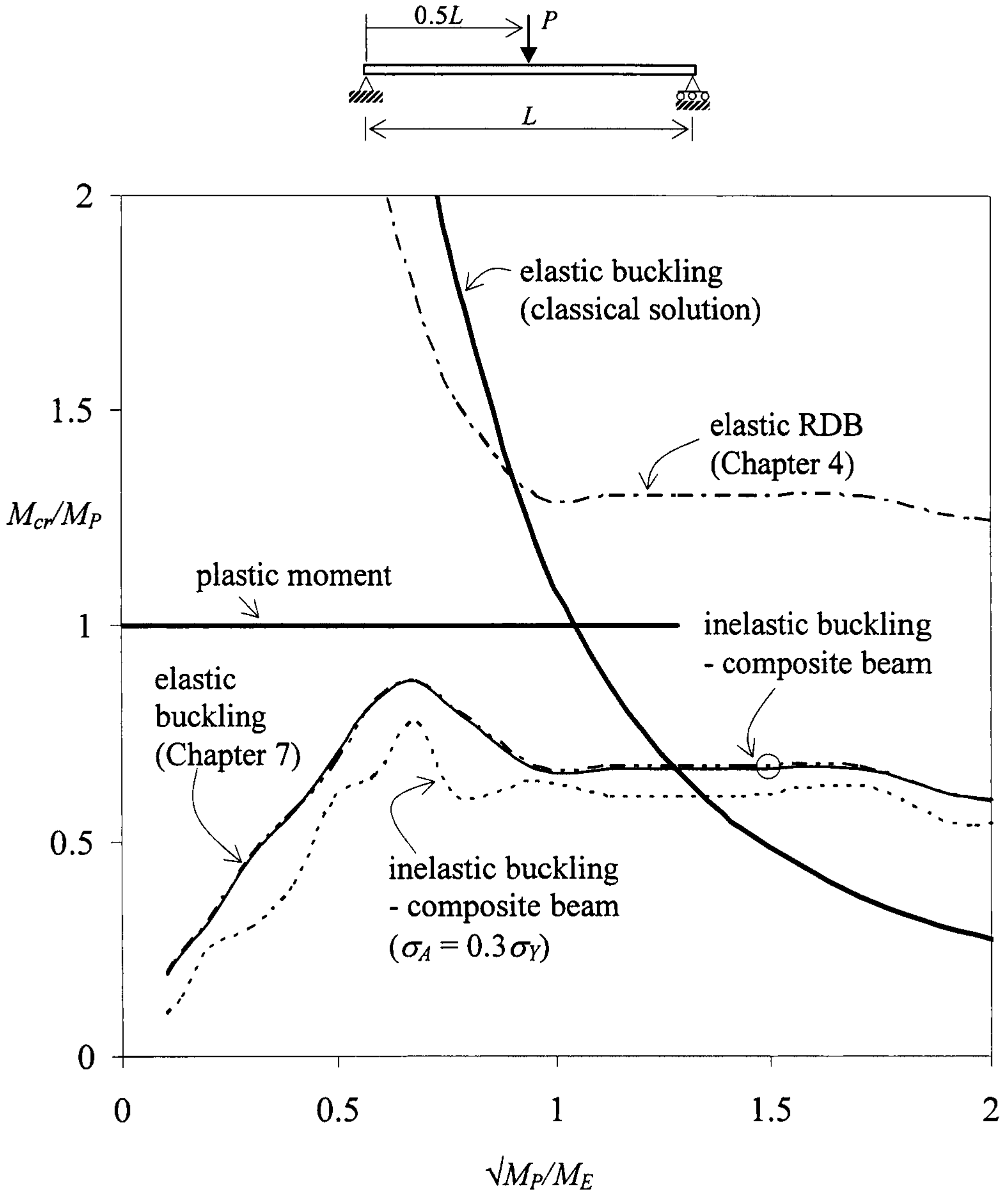

Figure 8.13 Critical buckling moments for simply supported composite beam subjected to mid-span point load

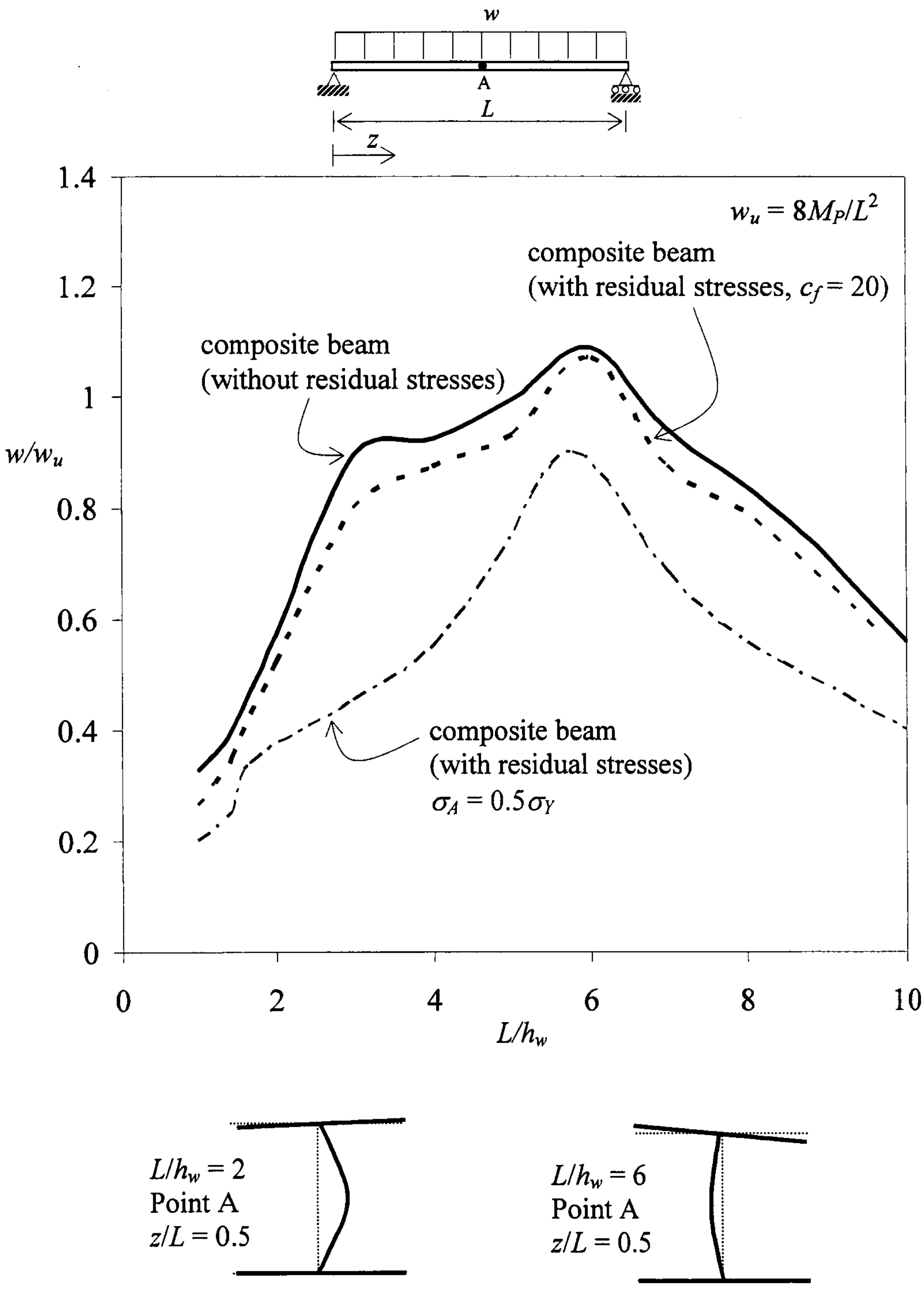

Figure 8.14 Inelastic buckling for simply supported beam subjected to uniformly distributed load

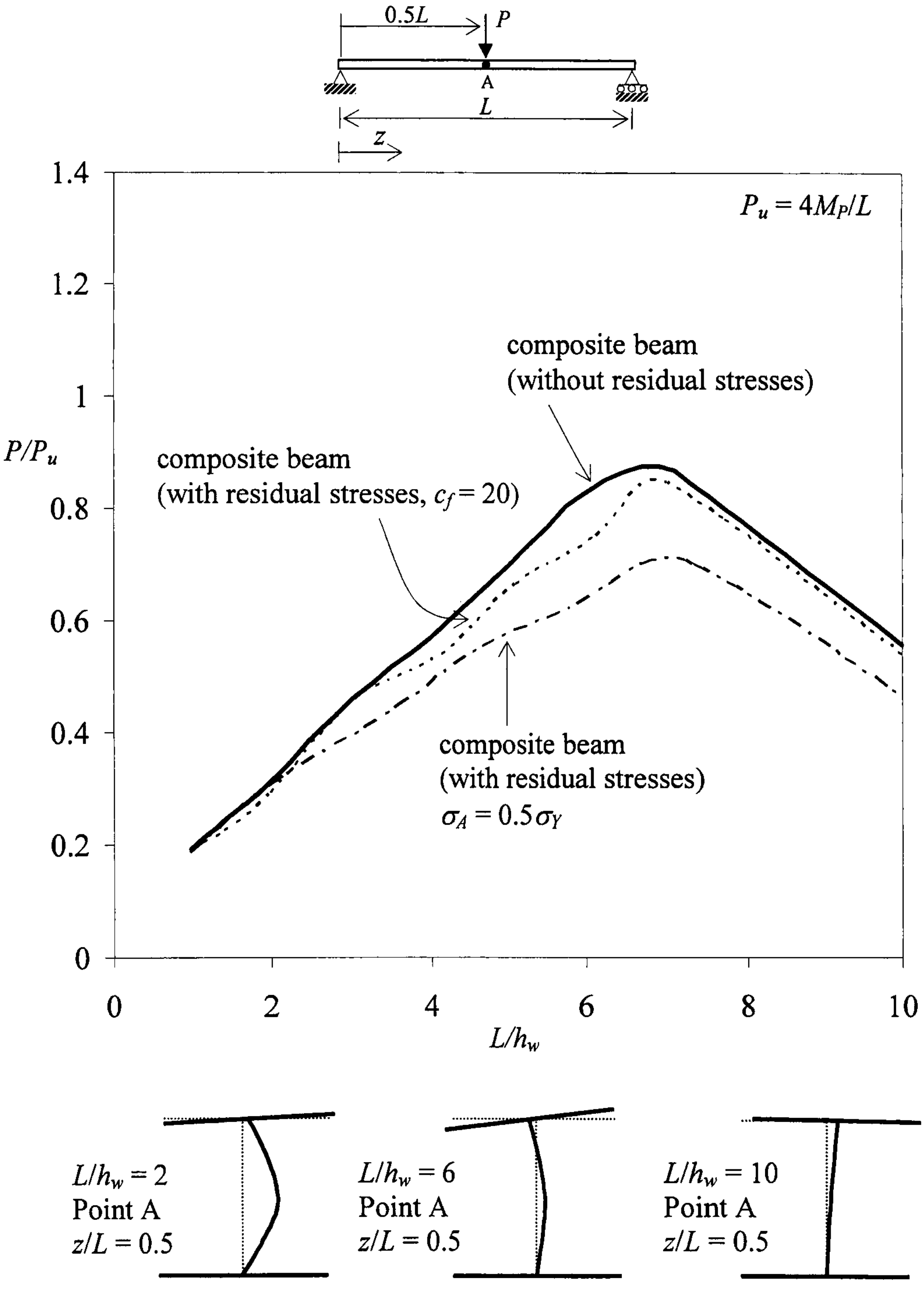

Figure 8.15 Inelastic buckling for simply supported beam subjected to mid-span point load

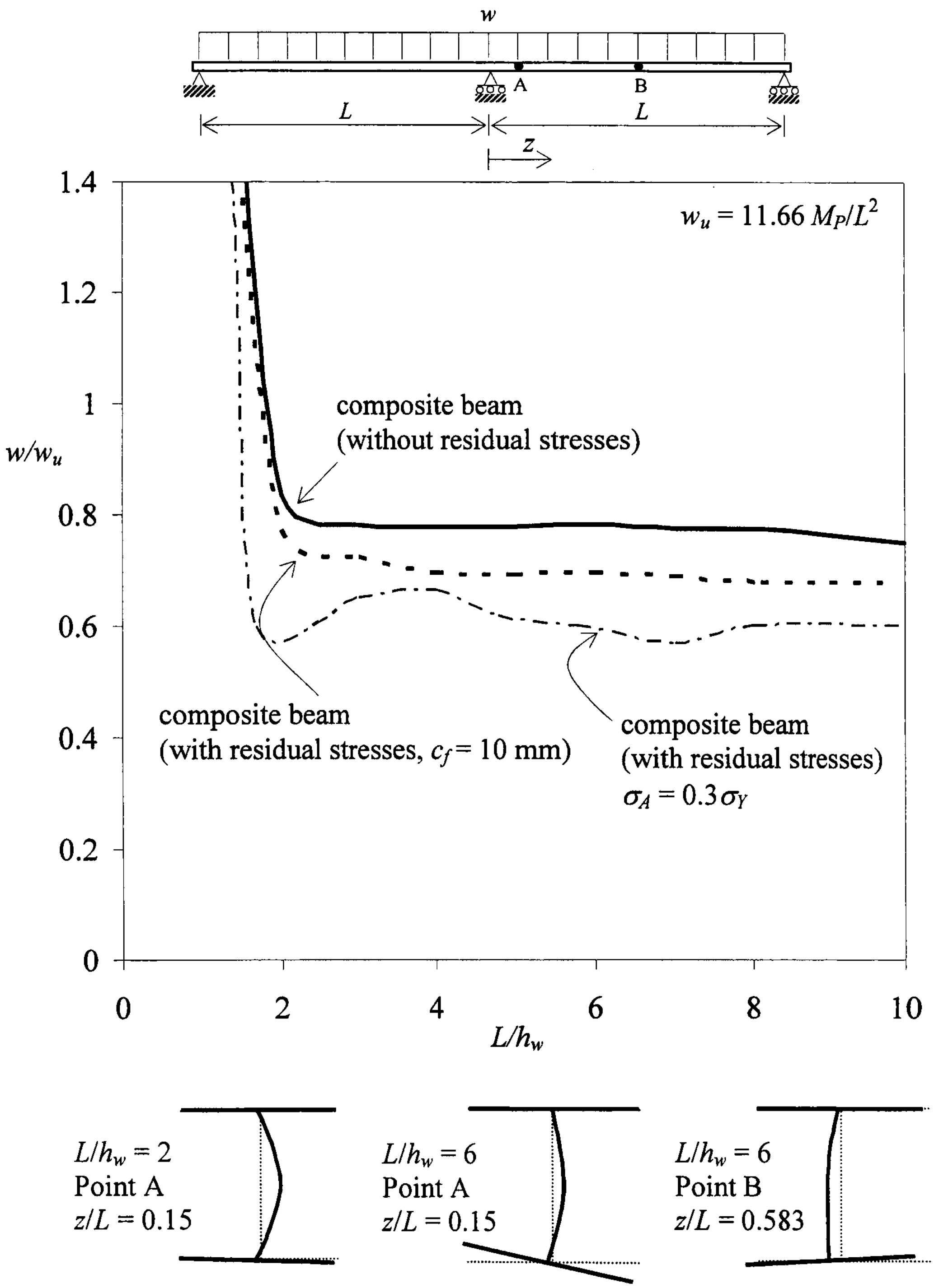

Figure 8.16 Inelastic buckling for two-span continuous beam subjected to uniformly distributed load

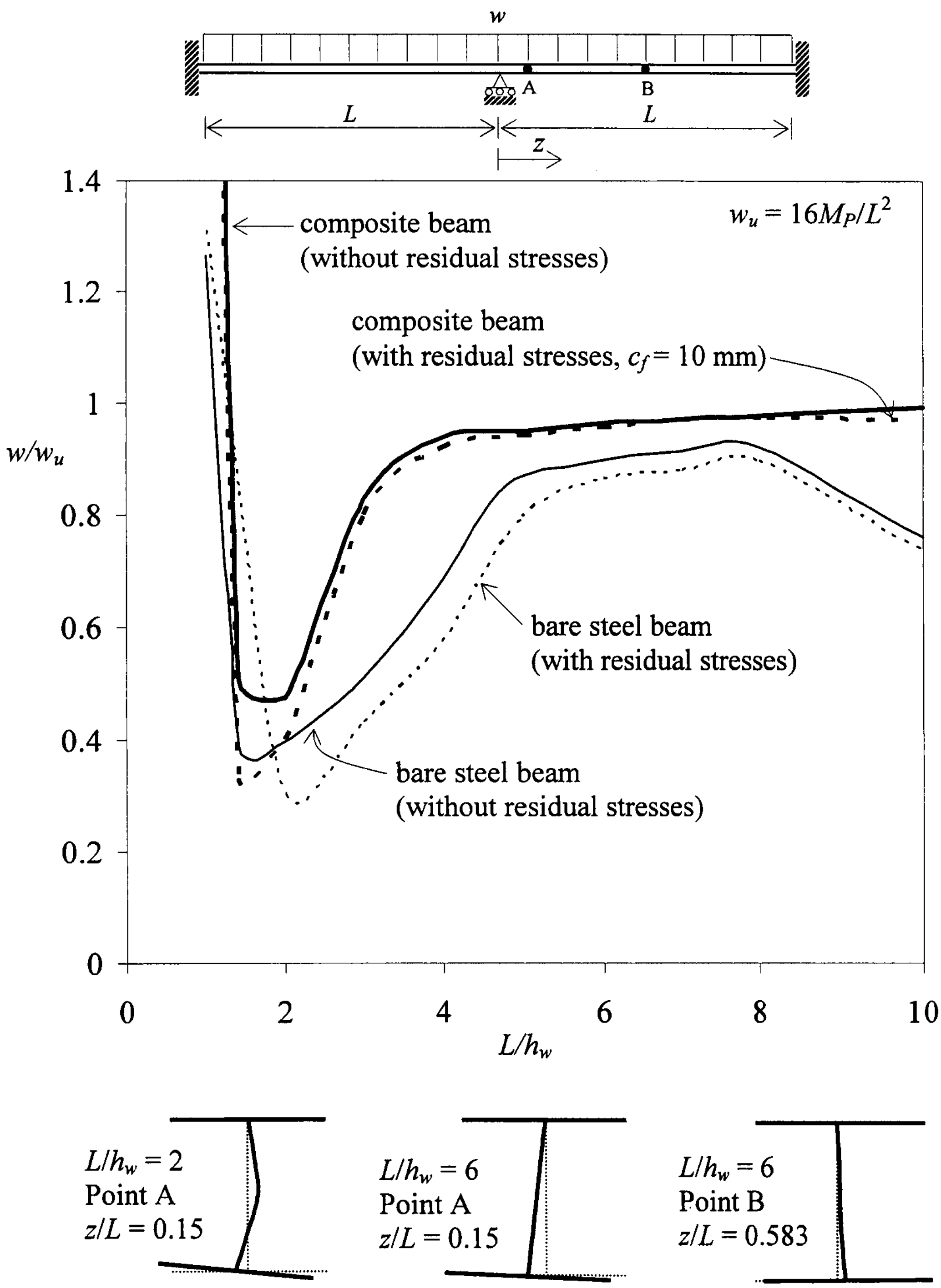

Figure 8.17 Inelastic buckling for two-span continuous beam subjected to uniformly distributed load

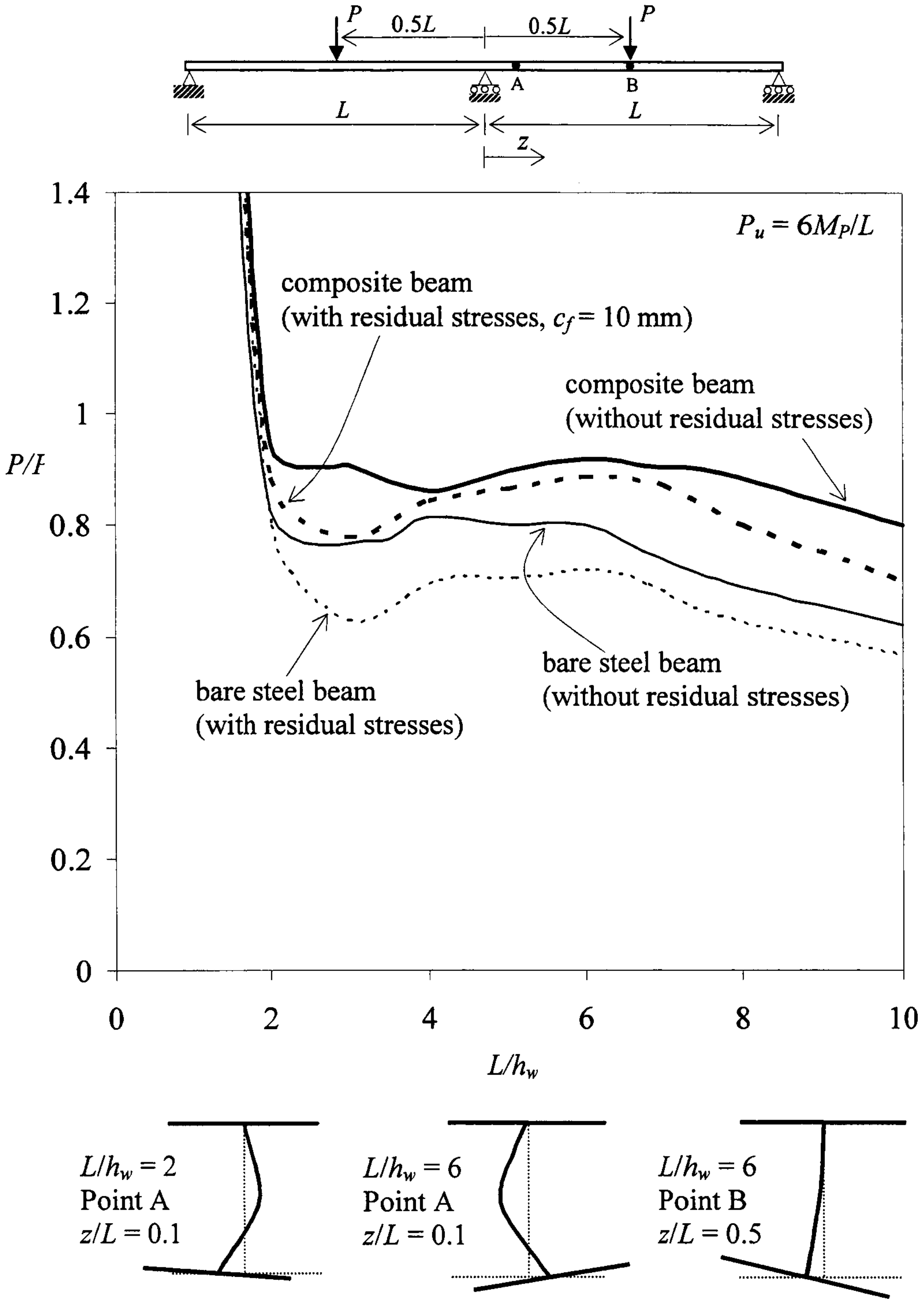

Figure 8.18 Inelastic buckling for two-span continuous beam subjected to mid-span point loads

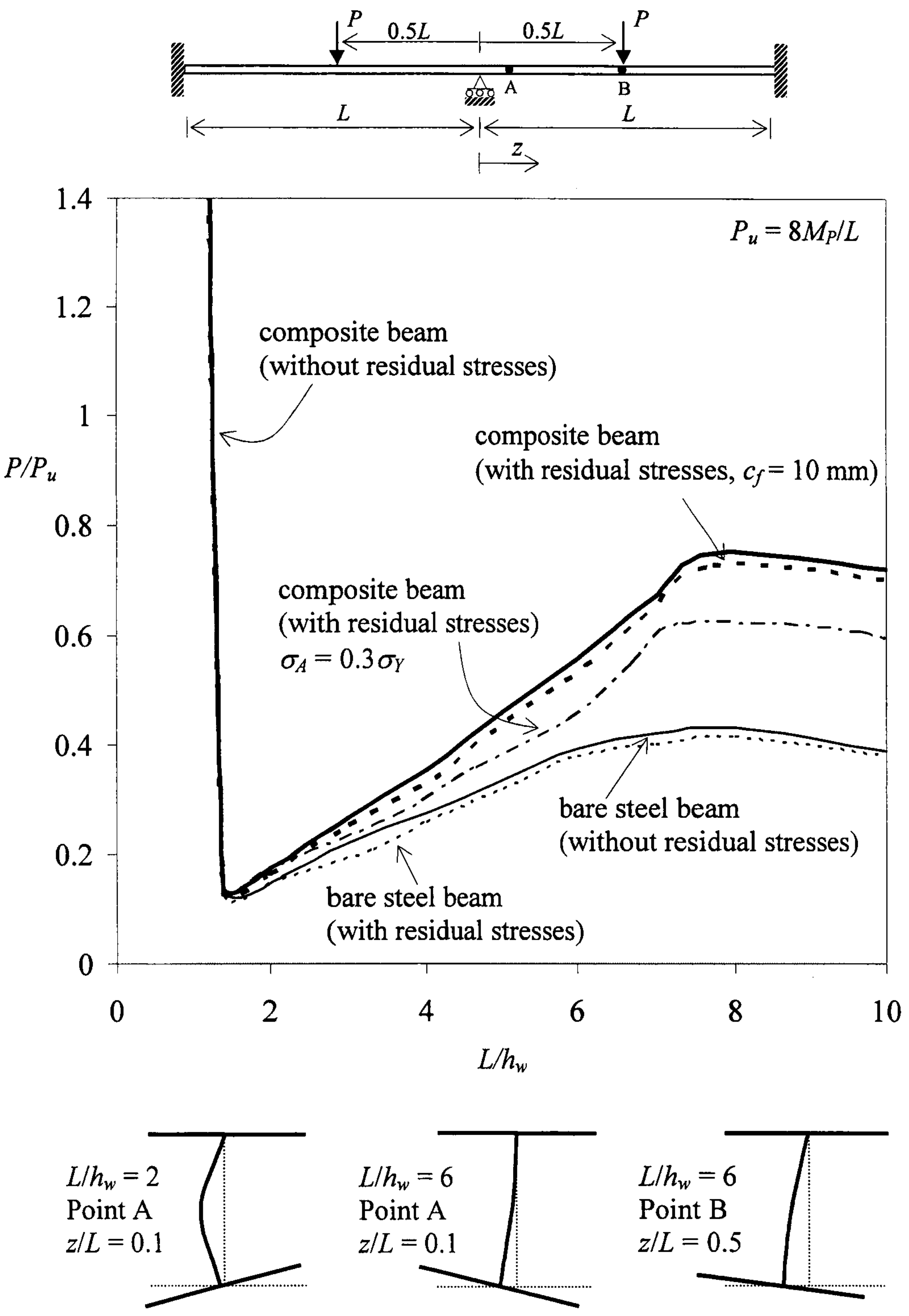

Figure 8.19 Inelastic buckling for two-span continuous beam subjected to mid-span point loads

Chapter 9

CONCLUSIONS

TABLE OF CONTENTS

9.1 CONCLUSIONS

The aim of the research presented in this thesis has been to study theoretically the elastic and inelastic restrained distortional buckling (RDB) of half-through bridge girders and continuous composite beams. This objective has been achieved by developing analytical methods, such as a Ritz-based procedure and a bubble augmented spline finite strip method, and employing them to carry out extensive parametric studies for the elastic and inelastic buckling of plates and plate assemblies. The intention of this chapter is to summarise briefly some of the most important conclusion which have resulted from this study.

When elastic restraint against twist rotation is applied to the cross-section along the beam length, as is the case for half-through bridge girders and continuous composite (steel-concrete) beams, the member is not free to twist during buckling and cross-sectional distortion must necessarily accompany the buckling deformation. The buckling mode for restrained members becomes distortional rather than lateral-torsional. Thus, Vlasov's assumption that the cross-section does not deform during the overall buckling is disputed for restrained members and that has been confirmed in this thesis.

In Chapter 3, the results of a numerical buckling analysis of a two-span composite tee-beam that is cast unpropped were presented. This study links two methods of analysis, a rational in-plane analysis of a two-span continuous beam, which may have different span lengths with arbitrary positions of the loads, and a rational out-of-plane beam-type finite element analysis to determine the elastic buckling load factors under short-term loading and to investigate the effects of shrinkage and creep on the elastic buckling load factor of a continuous composite beam. Extensive numerical investigations were carried out and a range of parameters such as the area of the steel section, beam slenderness, area of the concrete slab section, area of the secondary steel reinforcement, concrete compressive strength, propped and unpropped construction, symmetrical and asymmetrical beam configurations and different loading configurations were considered in this study. The in-plane analysis accounted for the variation of both bending and axial actions in the steel joist, the latter of which seems to have been ignored by many researchers, and not previously quantified. The analysis also indicated that there is a discrepancy between the results of the rational buckling analysis used in this chapter, which includes the effect of concrete cracking, and other techniques available in the literature which do not include this effect or which are overly simplistic.

A quasi-viscoelastic model was also used in Chapter 3 to determine the redistribution of bending moment and axial force within the steel joist in the time domain. The results of this in-plane analysis were then used as input data for a finite element method for analysing elastic distortional buckling. It was shown that the buckling load factor in the long term decreased somewhat from its short-term value owing to the quasi-viscoelastic rheology of the concrete slab. The effects of shrinkage and creep in conventional reinforced and prestressed concrete members are quite well understood, and the effects of these time-varying characteristics of the concrete component on the deflections of composite beams and columns have received a good deal of attention in recent years. However, creep and shrinkage effects may cause a redistribution of internal actions within a composite member, which increases significantly the compression within the steel component, and that may therefore lead to considerations of the possible buckling instability of the steel component. The importance of this phenomenon lies in the quest for refining composite structural members to best optimise their performance and economy, and to attempt to formulate design rules that are less conservative, but more accurate, than those in most national structural standards. While the propensity of the steel component to buckle as a result of the time-dependent actions of the concrete has hitherto been all but ignored in design, it is felt that ignoring this phenomenon has been justified by overly conservative designs and/or the use of stocky thin-walled steel sections.

An energy-based method was developed in Chapter 4 to study the elastic buckling of I-section members subjected to axial load and moment gradient. When restraint against twist rotation is applied to the cross-section along the beam length, the member is not free to twist during buckling and cross-sectional distortion must necessarily accompany the buckling deformation. This effect is difficult to quantify, and depends on such factors as the topology of the cross-sectional profile, the beam length, the loading configuration and the stiffness of the torsional restraint. By invoking a Ritz-based procedure, a simple generic model is developed that may be used for studying the elastic RDB of I-beams restrained completely and continuously against lateral translation and lateral rotation at one flange level, but elastically against twist rotation at this flange level, when subjected to moment gradient. This situation is commonly encountered in half-through girder bridges. The analysis is applicable to members under various conditions of loading and degree of continuous restraint. The results of the energy method have been used to develop a design procedure. Firstly, a unique dimensionless parameter that quantifies the influence of a number of material and geometric factors on the restrained-distortional buckling solutions was identified in the model, and was then employed to produce useful design graphs. The proposed design curves provide accurate estimates of the elastic restrained distortional buckling capacity over a practical range of cross-sectional geometry. It was concluded that the design method developed in this chapter, due to its generality and simplicity, provides an accurate and quick method for solving complex restrained-distortional buckling problems of half-through girder bridges. A parametric study was also undertaken to investigate the factors influencing the lateral-distortional buckling behaviour of simply supported continuously restrained monosymmetric I-beams. The results of this analysis demonstrated the beneficial effect of twist restraint and significant effect of web distortion caused by the combination of the degree of monosymmetry and distortion of the web imposed by the restraint at the tension flange level. The developed method was then further modified to account for geometric nonlinearity and was used to investigate the effects of combined uniform axial force and moment gradient on the critical buckling load of simply supported isolated beam-columns. The results obtained in this study demonstrated that a linear interaction equation is suitable in determining the out-of-plane buckling capacity of beam-columns. It was also confirmed that the stability criteria for beam-columns under moment gradient are greatly influenced by the beam parameter, K, torsional restraint parameter, α, distortional buckling parameter, γ and the loading configuration.

The analysis developed in Chapter 4 was expanded in Chapter 5 to include inelasticity as well as residual stresses, so that predictions of buckling strengths may be made. The method incorporates the residual stresses caused by the process of fabrication, the so-called Cambridge residual stress model, to include the effects of inelasticity. Inelasticity is of particular significance in fabricated I-section members, such as welded plate girders, because the welding process results in levels of residual stresses that are usually higher than those in hot-rolled beams. The variations of the residual stresses across the flanges are nearly uniform in welded beams, and once flange yielding is initiated, it spreads quickly through the flange with little increase in moment. This causes large reductions in the inelastic buckling moments of members. In this chapter, the results were reported for the inelastic RDB of doubly symmetric beams, monosymmetric beams and beam-columns. The nominal buckling load obtained from the modified 'design by buckling analysis' in AS4100 was compared with inelastic RDB solutions obtained from the current model. Overall, the energy method demonstrated an excellent agreement with the proposed method. The distortional buckling parameter, γ identified in Chapter 4 once more allowed the high multiplicity of buckling curves associated with inelastic distortional instability to be reduced to only few. The influences of the degree of beam monosymmetry, torsional twist restraint, and the width of the tensile stress block in the flange were also examined in this chapter. It was shown that the inelastic buckling capacities decrease by reducing the degree of beam monosymmetry and with increasing the width of tensile stress block. The numerical studies demonstrated the favourable effects of the elastic translational and minor axis rotational restraints applied at the tension flange of a simply supported beam, as normally employed in half-through bridge girders. The energy method was then employed to study the inelastic lateral buckling of isolated beam-columns under different loading configurations, and demonstrated that the inelastic RDB load-moment interaction curves are a little variable when compared with corresponding elastic curves. It was in general found that the effects of the residual stresses cause significant deviations in the inelastic RDB strength. The presence of the residual stresses leads to variations in the yielded regions in the cross-section, and results in variations in the cross-section rigidities. These variations cause quite considerable changes in the inelastic critical buckling moments. It was thus concluded that the process of fabrication of I-section members may have an adverse effect on their strength for the limit state of RDB. As residual stresses exist in all welded steel I-sections, these should be carefully quantified and designed for.

In Chapter 6, a numerical model based on the harmonic-based semi-analytical finite strip method and augmented with bubble functions in the form of orthogonal Legendre polynomials was developed in order to evaluate their efficiency in calculating the elastic buckling capacities of isolated plates and their assemblies, which may buckle locally, laterally or in a distortional mode. The numerical analyses undertaken have demonstrated the accuracy and versatility of the present approach for predicting elastic local buckling loads for simply supported thin-walled plates with different transverse end supports under in-plane compression and bending. The results were compared with those published elsewhere, and significant improvement in terms of discretization was observed. It was found that in some cases only one bubble strip for each flat was needed to model the topology, compared with several needed with conventional finite strips, in order to achieve comparable accuracy. It was further shown that augmentation of bubble terms, in modelling plate assemblies where membrane actions are significant, does not improve the efficiency of the finite strip method when measured by the topological discretization. In the same way, there was no significant improvement in convergence for members where overall buckling precedes local buckling.

In Chapter 7 a new bubble augmented spline finite strip method suitable for the analysis of general thin-plate structures was developed. The method allows for consideration of structures with intermediate supports and a variety of conditions that may be prescribed at the ends of a plate or plate assembly. The strip was formulated routinely by the displacement approach. The applications presented demonstrated the good convergence properties and numerical accuracy of the spline finite strip method in a range of situations. The present method gives not only excellent results for the local buckling coefficient, k, but the buckling coefficients computed also converged rapidly. In addition, the simplicity of the semi-analytical finite strip method is preserved, while the problems of dealing with non-periodic buckling modes, shear and non-simple support are eliminated. The method was employed to study local buckling of flat plates under longitudinally varying compression and bending with different boundary conditions at the ends. The results showed that the loaded edge's boundar conditions affect significantly the critical stresses when the aspect ratio of the plate is less than 2, while the restraint at the loaded edges in long plates has a minor effect on the buckling stresses. The method was then employed to study extensively elastic local and overall buckling modes in single span and two-span continuous steel-concrete T-beams under moment gradient. The study confirmed that RDB mode is a governing mode for steel I-sections with one flange fully restrained. It was shown that the deformations can be reasonably large in the proximity of the internal supports and near the concentrated forces. The numerical investigations also demonstrated that variations of the web slenderness parameter have a most pronounced influence on the elastic buckling capacity of composite T-section beams. The bubble augmented spline finite strip method was also employed to study the buckling behaviour of a composite T-section with a longitudinal stiffener under the action of moment gradient and shear.

Chapter 8 then modifies the bubble augmented spline finite strip method to account for inelastic behaviour, so that buckling strengths may be predicted. The method includes the so-called 'tendon force concept' model for residual stresses caused by the process of fabrication, and developed by the Cambridge researches. The numerical studies of this chapter focus on buckling characteristics of single span and two-span composite T-section beams in the inelastic range of structural response under the actions of moment gradient and shear. Significant reductions in the buckling capacity were observed and attributed to the coupling of local and RDB modes, material non-linearity, residual stresses and the presence of varying axial force in continuous steel-concrete composite beams. It was confirmed that governing buckling modes for such structural configurations are either local buckling, RDB buckling or the combination of the two.

9.2 FURTHER RESEARCH

The work undertaken in this thesis has established analytical methods for predicting the elastic and inelastic restrained distortional buckling. The extensive parameter studies for the I-sections and composite tee-beams, in the elastic and inelastic range of structural response have been presented.

The Ritz-based energy method and the bubble augmented spline finite strip method of buckling analysis developed in this thesis are applicable only to a bifurcation analysis. Thus, there is a need to exted the spline finite strip method to the post-buckling range. This type of anlaysis will be very useful for studying the post-buckling behaviour in the distortional mode, and for studying the interaction of restrained distortional buckling with local buckling.

The present study has concentrated on developing analytical methods. While the theoretical predictions have been compared with available experimental results, where possible, there is also a real need for more experimental work, particularly on the interaction buckling of beams subjected to moment gradient.

REFERENCES

REFERENCES

1. AASHTO (1998). *LRFD Bridge Design Specifications*, 2nd Edn., American Association of State Highway and Transportation Officials, Washington DC.

2. *ABAQUS User's Manual - Version 5.8*, (1998). Hibbitt, Karlsson & Sorensen Inc., Pawtucket, Rhode Island, USA.

3. Ahlberg, J.H., Nilson, E.M. and Walsh, J.L. (1967). *The theory of spline and their applications*, Academic Press, New York, 1967.

4. Akay, H.V., Johnson, C.P. and Will, K.M. (1977). Local and lateral buckling of beams and frames, *Journal of the Structural Division*, ASCE, **103**(ST9), 1821-1831.

5. Albert, C., Essa, H.S. and Kennedy, D.J.L. (1992). Distortional buckling of steel beams in cantilever-suspended span construction, *Canadian Journal of Civil Engineering*, **19**, 767-780.

6. Allen, H.B. and Bulson, P.S. (1980). *Background to buckling*, McGraw-Hill, London, England.

7. Ansourian, P. (1981). Experiments on continuous composite beams, *Proceedings of the Institution of Civil Engineers, Part* 2, **71**, 25-51.

8. Ansourian, P. (1982). Experiments on continuous composite beams, *Proceedings of The Institution of Civil Engineers London*, **73**(2), 25-51.

9. Aribert, J.M. (1994). Effect of the local plate buckling on the ultimate strength of continuous composite beams, *Thin-Walled Structures,* **20**(1-4) Part 2, 279-300.

10. AS4100 (1998). *Steel Structures*, Australian Standard, Standards Australia.

11. Azhari, M. (1993). Local and post-local buckling of plates and plate assemblies using the finite strip method, *PhD Thesis*, The University of New South Wales, Sydney.

12. Azhari, M. and Bradford, M.A. (1993). Local buckling of composite tee-beams with longitudinal stiffeners, *Canadian Journal of Civil Engineering*, **20**(6), 923-930.

13. Azhari, M.A. and Bradford, M.A. (1994a). Elastic local buckling of composite tee-beams with longitudinal stiffeners, *Canadian Journal of Civil Engineering*, **20**, 923-930.

14. Azhari, M.A. and Bradford, M.A. (1994b). Local buckling by complex finite strip method using bubble functions, *Journal of Engineering Mechanics*, ASCE, **120**(1), 43-57.

15. Azhari, M. and Bradford, M.A. (1995). The use of bubble functions for the post-local buckling of plate assemblies using the finite strip method, *International Journal for Numerical Methods in Engineering*, **38**(6), 955-968.

16. Azhari, M., Hoshdar, S. and Bradford, M.A. (2000). On the use of bubble functions in the local buckling analysis of plate structures by the spline finite strip method, *International Journal of Numerical Methods in Engineering*, **48**(4), 503-593.

17. Baar, S. (1968). Etude theorique et experimentale du deversment des pouters a membrure tubulaire, *Collection des Publications de la Faculte des Sciences Appliques de L'Universite de Liege*.

18. Barnard, P.R. and Johnson, R.P. (1965). Plastic behaviour of continuous composite beams, *Proceedings of the Institution of Civil Engineers*, **32**, 180-197.

19. Bartels, D. and Bos, C.A.M. (1973). Investigation of the boundary conditions on the lateral buckling phenomenon, taking account of cross-sectional deformation, *Heron*, **19**, 1-26.

20. Batdorf, S.B. and Budianski, B. (1949). A mathematical theory of plasticity based on concept of slip, *NACA Technical note* TN 1871.

21. Bedair, O.K. and Sherbourne, A.N. (1995). Unified approach to local stability of plate/stiffener assemblies, *Journal of Engineering Mechanics*, ASCE **121**, 214-229.

22. Bedair, O.K. (1997a). Stability, free vibration, and bending behaviour of multistiffened plates, *Journal of Engineering Mechanics*, ASCE, **123**(4), 328-337.

23. Bedair, O.K. (1997b). The elastic behaviour of multi-stiffened plates under uniform compression, *Thin-Walled Structures*, **27**(4), 311-335.

24. Benito, R. (1983). Static and dynamic interactive buckling of plate assemblies, *D.Sc. Thesis*, The University of St. Louis, USA.

25. Birkhoff, G. and de Boor, C.R. (1965). Piecewise polynomial interpolation and approximation, In *Approximation of Functions* (ed. H.L. Garabedian), Elsevier, Amsterdam, 164-190.

26. Bleich, F. (1952). *Buckling strength of metal structures*, McGraw-Hill, New York.

27. Booker, J.R. and Kitipornchai, S. (1971). Torsion of multi-layered rectangular section, *Journal of Engineering Mechanics,* ASCE, **97**(EM5), 1451-1468.

28. Bradford, M.A. and Trahair, N.S. (1981). Distortional buckling of I-beams, *Journal of the Structural Division*, ASCE, **107**(ST2), 355-370.

29. Bradford, M.A. and Trahair, N.S. (1982). Distortional buckling of thin-web beam-columns, *Engineering Structures*, **4**(1), 2-10.

30. Bradford, M.A. and Trahari, N.S. (1983). Lateral stability of beams on seats, *Journal of Structural Engineering*, ASCE, **109**(9), 2212-2215.

31. Bradford, M.A. (1983). Buckling of beams with flexible cross-sections, *PhD Thesis*, University of Sydney, Sydney.

32. Bradford, M.A. and Hancock, G.J. (1984). Elastic interaction of local and lateral buckling in beams, *Thin-Walled Structures*, **2**, 1-25.

33. Bradford, M.A. (1985a). Local and post-local buckling of fabricated box members, *Civil Engineering Transactions*, IEAust., **CE27**(4), 391-396.

34. Bradford, M.A. (1985b). Distortional buckling of monosymmetric I-beams, *Journal of Constructional Steel Research*, **5**, 123-136.

35. Bradford, M.A. and Trahair, N.S. (1985). Analysis of inelastic buckling tests on beam-columns, *Research Report R-489*, University of Sydney.

36. Bradford, M.A. (1986a). Inelastic distortional buckling of I-beams, *International Journal of Computers and Structures*, **24**(6), 922-933.

37. Bradford, M.A. (1986b). Local buckling analysis of composite beams, *Civil Engineering Transactions*, IEAust., **CE 28**(4), 312-317.

38. Bradford, M.A. and Trahair, N.S. (1986). Analysis of inelastic buckling tests on beam-columns, *Journal of Structural Engineering*, ASCE, **112**(3), 538-549.

39. Bradford, M.A. (1987). Inelastic local buckling of fabricated I-beams, *Journal of Constructional Steel Research*, **7**, 317-334.

40. Bradford, M.A. and Johnson, R.P. (1987). Inelastic buckling of composite bridge girders near internal supports, *Proceedings of The Institution of Civil Engineers London*, **83**(2), 143-159.

41. Bradford, M.A., Cuk, P.E., Gizejowski, M.A. and NS Trahair, N.S. (1987). Inelastic lateral buckling of beam-columns, *Journal of Structural Engineering*, ASCE, **113**(11), 2259-2277.

42. Bradford, M.A. and Waters, S.W. (1988). Distortional instability of fabricated monosymmetric I-beams, *International Journal of Computers and Structures*, **29**(4), 715-724.

43. Bradford, M.A. and Cuk, P.E. (1988). Elastic stability of tapered monosymmetric I-beams, *Journal of Structural Engineering*, ASCE, **114**(5), 977-996.

44. Bradford, M.A. (1988a). Buckling of elastically restrained beams with web distortions, *Thin-Walled Structures*, **6**, 287-304.

45. Bradford, M.A. (1988b). Buckling strength of deformable monosymmetric I-beams, *Engineering Structures*, **10**, 167-173.

46. Bradford, M.A. (1988c). Stability of tapered I-beams, *Journal of Constructional Steel Research*, **9**, 195-216.

47. Bradford, M.A. (1989a). Inelastic buckling of tapered monosymmetric I-beams, *Engineering Structures*, **11**(2), 119-126.

48. Bradford, M.A. (1989b). Buckling strength of partially restrained I-beams, *Journal of Structural Engineering*, ASCE, **115**(5), 1272-1276.

49. Bradford, M.A. (1989c). Buckling of beams supported on seats, *The Structural Engineer*, **67**(23/5), 411-414.

50. Bradford, M.A. (1989d). Buckling of longitudinally stiffened plates in bending and compression, *Canadian Journal of Civil Engineering*, **16**(5), 607-614.

51. Bradford, M.A. (1989e). Lateral-distortional buckling of tee-section beams, *Thin-Walled Structures*, 13-30.

52. Bradford, M.A. and Gilbert, R.I. (1989). Nonlinear behaviour of composite beams at service loads, *The Structural Engineer*, **67**(14), 263-268.

53. Bradford, M.A. (1990a). Distortional buckling strength of elastically restrained monosymmetric I-beams, *Thin-Walled Structures*, **9**, 339-350.

54. Bradford, M.A. (1990b). Stability of monosymmetric beam-columns with thin webs, *Journal of Constructional Steel Research*, **15**, 323-339.

55. Bradford, M.A. (1990c). Design of beams with partial end restraint, *Proceedings of the Institution of Civil Engineers*, London, Part 2, **89**, 163-181.

56. Bradford, M.A. (1990d). Inelastic buckling of beams with tension flange restraint, *Proceedings*, 4th *International Conference on Steel Structures and Space Frames*, Singapore, 31-34.

57. Bradford, M.A. (1990e). Elastic local buckling of trough girders, *Journal of Structural Engineering*, ASCE, **116**(6), 1594-1610.

58. Bradford, M.A. (1990f). Lateral-distortional buckling of tee-section beams, *Thin-Walled Structures*, **10**, 13-30.

59. Bradford, M.A. (1991). Buckling of prestressed steel girders, *Engineering Journal*, **28**(3), 98-101.

60. Bradford, M.A. (1992a). Lateral-distortional buckling of steel I-section members, *Journal of Constructional Steel Research*, **23**(1-3), 97-116.

61. Bradford, M.A. (1992b). Buckling of doubly-symmetric cantilevers with slender webs, *Engineering Structures*, **14**(5), 327-334.

62. Bradford, M.A. and Gao, Z. (1992). Distortional buckling solutions for continuous composite beams, *Journal of Structural Engineering*, **118**(1), 73-89.

63. Bradford, M.A. and Azhari, M. (1993). Inelastic local buckling of plates and plate assemblies using bubble functions, *Engineering Structures*, **17**(N2), 95-103.

64. Bradford, M.A. and Wee, A. (1994). Analysis of buckling tests on beams on seat supports, *Journal of Constructional Steel Research*, **28**, 227-242.

65. Bradford, M.A. and Azhari, M. (1995). Inelastic local buckling of plates and plate assemblies using bubble functions, *Engineering Structures*, **17**(N2), 95-103.

66. Bradford, M.A. (1996). Elastic distortional buckling of overhanging beams, *Structural Engineering and Mechanics*, **4**(1), 37-47.

67. Bradford, M.A. (1997a). Lateral-distortional buckling of continuously restrained columns, *Journal of Constructional Steel Research*, **42**(2), 121-139.

68. Bradford, M.A. (1997b). Shrinkage behavior of composite beams, *American Concrete Institute Structural Journal*, **94**(6), 625-632.

69. Bradford, M.A. (1997c). Service load analysis of slender R-C columns, *American Concrete Institute Structural Journal*, **94**(6), 675-685.

70. Bradford, M.A. and Azhari, M. (1997). The use of bubble functions for the stability of plates with different end conditions, *Engineering Structures*, **19**, 151-161.

71. Bradford, M.A. and Ronagh, H.R. (1997a). Generalised elastic buckling of restrained I-beams by the FEM, *Journal of Structural Engineering*, ASCE, **123**(12), 1631-1637.

72. Bradford, M.A. and Ronagh, H.R. (1997b). Elastic distortional buckling of tapered composite beams, *Structural Engineering and Mechanics*, **5**(3), 269-281.

73. Bradford, M.A. and Ge, X.P. (1997). Elastic distortional buckling of continuous I-beams, *Journal of Constructional Steel Research*, **41**, 249-266.

74. Bradford, M.A. (1998a). Inelastic buckling of I-beams with continuous elastic tension flange restraint, *Journal of Constructional Steel Research*, **48**, 63-67.

75. Bradford, M.A. (1998b). Distortional buckling of elastically restrained cantilevers, *Journal of Constructional Steel Research*, **47**, 3-18.

76. Bradford, M.A. (1998c). Analysis of slender R-C columns at service loads, *Proceedings of EASEC6*, Taipei, 14-16 Jan., Taipei: NTU, 925-931.

77. Bradford, M.A., Wright, H.D. and Uy, B. (1998). Short and long-term behaviour of axially loaded composite profiled walls, *Proceedings of the Institution of Civil Engineers, London, Structures and Buildings*, **128**(1), 26-37.

78. Bradford, M.A. (1999). Elastic distortional buckling of tee-section cantilevers, *Thin-Walled Structures*, **33**(1), 3-17.

79. Bradford, M.A. and Kemp, A.R. (2000). Lateral-distortional buckling of composite beams in hogging bending, *Progress in Structural Engineering and Materials*, **2**(2), 169-178.

80. Bradford, M.A. (2000). Strength of compact steel beams with partial restraint, *Journal of Constructional Steel Research*, **53**(2), 183-200.

81. Bradford, M.A., Vu Manh, H and Gilbert, R.I. (2002). Numerical analysis of continuous composite beams under service loading, *Advances in Structural Engineering*, **5**(1), 1-12.

82. BS5950 - 1990. Structural use of steelwork in building. Part 1: Code of practice for design in simple and continuous construction: hot rolled sections, *British Standards Institution*, London.

83. Carlsen, C.A. (1980). A parametric study of collapse of stiffened plates in compression, *The Structural Engineer*, **58**(2), 33-40.

84. Chen, W.F. and Lui, E.M. (1991). *Stability of steel frames*. CRC Press.

85. Cherry, S. (1960). The stability of beams with buckled compression flanges, *The Structural Engineer*, **38**(9), 277-285.

86. Cheung, Y.K. (1976). *Finite strip method in structural analysis,* Pergamon Press, Oxford.

87. Cheung, Y.K., Fan, S.C. and Wu, C.Q. (1982). Spline finite strip in structural analysis, *Proceedings of the International Conference on Finite Element Methods*, 704-709.

88. Cheung, Y.K. and Fan, S.C. (1983). Static analysis of right box girder bridges by spline finite strip method, *Proceedings of the Institution of Civil Engineers*, **75**(2), 311-323.

89. Clark, J.W. and Hill, H.N. (1960). Lateral buckling of beams, *Journal of the Strucutral Division*, ASCE, **86**(ST7), 175-196.

90. Climenhaga, J. J. and Johnson, R. P. (1972). Local buckling in continuous composite beams, *The Structural Engineer*, **50**(9), 367-375.

91. Cuk, P.E. (1984). Flexural-torsional buckling in frame structures, *PhD Thesis*, University of Sydney, Sydney.

92. Cuk, P.E., Rogers, D.F. and Trahair, N.S. (1986). Inelastic Buckling of Continuous Steel Beam-Columns, *Journal of Constructional Steel Research*, **6**, 21-52.

93. Dawe, J.L. and Kulak, G.L. (1984a). Plate instability of W-shapes, *Journal of the Structural Engineering Division*, ASCE, **110**(ST6), 1278-1291.

94. Dawe, J.L. and Kulak, G.L. (1984b). Local buckling of W-shape columns and beams, *Journal of the Structural Engineering Division*, ASCE, **110**(ST6), 1292-1304.

95. De Boor, C. (1978). *A Practical Guide to Splines*, Applied Mathematical Science, Vol.27.

96. Della, C. L. and Scapolla, T. (2000). Serendipity and bubble plus hierarchic finite elements for thin to thick plates, *Structural Engineering and Mechanics*, **9** (5), 433-448.

97. Dekker, N.W., Kemp, A.R. and Trinchero, K.P. (1995). Factors influencing the strength of continuous composite beams in negative bending, *Journal of Constructional Steel Research*, **34**, 161-185.

98. Dekker, N.W. and Kemp, A.R. (1998). Simplified distortional buckling model for doubly symmetrical I-sections, *Canadian Journal of Civil Engineering*, **25**(4), 718-727.

99. Desmond, T.P., Pekoz, T. and Winter, G. (1981). Edge stiffeners for thin-walled members, *Journal of the Engineering Structural Division*, ASCE, **107**(ST2), 329-353.

100. De Vries, K. (1947). Strength of beams as determined by lateral buckling, *Transactions*, ASCE, **112**, 1245-1271.

101. Dezi, L., Leoni, G. and Tarantino, A.M. (1998). Creep and shrinkage analysis of composite beams, *Progress in Structural Engineering and Materials*, **1**(2), 170-177.

102. Donald, I.B. (Ed.), (1990). *Thin-Walled Structures: Developments in Theory and Practice*, London, Elsevier Applied Science.

103. Dwight, J.B. and Moxham, K.E. (1969). Welded Steel Plates in Compression, *The Structural Engineer*, **47**(2).

104. Dwight, J.B. (1981). The effect of residual stresses on structural stability, *Residual Stresses and Their Effect*, Ed. Farlane, A.J.A., The Welding Institute, London, England, 21-27.

105. Essa, H.S. and Kennedy, D.J. (1994). Station Square revisited: distortional buckling collapse, *Canadian Journal of Civil Engineering*, **21**, 377-381.

106. Essa, H.S. and Kennedy, D.J. (1995). Design of steel beams in cantilever-suspended-span construction, *Journal of Structural Engineering*, **121**(11), 1667-1673.

107. Euler, L. (1759). Sur la force des colonnes, Acadamie Royale des Sciences et Belles Lettres de Berlin, *Memoires*, **13**, p.252. Translated in *American Journal of Physics* (1947), **15**, p.309.

108. Eurocode 3, ENV-1993-1-1: Background Document 5.05, *Design rules for thin-Walled plate girders for the ultimate and serviceability limit state taking account of the buckling phenomena*, CEN, Brussels.

109. Eurocode 4 (1996) – *Design of composite steel and concrete structures* – Part 2: Bridges, Draft.

110. *European Convention for Constructional Steelwork CECCS European recommendations for Composite Structures*. (1981). Construction Press.

111. Fan, S.C and Cheung, Y.K. (1983a). Analysis of shallow shells by spline finite strip method, *Engineering Structures*, **5**, 225-263.

112. Fan, S.C. and Cheung, Y.K. (1983b). Analysis of shallow shells by spline finite strip method, *Engineering Structures*, **5**, 311-323.

113. Fan, S.C. and Luah, M.H. (1992). New spline finite element for plate bending, *Journal of Engineering Mechanics*, **118**(6), 1065-1081.

114. Fisher, M. (1967). Das Kipp-Problem guebelasteter exzentrisch durch Normalkraft beanspruchter I-Trager bei Verzicht auf die Voraussetzung der Querschnittstreue, *Der Stahlbau*, Berlin, **36**(3), p.77.

115. Galambos, T.V. (1988). *Guide to stability criteria for metal structures*, 4th Edn., Structural Stability Research Council, John Wiley, New York.

116. Gallagher, R.H., Gellathy, R.A., Padlog, J. and Mallett, R.H. (1967). A discrete element procedure for thin-shell instability analysis, *American Institute of Aeronautics and Astronautics Journal*, **5**, 138-145.

117. Gallagher, R.H., and Yang, H.T.Y. (1969). Elastic instability predictions for doubly-curved shells, *Proceedings of Second Conference on Matrix Methods in Structural Analysis*, Ohio, 68-150.

118. Garbow, B.S. Boyle, J.M., Dongarra, J. and Cleve B. Moler, C.B. (1977). *Matrix Eigensystem Routines* - EISPACK Guide Extension Springer.

119. Gilbert, R.I. (1988). *Time effects in concrete structures*, Amsterdam: Elsevier.

120. Gilbert, R.I. and Bradford, M.A. (1990). Design of slender reinforced concrete columns for creep and shrinkage, *Proceedings of 2nd International Conference on Computer Aided Analysis and Design of Concrete Structures*, Zell am See, Austria, Swansea: Pineridge Press, 739-748.

121. Gilbert, R.I. and Bradford, M.A. (1995). Time-dependent behaviour of continuous composite beams at service loads, *Journal of Structural Engineering*, ASCE, **121**(2), 319-327.

122. Gioncu, V. and Peteu, D. (1997). Available rotation capacity of wide-flange beams and beam-columns, *Journal of Constructional Steel Research*, **43**, 161-218 and 219-244.

123. Goldberg, J.E., Bogdanoff, J.L. and Glauz, W.D. (1964). Lateral and torsional buckling of thin-walled beams, *Publications, IABASE*, **24**, 92-100.

124. Goltermann, P. and Svensson, S.E. (1987). Lateral distortional buckling: predicting elastic critical stress, *Journal of Structural Engineering*, **114**(7), 1606-1625.

125. Gradzki, R. and Kowal-Michalska, K. (1985). Elastic and elasto-plastic buckling of thin-walled columns subjected to uniform compression, *Thin-Walled Structures*, **3**(2), 93-108.

126. Graves-Smith, T.R. (1968). The postbuckling behaviour of thin-walled columns, *Eighth congress of the IABSE*, New York, U.S.A., p. 311.

127. Greville, T.N.E. (1969). *Theory and applications of spline functions*, Academic Press, New York.

128. Gronding, G.Y., Chen, Q., Elwi, A.E. and Cheng, J.J. (1998). Stiffened steel plates under compression and bending, *Journal of Constructional Steel Research*, **45**(2), 125-148.

129. Gronding, G.Y., Elwi, A.E. and Cheng, J.J.R. (1999). Buckling of stiffened steel plates – a parametric study, *Journal of Constructional Steel Research*, **50**(2), 151-175.

130. Guo, Y.L. and Lindner, J. (1993). Analysis of elasto-plastic interaction buckling of stiffened panels by spline finite strip method, *Computers and Structures*, **46**, 529-536.

131. Haaijer, G. (1957). Plate buckling in the strain-hardening range, *Journal of the Engineering Mechanics Division*, ASCE, **83**(EM2), 1212.1-47.

132. Hall, A.S. (1986). *An Introduction to the Mechanics of Solids*, SI Edn., John Wiley and Sons.

133. Hall, A.S. and Kabaila, A.P. (1986). *Basic concepts of structural analysis*, Greenwich Soft, Sydney.

134. Hamada, S. and Longworth, J. (1974). Buckling of composite beams in negative bending, *Journal of the Structural Division*, ASCE, **100**(ST11), 2205-2222.

135. Hancock, G.J. (1978). Local, distortional and lateral buckling of I-beams, *Journal of the Structural Division,* ASCE, **104** (ST11), 1781-1798.

136. Hancock, G.J. and Trahair, N.S. (1978). Finite element analysis of the lateral buckling of continuously restrained beam-columns, *Civil Engineering Transactions*, IEAust., **CE20**, 120-127.

137. Hancock, G.J. and Trahair, N.S. (1979). Lateral buckling of roof purlins with diaphragm restraint, *Civil Engineering Transactions*, IEAust., **CE21**, 10-15.

138. Hancock, G.J., Bradford, M.A. and Trahair, N.S. (1980). Web distortion and flexural-torsional buckling, *Journal of the Structural Division*, ASCE, **106**(ST7), 1557-1571.

139. Hancock, G.J. (1980). Web distortion and flexural-torsional buckling, *Proceedings of the American Society of Civil Engineers*, **106**(ST7), 1557-1569.

140. Hancock, G.J., Bradford, M.A. and Trahair, N.S. (1980). Web distortion and flexural-torsional buckling, *Journal of the Structural Division*, ASCE, **106**(ST7), 1557-1571.

141. Hanswille, G. and Kina, J. (1996). Lateral torsional buckling of composite beams, *Composite Construction in Steel and Concrete,* Engineering Foundation Irsee.

142. Hanswille, G. (2000). Lateral-torsional buckling of composite beams comparison of more accurate methods with Eurocode 4, *Proceedings of the International Conference on Composite Construction in Steel and Concrete IV*, Banff, Canada, May-June.

143. Johnson, R.P., van Dalen, K. and Kemp, A.R. (1967). Ultimate strength of continuous composite beams, *Proceedings of Conference on Structural Steelwork*, British Constructional Steelwork Association, London, 27-36.

144. Johnson, C.P. and Will, K.M. (1974). Beam buckling by finite element procedure, *Journal of the Structural Division*, ASCE, **100**(ST3), 669-680.

145. Johnson, R.P. and Hope-Gill, M.C. (1976). Tests on three three-span continuous composite beams, *Proceedings of The Institution of Civil Engineers*, **61**(2), 367-381.

146. Johnson, R.P. and Bradford, M.A. (1983). Distortional lateral buckling of stiffened composite bridge girders, *Int. Conf. on Instability and Plastic Collapse of Steel Structures,* Manchester, Granada, 569-580.

147. Johnson, R.P. and Buckby, R.J. (1986). *Composite structures of steel and concrete: Volume 2: Bridges*. Collins, London, 2nd Edn.

148. Johnson, R.P and Molenstra, V. (1990). Strength and stiffness of shear connections for discrete U-frame action in composite girders, *The Structural Engineer*, **68** (19), 386-392.

149. Johnson, R.P and Fan, C.K.R. (1990). Distortional lateral buckling of continuous beams, *Research Report CE* 30, University of Warwick.

150. Johnson, R.P. and Fan, C.K.R. (1991). Distortional lateral buckling of continuous composite beams, *Proceedings of Institution of Civil Engineers*, **91**(2), 131-161.

151. Johnson, R.P. and Chen, S. (1993). Stability of Continuous Composite Plate girders with U-frame action, *Proceedings of the Institution of Civil Engineers, Structures and Buildings*, **99**(2), 187-197.

152. Jonsson, J. (1999). Distortional theory of thin-walled beams, *Thin-Walled Structures*, **33**, 269-303.

153. Kapur, K.K. and Hartz, B.J. (1966). Stability of plates using the finite element method, *Journal of Engineering Mechanics* - ASCE, **92**, 177-195.

154. Kasagi, A. and Sridharan, S. (1992). Postbuckling analysis of layered composites using p-version finite strips, *International Journal of Numerical Methods in Engineering*, **33**, 2091-2107.

155. Kemp, A.R., Dekker, N.W. and Trincher, P. (1995). Differences in inelastic properties of steel and concrete beams, *Journal of Constructional Steel Research*, **34**(2-3), 187-206.

156. Kerensky, O.A., Flint, A.R. and Brown, W.C. (1956). The basis for design of beams and plate girders in the revised British standard 153, *Proceedings, ICE, Part* 3, **5**, 396-444.

157. Kitipornchai, S. and Trahair, N.S. (1972). Elastic stability of tapered I-beams, *Journal of the Structural Division*, **98**(ST3), 713-728.

158. Kitipornchai, S. and Trahair, N.S. (1975). Elastic behaviour of tapered monosymmetric I-beams, *Journal of the Structural Division*, **101**(ST8,) 1661-1678.

159. Kitipornchai, S. and Trahair, N.S. (1980). Buckling properties of monosymmetric I-beams, *Journal of the Structural Division*, (ST5), 941-957.

160. Kitipornchai, S., Wang, C.M. and Trahair, N.S. (1986). Buckling of monosymmetric I-beams under moment gradient, *Journal of Structural Engineering*, **112**(4), 781-799.

161. Kitipornchai, S. and Wong, C.M. (1986). Lateral buckling of tee beams under moment gradient, *Computers and Structures*, **23**(1), 69-76.

162. Kitipornchai, S. and Wong-Chung, A.D. (1987). Inelastic Buckling of Welded Monosymmetric I-Beams, *Journal of Structural Engineering*, ASCE, **113**(4), 740-756.

163. Kitipornchai, S., Wang, C.M. and Trahair, N.S. (1986). Buckling of monosymmetric I-beams under moment gradient, *Journal of Structural Engineering*, ASCE, **112**(4), 781-799.

164. Kitipornchai, S. and Wang, C.M. (1988a). Inelastic buckling of welded monosymmetric I-beams, *Journal of Structural Engineering*, **113**(4), 740-756.

165. Kitipornchai, S. and Wang, C.M. (1988b). Flexural-torsional buckling of monosymmetric beam-columns/tie-beams, *The Structural Engineer*, **66**(23/6), 393-399.

166. Koiter, W.T. (1945). Over the stabiliteit van het elastisch evenwicht (in dutch), *PhD Thesis*, University of Delft., Engl. Transl. NASA TTF 10, 833 (1967) and AFFDL TR 70-25 (1970).

167. Koiter, W.T. (1969). The nonlinear buckling problem of a complete spherical shell under uniform external pressure, *Proc. Kon. Ned. Ak. Wet.* **B72**, 40-123.

168. Koiter, W.T. and Kuiken, G.D.C. (1971). The interaction between local buckling and overall buckling and the behaviour of built-up columns, *Delft University of Technology Report*, WTHD-23.

169. Koiter, W.T. (1974). Current trends in the theory of buckling, *Proceedings IUTAM symposium on buckling of structures*, Harvard University.

170. Koiter, W.T. (1976). General theory of mode interaction in stiffened plate and shell structures, *Report WTHID*-91, Delft University of Technology, Delft.

171. Koko, T.S. and Olson, M.D. (1991). Nonlinear analysis of stiffened plates using superelements, *International Journal for Numerical Methods in Engineering*, **31**(2), 319-343.

172. Kollbrunner, C.F. and Hajdin, N. (1968). Die Verschiebungsmethode in der Theorie der dunnwandigen Stabe und ein neues Berechnungs model des Stabes mit in seinen Ebenen deformierbaren Querschnitten, *Publications*, IABSE, **28**(2), 87.

173. Kristek, V. and Studnicka, J. (1975). Stability Analysis of thin-walled structures considered as a folded plate structure (in Czechoslovakian), *Stavebnicky casopis*, **23**(6), 395.

174. Kwon, Y.B. and Hancock, G.J. (1986). A non-linear elastic spline finite strip analysis for thin-walled sections, *Research Report R*-532, University of Sydney.

175. Kwon, Y.B. and Hancock, G.J. (1993). Post-buckling analysis of thin-walled channels undergoing local and distortional buckling, *Computers and Structures*, **49**, 507-516.

176. Lau, S.C.W. and Hancock, G.J. (1986). Buckling of thin flat-walled structures by a spline finite strip method, *Thin-Walled Structures*, **4**, 269-294.

177. Lawther, R. (1990). On the use of bubble functions in stability analysis, *Thin-Walled Structures*, **9**, 377-387.

178. Lay, M.G. (1965). Flange local buckling in wide flange shapes, *Journal of the Structural Division*, ASCE, **91**(ST6), 95-116.

179. Lay, M.G. and Galambos, T.V. (1967). Inelastic beams under moment gradient, *Journal of the structural division*, ASCE, **91**(ST4), 381-399.

180. Leach, P. and Davies, J.M. (1996). An experimental verification of the generalized beam theory applied to interactive buckling problems, *Thin-Walled Structures*, **25**(1), 61-79.

181. Lee, G.C., Morrell, M.L. and Ketter, R.L. (1972). Design of tapered members, *Bulletin* 173, Welding Research Council, June.

182. Lee, D.S. (2001). Distortional buckling of I-section beams, *PhD Thesis*, University of New South Wales, Sydney.

183. Lindner, J. (1998). Lateral torsional buckling of composite beams, *Journal of Constructional Steel Research*, **46**(1-3), Paper No. 289.

184. Libove, C., Ferdman, S. and Reusch, J. (1949). *NACA Technical Note No.* 1124.

185. Liu, X.Y. and Zheng, J.J. (1987). Spline integral equation method for rotating disc of variable thickness, *BEM X* (Ed. C.A. Brebbia and W.S. Venturini), *Computational Mechanics Publications*, Southampton.

186. Loh, H.Y, Uy, B. and Bradford, M.A. (2004). Behaviour of partial strength composite steel-concrete joints incorporating various novel features, *The Seventh Pacific Structural Steel Conference,* Long Beach, USA.

187. Ma, M. and Hughes, O. (1996). Lateral distortional buckling of monosymmetric I-beams under distributed vertical load, *Thin-Walled Structures*, **26**(2), 123-145.

188. Michell, A.G.M. (1899). Elastic stability of long beams under transverse forces, *Philosophical Magazine*, **48**(5), p.298.

189. Naka, T. and Kato, T. (1961). *Buckling strength of single members.* (in Japanese), University of Tokyo Press, Japan.

190. Navaranta, D.R., Pain, T.H.H. and Witmer, E.A. (1968). Stability analysis of shells of revolution by the finite element method, *American Institute of Aeronautics and Astronautics Journal*, **6**(2), 355-361.

191. Nethercot, D.A. and Rockey, K.C. (1971). A unified approach to the elastic lateral buckling of beams, *The Structural Engineer*, **49**(7), 321-330.

192. Nethercot, D.A. (1973a). The solution of inelastic lateral stability problems by the finite element method, *Proceedings of 4th Australasian Conference on the Mechanics of Structures and Materials*, Brisbane, 183.

193. Nethercot, D.A. (1973b). Lateral buckling of tapered beams, *Publications*, IABSE, **33**(2), 173-192.

194. Nethercot, D.A. and Trahair, N.S. (1975). Design of diaphragm braced I-beams, *Journal of the Structural Division*, ASCE, **101**(ST10), 2045-2061.

195. Nethercot, D.A. and Trahair, N.S. (1976). Lateral buckling approximations for elastic beams, *Structural Engineer*, **54**(6), 197-204.

196. Nylander, H. (1943). Drehungsvorgange und Gebunde Kippung bei Geranden, Doppelt-symmetrishen I-Tragern, *Ingeriors Vetenskaps Akochtemein Handlinger*. 174, Stockholm.

197. Oehlers, D.J. and Bradford, M.A. (1995). *Fundamental behaviour of composite steel and concrete structural members*, Oxford: Butterworth-Heinemann.

198. Oehlers, D.J. and Bradford, M.A. (1999). *Elementary behaviour of composite steel and concrete structural members*, Oxford: Butterworth-Heinemann.

199. Okumura, T. (1950). Study on buckling of welded members – lateral buckling of I-shaped girders (in Japanese), *Journal of the Japan Welding Society*, **21**.

200. Pi, Y.L and Trahair, N.S. (1999). Distortional and warping at beam supports, *Journal of Structural Engineering*, ASCE, **126**(11), 1279-1287.

201. Pi, Y-L. and Bradford, M.A. (2001). Elastic flexural-torsional buckling and postbuckling of arches subjected to a central concentrated load, *Eighth International Conference on Civil and Structural Engineering Computing*, Eisenstadt, Austria, Civil-Comp Press:79.

202. Pifko, A. and Isakson, G. (1969). A finite element method for the plastic buckling analysis of plates, *AIAAJ*, **7**(10), 1950-1957.

203. Pignataro, M., Di Carlo, A. and Rizzi, N. (1985). Discussion on accurate determination of asymptotic postbuckling stresses by the finite element method by J. F. Olesen and E. Byskov, *Computers and Structures*, **21**(5), 933-935.

204. Pincus, G. and Fisher, G.P. (1966). Behaviour of diaphragm-braced columns and beams, *Journal of the Structural Division*, ASCE, **92**(ST2), 323-350.

205. Plank, R.J. (1973). The initial buckling of thin walled structures under combined loadings, *PhD Thesis*, The University of Birmingham, England.

206. Plank, R.J. and Wittrick, W.H. (1974). Buckling under combined loading of thin flat-walled structures by a complex finite strip method, *International Journal of Numerical Methods in Engineering*, **8**, 323-339.

207. Poowannachaikul, T. and Trahair, N.S. (1975). Inelastic buckling of continuous steel I-beams, *Civil Engineering Transactions*, IEAust., No. 3527, 134-139.

208. Prager, W. (1948). *Courant Anniversary Volume*, Interscience, New York, p. 289.

209. Prandtl, L. (1899). Kipperscheinungen, *Thesis*, Munich.

210. Prenter, P.M. (1975). *Splines and variational methods*, John Wiley, New York.

211. Protte, W. (1961). Ein Beitrag zum Problem der Gesamtstabilitat guerausgesteifter Trager im Kippbereich, *Der Stahlbau*, Berlin, **30**(4), p.103.

212. Przemieniecki, J.S. (1973). Finite element analysis of local instability, *American Institution of Aeronautical Journal*, **11**, 33-39.

213. Rajasekaran, S. And Murray, D.W. (1973). Coupled local buckling in wide-flange beam columns, *Journal of the Structural Division*, ASCE, **99**(ST6), 1003-1023.

214. Ranzi, G. (2004). Partial interaction analysis of composite beams using the direct stiffness method, *PhD Thesis*, The University of New South Wales, Sydney.

215. Reis, A. and Roorda, J. (1977). The interaction between lateral-torsional and local plate buckling in thin-walled beams, *Second International Colloquium On the Stability of Steel Structures*, Liege.

216. Roberts, T.M. and Jhita, P.S. (1983). Lateral, local and distortional bucking of I-beams, *Thin Walled Structures*, **1**, 289-308.

217. Ronagh, H.R. and Bradford, M.A. (1994a). Elastic distortional buckling of tapered beams, *Engineering Structures*, **16**(2), 97-110.

218. Ronagh, H.R. and Bradford, M.A. (1994b). Parameters affecting distortional buckling of tapered steel members, *Journal of Structural Engineering*, **120**(11), 3137-3155.

219. Ronagh, H.R. and Bradford, M.A. (1994c). Some notes on finite element buckling formulations for beams, *International Journal of Computers and Structures*, **52**(6), 1119-1126.

220. Ronagh, H.R. and Bradford, M.A. (1996). A rational model for the distortional buckling of tapered members, *Computer Methods in Applied Mechanics and Engineering*, **138**, 263-277.

221. Ronagh, H.R., Attard, M.M and Bradford, M.A. (1997). A new formulation for linear, nonlinear, buckling and postbuckling analysis of tapered symmetric beam-columns, *Proc., Seventh Int. Conf. on Computing in Civil and Building Engineering*, Seoul, Korea, 273-278.

222. Ronagh, H.R. and Bradford, M.A. (1998). Distortional buckling of I-shaped plate girders, a simple and efficient model, *Proceedings of 5th Pacific Structural Steel Conference*, Seoul, 1999-204.

223. Ronagh, H.R. (2001). Progress in the methods of analysis of restricted distortional buckling of composite bridge girders, *Progress in Structural Engineering and Materials*, **3**(2), 141-148.

224. Ronagh, H. R and Bradford, M.A. (2002). Instability of the steel joist in composite bridge girders: Review of current design methods, *Australian Journal of Structural Engineering*, **3**(3), 143-152.

225. Saadatpour, M.M, Azhari, M. and Bradford, M.A. (1998). Buckling of arbitrary quadrilateral plates with intermediate supports using the Galerkin method, *Computer Methods in Applied Mechanics and Engineering,* **164**, 297-306.

226. Salvadori, M.G. (1955). Lateral buckling of I-beams, *Transactions*, ASCE, **120**, 1165-1177.

227. Sangakkara, S.M.S.R. (1978). A comparative study of lateral-torsional buckling of I-Beams, *PhD Thesis*, The University of Sheffield, England.

228. Satsangi, S.K. and Mukhopadhyay, M. (1989). A review of static analysis of stiffened plates, *Journal of Structural Engineering*, **15**(4), 117-126.

229. Schafer, B.W. and Pekoz, T. (1997). The behaviour and design of longitudinally stiffened thin-walled compression elements, *Thin-Walled Structures*, **27**(1), 65-78.

230. Schaumann, P. (1991). Verbundbrücken unter Verwendung von Walzträgern - Konstruktiver Entwurf und Forschungserkenntnisse, in Vortragsband zu den Seminaren Verbundbrückentag in Bochum und Berlin, ARBED Recherches, Luxemburg, 1991

231. Scheer, J. (1959). Zum Problem der Gesamtstabilitat von einfach symmetrischen I-Tragern, *Der Stahlbau*, Berlin, **28**(5), p.113 and **128**(6), p.165.

232. Schmied, R. (1967). Die Gesamstabilitat von zweiachsig aussermittig gedruckten dunnwandigen I-Staben unter Berucksichtigung der Querschnittsverformung nach der nichlinearten Plattentheorie, *Der Stahlbau*, Berlin, **36**, p.1.

233. Schoenberg, I.J. (1946). Contributions to the problem of approximation of equidistant data by analytic functions, *Q. Appl. Math.*, **4**, 45-99 and 112-114.

234. Schultz, M.H. (1973). *Spline analysis*, Prentice-Hall, New Jersey.

235. Serrette, R.L. and Pekoz, T. (1995). Distortional buckling of thin-walled beams/panels. I: Theory, *Journal of Structural Engineering*, **121**(4), 757-776.

236. Shen, P.C. and Wang, J.G. (1987a). Static analysis of cylindrical shells by using B-spline functions, *Computers and Structures*, **25**, 809-816.

237. Shen, P.C. and Wang, J.G. (1987b). Vibration analysis of flat shells by using *B*-spline functions, *Computers and Structures*, **25**, 1-10.

238. Smith, S.T., Bradford, M.A. and Oehlers, D.J. (2000). Unilateral buckling of elastically restrained rectangular mild steel plates, *Computational Mechanics*, **26**(4), 317-324.

239. Sridharan, S. and Graves-Smith, T.R. (1981). Postbuckling analyses with finite strips, *Journal of the Engineering Mechanics Division*, ASCE, **107**(5), 869-888.

240. Sridharan, S. (1983). Doubly symmetric interactive buckling of plate structures, *International Journal of Solids and Structures*, **19**(7), 625-641.

241. Srinivasan, R.S. and Ramachandra, S.V. (1977). Linear and nonlinear analysis of stiffened plates, *International Journal of Solids and Structures*, **13**(10), 897-912.

242. SSRC (1988). *Guide to stability design criteria for metal structures*, Structural Stability Research Council, John Wiley and Sons, New York.

243. Standards Australia (1998). *AS*4100 *Steel Structures*. London: E & FN Spon.

244. Stefani, G. and Lawther, R. (1990). Bubble functions and the buckling analysis of frames, *Proceedings of* 2*nd* *EPMESC Conference*, Macau, 869-877.

245. Stroud, W.J. and Anderson, M.S., (1980). PASCO: structural panel analysis and sizing code capability and analytical foundations, NASA *TN* D 80181.

246. Stroud, W.J., Greene, W.H. and Anderson, M.S. (1981). Buckling loads for stiffened panels subjected to combined longitudinal compression and shearing loadings: results obtained with PASCO, EAL and STAGS computer programs, NASA *Technical Memorandum*, No. 83194.

247. Suzuki, Y. and Okumura, T. (1968). Influence of cross-sectional distortion on flexural-torsional buckling, *International Journal of Mechanical Sciences*, **17**, p. 307.

248. Svensson, S.E. (1985). Lateral buckling of beams analysed as elastically supported columns subjected to a varying axial force, *Journal of Constructional Steel Research*, **5**, 179-193.

249. Szabo, B.A. and Babuska, I. (1991). *Finite element analysis*, Wiley, New York.

250. Terrey, P.J., Bradford, M.A. and Gilbert, R.J. (1994). Creep and shrinkage of concrete in concrete-filled circular steel tubes, In P. Grundy *et al.* (Eds), Tubular Structures VI – *Proceedings of 6th International Symposium on Tubular Structures*, Melbourne, 14-16 Dec., Rotterdam, Balkema, 293-298.

251. Tham, L.G. and Szeto, H.Y. (1990). Buckling analysis of arbitrary shaped plates by spline finite strip method, *Computers and Structures*, **36**, 729-735.

252. Timoshenko, S.P. (1910). Einige Stabilitats – Probleme der Elasticitatstheorie, *Zeitschrift fur Mathematic und Physik*, **58**, 337-385. (also in *Collected Papers of Stephen P. Timoshenko.* McGraw-Hill, New York, 1953.)

253. Timoshenko, S.P. (1913). *Sur la stabilite des systemes elastiques, Annales des Ponts et Chaussees,* 1st *Part,* (also in *Collected Papers of Stephen P. Timoshenko.* McGraw-Hill, New York, 1953.)

254. Timoshenko, S.P. (1924). Beams without lateral support, *Transactions*, ASCE, **87**, 1247-1262.

255. Timoshenko, S.P. and Woinowsky-Krieger, S. (1959). *Theory of Plates and Shells*, 2nd Edn., McGraw Hill.

256. Timoshenko, S.P. and Gere, J.M. (1970). *Theory of Elastic Stability.*, 3rd Edn., McGraw-Hill, New York.

257. Trahair, N.S. (1966). The bending stress rules of draft A.S. CA1, *Journal of the Institution of Engineers*, Australia, **38**(6), 131-141.

258. Trahair, N.S. and Kitipornchai, S. (1972). Buckling of inelastic I-beams under uniform moment, *Journal of the structural division*, **98**(ST11), 2551-2566.

259. Trahair, N.S. (1979). Elastic lateral buckling of continuously restrained beam-columns, *The Profession of a Civil Engineer*, Edited by D. Campbell-Allen and E.H. Davis, Sydney University Press, Australia, 61-73.

260. Trahair, N.S. (1993). *Flexural-torsional buckling of structures*, London: E & FN Spon.

261. Trahair, N.S. and Bradford, M.A. (1998). *The behaviour and design of steel structures to AS*4100, 3rd Edn., E & FN Spon, London.

262. Trahair, N.S., Bradford, M.A. and Nethercot, D.A. (1998). *The behaviour and design of steel structures to BS*5950, E & FN Spon, London.

263. Tvergaard, V. (1973). Influence of postbuckling behaviour on optimum design of stiffened panels, *International Journal of Solids and Structures*, **9**, 177-192.

264. Usami, T. (1982). Post-buckling of plates in compression and bending, *Journal of Structural Division,* ASCE, **108**(3), 591-609.

265. Uy, B. and Bradford, M.A. (1995). Local buckling of cold formed steel sheeting in profiled composite beams at service load, *Structural Engineering Review*, 7(4), 289-300.

266. Uy, B. and Das, S. (1997). Wet concrete loading of thin-walled steel box columns during construction of a tall building, *Journal of Constructional Steel Research*, **42** (2), 95-119.

267. Van Erp, G.M. (1989). Advanced buckling analyses of beams with arbitrary cross sections, *PhD Thesis*, Eindhoven University of Technology.

268. Van Erp, G.M. and Menken, C.M. (1990). The spline finite strip method in the buckling analysis of thin-walled structures, *Communications in Applied Numerical Mehods*, **6**, 477-484.

269. Van Erp, G.M. and Menken, C.M. (1991). Initial post-buckling analysis with the spline finite strip method, *Computers and Structures*, **40**, 1193-1201.

270. Vlasov, V.Z. (1961). *Thin walled elastic beams*, 2nd Edn., Israel Program for Scientific Translation, Jerusalem, Israel.

271. Wang, C.M. and Kitipornchair, S. (1986a). Buckling capacities of monosymmetric I-beams, *Journal of Structural Engineering*, ASCE, **112**(11), 2373-2391.

272. Wang, C.M. and Kitipornchair, S. (1986b). On stability of monosymmetric cantilevers, *Engineering Structures*, **8**(3), 169-180.

273. Wang, S. and Dawe, D.J. (1999). Buckling of composite shell structures using the spline finite strip method, *Composites Part B* 30, 351-364.

274. Wang, S.T., Yost, M.I. and Tien, Y.L. (1977). Lateral buckling of locally buckled beams using finite element techniques, *Computers and Structures*, **7**(7), 469-475.

275. Wang, C.M. and Kitipornchai, S. (1986). Buckling capacities of monosymmetric I-beams, *Journal of Structural Engineering*, ASCE, **112**(11), 2372-2391.

276. Wang, Y.C., Liu, Z. and Wu, Y. (1984). All particular solution method in boundary element techniques, In Du QH, Tanaka M, Ji X Eds., *Theory and Applications of Boundary Element Methods*, International Academic Publishers.

277. Weston, G., Nethercot, D.A. and Crisfield, M.A. (1991). Lateral buckling in continuous composite bridge girders, *The Structural Engineer*, **69**(5), 79-87.

278. Williams, F.W. and Wittrick, W.H. (1968). Computational procedures for a matrix analysis of the stability and vibration of thin-walled structures in compression, *International Journal of Mechanical Sciences*, **11**, 979-998.

279. Williams, F.W. and Jemah, A.K. (1987). Buckling curves for elastically supported columns with varying axial force to predict lateral buckling of beams, *Journal of Constructional Steel Research*, **7**, 133-147.

280. Williams, F.W., Jemah, A.K. and Lam, D.H. (1993). Distortional buckling curves for composite beams, *Journal of Structural Engineering*, **119**(7), 2134-2149.

281. Wittrick, W.H., Curzon, P.L.V. (1968a). Stability functions for the local buckling of thin-walled structures in bending and compression, *Aeronautical Quarterly*, **19**, 327-351.

282. Wittrick, W.H., Curzon, P.L.V. (1968b). Local buckling of long polygonal tubes in combined bending and torsion, *International Journal of Mechanical Sciences*, **10**, 849-857.

283. Wittrick, W.H. and Williams, F.W. (1971). An algorithm for computing natural frequencies of elastic structures, *Journal of Mechanics and Applied Mathematics*, **24**, 263-284.

284. Wittrick, W.H. and Williams, F.W. (1973). An algorithm for computing the critical buckling loads of elastic structures, *Journal of Structural Mechanics*, 498-518.

285. Wittrick, W.H. and Williams, F.W. (1974). Buckling and vibration of anisotropic or isotropic plate assemblies under combined loading, *International Journal of Mechanical Sciences,* **16**, 209-239.

286. Woods, R.F. and Watson, S.D.C. (1977). The effects of beam support and web distortion on the flexural-torsional buckling of I-beams, *Honours Thesis*, School of Civil Engineering, University of Sydney.

287. Woolcock, S.T., Kitipornchair, S. and Bradford, M.A. (1999). *Design of portal frame buildings, 3rd Edition*, Australian Institute of Steel Construction, Sydney.

288. Young, B.W. and Schulz, G.W. (1977). Mechanical properties and residual stresses, *Second Int. Coll. On Stability of Steel Structures*, Leige, Belgium, Introductory Report, ECCS and IABSE, 31-46.

289. Zhao, X-L., Hancock, G.J., Trahair, N.S. and Pi Y-L. (1995). Lateral buckling of cold-formed RHS beams, In: Kitipornchai, S., Hancock, G.J. & Bradford, M.A.

(Eds.), *International Conference on Structural Stability and Design*. Balkema, 55-60.

290. Zhu, D.S. and Cheung, Y.K. (1989). Postbuckling analysis of shells by a spline finite strip method, *Computers and Structures*, **31**, 357-364.

291. Zhu, D.S. and Cheung, Y.K. (1996). Postbuckling analysis of circular cylindrical shell under combined loads, *Computers and Structures*, **58**(1), 21-26.

292. Zienkiewicz, O.C. and Taylor, R.L. (2000). *The Finite Element Method.* 5th Ed., Butterworth-Heinemann, Oxford.

APPENDIX

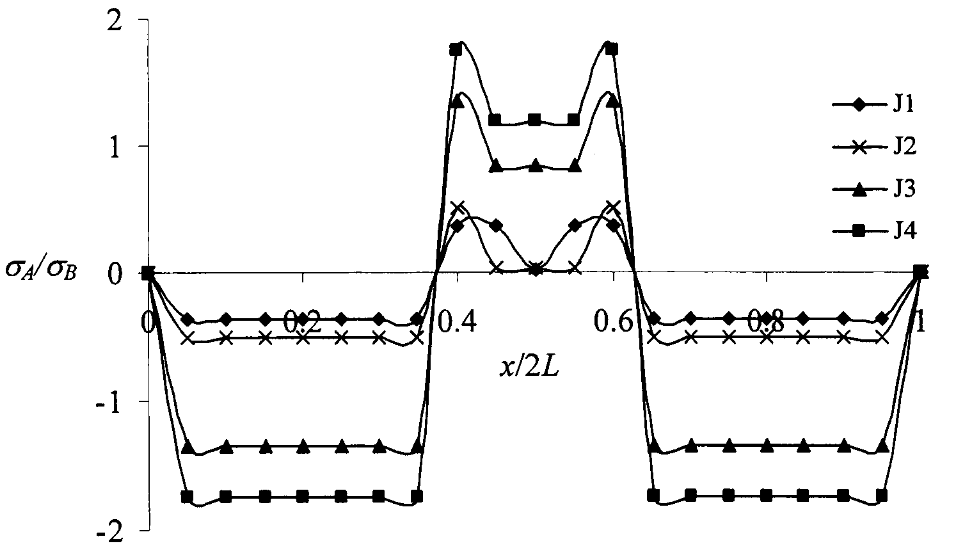

Figure A1.1 Stress ratio excluding self-weight (CASE 2, R1, S1)

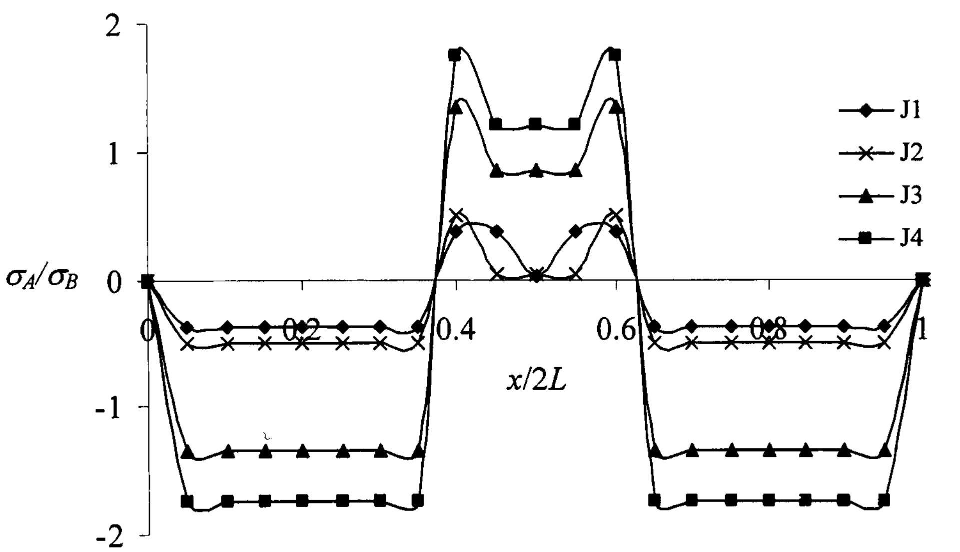

Figure A1.2 Stress ratio excluding self-weight (CASE 3, R1, S1)

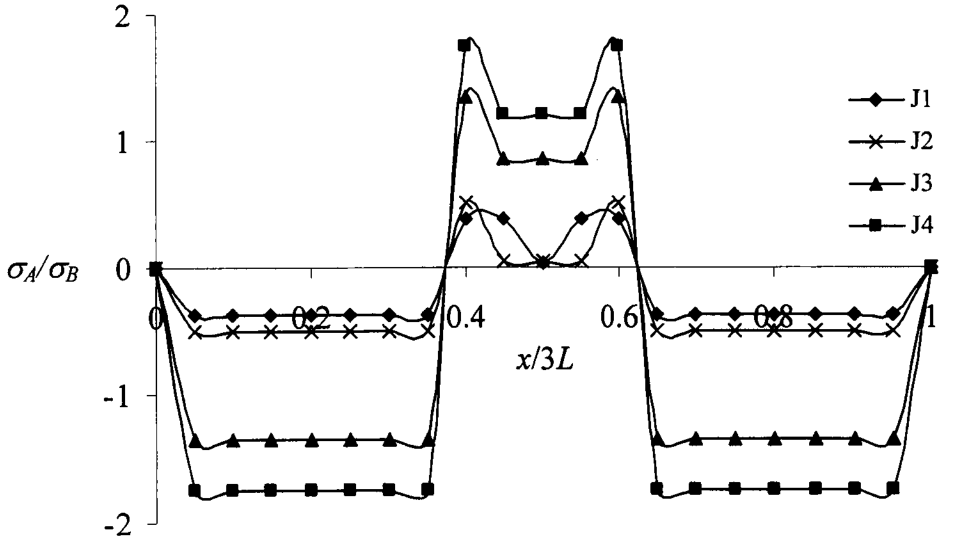

Figure A1.3 Stress ratio excluding self-weight (CASE 4, R1, S1)

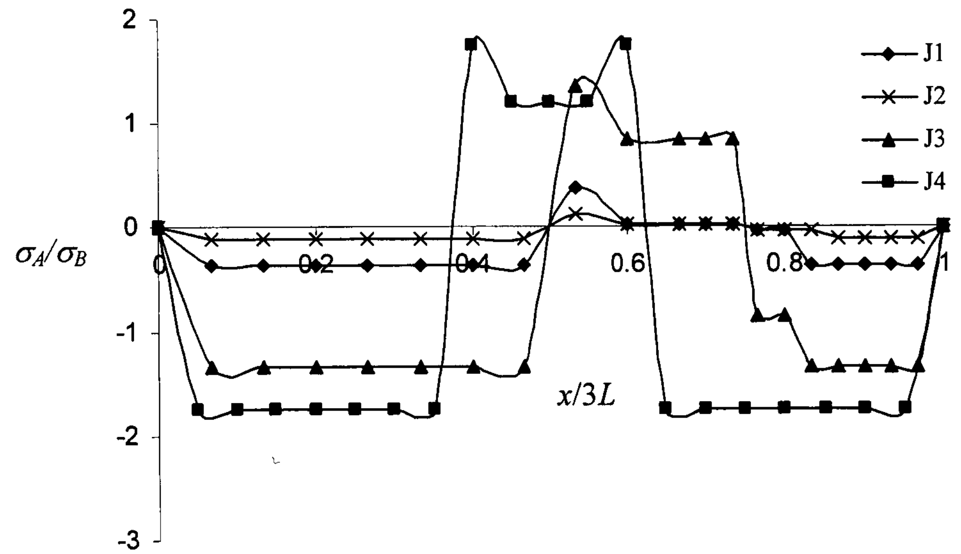

Figure A1.4 Stress ratio excluding self-weight (CASE 5, R1, S1)

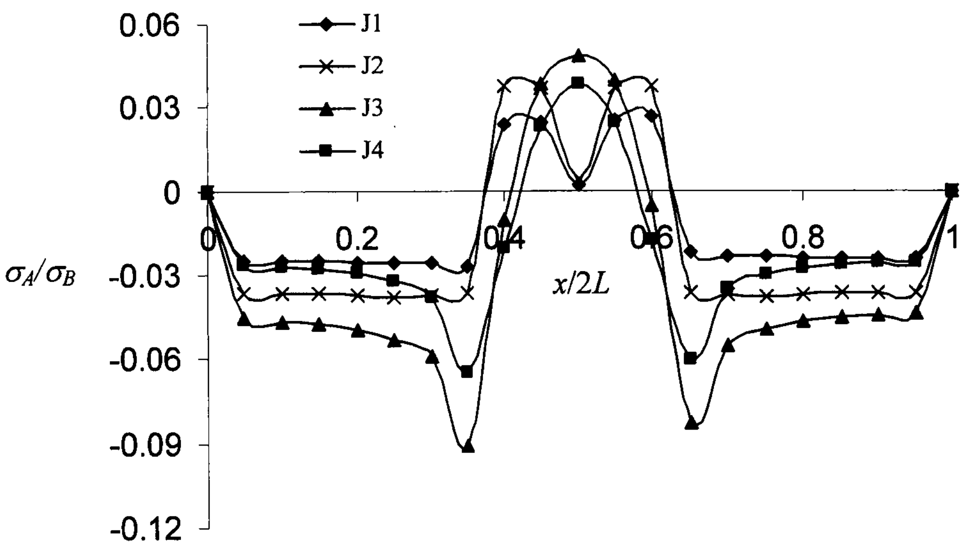

Figure A1.5 Stress ratio including self-weight (CASE 2, R1, S1)

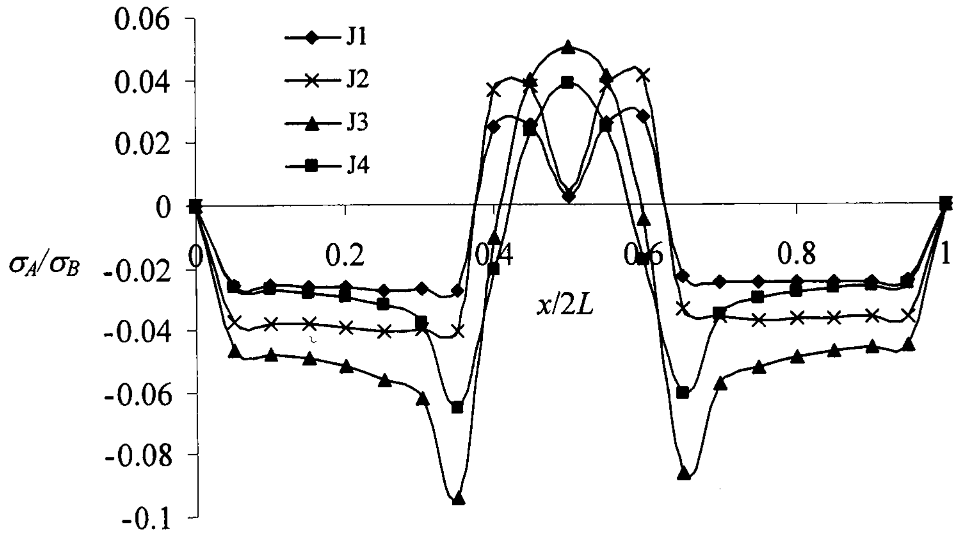

Figure A1.6 Stress ratio excluding self-weight (CASE 3, R1, S1)

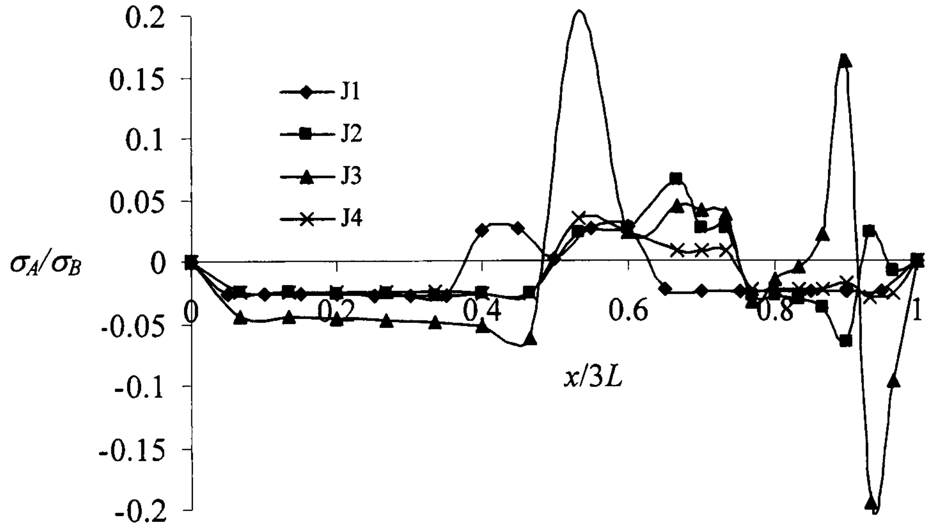

Figure A1.7 Stress ratio excluding self-weight (CASE 4, R1, S1)

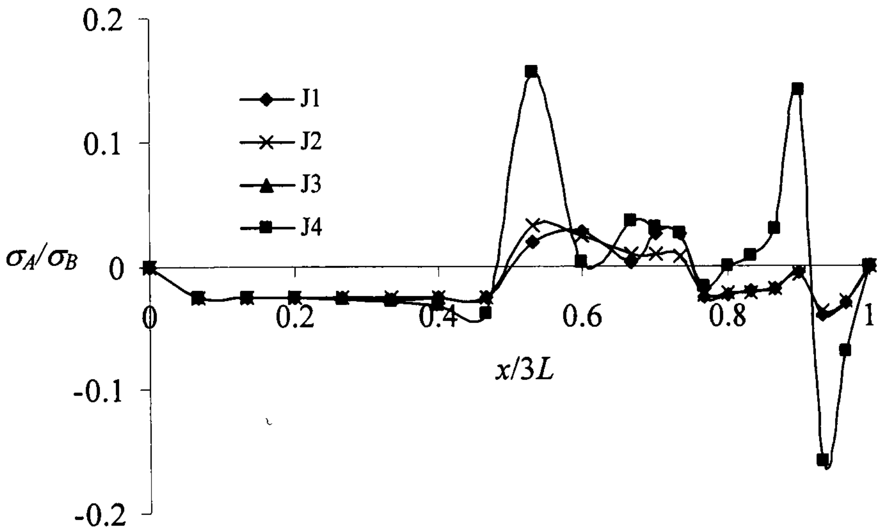

Figure A1.8 Stress ratio excluding self-weight (CASE 5, R1, S1)

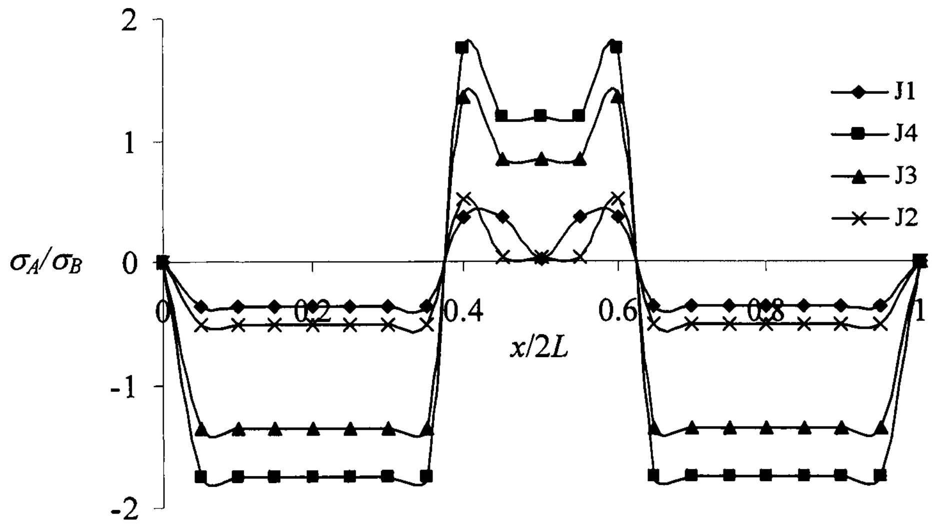

Figure A1.9 Stress ratio excluding self-weight (CASE 8, R1, S1)

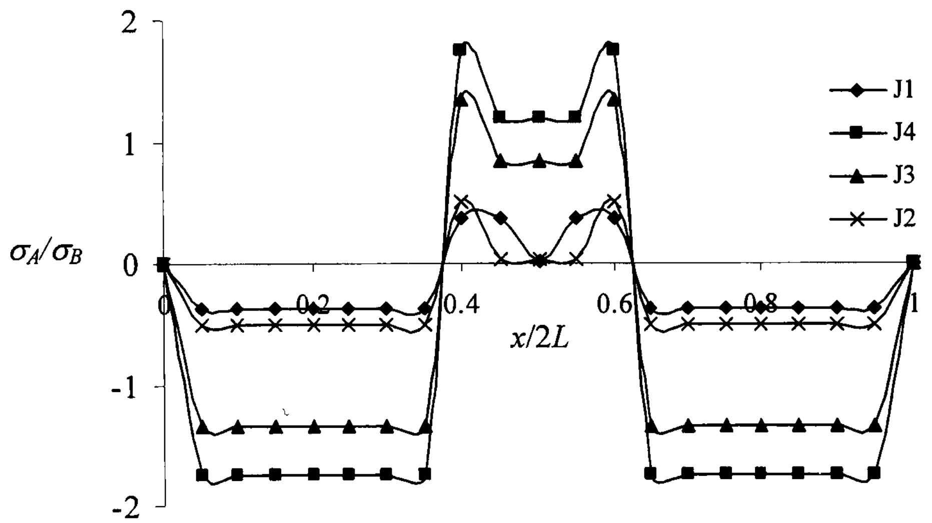

Figure A1.10 Stress ratio excluding self-weight (CASE 9, R1, S1)

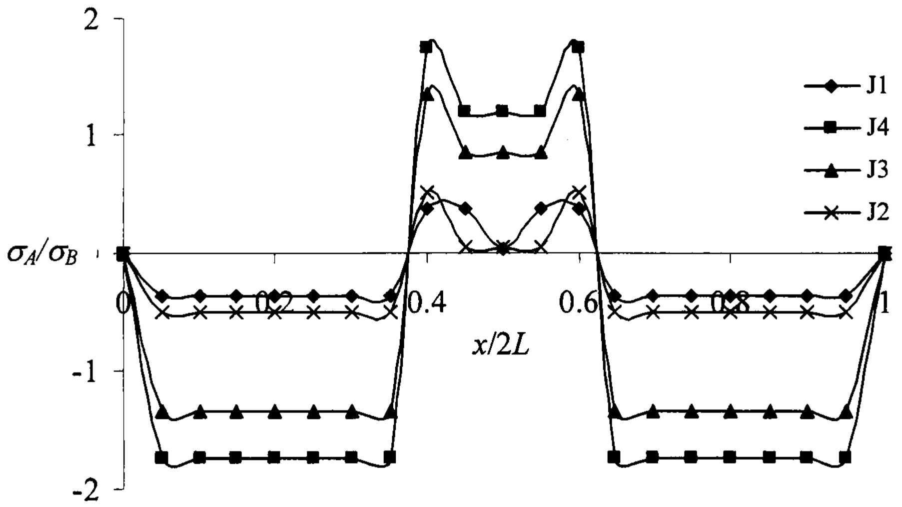

Figure A1.11 Stress ratio excluding self-weight (CASE 10, R1, S1)

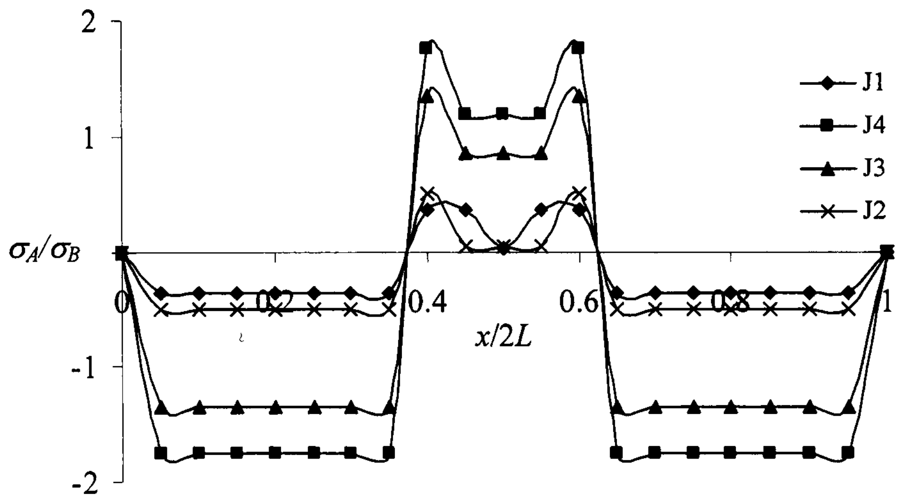

Figure A1.12 Stress ratio excluding self-weight (CASE 11, R1, S1)

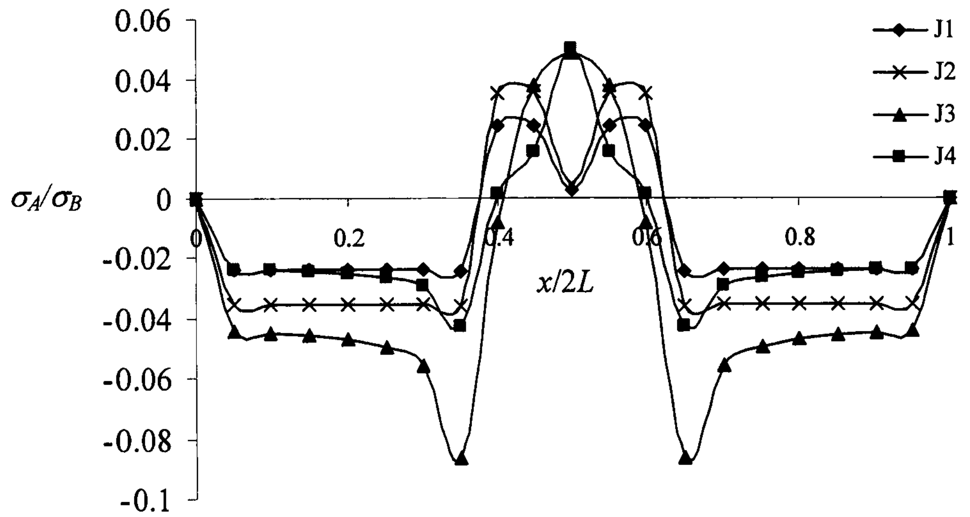

Figure A1.13 Stress ratio including self-weight (CASE 8, R1, S1)

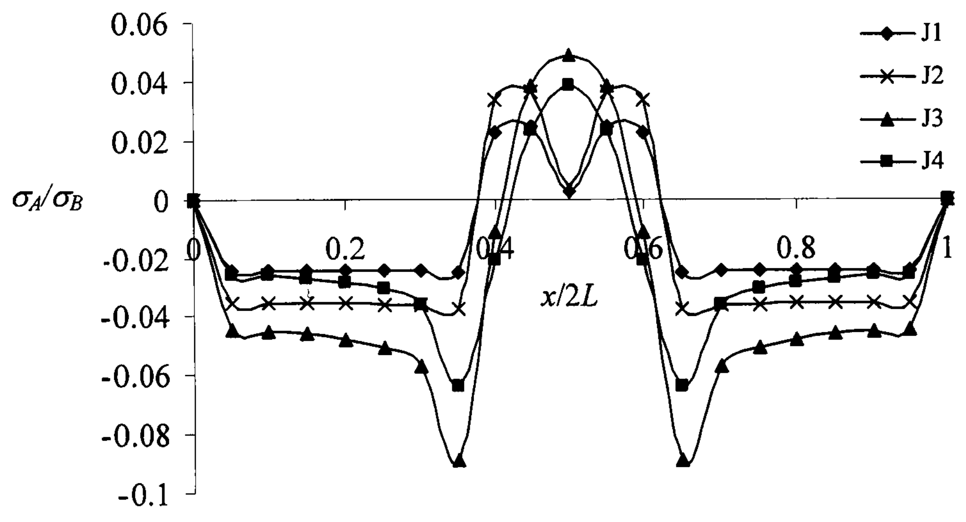

Figure A1.14 Stress ratio excluding self-weight (CASE 9, R1, S1)

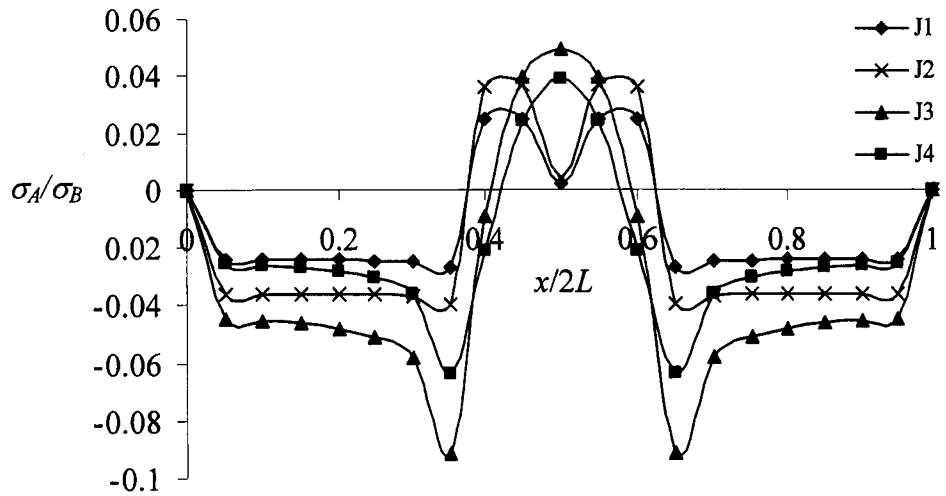

Figure A1.15 Stress ratio including self-weight (CASE 10, R1, S1)

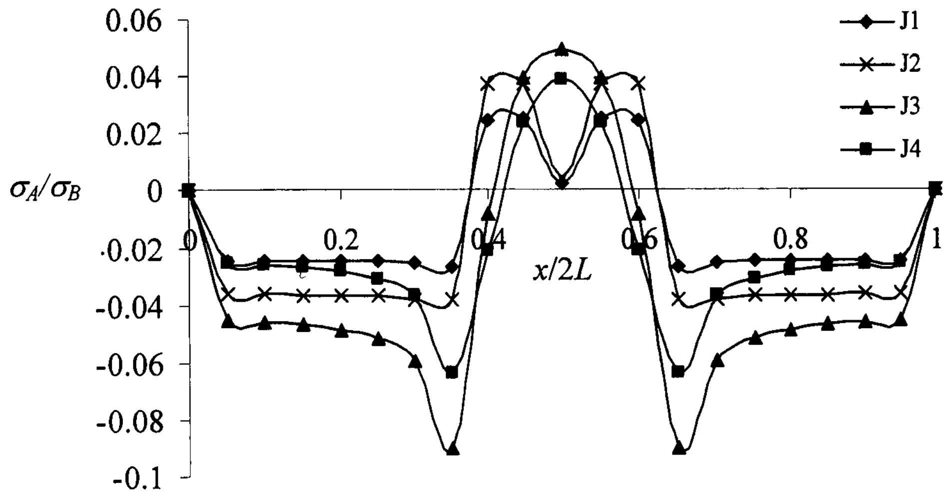

Figure A1.16 Stress ratio including self-weight (CASE 11, R1, S1)

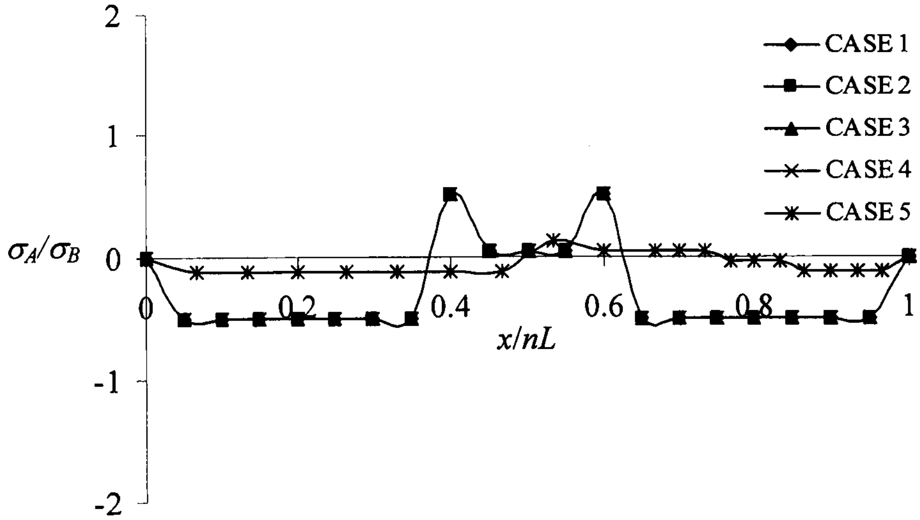

Figure A1.17 Stress ratio excluding self-weight (J2, R1, S1)

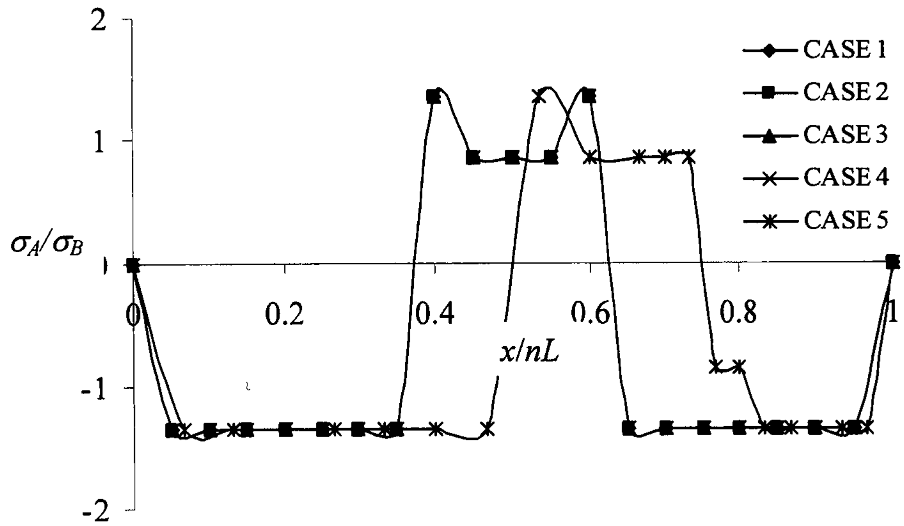

Figure A1.18 Stress ratio excluding self-weight (J3, R1, S1)

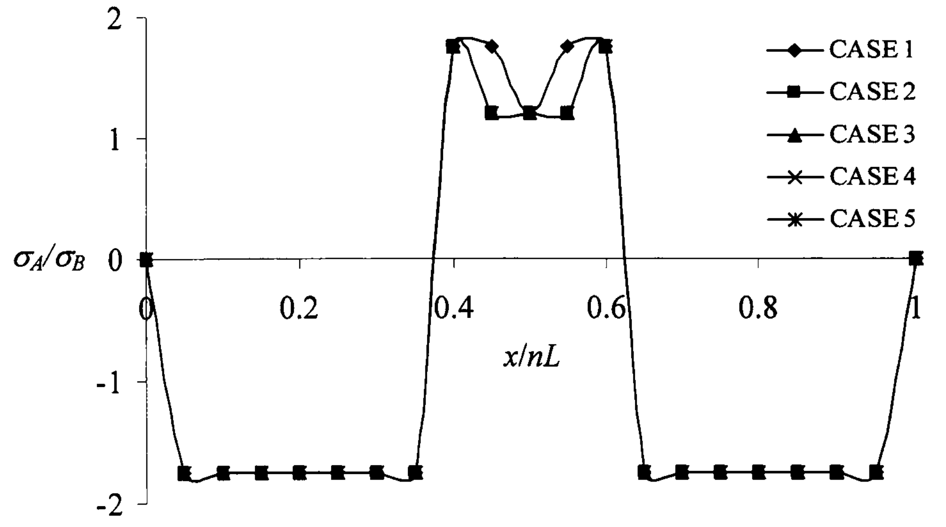

Figure A1.19 Stress ratio excluding self-weight (J4, R1, S1)

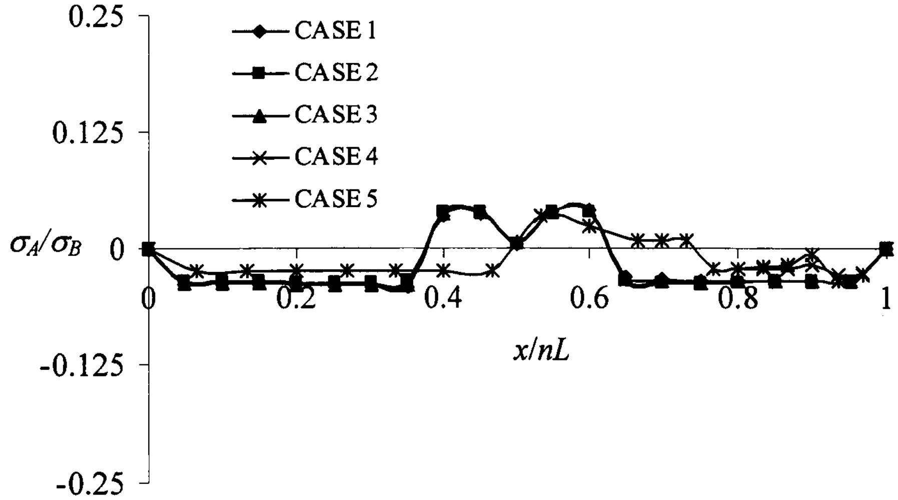

Figure A1.20 Stress ratio excluding self-weight (J2, R1, S1)

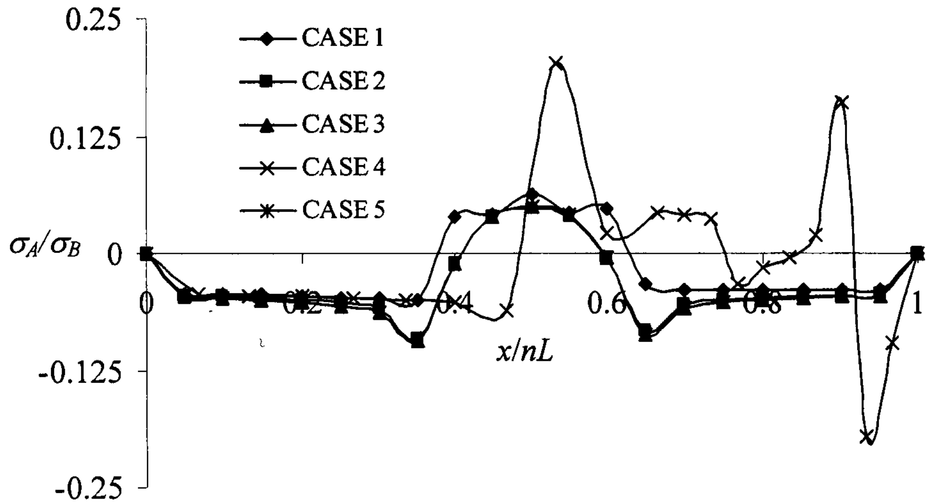

Figure A1.21 Stress ratio excluding self-weight (J3, R1, S1)

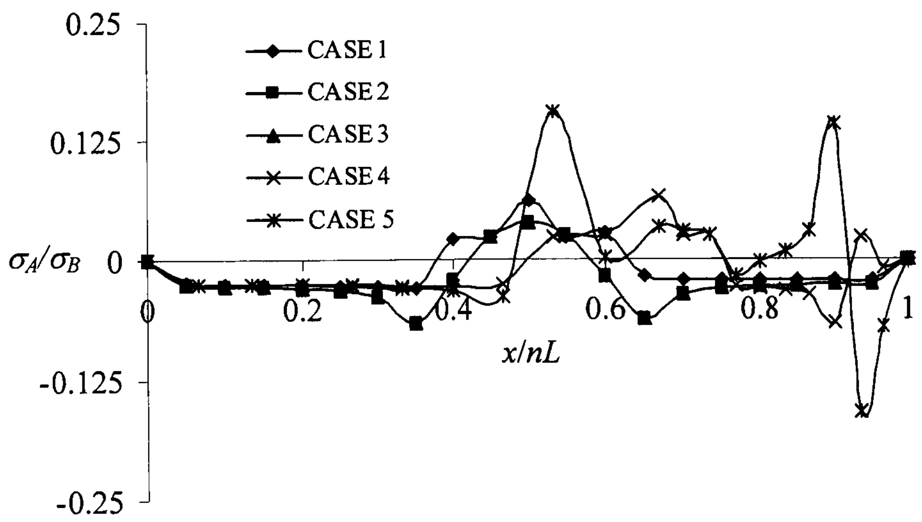

Figure A1.22 Stress ratio excluding self-weight (J4, R1, S1)

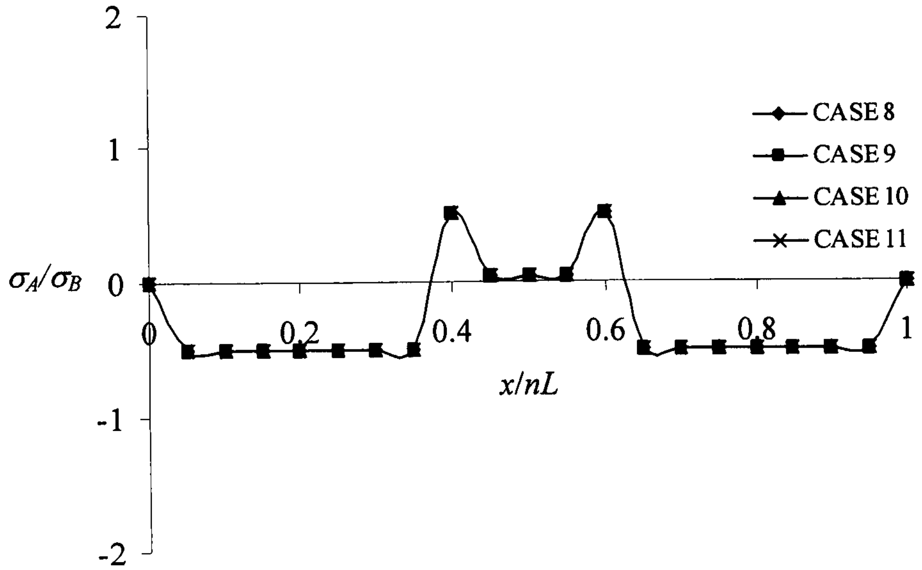

Figure A1.23 Stress ratio excluding self-weight (J2, R1, S1)

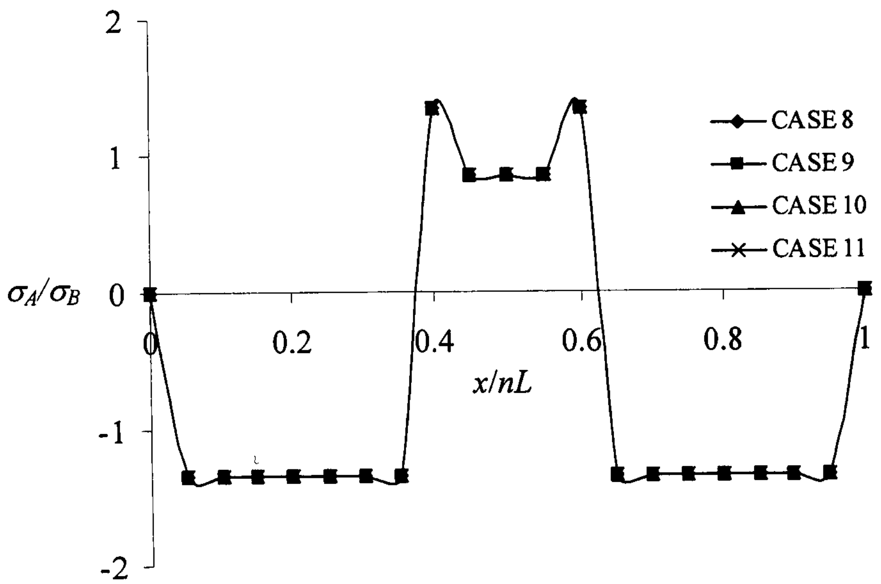

Figure A1.24 Stress ratio excluding self-weight (J3, R1, S1)

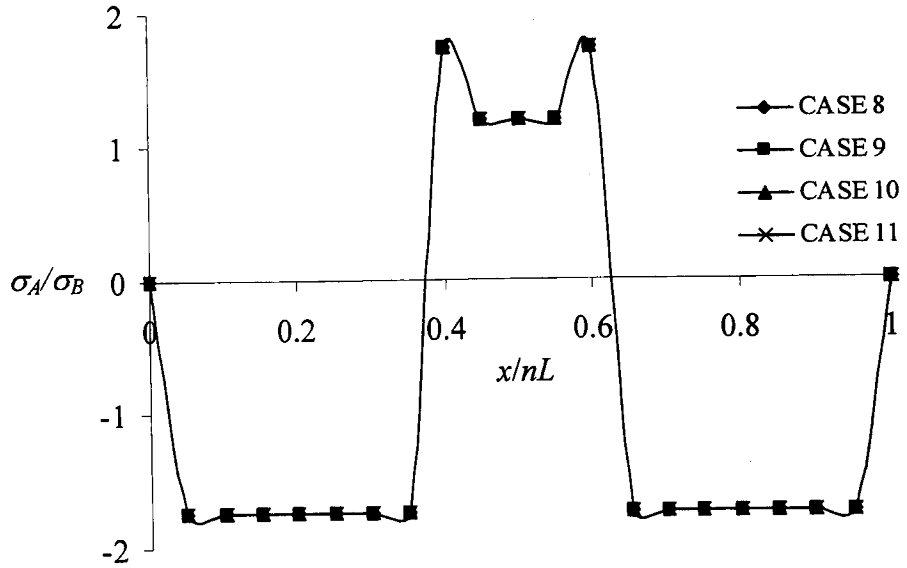

Figure A1.25 Stress ratio excluding self-weight (J4, R1, S1)

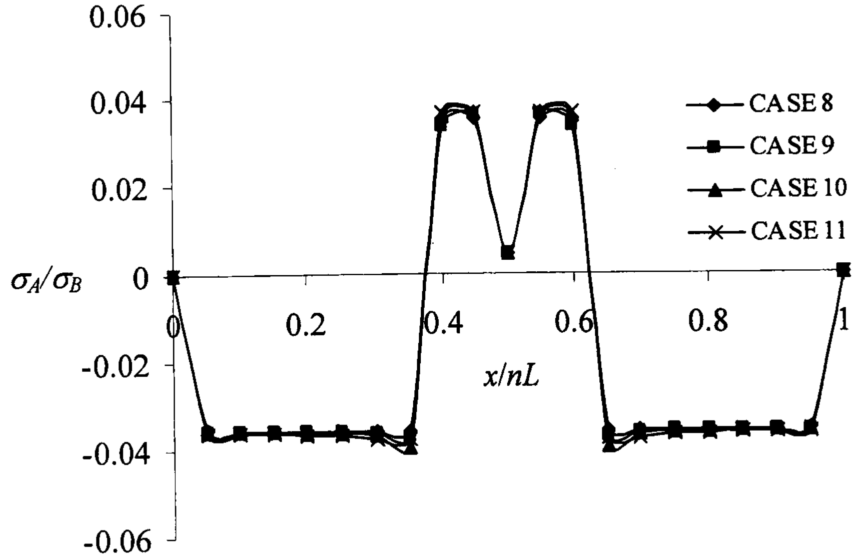

Figure A1.26 Stress ratio including self-weight (J2, R1, S1)

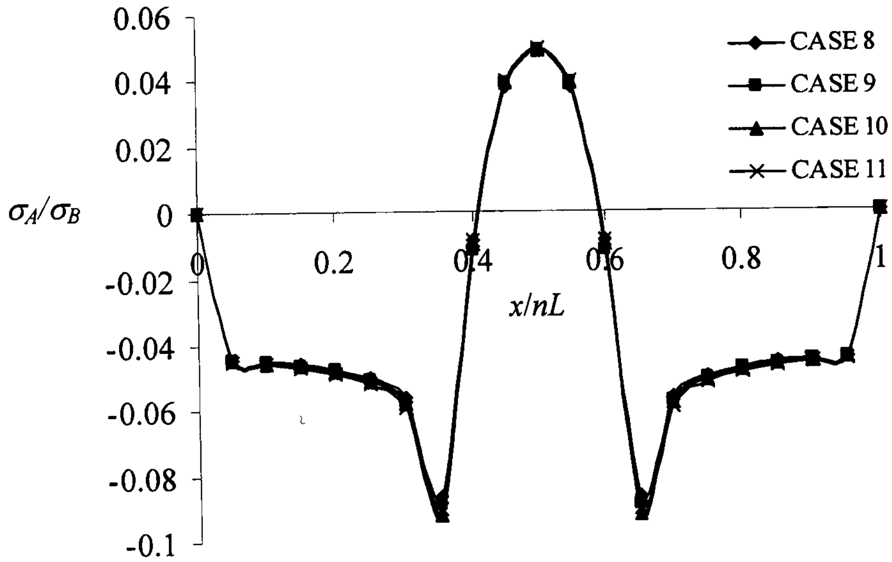

Figure A1.27 Stress ratio including self-weight (J3, R1, S1)

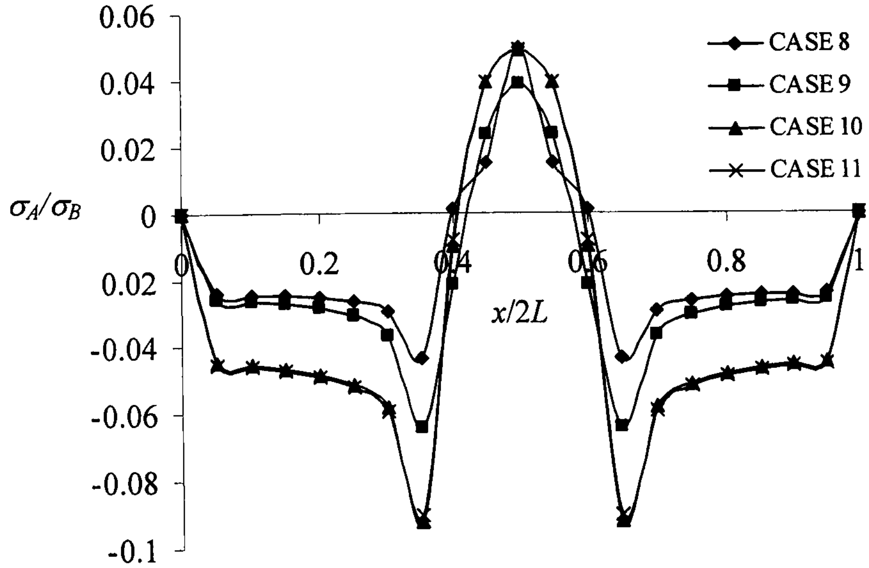

Figure A1.28 Stress ratio including self-weight (J4, R1, S1)

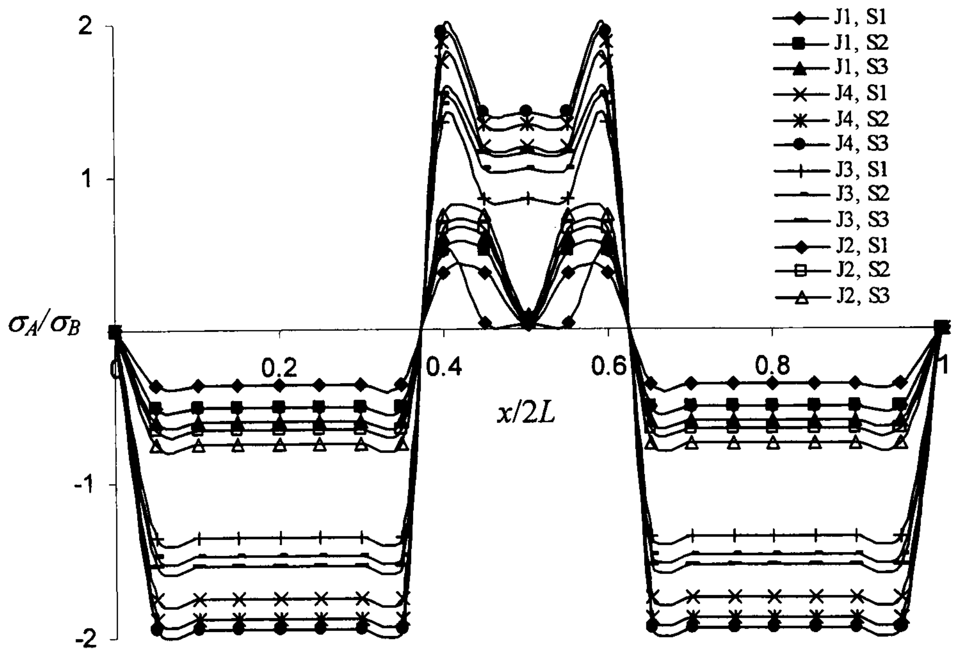

Figure A1.29 Stress ratio excluding self-weight (CASE 2, R1)

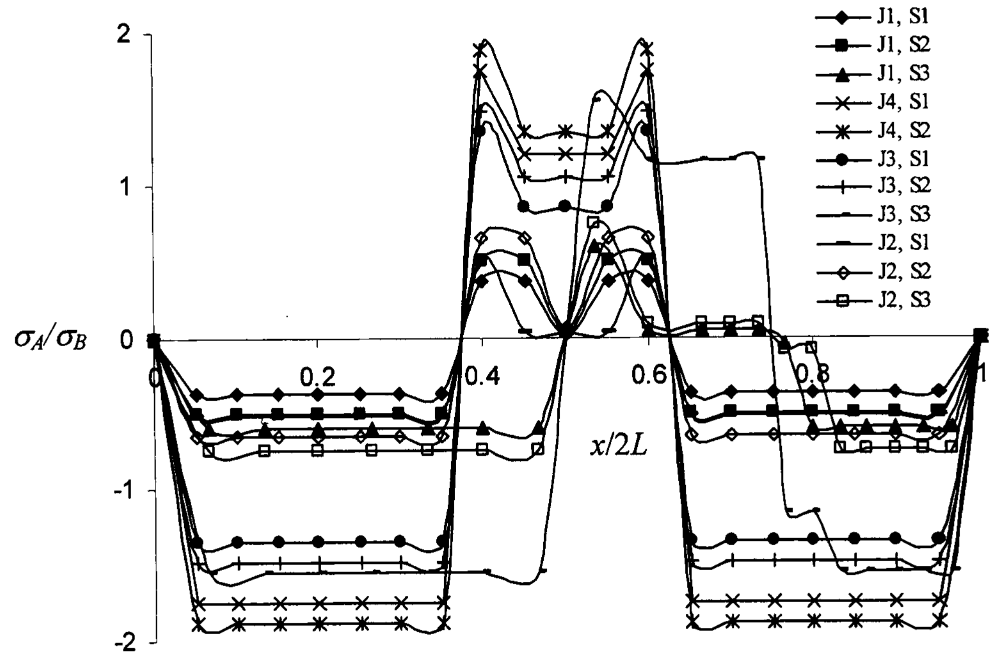

Figure A1.30 Stress ratio excluding self-weight (CASE 3, R1)

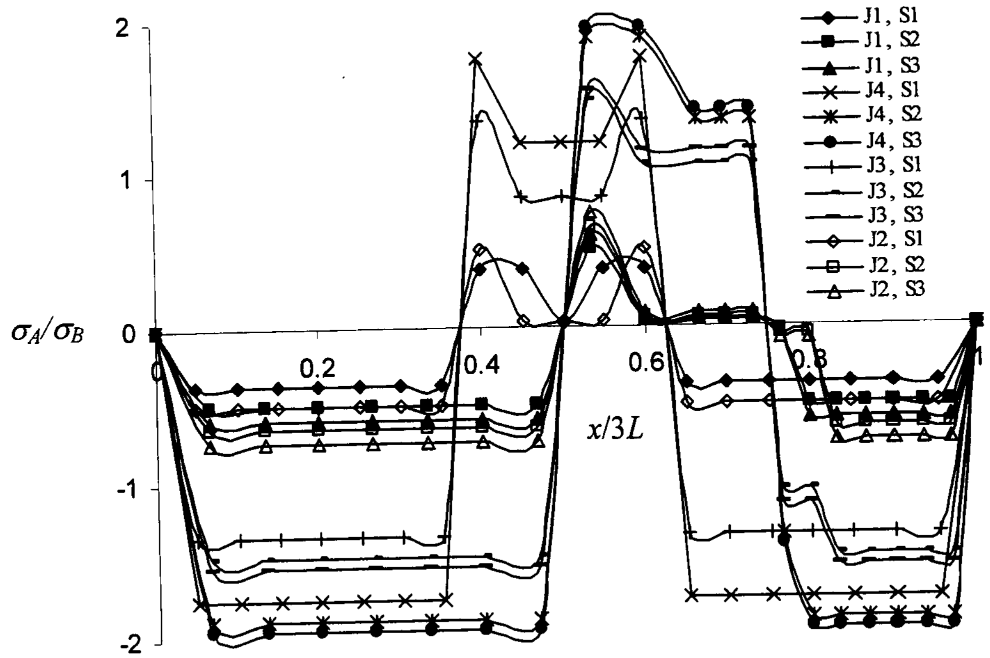

Figure A1.31 Stress ratio excluding self-weight (CASE 4, R1)

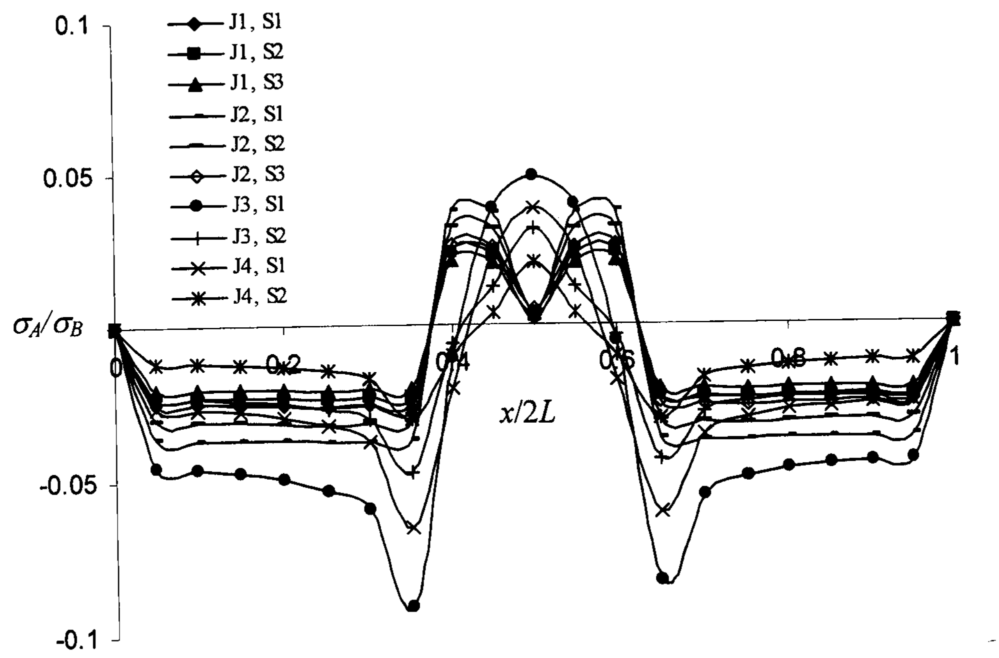

Figure A1.32 Stress ratio including self-weight (CASE 2, R1)

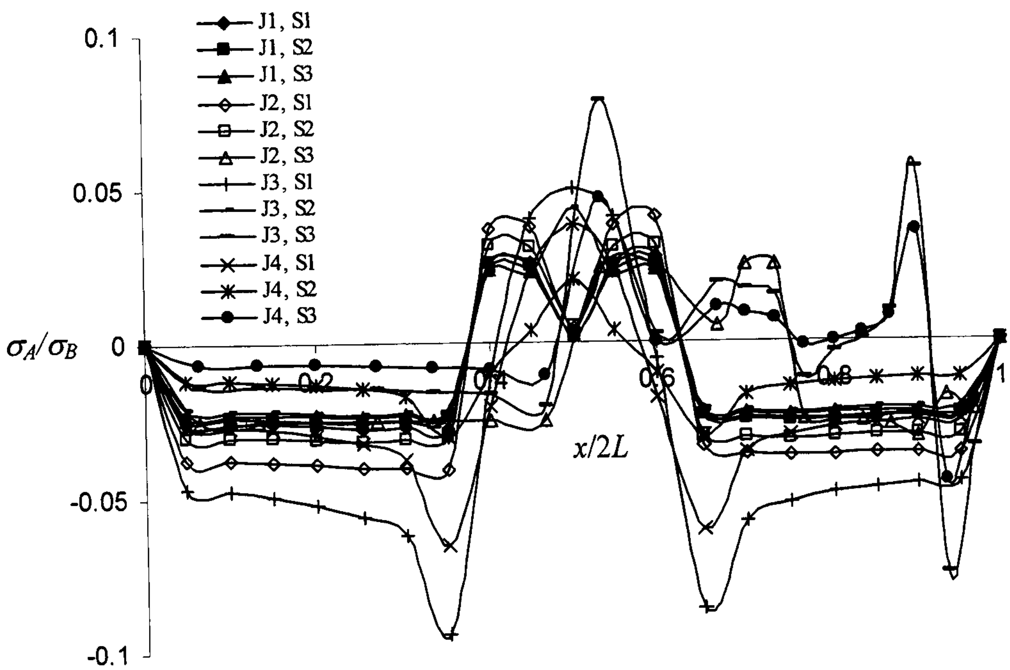

Figure A1.33 Stress ratio including self-weight (CASE 3, S1)

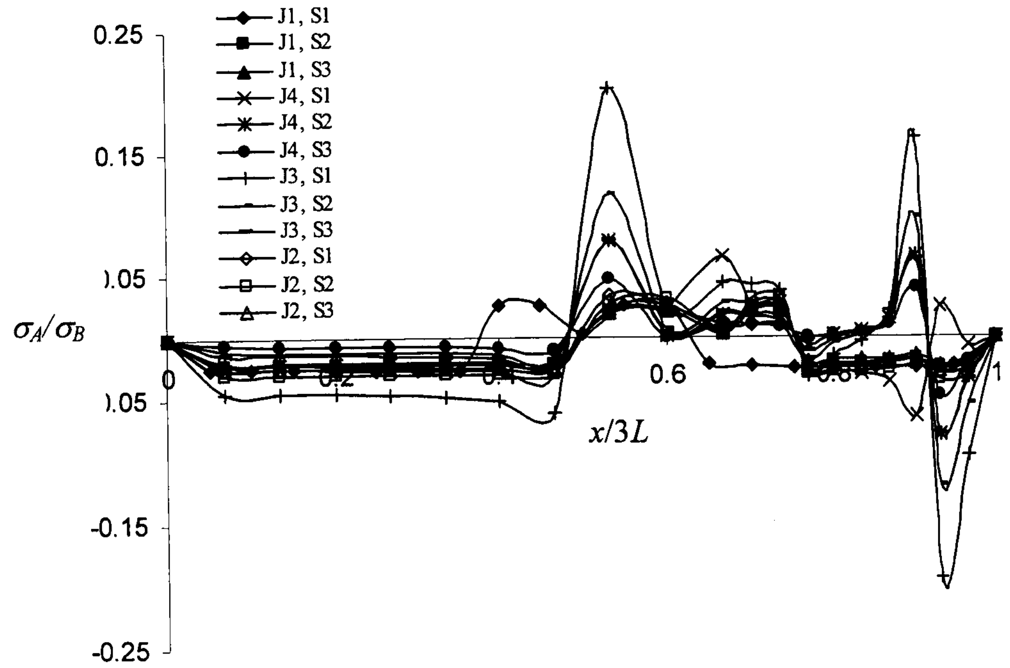

Figure A1.34 Stress ratio including self-weight (CASE 4, R1)

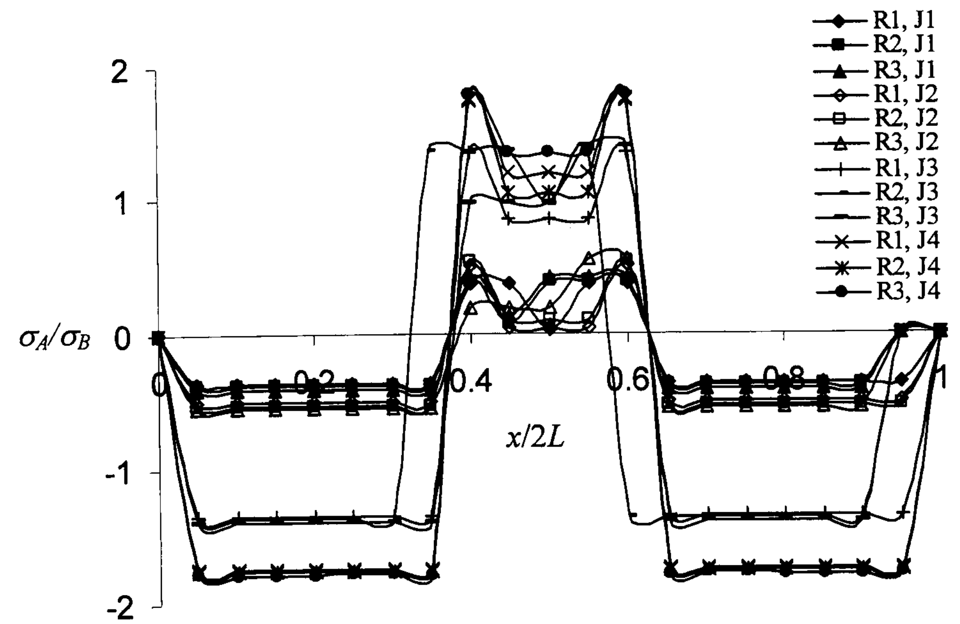

Figure A1.35 Stress ratio excluding self-weight (CASE 2, S1)

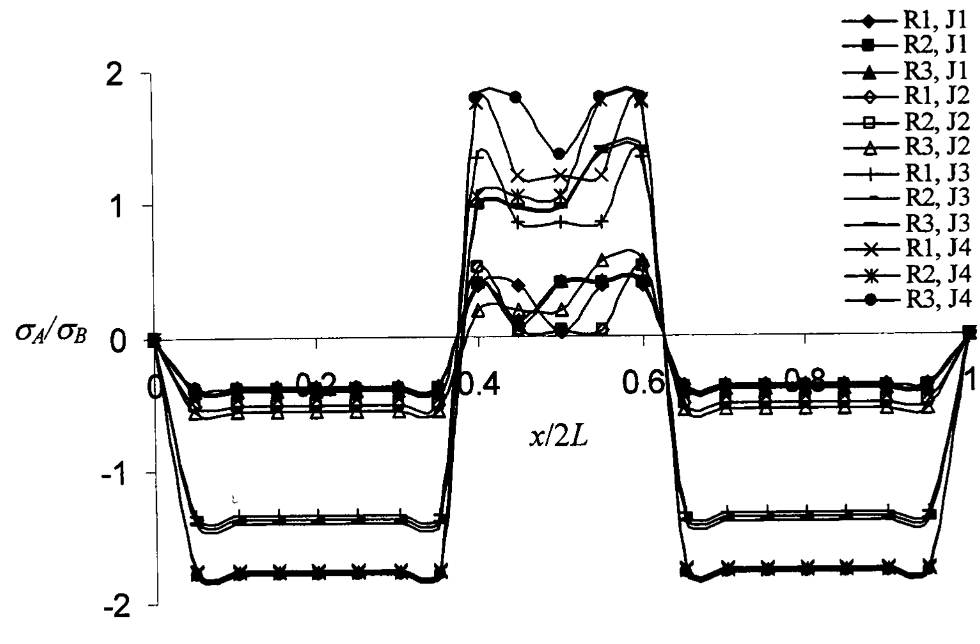

Figure A1.36 Stress ratio excluding self-weight (CASE 3, S1)

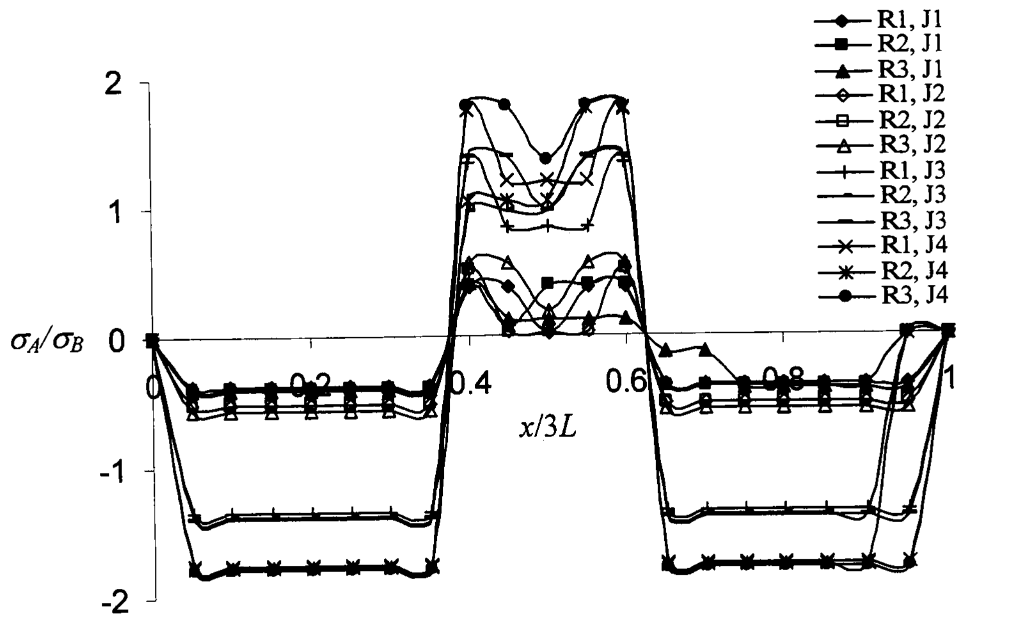

Figure A1.37 Stress ratio excluding self-weight (CASE 4, S1)

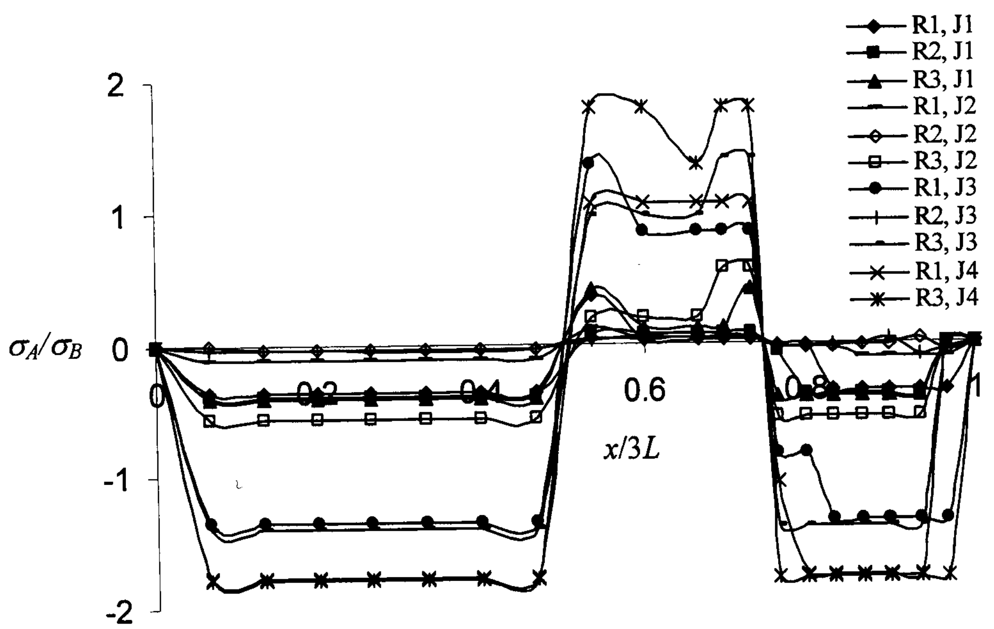

Figure A1.38 Stress ratio excluding self-weight (CASE 5, S1)

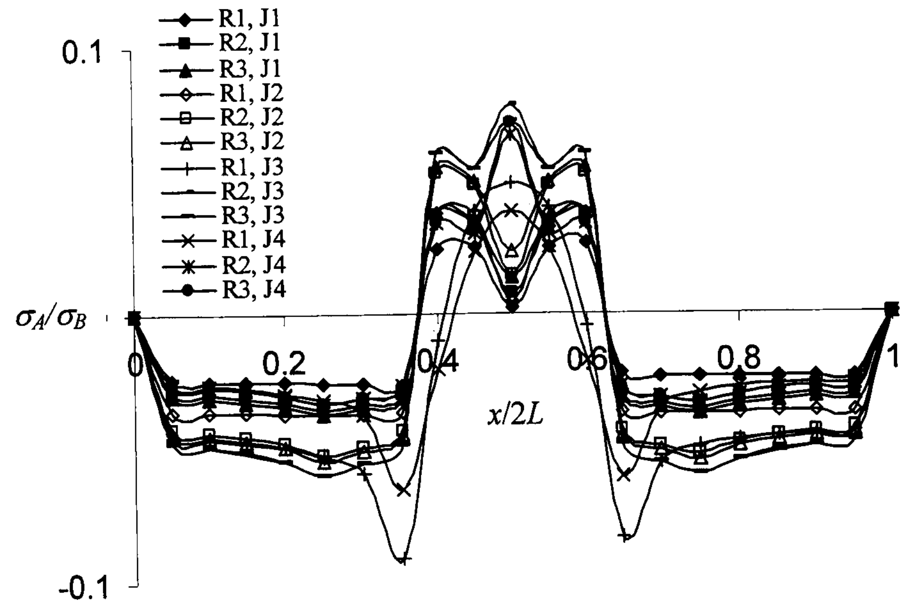

Figure A1.39 Stress ratio including self-weight (CASE 2, S1)

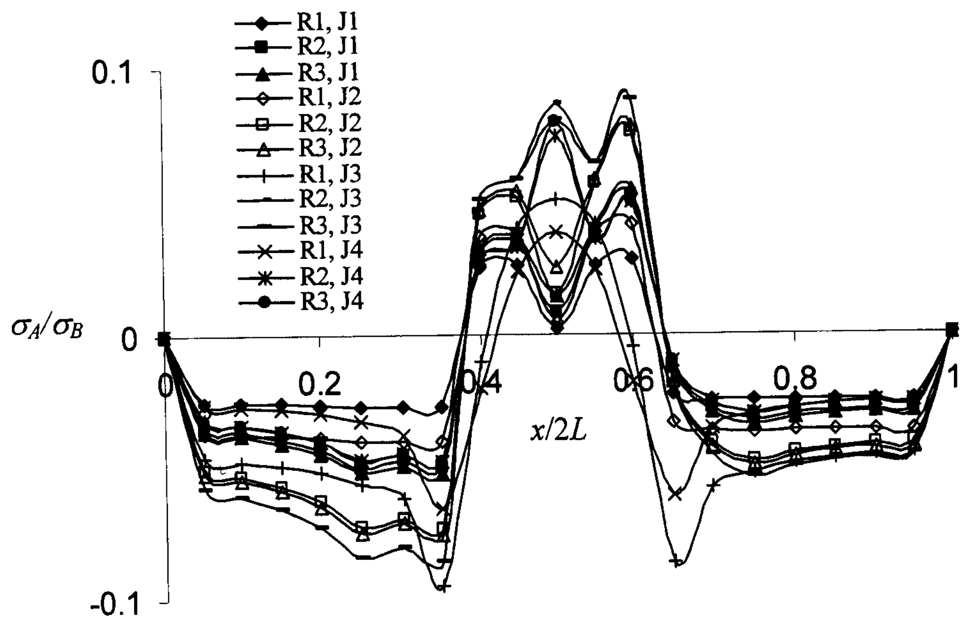

Figure A1.40 Stress ratio including self-weight (CASE 3, S1)

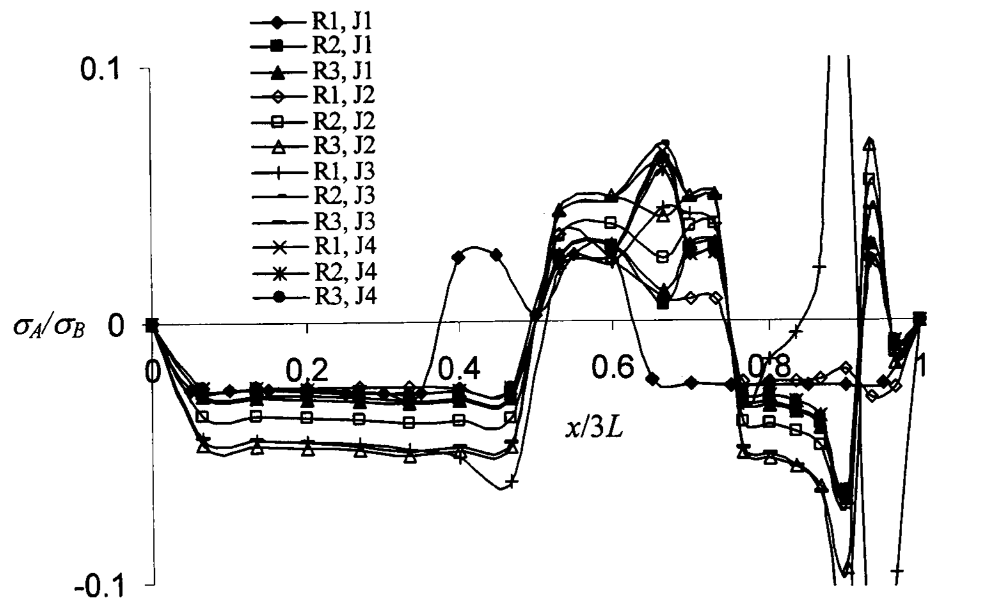

Figure A1.41 Stress ratio including self-weight (CASE 4, S1)

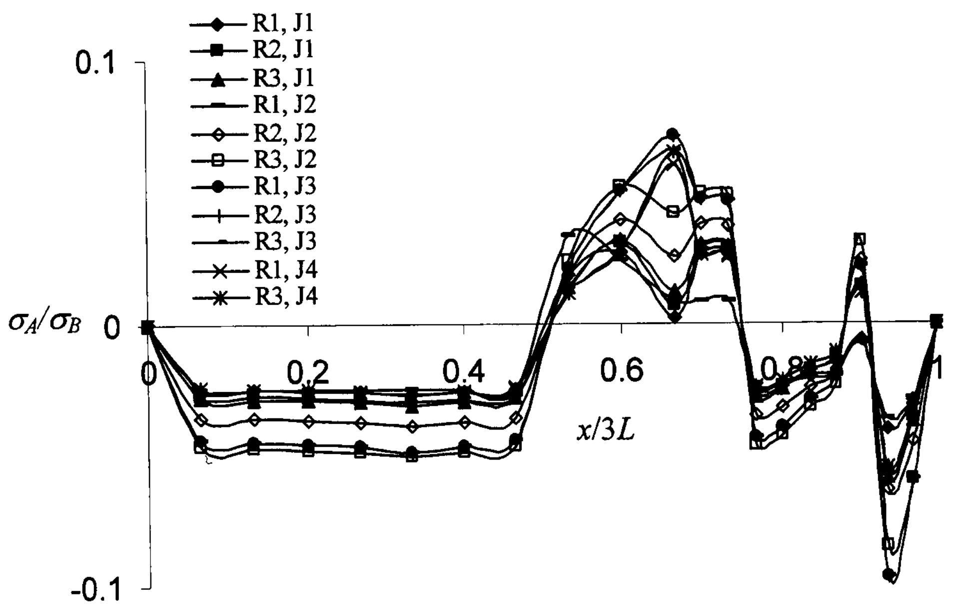

Figure A1.42 Stress ratio including self-weight (CASE 5, S1)

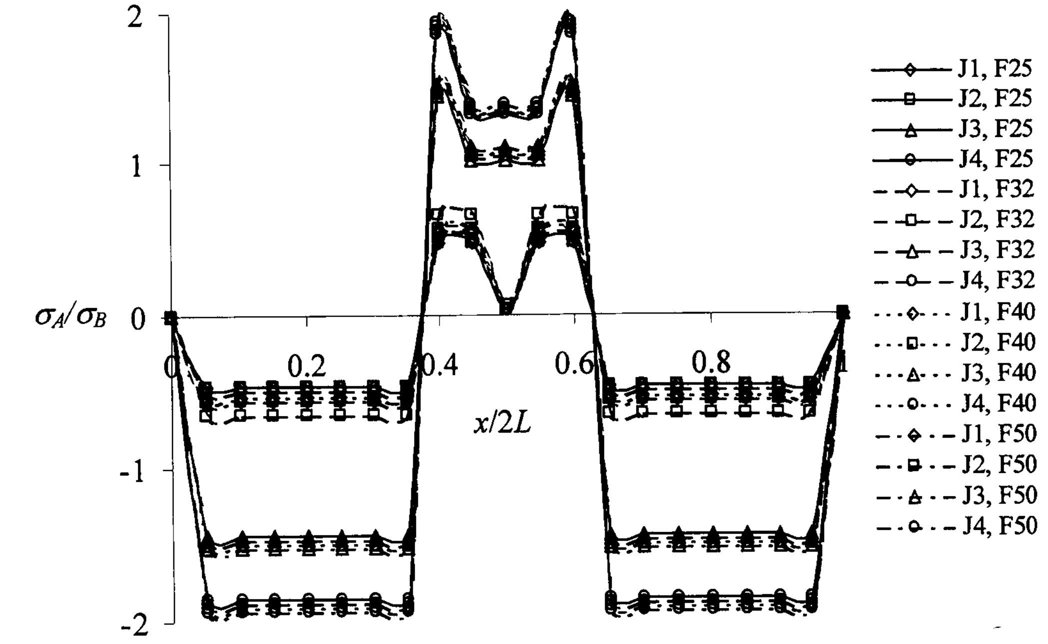

Figure A1.43 Stress ratio excluding self-weight (CASE 1, R1, S2)

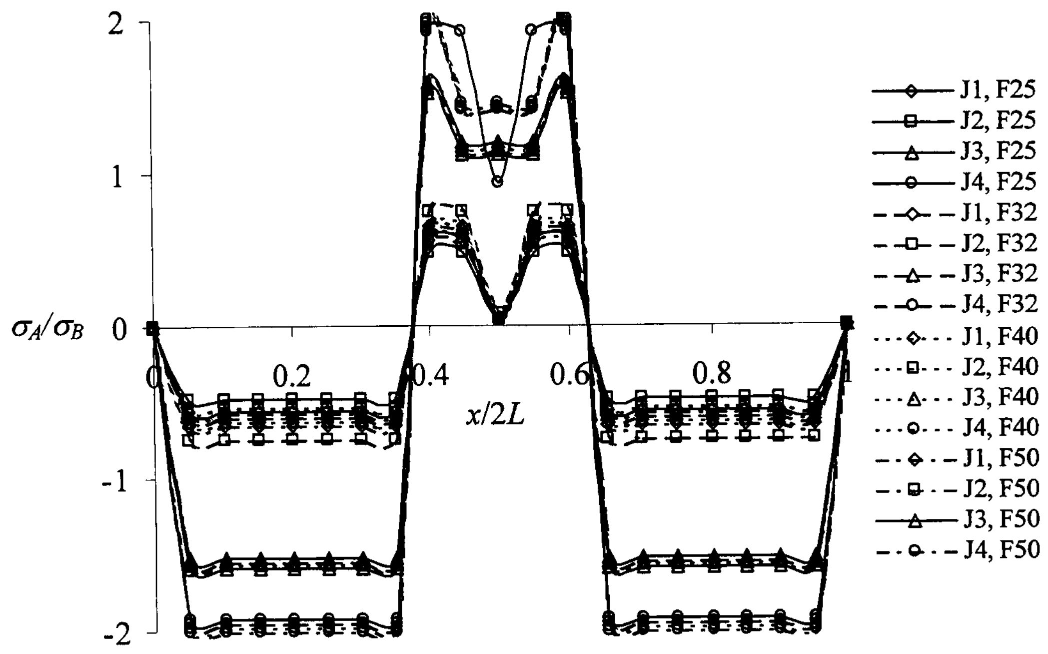

Figure A1.44 Stress ratio excluding self-weight (CASE 1, R1, S3)

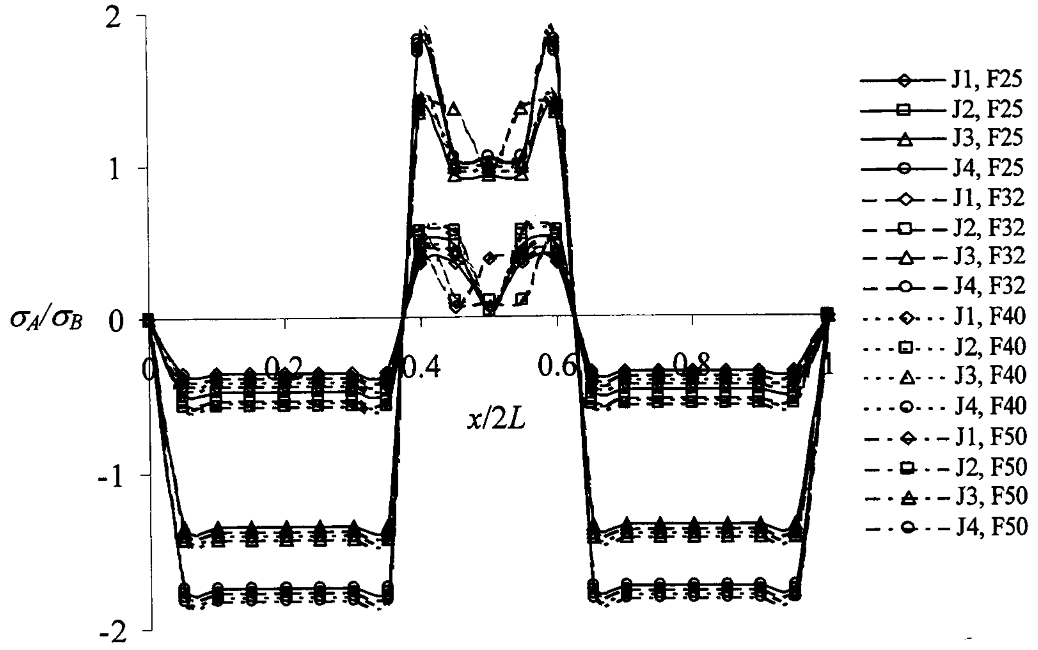

Figure A1.45 Stress ratio excluding self-weight (CASE 1, R2, S1)

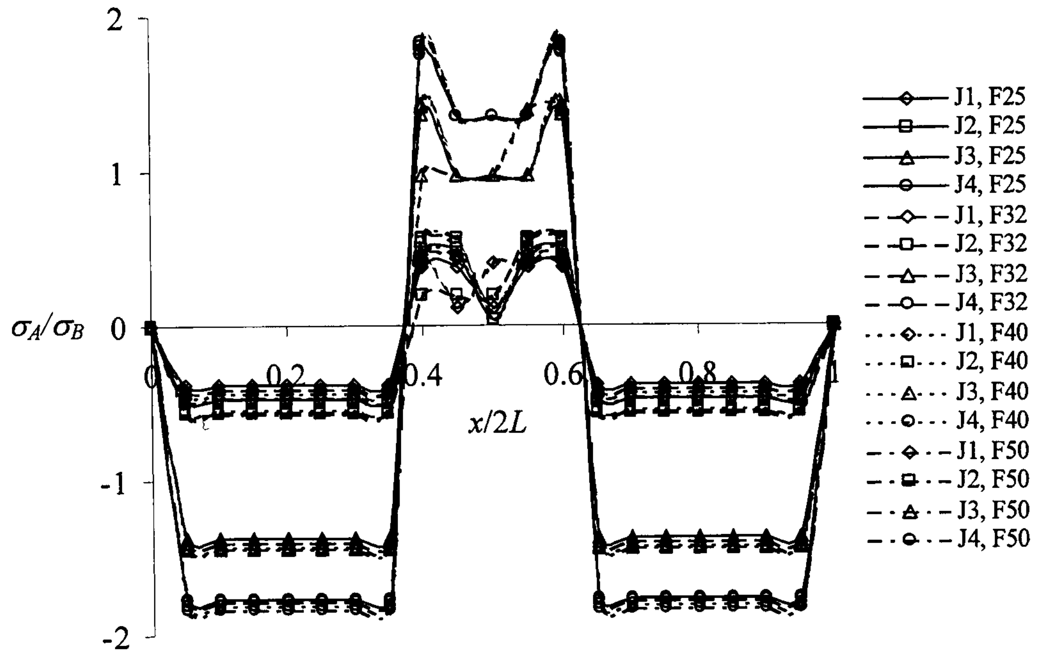

Figure A1.46 Stress ratio excluding self-weight (CASE 1, R3, S1)

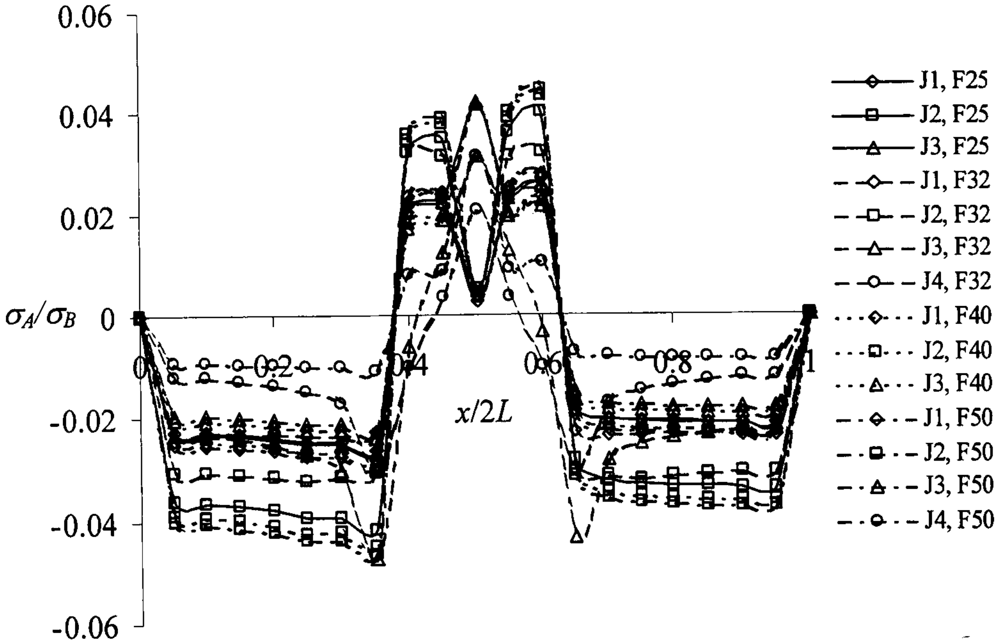

Figure A1.47 Stress ratio including self-weight (CASE 1, R1, S2)

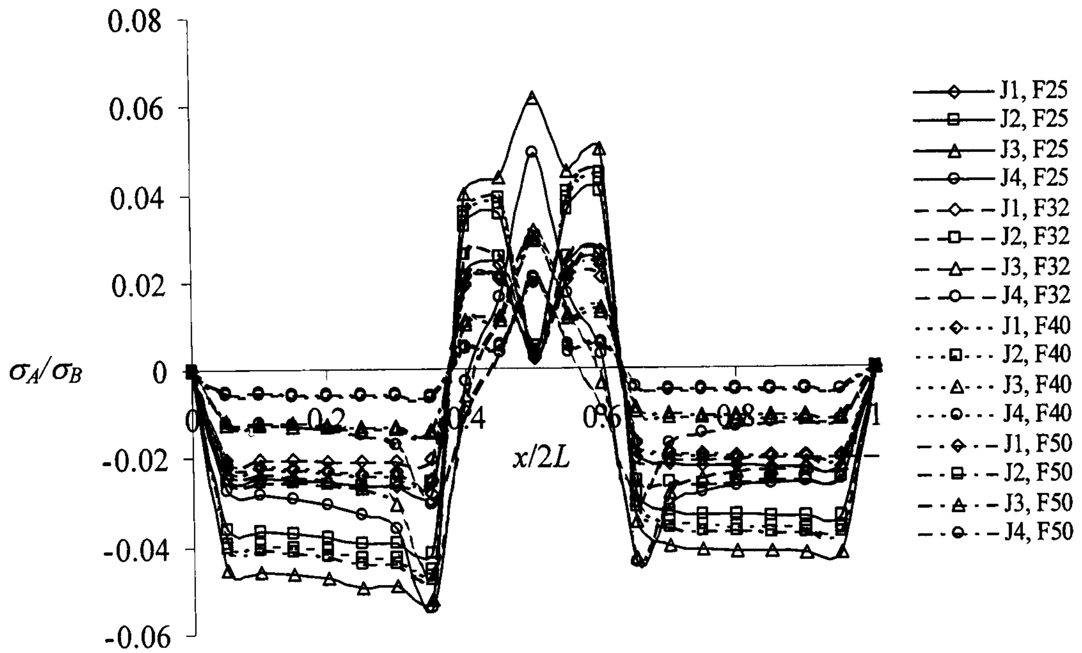

Figure A1.48 Stress ratio including self-weight (CASE 1, R1, S3)

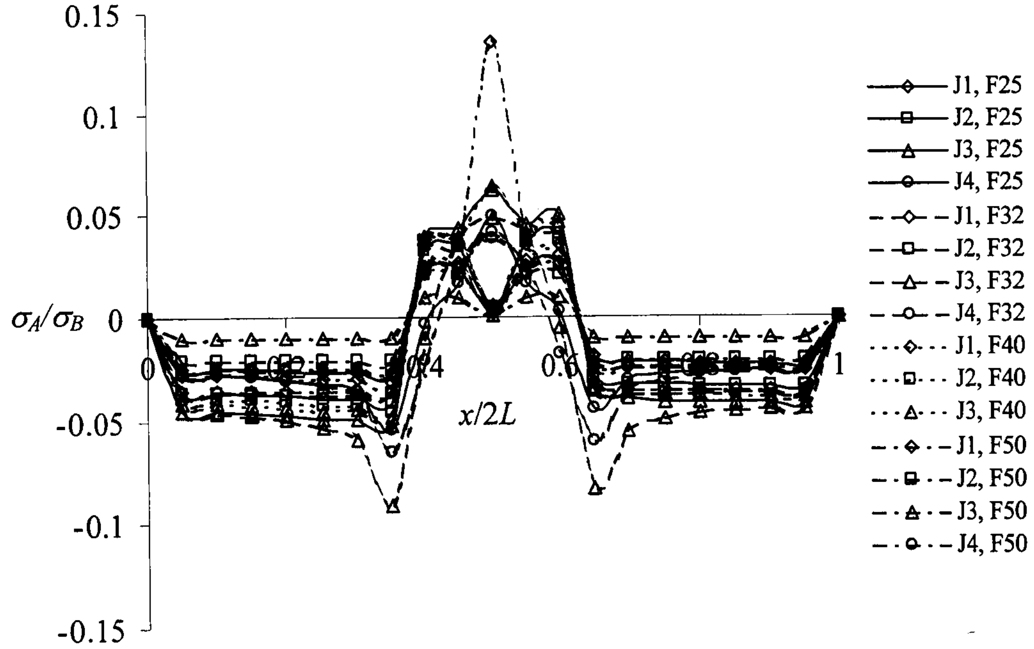

Figure A1.49 Stress ratio excluding self-weight (CASE 1, R2, S1)

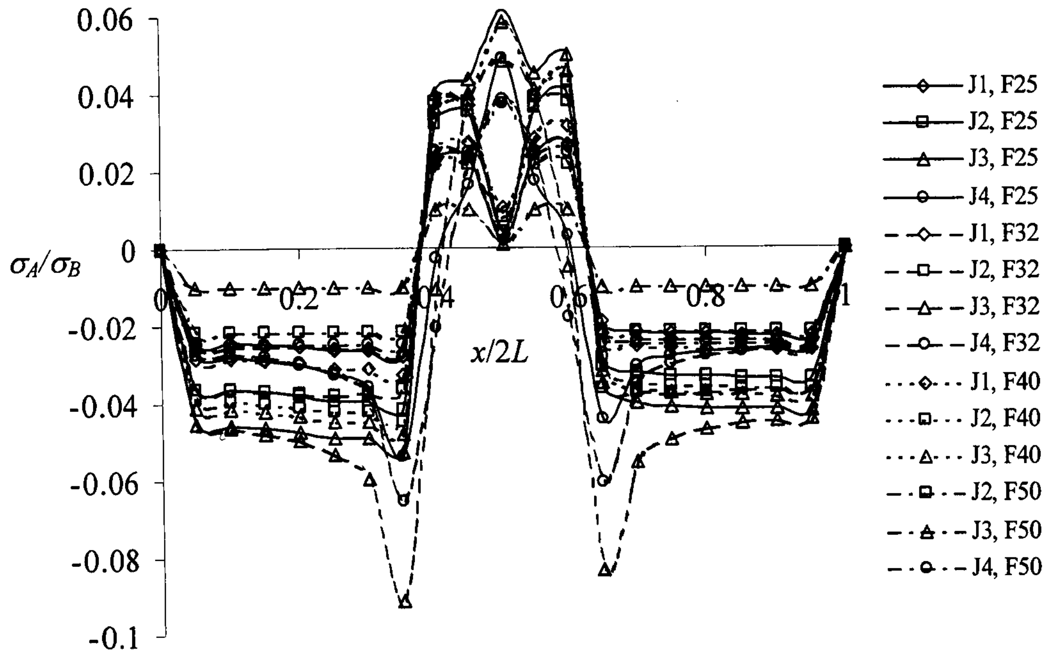

Figure A1.50 Stress ratio including self-weight (CASE 1, R3, S1)

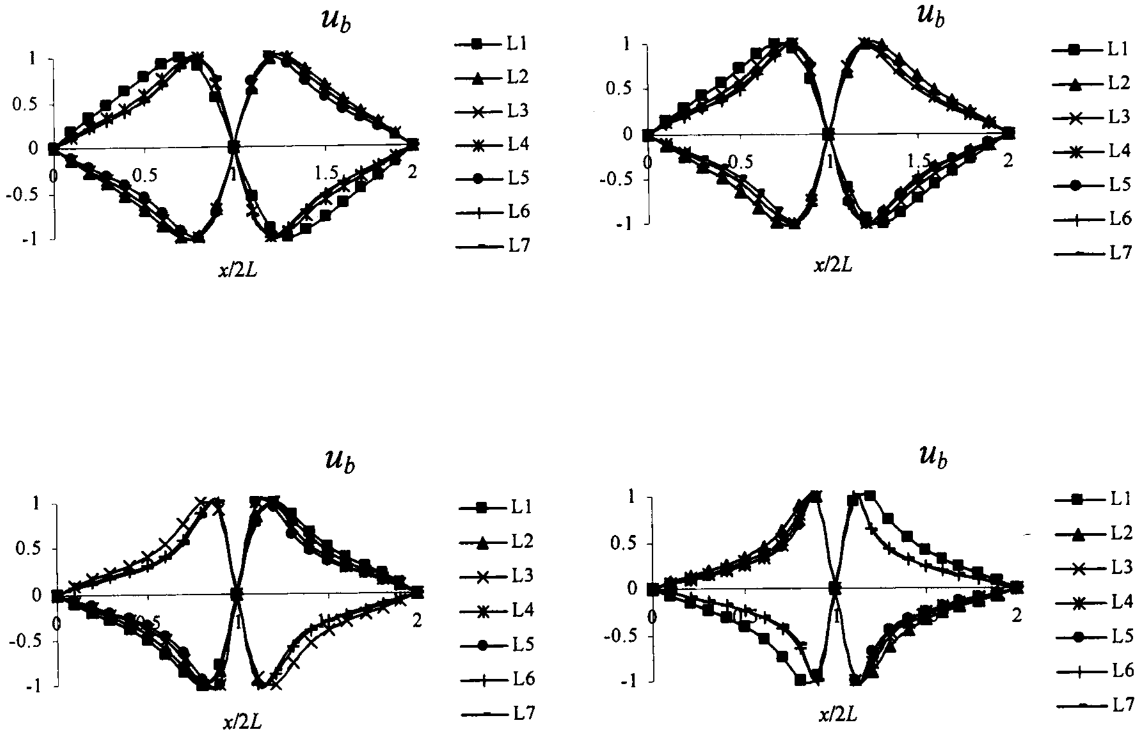

Figure A1.51 Buckling modes (CASE 2, R1, S1, unpropped construction): (i) J1, (ii) J2, (iii) J3 and (iv) J4

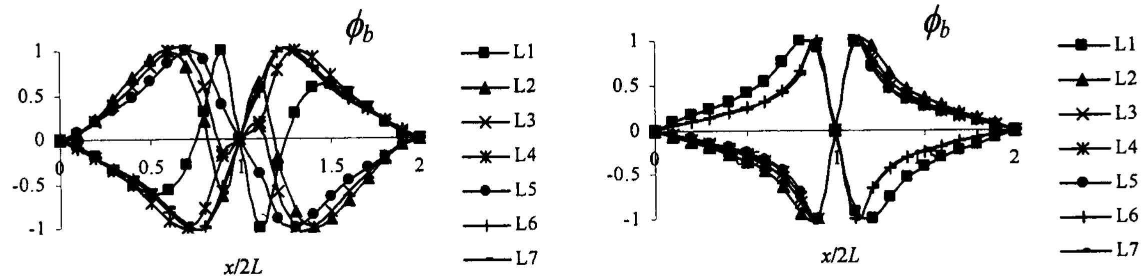

Figure A1.52 Buckling modes (CASE 2, R1, S1, unpropped construction): (i) J1 and (ii) J4

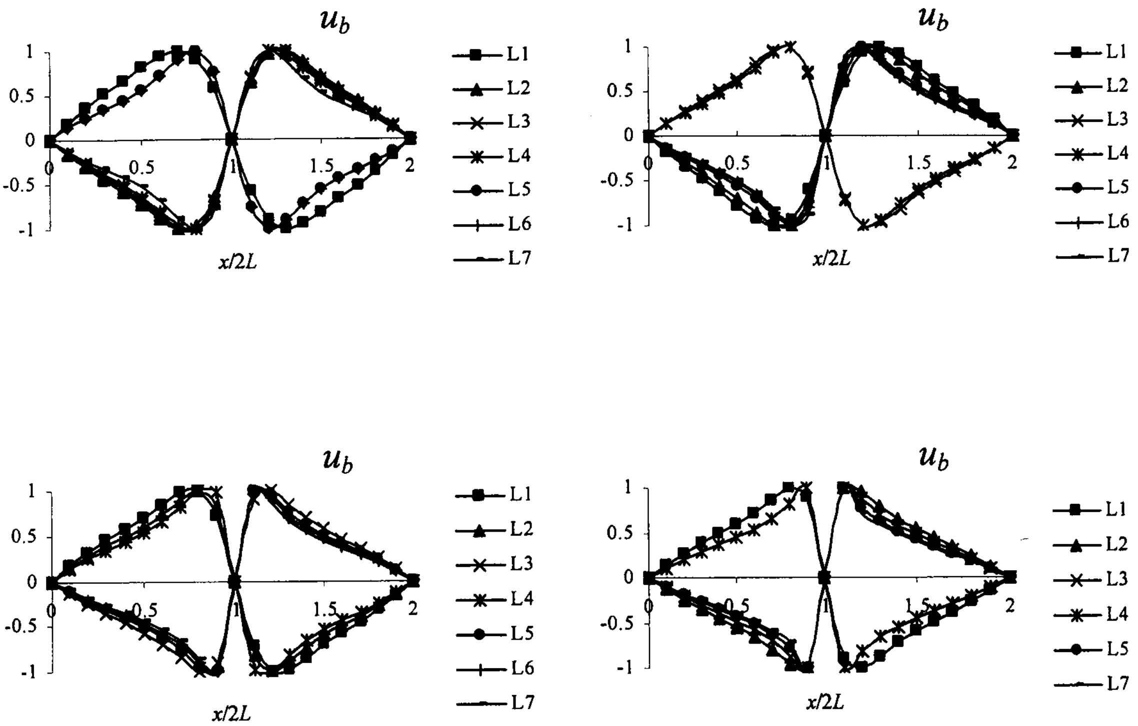

Figure A1.53 Buckling modes (CASE 2, R1, S1, propped construction): (i) J1, (ii) J2, (iii) J3 and (iv) J4

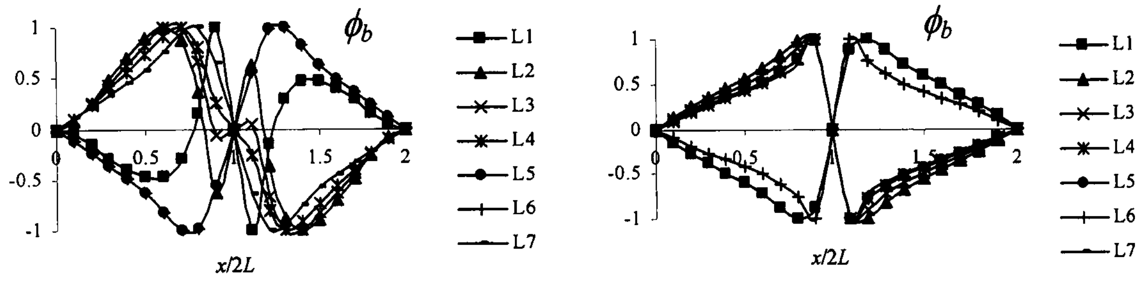

Figure A1.54 Buckling modes (CASE 2, R1, S1, propped construction): (i) J1 and (ii) J4

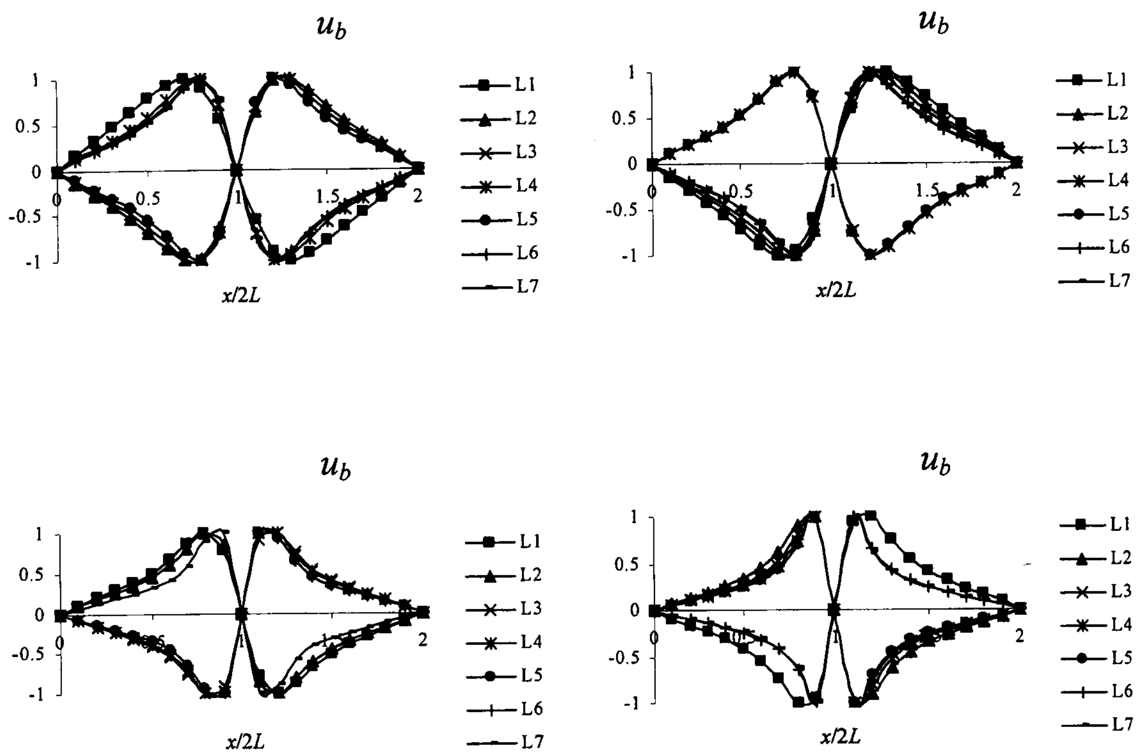

Figure A1.55 Buckling modes (CASE 3, R1, S1, unpropped construction): (i) J1, (ii) J2, (iii) J3 and (iv) J4

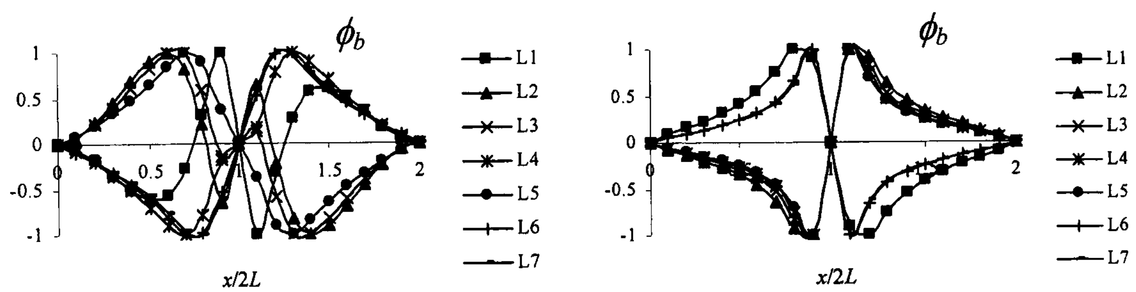

Figure A1.56 Buckling modes (CASE 3, R1, S1, unpropped construction): (i) J1 and (ii) J4

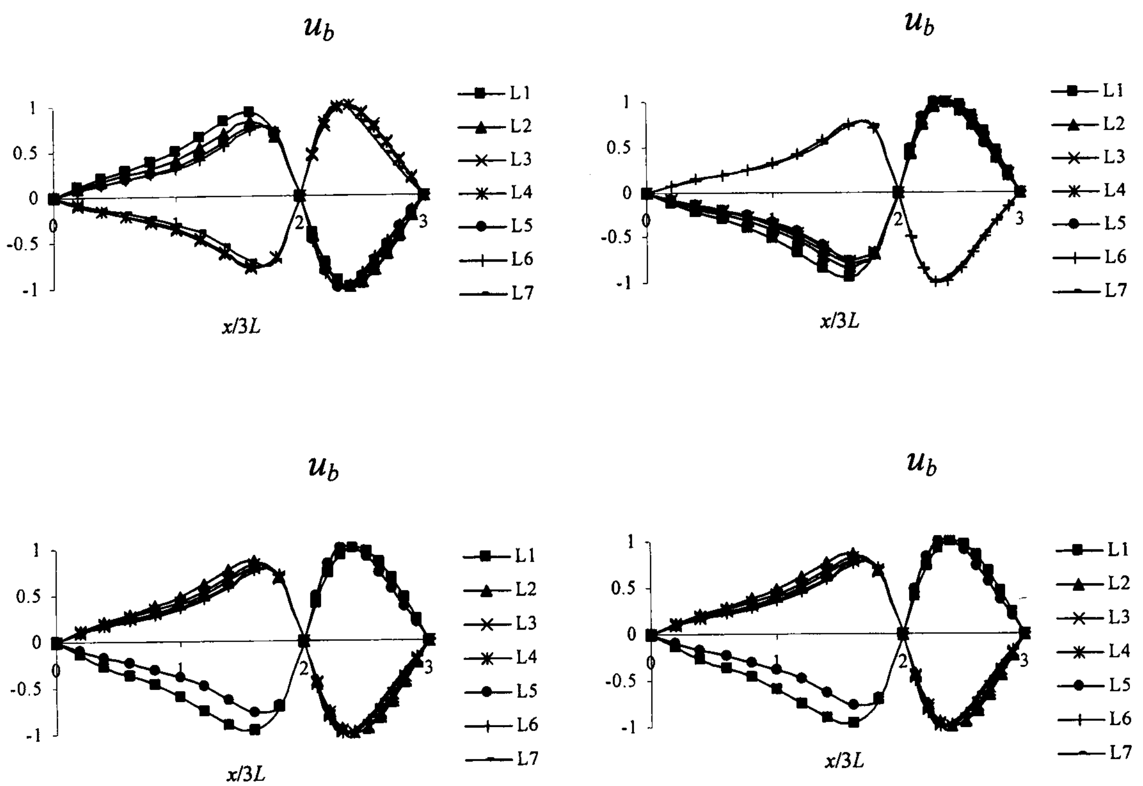

Figure A1.57 Buckling modes (CASE 5, R1, S1, unpropped construction):
(i) J1, (ii) J2, (iii) J3 and (iv) J4

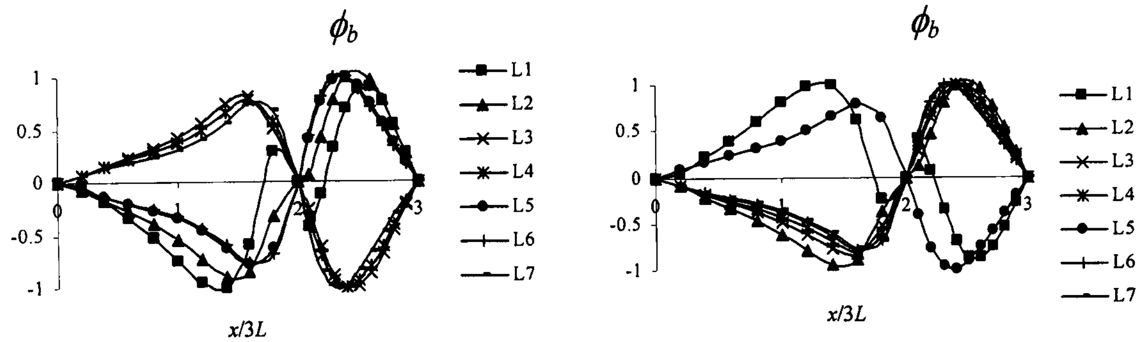

Figure A1.58 Buckling modes (CASE 5, R1, S1, unpropped construction):
(i) J1 and (ii) J4

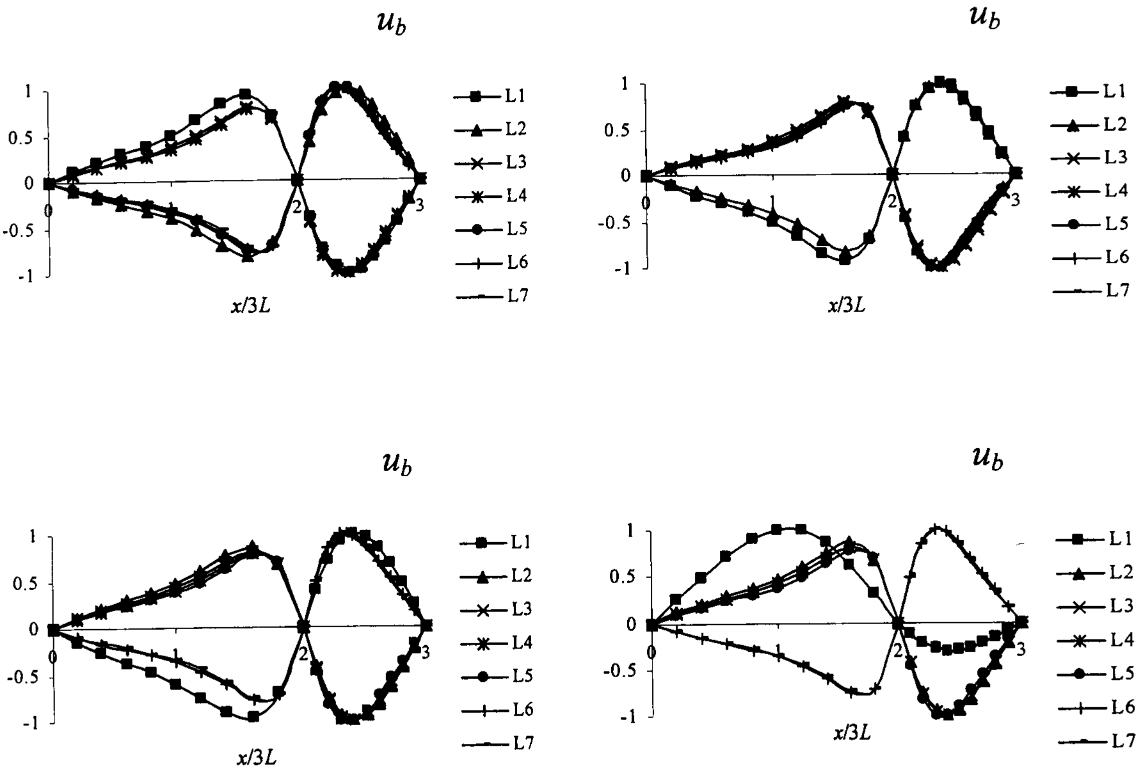

Figure A1.59 Buckling modes (CASE 6, R1, S1, unpropped construction):
(i) J1, (ii) J2, (iii) J3 and (iv) J4

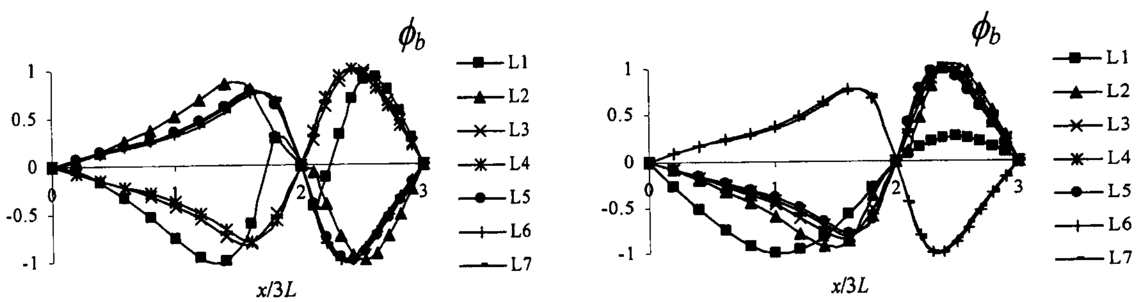

Figure A1.60 Buckling modes (CASE 6, R1, S1, unpropped construction):
(i) J1 and (ii) J4

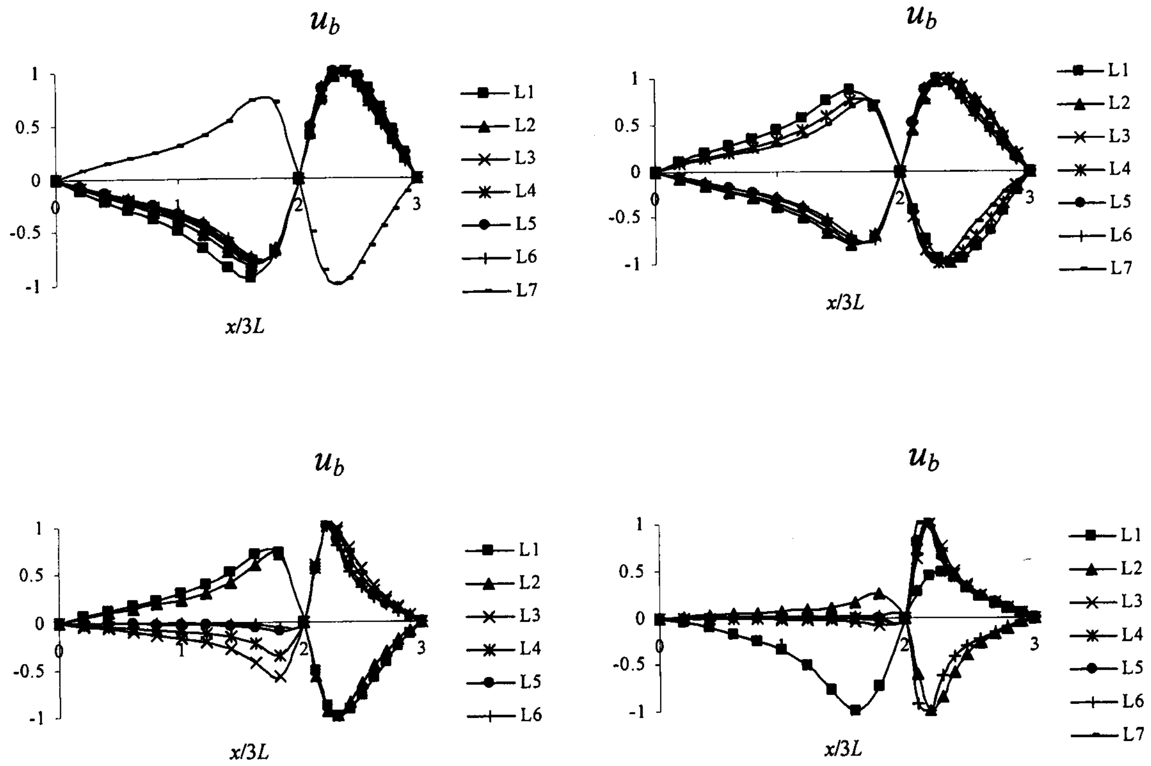

Figure A1.61 Buckling modes (CASE 7, R1, S1, unpropped construction):
(i) J1, (ii) J2, (iii) J3 and (iv) J4

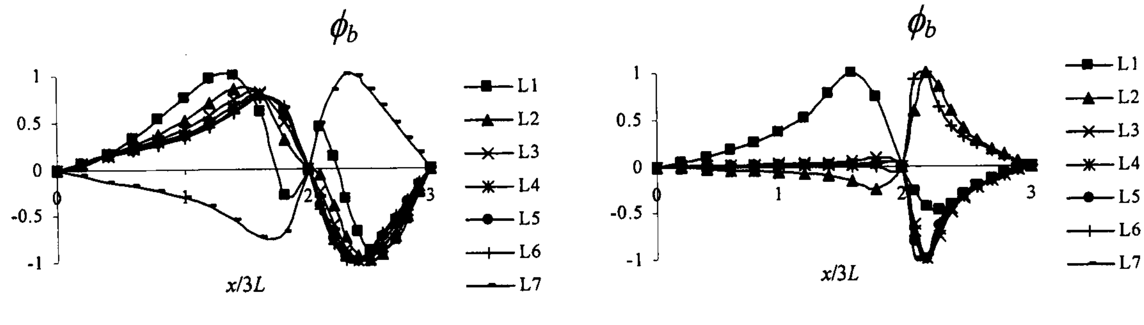

Figure A1.62 Buckling modes (CASE 7, R1, S1, propped construction):
(i) J1 and (ii) J4

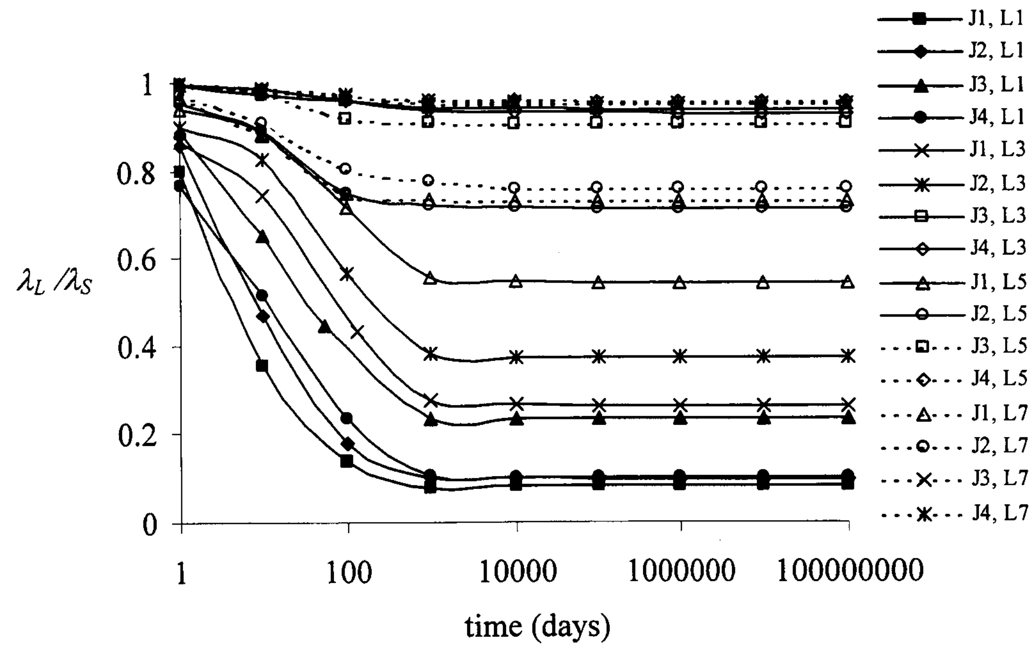

Figure A1.63 Creep and shrinkage effects (R1, S2, equal spans, unpropped construction)

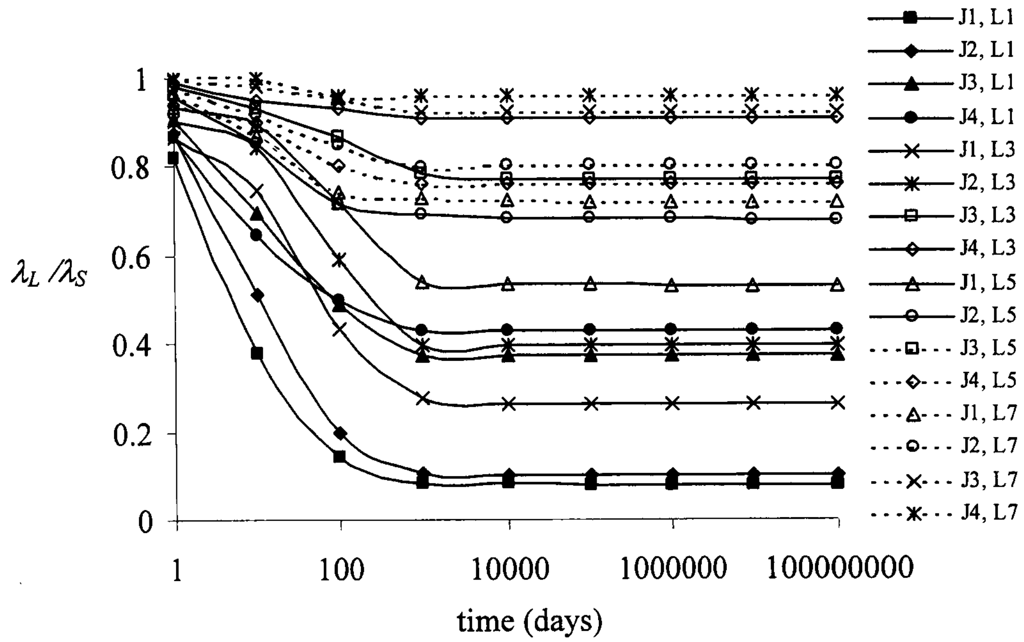

Figure A1.64 Creep and shrinkage effects (R1, S3, equal spans, unpropped construction)

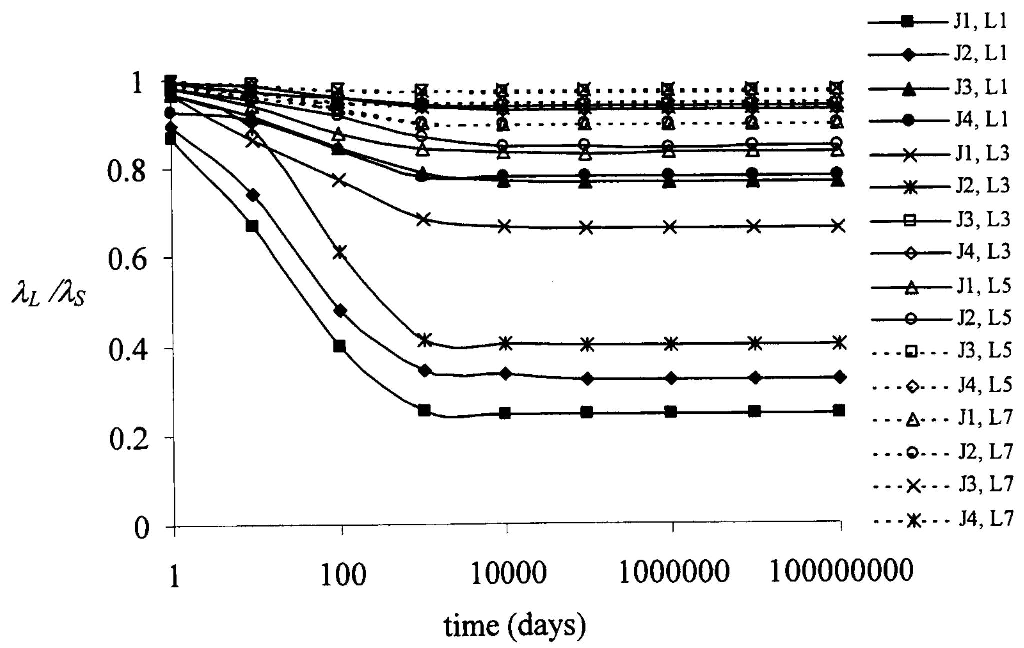

Figure A1.65 Creep and shrinkage effects (R1, S2, unequal spans, unpropped construction)

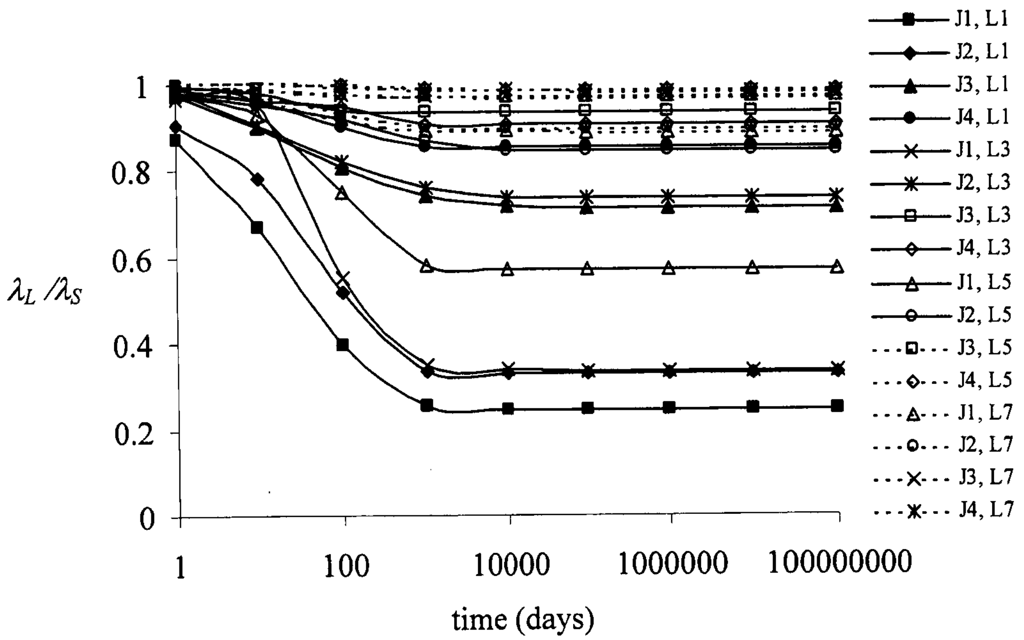

Figure A1.66 Creep and shrinkage effects (R1, S3, unequal spans, unpropped construction)

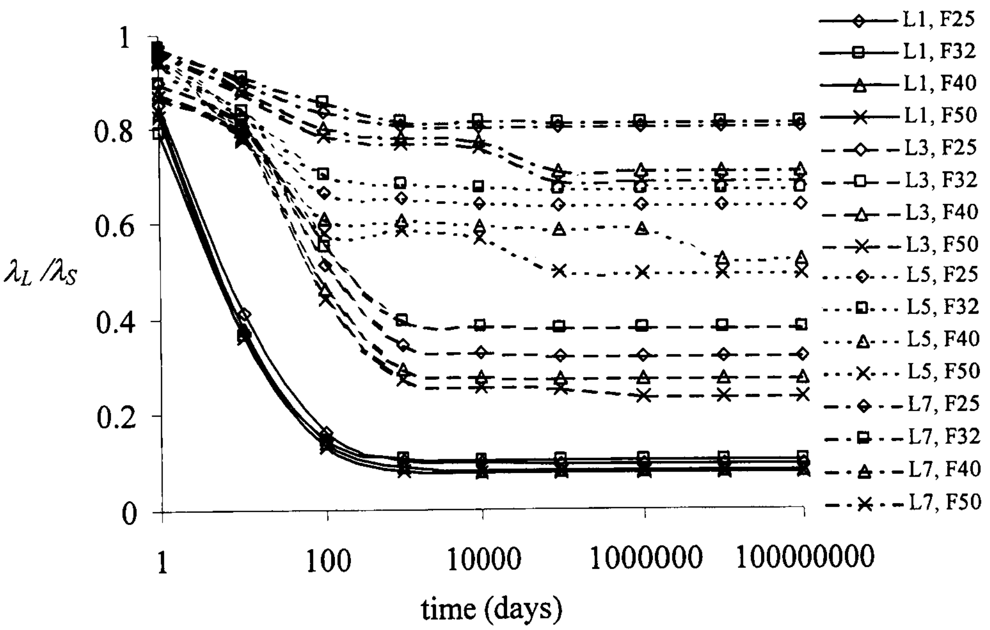

Figure A1.67 Creep and shrinkage effects (J2, R1, S1, equal spans, unpropped construction)

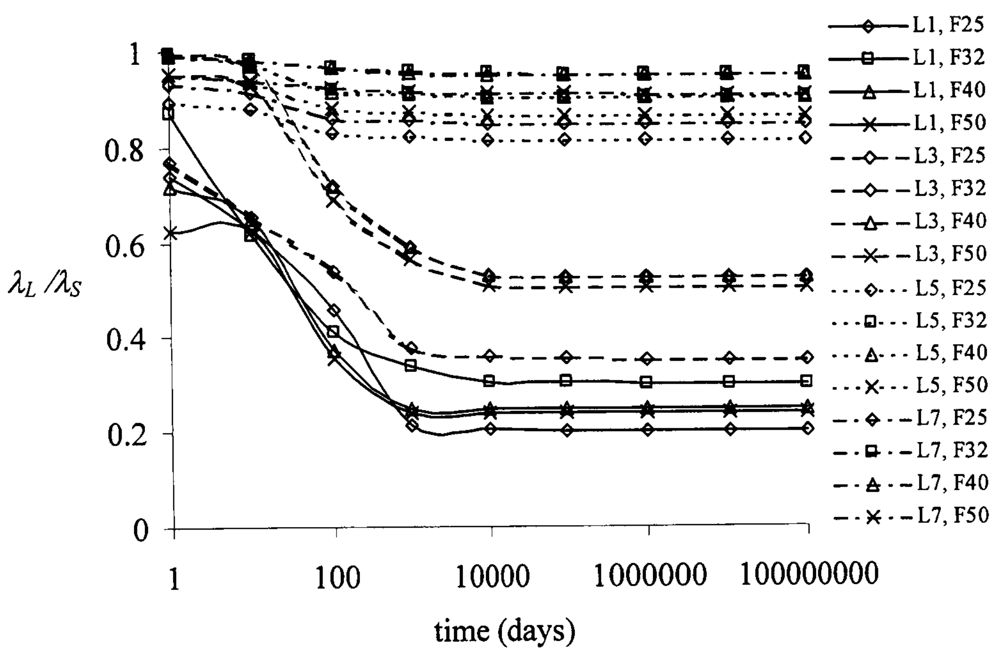

Figure A1.68 Creep and shrinkage effects (J3, R1, S1, equal spans, unpropped construction)

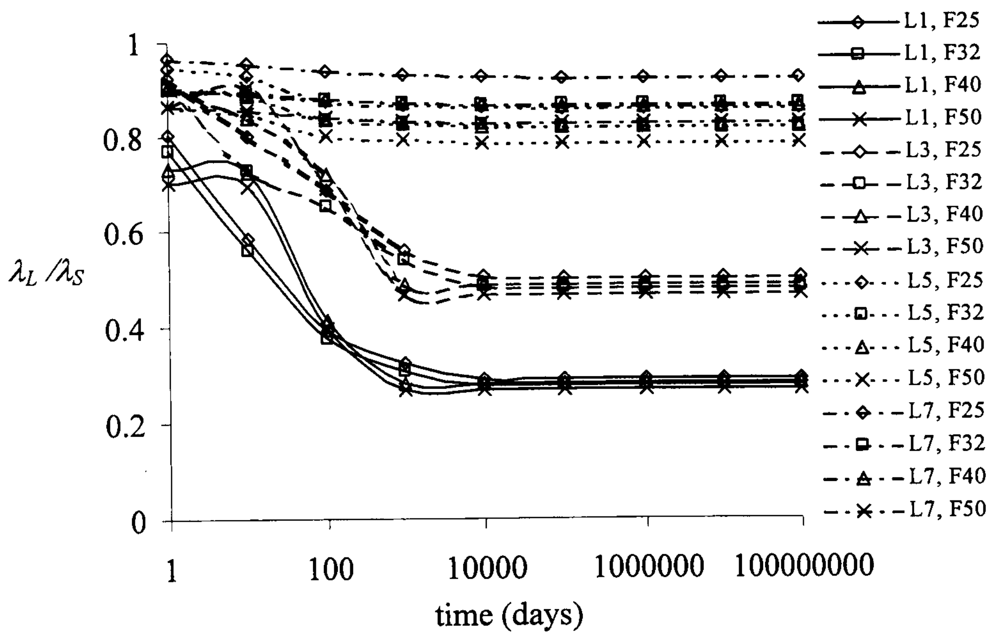

Figure A1.69 Creep and shrinkage effects (J4, R1, S1, equal spans, unpropped construction)